Bend Diversion to Minimise Sediment Intake

CJ Brink

Thesis presented in partial fulfilment of the requirements for the degree of Master of Engineering at the University of Stellenbosch.

PROF GR BASSON DECEMBER 2004

I, the undersigned, hereby declare that the work contained in this thesis is my own original work and that I have not previously in its entirety or in part submitted it at any university for a degree.

Signature: .....…..... Date: .....

SYNOPSIS

The primary aim of the research was to determine the optimum diversion location in a curved channel to minimise the abstraction of sediment. The secondary aim was to determine the optimum diversion angle for a diversion channel located on the outside of a bend at the optimum diversion location.

The velocity distribution in the curved channel was investigated to try obtain a better understanding of curvilinear flow. The scour patterns in the channel were monitored in order to compare them with the measured velocity distributions.

Simulations were carried out with the DELFT 3D (hydrodynamics) and Mike21C (sediment dynamics) modelling programmes and compared with the results obtained from laboratory experiments and with existing empirical formulas.

The optimum diversion location was found to be located on the outside of the bend in the downstream section of the bend. Three main scour zones were identified with the third scour zone at the location of the maximum velocity. The location of the maximum velocity was found to be relatively constant with varying Froude numbers, but moving in the downstream direction with increasing radius of curvature-to-width ratio. The velocity distributions in the horizontal and vertical planes are well defined and correspond to descriptions in the literature.

It is evident that the diverted discharge ratio increases with an increase in the diversion angle while it decreases with an increase in Froude number. Higher Froude numbers in the curved channel lead to more favourable conditions for the diversion of water. The diversion does not influence the secondary flow patterns (for the range of Diversion Discharge Ratio's tested) and that the maximum velocity zone stayed in the same location as in the tests without a diversion.

The hydrodynamics of the laboratory experiments were well simulated with the DELFT 3D hydrodynamic model, using three-dimensional and two-dimensional formulations. Mike21C was used to simulate the sediment dynamics of some of the

laboratory experiments that gave relatively good agreement with experimental data. A two-dimensional depth averaged model could therefore be used with reliability to simulate field conditions in relatively shallow rivers, and is preferred to empirical methods to predict maximum scour that were calibrated under very specific hydraulic conditions.

SAMEVATTING

Die primêre doel van navorsing was om die optimum uitkeer-posisie in ‘n draai te bepaal om sodoende sediment onttrekking te minimiseer. Die sekondêre doel was om die optimum uitkeringshoek vir ‘n uitkeerkanaal te bepaal wat geleë is aan die buitekant van ‘n draai by die voorgestelde optimum uitkeer-posisie.

Die snelheidsverspreiding in die draai was ook ondersoek om te probeer om spiraalvloei beter te verstaan. Die uitskuurpatrone in die kanaal is ook gemonitor om dit te kon vergelyk met die gemete snelheidsverspreiding.

Numeriese simulasies is gedoen met DELFT 3D (hidrodinamika) en Mike21C (sediment dinamika) modelleringsprogrammatuur en is vergelyk met die resultate van die laboratorium eksperimente asook met die van bestaande empiriese vergelykings.

Daar is gevind dat die optimum uitkeer-posisie aan die buitekant van ‘n draai aan die stroomaf-kant van die draai geleë is. Drie hoof uitskurings-areas is gevind terwyl die derde area ooreenstem met die posisie van maksimum snelheid. Die posisie waar die maksimum snelheid voorkom is relatief konstant met ‘n verandering in Froude-getal, maar beweeg in die stroomaf-rigting met ‘n styging in die radius-tot-wydte verhouding. Die vertikale en horisontale snelheidsverspreiding is goed gedefinieer en stem ooreen met soortgelyke beskrywings in die literatuur.

Die uitkeer-vloei verhouding styg met ‘n stygende uitkeerhoek terwyl dit daal met ‘n styging in Froude-getal. Daar is ook gevind dat groter Froude-getalle meer gunstige omstandighede skep vir die uitkeer van water. Die uitkeer-kanaal beïnvloed nie die sekondêre vloei-patrone nie (vir die reeks van uitkeer vloei-verhoudings wat getoets

is) en die sone van maksimum snelheid bly in dieselfde omgewing vir hierdie toetse as vir die toetse sonder ‘n uitkeer kanaal.

Die hidrodinamika van die laboratorium eksperimente is goed gesimuleer m.b.v die DELFT 3D numeriese program, terwyl Mike21C gebruik is om die sedimentdinamika te simuleer. Die resultate van die Mike21C simulasies vergelyk relatief goed met die eksperimentele data en kan met ‘n redelike graad van vertroue aangewend word om veldkondisies te simuleer in relatiewe vlak riviere. Dit word aanbeveel bo die empiriese vergelykings om maksimum uitskuring te voorspel aangesien die empiriese vergelykings gekalibreer is vir baie spesifieke hidroulise kondisies.

ACKNOWLEDGEMENTS

This document is dedicated to my wife, Elbè, for all her support and motivation that enabled me to persist in finishing my studies. Thank you for supporting me in realising one of my dreams, I will always be grateful to you.

To my parents, thank you for providing me with a solid foundation that I can apply in life and for all the sacrifices you made over the years. It is much appreciated.

Prof Gerrit Basson, your guidance and advice throughout my post-graduate studies are appreciated. Thank you for giving me the opportunity to be part of your research team.

I would like to acknowledge the following persons for all their support that enabled me to compile this document:

- The board of directors of Element Consulting Pty (Ltd) for giving me the opportunity to continue with my studies and for the partial funding of my postgraduate studies.
- Ms Onele Mngambi for her assistance with the laboratory work.
- Mr Frank Denys for his assistance with the Mike 21C simulations.
- Messrs Noël Combrinck and Andreas Hector of the Hydraulic Laboratory of the University of Stellenbosch for their support in building the model and always being available to lend a helping hand.
- Messrs Dries Rossouw and Louis Fredericks of the Department of Civil Engineering's Workshop of the University of Stellenbosch who helped with the preparation of the laboratory work.

TABLE OF CONTENTS

Page

LIST OF FIGURES

Page

LIST OF TABLES

Page

LIST OF SYMBOLS

Δh = change in water level

ξ = coefficient

ϕ = flow deviation angle

σ_g = standard deviation of the bed material

θ = diversion angle

θ_{sec} = angle for fully developed secondary flow

θ_{bend} = central bend angle

$\theta_{v,max}$ = the angle where the maximum velocity is located

$\overline{u}$ = radial velocity (xy plane)

b = bed width of the diversion

w = channel width

C = Chezy coefficient

D = flow depth

d = water depth

F_r = Froude number

g = acceleration due to gravity

G_0 = incoming sediment load from river

G_b = sediment concentration in the branch channel

G_d = diverted sediment load

G_m = sediment concentration in the main channel

h = flow depth

H = water level above V-notch

K = constant

K = diversion angle [rad]

L = distance to optimum diversion location

L_{tot} = length of the diversion bend

$L_{v,max}$ = location of the maximum velocity

$\overline{Q}$ = long-term average river flow

Q_c = the critical discharge for the beginning of sediment movement

Q = river flow

$Q_{\%}$ = frequency of the project's water demand

Q_0 = incoming discharge from river

Q_d = diverted discharge

r = distance from the centre of the bend

r_c / w = radius of curvature to-width-ratio

r = radius of curvature

r_c = average radius of curvature

r_o = outer radius

r_i = outer radius

R = mean radius of curvature

R = radius of curvature of the local streamline

$R1$ = inner radius

$R2$ = outer radius

R_c = average radius of curvature

S = slope of the river

S_{xy} = strength of the spiral

T = total length affected by secondary flow

V = average velocity

V_o = Q/A (mean velocity)

w = channel width

w/d = width-to-depth ratio

y = depth of water in channel

y_o = depth of flow [m]

1 INTRODUCTION

1.1 BACKGROUND

River diversion structures serve to divert water from river streams as well as to limit the sediment load that enters the diversion system. One of the key features of a diversion structure is the location. By ensuring that the structure is properly located i.e. on a stable bank in a stable river reach, the reliability of the delivered water can be enhanced. The effect of the diversion structure on the morphology of the river can also be limited by ensuring that sediment transport is maintained through the structure. This can be achieved by limiting the sediment that enters the diversion structure and by removing the sediments from the diverted water and returning them to the river.

River bends prove to be ideal for diversion structures and a diversion structure should be on the outside of the bend to take advantage of secondary (spiral) flow. Secondary (spiral) flow has the tendency to direct the heavy sediment laden bottom layers away from the diversion structure and to allow the top layers, with lower sediment concentration, to be directed towards the diversion structure. If the diversion structure can take advantage of the spiral flow, less sediment will be diverted. This is important in minimising sedimentation in the diversion structure.

The study presented in this thesis investigates two features associated with river bend diversion structures, i.e. the optimum diversion location to minimise the abstraction of sediment and the optimum diversion angle.

The present study commenced in January 2001 with a comprehensive literature study. Laboratory work was carried out between January 2002 and September 2002 followed by the simulation with DELFT 3D and MIKE21C.

One of the first descriptions of curvilinear flow was provided in the 19th century by *Thompson (1876)*. Thompson stated that the bend flow phenomenon will only occur if there is a horisontal pressure greater on the outside of a curved path than on the

inside. The result is that the water surface is super-elevated at the outer (concave) bank. Along any vertical section the pressure gradient acting towards the centre of the curvature has to be the same, since the cross slope of the water surface at the top determines it. Thus, the centrifugal acceleration has to be the same down any vertical section. This implies that the velocity is smaller near the bottom and the bottom filaments have to move in curves of smaller radius than the top ones thus giving rise to secondary (spiral) flow. The secondary (spiral) flow is directed towards the centre of curvature of the channel and will tend to move the bed sediment away from the outer (concave) bank towards the centre. For continuity there must exist an opposite cross flow at the surface that tend to push the filaments at the top to the outer (concave) bank. Figure 1-1 shows the developed secondary (spiral) flow. This fact being the explanation for diverting water from the outside of river bends. The remains of such diversion schemes date back to ancient Mediterranean civilizations.

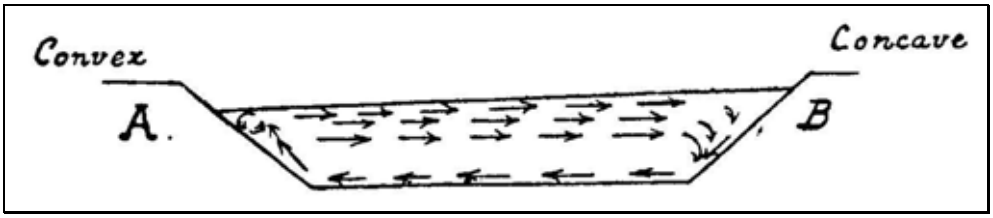

Figure 1-1: Secondary (Spiral) flow *(Thompson, 1876)*

Various classifications of intakes were found in the literature. Intakes are generally classified according to hydraulic or sediment principles. *Scheuerlein (1984)* classified intake types according to their hydraulic and sediment control principles. According to hydraulic principles the intakes were classified as lateral intakes, frontal intakes, bottom intakes and suction intakes. For sediment control a different classification seemed appropriate and the classification with respect to the mechanism of sediment transport is the control of bedload; sediment rejection; sediment extraction; sediment ejection; and the control of suspended load.

Raudkivi (1993) classified the different types of intakes according to their hydraulic and sediment control aspects as follows: intakes on river bends, intakes with dividing walls, intakes with under sluices, intakes with excluder tunnels, intakes with baffles,

guide vanes and deflectors. According to the above classification there is no clear subdivision apart from the hydraulic and sediment aspects. A clearer subdivision would distinguish between separate intakes and intakes connected to dams, weirs or barrages.

Vanoni (1977) stated that water should be diverted according to the following three principles: direct only water into the diversion structure and return the sediment to the river, design the canal system hydraulically so that the water with its sediment will be transported out onto the land with a minimum of sediment deposited in the diversion structure, design the diversion structure to direct as little sediment as practically possible into the diversion channel and remove the deposited sediment by the most inexpensive available method. Of the above-mentioned diversion principles, the third principle is recommended.

Scheuerlein (1984) recommended that the principle of sediment rejection be applied to diversion structures. The principle of sediment rejection is based on allowing the upper, clearer layers of the flow to enter the intake while the lower sediment laden layers are prevented from entering the intake. Advantage can be taken of the river bend phenomenon where the developed secondary current provides favourable flow patterns at the intake. Thus intakes should be located on the outer (concave) bank of a bend to take advantage of this phenomenon. When the intake does not operate in combination with a diversion dam or weir the sediment rejection technique can be applied to divert up to 50% of the total river flow without experiencing bedload problems *(Scheuerlein, 1984)*.

In summary, the principle of sediment rejection, where as little sediment as possible is abstracted from the main channel, is recommended. This can be achieved with the aid of the secondary flow that develops in bends and creates spiral motion. The spiral motion moves the sediment laden bottom flow towards the inside of the bend, while the upper flow with less suspended sediment move towards the outside of the bend where the diversion is located.

In South African rivers 60 to 80 % of the transported sediment does not consist of sand (“bedload”), but of silt and clay. These fine fractions (often called wash-load)

have a near uniform vertical and lateral distribution and therefore it is difficult to apply the sediment rejection principle, using secondary currents at a bend or elevated intakes. Diverted fine sediments could lead to sedimentation in the diversion structure, but it are often not harmful to pumps and pipelines. Pumps and pipelines are however generally sensitive to sand transport and bedload sediment rejection is an important consideration in South African river diversion designs.

1.2 OBJECTIVES

The primary aim of the research was to determine the optimum diversion location in a curved channel to minimise the abstraction of sediment. The secondary aim was to determine the optimum diversion angle for a diversion channel located on the outside of a bend at the proposed diversion location.

The velocity distribution in the curved channel was investigated to obtain a better understanding of curvilinear flow. The scour patterns in the channel were monitored in order to compare it with the measured velocity distribution.

Simulations were carried out with the DELFT 3D (hydrodynamics) and Mike21C (sediment dynamics) modelling programmes and compared them with the results obtained from laboratory experiments and to existing empirical formulas.

1.3 METHODOLOGY

Following a literature review of the hydraulics and sediment dynamics of river bend flow, laboratory experiments were carried out on a curved channel with varying radii preceded by a straight channel in each case, to determine the optimum diversion location. Three radii (r_c) with curvature-to-width (w) ratios r_c/w =*8.5, 11.8* and *15.2* were used with a range of Froude numbers of *0.1, 0.3, 0.5* and *0.7*. The sediment used in the test procedure was No 2 Consol sand that is commercially available with a median diameter of 0.2 mm.

The curved channel with r_c/w of *8.5* was reinstated for the series of experiments on the optimum diversion angle. Diversion angles of *20*°, *35*° and *50*° were tested with a range of Froude number of *0.3, 0.5* and *0.7*.

The DELFT 3D numerical program was used to simulate the hydrodynamics of the laboratory experiments. Two and three-dimensional computational models were used.

Mike21C was used to simulate the sediment dynamics of one of the laboratory experiments.

2 CONCEPTS OF CURVILINEAR FLOW

2.1 INTRODUCTION

During the extensive literature survey that was performed a number of references to curvilinear flow were found. Presenting all of this information is beyond the scope of the current research and only the relevant information that is applicable to the topic of the current research will be presented. The aspects that will be addressed in this section include a description of curvilinear flow, the position of the maximum velocity, the development of secondary flow and the strength of spiral flow.

However, the other related information that will not be addressed in this document is listed below. With regard to the various topics the reader is referred to:

Two-dimensional velocity distribution

Avery (1989), Chen and Shen (1983), Chow (1959), Henderson (1967), Hussein and Smith (1986), Kalkwijk and De Vriend (1980), Lee and Yu (1990), Leliavsky (1965), *Liu et al (1982)*, *Raudkivi (1993), Rozovskii (1957), Shen (1971), Shukry (1950)* and *Vriend and Struiksma (1983).*

Three-dimensional velocity distribution

Rozovskii (1957), Rozovskii (1962) and *Yalin (1992).*

Energy losses

Chang (1983), *Müller (1943), Shukry (1950)* and *(Yalin, 1992).*

Shear stress

Avery (1989), Bathurst (1979), Bridge and Jarvis (1982), Chen and Shen (1983), Choudhary and Narasimhan (1977), Francis and Asfari (1971), Khalid (1964), Mandouh and Townsend (1979), Okoye (1989), Shukry (1950) and *Varshney and Garde (1975).*

Scour depth relationships

Avery (1989), *Apmann (1972)*, *Blench (1969)*, *Bridge and Jarvis (1982), Chatley (1931), Lacey (1929)*, *Lacey (1930), Leliavsky (1965), Liu et al (1982)*, *Nelson and Smith (1989), Nwachukwu (1973), Ripley (1927)*, *Rzhanitsyn (1960), Sharma, Varshney and Tiagi (1973), Tyagi (1967)* and *Yen and Lee (1995).*

Bed configuration

Bridge (1983), Rzhanitsyn (1960) and *Shen (1971).*

2.2 CURVILINEAR FLOW CHARACTERISTICS

The characteristics of flow around a river bend are described by numerous researchers, among other *Avery (1989)*, *Bathurst (1979)*, *Bouvard (1992)*, *Bridge (1977)*, *Bridge (1983), Bridge and Jarvis (1982)*, *Chow (1959)*, *Christian (1988)*, *Henderson (1967)*, *Hussein and Smith (1986)*, *Jackson (1975)*, *Lee, Yu and Hsieh (1990)*, *Leliavsky (1965)*, *Minikin (1920)*, *Odgaard (1986)*, *Okoye (1989)*, *Raudkivi (1993)*, *Rzhanitsyn (1960)*, *Shen (1971)*, *Shukry (1950)*, *Snell (1994)*, *Thompson (1876)*, *Thorn and Hey (1979)*, *Varshney (1977)*, *Vriend and Struiksma (1983)* and *Yalin (1992)*.

The following is a summary of the characteristics of flow in river bends:

Consider open channel flow through a bend with outside radius (*R2*) and inside radius (*R1*) (see Figure 2-1). Centrifugal acceleration is generated by streamline curvature in the region of the flow where the velocity is approximately constant. The combination of the local accelerations at all the points across the stream leads to super-elevation of the water surface. The super-elevation is the increase in the elevation of the water surface on the outer (concave) bank of the bend and the decrease of the water surface on the inner (convex) bank of the bend. The order of magnitude being (*Bouvard, 1992*):

$$\Delta h = \int_{R1}^{R2} \frac{v^2}{gR} dR \quad \text{..... (2-1)}$$

where Δh = change in water level [m]

$R1$ = inner radius [m]

$R2$ = outer radius [m]

V = local velocity

R = radius of curvature of the local streamline

g = gravitational acceleration

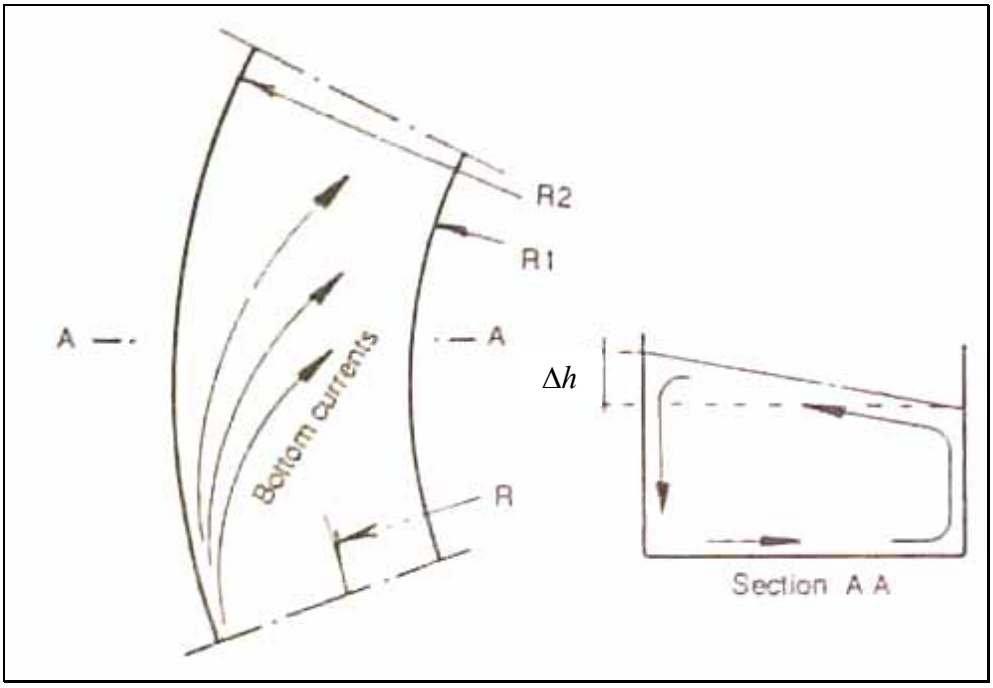

Figure 2-1: Curvilinear flow in an open channel bend *(Bouvard, 1992)*

The velocity (viewed in cross-section) near the walls is extremely low and vanishes at the wall itself. This has the effect that the centrifugal acceleration also virtually vanishes. The imbalance due to the greater hydrostatic pressure head on the outside wall will then force the heavily sediment laden bottom layers to move inwards towards the centre of the curvature of the channel. The rise in level (Δh) is thus countered by the wall friction associated with the centrifugal bottom flow. The result is that the top layers, where the sediment concentration is the least, will move towards the outside of the bend.

A spiral motion is created with the direction being anti-clockwise for a bend to the left (see Figure 2-1) and clockwise for a bend to the right looking in the downstream direction. The bedload will then mainly occur in the inside of the bends, the very reason for diverting water from the outside of river bends.

The spiral motion (secondary flow) changes the velocity distribution and is responsible for the development of higher local velocities and higher boundary shear stress on the channel bed. By forcing the streamlines of high velocities towards the outer bank, the centrifugal force creates a reduction in the effective flow area. This decrease in effective flow area as well as the increase in the form resistance due to the direction change of flow causes a backwater effect. The redistribution of shear stress in a channel bend with mobile boundary introduces bed deformation.

The point of maximum velocity moves close to the outer bank and also downward. Thus, the maximum velocity streamline is meandering not only in plan but also in elevation. The result of this phenomenon is that the increased velocity gradients, i.e. boundary shear stress at the outer boundary of the bend lead to increased erosion along the outer bank. The eroded material from the outer bank is carried by the bottom current towards the downstream side of the inner bank of the bend.

In natural rivers this flow pattern has a very important effect on the sedimentation processes. Natural rivers have the tendency to scour from the outside of the curve and to deposit on the inside. The consequence of this scouring mechanism is that if a branch channel is taken from the outside of the curve, the sediment concentration will be much less in the branch than in the main channel. This fact being the explanation for diverting water from the outside of river bends. The remains of such diversion schemes date back to ancient Mediterranean civilizations *(Henderson, 1967)*.

The resultant velocity due to the spiral motion is at an angle (ϕ), the flow deviation angle, to the velocity normal to the cross section. The flow deviation angle is defined as:

$$\tan\phi = \frac{Ky_o}{r} \quad \text{..... (2-2)}$$

where ϕ = flow deviation angle

y_o = flow depth [m]

r = radius of curvature [m]

K = constant

The *K*-values are dependant on the roughness of the bed with *C* being the Chezy coefficient. For smooth beds ($C/\sqrt{g} \approx 19$) the values are in the range of $-10.25 \le K \le -12.90$ with $\overline{K} = -11.58$ and rough beds ($C/\sqrt{g} \approx 10$) the values are within the range of $-4.6 \le K \le -12$ with $\overline{K} = -5.30$.

2.3 POSITION OF MAXIMUM VELOCITY

The position of the maximum velocity in river bends is described by a number of researches among other *Bridge (1977)*, *Bridge (1983)*, *Bridge and Jarvis (1982)*, *Christian (1988)*, *Hussein and Smith (1986)*, *Lee, Yu and Hsieh (1990)* and *Minikin (1920)* to shift from the inner (convex) bank upstream of the bend to near the outside of the bend downstream of the apex of the bend (see Figure 2-2).

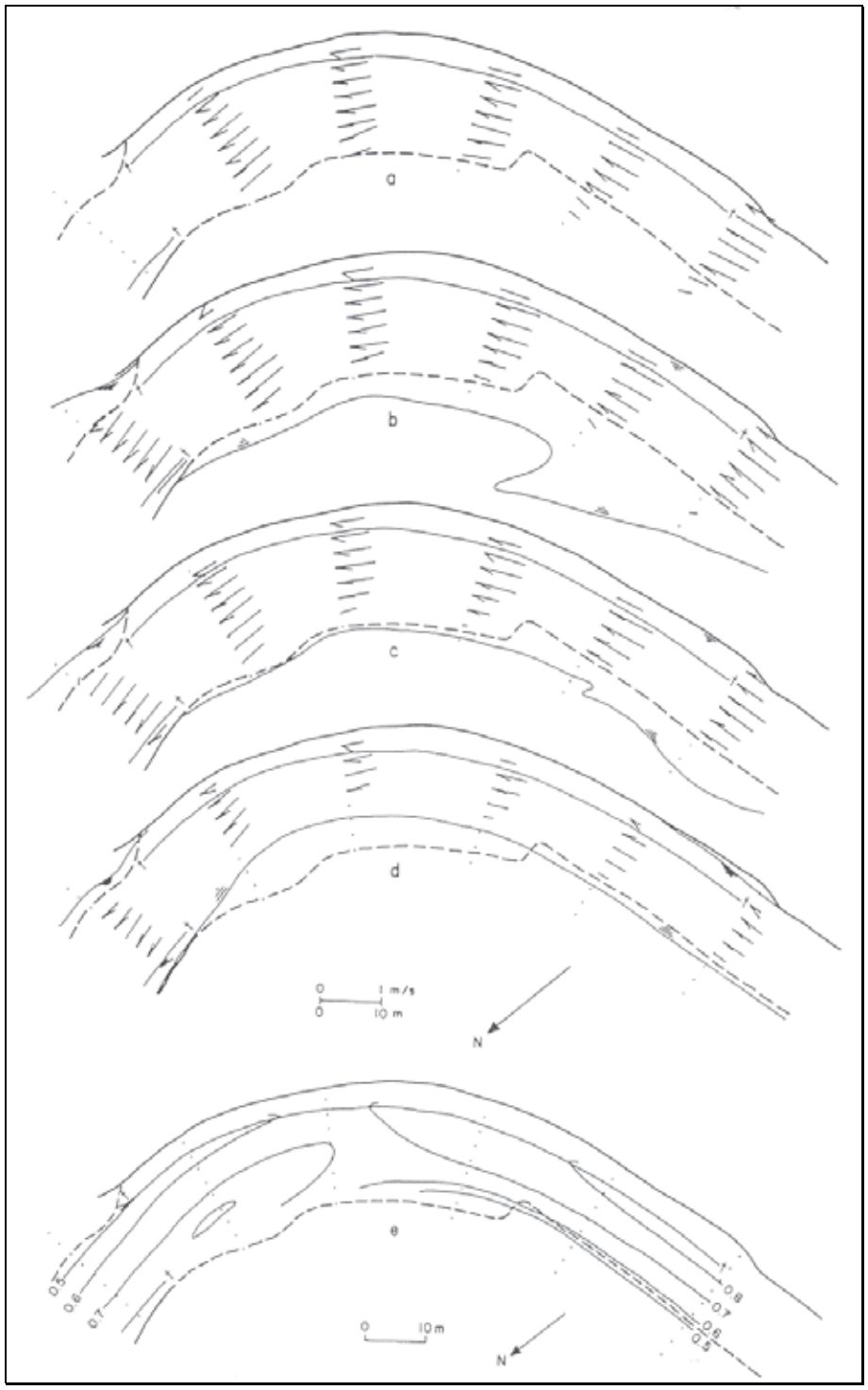

Figure 2-2: Aerial distribution of mean velocity vectors for a range of discharges (a)–(d) and contour map of mean velocity magnitudes for near bank full discharge (e) (*Bridge and Jarvis, 1982)*

The non-uniform flow features that change in time with discharge can explain the path of the maximum velocity (thalweg). In the flow direction there are convective

accelerations associated with the changing cross-sectional shapes, curvature and secondary flow. In the transverse direction a net convective momentum flux occurs due to stream-wise variations in secondary flow *Bridge (1983)*.

Christian (1988) found that during extreme floods, the highest velocity will be closer to the inner (convex) bank (Figure 2-3).

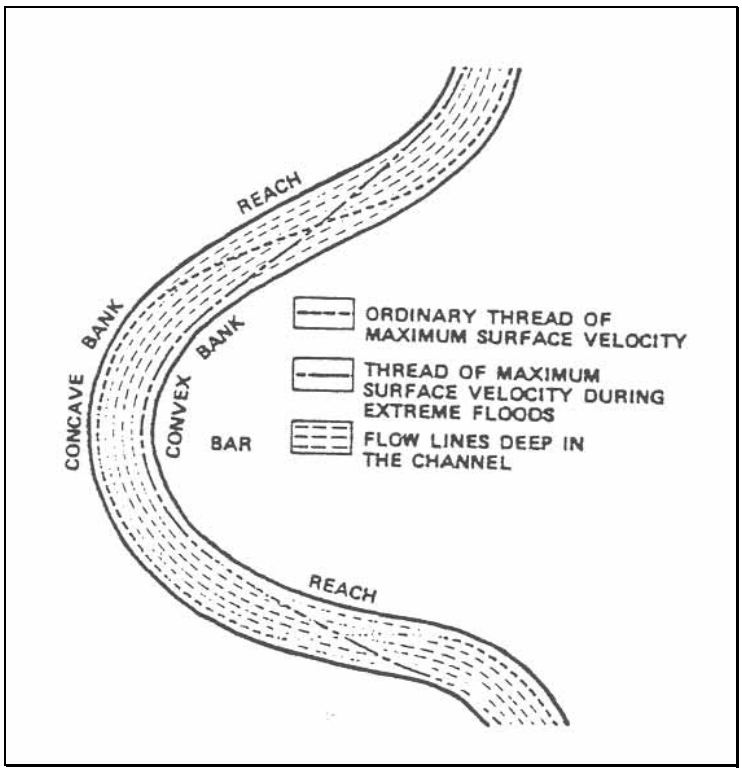

Figure 2-3: Location of maximum surface velocity during normal and flood flows *(Christian, 1988)*

Minikin (1920) found that the maximum velocity is located on the outer (concave) bank of the bend at a distance of one third of the width to the inner bank as is shown in Figure 2-4.

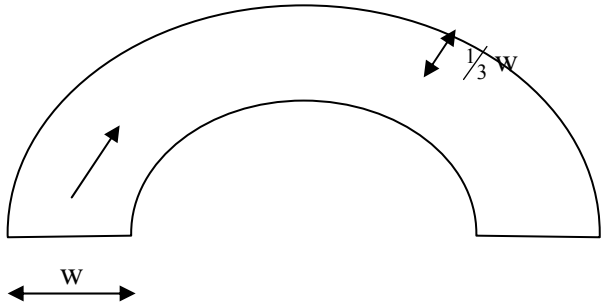

Figure 2-4: Maximum velocity location (*Minikin, 1920)*

The positions of the maximum velocity in river bends are related to the following:

- Curvature of the bend *(Minikin, 1920)*.
- The width to depth ratio *(Lee, Yu and Hsieh, 1990)*.
- The strength of the centrifugal force *(Lee, Yu and Hsieh, 1990)*.
- Position moves downstream with an increase in discharge *(Bridge, 1977)*.
- Location shifts downward from the water surface *(Lee, Yu and Hsieh, 1990)*.

2.4 DEVELOPMENT OF SECONDARY FLOW

The following guidelines were found in the literature survey to determine the status of the developed secondary (spiral) flow:

Raudkivi (1993) showed that the development of secondary flow (with reference to Figure 3-4) is essentially complete after

$$\theta = 1.5\frac{C}{\sqrt{g}}\frac{y_o}{r} \quad \text{..... (2-3)}$$

where θ_{sec} = angle after which secondary flow is completed [radians]

C = Chezy coefficient

y_o = depth of flow [m]

r = radius of curvature [m]

Raudkivi (1993) found that the secondary current in a river bend is not fully developed if the angle $\theta < 30°$ (Figure 2-5). Thus a longer bend with $\theta > 30°$ is required to ensure that the secondary currents are fully developed.

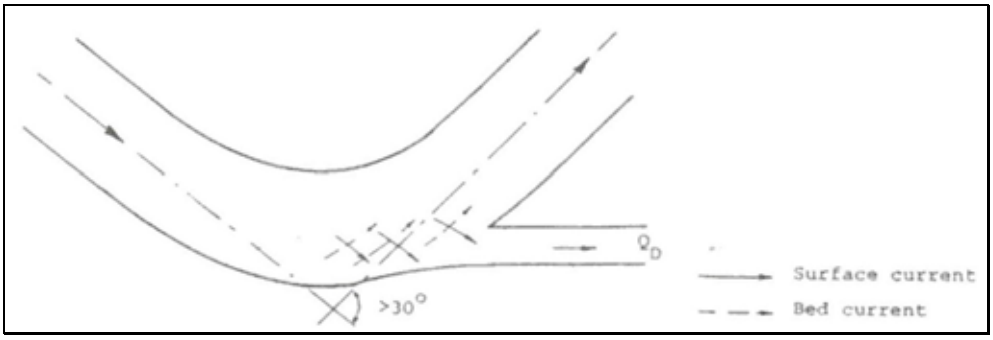

Figure 2-5: Secondary current development in a river bend *(Raudkivi, 1993)*

Mandouh and Townsend (1979) found that in a system that consists of a single bend followed by a straight section, the total length affected by secondary flow (T) can be calculated by means of the following equation where the second term represents the effective decay region that extends downstream of the bend.

$$T = \frac{\pi R \theta_{bend}}{180} + \frac{1.77Ch}{\sqrt{g}} \quad \text{..... (2-4)}$$

where T = total length
R = mean radius of curvature
θ_{bend} = central angle of bend in degrees
C = Chezy coefficient
h = flow depth

Rozovskii (1961) concluded that the flow is fully developed after it has progressed a certain distance downstream from the entrance. The angle for flow development can be given by

$$\theta = \frac{2.3CD}{\sqrt{g}r_c} \quad \text{..... (2-5)}$$

where θ = angle of flow development
C = Chezy coefficient
D = flow depth
r_c = mean channel radius

The magnitude of the secondary currents is up to 15% of the average channel velocity. *(Simons, 1971)*

2.5 STRENGTH OF THE SPIRAL FLOW

Choudhary and Narasimhan (1977) studied the strength of the spiral flow and found that it originates in the early reaches of the bend, develops to its full strength in the central region and then decays towards the exit reach of the bend. The bend can therefore be separated into the early developing, central developed and final decaying zones.

In the early developing zone, the spiral motion is very weak and its presence is confined to a region close to the surface of the flow. The origin appears to be at the free surface near the outer wall. The spiral motion develops earlier with an increase in Froude number and its intensity is higher for narrow than for wide channels.

In the central zone, the maximum intensity of the strength of the spiral is reached along the inner wall and changes slightly with the value of angle of the bend (θ) and r/r_c (where r is the distance from the centre of the bend and r_c the centreline radius of the bend). A typical result of fully developed spiral flow is shown in Figure 2-6.

In the decaying zone, the strength of the spiral decays from the inner to the outer wall and the decay spreads outward as the flow traverses downstream. The decaying rate is faster for wider than for narrow channels.

From the above, *Choudhary and Narasimhan (1977)* concluded that the boundary resistance has a predominant effect in the growth and decay of spiral motion. The Froude number plays a lesser part in the distribution of the spiral flow.

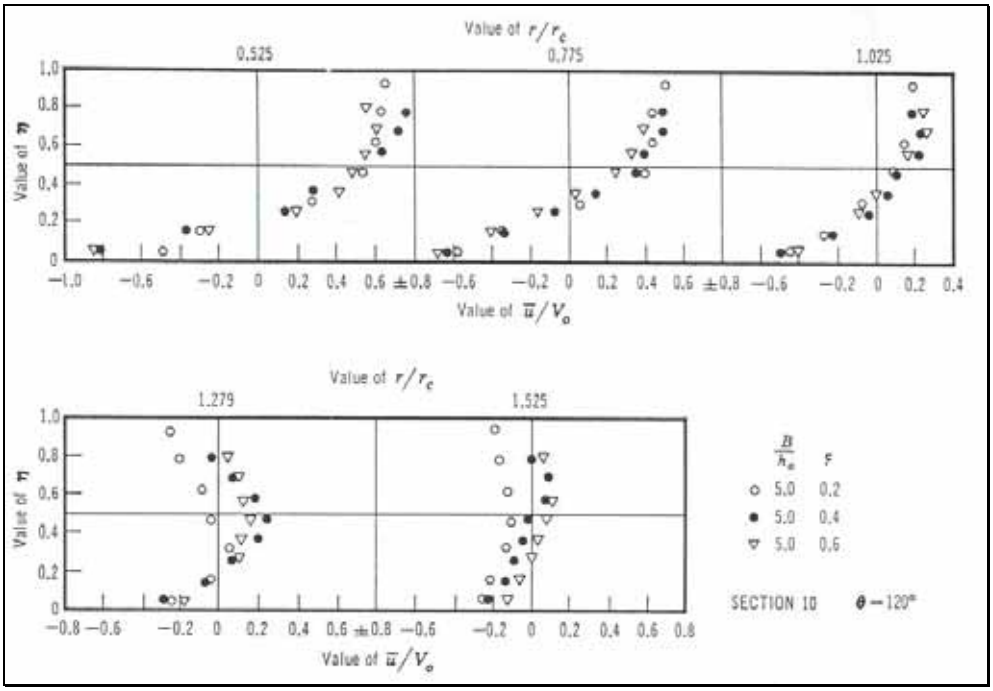

Figure 2-6: Distribution of Radial Mean Velocity $\bar{u}$ for B/h_o=5.0 *(Choudhary and Narasimhan, 1977)*

The strength of a spiral flow is defined as the percentage ratio of the mean kinetic energy of the lateral motion to the total kinetic energy of flow at a given cross-section. When the streamlines are all parallel to the axis of the channel, $S_{xy} = 0$. With reference to Figure 2-7 the strength of the spiral flow is given by *(Chow, 1959)*:

$$S_{xy} = \frac{\bar{u}}{V_o} * 100 \quad \text{..... (2-6)}$$

where S_{xy} = strength of the spiral

$\bar{u}$ = radial velocity (xy plane)

V_o = Q/A (mean velocity)

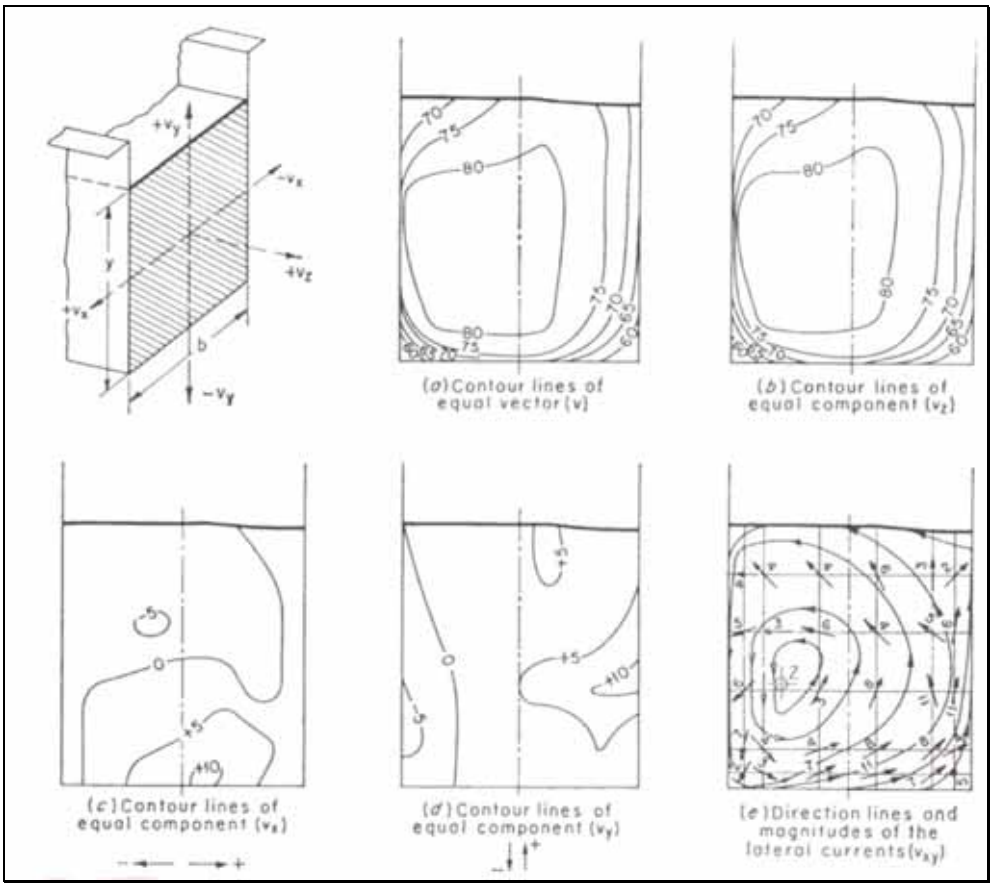

Figure 2-7: Distribution of velocity components *(Chow, 1959)*

In summary, the strength of the spiral flow (S_{xy}) after *Choudhary and Narasimhan (1977)*, *Chow (1959)*, *Shukry (1950)* and *Rozovskii (1963)* is characterised by the following:

i) S_{xy} is relative high at a low Reynolds number of the approach flow, but decreases with increasing Reynolds number.

ii) S_{xy} decreases with an increase of the radius-width ratio. The curve effect approaches its minimum at $r_c / w = 3.0$.

iii) S_{xy} decreases as the depth to width ratio increases.

iv) S_{xy} increases as the diversion angle of the bend (θ) becomes large (see Figure 4-1 for definition of θ). For the range ($\theta/180 = 0 - 0.5$) the increase in S_{xy} is nearly twice that of for the range ($\theta/180 = 0.5 - 1.0$).

v) The relative strength of the spiral increases with an increase in r/r_c.

vi) With an increase in Froude number the maximum spiral decreases and the rate of lateral spread of the spiral increases.

vii) The kinetic energy of the lateral currents in the bend is relatively small compared with the energy in the longitudinal currents. Thus, the lateral currents play a minor role in the energy loss due to bend resistance.

viii) The secondary circulation is the weakest at low and high discharges and is the strongest at medium discharges.

2.6 SUMMARY

Curvilinear flow is characterised by the development of secondary (spiral) flow. The centrifugal acceleration in bends leads to the super-elevation of the water surface and the formation of spiral flows.

The path of the maximum velocity (thalweg) shifts from the inside of the bend towards the outside in the downstream direction with the maximum velocity being near the outside of the bend, downstream of the apex.

The effect on the strength of the spiral flow can be summarised as follows:

i) The strength of the spiral flow increases in the downstream direction in the central developed zone *(Choudhary and Narasimhan, 1977)* and it increase with an increase in the diversion angle *(Shukry, 1950)*.

ii) The strength of the spiral flow decreases with an increase in the Reynolds number, with an increase in the depth to width ratio and with an increase in the radius of curvature ratio (r_c/w) *(Shukry, 1950)*.

iii) Secondary currents are the weakest at high and low discharges and the strongest at medium discharges *(Rozovskii, 1963)*.

The central bend angle that is necessary for the secondary flow to develop fully can be determined by one of the following relationships:

i) Equation 2-3 (*Raudkivi, 1993*)

ii) Equation 2-4 (*Mandouh and Townsend, 1979*)

iii) Equation 2-5 (*Rozovskii, 1963*)

3 THE FLUVIAL MORPHOLOGY OF RIVER BENDS

3.1 THE FORMATION OF BENDS

Shen (1971) described the formation of bends in alluvial channels to be usually part of a meander or deformed meander system. Bends are normally formed as a result of the natural tendency for sinuous flow in channels when the slope of the river (*S*) is less than $S = 0.0017Q^{1/4}$ (*Q* is in cubic feet per second and *S* in ft/1000). The tendency for bends to develop in alluvial channels that eventually flattens the slope has been demonstrated by *Lane (1955).*

The shape of the bend in natural alluvial channels varies from symmetrical patterns to deformed bends that is most frequently encountered in nature *(Shen, 1971)*.

A sharp bend subtends a deep, narrow section along the concave bank with a resultant intense attack on that bank. A long flat bend is associated with a wide, shallow unstable channel with a tendency toward the movement of travelling bars along the concave bank. A bend of optimum radius will subtend a section that approaches a rectangle. Figure 3-1 illustrates a typical cross-section of a sharp, optimum and flat bends *(Vanoni, 1977)*.

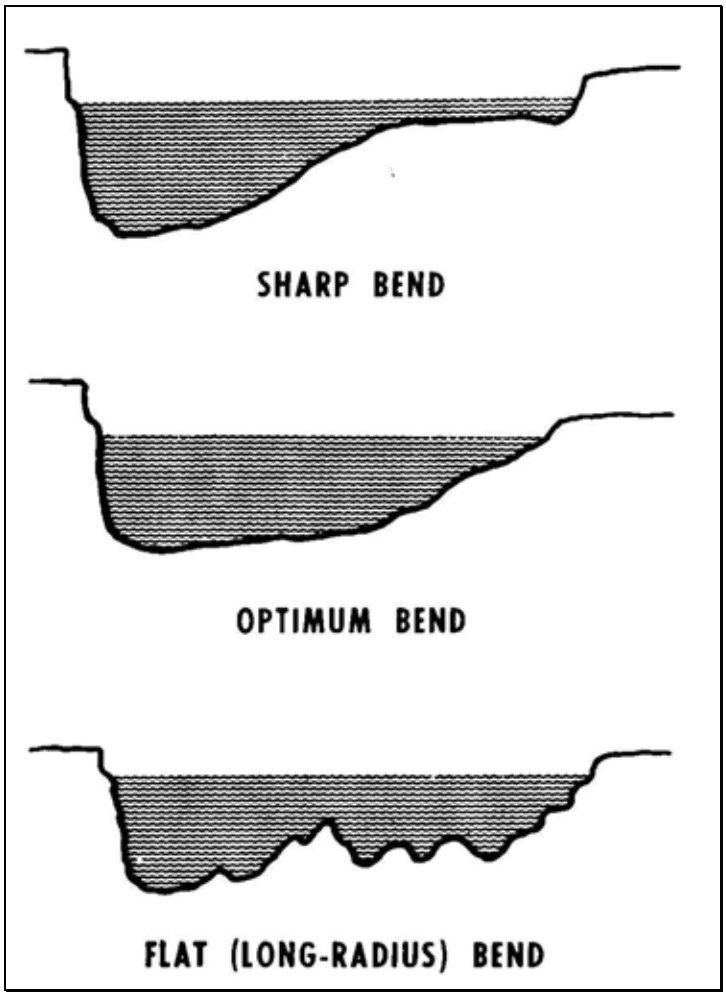

Figure 3-1: Cross-section of sharp, optimum and flat bends *(Vanoni, 1977)*

Shen (1971) classified the types of bends that form in alluvial channels to be of three types, i.e. entrenched bends, meandering surface bends and forced bends.

The entrenched or deepened bends also includes those that follow the curves of the valley so that each river bend includes a promontory of the parent plateau.

Meandering surface bends includes those that are formed only by the river on a flat, alluvium covered valley floor where the slopes of the valley are not involved in the formation of the bend.

Forced bends are often encountered under natural conditions in an alluvial river. This bend is formed when the stream impinging on a non-eroding parent bank that forms a

forced curve that is gradually transformed into a river bend of a more constricted shape.

In all types of bends the density of the material composing the banks is important and determines the radius of curvature to a certain degree. In a free bend the radius of curvature increases with the density of the material. The radius of curvature is the smallest in a forced bend *(Shen, 1971)*.

From the standpoint of the action of the stream and the interaction between the stream and the channel as well as from the general laws of their formation, one can distinguish between the following three types of bend, i.e. free, limited and forced bends.

Free bends are where both banks are composed of alluvial flood plain material that is usually quite mobile. This type of bend corresponds to the common concept of surface bends.

In the case of limited bends the banks of the stream are composed of consolidated parent material that limits the intensive development of lateral erosion by the stream. This corresponds to entrenched or deepened bends.

The formation of forced bends is due to the stream that impinges onto an almost straight parent bank at a large angle in the range of 60° to 100° *(Shen, 1971)*.

There are two characteristic features of all the different types of bends. Firstly, there is a close relationship between the type of bend and the radius of curvature. The forced bend has the smallest radius of curvature, followed by the free bends. The limited bends have the greatest radii. Secondly, there is a relation of the type of bend to the distribution of depths along the length of the bends. In the case of free and limited bends the depth gradually increases in a downstream direction and the maximum depth is found some distance downstream of the apex. As for forced bends, the depth sharply increases at the beginning of the bend and then gradually diminishes. The greatest depth is located in the middle third of the bend where there is a concentrated scour *(Shen, 1971)*.

3.2 THE MECHANICS OF SCOUR AT BENDS

Yen and Lee (1995) described the mechanics of sediment transport in river bends to have a twofold complexity. One the one hand, the non-uniform sediment is subjected to the longitudinal and transverse transport induced by the secondary flow associated with river bends. The other factor is the effect of the unsteadiness of flow in natural rivers that affect the motion of the sediment particles.

The channel in a bend is deep along the outer (concave) bank and shallower at the inner (convex) bank. The reason being that there is a concentration of stream power, turbulence, flow and sediment transport ability at the outer (concave) bank. The dimensions of the bend channel are dynamic. The length, width, depth, shape and position of deepest scour hole vary with sediment and water discharge, radius of curvature, angle of the bend, slope of the energy gradient, characteristics of the bed and bank material and other less significant variables *(Shen, 1971)*.

There are two characteristic features of all the different types of bends. Firstly, there is a close relationship between the type of bend and the radius of curvature. The forced bend has the smallest radius of curvature, followed by the free bends. The limited bends have the greatest radii. Secondly, there is a relationship between the type of bend and the distribution of depths along the length of the bends. In the case of free and limited bends the depth gradually increases in a downstream direction and the maximum depth is found some distance downstream of the apex. As for forced bends, the depth sharply increases at the beginning of the bend and then gradually diminishes. The greatest depth is located in the middle third of the bend where there is a concentrated scour *(Shen, 1971)*.

It is stated that a wide variation of the standard deviation of the bed material (σ_g) will affect the maximum scour depth and the rate of scour. *Rouse (1950)* observed that a larger value of σ_g would cause the coarser particles to remain in the scour hole and thus pave it with the coarser material. This reduces the rate of scour due the

armouring action. It was found that the value of σ_g lies between 1.2 and 1.7 for alluvial material up to a size of 0.6 mm.

3.3 LOCATION OF MAXIMUM SCOUR

The mechanics of scour in river bends have been widely studied by among other, *Kalkwijk and De Vriend (1980)*, *Mandouh and Townsend (1979)*, *Minikin (1920)* and *Raudkivi (1993)*. It is concluded that the path of maximum scour in river bends will gradually shift from the middle of the cross-section to the outside of the bend in the downstream direction, reaching a maximum just downstream of the apex (see Figure 3-2). Typical bed topography of a river bend is shown in Figure 3-3 where it can be seen how the maximum scour shifts towards the outside of the bend in the downstream direction.

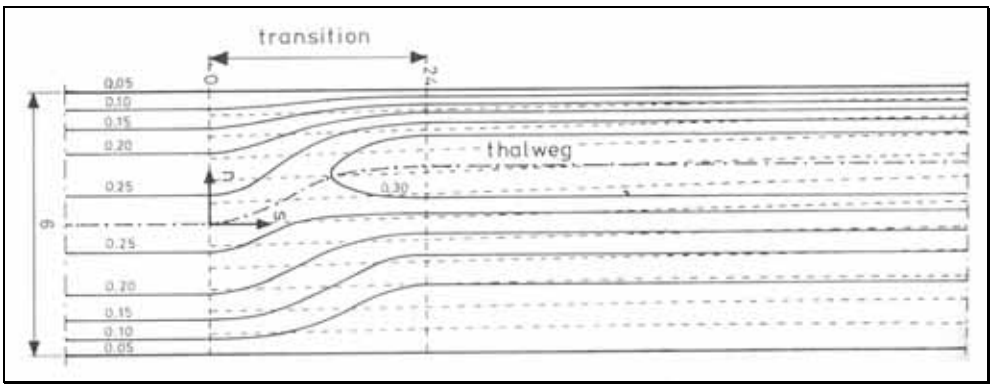

Figure 3-2: Typical depth contours obtained in experiments
(Kalkwijk and De Vriend, 1980)

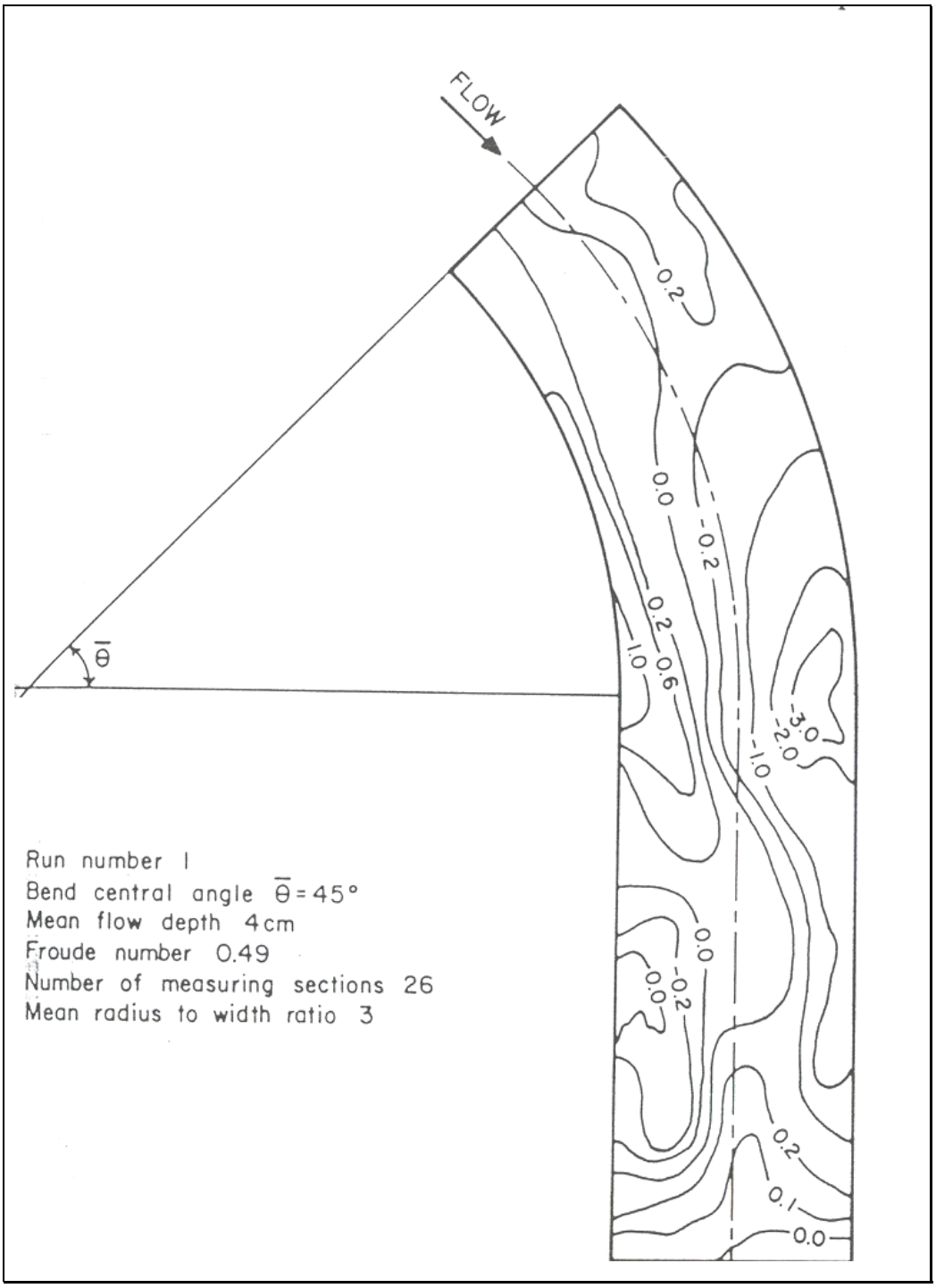

Figure 3-3: Bed topography [cm] for r_c / w =3.0 with $\bar{\theta}$ = 45° and w = 0.3 m *(Mandouh and Townsend, 1979)*

Raudkivi (1993) quantified the position of maximum scour to be at the outer (concave) bank with its deepest point approximately twice the river width downstream

of the intersection of the upstream axis with the bank. The location of the deepest scour hole is shown in Figure 3-4.

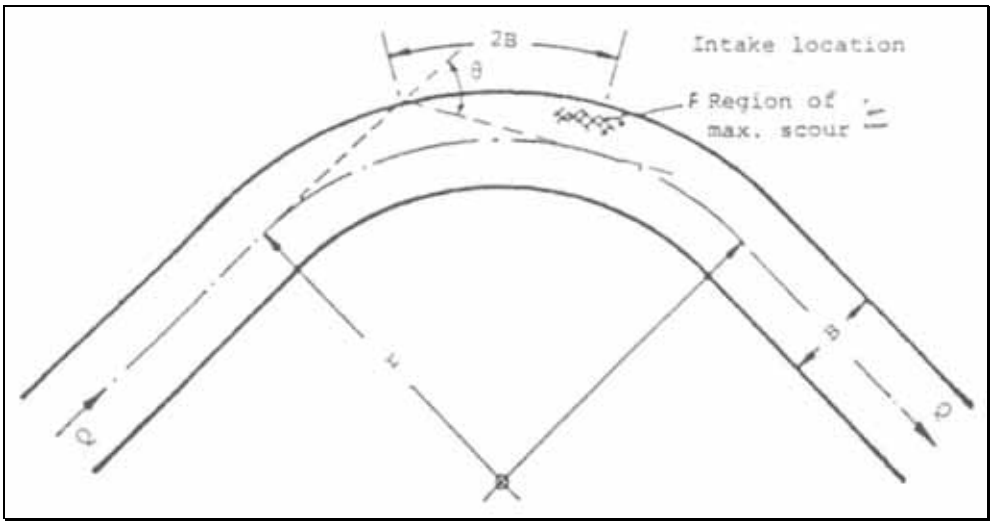

Figure 3-4: Location of maximum scour hole in a river bend *(Raudkivi, 1993)*

The effect on scour in river bends due to the change in the following parameters were found in the literature by among other, *Kalkwijk and De Vriend (1980)*, *Minikin (1920)*, *Mandouh and Townsend (1979)*, *Nwachukwu (1973)*, *Thompson (1876)* and *Yalin (1992)* as:

- The position of maximum scour moved downstream with an increase in bend angle.
- The position of maximum scour is at the outside of the bend downstream of the apex.
- Scour depth increases with increase in Froude number.
- Scour depth decreases with increase in the depth to width ratio.
- Scour depth increases as the relative curvature increases.

3.4 THE EFFECT OF DIVERSION STRUCTURES ON RIVERS

Diversion structures affect the long-term morphology of a river. There is a difference in the impact on the morphology between a diversion with and without a weir.

When the diversion structure is constructed with a weir, the weir divides the river into an upstream and downstream reach. The weir will act as a reservoir with a backwater effect that leads to the formation of a delta at the upstream end. Ultimately, it will lead to the weir being silted up to near the spillway crest level while the upstream river level continues to change until the initial slope and sediment carrying capacity is re-established.

A consequence of the backwater effect moving gradually upstream is that groundwater is affected. This will change the conditions for vegetation and make additional areas flood prone. Downstream of the bend degradation will initially prevail due to the sediment that is trapped upstream of the weir. The effect of degradation on the groundwater and vegetation is just the opposite of aggradation. In addition, it may also effect the foundation of river structures and contribute to slumping and slip of the riverbanks. Degradation will change into aggradation once the weir is silted to the spillway crest level and sediment is once again passed over the weir and transported further downstream *(Raudkivi, 1993)*.

A diversion without a weir will in most cases lead to aggradation of the river downstream of the diversion structure. This is the case since the aim of a diversion structure is to divert water with as little sediment as possible. Thus, the flow that does not enter the diversion structure is overloaded with sediment and deposits the excess sediment. The deposited sediment downstream of the diversion gradually creates a backwater effect that promotes aggradation in the upstream direction. This process will continue until the downstream river slope has increased to the extent that the reduced flow is again capable of transporting the sediment that arrives upstream. If the river was eroding before the diversion structure was constructed, the additional sediment input and reduced flow can be beneficial to the downstream reach of the river *(Raudkivi, 1993)*.

4 RIVER BEND DIVERSION STRUCTURES

4.1 GENERAL

Raudkivi (1993) gave three guidelines when designing a diversion structure. The first is that the diverted discharge (Q_d) has to be less than the long-term average river flow ($\overline{Q}$). The second is that Q_d should be less than the critical discharge for the beginning of bed-load transport (Q_c). The third factor is the river flow relative to the frequency of the project's water demand ($Q_{\%}$), i.e. for example the 95% value of the demand. It was concluded that a weir is necessary if $Q_d / Q_{\%} > 0.25$. If the result is smaller, diversion can be achieved without a weir provided that the flow depth in the river, at demand, is large enough. The flow depth should preferable not be less than 1.5 m.

The intake velocity should also be less than the river velocity for $\overline{Q} > Q_c$. Bottom currents should be prevented from entering the intake since it is most heavily laden with sediment. Surface currents should also be prevented from entering the intake since it could carry large quantities of floating debris. One of the most important requirements of diversion works is that the diverted flow should carry as little sediment as possible. Methods to achieve this can be classified into passive and active control. Passive control consists of locating the diversion structure at the optimum location and therefore taking preventive measures to ensure the optimum operation of the structure. Active control conditions refer to the optimum operation of the diversion structure *(Raudkivi, 1993)*.

The general objective of diversion works for irrigation is to divert water that does not carry course sediment, but water that is laden with fine sediment (silt) that plays a significant role as fertilizer for agricultural land use. Coarse particles are mainly concentrated near the bed, while the fine sediment is more evenly distributed at all levels. Therefore it is fairly obvious that the abstraction of water should be from the top layers in order to prevent the coarse sediment from entering the diversion works *(Leliavsky, 1965)*.

The most unfavourable condition for preventing sediment from entering the intake is for the scenario of a high diverted discharge ratio (DDR) with large incoming sediment load. The aim of the diversion structure should be to minimise the diverted sediment ratio (DSR) for all the incoming flows from the river *(Tan, 1996)*.

Avery (1982) made the following recommendations for designing diversion works:

i) The location of the diversion works should be on the outside (concave) bank of the bend where the flow velocities are higher and where the sediment is unlikely to settle out.

ii) The diversion angle should be as small as possible. The diversion angle should be between 0° and 90°, i.e. between the direction of main flow and the direction of abstracted flow (Figure 4-1).

iii) Stagnation areas should be avoided since they will encourage accumulation of sediment.

iv) When the pumps can convey sediment in suspension, the approach flow should be uniform at a constant velocity and high enough to keep the sediment from settling out.

v) The sediment settling technique that is used, should be adequately designed to avoid possible problems such as too small settling basins or insufficient spare water for flushing or sluicing.

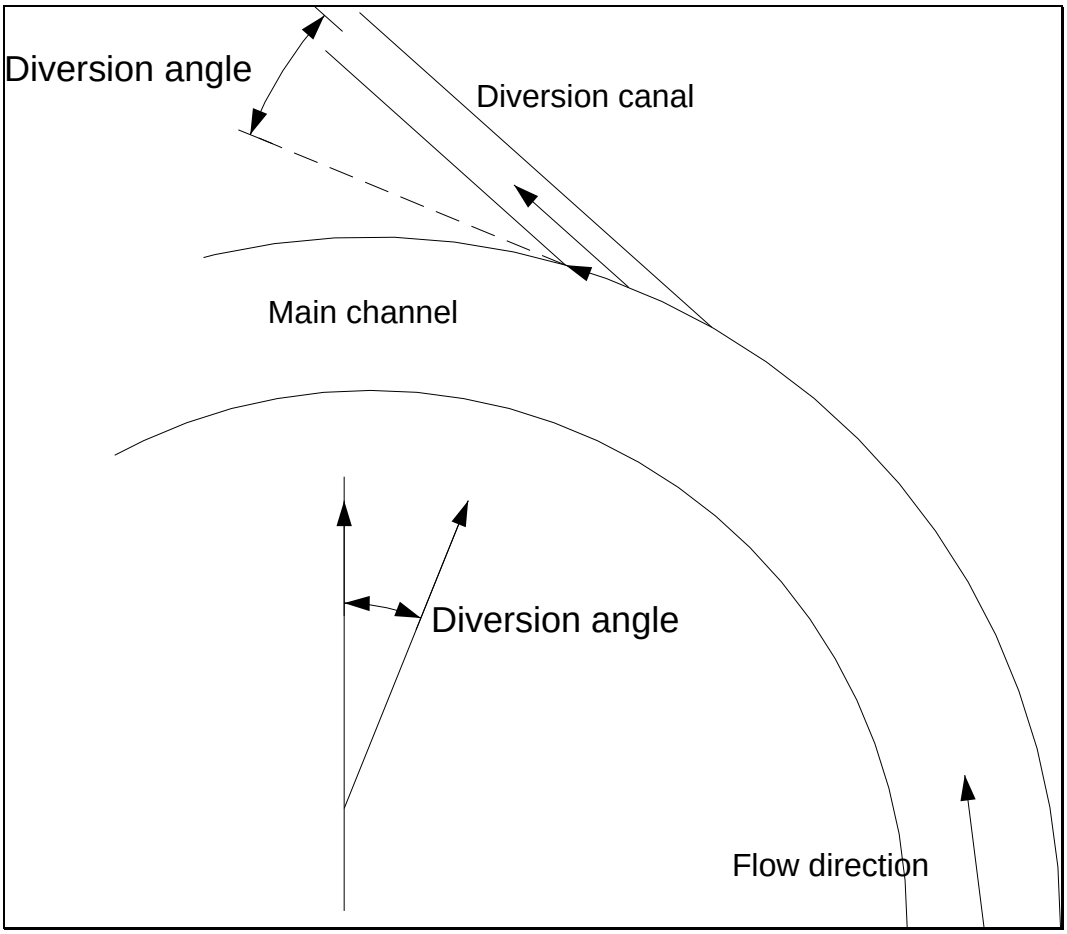

Figure 4-1: Diversion angle

4.2 BEND DIVERSION LOCATION

The local geology of the proposed diversion structure is an important parameter to take into account. Factors such as the stability of the riverbanks and additional stabilisation measures to stabilise the intake should be taken into account when selecting the diversion location to ensure that the intake is directed to the main current and that the flow path does not wander often *(Tan, 1996)*.

Special attention should be given to bends of meandering rivers since they generally erode rapidly and cut-offs could occur that may lead to the river bypassing an intake altogether. Braided gravel-rivers can create essentially the same problems as meandering rivers. The individual stream channels change their locations and

therefore the channel pattern could be different from that before. Therefore, favourite locations for diversion structures include stable bends, cliff faces and gorges *(Raudkivi, 1993)*.

Figure 4-2 shows the natural locations for diversion structures. The points marked (1) indicate locations making use of the bend effect and (2) indicates gorges, where there are fixed deep-water cross-sections with deep and relative tranquil flow. Cliff faces with flow curvature and down flow are marked (3) and rapids where the suspended sediment is low are marked as (4) *(Raudkivi, 1993)*.

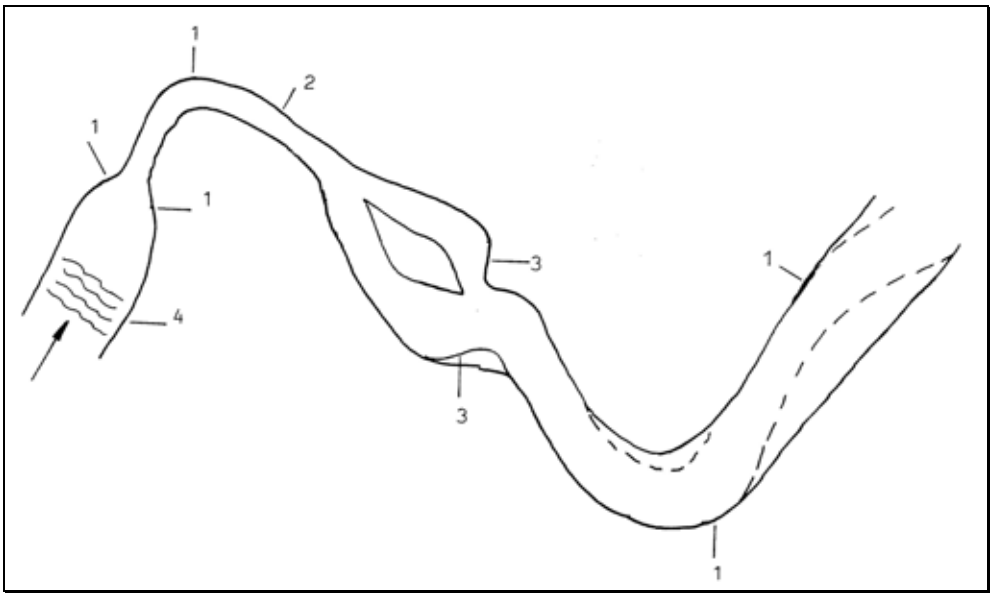

Figure 4-2: Natural locations for diversion structures on a natural river *(Raudkivi, 1993)*

Apart from the hydraulic aspects that determine diversion location, the economical aspects should also be taken into account. The selected diversion location will have an important bearing on the amount of sediment that enters the diversion structure. Generally rivers have a much higher transporting capacity per unit of flow than the diversion channel. Therefore, specific measures for sediment exclusion must usually be made. The characteristic of river behaviour that makes the selection of the point of diversion very important is the control of the sediment that will enter the diversion structure. The flow phenomena in river bends (particularly the presence of secondary

flow) can therefore be used to minimise the sediment entering the diversion structure *(Shen, 1971)*.

The optimum diversion location where studied by among other, *Avery (1989)*, *Bouvard (1992)*, *Bulle (1926)*, *Cecen (1988)*, *Joglekar, Gotankar and Kulkarni (1951), SC and CHES (1992)*, *Shen (1971)*, *Snell (1994)*, *Thompson (1876)*, *Vanoni (1977)*, *Yalin (1992)*. Considering their comments and taking into account the discussion in Section 2 and 3, the following is recommended:

The principle of sediment rejection should be applied in determining the location of the diversion works. The point of diversion should be located on the outer (concave) bank to effectively utilise the effect of the secondary (spiral) flow as were described in Section 2.4. This will ensure that the top layers of the water, where the sediment concentration is the least, be diverted as were discussed in Section 3.2.

The relation between the central angle of a bend and the optimal location based on experimental data *(SC and CHES, 1992)* is given in Table 4-1 and the angles are defined in Figure 4-3.

Central angle of bend (˚) (describing the length of the bend)	<45	60	90	120	150	180
Optimal location of intake (˚)	0 (end)	45	60	80	95	110

Table 4-1: Relationship between the central angle of a bend and the optimal location of the intake *(SC and CHES, 1992)*

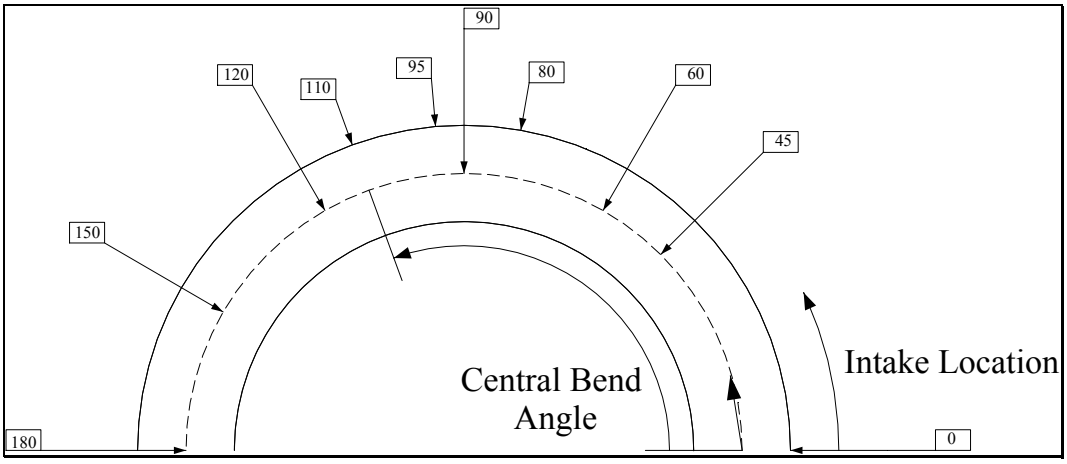

Figure 4-3: Definition sketch related to Table 4-1

SC and CHES (1992) found that the optimal location of an intake can also be related to the width and radius of curvature of a bend by means of the following empirical equation.

$$L = \xi\, w \sqrt{\frac{4r_c}{w} + 1} \quad \text{..... (4-1)}$$

where L = distance to optimum diversion location

ξ = 0.8 (coefficient)

r_c = average radius of curvature

w = width

4.3 DIVERSION ANGLE

The diversion angle is defined as the angle between the intake and the tangent of the radius of curvature as shown in Figure 4-1.

The intake location should be aligned to produce a suitable curvature of flow into the intake. Thus, changing the flow direction as little as possible. When the flow is diverted through a large angle, the flow patterns will be disturbed and bedload will be attracted to the intake.

Avery (1989) found that the optimal angle of diversion is inter alia dependent on, the diverted discharge ratio (*DDR*) and the width of the river and intake. *Bulle (1926)* found that there is no such thing as an optimum diversion angle since the angle varies with the diversion ratio and the location of the intake. It was also found that the optimum diversion angle increases as the diversion ratio decreases.

Leliavsky (1965) described the movement of a particle of water through a diversion structure (see Figure 4-4). It can be seen that the change in direction of a moving particle of water that is diverted from its natural path *ab* to *bc* cannot take place abruptly at the apex *b*, but must occur gradually as indicated by the dotted lines. The range of tests performed is shown in Figure 4-5. From the tests it was found that the average radius of the curved trajectory depends on the diversion angle. If the radius of curvature is correlated with the diversion angle, it is shown that the centrifugal force is also correlated with the diversion angle. This point is illustrated in Figure 4-6. Although the above were done for straight channels with diversions it is similar to that occurring in a bend of an alluvial river. *Leliavsky (1965)* suggested that the relationship between the radius of curvature, width of the diversion and the diversion angle could be given by

$$r = \frac{b}{2}\tan\left(\frac{\pi - K}{2}\right) \quad \text{..... (4-2)}$$

where r = average radius of curvature [m]
b = bed width of the diversion [m]
K = diversion angle [rad]

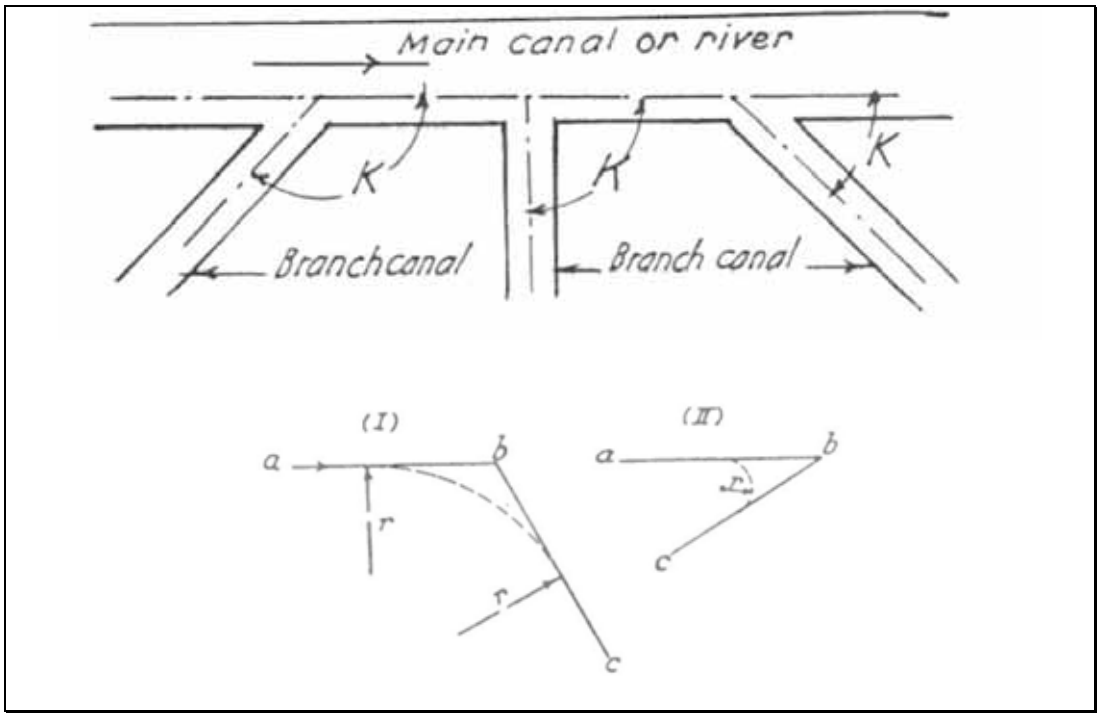

Figure 4-4: Diversion angle *(Leliavsky, 1965)*

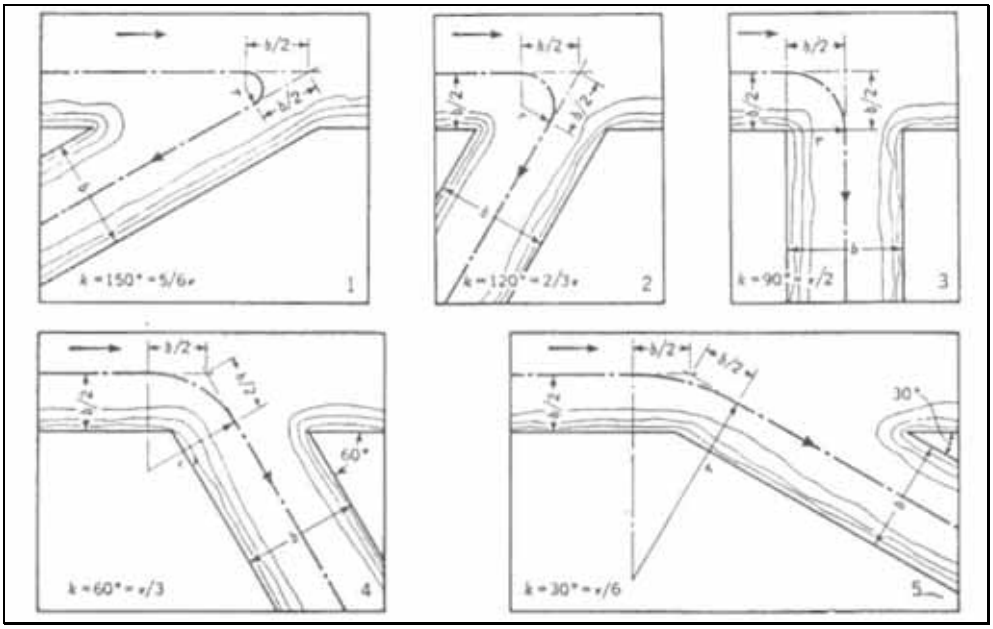

Figure 4-5: Plan layout of tests on the diversion angle *(Leliavsky, 1965)*

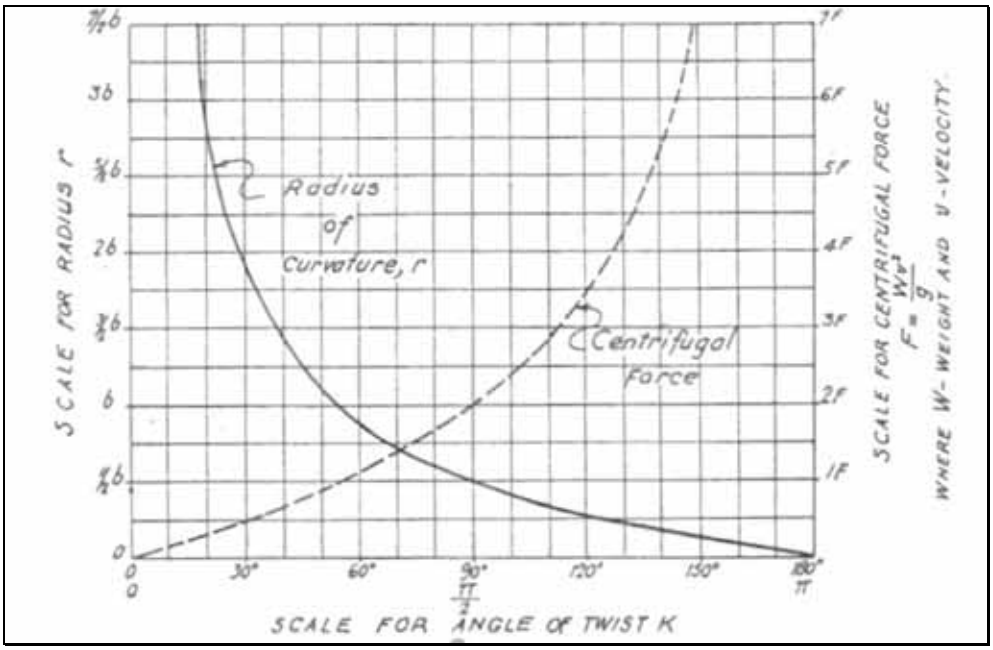

Figure 4-6: Test results on the diversion angle *(Leliavsky, 1965)*

The following diversion angles are recommended:

- *Avery (1989)* recommends a diversion angle between 10º and 45º.
- *Liu et al (1982)* recommends a diversion angle between 5˚ and 40˚.
- *Hufferd* and *Watkins (1972)* recommends a diversion angle between 30° and 45° if a model study is not carried out.

4.4 DIVERSION RELATED PARAMETERS

4.4.1 RADIUS OF CURVATURE-TO-WIDTH RATIO

The following radius of curvature-to-width ratios (r_c / w) were found in the literature and is summarised in Figure 5-1.

Liu et al (1982) recommends that the radius of curvature for a diversion bend be in the order of 4-8 times the average width of the bend (r_c / w = 4-8). *Chow (1959)* recommends the ratio to be equal to three (r_c / w = 3), since it will give the smallest radius at which the effect due to spiral flow is minimized. *Avery (1989)* suggested

that the ratio be in the range of 3 to 5 (r_c / w = 3-5). *Shen (1971)* found a relationship between the type of bend and the ratio of curvature-to-width for a bend. For free bends the ratio is r_c / w = 4.5-5.0, for limited bend r_c / w = 7-8 and for forced bends the ratio is r_c / w = 2.5-3.0. *Bagnold (1960)* made a theoretical evaluation indicating that an optimum channel curvature should exist with a ratio of bend radius (r) to channel width (w) between 2 to 3 ($r_c / w = 2$-3).

On the Missouri River bend radii varying between 10 and 20 times the controlled width (r_c / w = 10 – 20) have been associated with minimum maintenance, while ratios of up to six (r_c /b = 6) have been extremely difficult to hold. *Rzhanitsyn (1960)* did an analysis on a number of European streams and showed that the ratio decreases to become relatively constant at 10 to 14 (r_c / w = 10 - 14).

Varshney (1977) analysed some of the North Indian rivers and concluded that their bends have an average ratio of 2.45 (r_c / w = 2.45). A similar study of American rivers by *Yen (1965)* showed that their rivers have an average ratio of 2.3 (r_c / w = 2.3).

The length of the diversion bend is usually adopted to be 1.1 – 1.4 times the radius of curvature ($L_{tot} / r_{avg} = 1.1 - 1.4$) *(Tan, 1996)*.

4.4.2 DIVERTED DISCHARGE RATIO (DDR)

The discharge for sediment releasing is equal to 1-1.2 times the diversion discharge (Q_d). The bend should also be able to convey the typical flood of the river that, for example, occurs at least for 2-5 days of each year *(Tan, 1996)*.

The diversion flow rate (Q_d) should be less than the long-term average river flow ($\overline{Q}$) and less than the critical discharge required (Q_c) that initiates bedload transport. The discharge necessary to transport coarse sediment from upstream of the intake to downstream, and still continuing transport further downstream is the difference ($Q_c - Q_d$) *(Raudkivi, 1993)*.

The diverted discharge ratio (*DDR*) is calculated by the following equation

$$DDR = \frac{Q_d}{Q_o} \quad \text{..... (4-3)}$$

Where Q_d = diverted discharge

Q_0 = incoming discharge from river

Tan (1996) recommended a DDR within the range of 45% to 50% for Chinese rivers and *Avery (1989)* a DDR of between 66% to 77% for rivers in England.

4.4.3 DIVERTED SEDIMENT RATIO (DSR)

Avery (1989) stated that it is often the case that the proportion of sediment abstracted with relation to the total river sediment load (DSR) is greater than the proportion of water abstracted (DDR). *Tan (1996)* noted that the DSR is directly proportional to the DDR in China.

Habermaas (1935) did a series of model experiments to measure the diverted sediment ratio (DSR). The DDR of these tests was constant at 50%. These results are summarised by *Mosoyi (1965)* and are shown in Figure 4-7. The result of model 1 is noteworthy since all the sediment was diverted. The reason being that the curvature of flow into the offtake swept essentially the entire bedload against the convex face and into the branch channel.

The diverted sediment ratio (*DSR*) is calculated with the following equation

$$DSR = \frac{G_d}{G_o} \quad \text{..... (4-4)}$$

Where G_d = diverted sediment load

G_0 = incoming sediment load from river

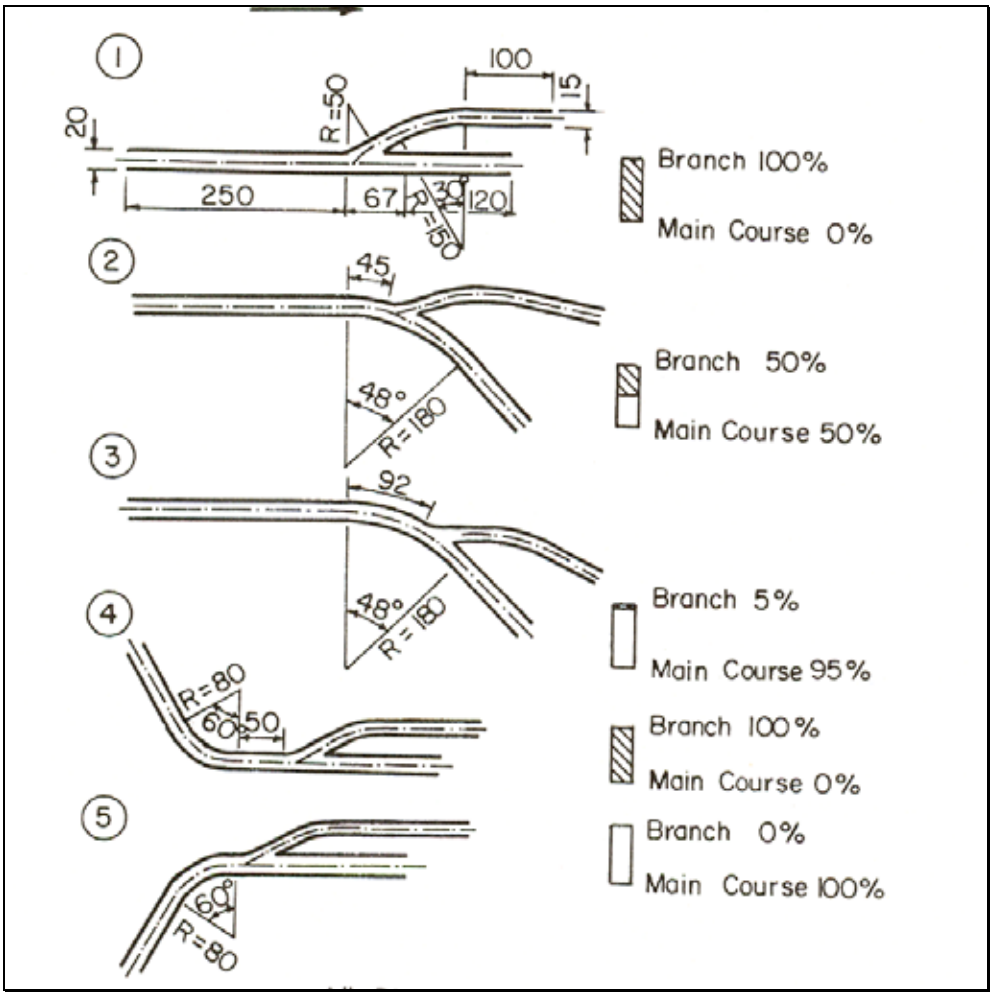

Figure 4-7: Model experiments of diversion structures (*Mosoyi, 1965)*

Bulle (1926) developed Figure 4-8 that shows the relationship between the sediment concentration in the main channel (G_m) and in the branch channel (G_b) and the Diverted Discharge Ratio (DDR).

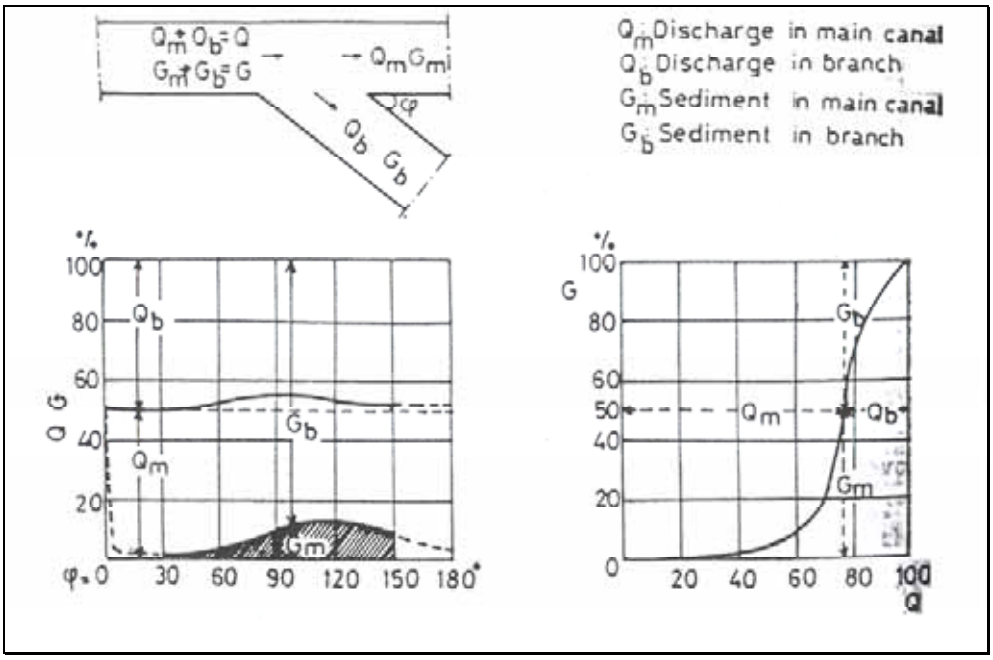

Figure 4-8: Sediment entry into the diversion channel *(Bulle, 1926)*

5 LABORATORY TESTS AND ANALYSIS ON OPTIMUM DIVERSION LOCATION

5.1 EXPERIMENTAL SET-UP

A series of laboratory experiments were carried out in the Hydraulic Laboratory of the University of Stellenbosch to determine the optimum diversion location by assessing the position of the maximum velocity. Scour patterns were also monitored so that the location of the maximum scour hole could be compared with the location of the maximum velocity. A model was constructed to simulate the flow behaviour in a river bend that is preceded by a straight section.

It was decided to aim for a water level of 100 mm above the model bed to be able to perform velocity measurements at 30, 50 and 70 mm above the bed. The width of the model was 0.3 m to ensure a width to depth ratio (*w/d)* of 3. This is a minimum *w/d* ratio where the side effects of the model walls will be minimised.

The choice of the range of r_c/w ratios that were to be tested was based on the recommended ratios that were found in the literature (Section 4.4.1). With the available laboratory space and with the range of recommended length to radius ratios (L_{tot}/r_c) of 1.0 to 1.4 *(Tan, 1996)* it was decided to construct three bends with r_c/w of 8.5, 11.8 and 15.2, the total length of the bend being 4.9 m. This resulted in an acceptable L_{tot}/r_c of 1.1 to 1.9. Larger r_c/w ratios are more representative of South African rivers. A summary of the recommended r_c/w ratios that were found in the literature compared to the r_c/w ratios that were used in the current research is shown in Figure 5-1.

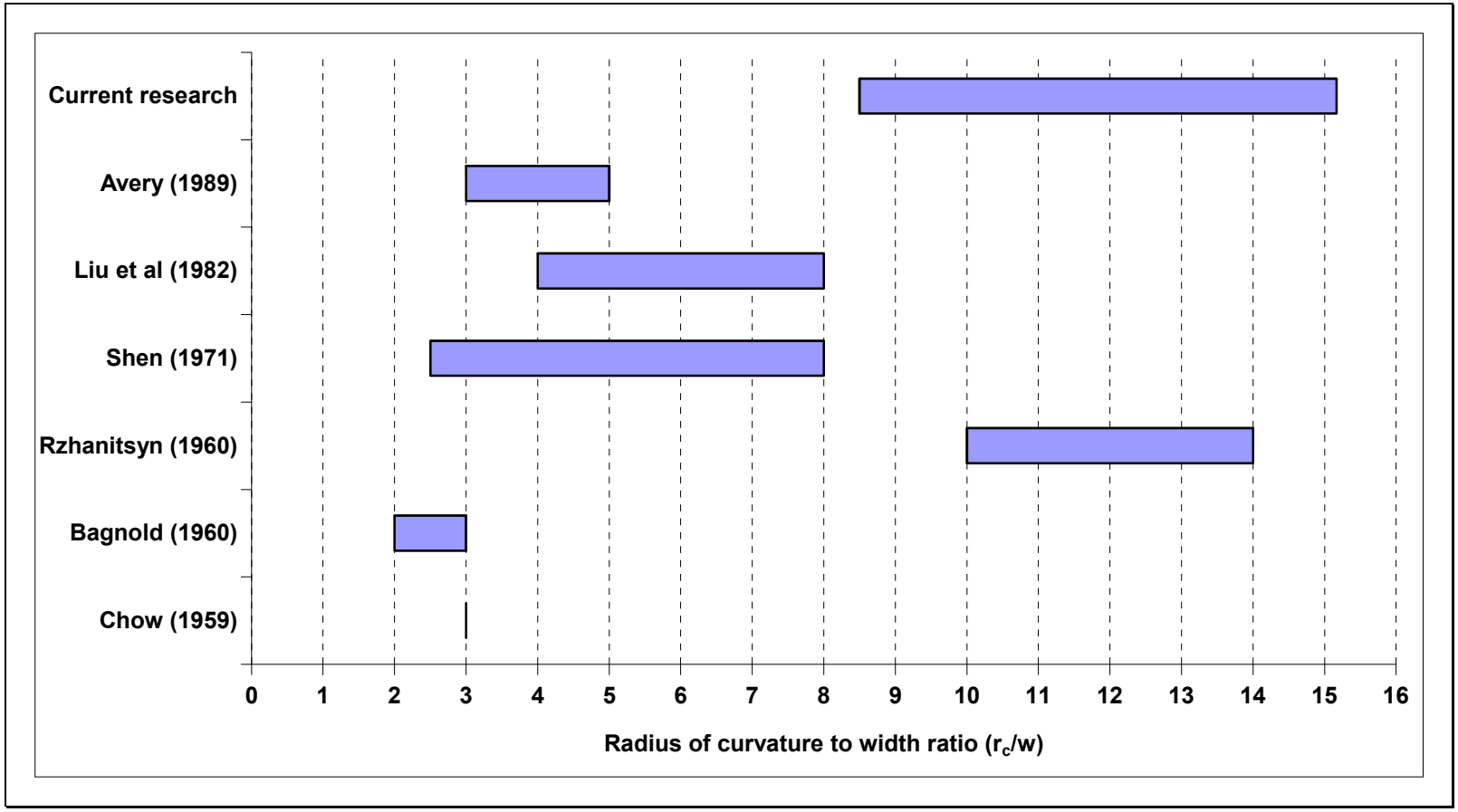

Figure 5-1: Summary of radius of curvature-to-width ratios (r_c/w)

The plan layout of the model is presented in Figure 5-2.

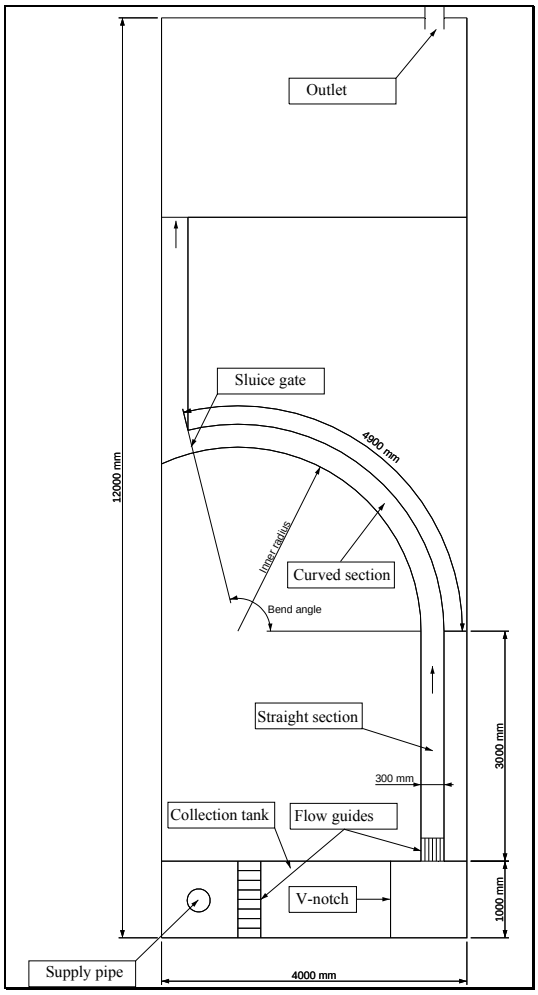

Figure 5-2: Plan layout of model to determine the optimum diversion location (not to scale)

The model consisted of a straight channel, followed by a curved section. The straight section was 3.0 m in length, 0.3 m wide and 0.3 m in depth. The curved section varied in length for the different tests and was also 0.3 m wide and 0.3 m deep. Obtaining the water from a constant pressure head tank ensured constant discharge. The water entered the collection tank through a 150 mm diameter pipe.

The discharge was measured using a 90° V-notch that was located upstream of the straight section in the collection tank. Flow directors were placed in the collection tank to dampen turbulence and to ensure uniform flow conditions. This was done to ensure correct readings at the V-notch. An A. Ott-meter was used to measure the

velocities in the straight and curved channel. At the downstream end of the curved section a sluice gate was inserted to control the water level in the channel. By ensuring a control section at the downstream end of the channel the possibility of a control section developing in the bend was prevented. Flow directors were placed at the entrance to the straight channel to dampen turbulence and to ensure uniform flow conditions. Photos of the model are shown in Figure 5-3 and Figure 5-4.

Figure 5-3: Photo of straight section

Figure 5-4: Photo of curved section

5.2 TEST PROCEDURE

5.2.1 VELOCITY RELATED TESTS

It was decided to use three different centreline radii, i.e. r_c = 2.55, 3.55 and 4.55 m. For each radius, conditions were set-up to represent a range of Froude numbers (F_r). Tests were carried out for F_r = 0.1, 0.3, 0.5 and 0.7 with no sediment in the channel and one sediment related test with a F_r = 0.3. Only sub-critical flow conditions were modelled since it is the prevailing condition in natural rivers. The water level in the channel was controlled by the downstream sluice gate. The aimed water level for all tests was 100 mm. With the aimed Froude numbers known, the corresponding discharges and water levels above the V-notch were calculated with the following equations:

$$F_r = \frac{V}{\sqrt{gy}} \quad \text{(5-1)}$$

From continuity,

$$V = \frac{Q}{by} \quad \text{(5-2)}$$

Substituting equation 5-2 in equation 5-1 yields,

$$F_r = \frac{Q}{by\sqrt{gy}} \quad \text{(5-3)}$$

The V-notch equation that was used were as follow

$$Q = \tfrac{8}{15} C_d \sqrt{2g} \tan\left(\tfrac{\theta}{2}\right) H^{\frac{5}{2}} \quad \text{(5-4)}$$

Substituting equation 5-3 into equation 5-4 and rearranging to get H:

$$H = \left[\frac{15 F_r by \sqrt{gy}}{8 C_d \sqrt{2g} \tan\left(\tfrac{\theta}{2}\right)} \right]^{\frac{2}{5}} \quad \text{(5-5)}$$

where H = water level above V-notch
F_r = Froude number
y = depth of water in channel
C_d = 0.61
θ = 90°
V = average velocity

From equation 5-5, H is solved to obtain the desired water level above the V-notch.

Velocities were measured in 50 mm intervals across the channel at 14 cross sections that were perpendicular to the channel direction and at three depths, i.e. 30, 50 and 70 mm above the channel bed. The cross-sections were at 500 mm intervals except at the change over from the straight to the curved channel where the spacing was 190 mm between the last cross-section of the straight and the first cross-section on the

bend. Thus, a total number of 210-point velocities was measured for each test run. Water levels were also measured at the same grid as previously explained by means of a needle gauge that was fitted to the measuring unit. The grid layout of positioning where measurements were made is shown in Figure 5-5.

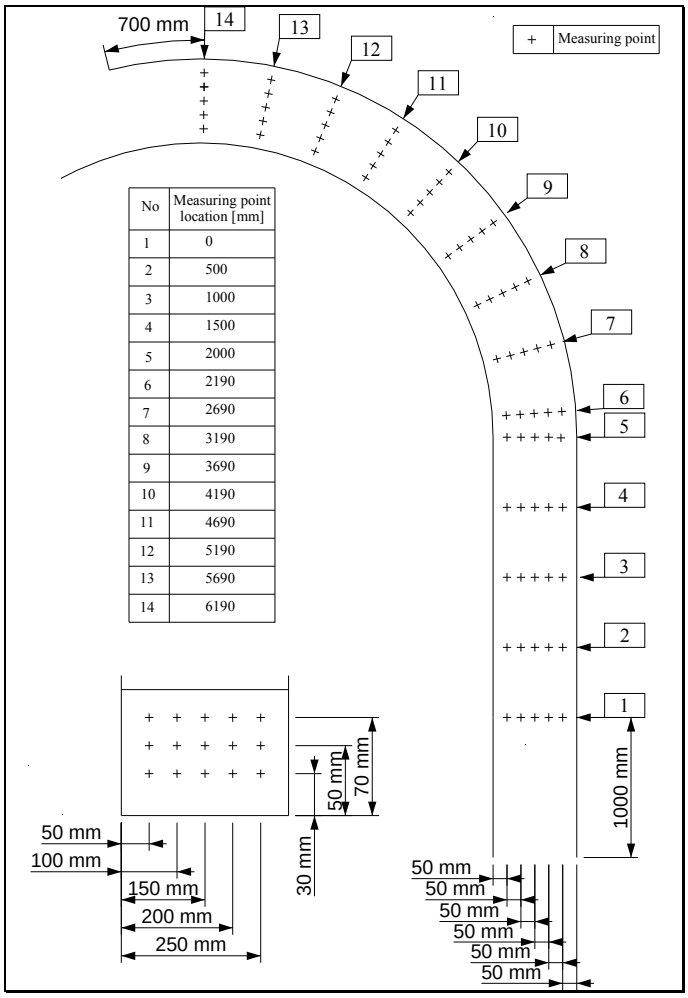

Figure 5-5: Velocity measurement positions for diversion location related tests (not to scale)

An A.Ott-meter (Figure 5-6) was used to measure the velocities. The A.Ott-meter consisted of a propeller and a counting device that counted the number of rotations. At every measuring point the number of revolutions in a 30-second interval were obtained. At each measuring point, the revolutions in three 30-second intervals was taken in order to obtain a reliable average number of revolutions. The average duration of a test was approximately 12 hours.

The unit was mounted on a trolley that could move across the model and also move in the longitudinal direction. The measuring unit could also change direction to accommodate measuring in the curved section, since measurements were made perpendicular to the direction of flow. A protractor was fitted to this unit to ensure that the propeller was perpendicular to the flow direction.

Figure 5-6: Velocity measurements with an A.Ott-meter

Two types of propellers were used. A bigger propeller was used for the tests where $F_r = 0.1$ and 0.3 and a smaller propeller was used for $F_r = 0.5$ and 0.7. The number of revolutions where converted to point velocities by the following equations for the smaller and bigger propeller respectively:

$$V = 0.0923n + 0.035 \quad \text{for } n < 1.13 \quad (5\text{-}6)$$

$$V = 0.1020n + 0.024 \quad \text{for } n > 1.13 \quad (5\text{-}7)$$

$$V = 0.0583n + 0.030 \quad \text{for } n < 7.11 \quad (5\text{-}8)$$

$$V = 0.0545n + 0.057 \text{ for } n > 7.11 \quad \text{(5-9)}$$

A typical test can be described as follows:

- The valve in the 150 mm diameter pipe was adjusted to obtain the required water level above the V-notch.
- Once the required water level has been reached, the valve was left in that position to let the water level stabilise. Continuous adjustments were made at the valve until the water at the V-notch stabilised at the required level.
- The measuring unit was placed at section 6 and the needle gauge was adjusted to represent a water level of 100 mm above the model bed.
- The sluice gate at the downstream end of the curved section was then adjusted to obtain the required water level in the model. Time was given for the water level to stabilise before measurements commenced.
- At every measuring point the water level was first measured.
- The measuring unit was then rotated until the propeller was perpendicular to the direction of the channel and the counter was activated to get the number of revolutions. This was repeated three times to obtain a reliable average.
- Before moving the unit the water level at that particular point was measured again to ensure that a constant supply of water was obtained.
- The unit was then moved to the next measuring point where the above-mentioned steps were carried out.
- After all the measurements were completed, the water level at the V-notch was once again verified.

On the completion of each test a continuity check was done. The measured velocities were integrated over area to determine the measure discharge ($Q_{avg,\ measured}$) and compared with the input discharge (Q_{in}) as were at the V-notch. The comparison is shown in Figure 5-7 from where it can be seen that the measured discharges were over measured by approximately 9%, when considering the average for the whole series of experiments that were done. The figure of 9% was deemed as being reasonable when considering the accuracy of the measured waterlevels that is within the range of 1 mm.

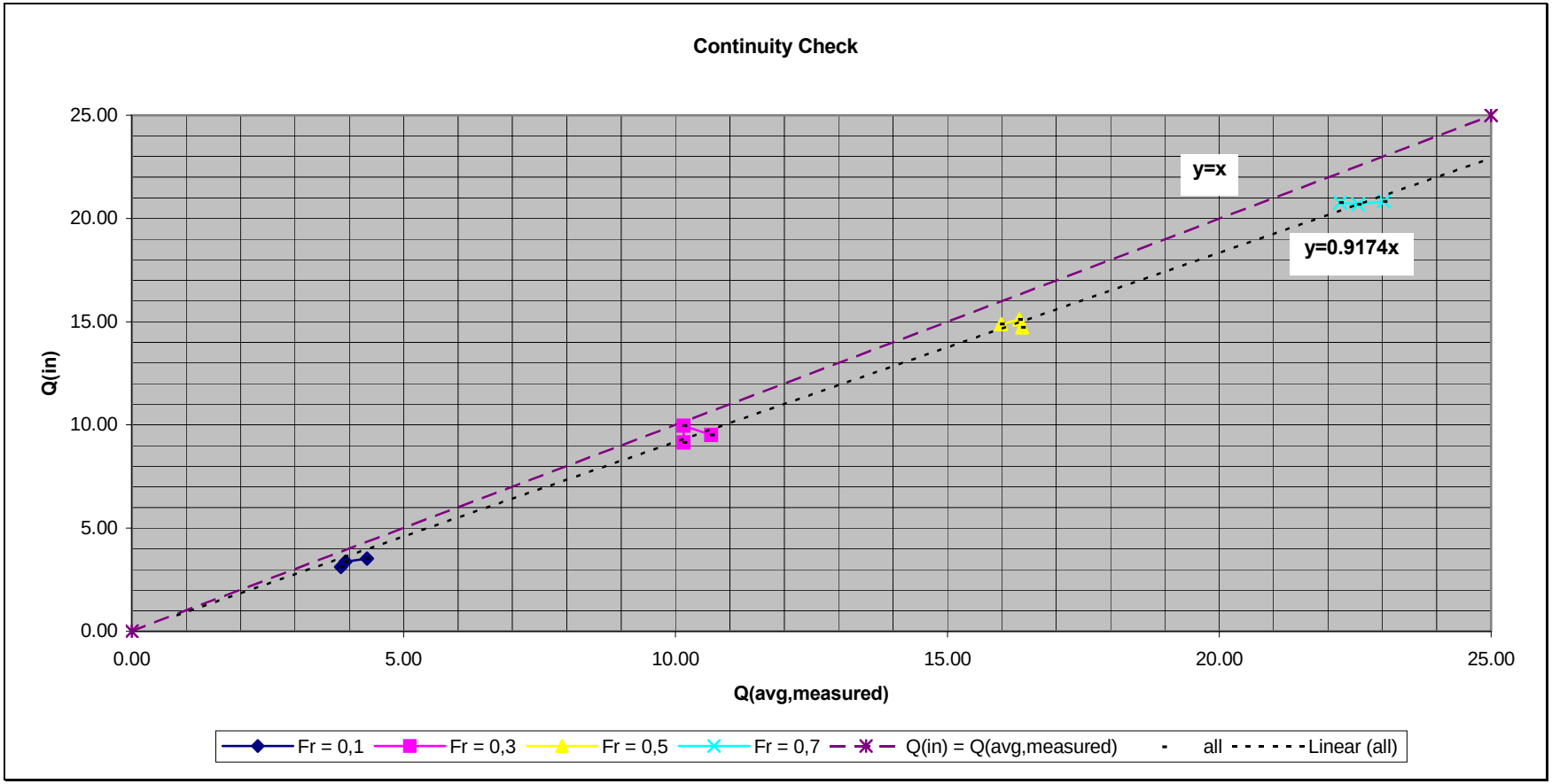

Figure 5-7: Evaluation of measured flow

5.2.2 SEDIMENT RELATED TESTS

The sediment used for the sediment related tests was No.2 Console sand that is commercially available. The same needle gauge set-up that was used for the velocity related tests were again used.

Measurements were taken at 20 cross-sections. For the straight section of the channel the cross-sections were at a 500 mm intervals and sediment levels were only recorded at 5 positions across each section i.e. at 50, 100, 150, 200 and 250 mm from the inside of the bend. For the curved section, measurements were made at the cross-sections that were at 250 mm intervals. Across the section 11 measurements were made at 25 mm intervals i.e. at 25, 50, 75, 100, 125, 150, 175, 200, 225, 250 and 275 mm from the inside of the bend. A total of 175 sediment levels was measured for each test while the typical duration was between 6 to 9 hours. The location of the measurement positions is shown in Figure 5-8.

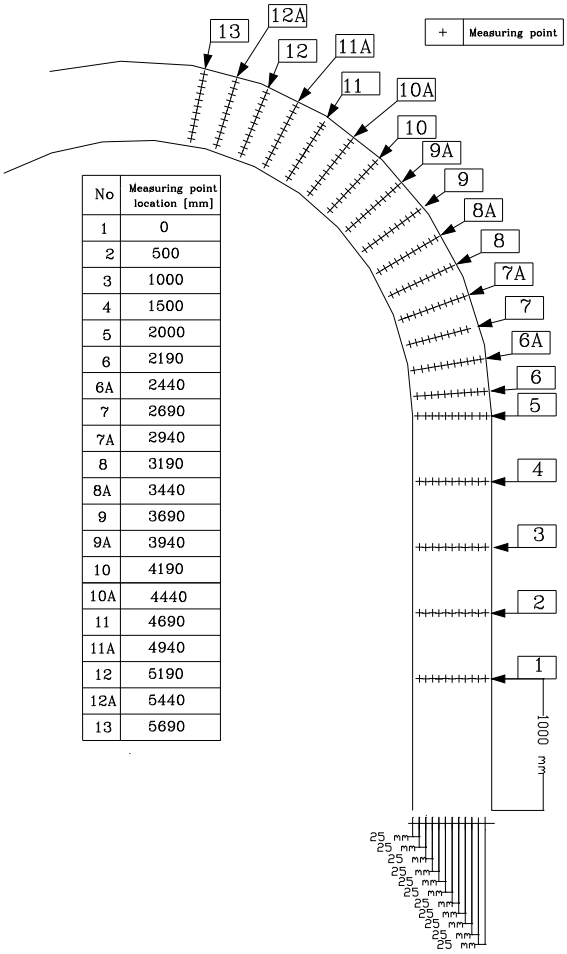

No	Measuring point location [mm]
1	0
2	500
3	1000
4	1500
5	2000
6	2190
6A	2440
7	2690
7A	2940
8	3190
8A	3440
9	3690
9A	3940
10	4190
10A	4440
11	4690
11A	4940
12	5190
12A	5440
13	5690

Figure 5-8: Measurement positions of sediment levels for diversion location related tests (not to scale)

A typical test procedure can be summarised as follows:

- The model was filled with sand to a level of approximately 100 mm above the model bed.
- The downstream sluice gate was closed to allow initial ponding of the water and to prevent excessive initial scouring in the bend.
- The needle gauge was set to the required level at cross-section no 5 (2.0 m stake value).
- The valve was slowly opened to prevent excessive scouring and to allow for the sand to be saturated.
- The downstream sluice gate was kept closed until the sand was saturated and the required water level was obtained.

- The next step was to simultaneously lift the downstream sluice gate (slowly) and to open the valve to reach the required discharge while the required water level was maintained.
- The process was left until the water level was in equilibrium i.e. when no change in water level could be measured.
- Then the downstream sluice gate and valve was once again simultaneously lowered while maintaining a constant water level.
- Once the valve and sluice gate were closed the sluice gate was fractionally opened to allow the water to flow out of the model with as little as possible disturbance to the scouring patterns.
- Once the model was free of standing water the sediment levels were measured.
- This process was repeated until the bed was exposed due to scouring.

5.3 TEST A (AVERAGE RADIUS = 2.55 M)

5.3.1 VELOCITY RELATED TESTS

5.3.1.1 TEST A1 (F_R = 0.1)

The test was carried out with an average water level of 106.4 mm above the model bed and a discharge of 3.38 l/s.

The velocities that were measured at 70 mm (*V70*), 50 mm (*V50*) and 30 mm (*V30*) from the bed are presented in Appendix A: Figure A-1. From this figure it is clear that the velocity distribution develops in such a manner that the velocity on the outer (concave) bank is greater than on the inner (convex) bank. The highest velocities were measured on the outer bank near the downstream end of the bend. A maximum velocity of 0.137 m/s was measured between 5.19 m and 5.69 m on the outer bank of the bend.

The presence of a secondary current that creates a clockwise spiral flow is noted when studying the path of maximum velocity. It is once again clear that the maximum velocity is located on the outside of the bend near the bend exit (see Appendix A: Figure A-2).

A cross-sectional plot of the velocity distribution that was measured at the 14 sections is presented in Appendix A: Figure A-3. The cross-sections are plotted in a downstream direction from top left to bottom right. From this figure it is also evident that the maximum velocity is situated on the outside of the bend near the bend exit and that it shifts downwards in the downstream direction.

From Figures A-1 to A-3 a three-dimensional view of the velocity distribution in the curved section can be formed. It is clear that higher velocities develop in the downstream direction of the bend; the velocity is higher on the outside of the bend than on the inside and that it shifts downwards in the downstream direction. Thus confirming the presence of a clockwise spiral flow in the bend.

The velocity distribution is presented as a line graph in Figures A-4 to A-8 (see Appendix A) with the location of the turning points in Figure D-2 (see Appendix D). The turning points are where *V30>V50*, *V30>V70* and *V50>V70*.

5.3.1.2 TEST A2 (F_R = 0.3)

The discharge during the test was 10.15 l/s and the average water level was 108.9 mm. A maximum velocity of 0.34 m/s was measured at the location 5.69 m on the outside of the bend.

The path of maximum velocity follows the centre of the channel up to 2.0 m where it gradually shifts towards the outside of the bend in the horizontal plane. In the vertical it dives downward from approximately 2.19 m towards the bottom in the downstream direction (see Appendix A: Figures A-9 to A-11).

The velocity distribution is presented as a line graph in Figures A-12 to A-16 (see Appendix A) with the location of the turning points in Figure D-3 (see Appendix D).

5.3.1.3 TEST A3 (F_R = 0.5)

The measured discharge was 14.88 l/s and a maximum velocity of 0.477 m/s was measured on the outside of the bend between 5.19 m and 5.69 m with an average water level of 125.6 mm.

The path of maximum velocity follows the centre of the channel towards chainage 2.19 m where it shifts towards the outside of the bend in the horizontal plane. It remains near the outside of the bend throughout the curved section. In the vertical plane it moves downward in the downstream direction (see Appendix A: Figures A-17 to A-19).

The locations of the turning points are presented in Figure D-3 (see Appendix D) and the line graph velocity distributions in Figures A-20 to A-24 (see Appendix A).

5.3.1.4 TEST A4 (F_R = 0.7)

In the horizontal plane the path of maximum velocity is near the centre of the channel up to 1.5 m where it shifts towards the inside of the channel. In the region of 2.69 m it gradually shifts towards the outside of the bend until the end of the curved section is reached and in the vertical plane it shifts downwards in the downstream direction.

The maximum velocity measured was 0.52 m/s between 5.19 m and 5.69 m with a discharge of 20.77 l/s and an average water level of 156.9 mm (see Appendix A: Figures A-25 to A-27).

The velocity distribution is presented as a line graph in Figures A-28 to A-32 (see Appendix A) with the location of the turning points in Figure D-4 (see Appendix D).

5.3.2 SEDIMENT RELATED TESTS

5.3.2.1 TEST A5 (FR = 0.3)

Several small scouring holes were observed with three main areas of scouring that can be identified. The first area was located between 2.94 m and 4.44 m. This area contained several small scouring holes with the maximum scouring occurring depth at 3.44 m. The width of the scour hole was approximately 100 mm.

The second area of scour is much smaller and is located between 4.94 m and 5.44 m. The point of maximum scour was at 5.19 m and the width of the scour hole was approximately 50 mm.

The third scour area was between 5.69 m and 6.19 m where the measurements stopped. The deepest scour hole occurred at 6.19 m and the width of the scour was

approximately 75 mm. The development of the scour holes is depicted in Appendix A: Figures A-33 to A-35.

5.4 TEST B (AVERAGE RADIUS = 3.55 m)

5.4.1 VELOCITY RELATED

5.4.1.1 TEST B1 (F_R = 0.1)

The discharge during the test was 3.12 l/s with a maximum velocity of 0.14 m/s at the outside of the bend between 5.69 m and 6.19 m. The average water level in the canal was 99.9 mm.

The path of maximum velocity in the horizontal plane can be described as being along the centre of the canal for the first 1.5 m. Then upon entering the bend at 2.19 m it shifted towards the inside of the bend up to 3.19 m where it changed direction and moved towards the outside of the bend. In the vertical plane it can also be seen that it dives from 2.19 m towards the end of the measurements at 6.19 m. Thus, the maximum velocity shifts towards the outside of the bend and dives towards the lower measuring points as it moves in a downstream direction towards the end of the bend (see Appendix A: Figures A-36 to A-43 and Appendix D: Figure D-7).

5.4.1.2 TEST B2 (F_R = 0.3)

The maximum velocity that was measured was 0.37 m/s at the outside of the bend between 5.19 m and 5.69 m. The average water level was 108.8 mm with a discharge of 9.51 l/s.

The path of the maximum velocity follows essentially the same pattern as described above. In the horizontal plane it moves from the centre of the channel towards the inside at 2.19 m and then shifts rapidly towards the outside of the bend at 3.69 m where it follows the outside of the bend up to the end of the bend. From the vertical velocity distribution it is seen how it moves downwards from 2.69 m up to the end of the measurements at 6.19 m (see Appendix A: Figures A-44 to A-51). The locations of the turning points are presented in Figure D-8 (see Appendix D).

5.4.1.3 TEST B3 (F_R = 0.5)

The average water level during the test was 107.1 mm with a discharge of 14.72 l/s. Between 5.19 m and 5.69 m a maximum velocity of 0.58 m/s was measured along the outside of the bend.

In the horizontal plane the path of maximum velocity was once again in the middle of the channel up to 2.19 m where it moved towards the inside of the bend as shown in Appendix A: Figure A-52. At 3.19 m it gradually moved towards the outside of the bend where it followed the outside of the bend until the end. It is noted that the maximum velocity moves downwards from 2.690 towards the end of the curved section in the vertical plane (see Appendix A: Figures A-53 and A-54).

The velocity distribution is presented as a line graph in Figures A-55 to A-59 (see Appendix A) with the location of the turning points in Figure D-9 (see Appendix D).

5.4.1.4 TEST B4 (F_R = 0.7)

A maximum velocity of 0.63 m/s was measured around 5.69 m at the outside of the bend. The discharge was 20.69 l/s with an average water level of 135.4 mm.

The velocity distribution is presented as a line graph in Figures A-63 to A-67 (see Appendix A) with the location of the turning points in Figure D-10 (see Appendix D).

The maximum velocity followed the route of being fairly in the centre of the channel in the horizontal plane up to 1.5 m where it suddenly shifted towards the inside of the bend and then at 3.19 m it shifted towards the outside of the bend up to the end of the bend. In the vertical plane it also moved downwards from about 2.69 m in the downstream direction (see Appendix A: Figures A-60 to A-62).

5.4.2 SEDIMENT RELATED

5.4.2.1 TEST B5 (F_R = 0.3)

In this case only one scour area can be identified between 2.94 m and 4.44 m being in the order of 50 mm wide (see Appendix A: Figures A-68 to A-69). The reason for only being able to identify one scour region is that the test must have been stopped too early when the scour was not completely finished. This can be said with a reasonable degree of confidence, since this scour pattern corresponds to the scour patterns during the initial stages of the other sediment related tests. Figure 5-9 is a photo of the a typical observed scour pattern in the curved section of the channel.

Figure 5-9: Photo of observed scour pattern

5.5 TEST C (AVERAGE RADIUS = 4.55 m)

5.5.1 VELOCITY RELATED TESTS

5.5.1.1 TEST C1 (F_R = 0.1)

In the horizontal plane the maximum velocity moved from being in the centre of the channel towards the inside at about 2.69 m and shifted swiftly towards the outside of the bend at 4.19 m where it followed the outside of the bend up to the point where measurements were taken. It shifted downwards from around 2.69 m towards the bottom in the downstream direction in the vertical plane.

The average water level during the test was 128.3 mm with a discharge of 3.53 l/s. A maximum velocity of 0.127 m/s was recorded in the region of 6.19 m near the outside of the bend (see Appendix A: Figures A-70 to A-77). The location of the turning points is presented in Figure D-12 (see Appendix D).

5.5.1.2 TEST C2 (F_R = 0.3)

A maximum velocity of 0.31 m/s was measured at the outside band at 6.19 m while the average water level was 122.6 mm with a discharge of 9.14 l/s.

The path of the maximum velocity in the horizontal plane was in the middle of the channel up to 3.19 m where it slightly shifted towards the inside of the bend before moving towards the outside of the bend in the vicinity of 4.19 m. It remained on the outside of the bend towards the end of the curved section. In the vertical plane it moves downward in the downstream direction (see Appendix A: Figures A-78 to A-80).

The velocity distribution is presented as a line graph in Figures A-81 to A-85 (see Appendix A) with the location of the turning points depicted in Figure D-13 (see Appendix D).

5.5.1.3 TEST C3 (F_R = 0.5)

The discharge during the test was 15.11 l/s with an average water level of 103.8 mm. The maximum velocity followed the centre of the channel up to 3.19 m where it shifted towards the outside of the bend in the horizontal plane. It followed the outside of the bend up to 6.19 m where the maximum velocity of 0.591 m/s was recorded. In the vertical plane the position of the maximum velocity also shifted from being in the upper region to the lower region in the downstream direction (see Appendix A: Figures A-86 to A-88).

The velocity distribution is presented as a line graph in Figures A-89 to A-93 (see Appendix A) with the location of the turning points in Figure D-14 (see Appendix D).

5.5.1.4 TEST C4 (F_R = 0.7)

The discharge during the test was 20.82 l/s with an average water level of 168.7 mm. At 6.19 m the maximum velocity was measured on the outside of the bend.

In the horizontal plane the maximum velocity shifted from being essentially in the centre of the channel up to 2.69 m towards to outside of the bend at 3.19 m where it remained until the end of the bend and in the vertical plane it moved downwards from 2.19 m towards the bottom in the downstream direction (see Appendix A: Figures A-94 to A-101). The location of the turning points is presented in Figure D-15 (see Appendix D).

The exceptionally low velocity indicated on the velocity distribution figures at 3.19 m near the inside of the bend is due to a measuring mistake and does not reflect the actual velocity.

5.5.2 SEDIMENT RELATED TESTS

5.5.2.1 TEST C5 (F_R = 0.3)

Three areas of major scour near the outside of the bend can be identified. The first big area is situated between 3.19 m and 4.69 m. It consists of several small scour holes that form the big scour area which is approximately 75 mm in width. The region of deepest scour is at 3.44 m.

The second scour area is in the region of 5.19 m and is much smaller and only 50 mm wide.

The third scour area is in the region between 5.69 m and 6.19 m. It consists of two scour holes that are about 75 mm wide. The area of deepest scour is at 6.19 m where the end of measurements is reached (see Appendix A: Figures A-102 to A-104).

5.6 ANALYSIS OF TESTS ON DIVERSION LOCATION

5.6.1 FLOW PATTERN

A summary of the positions of the maximum velocities as were measured is provided in Table 5-1. The locations of the maximum velocity ($L_{v,max}$) for r_c = 2.55 m were found to be in the region of 3.19 m from the beginning of the bend. When this length is converted into an angle, with zero being at the beginning of the bend, the angle where the maximum velocity is located ($\theta_{v,max}$) is at 68°. The ratio of the position of the maximum velocity to the total bend angle ($\theta_{v\max}/\theta_{bend}$) was calculated at 0.65.

Test No	r_c [m]	F_r	L_{vmax} [m]
A1	2.55	0.1	3.19-3.69
A2	2.55	0.3	3.69
A3	2.55	0.5	3.19-3.69
A4	2.55	0.7	3.19-3.69
B1	3.55	0.1	3.69-4.19
B2	3.55	0.3	3.19-3.69
B3	3.55	0.5	3.19-3.69
B4	3.55	0.7	3.69
C1	4.55	0.1	4.19
C2	4.55	0.3	4.19
C3	4.55	0.5	4.19
C4	4.55	0.7	4.19

Table 5-1: Summary of maximum velocity locations in curved section

Similarly, the location of the maximum velocity for a r_c = 3.55 m was at 3.69 m with $\theta_{v,max} = 57°$ and ($\theta_{v\max}/\theta_{bend} = 0.75$). For a r_c = 4.55 m the maximum velocity was measured at 4.19 m with $\theta_{v,max} = 51°$ and ($\theta_{v\max}/\theta_{bend} = 0.85$). A summary of the

relationship between the radius of curvature and the maximum axial flow velocity position is given in Table 5-2.

r_c	θ_{bend} [°]	$\theta_{v\max}$ [°]	$\theta_{v\max}/\theta_{bend}$
2.55	104	68	0.65
3.55	76	57	0.75
4.55	60	51	0.85

Table 5-2: Relationship of radius of curvature to maximum velocity position

It follows from Table 5-1 and Table 5-2 that the position of the maximum velocity moves in the downstream direction with an increase in the radius of curvature of the bend. It is also noted that the position of the maximum velocity does not vary much for different Froude numbers, for a specific radius.

In general, the velocity distributions obtained from the laboratory experiments seem to follow the same pattern. In the horizontal plane a fairly uniform velocity distribution is obtained in the first part of the straight section. Towards the end of the straight section the maximum velocity moves slightly towards the inside of the bend. The maximum velocity then gradually shifts towards the outside of the bend and reaches the outside of the bend between 3.19 m and 3.69 m. Further downstream it remains near the outside of the bend. A typical velocity distribution in the horizontal plane is presented in Figure 5-10.

In the vertical plane the general tendency is that the maximum velocity dives towards the bottom while moving towards the outside of the bend in the downstream direction. A typical velocity distribution in the vertical plane is presented in Figure 5-11 with a typical cross-sectional distribution in Figure 5-12.

In summary, the maximum velocity was found on the outside of the bend near the end of the bend; the velocities are higher on the outside of the bend than on the inside and the maximum velocity shifts downwards while moving towards the outside of the

bend in the downstream direction. This confirms the presence of a clockwise spiral that develops in the bend as was found in the literature.

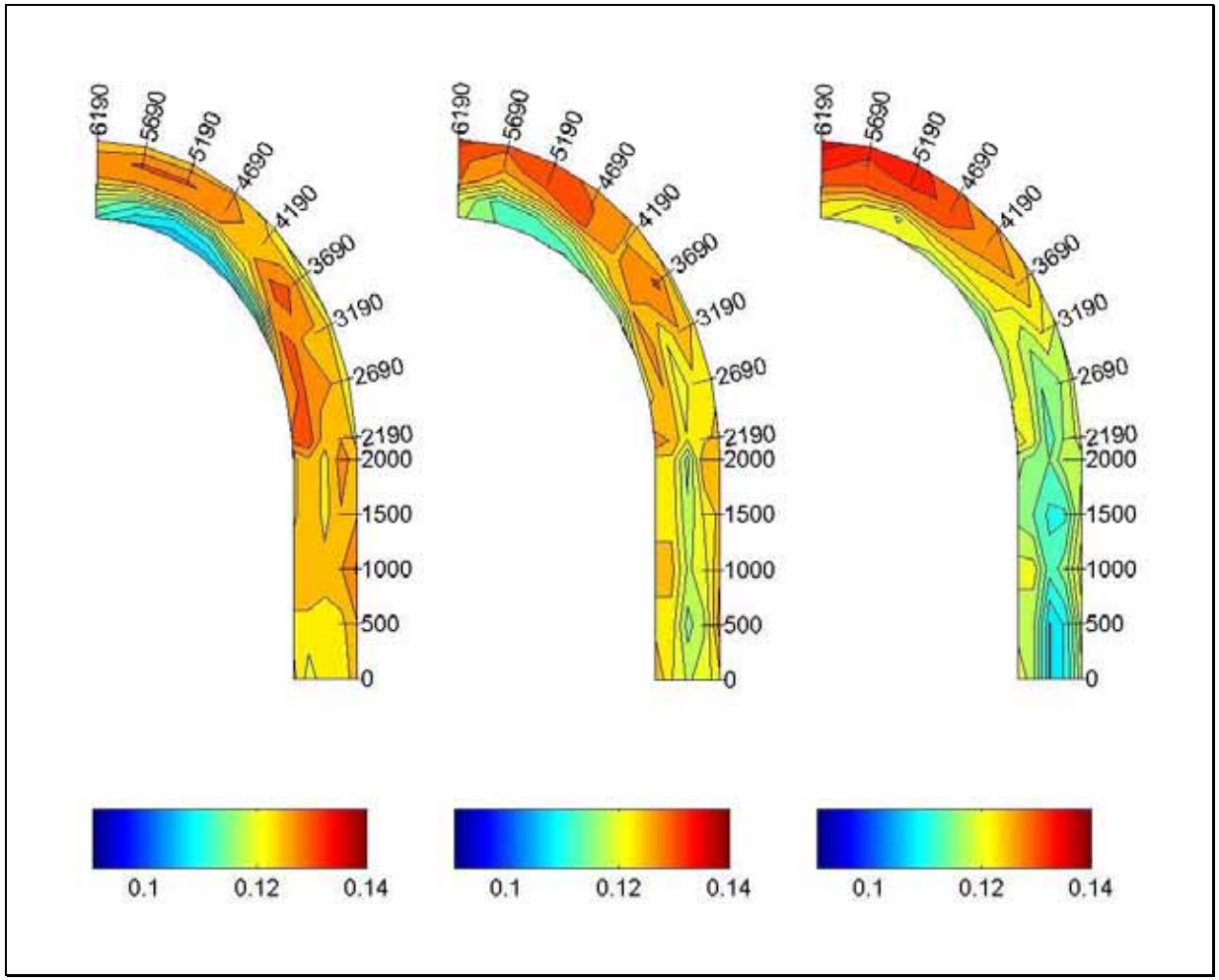

Figure 5-10: Typical velocity distribution in the horizontal plane measured at 70, 50 and 30 mm

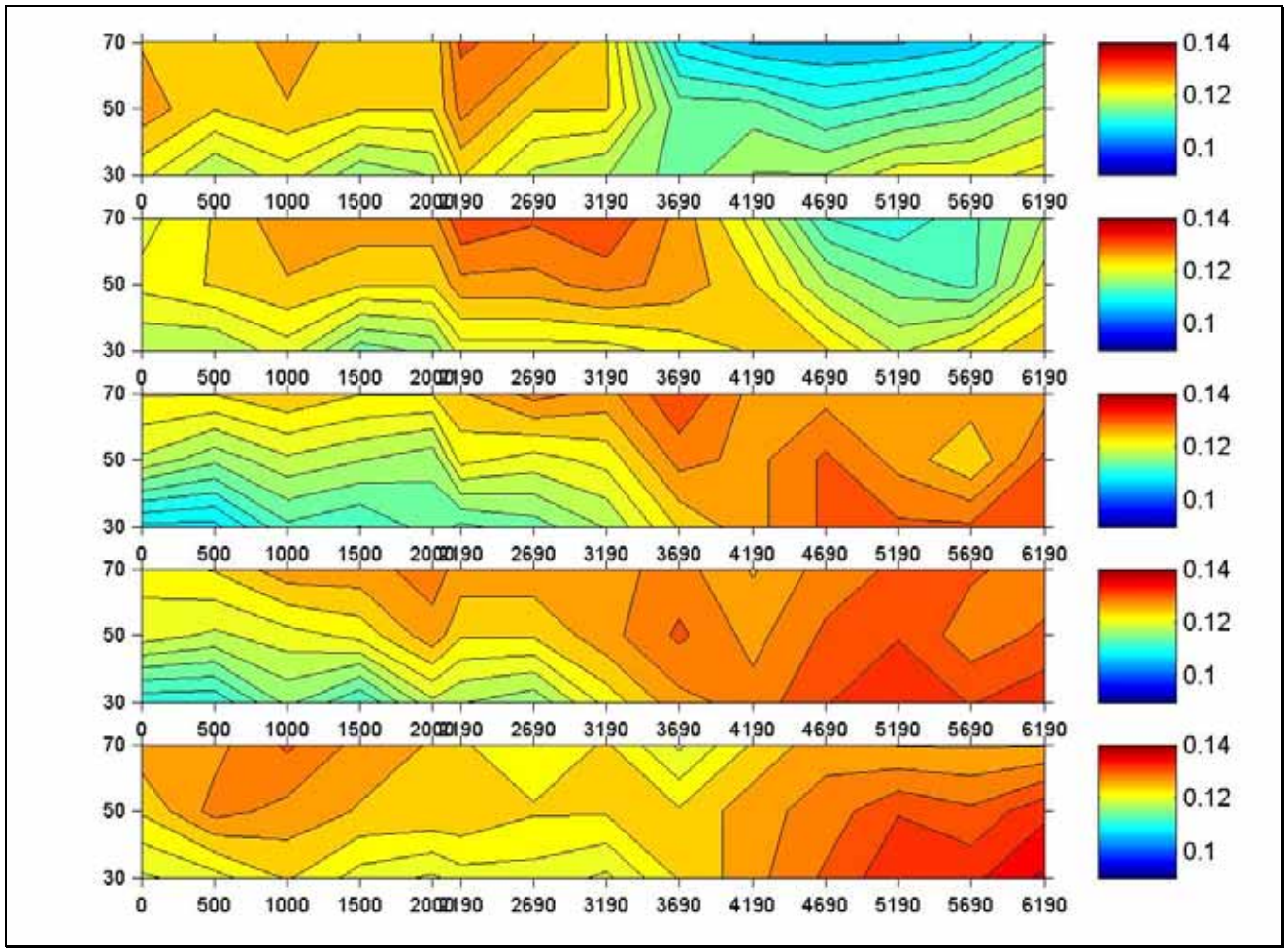

Figure 5-11: Typical velocity distribution in the vertical plane [m/s]

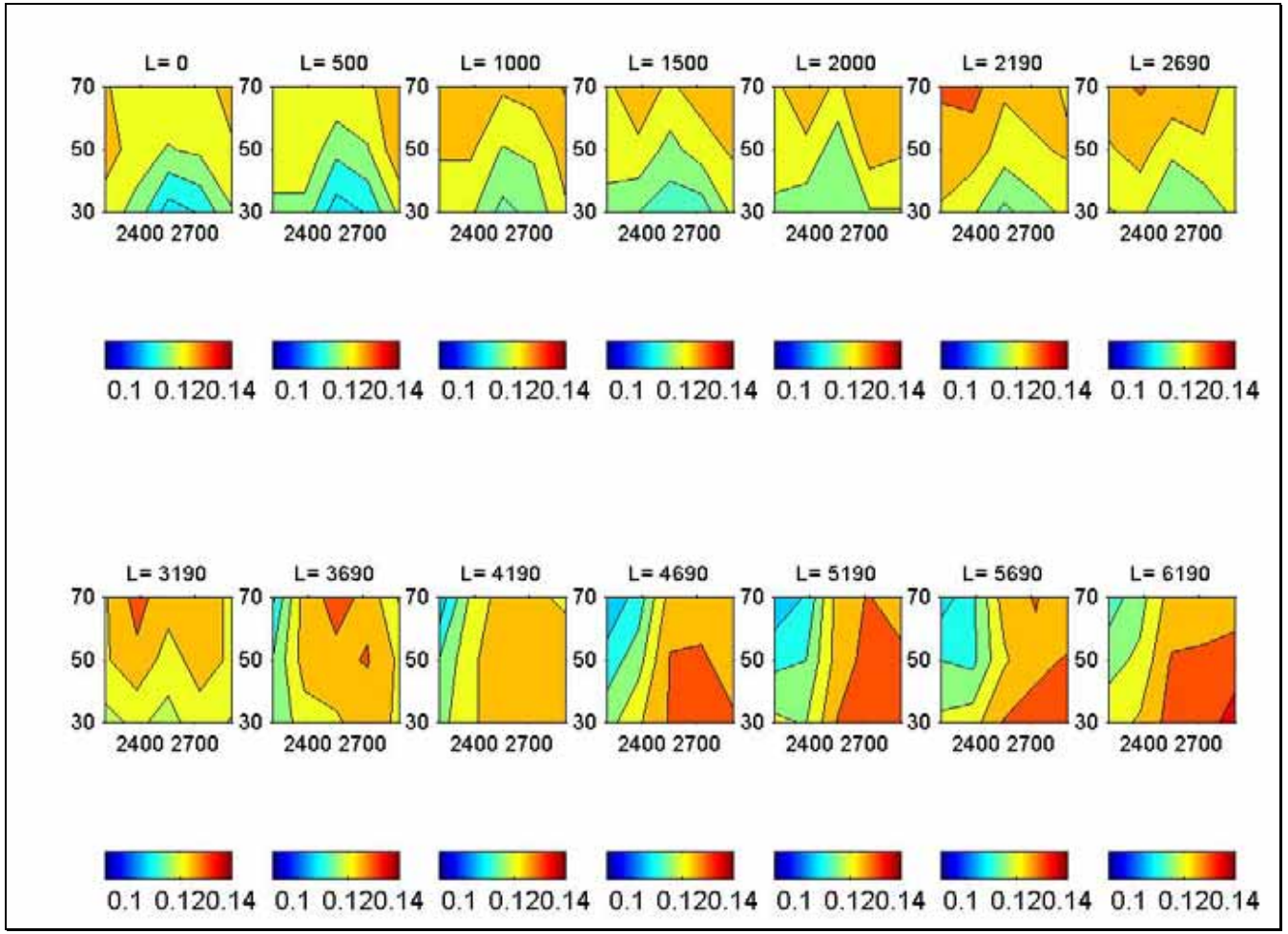

Figure 5-12: Typical cross-sectional velocity distribution [m/s]

The vertical velocity distributions obtained from the laboratory experiments were plotted as a line graph to further analyse the diving phenomenon that was observed from the vertical velocity distributions. Typical figures are presented in Figures 5-13, 5-14 and 5-15. The velocity measured at 70 mm above the bed is represented as *V70* while the velocity measured at 50 mm is represented as *V50* and the velocity measured at 30 mm above the bed as *V30*.

The following characteristics in the downstream direction are noted from the above mentioned figures:

i) The measured velocity at 70 mm from the bottom (*V70*) has a decreasing tendency near the inside of the bend.
ii) In the centre of the bend all the measured velocities show an increasing tendency.
iii) Near the outside of the bend the measured velocity at 30 mm from the bottom (*V30*) shows an increasing tendency.

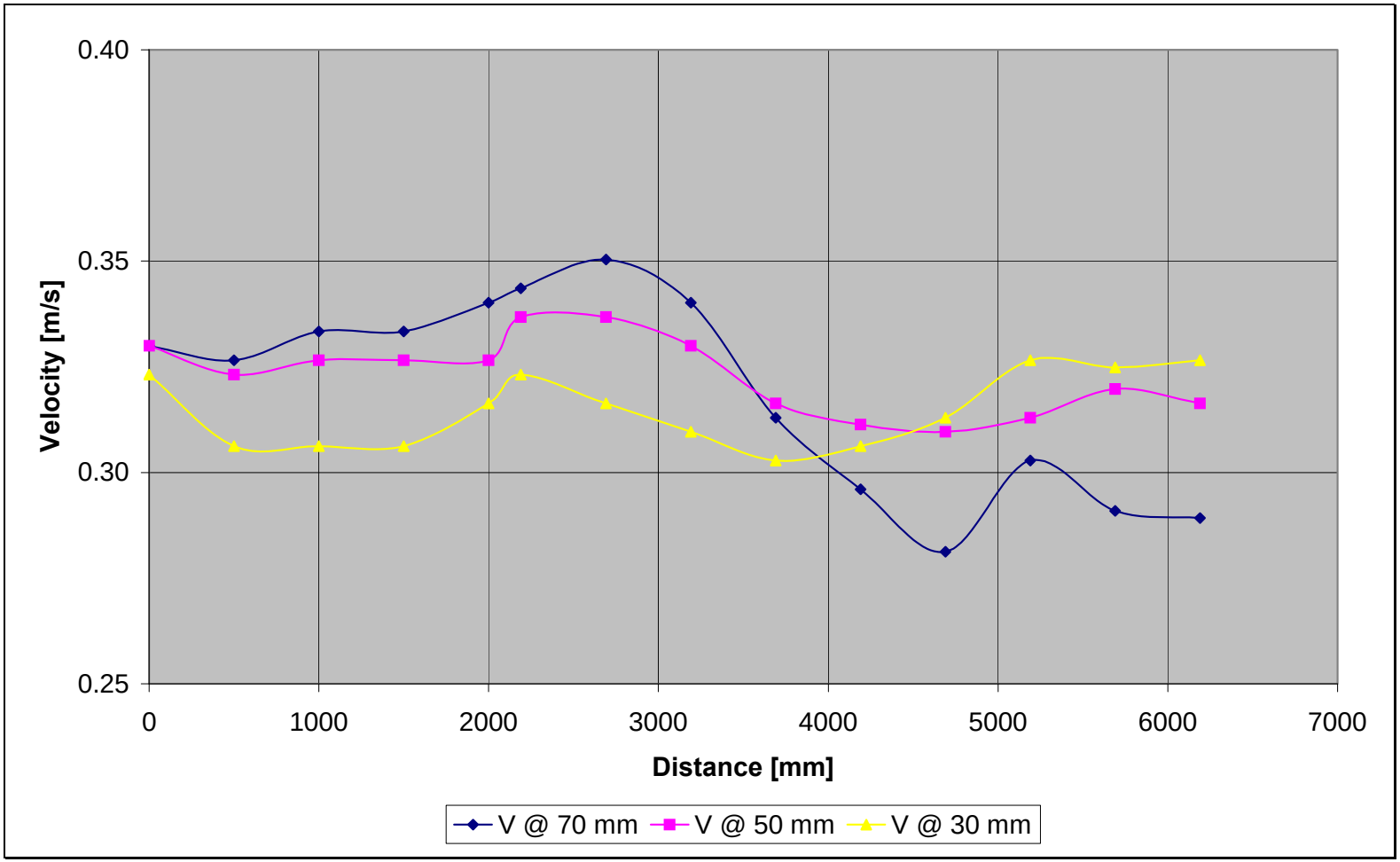

Figure 5-13: Decreasing tendency of *V70* near the inside of the bend with $r_c/w = 11.8$ and $F_r = 0.3$

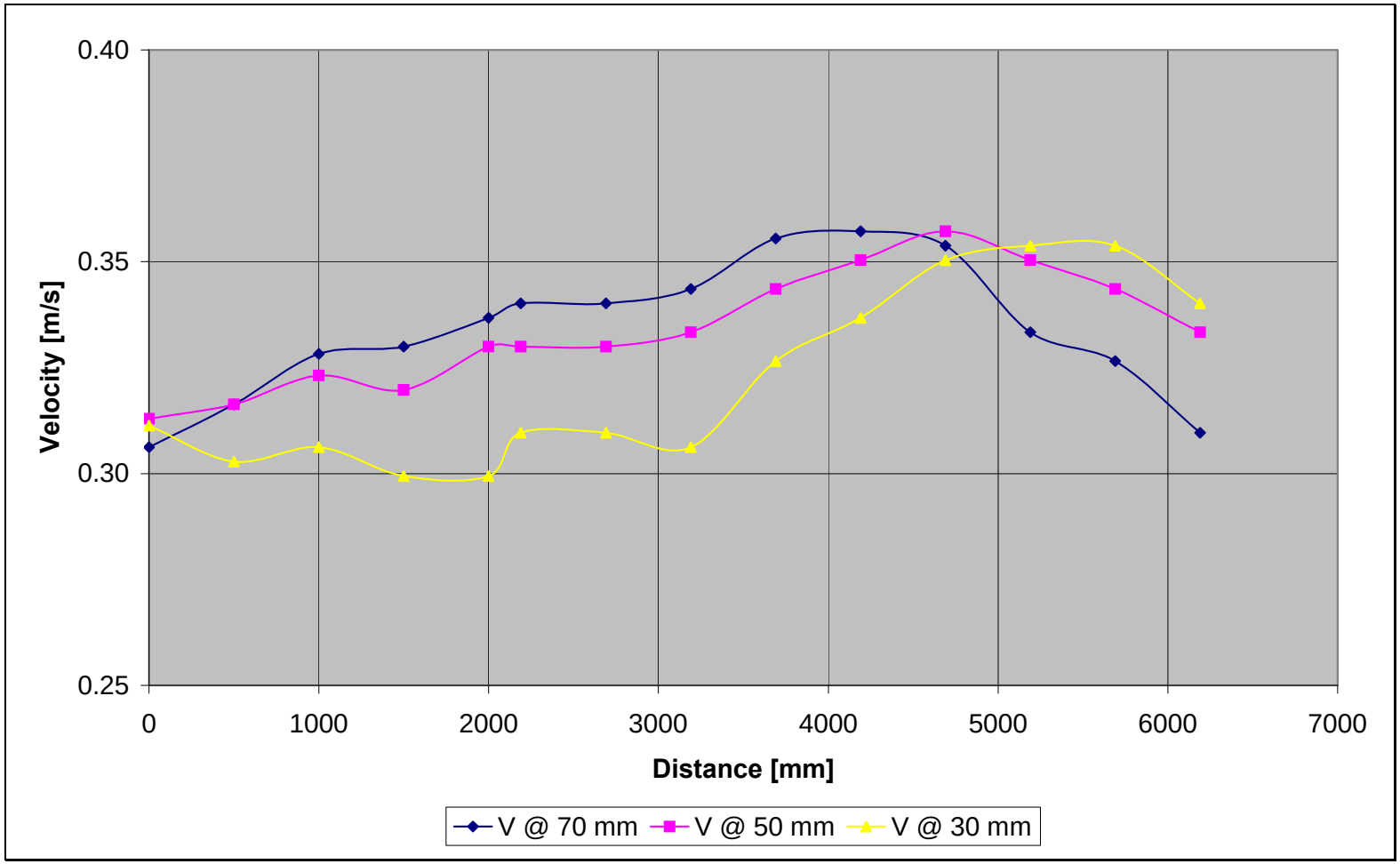

Figure 5-14: Increasing tendency of *V70, V50 and V30* at the centre of the bend with $r_c/w = 11.8$ and $F_r = 0.3$

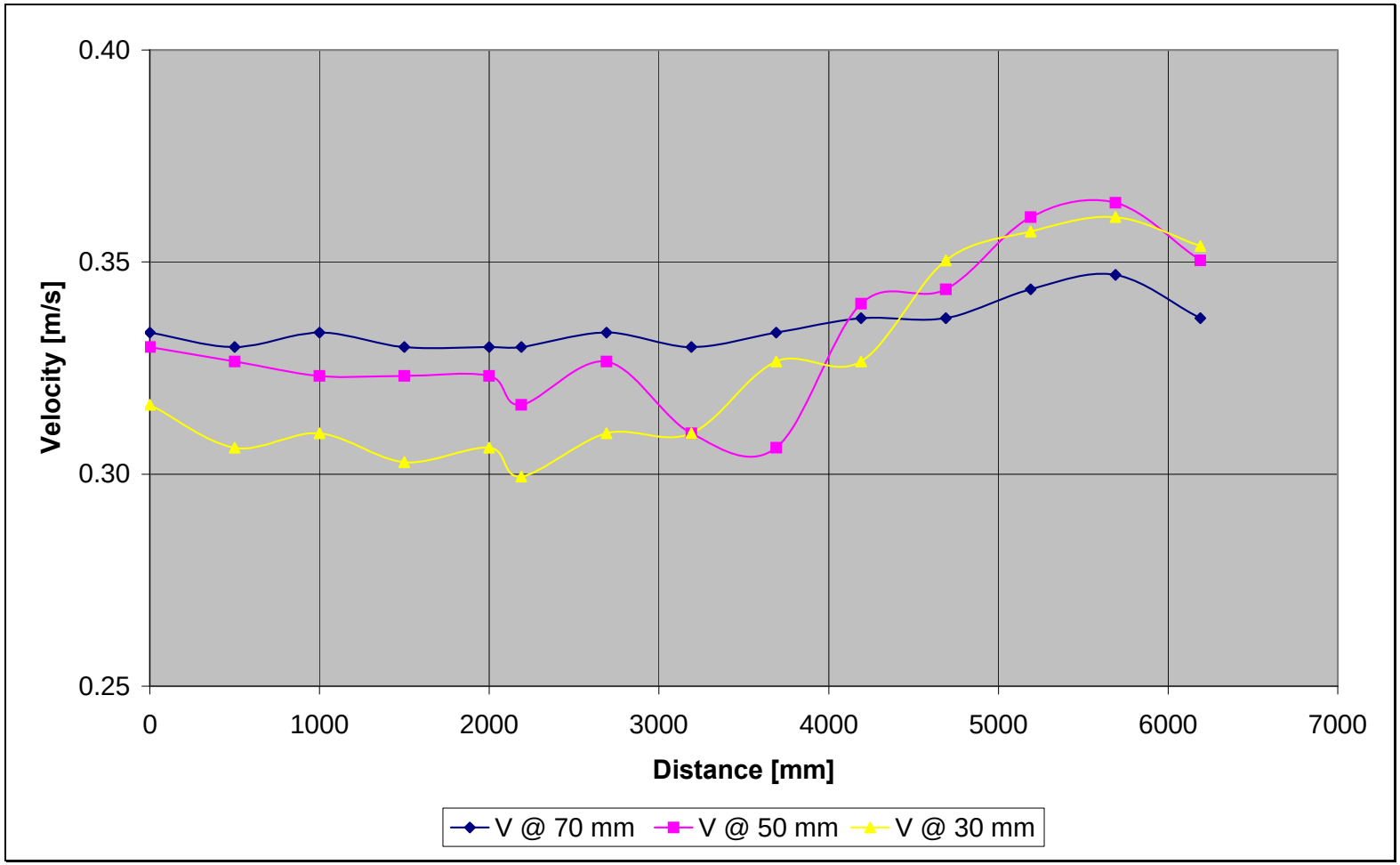

Figure 5-15: Increasing tendency of *V30* near the outside of the bend with $r_c/w = 11.8$ and $F_r = 0.3$

The typical tendency of the location of the turning points, i.e. where *V30>V50*, *V30>V70* and *V50>V70* is presented in Figure 5-16. It is noted that the turning points where *V30>V50*, *V30>V70* and *V50>V70* stay relatively constant near the inside of the bend but at the outside of bend they move in the downstream direction with an increase in Froude number. When comparing the location of these turning points of Tests A, B and C, it is noted that the turning points also move in the downstream direction with an increase of the radius of curvature. The range of the location of the turning points increase on the inside and outside of the bend for an increase in the radius of curvature (see Appendix D: Figures D-1, D-6, D-11). This turning phenomenon of *V30*, *V50* and *V70* can only occur due to the presence of the secondary (spiral) flow.

5.6.2 SCOUR PATTERN

In general the observed scour patterns for r_c / w = 8.5, 11.8 and 15.2 have the same tendency. Three main scour areas at the outside of the bend can be identified. The first area is located approximately between 3.19 m and 4.44 m with the maximum scour at 3.44 m. The second scour area is much smaller than the first one and occurs around 5.19 m. The third scour area is of the same scale as the second area and is located between 5.69 m and 6.19 m. The location of the third scour hole is in good agreement with the location of the maximum measured velocity in the bend. Figure 5-17 indicates a typical observed scour pattern (with the bend shown as a straight channel, starting at 2000 mm).

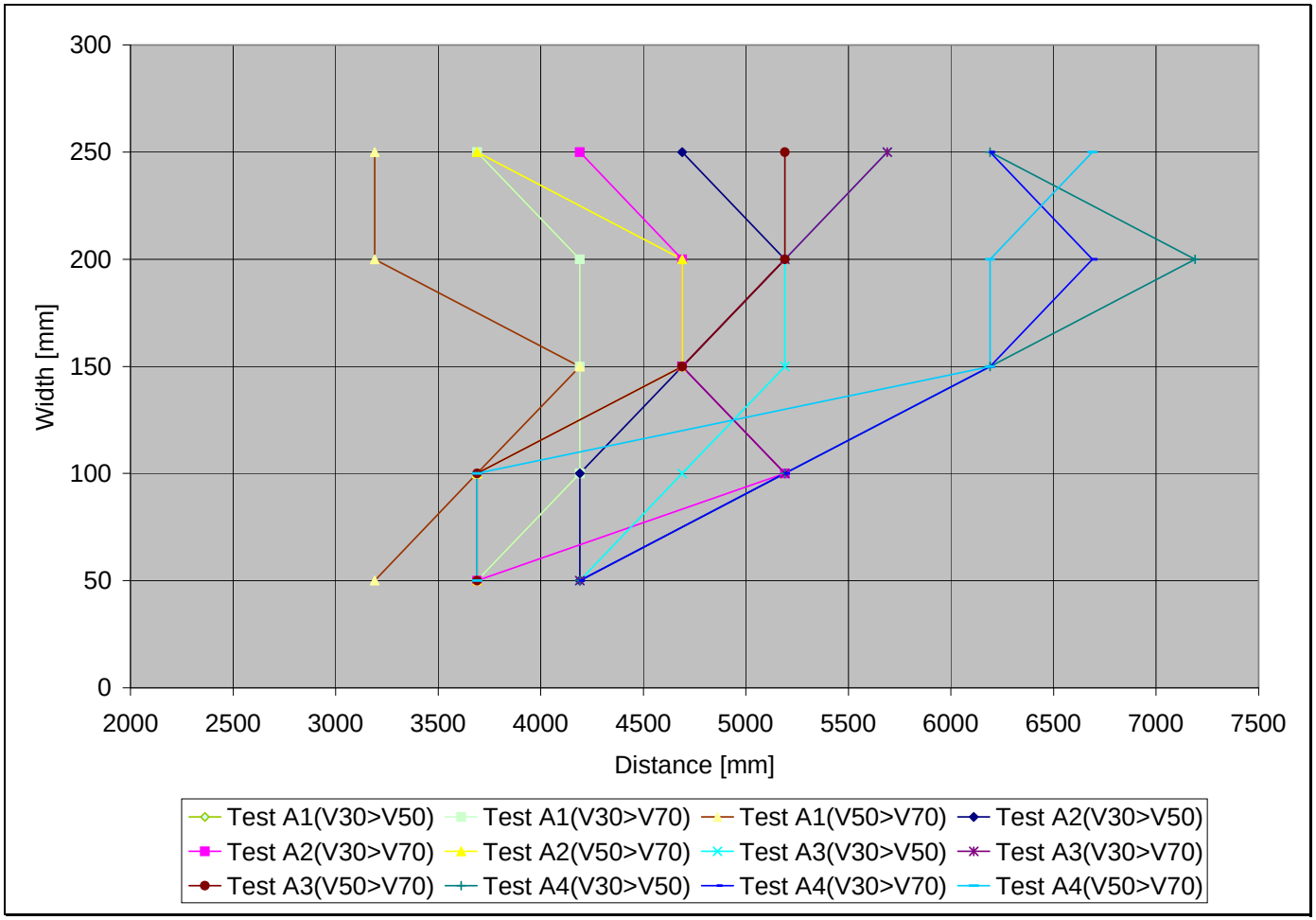

Figure 5-16: Typical location of turning points for *V30>V50*, *V30>V70* and *V50>V70*

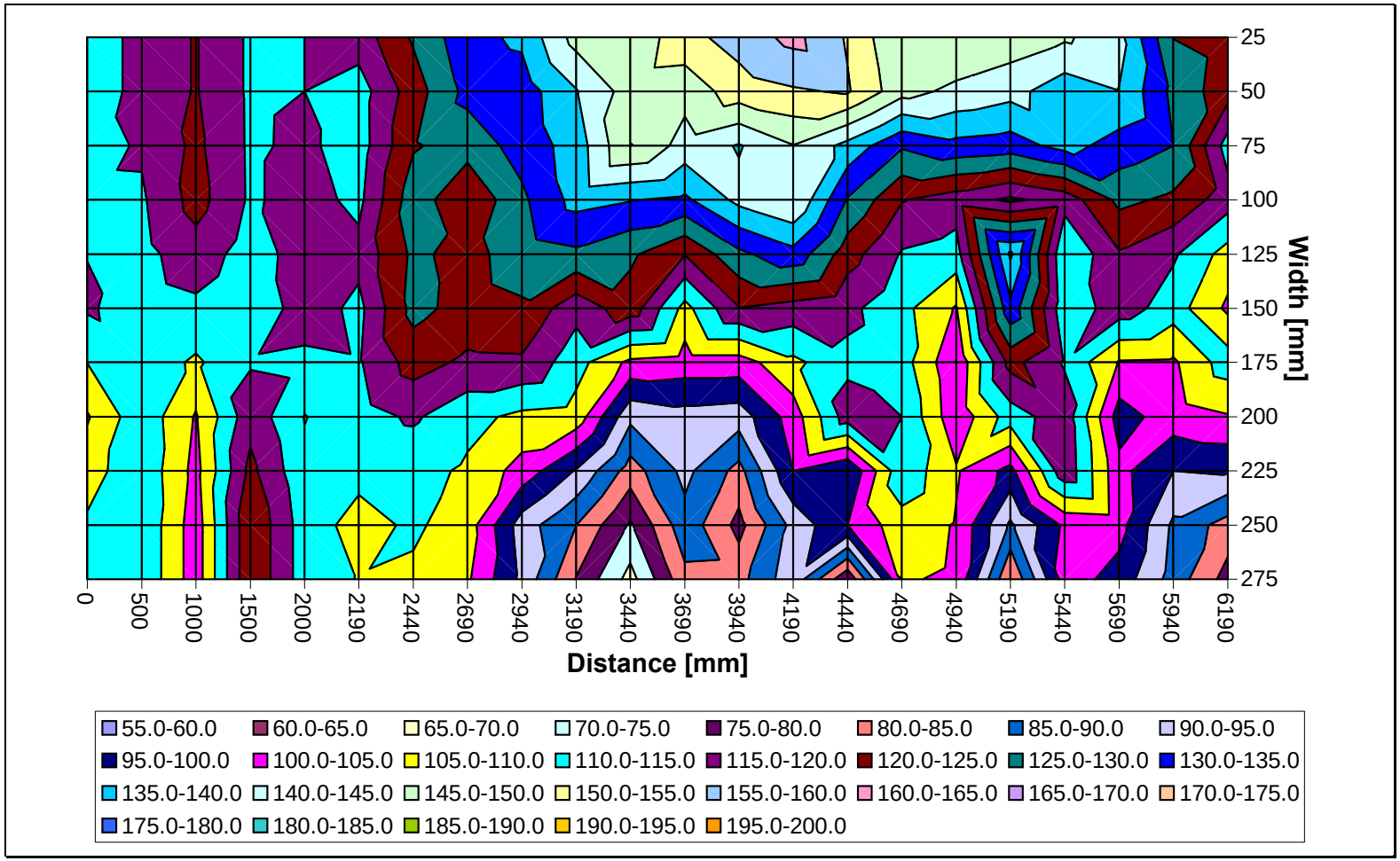

Figure 5-17: Typical observed scour pattern in straight and curved section for $r_c/w = 8.5$ and $F_r = 0.3$ measured from the bed [mm]

5.6.3 DEVELOPMENT OF SECONDARY FLOW

The recommendation by *Raudkivi (1993)* (see Figure 2-5), that the angle has to be greater than 30° for secondary flow to develop fully was applied to the data of the laboratory experiment carried out in the current research. With reference to Figure 5-18 the calculations were done as follows:

$$180^{\circ} = \theta_{\text{sec}} + \beta + \gamma$$

$$\gamma = 90° - \alpha$$

$$\alpha = \cos^{-1}\left(r_c / r_o\right)$$

$$\beta = \sin^{-1}\left(r_c / r_o\right)$$

where θ_{sec} = angle for fully developed secondary flow [°]

r_c = centerline radius [m]

r_o = outside radius [m]

therefore $180^{\circ} = \theta_{\text{sec}} + \beta + (90° - \alpha)$

and $90^{\circ} = \theta_{\text{sec}} + \beta - \alpha$

$$\theta_{\text{sec}} = 90^{\circ} - \beta + \alpha$$

thus,

$$\theta_{\text{sec}} = 90^{\circ} - \sin^{-1}\left(r_c / r_o\right) + \cos^{-1}\left(r_c / r_o\right) \quad \text{..... (5-10)}$$

The results are shown in Table 5-3 and it can be seen that the secondary flow was fully developed based on (*Raudkivi, 1993*) for the tests with a r_c/w of 8.5 and 11.8 and that the secondary flow was not fully developed for Test C with r_c/w = 15.2.

Evaluating equation 5-10 and solving r_c and r_o for θ = 30° resulted in the relationship of $r_c/r_o < 0.9659$ for the secondary flow to develop fully ($\theta_{sec} > 30°$). Expressing this

in terms of the centerline radius (r_c) and the width of the channel (w) yields, $r_c/w <$ 14.16 to ensure that $\theta > 30°$.

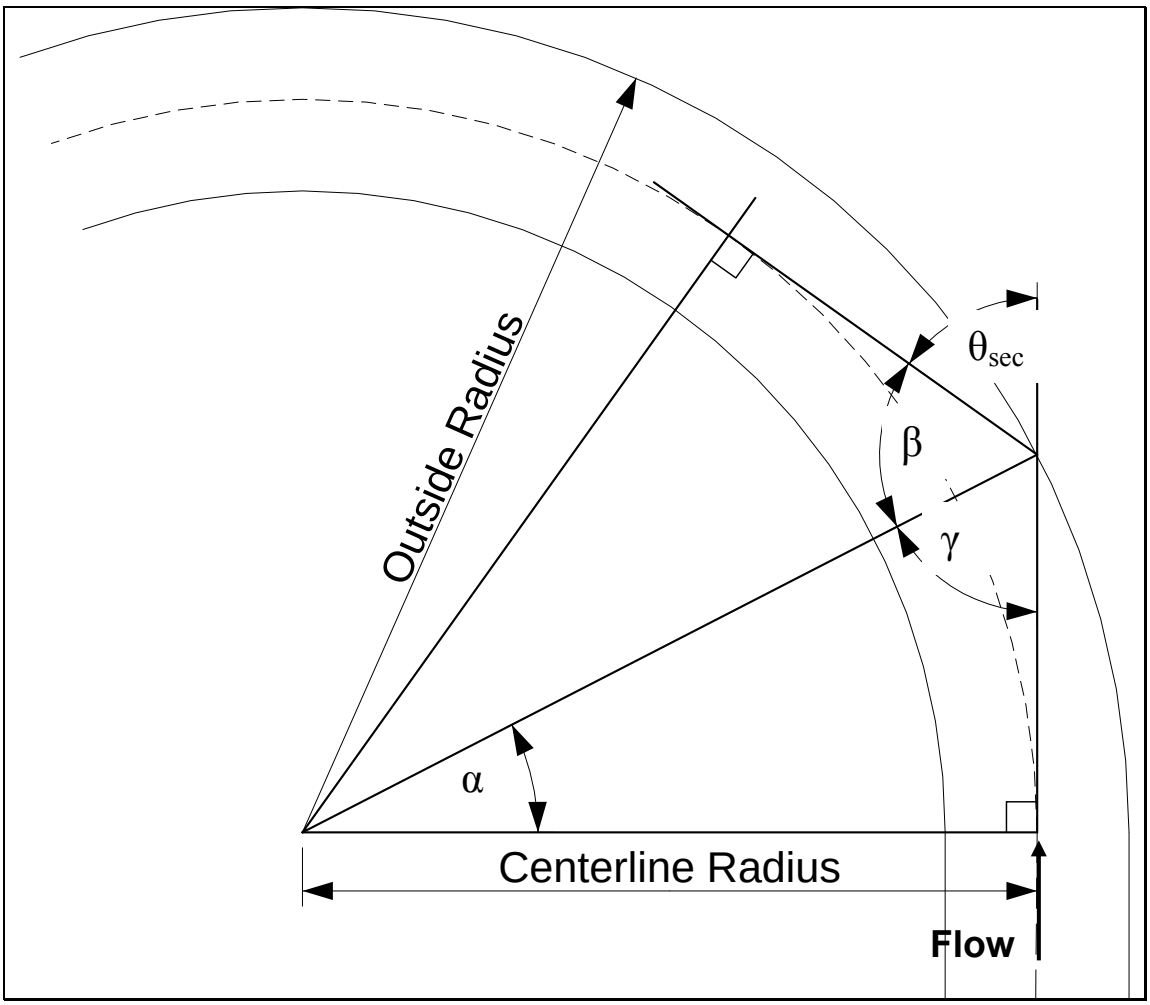

Figure 5-18: Calculations for fully developed secondary flow (Figure 2-5)

Test	r_c	W	r_c / w	θ_{sec} [°]
A	2.55	0.3	8.5	38.4
B	3.55	0.3	11.8	32.7
C	4.55	0.3	15.2	29

Table 5-3: Angle for fully developed secondary flow (Figure 5-18)

Equations 2-4 (*Mandouh and Townsend, 1979*) and 2-5 (*Rozovskii, 1963*) were applied to the data obtained from the current research and the results thereof are

shown in Figure 5-19. The Chezy coefficient (C) was calculated with $C = R^{\frac{1}{6}} / n$ *(Featherstone and Nalluri, 1995),* where R is the wetted perimeter and n is the Manning value of 0.013 (concrete with bends). The results obtained from the current research were also plotted on Figure 5-19 under the assumption that the secondary flow was fully developed at the location of the maximum measured velocity (Table 5-2).

From Figure 5-19 it is noted that equation 2-4 resulted in the angle where the secondary flow is fully developed being bigger than the central bend angle. The data of the current research takes the shape of equation 2-5, except for Test C with a central bend angle of 104° and r_c/w = 15.2.

Equation 2-5 was calibrated with the data of the current research and it was found that an average constant of 1.97 is generally in good agreement with the data range of this study except for Test C with a central bend angle of 104° which could possibly be ascribed to the fact that the secondary flow pattern has not developed fully for this case based on the equation 5-10 (*Raudkivi, 1993*).

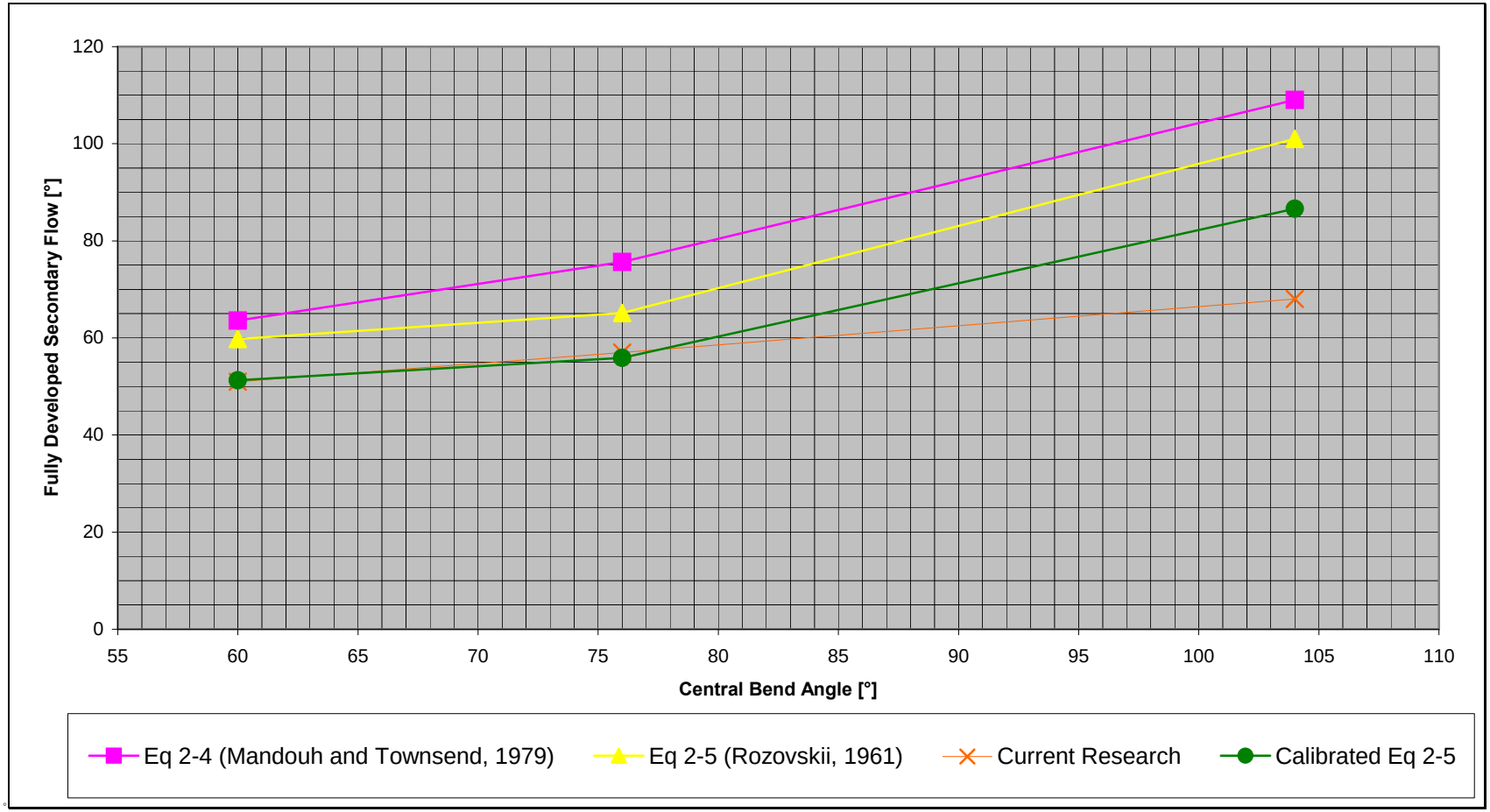

Figure 5-19: Central bend angle (θ_{sec}) needed for secondary flow to develop fully

5.6.4 DIVERSION LOCATION

In analysing the optimum diversion location, the diversion location predictors as recommended by *SC and CHES (1992)* (see Table 4-1), *SC and CHES (1992)* (see equation 4-1) and *Raudkivi (1993)* (see Figure 3-4) were applied to the data of the current research. The diversion location as were recommended by *SC and CHES (1992)* (Table 4-1) were found to be in very good agreement with the diversion location of the current research, while the diversion location from equation 4-1 and Figure 3-4 were not in good agreement. This is shown in Figure 5-20.

Raudkivi (1993) found that the diversion location is approximately twice the river width downstream of the intersection of the upstream axis with the outer bank (Figure 3-4). This location was calibrated on the data of the current research and it was found that the diversion location could be reasonably well-predicted with the distance being 8.8 times the width of the channel downstream of the intersection of the upstream axis with the outer bank (Figure 5-21). It is clear that the equation proposed by *Raudkivi (1993)* is not applicable to the hydraulic conditions of the tests of this research and it is not recommended that the new calibrated equation be applied for general use.

The equation by *SC and CHES (1992)* to determine the optimum diversion location (equation 4-1) was calibrated with the data of the current research. Replacing the constant of 0.8 in equation 4-1 with 1.71 resulted in a good fit to the data of the current research (Figure 5-21). As with *Raudkivi's* equation, the new calibrated equation varies too much from the original equation and is therefore not applicable to a wide range of conditions.

Evaluating the above-mentioned equations and the data of the current research in terms of the radius of curvature-to-width ratio (r_c/w) resulted in Figure 5-22. From this figure the diversion location can be found in terms of the radius of curvature-to-width ratio (r_c/w). A new equation was derived from the data of the current research to express the ratio of the diversion location and central bend angle ($\theta_{v,max}/\theta_{bend}$) as a

function of the radius of curvature-to-width ratio (r_c/w). Linear regression analysis on the data led to the following relationship (see Figure 5-22.):

$$\frac{\theta_{v,\max}}{\theta_{bend}} = 0.03\left(\frac{r_c}{w}\right) + 0.4 \quad \text{..... (5-11)}$$

where $\theta_{v,max}$ = location of maximum velocity [°]

θ_{bend} = central angle of bend [°]

r_c = average radius of curvature [m]

w = channel width [m]

In summary, the correlation with the observed data and empirical equations (except for Eq 5-11) is however not good and in general it is recommended that the methodology of Table 4-1 (*SC and CHES, 1992*) is used which was calibrated against a wide range of field conditions in China and shows good agreement with the research data of this thesis.

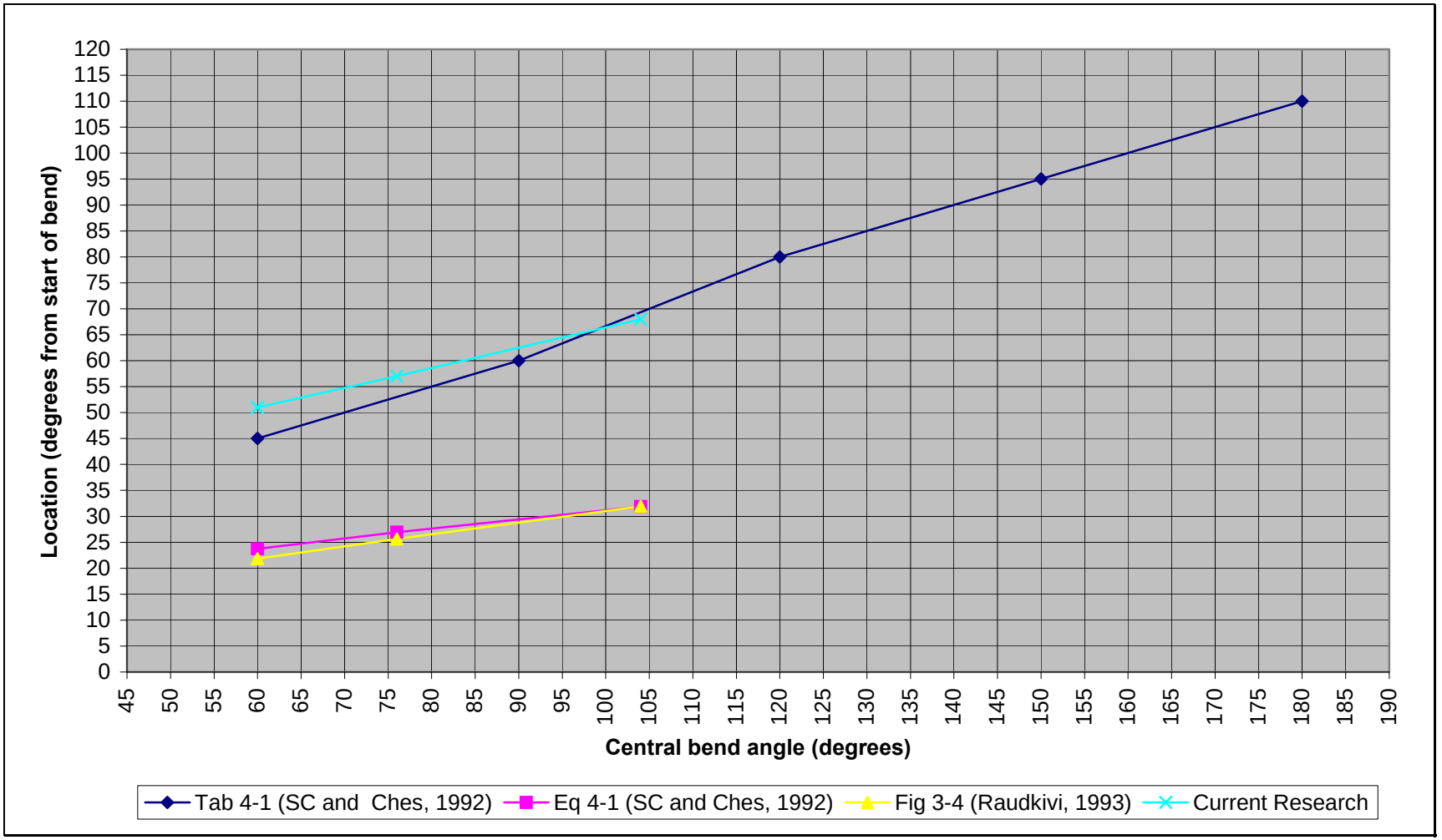

Figure 5-20: Diversion location in terms of the central bend angle

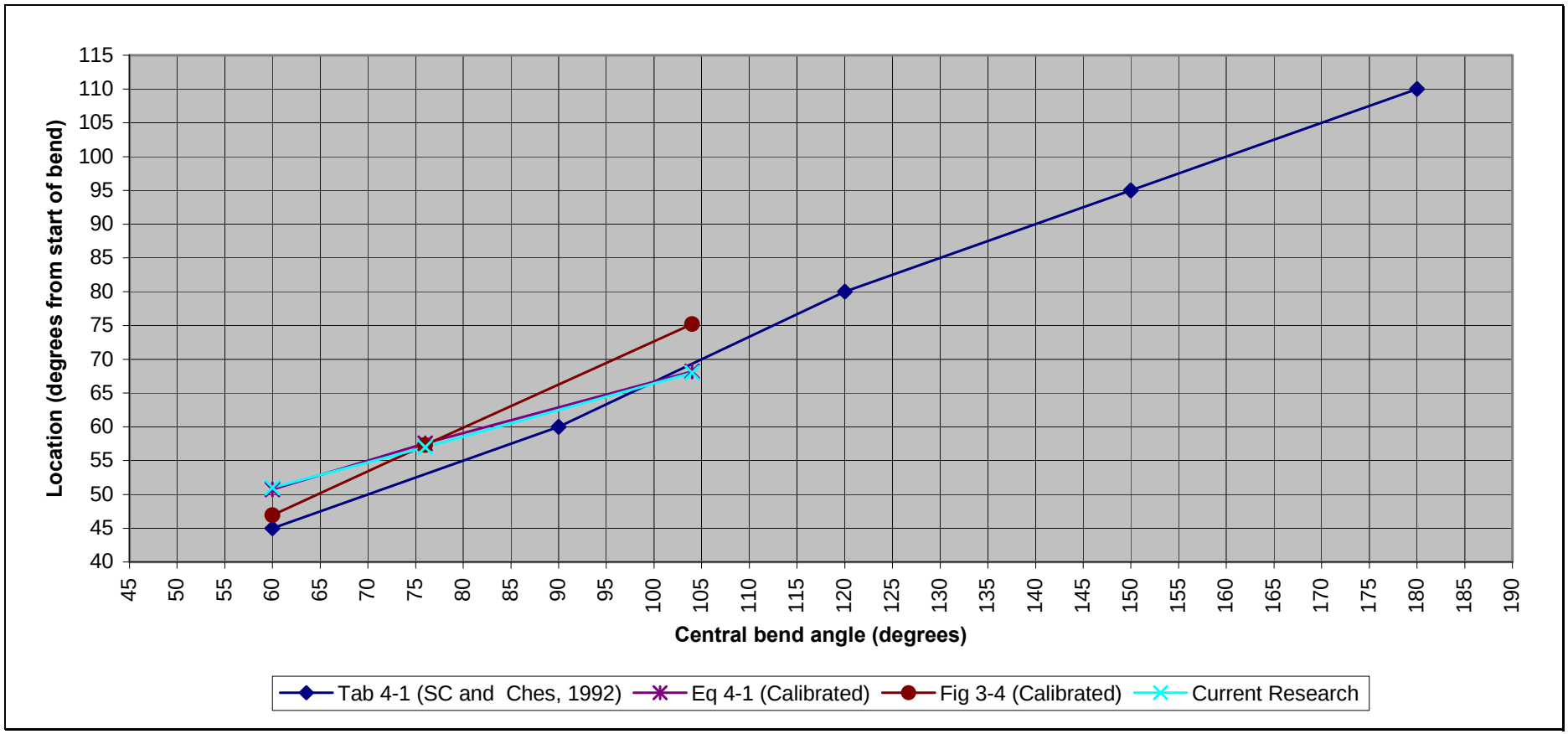

Figure 5-21: Calibrated diversion location in terms of the central bend angle

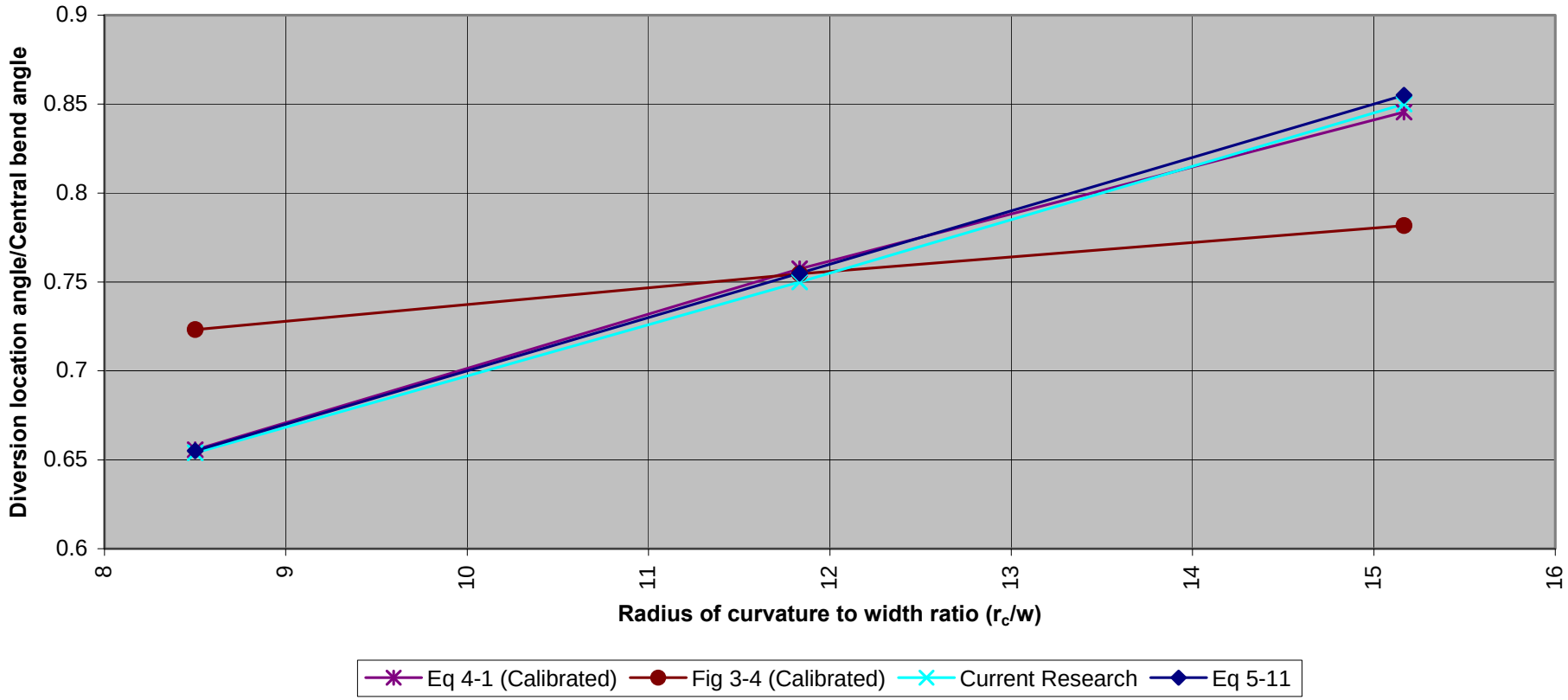

Figure 5-22: Diversion location in terms of the radius of curvature-to-width ratio (r_c/w)

5.6.5 SUMMARY

The position of the maximum velocity moves in the downstream direction with an increase in the radius of curvature (r_c) while the position is not much affected by varying Froude numbers for a specific radius (Table 5-1 and Table 5-2).

The observed scour patterns show the same tendency with varying radius of curvature-to-width ratio (r_c/w). Three main scour holes were identified with the location of the third scour hole being in good agreement with the location of the maximum velocity.

The maximum velocity zone was found near the outside of the bend exit with higher velocities on the outside of the bend than on the inside of the bend. The maximum velocity shifts downwards while moving towards the outside of the bend in the downstream direction. This confirms the presence of a clockwise spiral motion.

Evaluation of the development of secondary flow according to *Raudkivi (1993)* (Figure 2-5) leads to the relationship that r_c/w <14.6 for secondary flow to develop fully in the bend.

Equation 2-5 (*Rozovskii, 1961*) was calibrated with the data from the current research and it was found that the above-mentioned equation with a constant of 1.97 results in a good fit (Figure 5-19). This was done with the assumption that the secondary flow is fully developed where the maximum velocity was measured.

From Figure 5-20 it can be seen that the recommended diversion location (Table 4-1) by *SC and CHES (1992)* is in very good agreement with the diversion location found in the current research, and is the recommended approach to follow, covering a wide range of r_c/w and hydraulic conditions. A possible reason for this good agreement is that the L_{tot}/r_c range used in this research and in Table 4-1 is similar, with L_{tot}/r_c ranging from 1.1 to 1.9, a similar range as proposed by *Tan (1996)* as 1.1 to 1.4.

The recommended diversion location (Figure 3-4) by *Raudkivi (1993)* were calibrated on the laboratory data and it was found that the diversion location could be reasonable well-predicted with the distance being 8.8 times the width of the channel downstream of the intersection of the upstream axis with the outer bank (Figure 5-21). It is clear that the empirical relationship proposed by *Raudkivi (1993)* is only applicable to a certain range of hydraulic conditions and is therefore not generally applicable.

Equation 4-1 by *SC and CHES (1992)* to determine the optimum diversion location was calibrated with the data of the current research and by replacing the constant of 0.8 with 1.71, resulted in a good fit with the data from the current research (Figure 5-21).

Figure 5-22 shows the angle of the diversion location as a function of the central bend angle and the radius of curvature-to-width ratio (r_c/w).

6 LABORATORY TESTS AND ANALYSIS ON DIVERSION ANGLE

6.1 EXPERIMENTAL SET-UP

Three diversion angles were studied, i.e. diversion angles (θ) of 20°, 35° and 50° which are in good agreement with the recommended range of diversion angles found in the literature (Figure 6-1). The diversion angle (θ) is zero on the centreline in the channel direction, looking downstream, as shown in Figure 6-2.

The basic experimental set-up of Test A with r_c = 2.55 *m* as described in Section 5 was used for all the tests on the optimum diversion angle. The diversion channel was installed at 3.69 m from the beginning of the bend on the outside of the bend that coincides with the location of the maximum velocity zone (see Table 5-1). The diversion channel was 1.5 m in length and the width varied according to the diversion angle. The width at the entrance of the diversion channel was 150 mm measured on the tangent.

A second V-notch was erected at the downstream end of the main channel in order to be able to calculate the discharge through the diversion channel. The plan layout of the model is presented in Figure 6-2 and a photo of the diversion channel is shown in Figure 6-3.

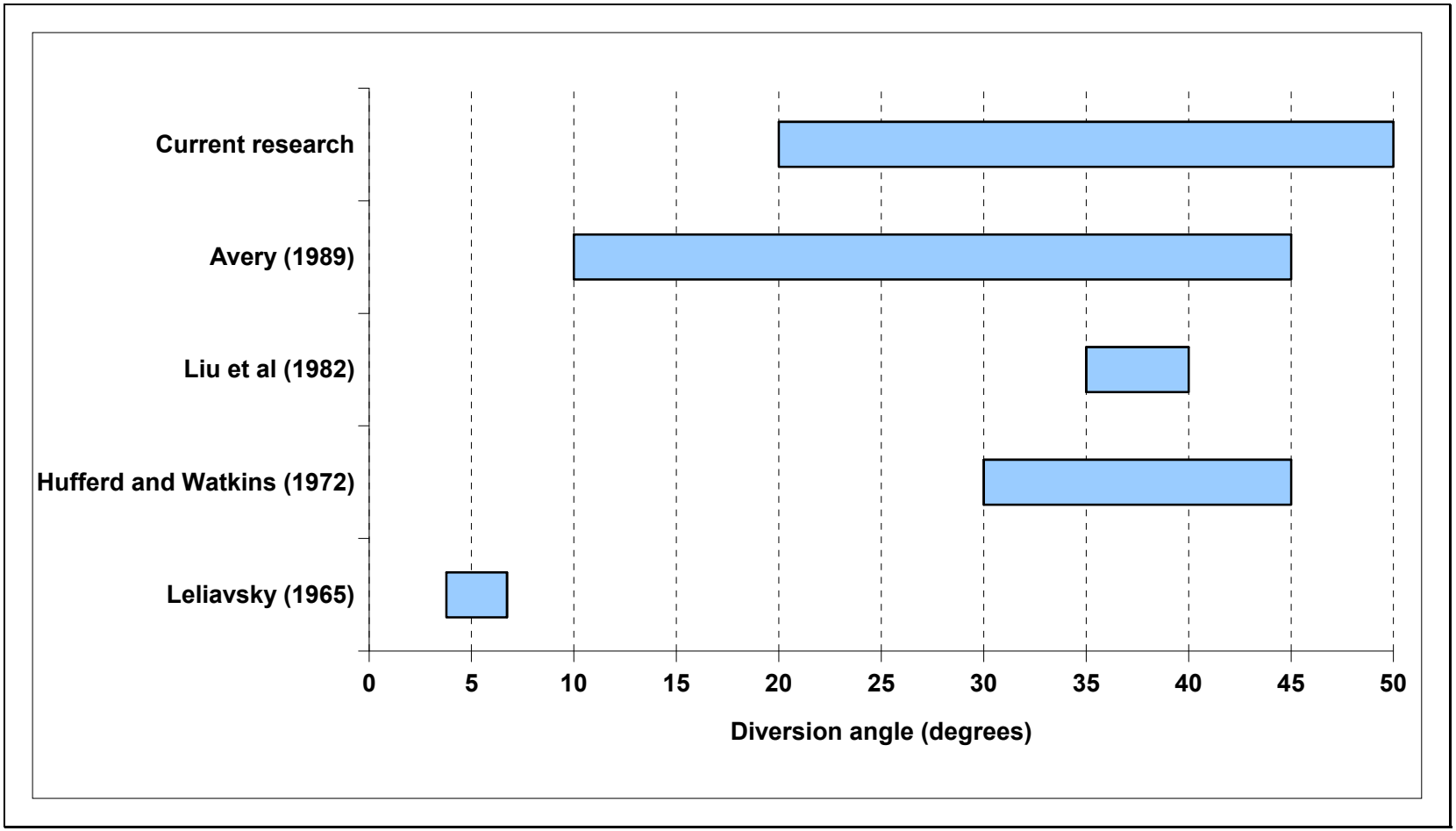

Figure 6-1: Summary of diversion angles in literature

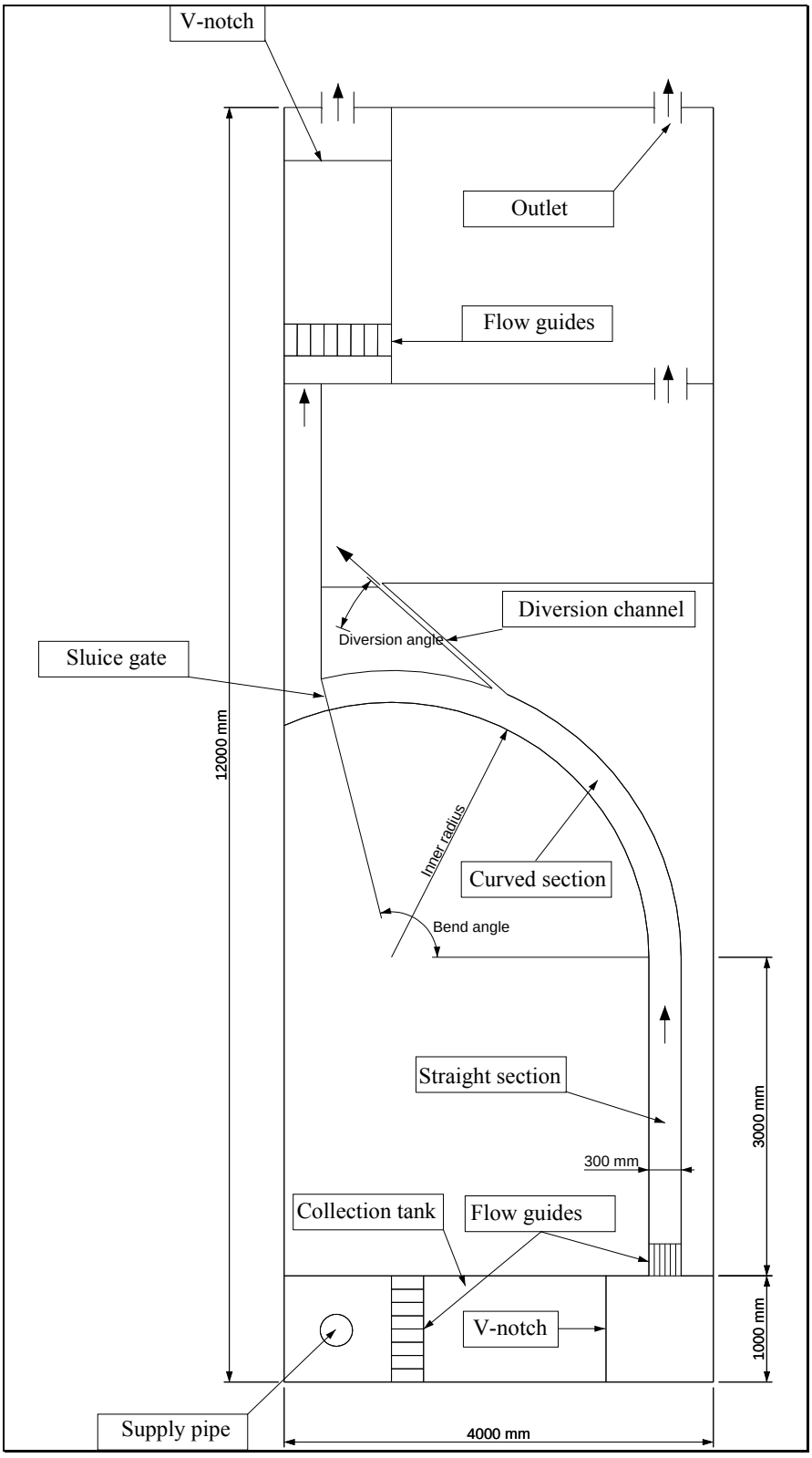

Figure 6-2: Plan layout of model for determining the optimum diversion angle (not to scale)

Figure 6-3: Photo of the diversion channel

6.2 TEST PROCEDURE

Point velocities were measured in the curved section at 13 cross-sections perpendicular to the direction of flow. The cross-sections were located at 500 mm intervals from 2.19 m to 4.19 m and then at 250 mm intervals from 4.44 m to 6.19 m. Across the width of the channel, velocities were measured at 50 mm, 100 mm, 150 mm, 200 mm and 250 mm from the inside of the bend and in the vertical plane velocities were measured at 30 mm, 50 mm and 70 mm from the bed of the model. Thus, a total of 195 point-velocities were measured during each test. Figure 6-4 shows the plan layout where measurements were taken.

For each diversion angle four scenarios were studied. For the first three scenarios the sluice gate at the downstream end of the diversion channel was completely opened to allow the maximum diversion of water. For the fourth scenario the sluice gate was closed to ensure that no water was diverted. This was done to simulate a scenario

where for example the pumps in a diversion channel were shut down and no water was abstracted from the main channel. The four scenarios tested were for Froude numbers *(F_r)* of 0.3, 0.5 and 0.7, in the main channel upstream of the diversion, with maximum diversion and $F_r = 0.3$ with no abstraction from the main channel.

The test description is the same as in Section 5-5 with the addition of measuring the discharge at the second V-notch to determine the diverted discharge.

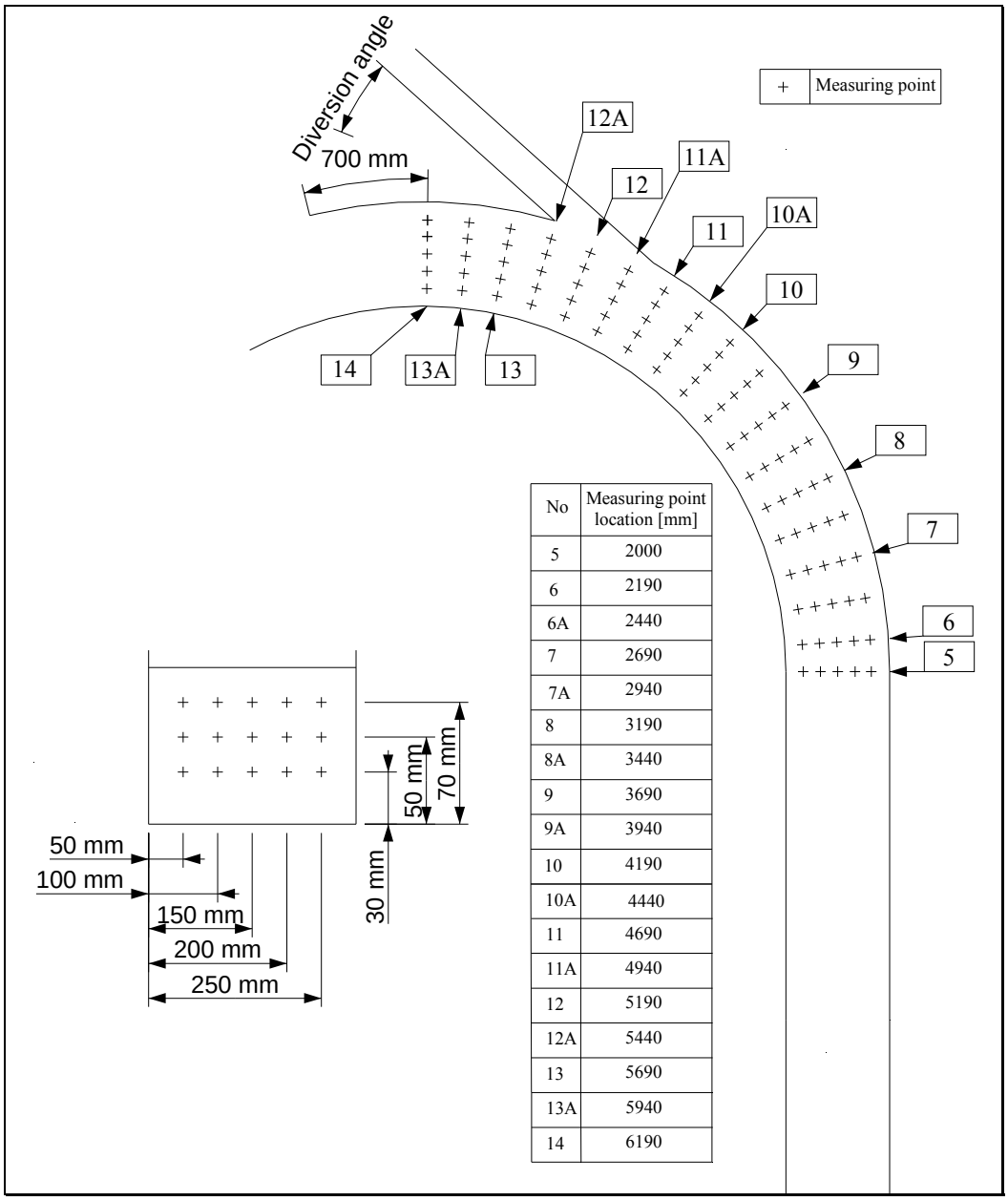

No	Measuring point location [mm]
5	2000
6	2190
6A	2440
7	2690
7A	2940
8	3190
8A	3440
9	3690
9A	3940
10	4190
10A	4440
11	4690
11A	4940
12	5190
12A	5440
13	5690
13A	5940
14	6190

Figure 6-4: Velocity measurement positions for diversion angle related tests (not to scale)

6.3 TEST D (Θ = 20˚)

The diversion location was installed at 3.69 m from the beginning of the bend.

6.3.1 TEST D1 (F_R = 0.3)

The total discharge during the test was 10.35 l/s with an average water level of 110.3 mm. A maximum velocity of 0.39 m/s was measured at 5.69 m on the outside of the bend. The diverted discharge was 3.97 l/s with a diverted discharge ratio (DDR) of 38.4 %.

The velocity distribution in the horizontal plane measured at 70 mm, 50 mm and 30 mm is presented in Appendix B: Figure B-1. It is interesting to note that the path of maximum velocity shifts from being near the inside of the bend between 2.19 m and 3.69 m to the outside of the bend downstream of 3.69 m up to 5.69 m where the maximum velocity is obtained.

When studying the velocity distribution in the vertical plane (see Appendix B: Figure B-2) it is clear that the path dives towards the bottom of the model bed while it moves towards the outside of the bend (see Appendix B: Figure B-3) where the diversion channel is situated.

The velocity distribution is presented as a line graph in Figures B-4 to B-8 (see Appendix B) with the location of the turning points in Figure E-2 (see Appendix E).

6.3.2 TEST D2 (F_R = 0.5)

The test was carried out with an average water level of 125 mm and a total discharge of 15.53 l/s. A DDR of 31.2 % was obtained with the diverted discharge being 4.85 l/s.

The path of maximum velocity shifts from near the inside of the bend up to 3.19 m to the outside of the bend in the horizontal plane where it remains up to 5.69 m where

the maximum velocity of 0.53 m/s was measured. In the vertical plane it moves downwards in the downstream direction (see Appendix B: Figures B-9 to B-16). The location of the turning points is presented in Figure E-3 (see Appendix E).

6.3.3 TEST D3 (F_R = 0.7)

A DDR of 32.1 % was obtained with the diverted discharge calculated at 6.86 l/s. The average water level during the test was 170.9 mm while the total discharge was 21.36 l/s.

The velocity distribution is presented as a line graph in Figures B-20 to B-24 (see Appendix B) with the location of the turning points in Figure E-4 (see Appendix E).

Once again the maximum velocity followed the same path as for the scenarios of F_r = 0.3 and 0.5, i.e shifting from near the inside of the bend towards the outside while diving towards the bottom in the downstream direction (see Appendix B: Figures B-17 to B-19).

6.4 TEST E (Θ = 35˚)

The diversion location was installed at 3.69 m from the beginning of the bend.

6.4.1 TEST E1 (F_R = 0.3)

The diverted discharge of 4.7 l/s was measured with a DDR of 46.8 %. The total discharge during the test was 10.04 l/s with an average water level of 108.5 mm and a maximum velocity of 0.42 m/s.

The path of maximum velocity moved on the inside of the bend up to 3.69 m where it shifted towards the outside of the bend at 4.19 m. It remained on the outside of the bend up to 5.69 m where the maximum velocity was measured. In the vertical plane the maximum velocity moved gradually towards the bottom of the bed in the downstream direction (see Appendix B: Figures B-25 to B-27).

The velocity distribution is presented as a line graph in Figures B-28 to B-32 (see Appendix B) with the location of the turning points in Figure E-6 (see Appendix E).

6.4.2 TEST E2 (F_R = 0.5)

The total discharge during the test was 14.9 l/s with a diverted discharge of 5.3 l/s, thus resulting in a DDR of 35.6 %. The average water level was 123.1 mm. The velocity distribution in the horizontal and vertical plane as well as the cross-sectional velocity distribution are presented in Appendix B: Figures B-33 to B-35. In this case a more uniform distribution across the width of the channel was obtained up to 3.19 m where the maximum velocity shifted towards the outside of the bend at 3.69 m. The maximum velocity moved downward in the downstream direction until the diversion channel is reached where the maximum velocity of 0.45 m/s was measured.

The velocity distribution is presented as a line graph in Figures B-36 to B-40 (see Appendix B) with the location of the turning points in Figure E-7 (see Appendix E).

6.4.3 TEST E3 (F_R = 0.7)

A DDR of 33.9 % was calculated with the diverted discharge of 7.49 l/s that was obtained while the total discharge was 22.08 l/s. The average water level during the test was 134.5 mm.

Between 2.19 m and 2.69 m higher velocities were measured on the inside of the bend than on the outside. The maximum velocity then shifted towards the outside of the bend at 3.69 m where it remained until the location of the diversion channel was reached at 5.69 m. The maximum velocity of 0.7 m/s was measured at this point. From the vertical velocity distribution it is noted that the maximum velocity shifted downward to the outside of the bend in the downstream direction (see Appendix B: Figures B-41 to B-48). The location of the turning points is presented in Figure E-8 (see Appendix E).

6.4.4 TEST E4 (F_R = 0.3, DDR = 0)

The average water level during the test was 113.5 mm while the discharge was 9.6 l/s. The velocity distribution is presented as a line graph in Figures B-52 to B-56 (see Appendix B).

The path of the maximum velocity in the horizontal plane can be described with reference to Figure B-49 (see Appendix B). The maximum velocity moves from being near the inside of the bend up to 3.69 m towards the outside of the bend at 4.94 m. The maximum velocity of 0.34 m/s. was measured at 5.94 m near the outside of the bend. Figures B-50 and B-51 (see Appendix B) represent the velocity distribution in the vertical plane. From these figures it is noted that the maximum velocity moves down towards the outside of the bend in the downstream direction.

6.5 TEST F (Θ = 50˚)

The diversion location was installed at 3.69 m from the beginning of the bend.

6.5.1 TEST F1 (F_R = 0.3)

With reference to Figures B-57 to B-59 (see Appendix B), the path of the maximum velocity can be described as follows:

In the horizontal plane the maximum velocity is near the inside of the bend between 2.19 m and 3.96 m where it then shifts towards the outside of the bend up to 4.96 m. Further downstream it remains on the outside of the bend until 5.69 m where the diversion channel is positioned. The maximum velocity of 0.45 m/s was measured at this location.

In the vertical plane the maximum velocity moves downward and to the outside of the bend in the downstream direction.

The average water level during the test was 111.2 mm with a total discharge of 11.04 l/s. The diverted flow was 5.25 l/s, representing a DDR of 47.6 %. The velocity distribution is presented as a line graph in Figures B-60 to B-64 (see Appendix B) with the location of the turning points in Figure E-10 (see Appendix E).

6.5.2 TEST F2 (F_R = 0.5)

A DDR of 40.6 % was obtained with the total discharge of 15.7 l/s and the diverted discharge of 6.37 l/s. The average water level during the test was 123.4 mm.

The maximum velocity follows the outside of the bend throughout the bend although there is a zone of high velocities near the inside of the bend between 2.19 m and 2.69 m. The maximum velocity of 0.56 m/s was measured at the diversion location of 5.69 m (see Appendix B: Figures B-65 to B-67).

The velocity distribution is presented as a line graph in Figures B-68 to B-72 (see Appendix B) with the location of the turning points in Figure E-11 (see Appendix E).

6.5.3 TEST F3 (F_R = 0.7)

The average water level during the test was 124.5 mm with a total discharge of 21.6 l/s. A DDR of 34.4 % was obtained with the diverted discharge being 7.44 l/s. The velocity distribution is presented as a line graph in Figures B-76 to B-80 (see Appendix B) with the location of the turning points in Figure E-12 (see Appendix E).

The path of the maximum velocity in the horizontal plane can be described with reference to Figure B-73 (see Appendix B). The maximum velocity is on the inside of the bend up to 3.19 m where it shifts outwards to the outside of the bend at 4.19 m. The maximum velocity remains on the outside until the diversion point is reached at 5.69 m where the maximum velocity of 0.74 m/s was measured.

In the vertical plane the maximum velocity gradually moves downward in the downstream direction up to the diversion location (see Appendix B: Figures B-74 and B-75).

6.5.4 TEST F4 (F_R = 0.3; DDR = 0)

The total discharge during the test was 9.6 l/s with an average water level of 115.8 mm.

In the horizontal plane the maximum velocity moves along the inside of the bend until 3.19 m where it steadily shifts towards the outside of the bend. From 4.94 m it remains on the outside of the bend up to the diversion location at 5.69 m. The maximum velocity of 0.32 m/s was measured at 6.19 m.

In the vertical plane the maximum velocity dives to the bottom while shifting towards the outside of the bend in the downstream direction (see Appendix B: Figures B-81 to B-88).

6.6 ANALYSIS OF TESTS ON DIVERSION ANGLE

In general the velocity distributions obtained form the laboratory experiments shows the same tendency. The maximum measured velocity during the series of test was located at the point of diversion. In the horizontal plane the maximum velocity is near the inside of the bend up to 3.19 m. It then shifts towards the outside of the bend and at approximately 3.69 m it reaches the outside of the bend where it remains up the point of diversion at 5.69 m (3.69 m from the beginning of the bend). A typical observed velocity distribution is presented in Figure 6-5.

From the vertical velocity distribution it is noted that the path of the maximum velocity dives towards the bottom in the downstream direction while moving towards the outside of the bend. A typical velocity distribution in the vertical is presented in Figure 6-6 and the cross-sectional distribution in Figure 6-7.

Presenting the vertical velocity distribution as a line graph, the following tendencies are observed in the downstream direction (see Figure 6-8 to Figure 6-10):

- The velocity measured at 70 mm from the bottom (*V70*) decreases near the inside of the bend.
- All the measured velocities (*V70*, *V50* and *V30*) increase at the centre of the bend.
- All the measured velocities (*V70*, *V50* and *V30*) increase near the outside of the bend with a sharp increase at the diversion location followed by a sharp decrease immediately downstream of the diversion.

The typical tendency of the location of the turning points, i.e where *V30>V50*, *V30>V70* and *V50>V70,* is reflected in Figure 6-11.

In analysing the location of the turning points where *V30>V50*, *V30>V70* and *V50>V70* the following conclusions can be made (see Appendix E: Figures E-1, E-5 and E-9):

- The location of the turning points where *V30>V50*, *V30>V70* and *V50>V70* stays relatively constant near the inside of the bend but at the outside of bend it moves in the downstream direction with an increase in Froude number.
- The range of the location of the turning points near the inside of the bend increases with an increase in the diversion angle.
- The range of the location of the turning points at the near outside of the bend decreases with an increase in the diversion angle.
- The location of the turning points for *V30>V50*, *V30>V70* and *V50>V70* was always upstream of the diversion location of 5.69 m.

The velocity distributions of Test E4 and Test F4 (DDR=0) and those with a DDR>0 is essentially the same. The only difference is that there exists a small area with lower velocities around the point of diversion for the tests with DDR=0 than for the tests with DDR>0.

Base on the above-mentioned results no real conclusion can be made regarding the optimum diversion angle. This is due to the fact that the results obtained from the three diversion angles that were analysed is essentially the same. It is well-evident that the diverted discharge ratio (DDR) increases with an increase in the diversion angle while it decreases with an increase in Froude number. The velocity distribution obtained with a Froude number of 0.3 and 0.5 is also more favourable than those obtained with a Froude number of 0.1 since the bend effect is more prominent. An important conclusion from the tests is that the diversion does not influence the secondary flow patterns (for the range of DDR's tested) and that the maximum velocity zone stayed in the same location as in the tests without a diversion.

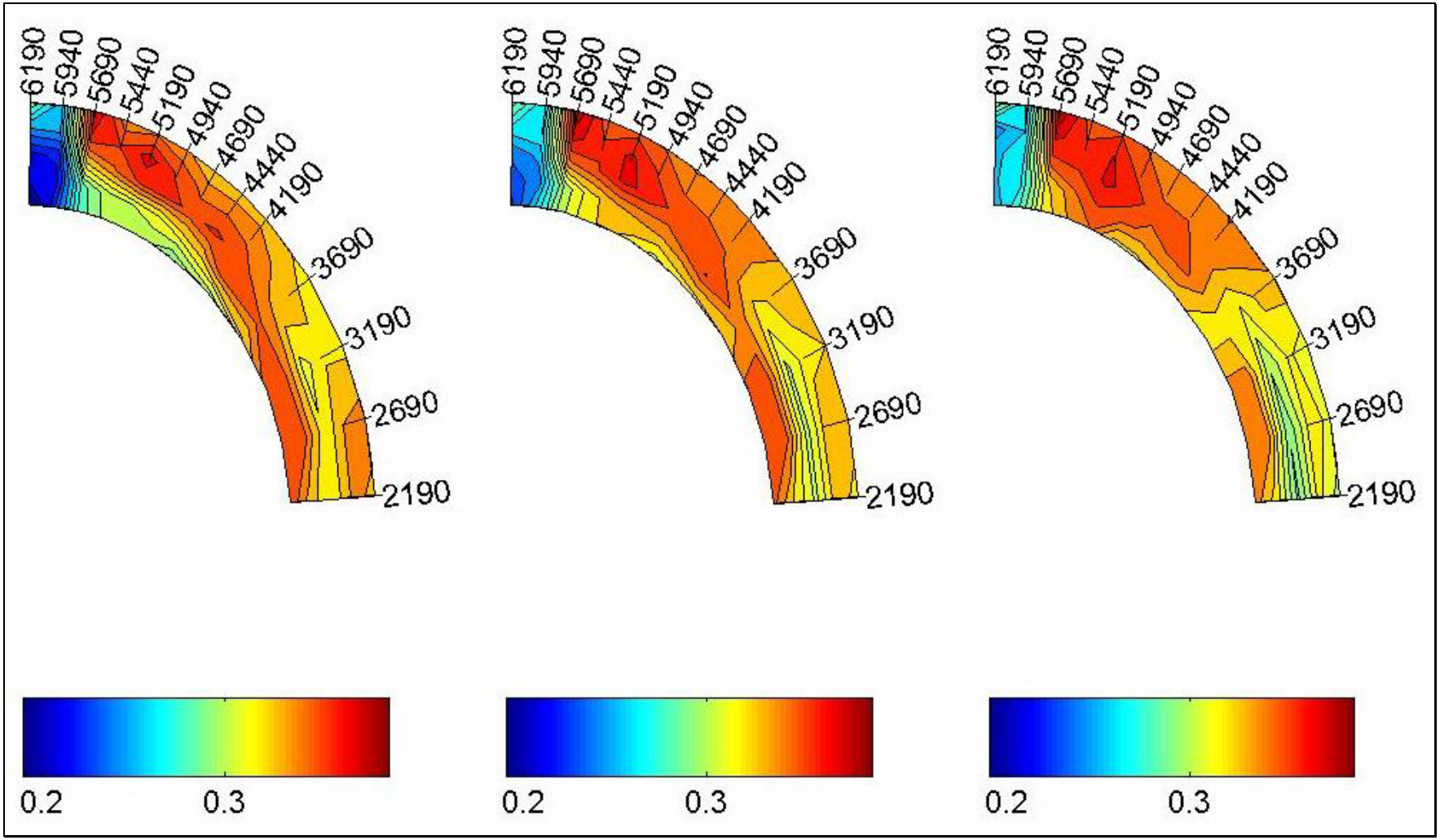

Figure 6-5: Typical velocity distribution in the horizontal plane measured at 70, 50 and 30 mm above the bed [m/s]

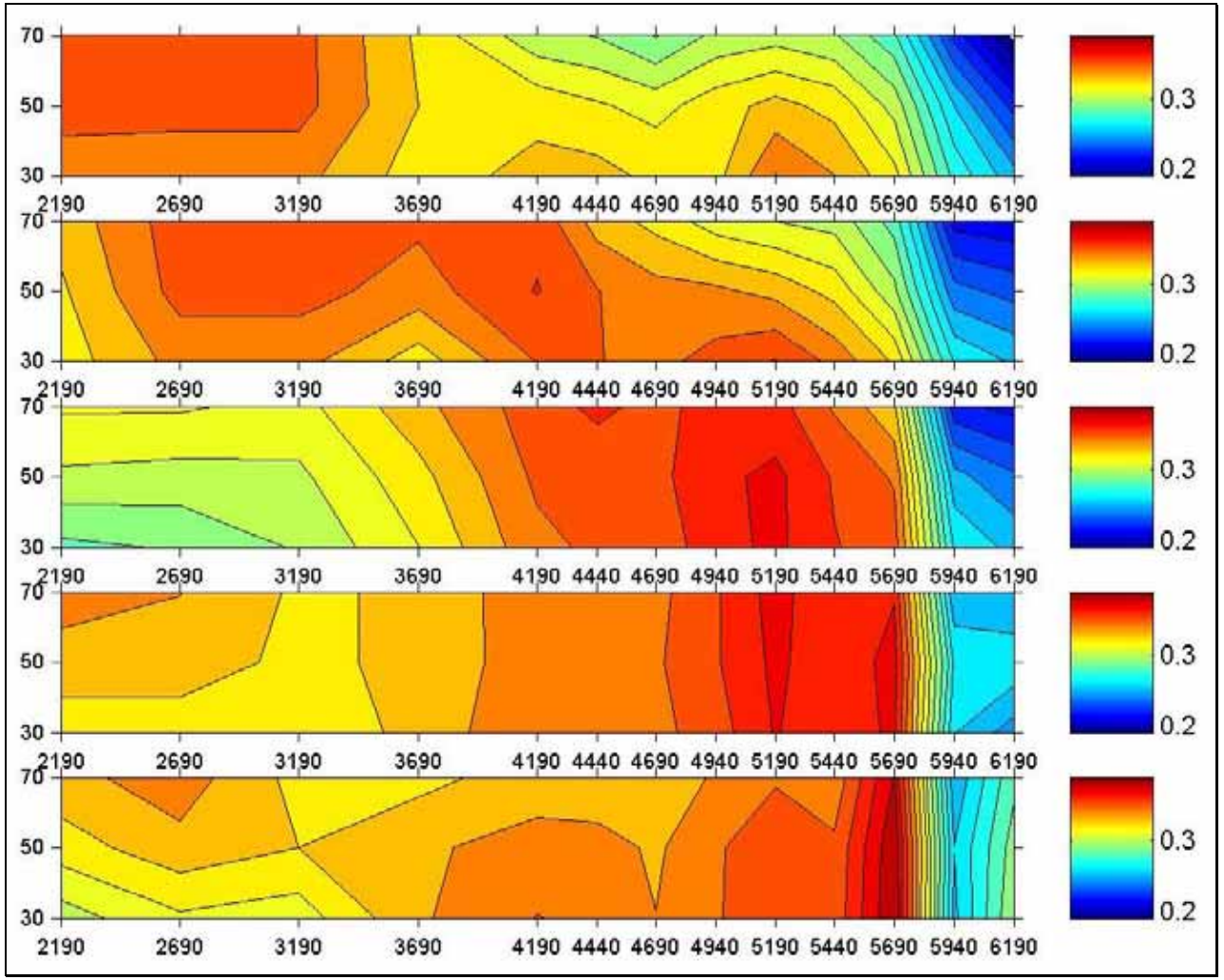

Figure 6-6: Typical velocity distribution in the vertical plane [m/s]

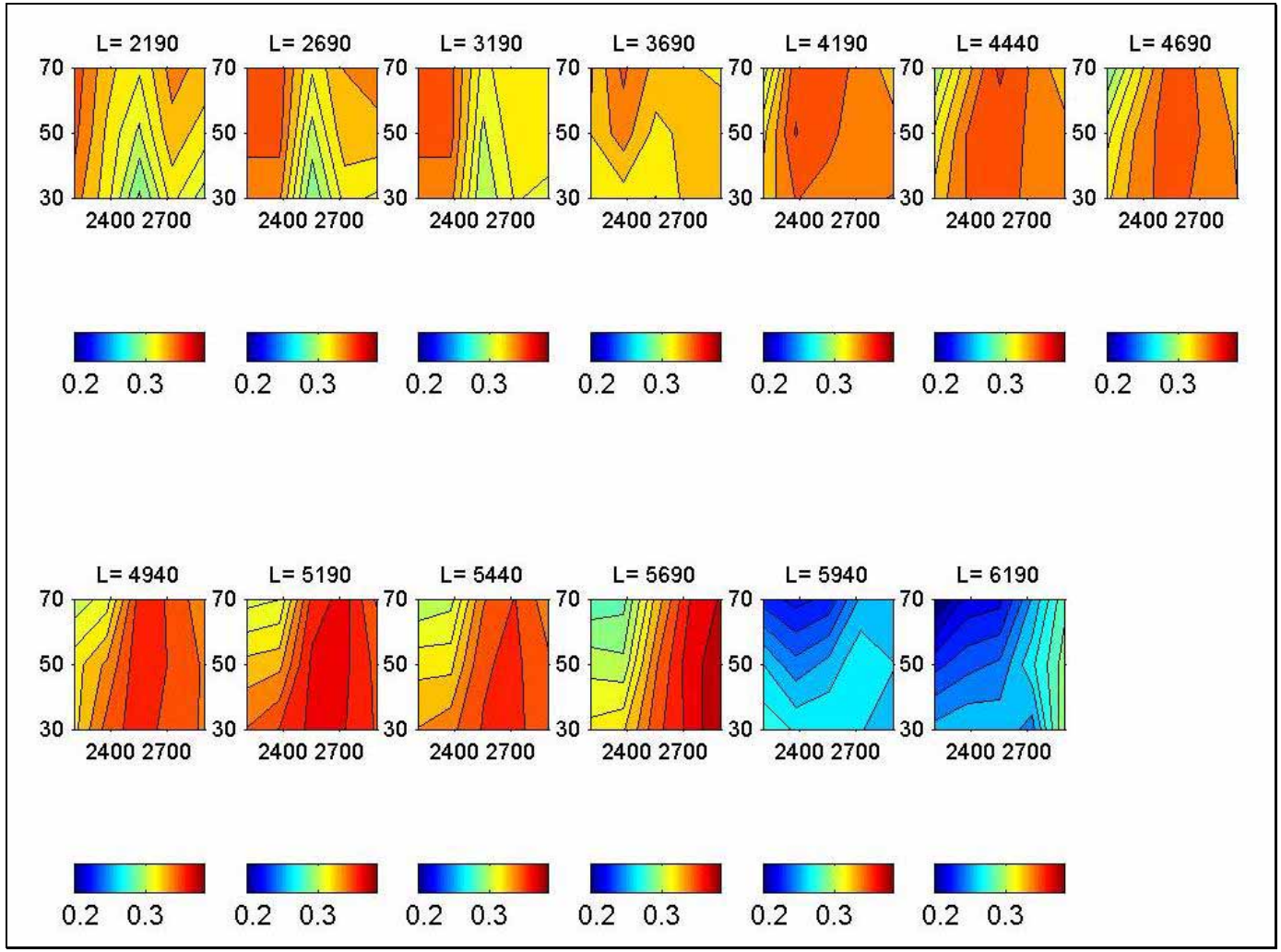

Figure 6-7: Typical cross-sectional velocity distribution [m/s]

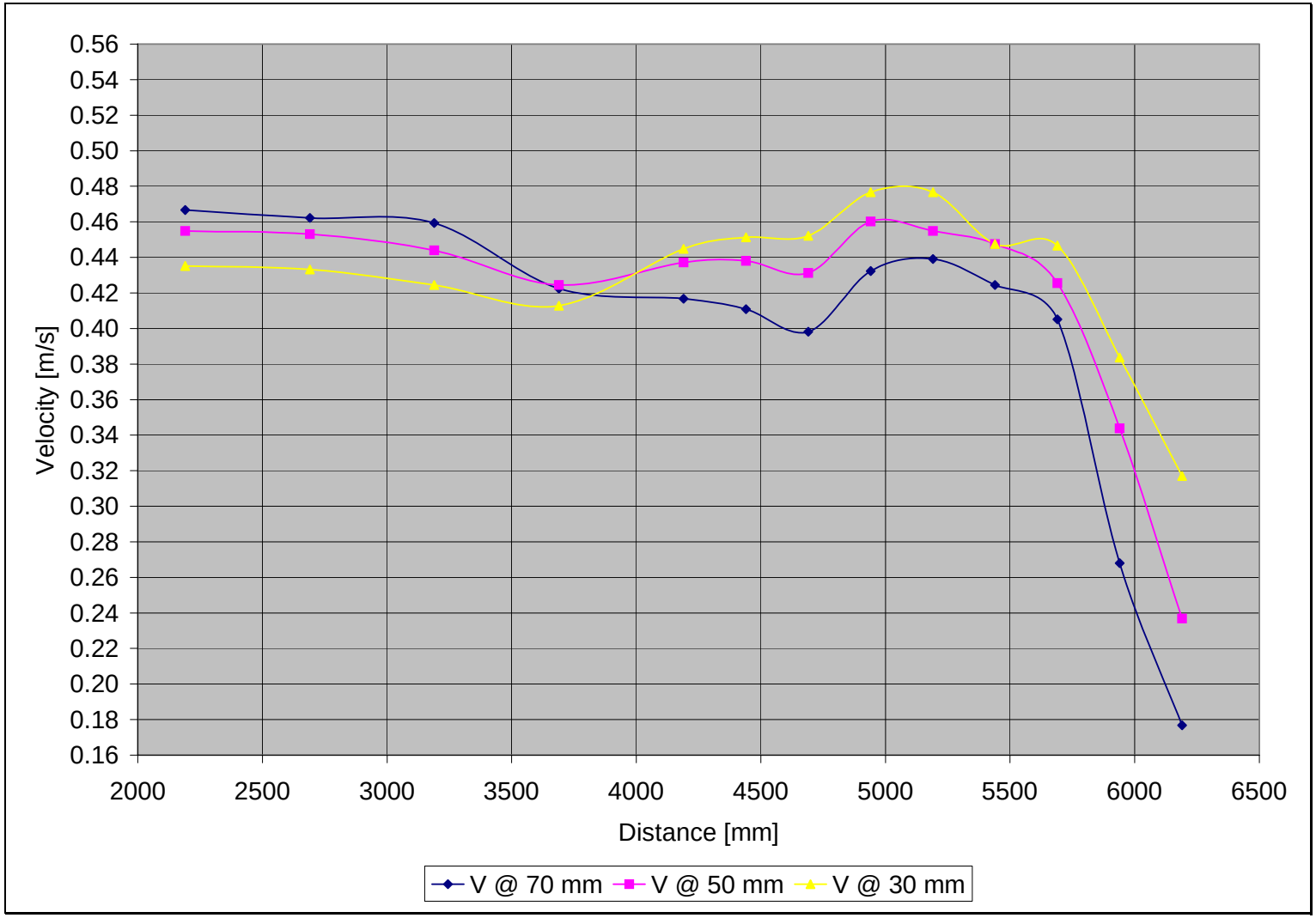

Figure 6-8: Decreasing tendency of *V70* near the inside of the bend with $r_c/w = 8.5$, $F_r = 0.3$ and $\theta = 50°$

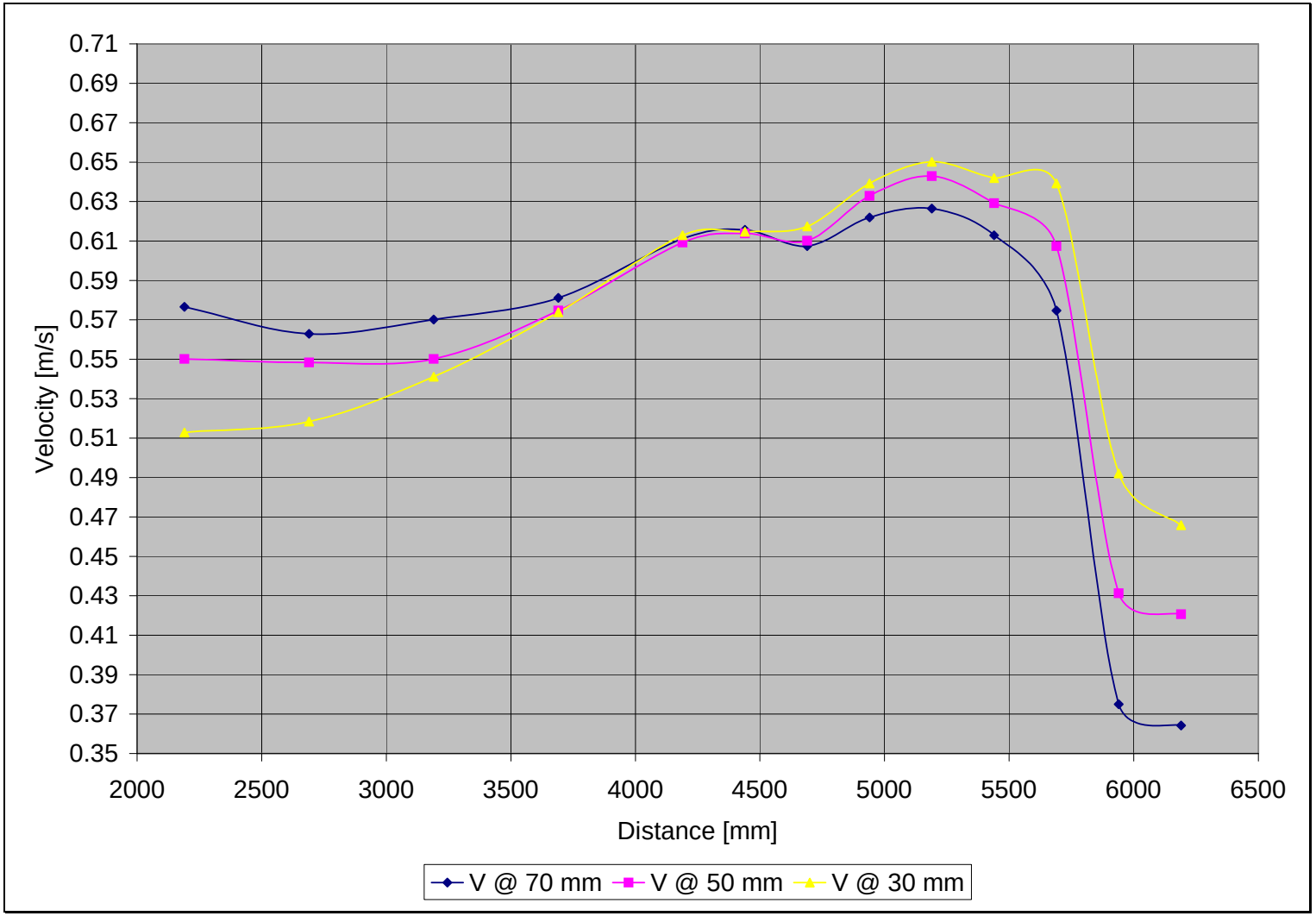

Figure 6-9: Increasing tendency of *V30, V50 and V70* at the centre of the bend with $r_c/w = 8.5$, $F_r = 0.5$ and $\theta = 35°$

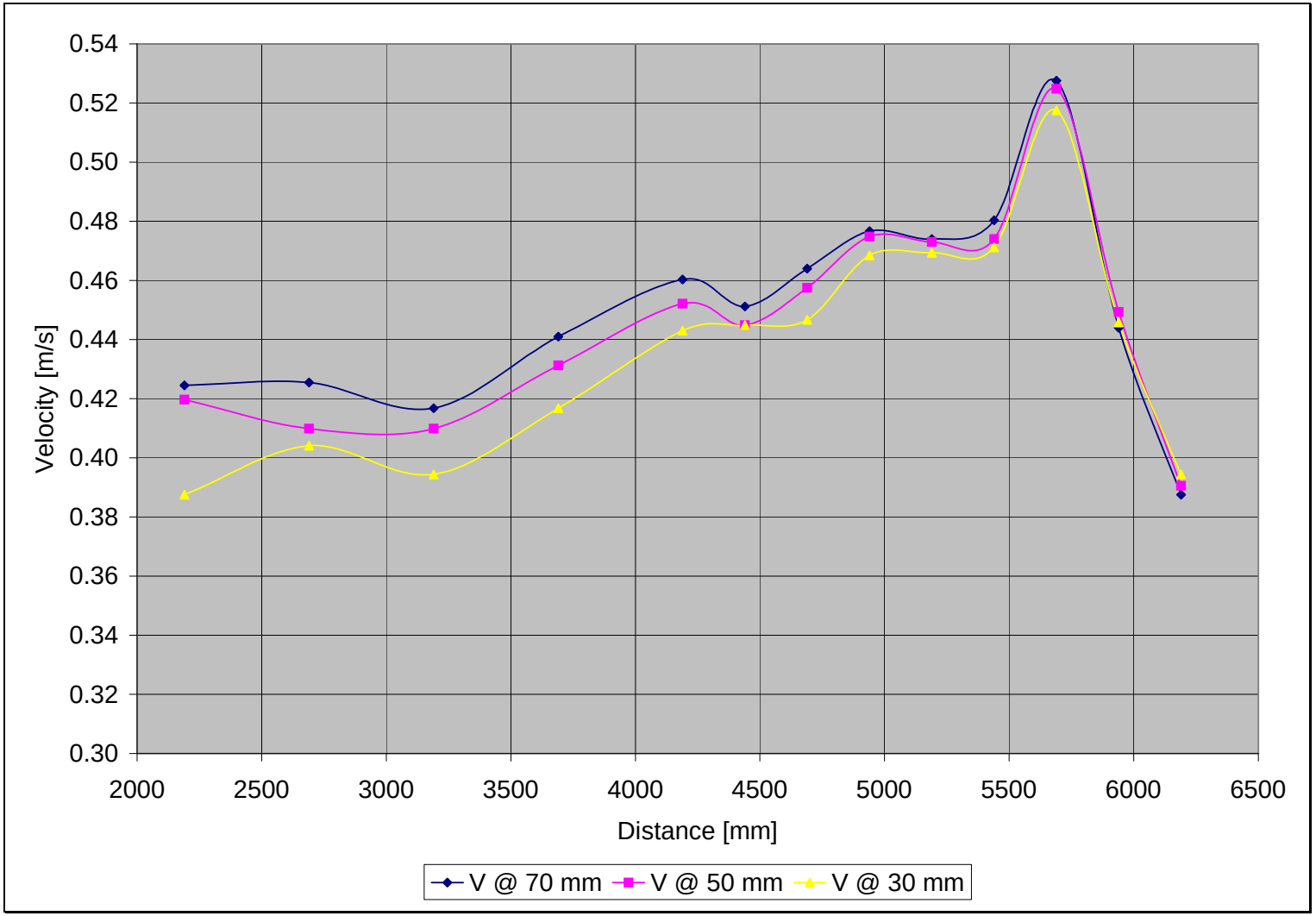

Figure 6-10: Increasing tendency of *V30, V50 and V70* near the outside of the bend with $r_c/w = 8.5$, $F_r = 0.7$ and $\theta = 20°$

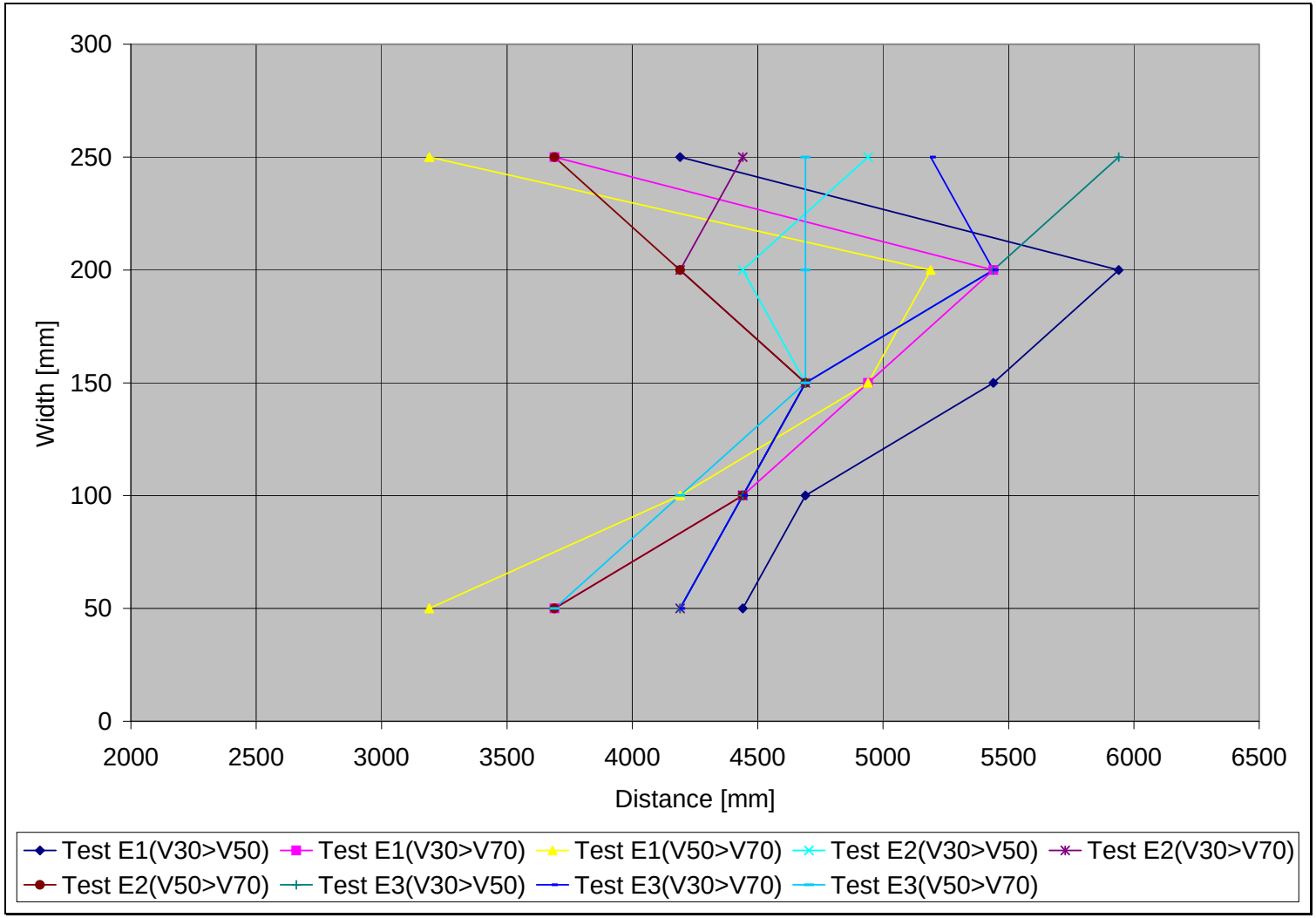

Figure 6-11: Location of turning points for *V30>V50*, *V30>V70* and *V50>V70*

7 MATHEMATICAL MODELLING

7.1 INTRODUCTION

The hydrodynamic programme DELFT 3D was used to simulate the hydrodynamics of the laboratory experiments for the case where $r_c = 2.55\ m$ (Test A). The aim of the simulation was to establish whether the programme could be used to simulate the laboratory experiments and secondary flow patterns with reliability.

The software Mike 21C was used to simulate the sediment dynamics of Test A5. Mike 21C is a two-dimensional vertically integrated programme (2DH) with advantages over DELFT 2D for sediment transport by using a curvilinear grid, secondary flow relationships for the bend sediment transport, where bank stability and bed slope are considered.

7.2 DELFT 3D (HYDRODYNAMICS)

7.2.1 DESCRIPTION OF HYDRODYNAMIC COMPONENT OF MODEL

The hydrodynamic model (DELFT3D-FLOW), capable of solving the time-dependent shallow water equations in three dimensions, is designed to simulate tidally and wind-driven flows in shallow seas, coastal areas, estuaries, rivers and lakes. The model includes formulations and equations that consider:

- tidal forcing
- wind shear stress on the water surface
- wave-driven flows
- the effect of the earth's rotation (Coriolis force)
- free surface gradients (barotropic effects)
- secondary currents

- bed shear stresses on the seabed
- drying and flooding on tidal flats
- turbulence induced mass and momentum fluxes (k-ε turbulence closure model).

The system of equations in Delft3D-FLOW comprises the horizontal momentum equations and the continuity equation, the equation of state and the advection-diffusion equation for heat, salt and other conservative tracers which are solved using the Alternating Direct Implicit scheme. The computation grid is an irregularly-spaced, orthogonal, curvilinear grid in the horizontal and a sigma coordinate grid in the vertical.

The equations and their numerical implementation are described in detail in the DELFT3D-FLOW user manual (WL|Delft Hydraulics, 2003a) of which simplified versions are provided below:

Conservation of momentum in x-direction:

$$\frac{\partial u}{\partial t} + u\frac{\partial u}{\partial x} + v\frac{\partial u}{\partial y} + g\frac{\partial \eta}{\partial x} - f.v + \frac{g.u\,|U|}{C^2(d+\eta)} - \frac{F_x}{\rho(d+\eta)} - \upsilon\left(\frac{\partial^2 u}{\partial^2 x} + \frac{\partial^2 u}{\partial^2 y}\right) = 0$$

Conservation of momentum in y-direction:

$$\frac{\partial v}{\partial t} + u\frac{\partial v}{\partial x} + v\frac{\partial v}{\partial y} + g\frac{\partial \eta}{\partial y} + f.u + \frac{g.v\,|U|}{C^2(d+\eta)} - \frac{F_y}{\rho(d+\eta)} - \upsilon\left(\frac{\partial^2 v}{\partial^2 x} + \frac{\partial^2 v}{\partial^2 y}\right) = 0$$

Conservation of mass, continuity equation:

$$\frac{\partial \eta}{\partial t} + \frac{\partial[(d+\eta)u]}{\partial x} + \frac{\partial[(d+\eta)v]}{\partial y} = 0$$

7.2.2 HYDRODYNAMIC MODELLING

The numerical model was set up to simulate only the hydrodynamics of the laboratory experiments for Test A (Section 5.3). Initial problems were encountered regarding the choice of some of the variables for the model. Special attention was given to the horizontal viscosity that determine the interaction of the different 'layers' of water with each other in order to simulate the spiral flow in the curved section. Once these initial constraints were overcome, the Chezy coefficient was adjusted until the simulated and measured water levels were in good agreement. Some of the important parameters used in the simulation are given in Table 7-1.

Parameter	**Value**
Time step	0.25 minutes
Chezy coefficient (C)	55 $m^{1/2}/s$
Uniform flow depth	Average measured water level from laboratory experiments
Horizontal viscosity	0.01 m^2/s

Table 7-1: Hydrodynamic model parameters

The simulated results compared well with those obtained from the laboratory experiments and the programme was then applied with a great degree of confidence.

Three-dimensional simulations were carried out first, followed by two-dimensional (in plan) simulations. Two-dimensional vertically integrated models are often used in sediment transport in river systems that are relatively shallow to save computational time. With a two-dimensional approach, empirical coefficients are incorporated in the software, calibrated against three-dimensional simulations during model development.

7.2.3 SIMULATION RESULTS

7.2.3.1 3D-SIMULATION

7.2.3.1.1 Test H1 (F_R = 0.1)

The simulated velocity distribution shows that higher velocities on the outside of the bend develop from halfway through the curved section up to the end of the curved section. The maximum velocities are found on the outside of the bend near the end. When the simulated and laboratory velocity distributions are compared it is in good agreement. The simulated water levels show the super elevation of the water level on the outside of the bend and were found to be as expected (see Appendix C: Figures C-7 to C-11).

7.2.3.1.2 Test H2 (F_R = 0.3)

The simulated velocity distributions are in good agreement with the measured laboratory velocity distributions. The maximum velocity is found on the outside of the bend near the end of the curved section with higher velocities on the outside of the bend from approximately the middle of the bend up to the end. The water levels generated were as expected with higher water levels on the outside of the bend indicating the super elevation of the water (see Appendix C: Figures C-12 to C-16).

7.2.3.1.3 Test H3 (F_R = 0.5)

The simulated velocity distributions at the surface (see Appendix C: Figure C-17) and at a distance of 70 mm, 50 mm and 30 mm from the bed are shown in Figures 7-1 to 7-3 respectively. From these figures it is clear that higher velocities on the outside of the bend start to develop from about halfway through the bend and remain higher on the outside until the end of the curved section is reached. The zone of highest velocities is found on the outside of the bend near the bend exit.

Figure C-21 (see Appendix C) indicates that the simulated water levels and the higher water levels on the outside of the bend are once again prominent indicating the super elevation of the water levels on the outside of the bend.

Figure 7-1: Test H3-Simulated velocity distribution in the horizontal plane at 70 mm above the bed

Figure 7-2: Test H3-Simulated velocity distribution in the horizontal plane at 50 mm above the bed

Figure 7-3: Test H3-Simulated velocity distribution in the horizontal plane at 30 mm above the bed

7.2.3.2 2D-SIMULATION

7.2.3.2.1 Test G1 (F_R = 0.1)

The simulated velocity distribution indicates that there is a zone towards the end of the curved section where the velocities are higher on the outside of the bend than on the inside. It is also noted that there are some places near the end of the straight section and at the beginning of the curved section where the simulated velocity distribution indicates higher velocities on the inside of the curve. This is in disagreement with the results from the laboratory experiments and is not as expected (see Appendix C: Figure C-1).

The simulated water levels show good agreement with laboratory work. The elevated water levels on the outside of the curved section can clearly be seen from Figure C-2 (see Appendix C).

7.2.3.2.2 Test G2 (F_R = 0.3)

The simulated velocity distribution (see Figure 7-4) for this scenario is in good agreement with the laboratory experiments. Approximately halfway through the curved section higher velocities developed on the outside of the bend with the highest velocities near the end of the curved section on the outside of the bend. However, there is still a zone at the beginning of the curved section where higher velocities are present on the inside of the bend contrary to the laboratory experiments.

Figure C-4 (see Appendix C) indicates that the simulated water levels were as expected, higher on the outside of the bend.

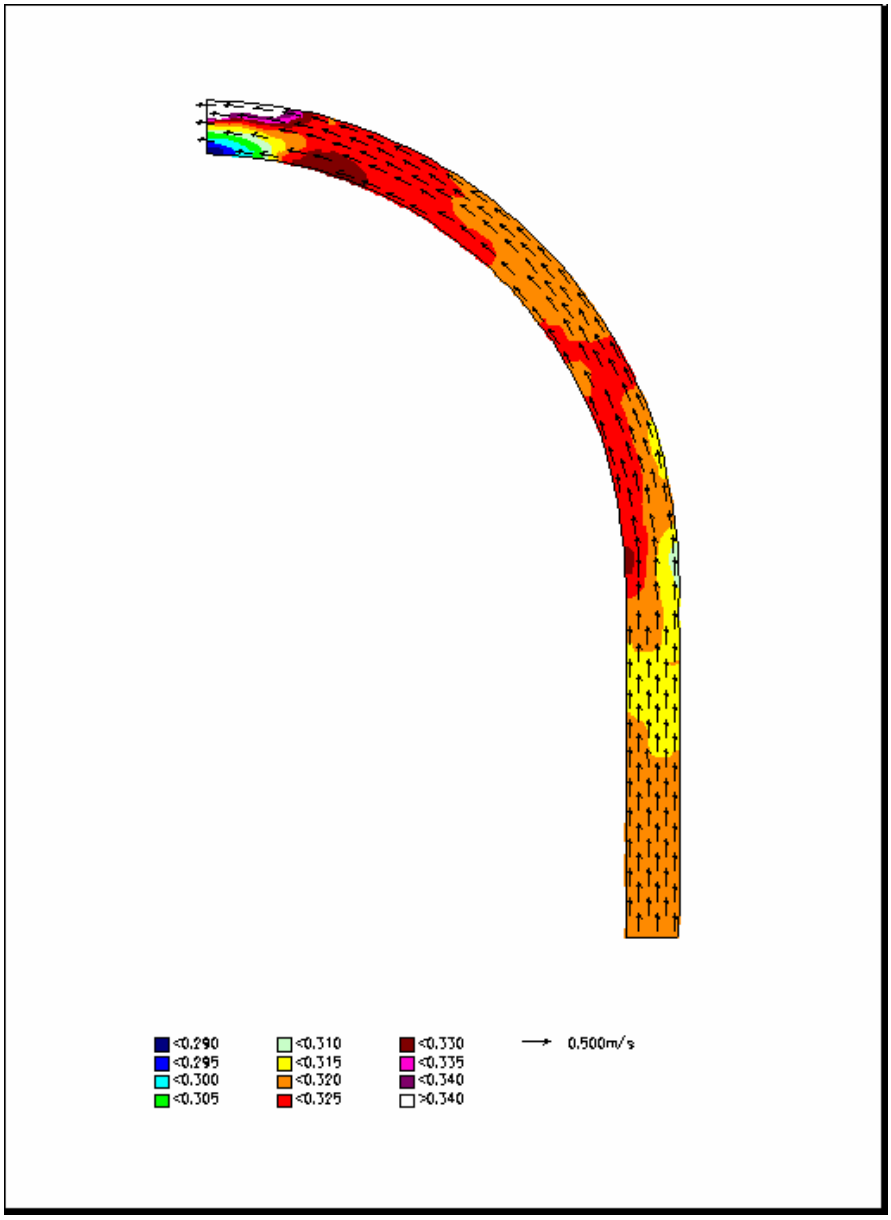

Figure 7-4: Test G2-Simulated velocity distribution in the horizontal plane

7.2.3.2.3 Test G3 (F_R = 0.5)

The simulated velocity distributions and water levels were in total disagreement with the laboratory experiments. The velocities seem to increase in the downstream direction throughout the straight and curved section. It is therefore the opinion of the author that the simulation time was too short and therefore the velocities were not

fully developed when the simulation was stopped (see Appendix C: Figures C-5 to C-6).

7.3 MIKE 21C (SEDIMENT DYNAMICS)

7.3.1 DESCRIPTION OF MODEL

For the computational modelling, the two-dimensional model MIKE 21C, developed by the DHI Water and Environment (DHI, 2003), was used. MIKE 21 is a software package for simulating free-surface flows, water quality, sediment transport and waves in rivers, lakes, estuaries, bays, coastal seas and other water bodies. In particular MIKE 21C, a special module developed to simulate river morphology, was used. MIKE 21C is based on a curvilinear grid, and hydrodynamics, sediment transport and river morphology can be simulated, with modules to describe:

- Flow hydrodynamics – water levels and flow velocities are computed over a curvilinear or rectangular grid.
- Helical flow (secondary currents).
- Sediment transport – based on various model types, capable of graded sediment transport computations.
- Alluvial resistance due to bed material and bed forms.
- Scour and deposition – large-scale movement of bed material is computed and the effect of supply limited sediment layers can be incorporated.
- Bank erosion and planform changes – bank lines as well as the curvilinear grid can be updated.

The bed slope effect on the sediment transport is very important and is incorporated into MIKE 21C as a transverse and longitudinal component.

The model Mike 21C is used for two-dimensional hydrodynamic and sediment transport of the typical field conditions. The model has the following characteristics:

- It solves the two-dimensioal Saint-Venant equations
- Dynamic acceleration, spatial acceleration, bed friction, water level gradients and horizontal shear.
- The flow is assumed to be friction dominated, the eddy viscosity is thus set at a small value.

- Transformed to curvilinear coordinates, solved as scalar equations (avoid grid curvature terms).
- The model can simulate both cohesive and non-cohesive sediment transport. Most of the sediment transported during floods in sand bedded rivers consists of silt and clay (about 70 %). In this research, however, limiting sand diversion was of importance and therefore cohesive sediment was not simulated.

7.3.2 SIMULATION RESULTS

The parameters used in the simulation are shown in Table 7-2. Figure 7-5 is the result of a Mike21C simulation of the laboratory tests (Test A5). It is clearly evident that the measured bed profiles and the simulated versions thereof only vaguely resemble each other. The reason for the discrepancy is that the model was unable to accurately simulate the sluice gate at the end of the channel. This problem was remedied by adding another straight section downstream of the bend (see Figure 7-6), which adds stability to the simulated water flows with the boundary in the computational model further downstream. Hydraulic conditions at the test section were however still simulated accurately.

Mike21C parameter	Description	Value assigned
Modelling period	Length of simulation	2 hours
Timestep	Length of calculation iteration	0.01 seconds
Boundaries	Water levels and discharges	Q = 0.0102 m^3/s H = 0.1 m
D_{50} of sediment	Size of sediment	0.12 mm
Transport mode	Type of sediment movement	Both bed and suspended sediment
Transport formulation	Theory behind sediment movement	Van Rijn
Horizontal eddy viscosity (ν)	Velocity or flux based viscosity	0.03 m^2/s
Manning n value	Roughness of channel	0.025 $s/m^{1/3}$
Threshold for drying and flooding	Water depth at which model begins calculating the hydrodynamics for that point	0.006 m

Table 7-2: Mike 21C properties for simulation of Test A5

The scour position corresponds with that of the laboratory test and the scour hole closes up as it moves downstream as was observed in the measured profile. The deepest scour hole achieved during the simulation is 0.094 m below the original bed level, compared with the observed maximum depth of 0.082 m below the original bed. The simulation produced an accurate prediction of the observed bed levels.

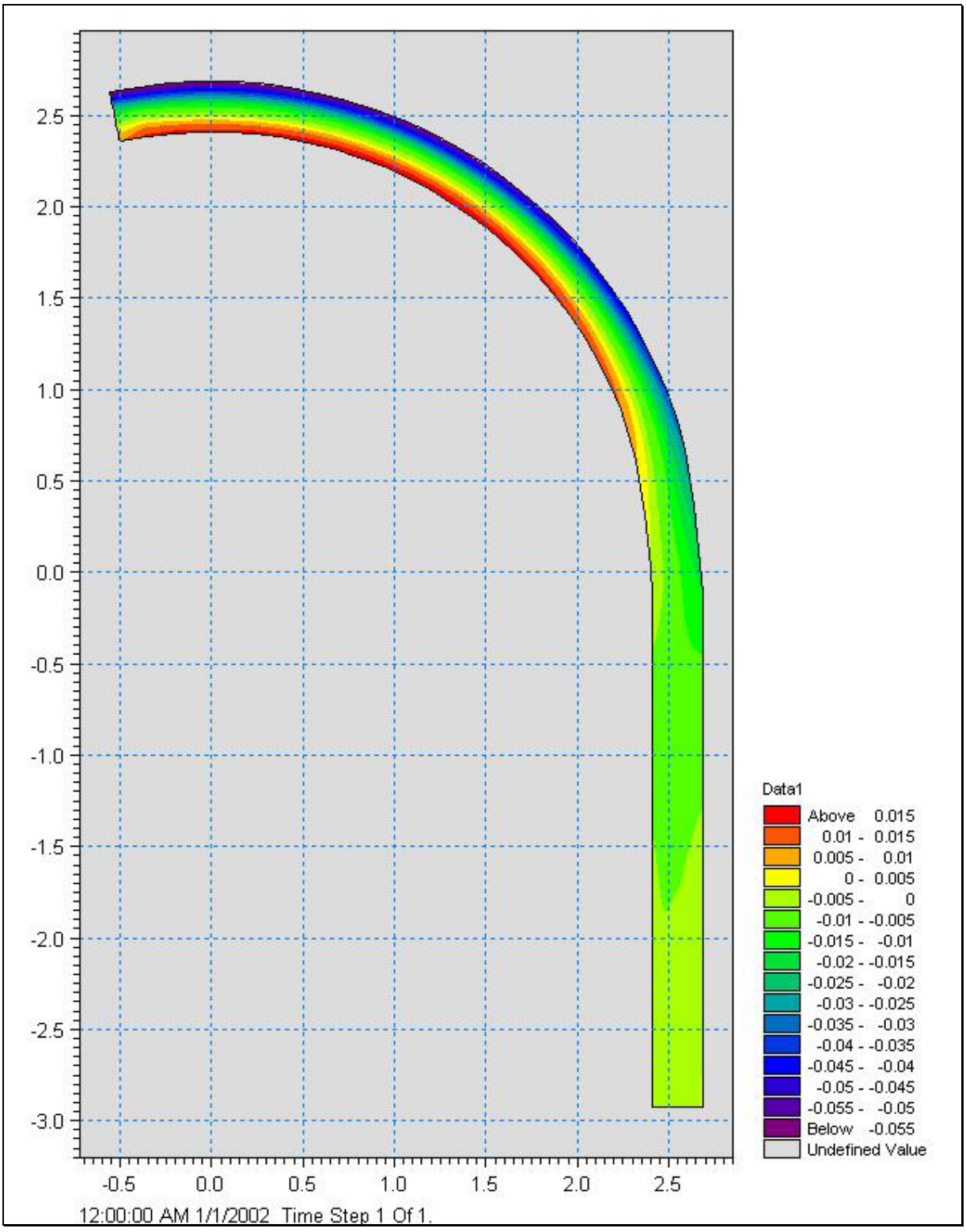

Figure 7-5: Initial simulation of Test A5

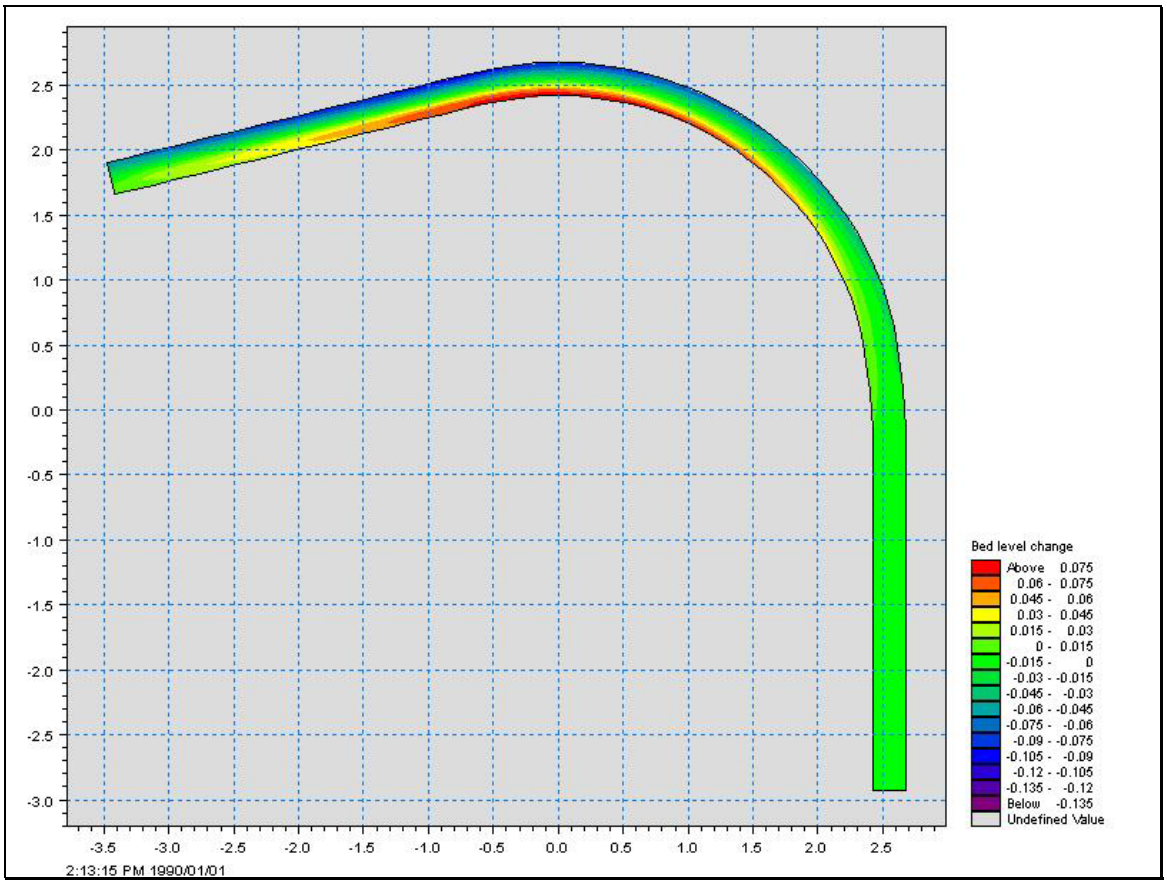

Figure 7-6: Simulated bed levels of Test A5

7.4 ANALYSIS OF MATHEMATICAL MODEL SIMULATION RESULTS

7.4.1 MODELLING OF HYDRODYNAMICS

The three-dimensional simulation results in higher velocities being indicated on the outside of the bend from approximately halfway through the bend with the maximum velocity being near the end of the curved section. Higher velocities are also found closer to the inside of the bend in the region near the end of the straight section and the beginning of the curved section. A typical simulated velocity distribution is presented in Figure 7-7(b). This is essentially the same as were obtained from the laboratory experiments (see Figure 7-7 (a)). Figure 7-7 (a) is not to scale (n.t.s) whereas Figure 7-7 (b) is to scale. From Figure 7-7 it can be seen that the simulated flow pattern is in good agreement with the observed flow pattern. Figure 7-8 is an enlarged view of the observed and simulated flow patterns in the curved section. The

zone of the maximum velocity is at 5.19 m near the outside of the bend. The velocity distribution obtained from the two-dimensional simulation indicates higher velocities on the outside of the bend only develop at the very end of the curved section.

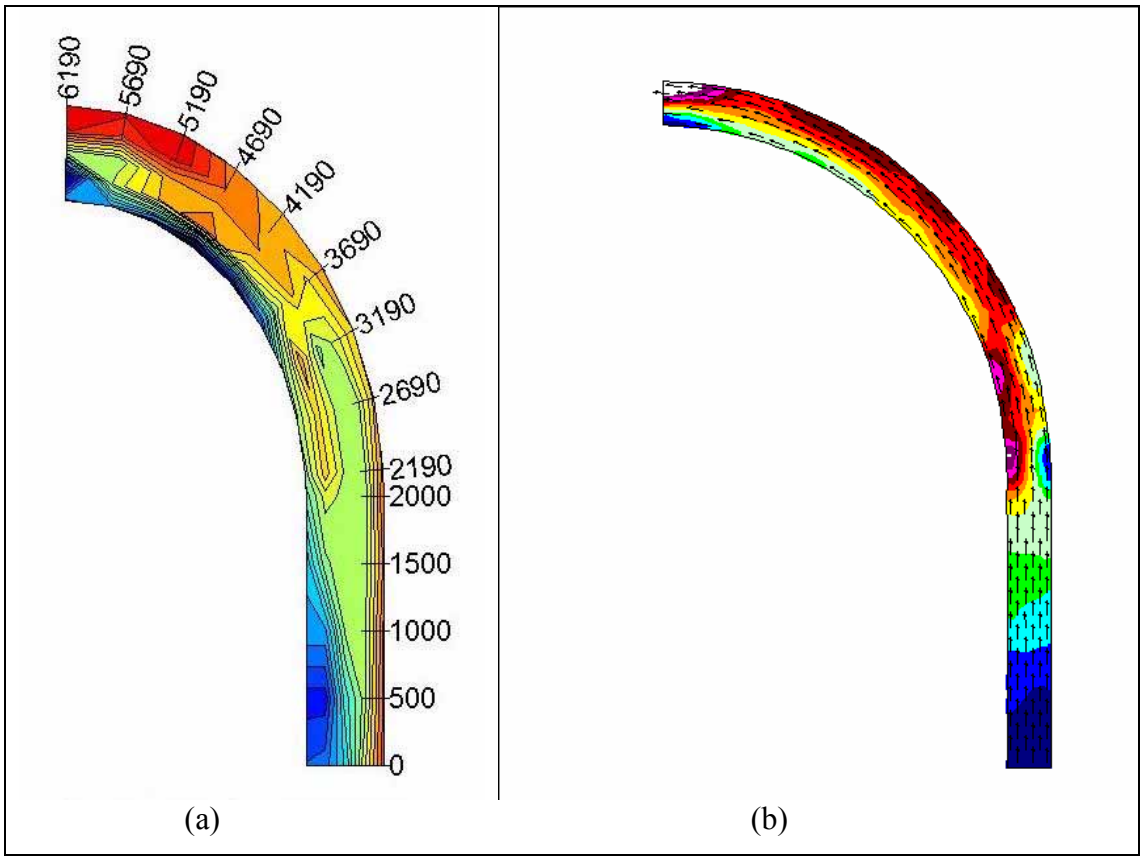

Figure 7-7: (a) Observed (n.t.s) and (b) simulated flow patterns measured at 70 mm above the bed (r_c/w =8.5 ,F_r =0.5)

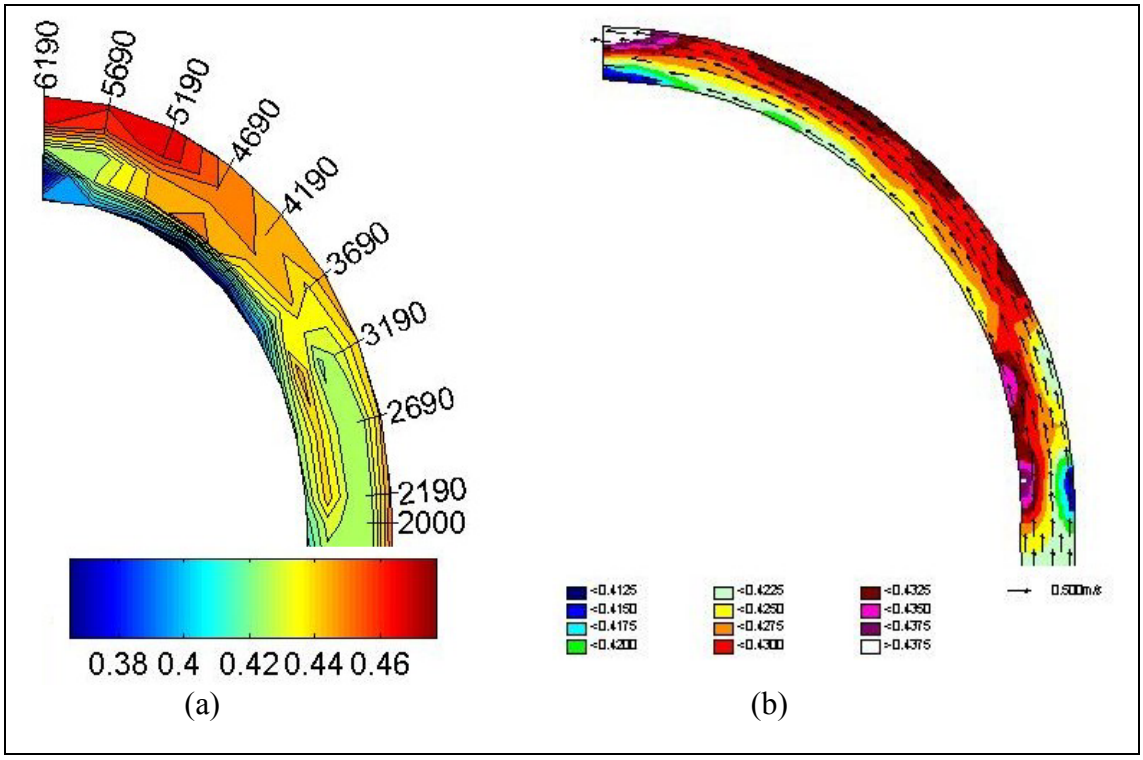

Figure 7-8: Enlarged view of the observed (a) and simulated (b) flow patterns in the curved section measured at 70 mm above the bed (r_c/w =8.5 ,F_r =0.5)

The simulated water levels are also in good agreement with the observed water levels. The super elevation of the water level on the outside of the bend is more evident in the case of the three dimensional simulation than for the two dimensional simulation.

In summary, it was found that the three-dimensional hydrodynamic model simulation results in a velocity distribution and simulated water levels that are in good agreement with those obtained from the laboratory experiments. The simulations with a Froude number of 0.3 and 0.5 were also in better agreement with the laboratory results than the simulation with a Froude number of 0.1.

7.4.2 MODELLING OF SEDIMENT DYNAMICS

A curvilinear grid that resembles a flow net of the river is set-up and at each of the nodes of this grid a value is then assigned, usually representing height. In other words the bathymetry of a river can be accurately incorporated. The grid was set-up to

represent the points where the sediment levels were measured (see Section 5.2.2 and Figure 5-8)

Several other parameters can be adjusted in the model and some are more important than others. Some of the more important parameters include discharge into the channel, water depth at the end of the channel, eddy viscosity, resistance (Chezy or Manning) and sediment grain size, among many others. Those mentioned parameters were seen to have the greatest effect on the simulations.

Initial simulation problems were remedied by the addition of a straight section downstream of the sluice gate. The addition of the straight section acted in some way as a sluice gate that allowed the water levels to be simulated more accurately, that in return produced results that are in good agreement with the measured sediment levels of the laboratory experiment.

Figure 7-9 (a) contains the measured sediment levels with (b) being the simulated sediment levels for Test A5 with r_c/w=8.5 and F_r=0.3. In general the simulation is in good agreement with the measured sediment levels with the centre of the sour zone corresponding olang the outside of the bend. However, the simulated sediment levels indicate a much smaller scour zone in comparison with the measured bed profile and earlier deposition is noted on the inside of the bend. A possible reason for this difference may be due to Van Rijn's sediment transport formula that was selected for the simulations and due to the fact that the sediment transport formula was not calibrated on the measured data from the laboratory.

It can be concluded that the three-dimensional hydrodynamics of the channel can be well-imitated with the two-dimensional depth averaged model (2DH) as well as the sediment dynamics of the curved section. Therefore this model can be applied with greater reliability on field conditions. The advantages of the 2DH model to simulate field conditions lies in the shorter simulation times for the often large models especially if a long term analysis is carried out that is longer as 6 months with rivers being longer than 10 km.

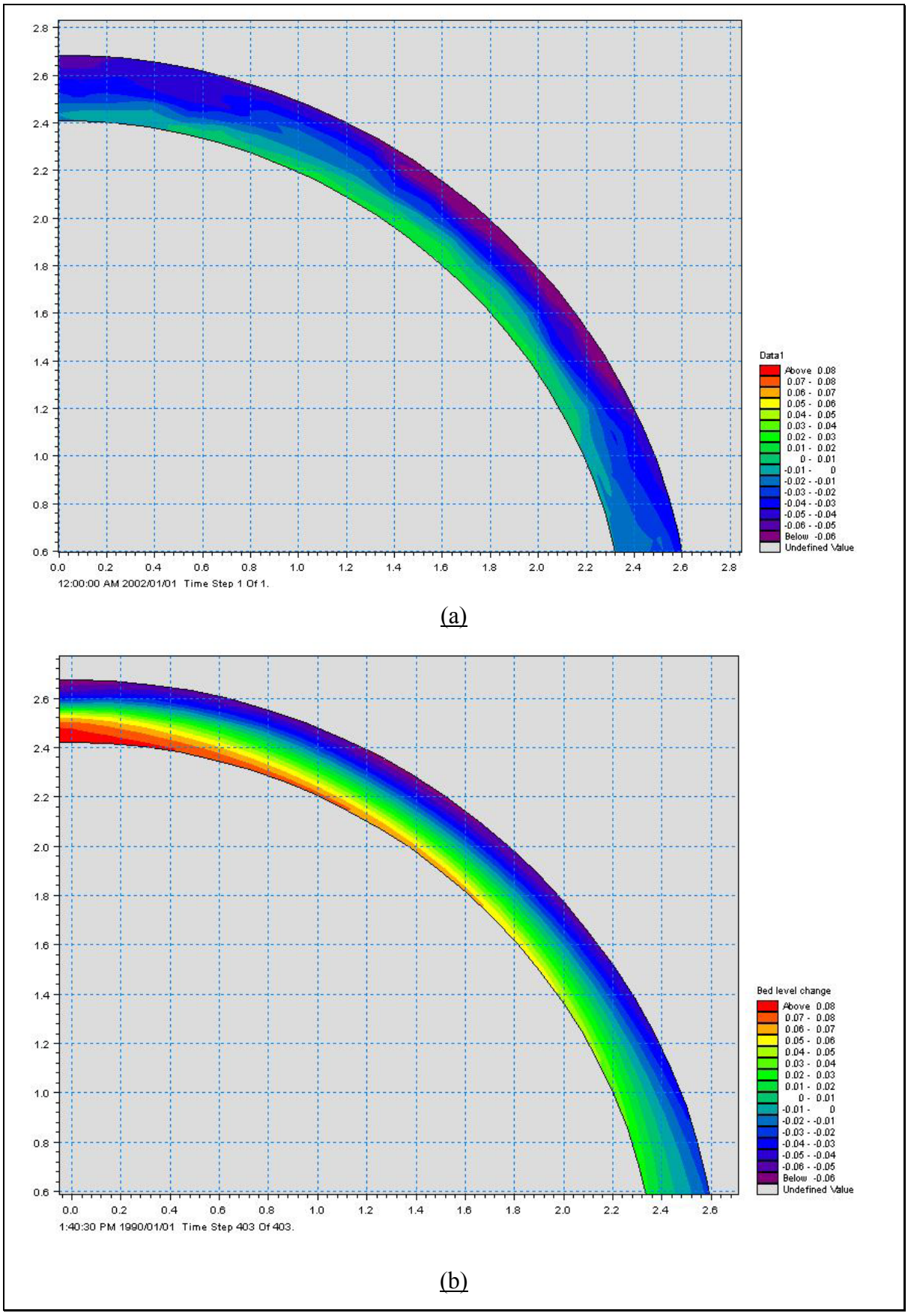

Figure 7-9: (a) Measured and (b) Simulated sediment levels (r_c/w=8.5, F_r=0.3)

8 CONCLUSIONS AND RECOMMENDATIONS

The optimum diversion location was determined in a laboratory canal by assessing the location of the maximum measured velocity. It was found that the maximum velocity value is located near the outside of bend at the bed, with higher velocities on the outside of the bend than on the inside. Three main scour areas could be identified and the location of the third scour hole (the deepest) is in good agreement with the maximum velocity.

The velocity distributions obtained from the measured data can be summarised as follows:

In the horizontal plane a fairly uniform velocity distribution is obtained in the first part of the straight section. Towards the end of the straight section the maximum velocity moves slightly towards the inside of the bend. The maximum velocity then gradually shifts towards the outside of the bend and reaches the outside of the bend between 3.19 m and 3.69 m. Further downstream it remains near the outside of the bend up to the end of the measurements (see Figure 8-1). The horizontal velocity distribution as described above is in good agreement with that described by *Bridge and Jarvis (1982)* and *Bridge (1983).*

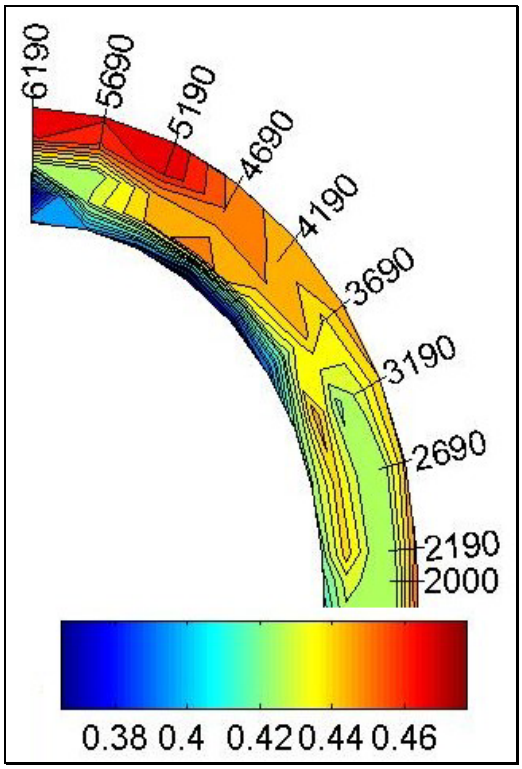

Figure 8-1: Flow pattern in the curved section (n.t.s)

In the vertical plane the general tendency is that the maximum velocity dives towards the bottom while moving towards the outside of the bend in the downstream direction. This is in good agreement with *Lee, Yu and Hsieh (1990)*. The vertical velocity distribution can be characterised by the following:

i) The measured velocity at 70 mm from the bottom (*V70*) has a decreasing tendency near the inside of the bend.

ii) In the centre of the bend all the measured velocities show an increasing tendency.

iii) Near the outside of the bend the measured velocity at 30 mm from the bottom (*V30*) shows an increasing tendency.

iv) The locations of the turning points where *V30>V50*, *V30>V70* and *V50>V70* stay relatively constant near the inside of the bend but move in the downstream direction with an increase in Froude numbers.

v) The locations of the turning points where *V30>V50*, *V30>V70* and *V50>V70* move downstream near the inside and outside of the bend with an increase in the radius of curvature ratio (r_c/w).

vi) The range of the location of the turning points increase on the inside and outside of the bend for an increase in the radius of curvature

The location of the maximum velocity was found to be relative constant with varying Froude number, whilst moving in the downstream direction with an increase in the radius of curvature-to-width ratio (r_c/w). Table 5-2 contains a summary on the diversion locations as obtained from the laboratory data.

The development of secondary flow can be predicted with equation 2-3 *(Raudkivi, 1993)* and equation 2-5 *(Rozovskii, 1961)* with a constant of 1.97. A radius of curvature-to-width ratio (r_c/w) smaller than 14.6 is required to ensure that the secondary flow can develop fully in a bend according to Figure 8-2 *(Raudkivi, 1993)*. From this figure it is noted that the secondary flow was not fully developed for the range of tests with r_c/w=15.2, applying the principles of *Raudkivi (1993).*

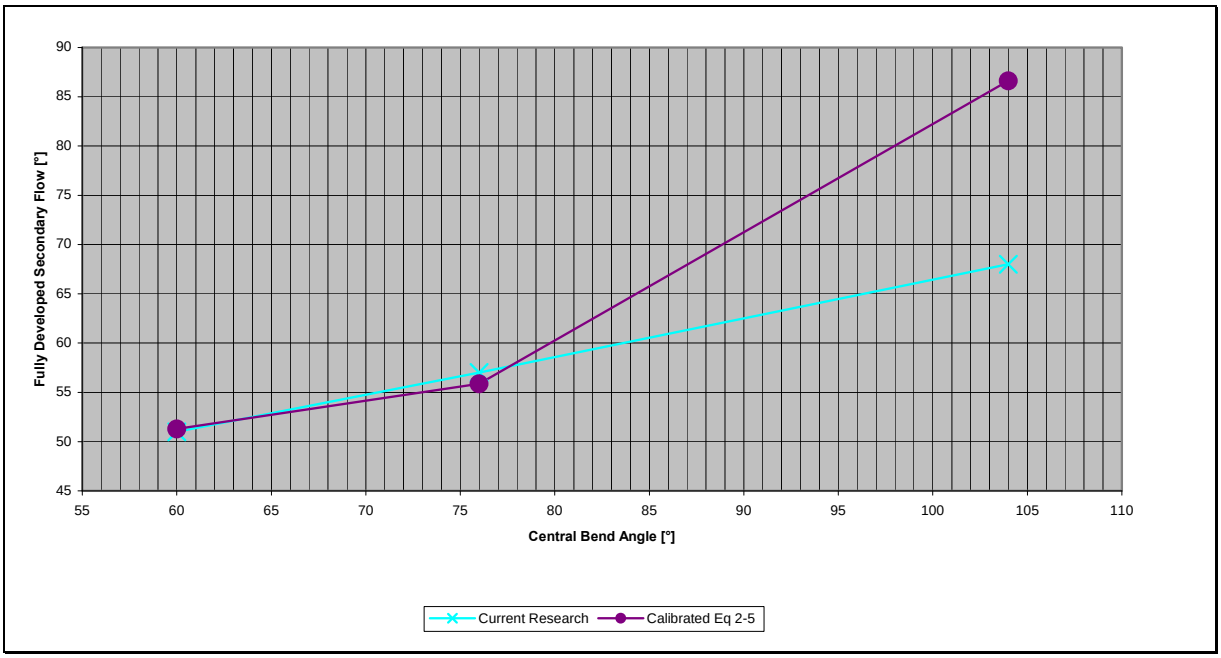

Figure 8-2: Fully developed secondary flow

The optimum diversion location from the current research is in good agreement with the recommended diversion location of Table 4-1 *(SC and CHES, 1992)* (see Figure 8-3). Applying Figure 3-4 *(Raudkivi, 1993)* to the data of the current research

resulted in the diversion location being 8.8 times the width of the channel downstream of the intersection of the upstream axis with the outer bank. Equation 4-1 *(SC and CHES, 1992)* was calibrated on the data of the current research with a constant of 1.71 (see Figure 8-4).

The diversion location can also be predicted with Figure 8-4 where the diversion location is expressed as a ratio of the diversion location and the central bend angle in relation to the radius of curvature-to-width ratio (r_c/w), as derived in this research.

It is recommended that Table 4-1 (*SC and CHES, 1992)* be used in predicting the optimum diversion location that covers a wide range of radius of curvature-to-width ratios (r_c/w) and hydraulic conditions. The empirical relationships by *SC and CHES (1992)* (Equation 4-1) and *Raudkivi (1993)* (Figure 3-4) were found to be only applicable on specific hydraulic conditions and cannot be applied the general.

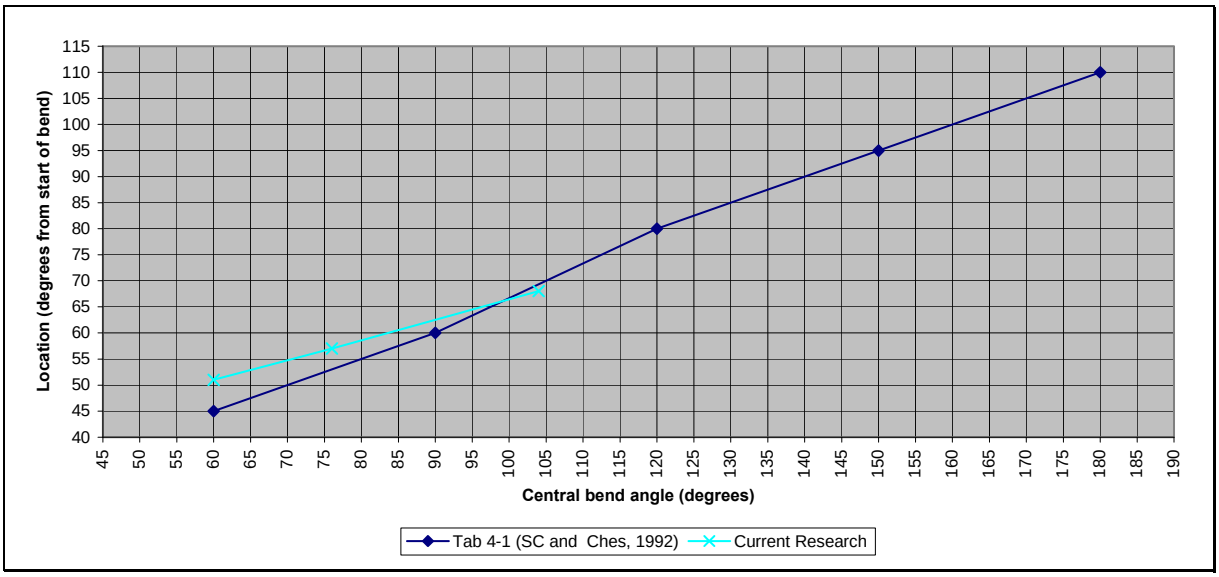

Figure 8-3: Relation between the optimum diversion location and the central bend angle

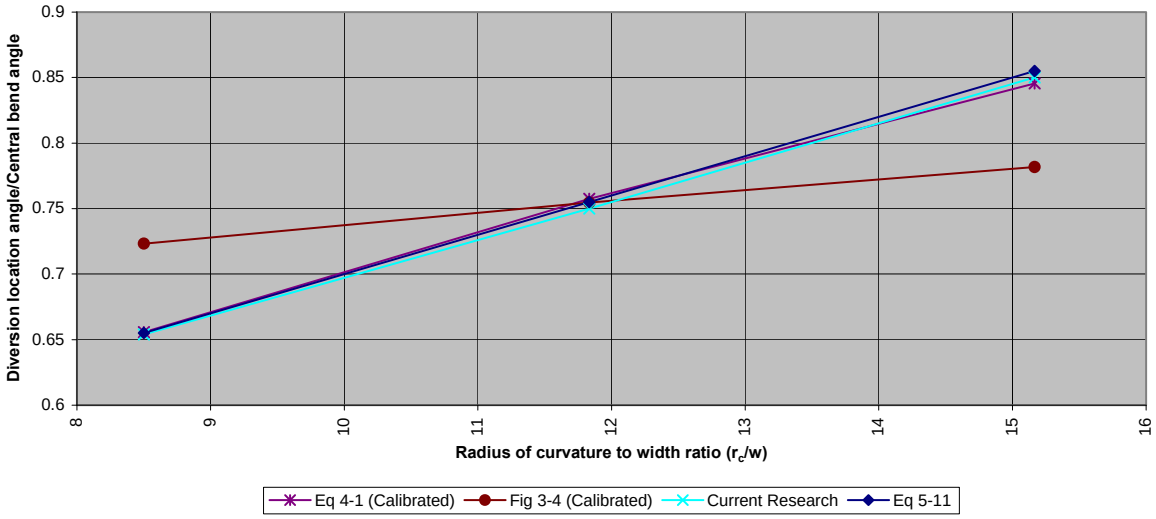

Figure 8-4: Relationship between the optimum diversion location and the radius of curvature-to-width ratio (r_c/w)

The three-dimensional simulation of the DELFT 3D mathematical model provided good simulation of the laboratory experiments (see Figure 8-5). The simulated velocity distributions obtained showed the same tendency as those measured in the laboratory. The simulations of the sediment dynamics with Mike21C provided results that are in good agreement with the measured sediment levels (see Figure 8-6).

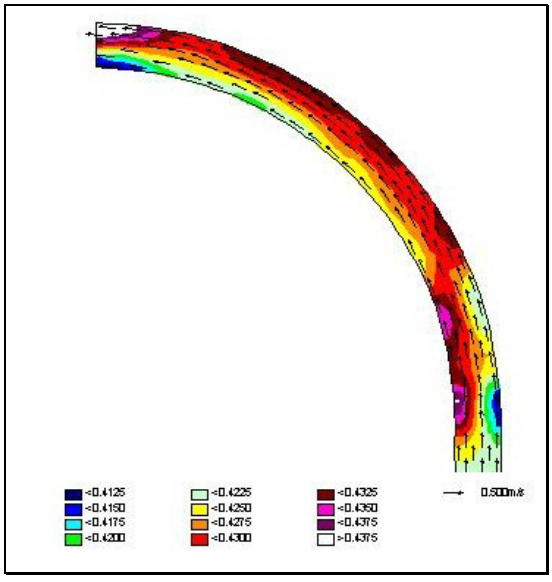

Figure 8-5: Simulated flow pattern in the curved section

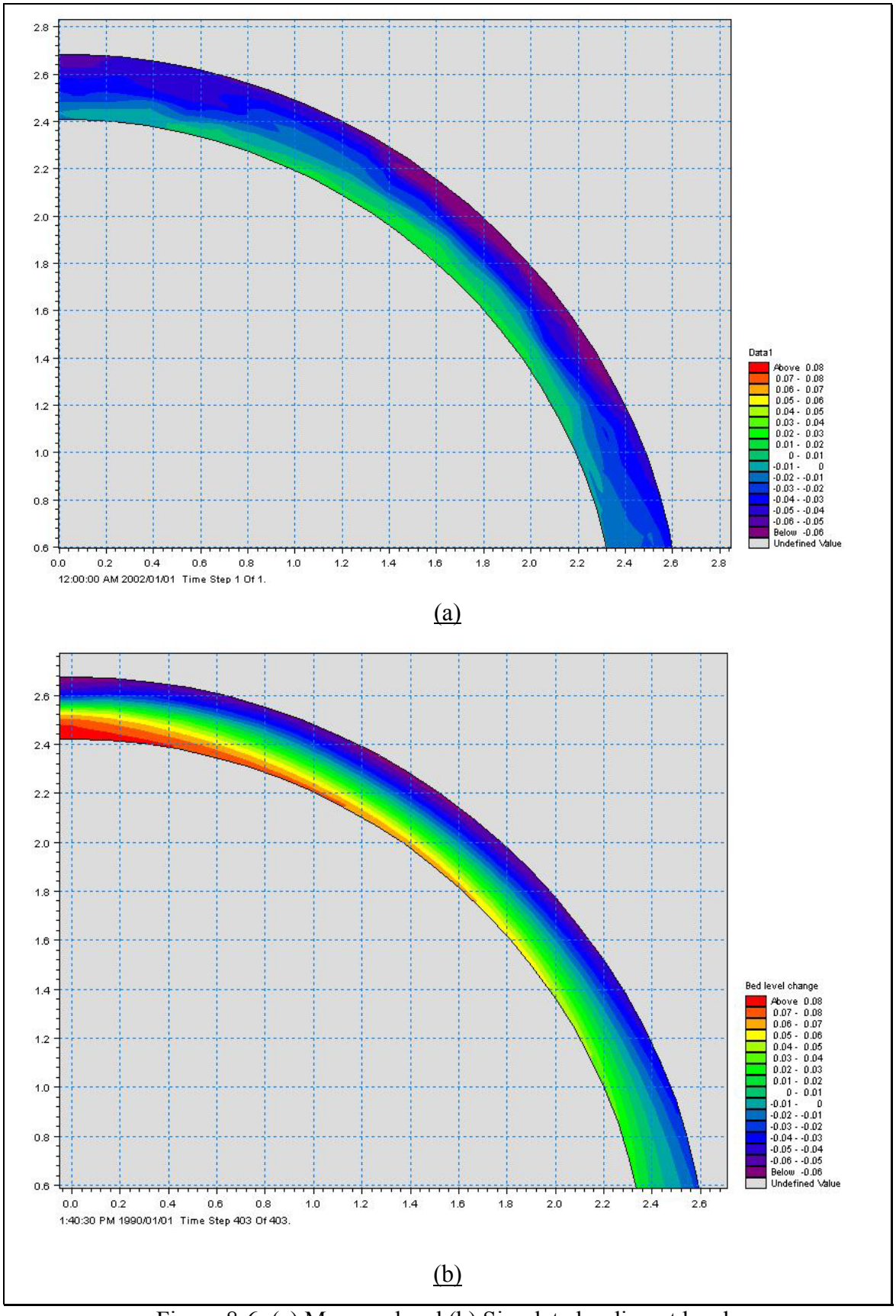

Figure 8-6: (a) Measured and (b) Simulated sediment levels

It is well-evident that the diverted discharge ratio (DDR) increases with an increase in the diversion angle while it decreases with an increase in Froude number. The velocity distribution obtained with a Froude number of 0.3 and 0.5 is also more favourable than those obtained with a Froude number of 0.1 since the bend effect is more prominent. This is in agreement with *Avery (1989)* who suggested a Froude number of 0.5-0.8 in the main curved channel. An important conclusion from the tests is that the diversion does not influence the secondary flow patterns (for the range of DDR's tested) and that the maximum velocity zone stayed in the same location as in the tests without a diversion.

In summary, the recommended approach to determine the optimum diversion location is by applying Table 4-1 (*SC and CHES, 1992)* which is applicable on a wide range of hydraulic conditions. The two-dimensional depth averaged model (2DH) can be used with great reliability to simulate the hydrodynamics of the channel as well as to predict scour patterns in the curved section. The results from these simulations are in good agreement with the data obtained from the laboratory experiments. In the case of empirical formulas, calibrated Equation 4-1 (*SC and CHES, 1992)* and Equation 5-11, that were derived from the data of the current research, can be used in determining the diversion location on the condition that the same hydraulic conditions apply.

There are still a number of outstanding issues that needs to be investigated to improve the understanding of curvilinear flow. Suggestions for future research are summarised below:

i) Curved channel

- The effect of different sediment sizes and non-uniform sediment on the scour characteristics can be investigated. This can lead to a relationship between the sediment characteristics and the depth of scour in a curved channel.
- More tests with varying radius to width ratios can lead to an even better understanding of the velocity profile in curved channels.

- The effect of the width-to-depth ratio needs to be investigated in order to obtain an idea whether it will influence the velocity distribution.
- Different cross-sectional properties of the curved channel can lead to a more favourable velocity distribution that will result in even less sediment being diverted. A trapezoidal cross-section with a bottom slope that falls away from the outside of the curve will promote the development of secondary flow that will lead to greater velocities along the outside of the curve. This will also minimise the entrainment of coarse material into the diversion works.
- A curved channel a with narrowing width in the downstream direction will also lead to the development of higher velocities in the downstream section of the curve i.e. at the diversion location.
- The effect of the bottom slope in the longitudinal direction on the velocity distribution can be determined.
- The effect of a side weir, for flood control, upstream of the diversion works can be investigated where an artificial curved channel is constructed.

ii) Diversion channel

- According to the current research there was no significant influence on the velocity distribution in the main channel with varying diversion angles. This aspect needs more attention to develop an understanding of the effect of the diversion angle on the velocity distribution.
- The development of diverted sediment ratios (DSR) for curved channels in order to compare existing DSR's for straight channel diversions with that of curved channels.
- Sediment flushing in the diversion channel can be studied to determine the effect on the velocity distribution in the curved channel while flushing the diversion channel.
- The oscillation phenomenon in the diversion channel for the non-pumping scenario of a diversion works can be studied.

9 REFERENCES

Apmann, R.P. (1972). Cited in Nwachukwu (1973).

Avery, P. (1989). Sediment control at intakes – a design guide. BHRA (The Fluid Engineering Centre), England.

Avery, P. (ed.) (1982). The problems of sedimentation modelling with particular reference to river intake models. *Int. Conf. On the Hydraulic Modelling of Civil Engineering Structures*, Coventry, England, pp. 167-180.

Bagnold, R.A. (1960). Cited in Vanoni (1977).

Bathurst, J.C. (1979). Secondary flow and shear stress at river bends. *Journ. of the Hydr Proc ASCE (New York).* Vol 105, No 10, pp. 1277 – 1295.

Blench, T. (1969). Mobile-Bed Fluviology. The University of Alberta Press, Canada.

Bouvard, M. (1992). Mobile Barrages and Intakes on Sediment Transporting Rivers. A.A. Balkema, Brookfield.

Bridge, J.S. (1977). Cited in Bridge (1983).

Bridge, J.S. (1983). Flow and Sedimentary Processes in River Bends: Comparison of Field Observations and Theory. *Proc. Conf.on River Meandering*, New Orleans, New York, pp.857-872.

Bridge, J.S. and Jarvis, J. (1982). The dynamics of a river bend: a study of flow and sedimentary processes. *Sedimentology (Amsterdam)*. Vol. 29, No 4, pp. 499 – 541.

Bulle, H. (1926). Cited in Cecen (1988).

Cecen, M.K. (1988). Reduction of Sediment Entrainment: Its Trapping and Flushing. Water Resources Publications, USA, Littleton, pp. 398-425. (Mahmood editor).

Chang, H.H. (1983). Energy expenditure in curved open channels. *Journ. of Hydr. Eng*, Vol 109, No 7, pp. 1012 – 1022.

Chatley, H. (1931). Cited in Nwachukwu (1973).

Chen, G.X. and Shen, H.W. (1983). River Curvature-Width Ratio Effect on Shear Stress. *Proc. Conf.on River Meandering*, New Orleans, New York, pp.687-699.

Choudhary, U.K. and Narasimhan, D. (1977). Flow in 180 Degrees Open Channel

Rigid Boundary Bends. *Journal of the Hydr Proc ASCE (New York)*, Vol 103, No 6, pp 651 – 657.

Chow, V.T. (1959). Open-channel hydraulics, McGraw-Hill Book Co. INC, London.

Christian, H.E. (1988). Streambank Erosion and Bank Stabilization. Reduction of Sediment Entrainment: Its Trapping and Flushing. Water Resources Publications, USA, Littleton, pp. 450-471. (Mahmood editor).

DHI (2003). MIKE 21C - River Hydrodynamics and Morphology - User Guide. DHI Water and Environment. Denmark.

Featherstone, R.E. and Nalluri, C. (1995). Civil Engineering Hydraulics, Blackwell Science, London.

Francis, J.R.D and Asfari, A.F. (1971). Cited in Chen and Shen (1983).

Habermaas, F. (1935). Cited in Shen (1971).

Henderson, F.M. (1967). Open Channel Flow. The Macmillan Company, New York.

Hufferd, J.A., Watkins, J.S. (1972) Joglekar, D.V., Gotankar, S.T. and Kulkarni, P.K. (1951).

Hufferd, J.A., Watkins, J.S. (1972). Chapter V: Sediment Control Methods: C. Control of sediment in Canals. Am. Soc. Civ Engrs Task Committee for the Preperation of the Manual of Sedimentation, USA, New York.

Hussein, A.S.A and Smith, K.V.H. (1986). Flow and bed diversion angle in curved open channels. *Journ. of Hydr. Res. (Delft; Neterlands)*. Vol. 24, No. 2, pp. 93 – 108.

Jackson, R.G. (1975). Cited in Chen and Shen (1983).

Joglekar, D.V., Gotankar, S.T. and Kulkarni, P.K. (1951). Cited in Hufferd and Watkins (1972).

Kalkwijk, J.P. and De Vriend, H.J. (1980). Computation of the flow in shallow river bends. *Journ. of Hydr. Research.* Vol 18, No. 4, pp. 327 – 342.

Khalid, S.A. (1964). Cited in Chen and Shen (1983).

Lacey, G. (1929). Cited in Raudkivi (1993).

Lacey, G (1930). Cited in Nwachukwu (1973).

Lane, E.W. (1955). Cited in Shen (1971).

Lee, H.Y. and Yu, W.S. (1990). Cited in Lee, Yu and Hsieh (1990).

Lee, H.Y., Yu, W.S. and Hsieh, K.C. (1990). Flow Characteristics of Sand-Silt River Bend. *Int. conf. of Physical Modelling of Transport and Dispersion*, Massachusetts, USA, pp.11B.19-11B.24.

Leliavsky, S. (1965). Irrigation Engeneering: Syphons, Weirs and Locks. Chapman and Hall Ltd, London.

Liu, X. et al. (1982). Cited in Tan (1996).

Mandouh, A.N. and Townsend, R.D. (1979). Shear-stress distributions in stable channel bends. *Journ. of the Hydr Proc ASCE (New York).* Vol 105, No 10, pp. 1233 – 1245.

Minikin, R.C.R. (1920). Practical River and Canal Engineering. Bedford Court Mansions, London.

Mosoyi, E. (1965). Cited in Shen (1971).

Müller, R. (1943). Cited in Chow (1959)

Nelson, J.M. and Smith, J.D. (1989). Cited in Yalin (1992)

Nwachukwu, B.A. (1973). Laboratory Study of Scour at Channel Bends. *Proc. of First Canadian Hydraulics Conf*, Edmonton, Canada, pp.144-164.

Odgaard, A.J. (1986). Cited in Baird and Achterberg (1989).

Okoye, K.G. (1989). Mean Flow Structure in Model Alluvial Channel Bends. *Proc. of Tech. Session B: Fluvial Hydraulic, IAHR 23rd Congress*, Ottawa, pp.B-81–B-90.

Raudkivi, A.J. (1993). Sedimentation: Exclusion and removal of sediment from diverted water. A.A. Balkema, Brookfield.

Ripley, H.C. (1925). Cited in Nwachukwu (1973).

Rouse, H. (1950). Cited in Varshney (1977).

Rozovskii, I.L. (1957). Cited in Shen (1971).

Rozovskii, I.L. (1961). Cited in Chang (1983).

Rozovskii, I.L. (1962). Cited in Yalin (1992).

Rozovskii, I.L. (1963). Cited in Bathurst (1979).

Rzhanitsyn, N.A. (1960). Cited in Shen (1971).

SC (Sediment Committee) and CHES. (1992). Sedimentation Handbook. Environment Science Press, Beijing (in Chinese).

Scheuerlein, H. (1984). Die Wasserentnahme aus geschiebeführenden Flüssen,

Ernst and Sohn, Berlin, Germany. (In German).

Sharma, H.D., Varshney, D.V. and Tiagi, S.S. (1973). Cited in Varshney (1977).

Shen, H.W. (1971). River Mechanichs: Volume 2, Shen, USA.

Shukry, A. (1950). Cited in Chow (1959).

Simons, D.B. (1971). Cited in Baird and Achterberg (1989).

Snell, E.F.A. (1994). The Design of River Intakes to minimise Abstraction of Sediment. *Proc. Conf. Fifty Years of Water Engineering in South Africa. A Tribute to Prof Des Midgley*, Johannesburg, South Africa, pp.467-500.

Tan, Y. (1996). Design of silt related hydraulic structures, Int conf on Reservoir Sedimentation.

Thompson, J. (1876). Cited in Vanoni (1977).

Thorn, C.R. and Hey, R.D. (1979). Cited in Bridge and Jarvis (1982).

Tyagi, A.K. (1967). Cited in Varshney (1977).

Vanoni, V.A. (1977). Sedimentation Engineering. Am. Soc. Civ Engrs Task Committee for the Preperation of the Manual of Sedimentation, USA, New York.

Varshney, D.V. (1977). Scour around Bends in Alluvial Channels. *Journ. of the Institution of Engineering (India)*. Vol 58, No CI2 & CI3, pp.91 – 98.

Varshney, D.V. and Garde, R.J. (1975). Cited in Chen and Shen (1983).

Vriend, H.J. and Struiksma, N. (1983). Flow and Bed Deformation in River Bends. *Proc. Conf.on River Meandering*, New Orleans, New York, pp.810-828.

WL|DELFT Hydraulics (2003a). DELFT3D-FLOW User Manual Version 3.10. WL|Delft Hydraulics, Delft, The Netherlands.

Yalin, M.S. (1992). River Mechanics. Pergamon Press, New York.

Yen, B.C. (1965). Cited in Varshney (1977).

Yen, C and Lee, K. T. (1995). Bed topography and sediment sorting in channel bend with unsteady flow. *Journ. of Hydr. Eng.* Vol. 121, No. 8, pp. 591 – 599.

APPENDIX A-DIVERSION LOCATION

APPENDIX A-DIVERSION LOCATION

TABLE OF CONTENTS

LIST OF FIGURES

LIST OF TABLES

A.1 TEST A (AVERAGE RADIUS = 2.55 M)

A.1.1 VELOCITY RELATED

A.1.1.1 TEST A1 (F_R = 0.1)

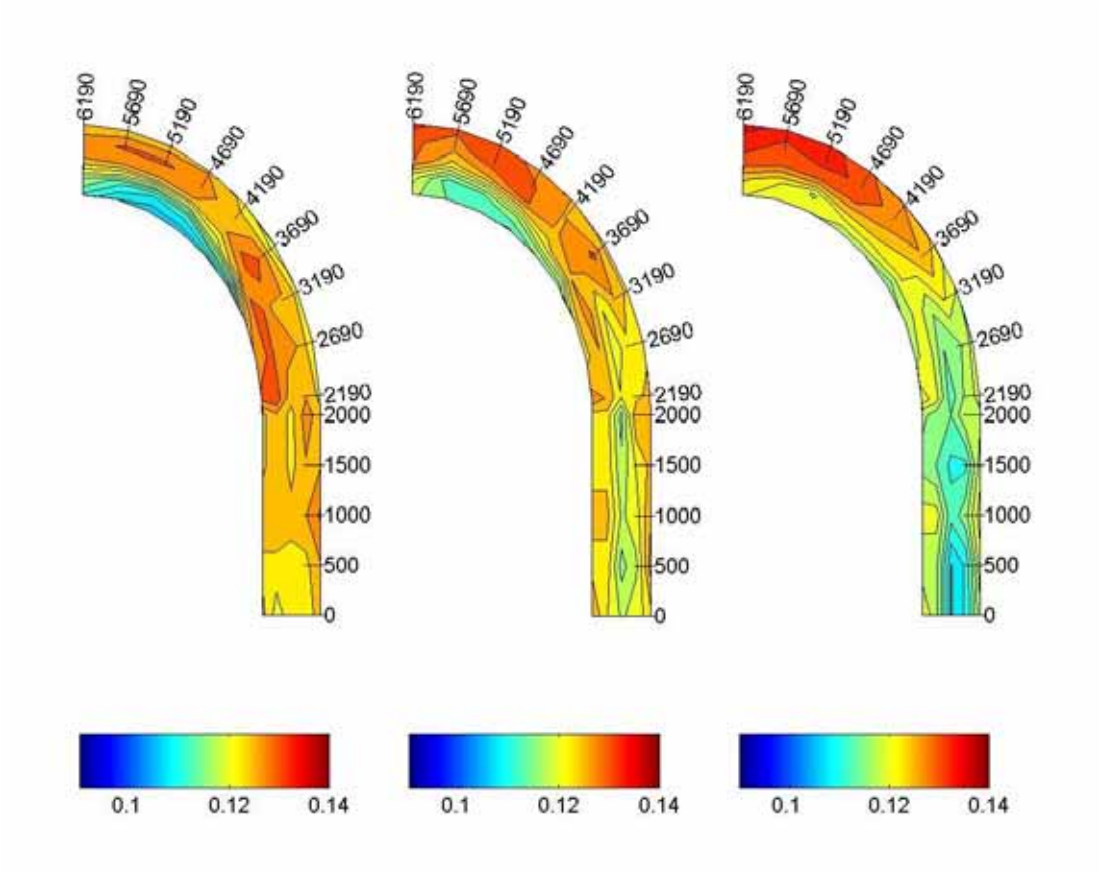

Figure A - 1: Test A1-Velocity distribution in the vertical plane measured at 70, 50 and 30 mm

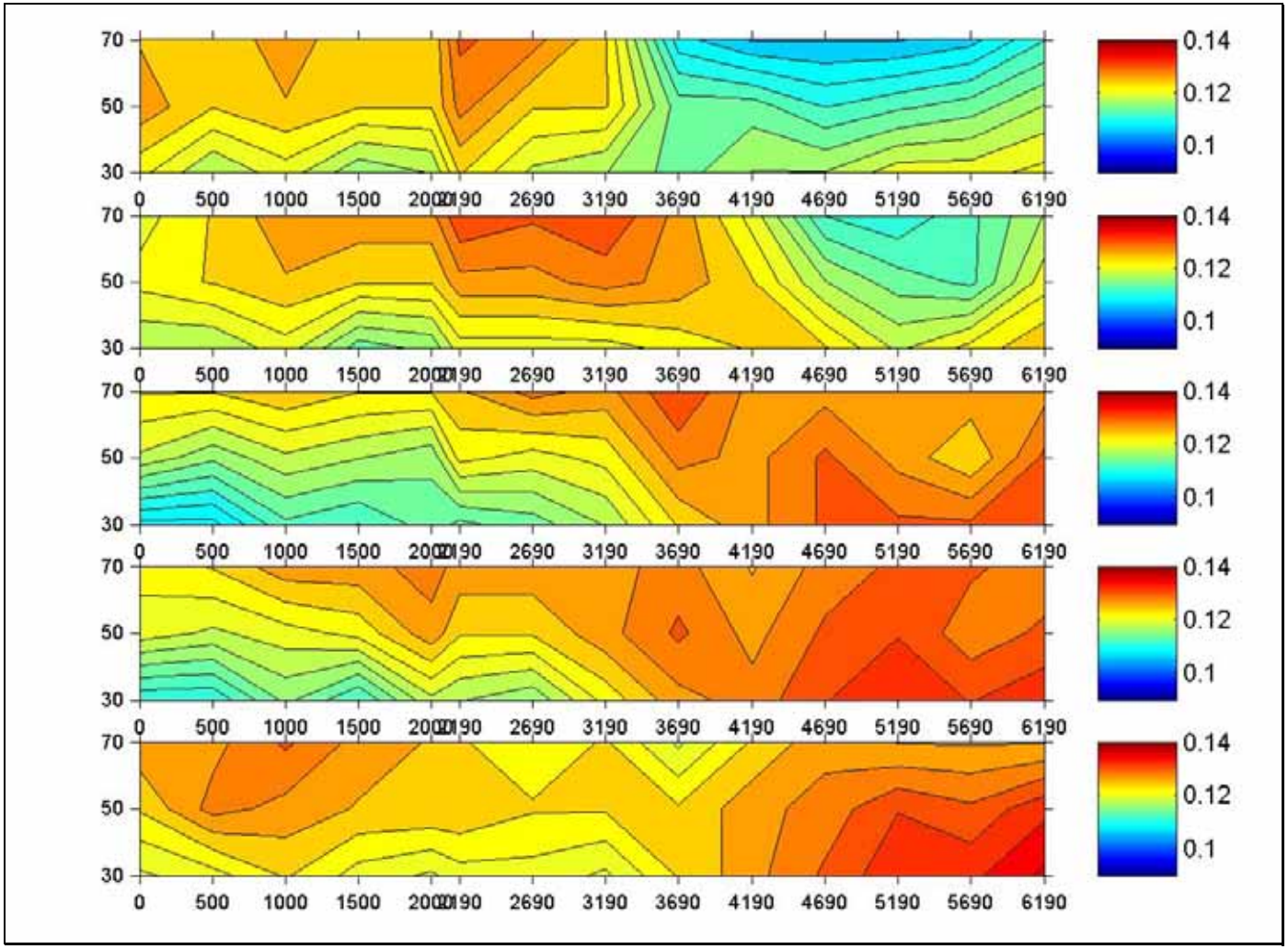

Figure A - 2: Test A1-Velocity distribution in the vertical plane

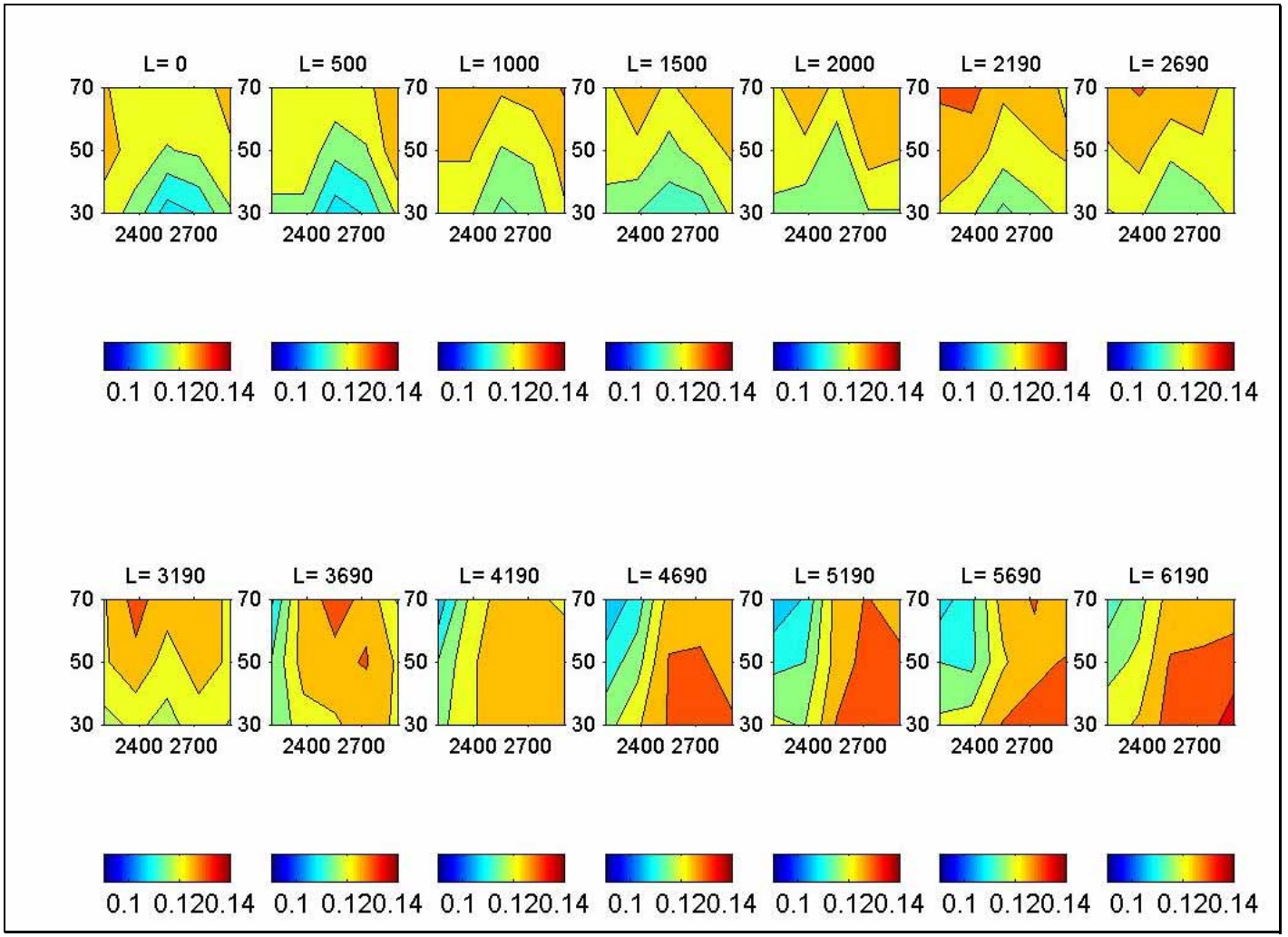

Figure A - 3: Test A1-Cross-sectional velocity distribution

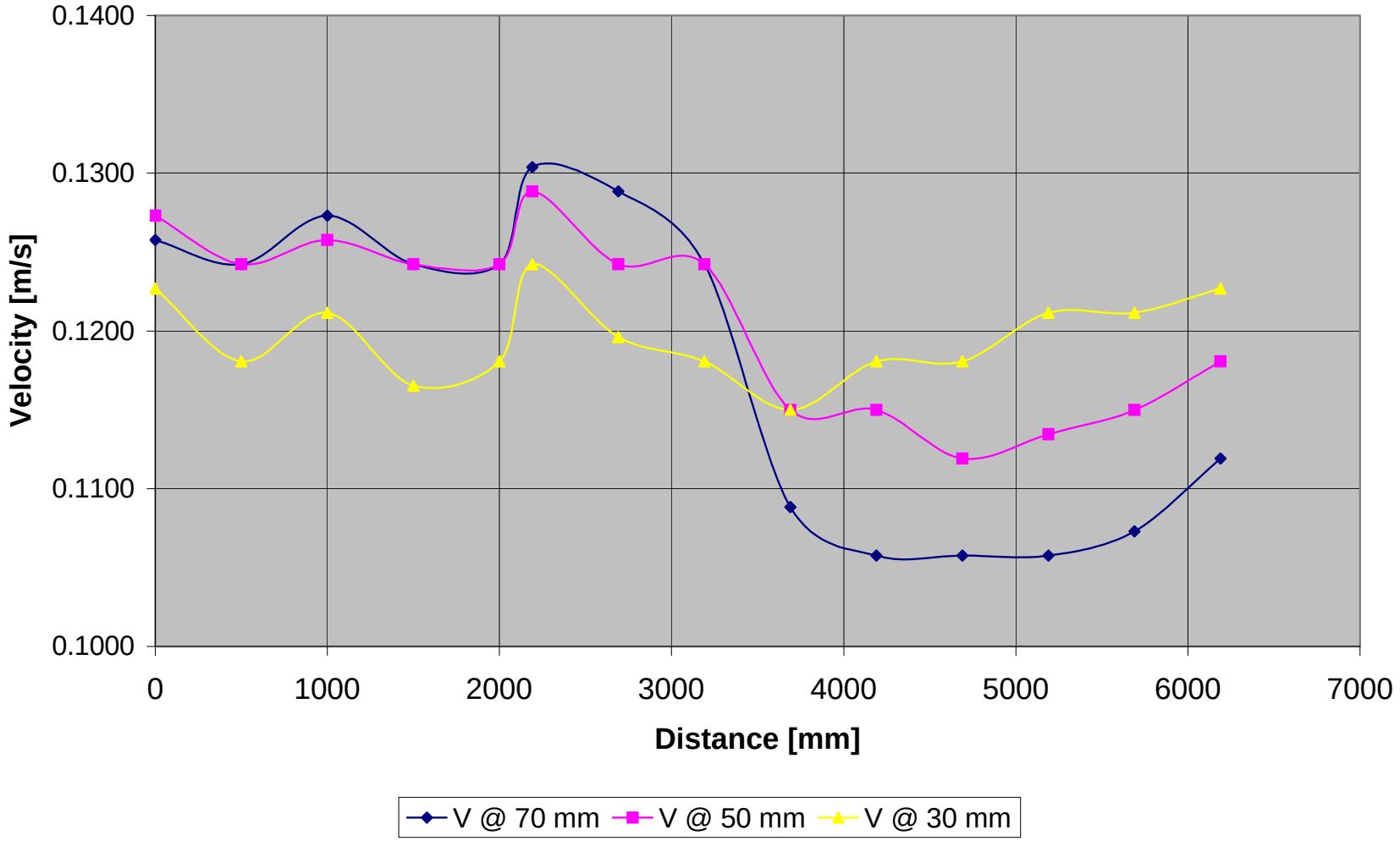

Figure A - 4: Test A1-Vertical velocity distribution measured at 50 mm from inner bank of bend

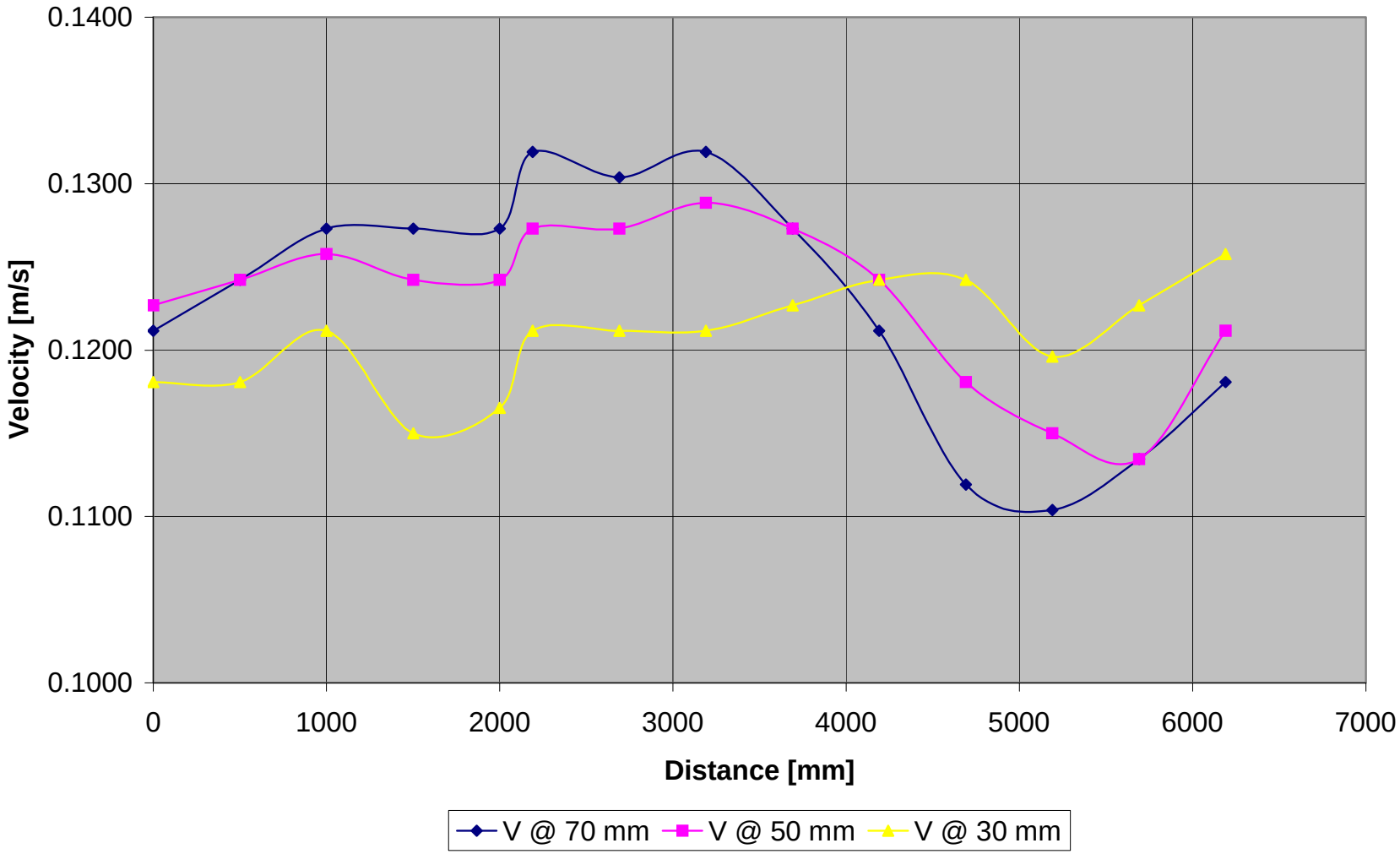

Figure A - 5: Test A1-Vertical velocity distribution measured at 100 mm from inner bank of bend

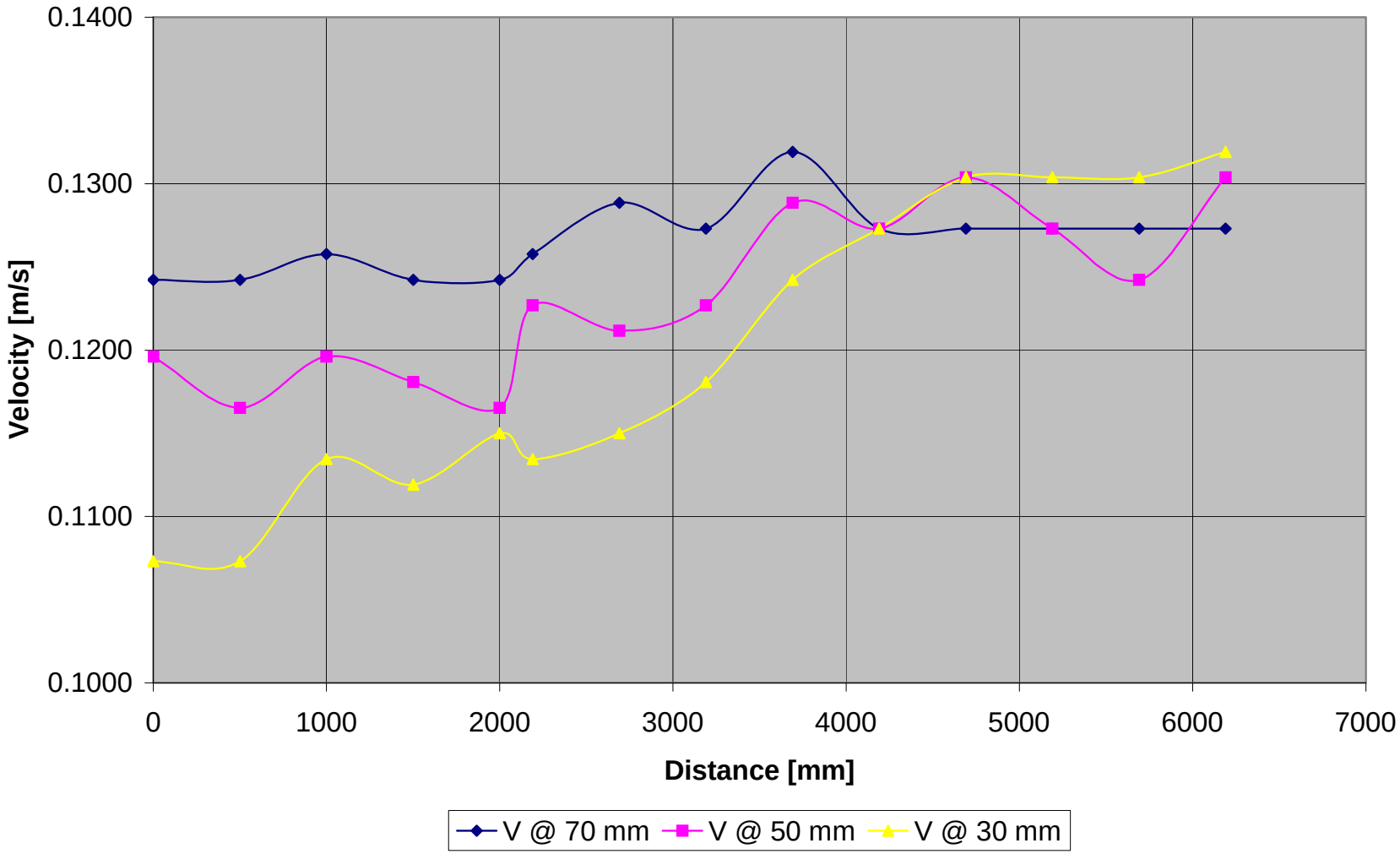

Figure A - 6: Test A1-Vertical velocity distribution measured at 150 mm from inner bank of bend

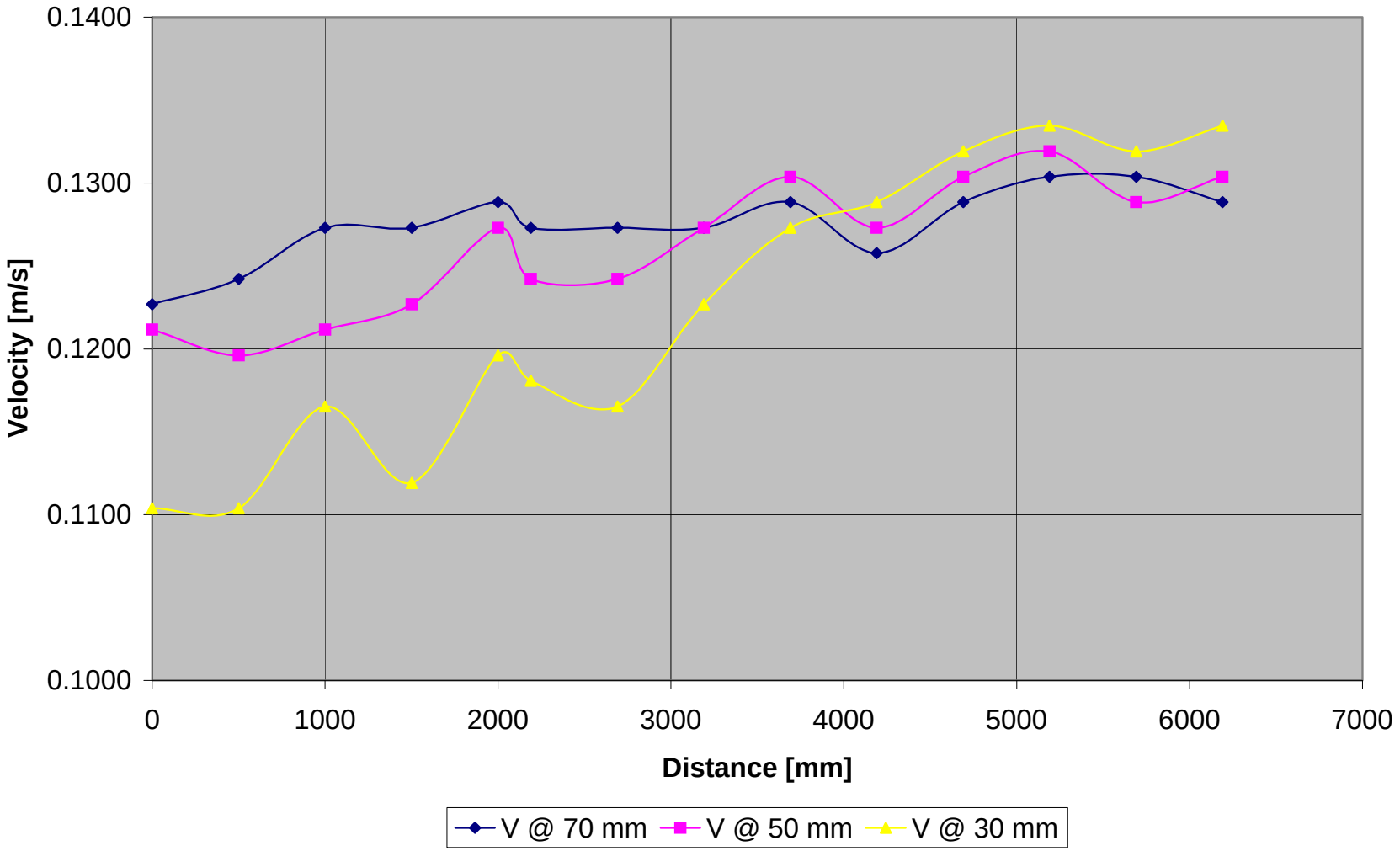

Figure A - 7: Test A1-Vertical velocity distribution measured at 200 mm from inner bank of bend

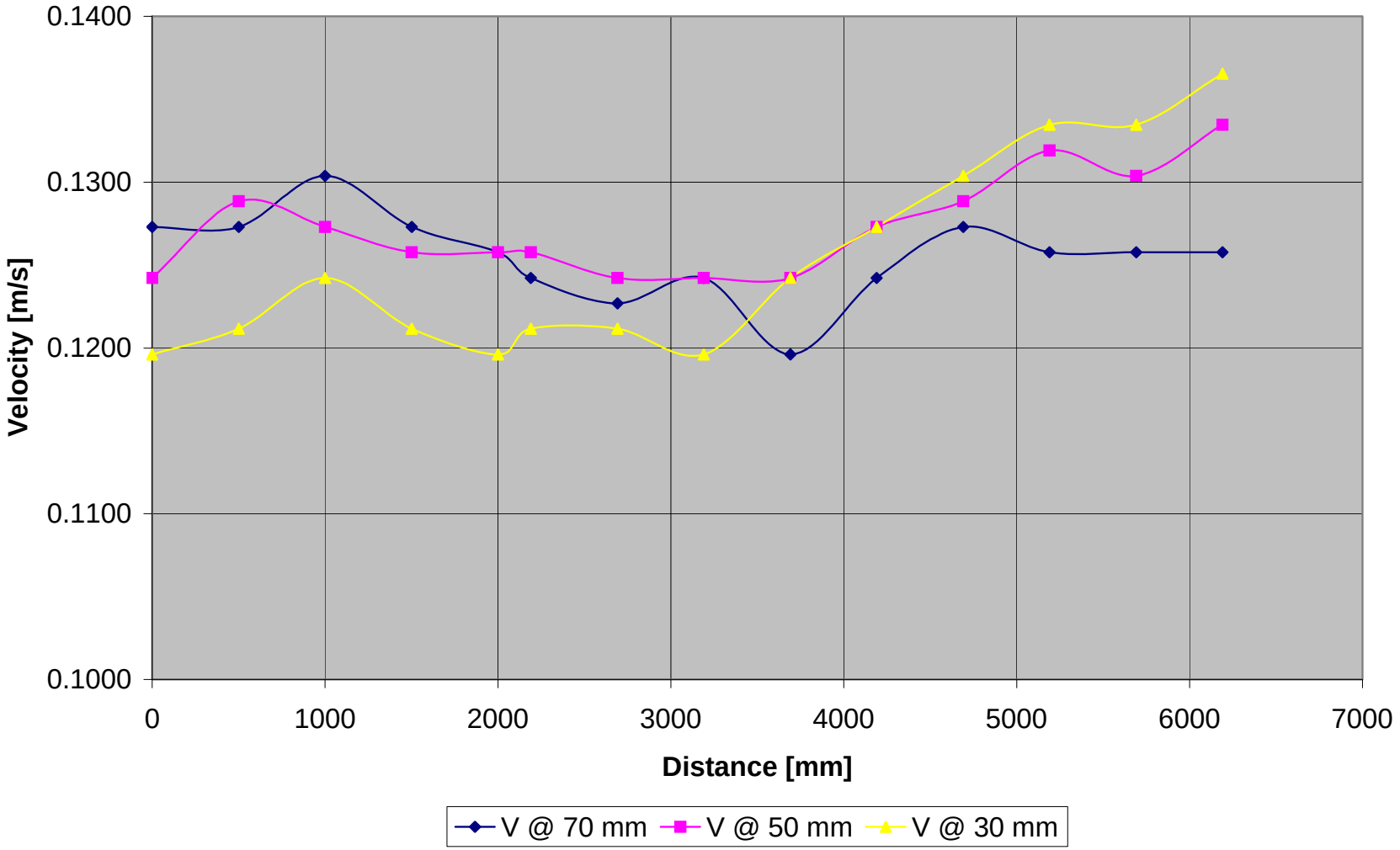

Figure A - 8: Test A1-Vertical velocity distribution measured at 250 mm from inner bank of bend

	Point	1	2	3	4	5	6	7	8	9	10	11	12	13	14
Width	**L**	**0**	**500**	**1000**	**1500**	**2000**	**2190**	**2690**	**3190**	**3690**	**4190**	**4690**	**5190**	**5690**	**6190**
	h														
50	**70**	0.126	0.124	0.127	0.124	0.124	0.130	0.129	0.124	0.109	0.106	0.106	0.106	0.107	0.112
	50	0.127	0.124	0.126	0.124	0.124	0.129	0.124	0.124	0.115	0.115	0.112	0.113	0.115	0.118
	30	0.123	0.118	0.121	0.117	0.118	0.124	0.120	0.118	0.115	0.118	0.118	0.121	0.121	0.123
100	**70**	0.121	0.124	0.127	0.127	0.127	0.132	0.130	0.132	0.127	0.121	0.112	0.110	0.113	0.118
	50	0.123	0.124	0.126	0.124	0.124	0.127	0.127	0.129	0.127	0.124	0.118	0.115	0.113	0.121
	30	0.118	0.118	0.121	0.115	0.117	0.121	0.121	0.121	0.123	0.124	0.124	0.120	0.123	0.126
150	**70**	0.124	0.124	0.126	0.124	0.124	0.126	0.129	0.127	0.132	0.127	0.127	0.127	0.127	0.127
	50	0.120	0.117	0.120	0.118	0.117	0.123	0.121	0.123	0.129	0.127	0.130	0.127	0.124	0.130
	30	0.107	0.107	0.113	0.112	0.115	0.113	0.115	0.118	0.124	0.127	0.130	0.130	0.130	0.132
200	**70**	0.123	0.124	0.127	0.127	0.129	0.127	0.127	0.127	0.129	0.126	0.129	0.130	0.130	0.129
	50	0.121	0.120	0.121	0.123	0.127	0.124	0.124	0.127	0.130	0.127	0.130	0.132	0.129	0.130
	30	0.110	0.110	0.117	0.112	0.120	0.118	0.117	0.123	0.127	0.129	0.132	0.133	0.132	0.133
250															
	70	0.127	0.127	0.130	0.127	0.126	0.124	0.123	0.124	0.120	0.124	0.127	0.126	0.126	0.126
	50	0.124	0.129	0.127	0.126	0.126	0.126	0.124	0.124	0.124	0.127	0.129	0.132	0.130	0.133
	30	0.120	0.121	0.124	0.121	0.120	0.121	0.121	0.120	0.124	0.127	0.130	0.133	0.133	0.137

Table A - 1: Test A1-Measured velocities [m/s]

A.1.1.2 TEST A2 (F_R = 0.3)

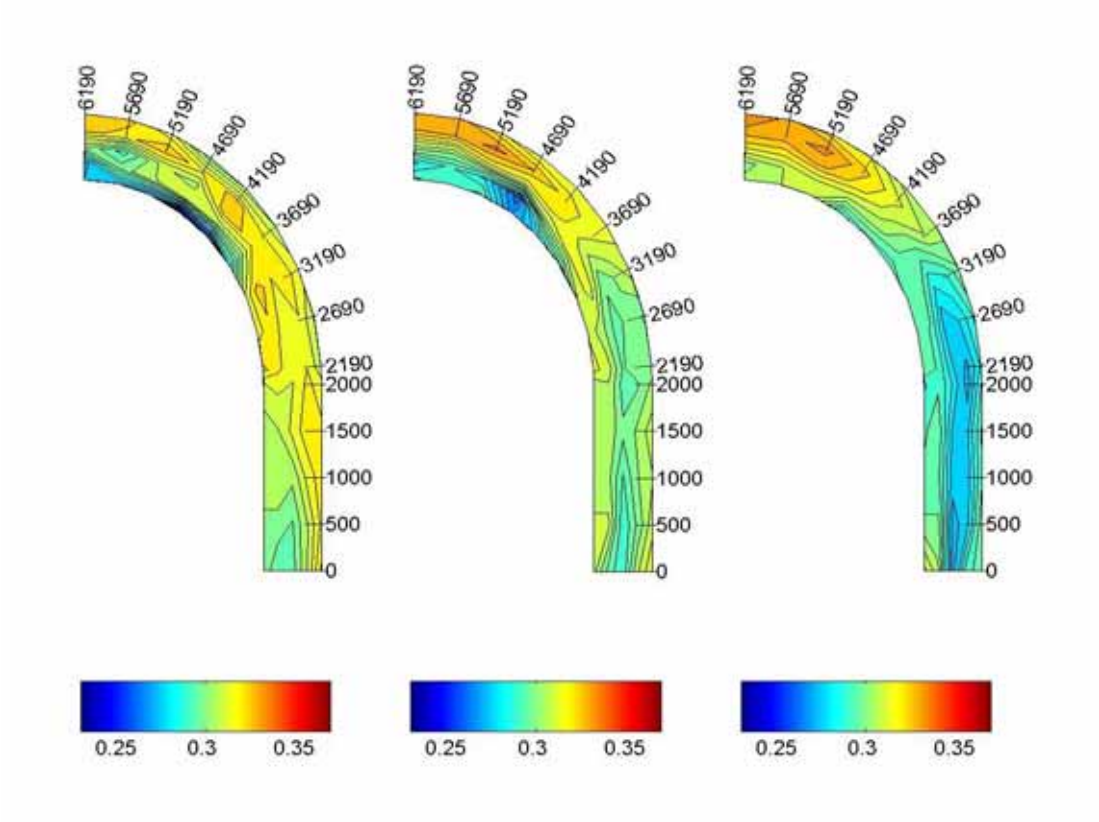

Figure A - 9: Test A2-Velocity distribution in the horisontal plane measured at 70, 50 and 30 mm

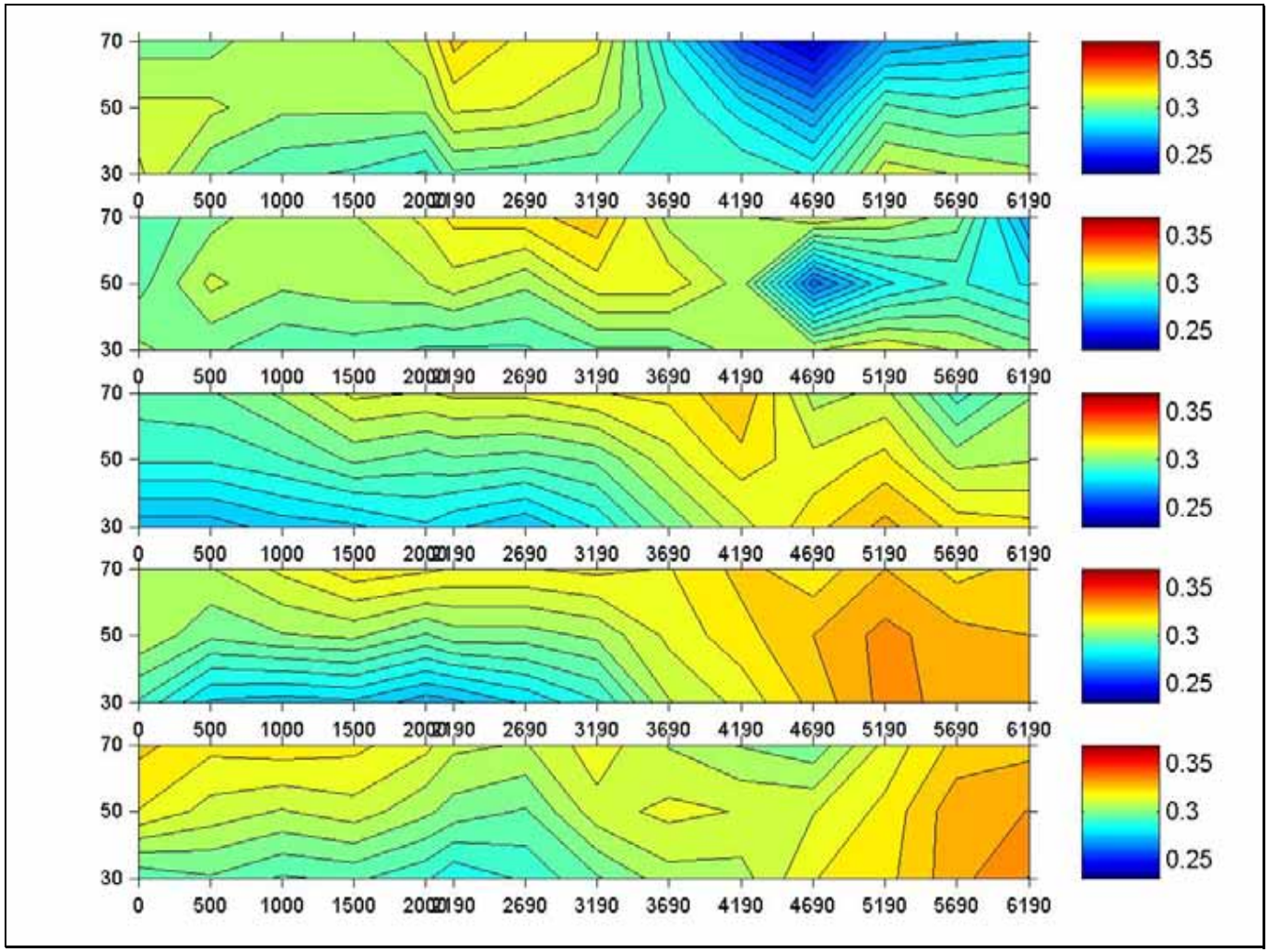

Figure A - 10: Test A2-Velocity distribution in the vertical plane

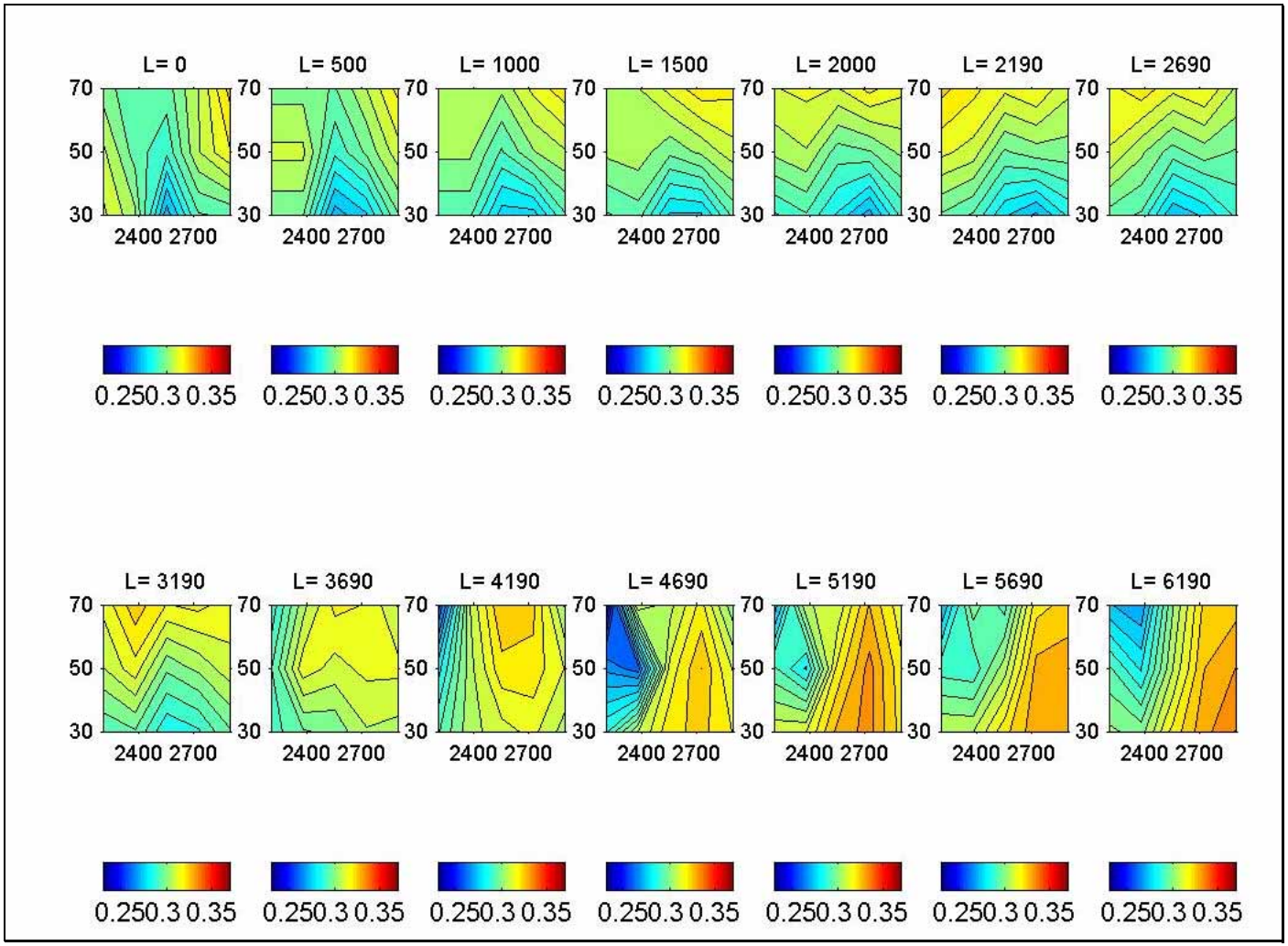

Figure A - 11: Test A2-Cross-sectional velocity distribution

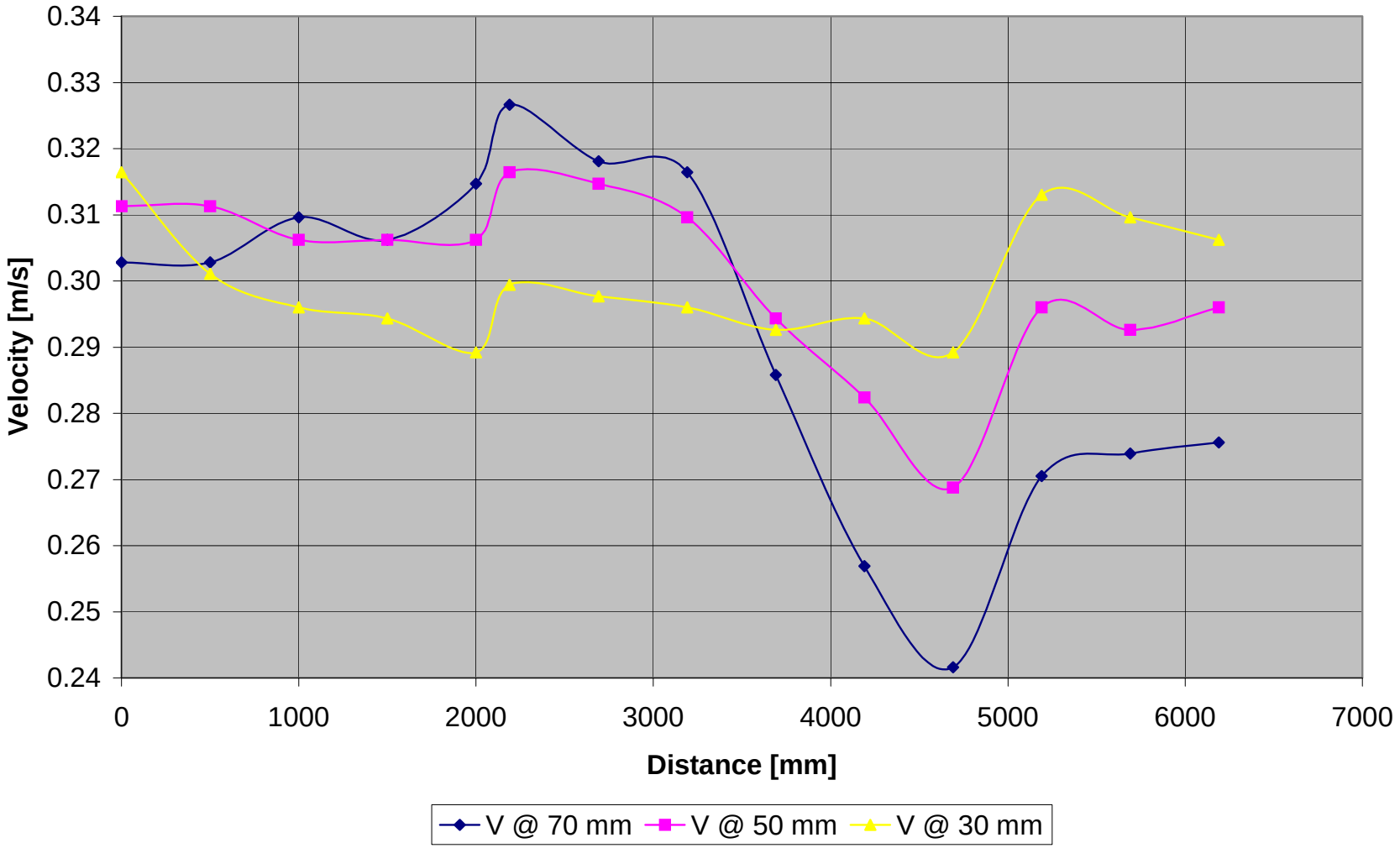

Figure A - 12: Test A2-Vertical velocity distribution measured at 50 mm from inner bank of bend

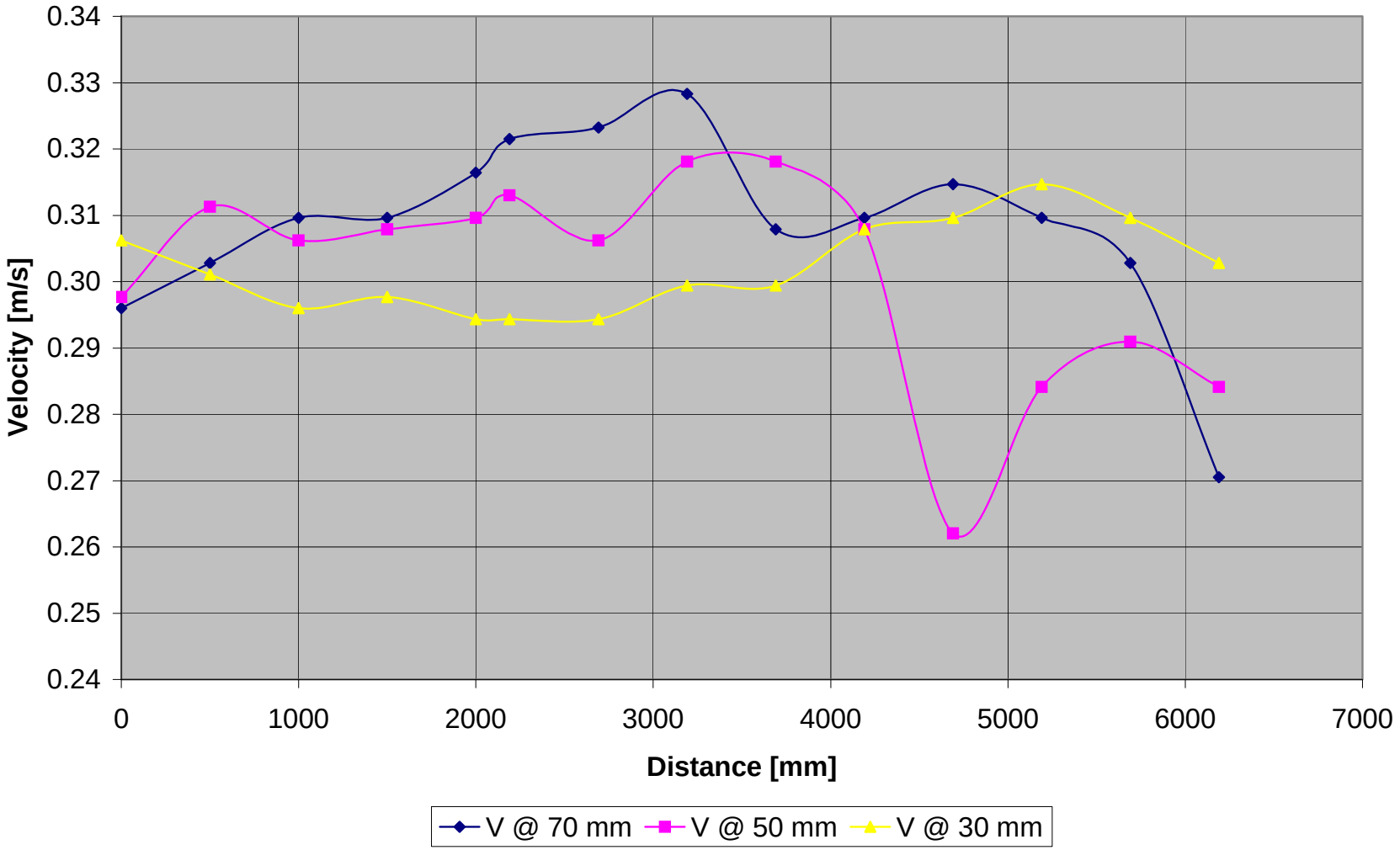

Figure A - 13: Test A2-Vertical velocity distribution measured at 100 mm from inner bank of bend

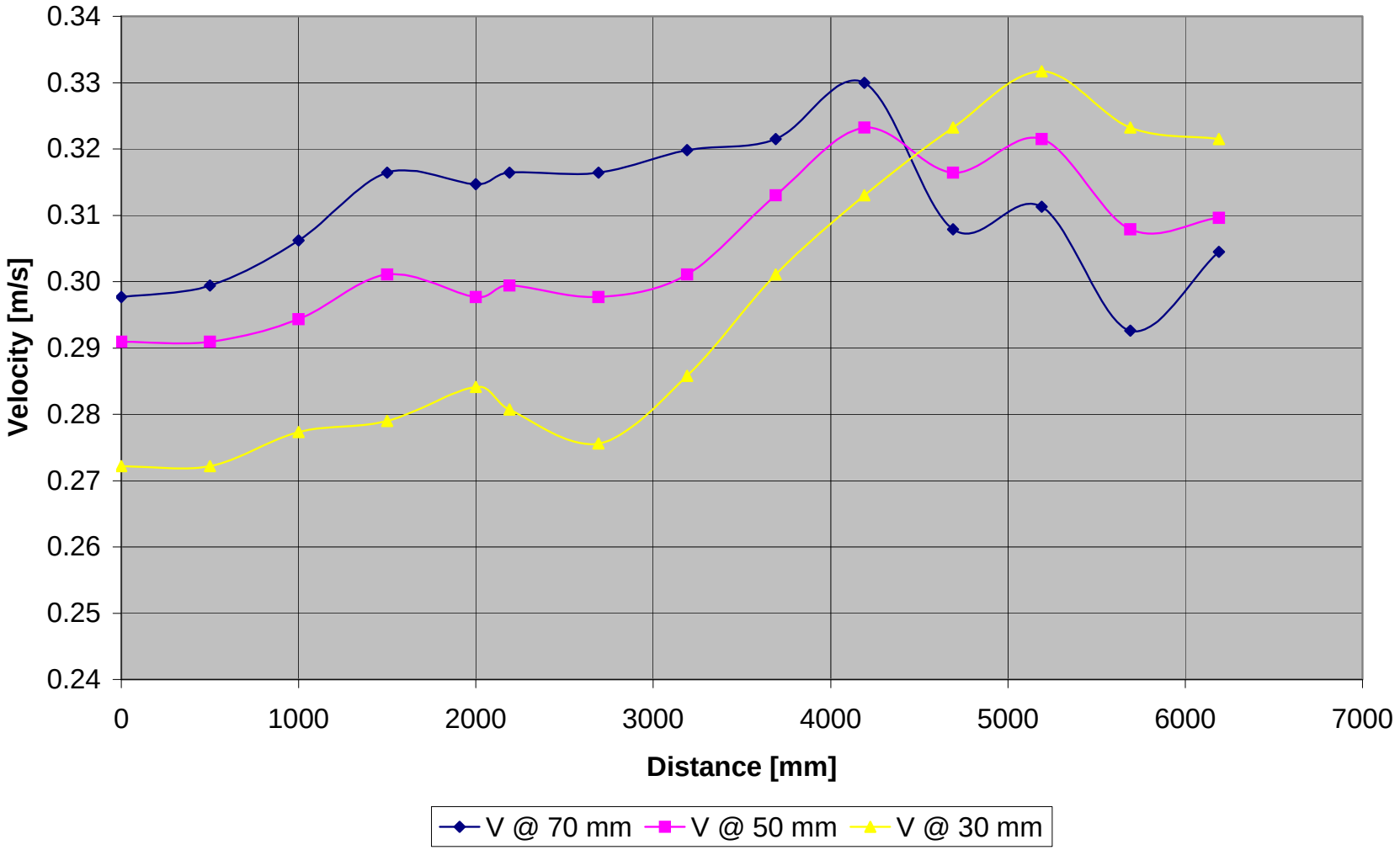

Figure A - 14: Test A2-Vertical velocity distribution measured at 150 mm from inner bank of bend

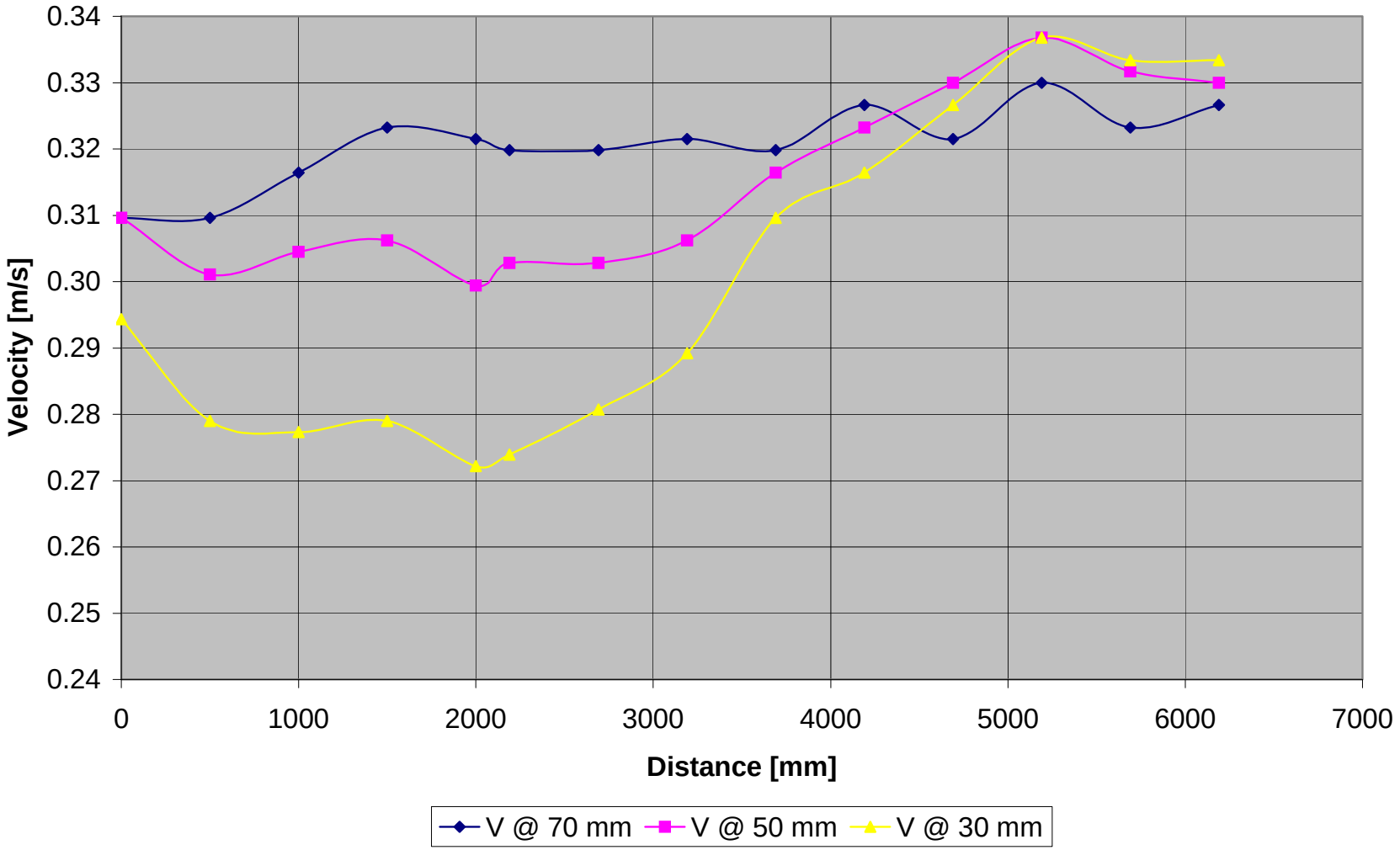

Figure A - 15: Test A2-Vertical velocity distribution measured at 200 mm from inner bank of bend

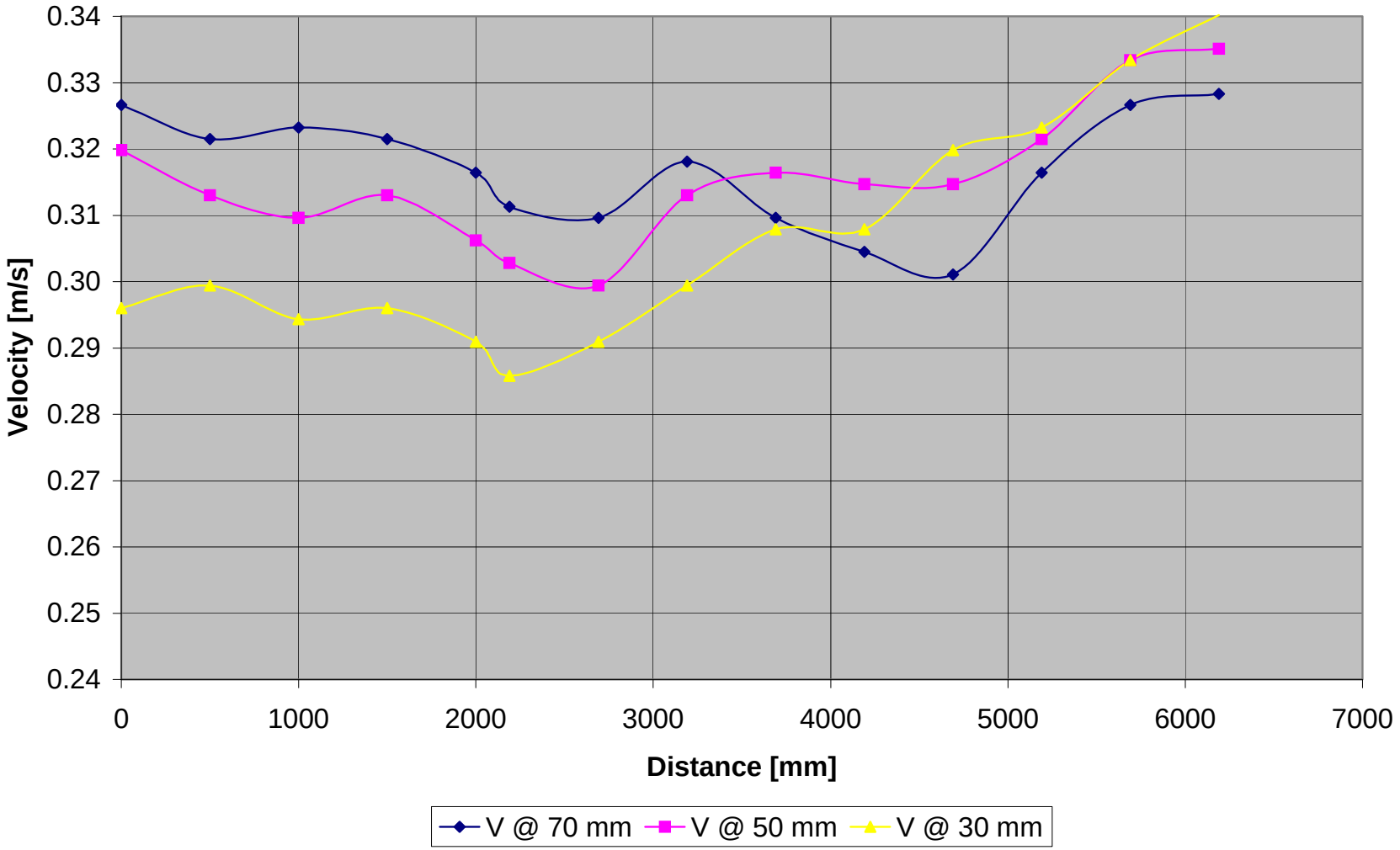

Figure A - 16: Test A2-Vertical velocity distribution measured at 250 mm from inner bank of bend

	Point	1	2	3	4	5	6	7	8	9	10	11	12	13	14
Width	L	0	500	1000	1500	2000	2190	2690	3190	3690	4190	4690	5190	5690	6190
	h														
50	70	0.303	0.303	0.310	0.306	0.315	0.327	0.318	0.316	0.286	0.257	0.242	0.271	0.274	0.276
	50	0.311	0.311	0.306	0.306	0.306	0.316	0.315	0.310	0.294	0.282	0.269	0.296	0.293	0.296
	30	0.316	0.301	0.296	0.294	0.289	0.299	0.298	0.296	0.293	0.294	0.289	0.313	0.310	0.306
100	70	0.296	0.303	0.310	0.310	0.316	0.322	0.323	0.328	0.308	0.310	0.315	0.310	0.303	0.271
	50	0.298	0.311	0.306	0.308	0.310	0.313	0.306	0.318	0.318	0.308	0.262	0.284	0.291	0.284
	30	0.306	0.301	0.296	0.298	0.294	0.294	0.294	0.299	0.299	0.308	0.310	0.315	0.310	0.303
150	70	0.298	0.299	0.306	0.316	0.315	0.316	0.316	0.320	0.322	0.330	0.308	0.311	0.293	0.305
	50	0.291	0.291	0.294	0.301	0.298	0.299	0.298	0.301	0.313	0.323	0.316	0.322	0.308	0.310
	30	0.272	0.272	0.277	0.279	0.284	0.281	0.276	0.286	0.301	0.313	0.323	0.332	0.323	0.322
200	70	0.310	0.310	0.316	0.323	0.322	0.320	0.320	0.322	0.320	0.327	0.322	0.330	0.323	0.327
	50	0.310	0.301	0.305	0.306	0.299	0.303	0.303	0.306	0.316	0.323	0.330	0.337	0.332	0.330
	30	0.294	0.279	0.277	0.279	0.272	0.274	0.281	0.289	0.310	0.316	0.327	0.337	0.333	0.333
250															
	70	0.327	0.322	0.323	0.322	0.316	0.311	0.310	0.318	0.310	0.305	0.301	0.316	0.327	0.328
	50	0.320	0.313	0.310	0.313	0.306	0.303	0.299	0.313	0.316	0.315	0.315	0.322	0.333	0.335
	30	0.296	0.299	0.294	0.296	0.291	0.286	0.291	0.299	0.308	0.308	0.320	0.323	0.333	0.340

Table A - 2: Test A2-Measured velocities [m/s]

A.1.1.3 TEST A3 (F_R = 0.5)

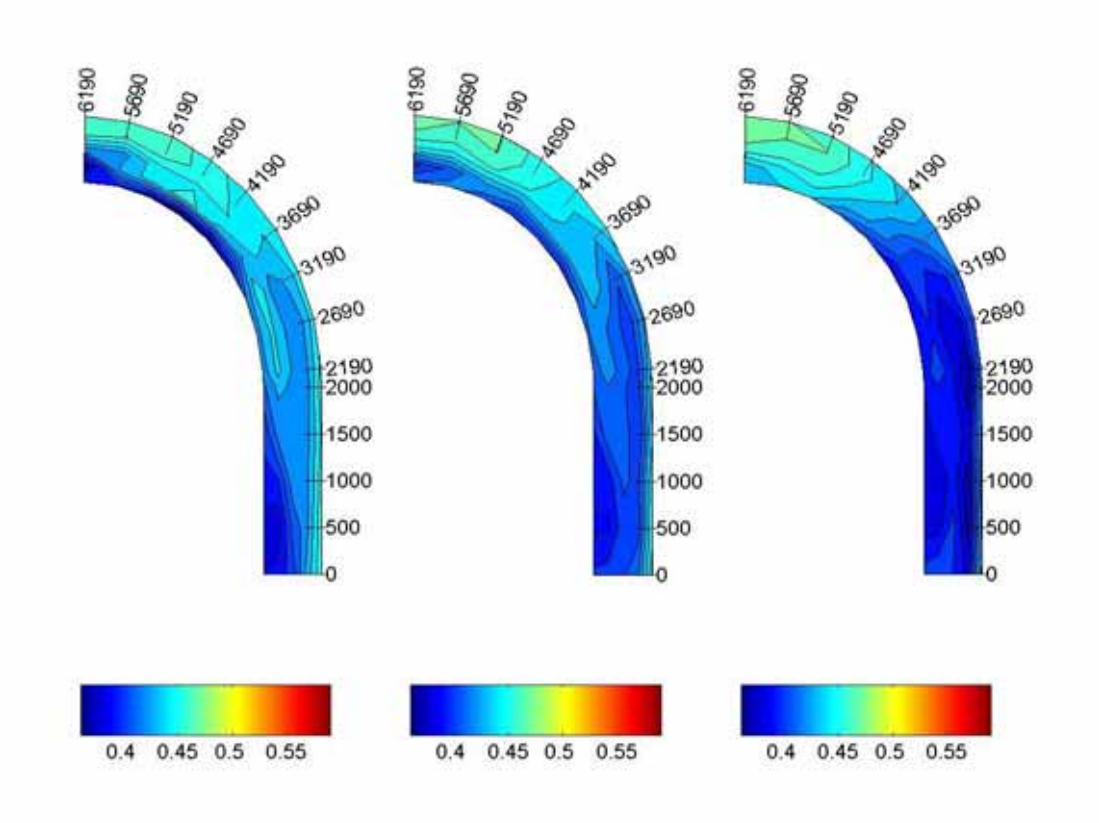

Figure A - 17: Test A3-Velocity distribution in the horizontal plane measured at 70, 50 and 30 mm

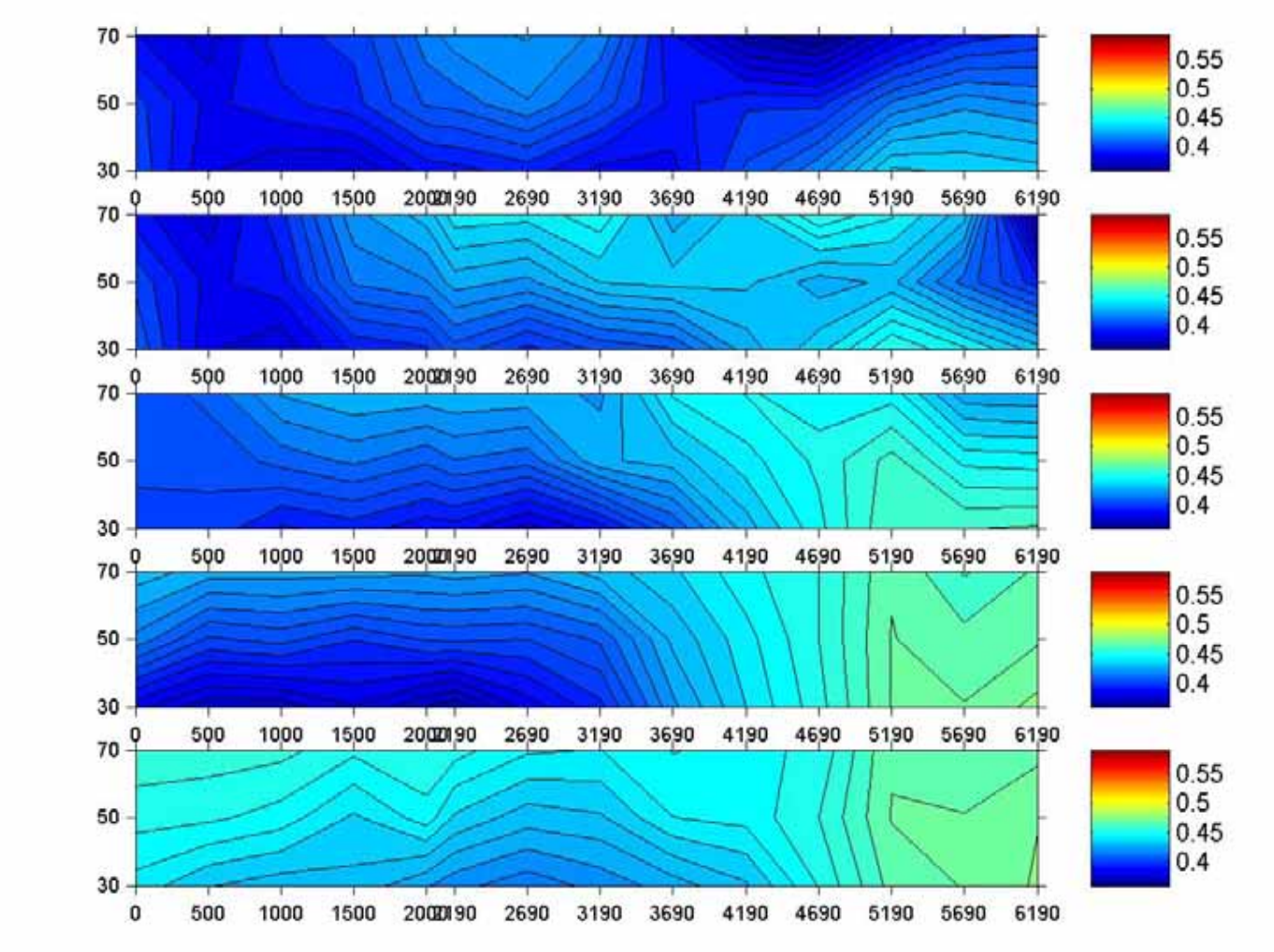

Figure A - 18: Test A3-Velocity distribution in the vertical plane

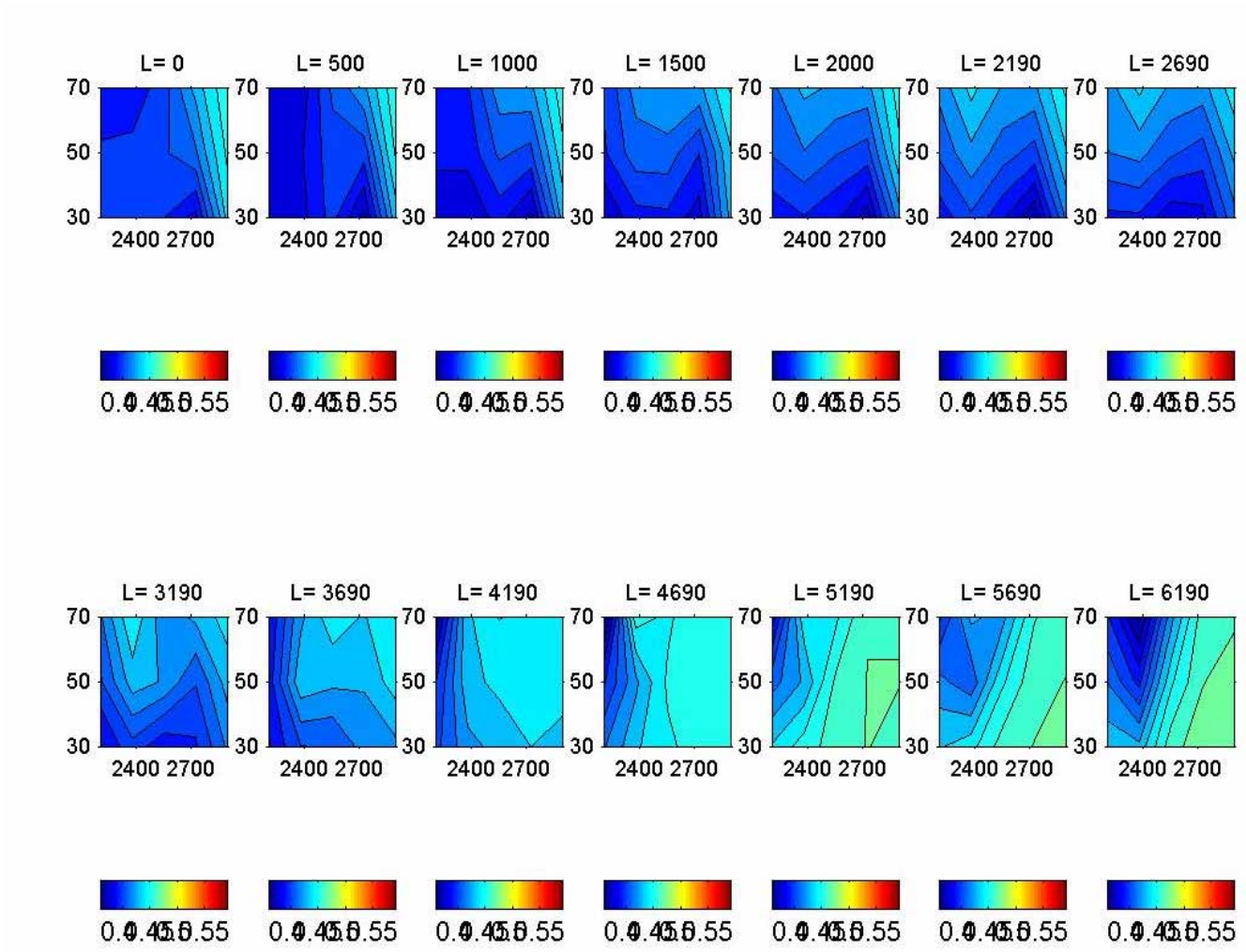

Figure A - 19: Test A3-Cross-sectional velocity distribution

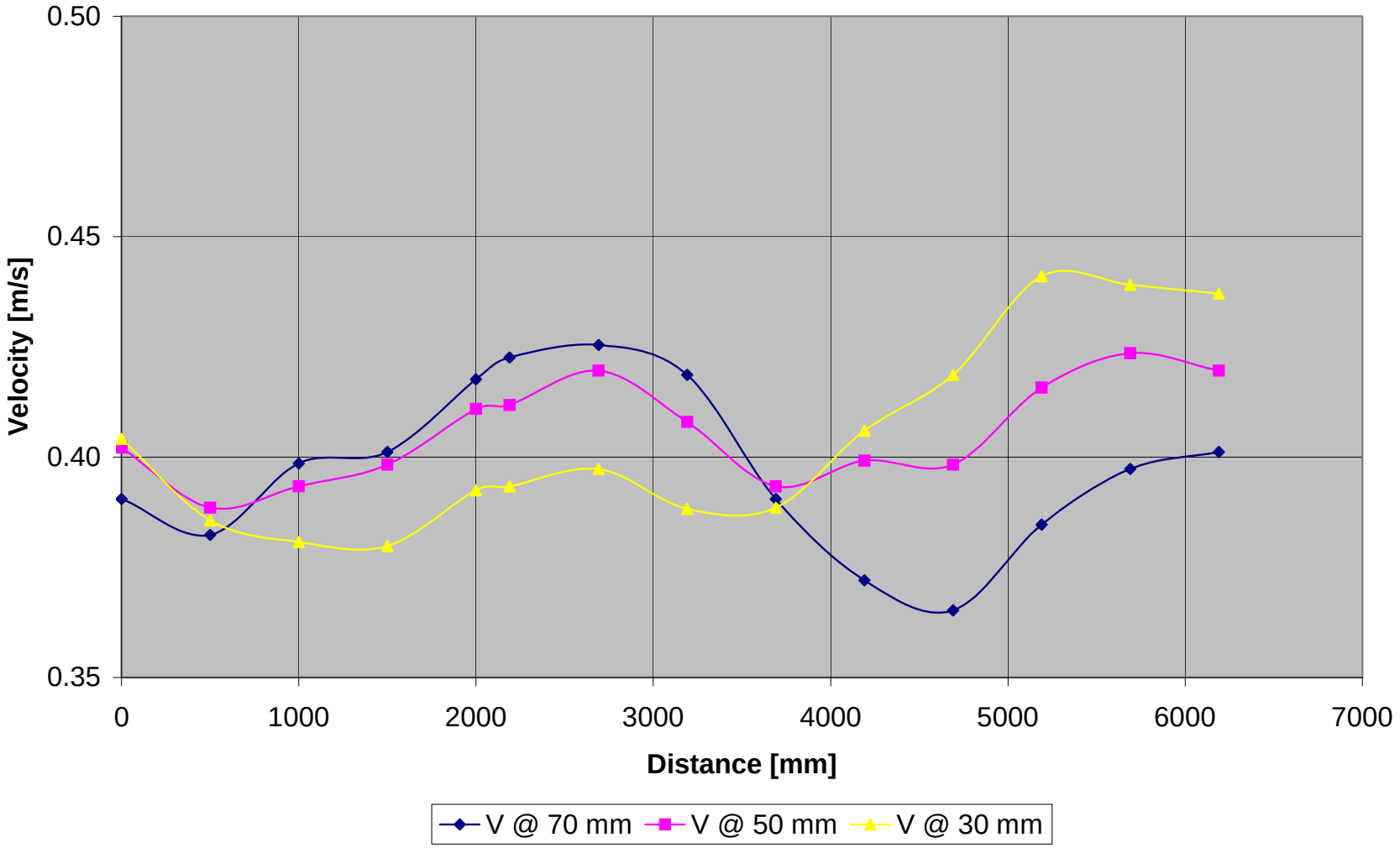

Figure A - 20: Test A3-Vertical velocity distribution measured at 50 mm from inner bank of bend

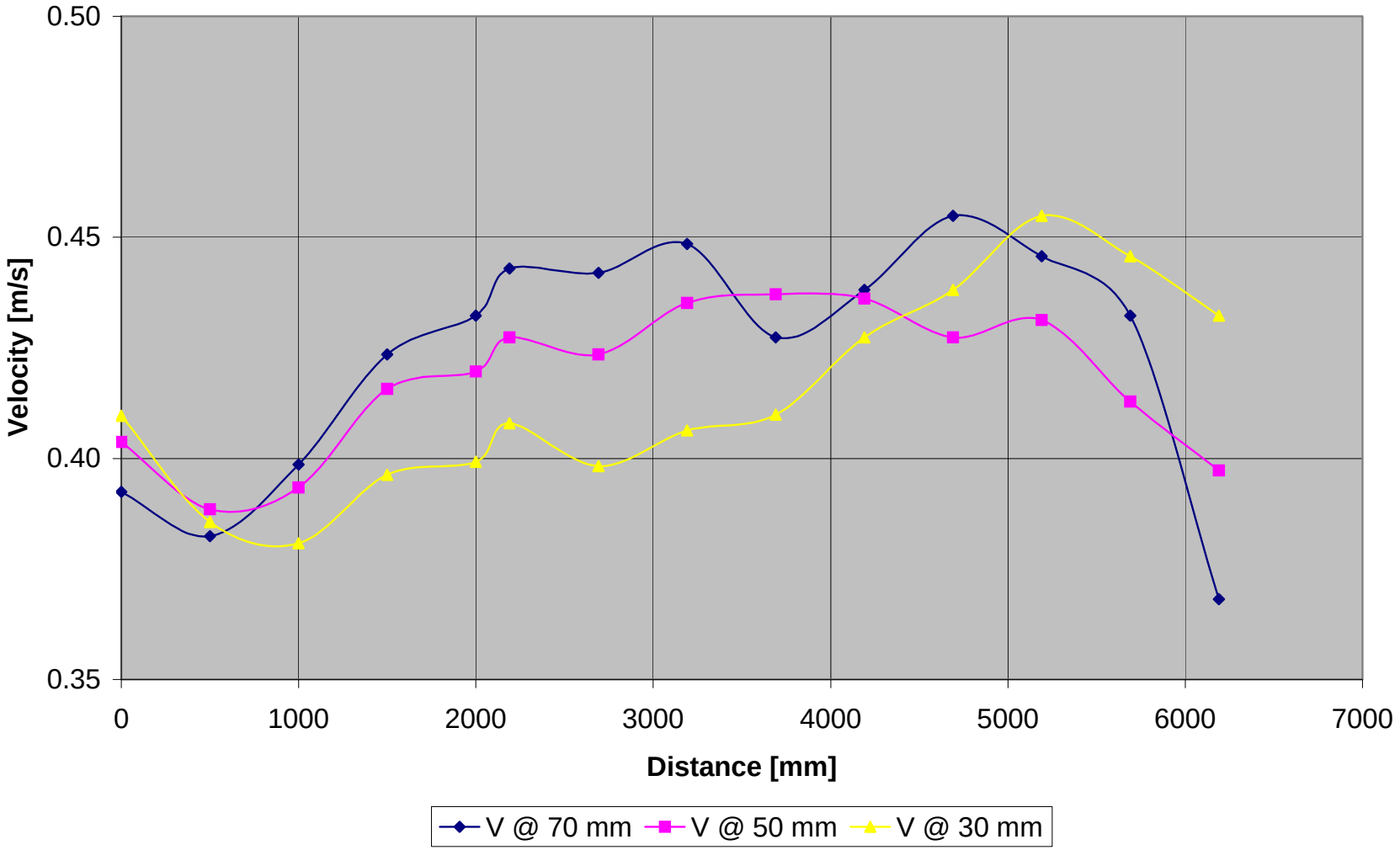

Figure A - 21: Test A3-Vertical velocity distribution measured at 100 mm from inner bank of bend

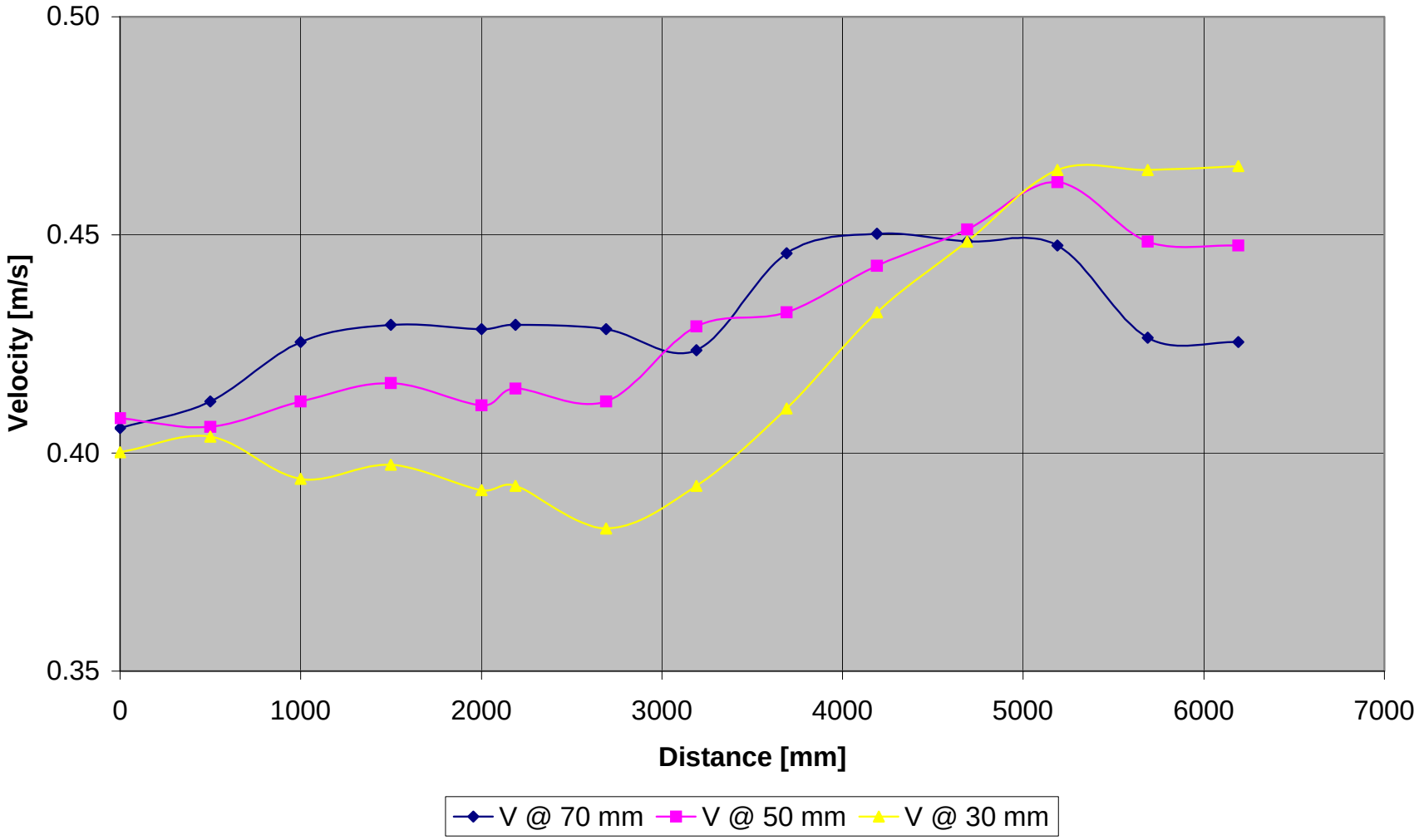

Figure A - 22: Test A3-Vertical velocity distribution measured at 150 mm from inner bank of bend

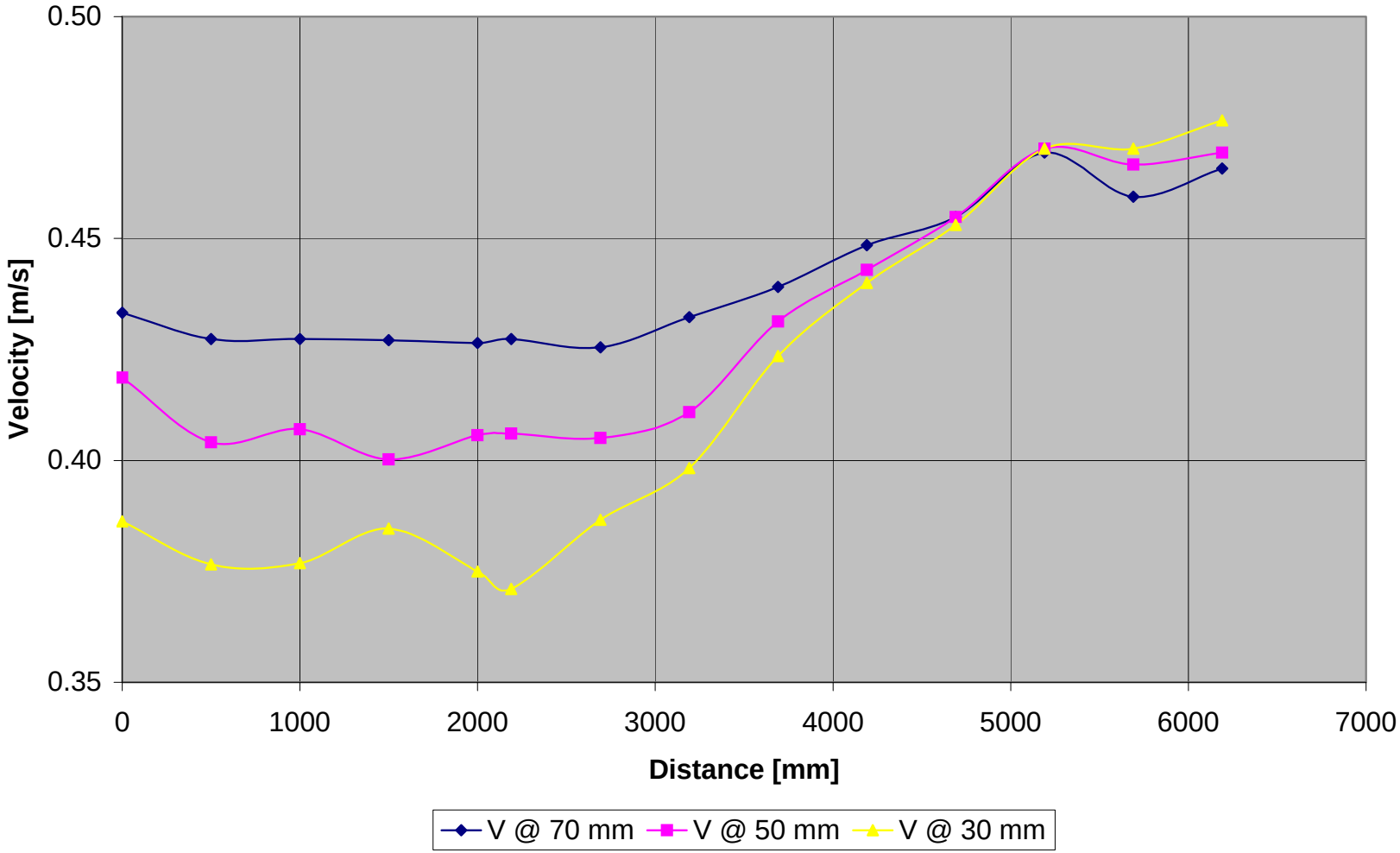

Figure A - 23: Test A3-Vertical velocity distribution measured at 200 mm from inner bank of bend

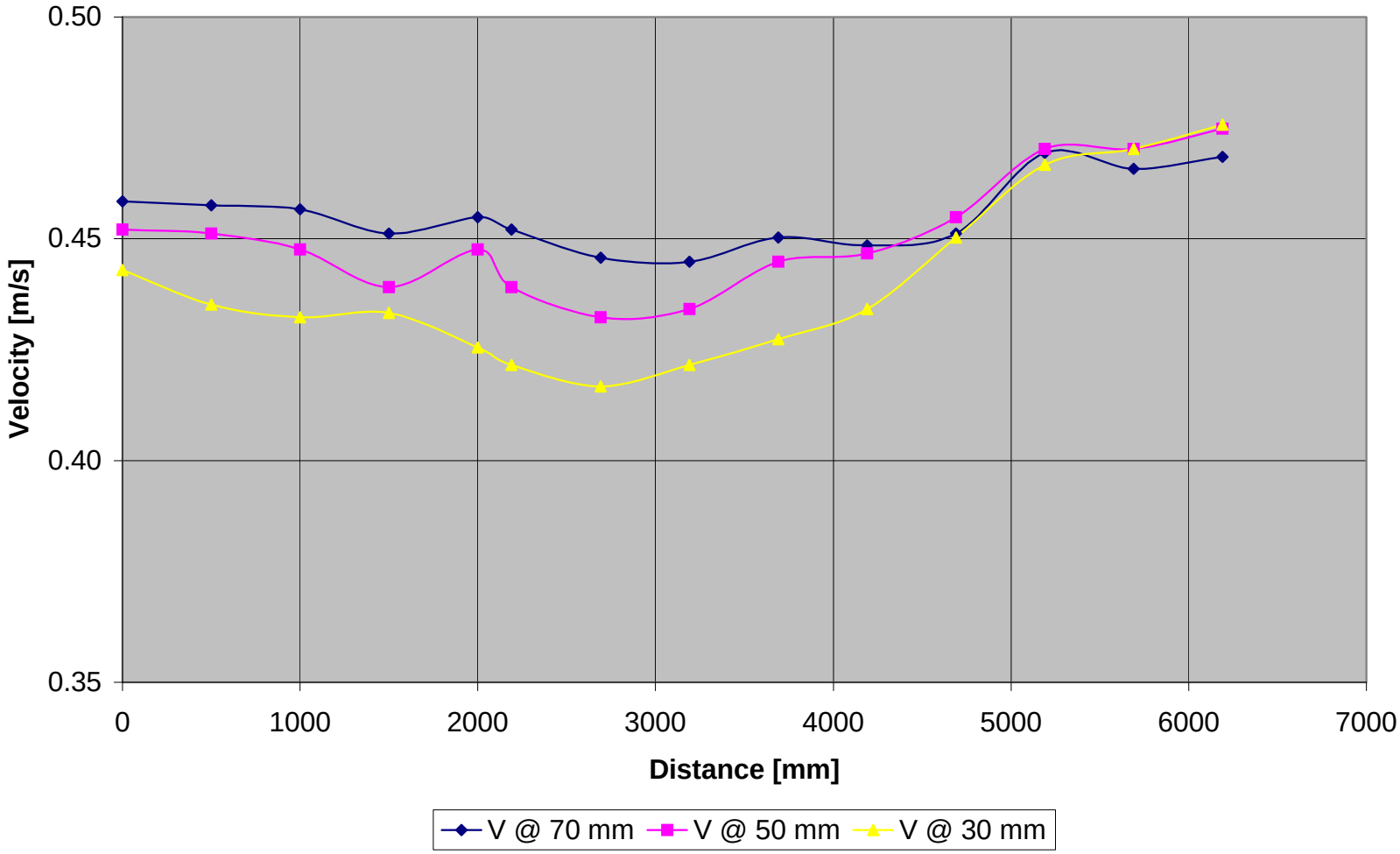

Figure A - 24: Test A3-Vertical velocity distribution measured at 250 mm from inner bank of bend

	Point	1	2	3	4	5	6	7	8	9	10	11	12	13	14
Width	L	0	500	1000	1500	2000	2190	2690	3190	3690	4190	4690	5190	5690	6190
	h														
50	70	0.390	0.382	0.399	0.401	0.418	0.423	0.425	0.419	0.390	0.372	0.365	0.385	0.397	0.401
	50	0.402	0.389	0.393	0.398	0.411	0.412	0.420	0.408	0.393	0.399	0.398	0.416	0.424	0.420
	30	0.404	0.386	0.381	0.380	0.392	0.393	0.397	0.388	0.389	0.406	0.419	0.441	0.439	0.437
100	70	0.392	0.382	0.399	0.424	0.432	0.443	0.442	0.448	0.427	0.438	0.455	0.446	0.432	0.368
	50	0.404	0.389	0.393	0.416	0.420	0.427	0.424	0.435	0.437	0.436	0.427	0.431	0.413	0.397
	30	0.410	0.386	0.381	0.396	0.399	0.408	0.398	0.406	0.410	0.427	0.438	0.455	0.446	0.432
150	70	0.406	0.412	0.425	0.429	0.428	0.429	0.428	0.424	0.446	0.450	0.448	0.448	0.426	0.425
	50	0.408	0.406	0.412	0.416	0.411	0.415	0.412	0.429	0.432	0.443	0.451	0.462	0.448	0.448
	30	0.400	0.404	0.394	0.397	0.391	0.392	0.383	0.392	0.410	0.432	0.448	0.465	0.465	0.466
200	70	0.433	0.427	0.427	0.427	0.426	0.427	0.425	0.432	0.439	0.448	0.455	0.469	0.459	0.466
	50	0.419	0.404	0.407	0.400	0.406	0.406	0.405	0.411	0.431	0.443	0.455	0.470	0.467	0.469
	30	0.386	0.377	0.377	0.385	0.375	0.371	0.387	0.398	0.424	0.440	0.453	0.470	0.470	0.477
250															
	70	0.458	0.458	0.457	0.451	0.455	0.452	0.446	0.445	0.450	0.448	0.451	0.469	0.466	0.468
	50	0.452	0.451	0.448	0.439	0.448	0.439	0.432	0.434	0.445	0.447	0.455	0.470	0.470	0.475
	30	0.443	0.435	0.432	0.433	0.425	0.422	0.417	0.422	0.427	0.434	0.450	0.467	0.470	0.476

Table A - 3: Test A3-Measured velocities [m/s]

A.1.1.4 TEST A4 (F_R = 0.7)

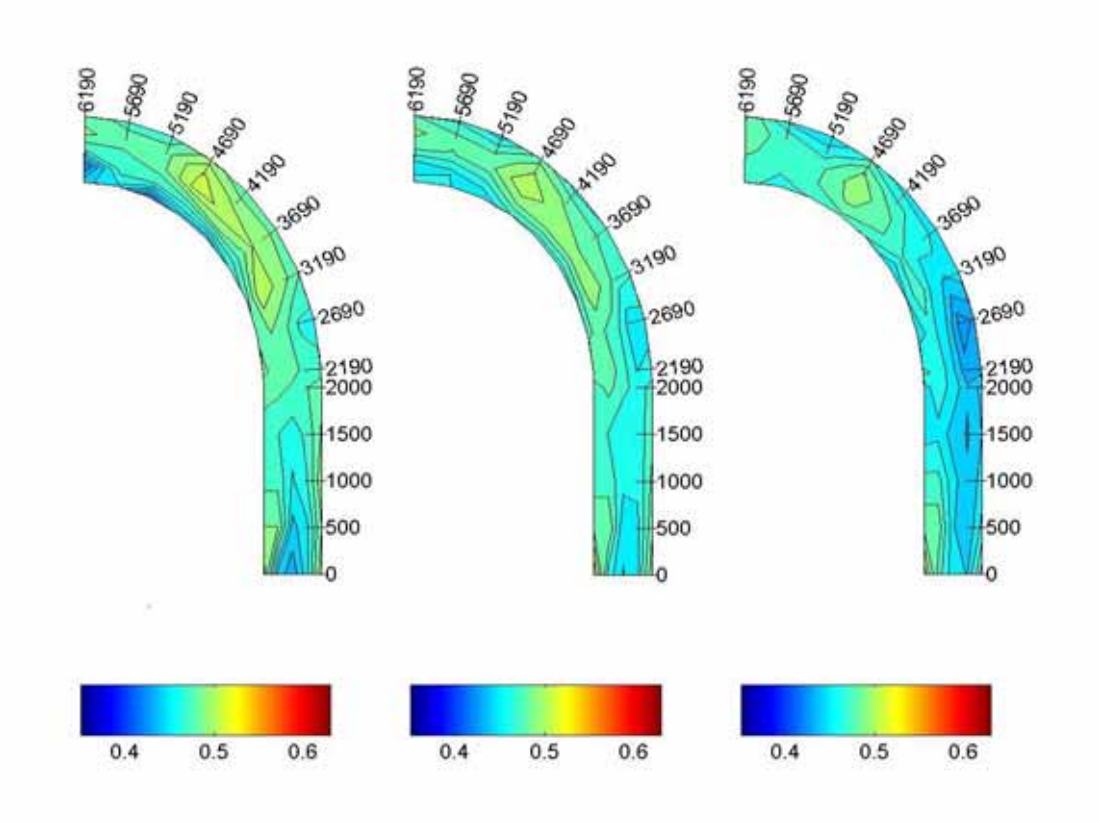

Figure A - 25: Test A4-Velocity distribution in the horisontal plane measured at 70, 50 and 30 mm

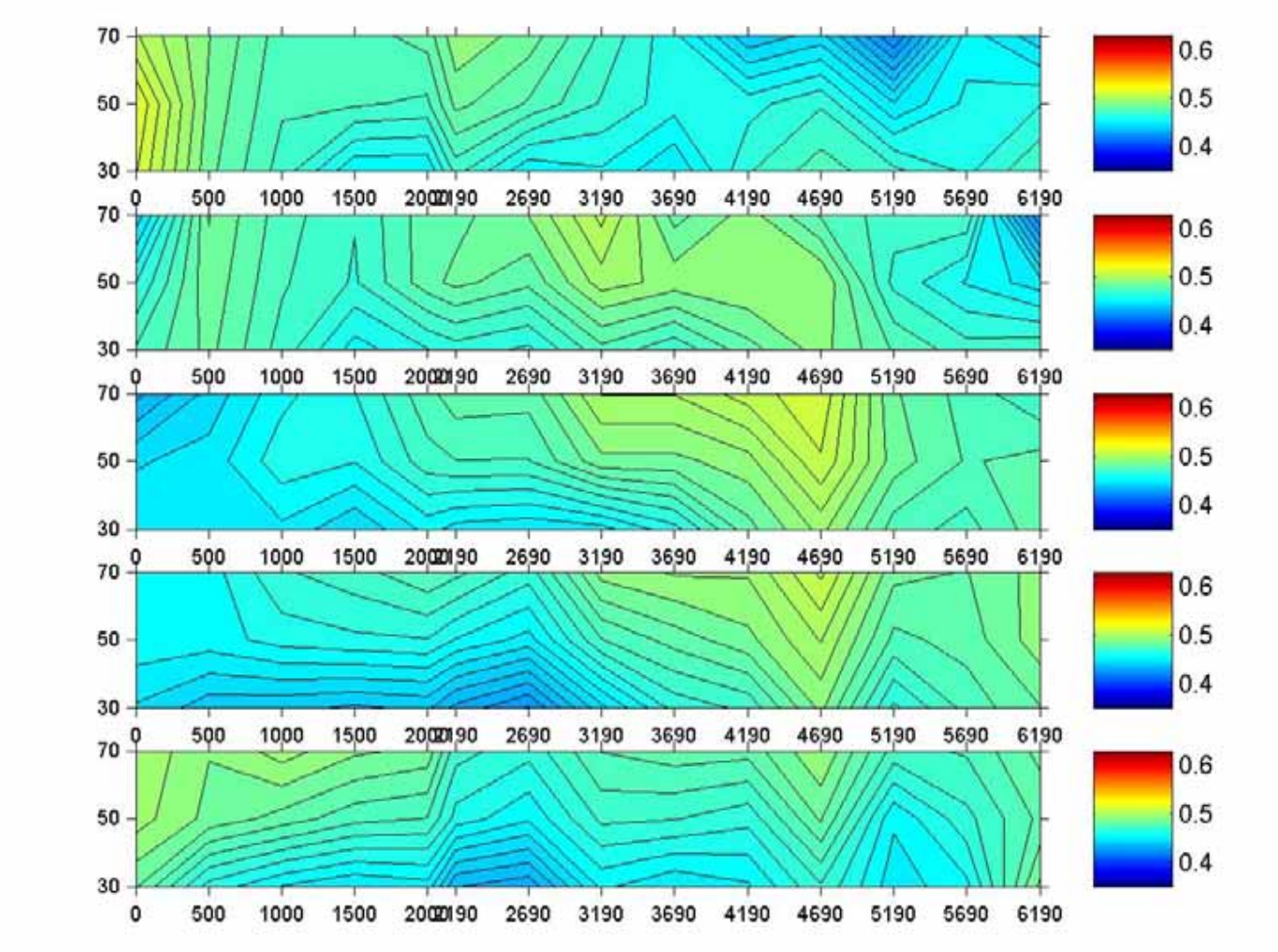

Figure A - 26: Test A4-Velocity distribution in the vertical plane

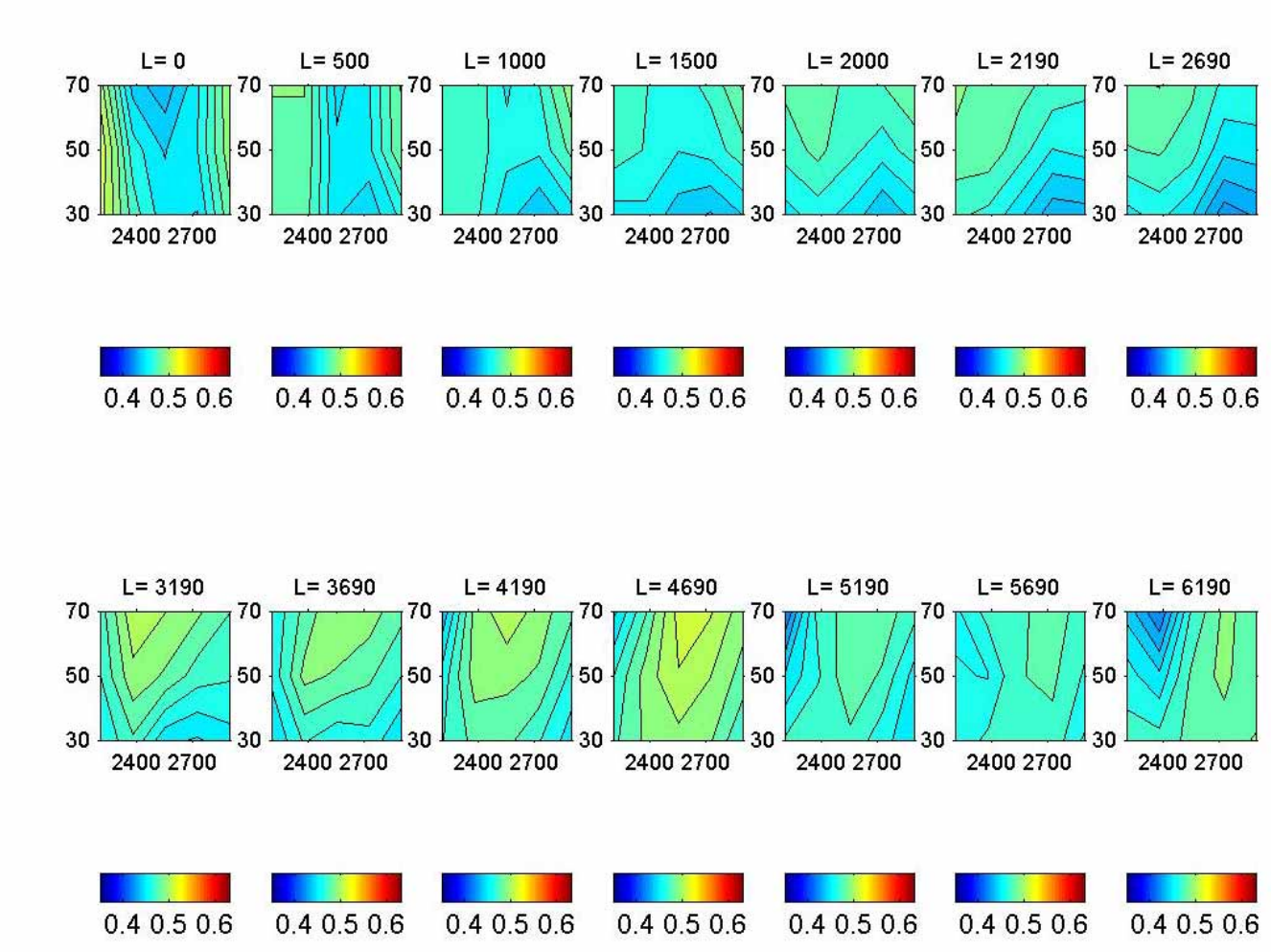

Figure A - 27: Test A4-Cross-sectional velocity distribution

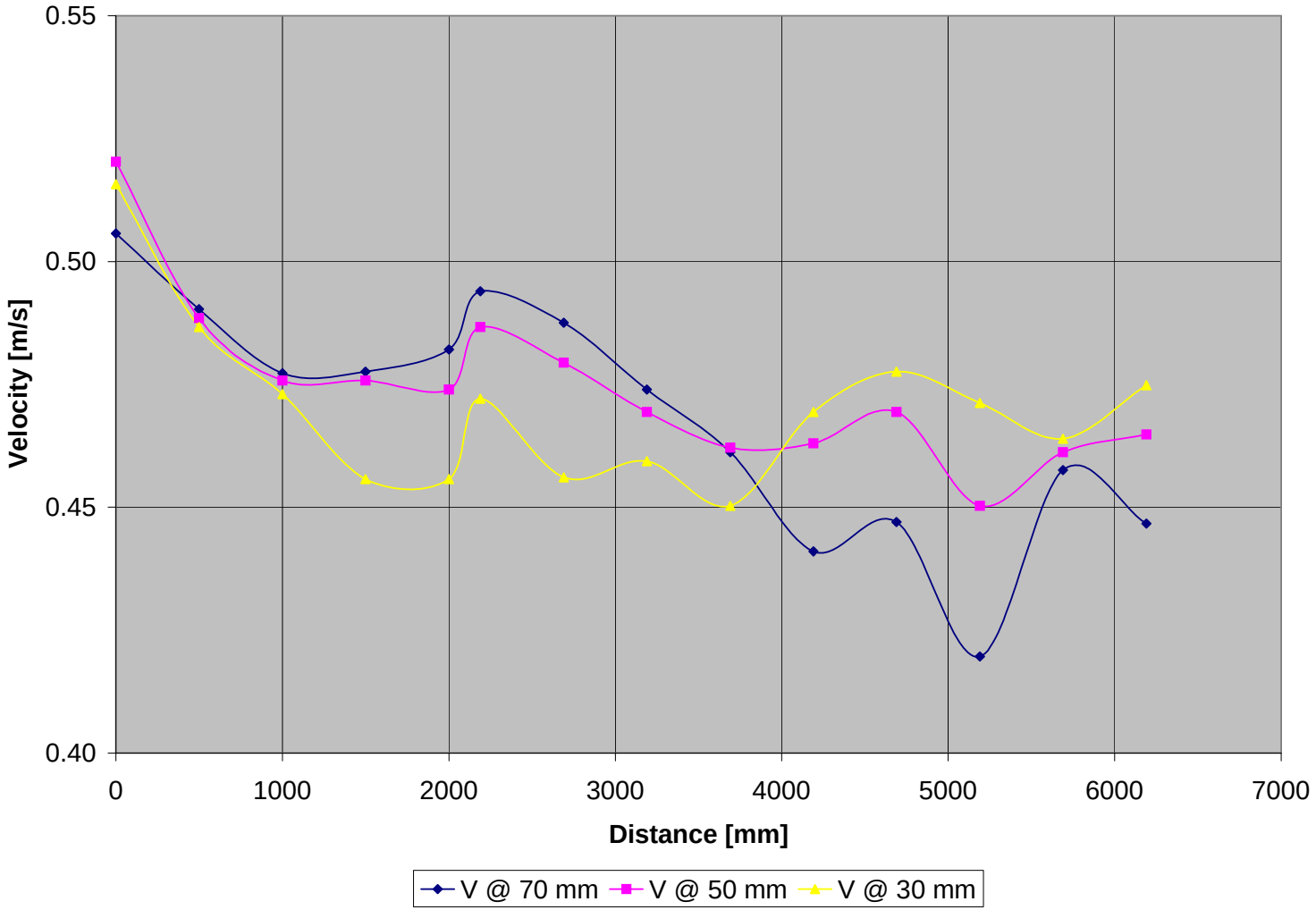

Figure A - 28: Test A4-Vertical velocity distribution measured at 50 mm from inner bank of bend

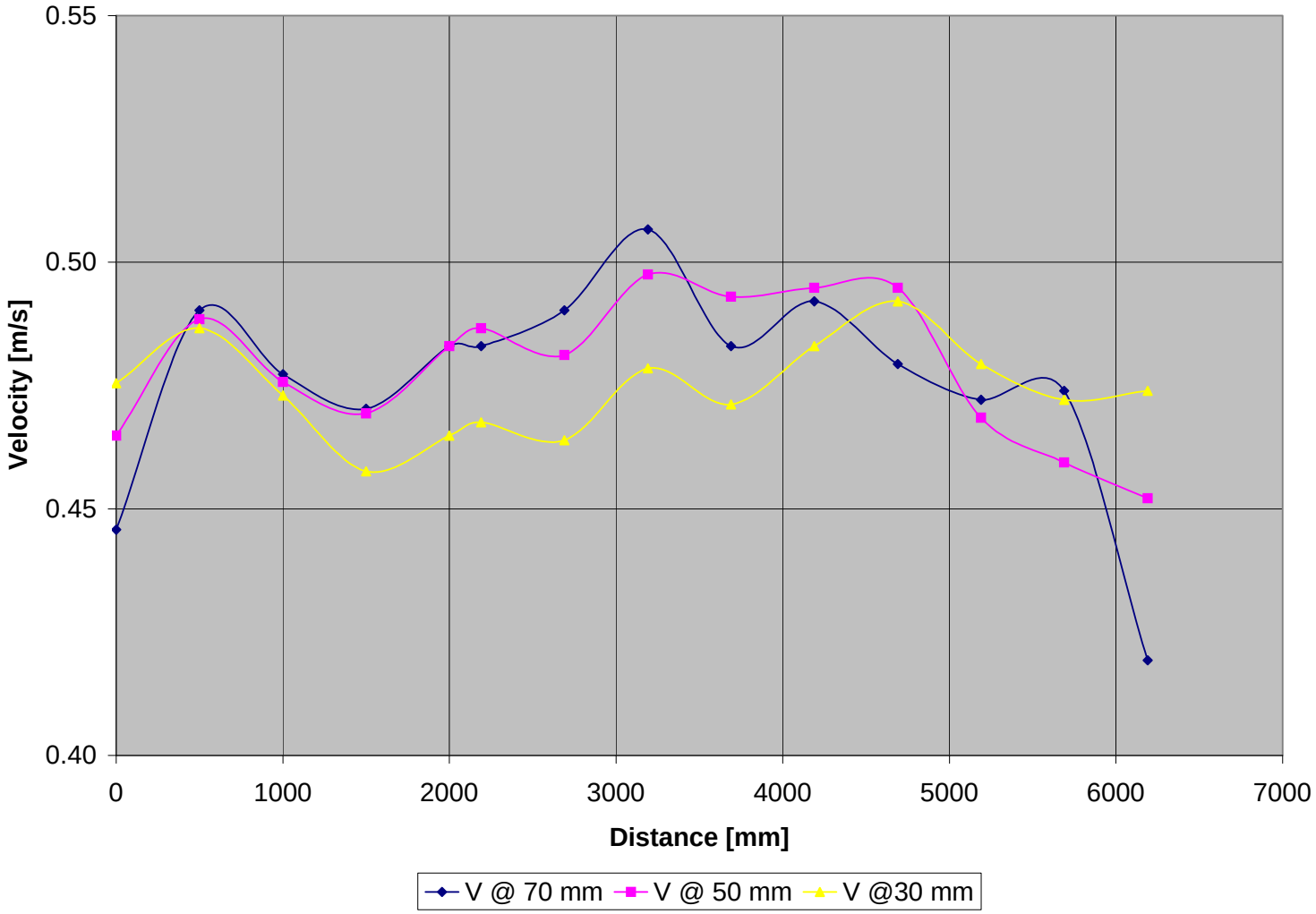

Figure A - 29: Test A4-Vertical velocity distribution measured at 100 mm from inner bank of bend

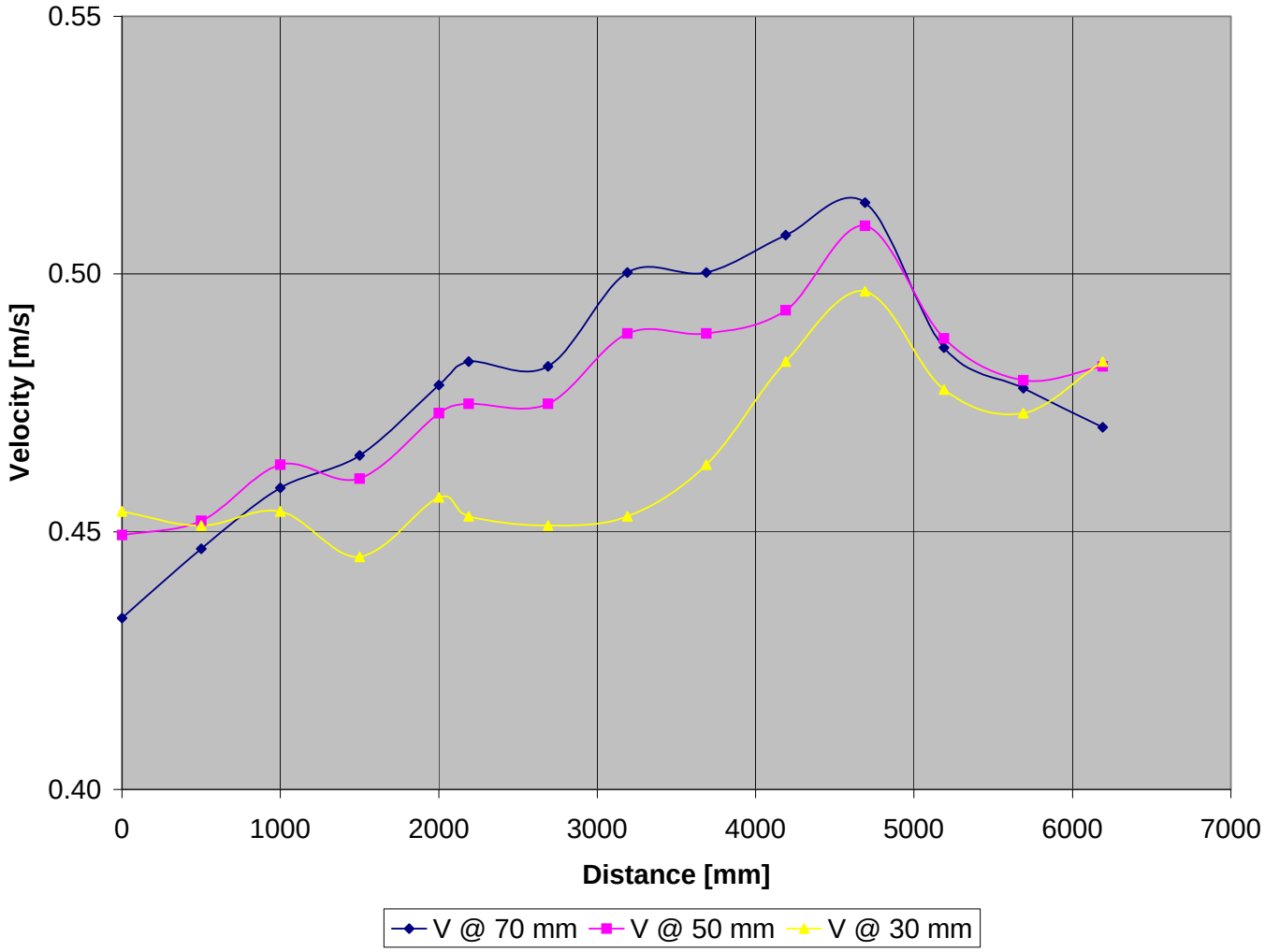

Figure A - 30: Test A4-Vertical velocity distribution measured at 150 mm from inner bank of bend

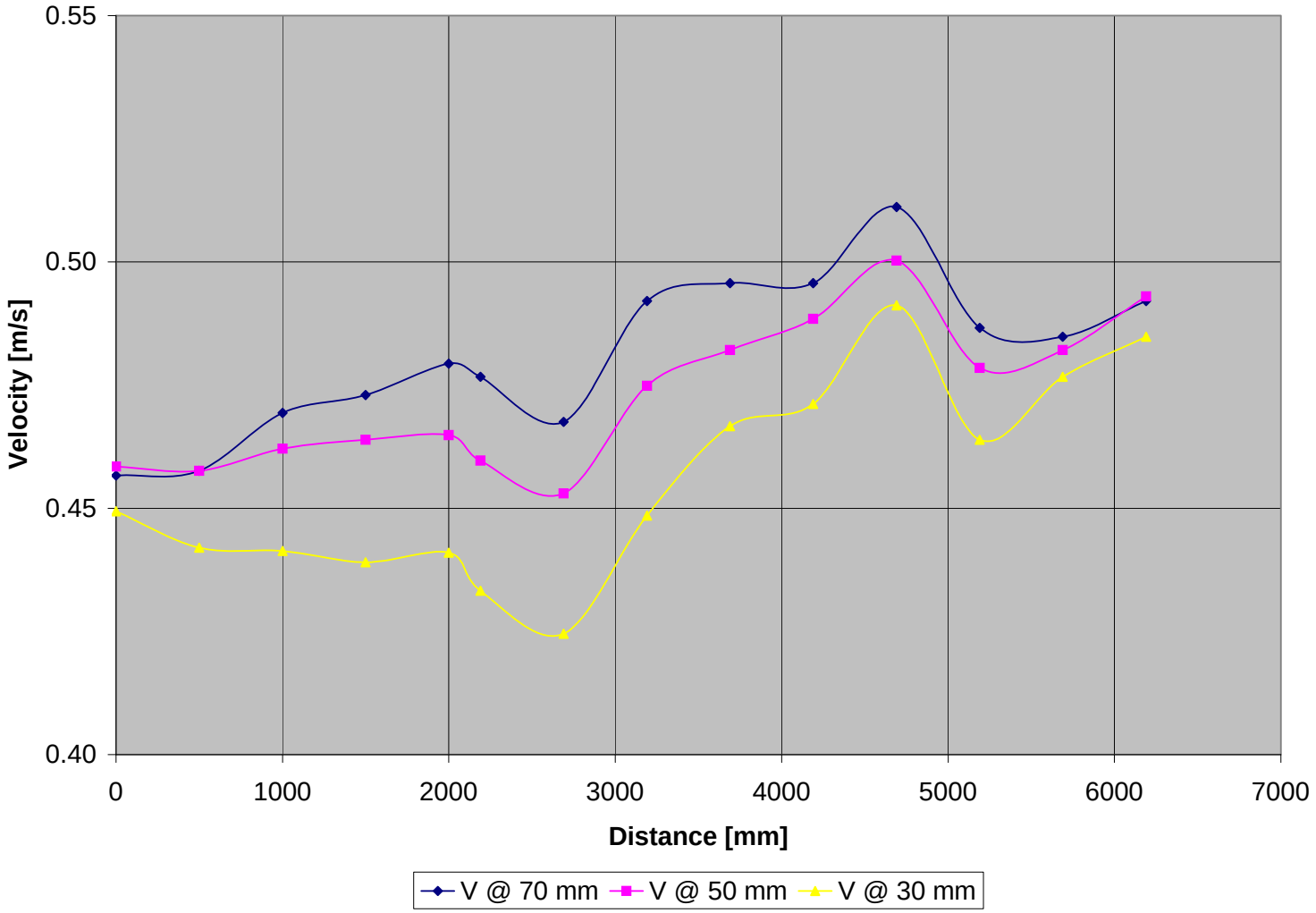

Figure A - 31: Test A4-Vertical velocity distribution measured at 200 mm from inner bank of bend

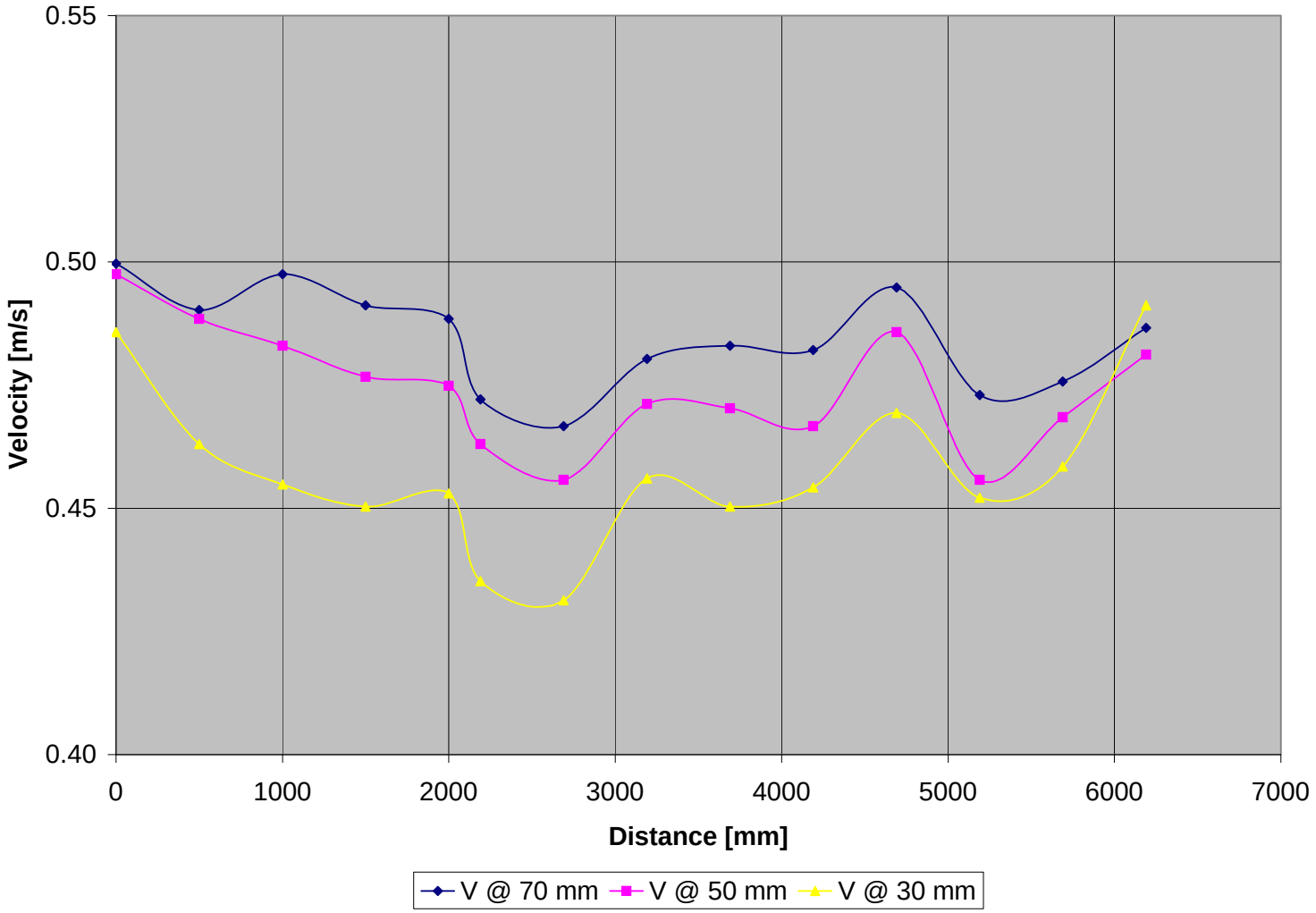

Figure A - 32: Test A4-Vertical velocity distribution measured at 250 mm from inner bank of bend

	Point	1	2	3	4	5	6	7	8	9	10	11	12	13	14
Width	**L**	**0**	**500**	**1000**	**1500**	**2000**	**2190**	**2690**	**3190**	**3690**	**4190**	**4690**	**5190**	**5690**	**6190**
	h														
50	**70**	0.506	0.490	0.477	0.478	0.482	0.494	0.488	0.474	0.461	0.441	0.447	0.420	0.458	0.447
	50	0.520	0.488	0.476	0.476	0.474	0.487	0.479	0.469	0.462	0.463	0.469	0.450	0.461	0.465
	30	0.516	0.487	0.473	0.456	0.456	0.472	0.456	0.459	0.450	0.469	0.478	0.471	0.464	0.475
100	**70**	0.446	0.490	0.477	0.470	0.483	0.483	0.490	0.507	0.483	0.492	0.479	0.472	0.474	0.419
	50	0.465	0.488	0.476	0.469	0.483	0.487	0.481	0.498	0.493	0.495	0.495	0.468	0.459	0.452
	30	0.475	0.487	0.473	0.458	0.465	0.468	0.464	0.478	0.471	0.483	0.492	0.479	0.472	0.474
150	**70**	0.433	0.447	0.458	0.465	0.478	0.483	0.482	0.500	0.500	0.508	0.514	0.486	0.478	0.470
	50	0.449	0.452	0.463	0.460	0.473	0.475	0.475	0.488	0.488	0.493	0.509	0.488	0.479	0.482
	30	0.454	0.451	0.454	0.445	0.457	0.453	0.451	0.453	0.463	0.483	0.497	0.478	0.473	0.483
200	**70**	0.457	0.458	0.469	0.473	0.479	0.477	0.468	0.492	0.496	0.496	0.511	0.487	0.485	0.492
	50	0.458	0.458	0.462	0.464	0.465	0.460	0.453	0.475	0.482	0.488	0.500	0.478	0.482	0.493
	30	0.449	0.442	0.441	0.439	0.441	0.433	0.424	0.448	0.467	0.471	0.491	0.464	0.477	0.485
250															
	70	0.500	0.490	0.498	0.491	0.488	0.472	0.467	0.480	0.483	0.482	0.495	0.473	0.476	0.487
	50	0.498	0.488	0.483	0.477	0.475	0.463	0.456	0.471	0.470	0.467	0.486	0.456	0.468	0.481
	30	0.486	0.463	0.455	0.450	0.453	0.435	0.431	0.456	0.450	0.454	0.469	0.452	0.458	0.491

Table A - 4: Test A4-Measured velocities [m/s]

A.1.2 SEDIMENT RELATED

A.1.2.1 TEST A5 (F_R = 0.3)

L	Width										
	25	50	75	100	125	150	175	200	225	250	275
0	125.5	125.5	124.2	122.9	123.8	124.7	124.4	124.0	122.0	120.0	120.0
500	120.0	120.0	119.9	119.8	120.1	120.4	121.0	121.5	120.7	119.9	119.9
1000	132.4	132.4	132.1	131.7	132.9	134.0	133.5	133.0	133.0	132.9	132.9
1500	146.7	146.7	146.4	146.0	147.1	148.1	147.9	147.6	147.1	146.5	146.5
2000	156.4	156.4	156.6	156.7	157.4	158.1	158.6	159.0	156.8	154.5	154.5
2190	154.3	152.2	152.1	150.8	152.6	153.7	153.2	151.4	152.2	150.5	150.0
2440	148.3	148.7	149.8	150.8	150.8	150.8	151.5	151.3	150.0	149.0	149.4
2690	151.5	154.2	152.2	152.0	150.3	150.8	150.1	151.2	150.2	149.8	145.8
2940	154.2	152.4	161.8	152.6	152.0	152.4	151.9	150.8	151.1	151.3	150.2
3190	159.8	159.0	158.1	156.7	156.3	153.7	153.0	151.9	149.5	150.7	148.3
3440	164.1	163.6	161.5	160.5	159.4	157.6	155.7	155.0	154.1	151.2	150.5
3690	165.0	162.2	161.0	159.3	158.9	158.7	157.6	157.7	156.5	155.0	154.3
3940	159.6	158.9	158.1	158.6	159.0	159.7	159.2	160.2	160.1	160.5	160.1
4190	163.1	162.8	161.2	161.7	169.4	157.9	159.0	158.6	158.6	158.5	161.0
4440	151.0	151.5	152.4	153.2	155.8	156.0	156.0	156.3	156.5	157.1	156.5
4690	145.0	145.1	145.8	147.0	147.1	147.5	149.5	151.2	152.1	151.5	155.0
4940	141.0	140.8	140.8	142.0	142.9	143.3	145.2	146.7	144.4	146.7	145.5
5190	139.6	139.2	137.8	137.6	138.8	140.0	138.6	141.5	142.3	143.7	145.0
5440	135.3	134.2	133.8	134.4	136.0	136.7	137.0	138.3	137.9	137.7	137.7
5690	142.1	138.6	137.4	139.1	137.6	138.7	138.0	139.6	141.7	140.1	141.0
5940	144.2	138.5	138.3	139.4	136.9	137.6	137.8	138.0	138.4	137.9	139.8
6190	131.2	129.2	131.1	131.0	131.0	131.3	131.1	133.7	134.3	131.2	133.6

Table A - 5: Test A5-Sediment levels (zero readings)

L	Width										
	25	50	75	100	125	150	175	200	225	250	275
0	119.6	119.6	116.1	112.5	114.3	116.0	117.4	118.8	114.6	110.3	110.3
500	116.0	116.0	115.0	113.9	114.4	114.8	116.0	117.2	113.2	109.2	109.2
1000	116.4	116.4	118.0	119.5	116.8	114.1	117.2	120.2	118.6	117.0	117.0
1500	122.7	122.7	121.8	120.8	116.1	111.4	114.8	118.2	121.1	124.0	124.0
2000	117.2	117.2	124.7	132.1	128.7	125.3	123.6	121.8	125.1	128.4	128.4
2190	120.3	111.2	114.8	120.8	123.5	122.4	116.5	126.2	130.2	121.4	124.3
2440	136.2	134.8	130.2	122.4	124.5	127.9	123.0	129.4	132.4	123.2	118.6
2690	138.1	131.4	128.6	130.3	126.6	123.2	127.0	122.4	126.2	119.1	109.0
2940	135.5	133.4	130.7	125.8	127.2	119.5	121.9	115.5	109.8	114.8	101.5
3190	152.0	150.8	147.0	134.0	128.5	125.8	116.5	112.9	112.7	97.0	91.2
3440	158.2	149.8	149.5	142.9	132.4	114.1	100.0	91.0	86.2	76.2	67.8
3690	159.7	157.0	143.2	147.0	131.5	115.3	105.0	102.4	100.0	88.5	74.5
3940	156.0	158.8	154.2	150.3	136.7	124.7	113.3	105.2	95.7	82.2	68.2
4190	164.6	162.8	157.6	142.5	130.0	120.0	113.7	101.2	83.5	68.8	59.5
4440	158.2	155.2	153.0	139.2	128.2	123.9	116.9	106.3	106.0	89.6	75.8
4690	160.0	160.2	148.0	130.7	132.1	130.5	129.9	117.6	104.0	99.2	92.6
4940	155.6	147.0	139.0	136.8	132.1	119.0	112.9	111.2	108.3	98.0	91.8
5190	148.3	144.0	133.2	135.3	116.0	106.1	98.2	98.0	104.6	101.0	98.7
5440	140.0	135.2	132.9	121.6	115.2	114.0	113.8	107.3	94.8	97.3	96.0
5690	133.7	133.3	122.5	119.2	111.0	115.3	109.1	105.8	92.2	95.0	88.4
5940	130.0	123.0	120.0	113.0	109.5	101.0	104.6	99.0	94.0	81.5	80.5
6190	115.8	114.7	118.0	112.2	106.5	105.5	101.2	94.1	90.5	90.5	89.1

Table A - 6: Test A5-Sediment levels (Run 1)

L	Width										
	25	50	75	100	125	150	175	200	225	250	275
0	114.5	114.5	117.3	120.0	113.7	107.3	106.5	105.7	105.9	106.0	106.0
500	109.1	109.1	106.6	104.1	108.6	113.0	112.8	112.6	113.3	113.9	113.9
1000	114.0	114.0	115.3	116.6	119.8	123.0	122.6	122.1	112.8	103.5	103.5
1500	129.3	129.3	128.2	127.0	127.7	128.4	120.2	112.0	114.5	116.9	116.9
2000	126.4	126.4	124.3	122.2	114.5	106.7	114.9	123.0	123.7	124.3	124.3
2190	123.5	119.5	120.7	124.5	121.8	124.3	121.6	125.8	121.5	112.8	115.1
2440	133.4	126.2	131.0	129.9	119.7	117.8	120.6	120.5	117.2	110.8	109.6
2690	140.0	133.7	127.5	131.2	126.5	121.0	118.8	115.6	107.5	106.0	106.2
2940	136.6	135.0	126.9	133.6	122.2	118.6	117.0	118.2	105.2	99.8	98.4
3190	146.6	142.7	134.0	120.6	128.9	112.7	100.8	112.1	100.2	93.1	94.6
3440	148.1	136.6	144.6	137.3	134.8	121.5	112.2	96.6	79.6	70.0	69.3
3690	156.8	148.2	138.4	131.1	125.2	112.0	106.6	94.0	80.0	74.0	72.3
3940	157.2	154.1	150.0	133.2	131.5	117.2	102.0	88.9	79.0	74.0	70.4
4190	162.9	156.5	152.0	143.6	140.5	126.4	115.3	102.2	93.6	80.4	78.0
4440	155.5	147.7	146.2	137.0	120.0	115.7	135.0	109.5	103.1	101.0	101.7
4690	153.9	148.5	141.9	136.0	133.0	134.0	122.4	119.0	112.6	105.3	95.5
4940	153.4	143.5	138.4	116.8	102.6	98.5	94.0	97.2	107.7	107.9	100.3
5190	150.6	146.5	143.8	144.0	124.9	111.4	96.6	85.0	78.6	82.1	96.0
5440	130.2	140.0	140.2	132.7	122.4	113.7	112.0	109.8	103.3	103.0	99.5
5690	135.3	131.2	130.0	128.2	125.2	119.7	114.2	105.0	98.5	74.2	93.8
5940	130.0	120.3	121.6	121.8	120.6	114.7	107.4	101.6	99.5	87.8	86.8
6190	122.5	126.4	117.0	115.1	120.5	107.2	101.1	102.8	100.9	79.5	79.1

Table A - 7: Test A5-Sediment levels (Run 2)

L	Width										
	25	50	75	100	125	150	175	200	225	250	275
0	111.3	111.3	112.8	114.2	114.9	115.6	110.1	104.5	107.7	110.8	110.8
500	117.0	117.0	115.7	114.3	113.5	112.6	113.1	113.5	114.0	114.4	114.4
1000	120.3	120.3	121.1	121.9	117.9	113.9	109.2	104.5	103.4	102.2	102.2
1500	114.2	114.2	114.3	114.3	112.6	110.8	114.5	118.2	121.4	124.5	124.5
2000	115.0	115.0	116.0	117.0	117.4	117.7	113.8	109.8	111.1	112.4	112.4
2190	117.3	112.7	112.6	113.7	116.5	113.7	114.5	113.0	111.4	108.2	109.8
2440	125.6	122.5	124.5	127.9	126.0	126.6	122.1	115.7	111.8	110.8	109.1
2690	133.3	131.5	127.0	120.5	123.3	123.0	119.0	111.5	109.2	107.5	105.7
2940	136.0	132.4	132.0	129.0	127.5	124.3	119.2	108.8	103.0	92.5	93.8
3190	146.9	139.6	137.2	136.7	129.0	116.6	112.0	108.0	94.6	85.0	79.7
3440	146.0	147.3	150.1	135.2	125.8	123.0	103.7	91.2	82.6	74.3	68.1
3690	153.4	146.7	143.0	134.0	120.2	108.3	102.7	93.1	91.4	88.2	83.5
3940	157.0	152.7	139.6	141.4	128.8	119.8	102.7	92.3	83.3	78.4	83.2
4190	161.5	154.4	144.8	145.0	133.3	118.0	108.8	102.4	100.0	91.6	93.4
4440	154.4	155.5	138.4	129.6	122.2	116.2	113.8	117.5	95.1	100.0	75.5
4690	145.0	146.7	130.6	120.3	114.5	111.5	112.3	115.0	113.7	108.0	105.5
4940	149.6	143.8	133.5	117.4	112.9	104.5	100.6	101.3	105.5	104.6	104.2
5190	147.9	141.7	132.6	114.0	140.7	133.6	121.7	112.5	98.3	89.0	80.0
5440	145.7	137.0	136.8	117.0	110.0	111.3	114.4	118.0	118.6	101.0	102.5
5690	141.7	139.8	132.9	126.2	119.5	117.7	104.5	97.6	101.5	101.8	98.0
5940	124.9	128.7	130.0	124.0	115.7	112.4	104.2	102.7	95.0	89.0	87.9
6190	122.8	122.0	112.7	117.3	107.9	104.0	112.5	104.6	95.5	82.8	78.0

Table A - 8: Test A5-Sediment levels (Run 3)

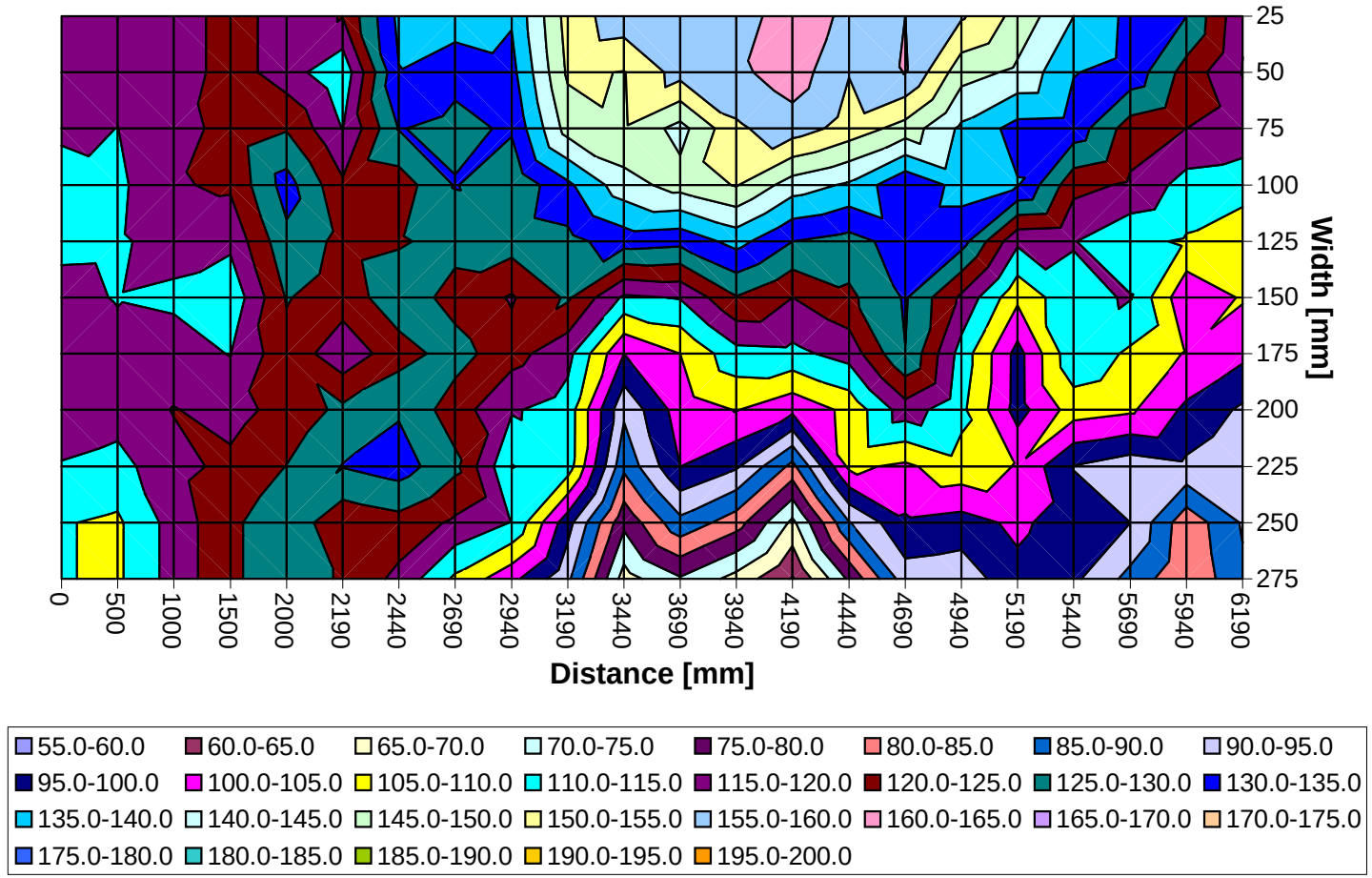

Figure A - 33: Test A5-Sediment levels after Run 1

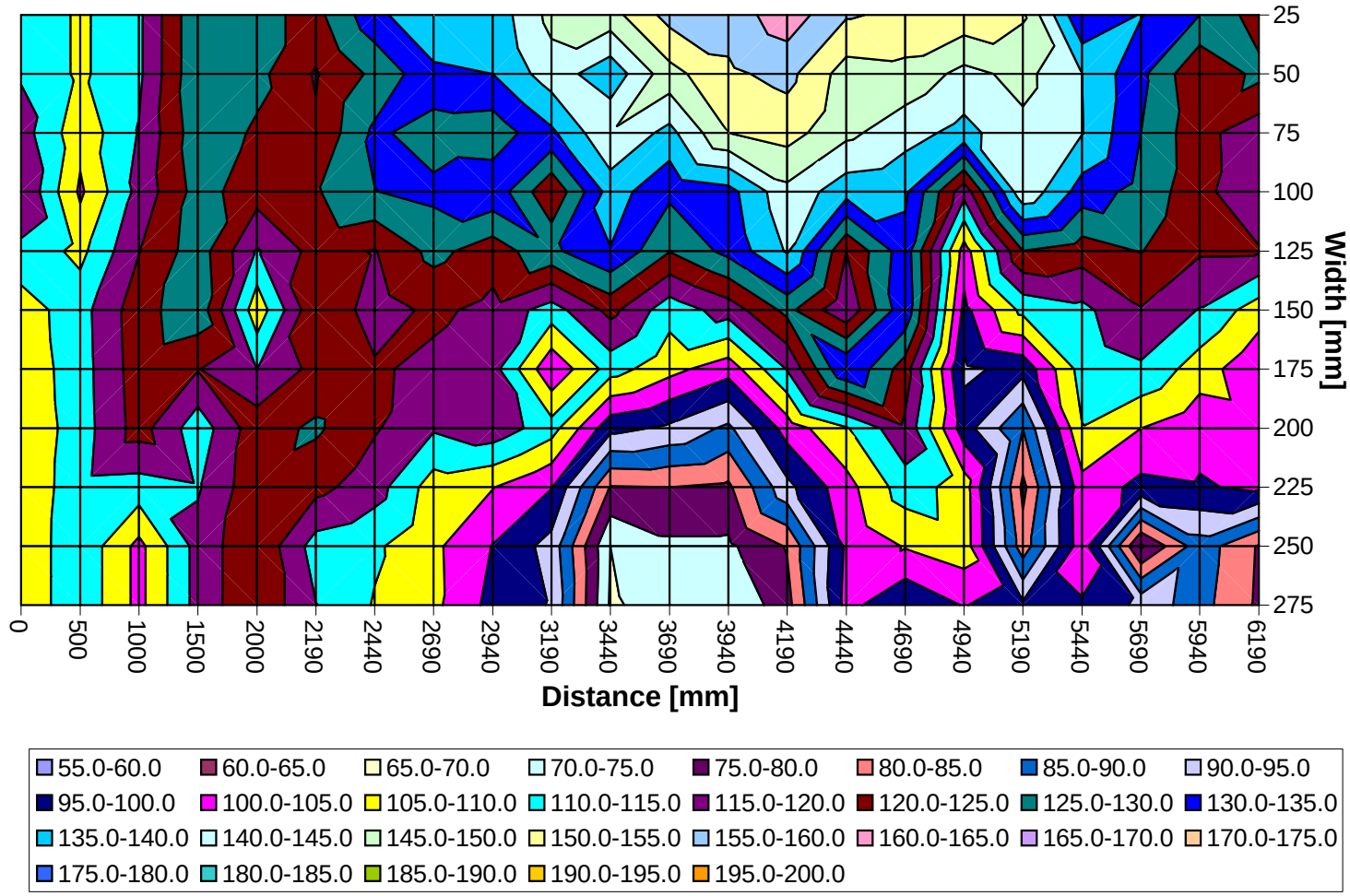

Figure A - 34: Test A5-Sediment levels after Run 2

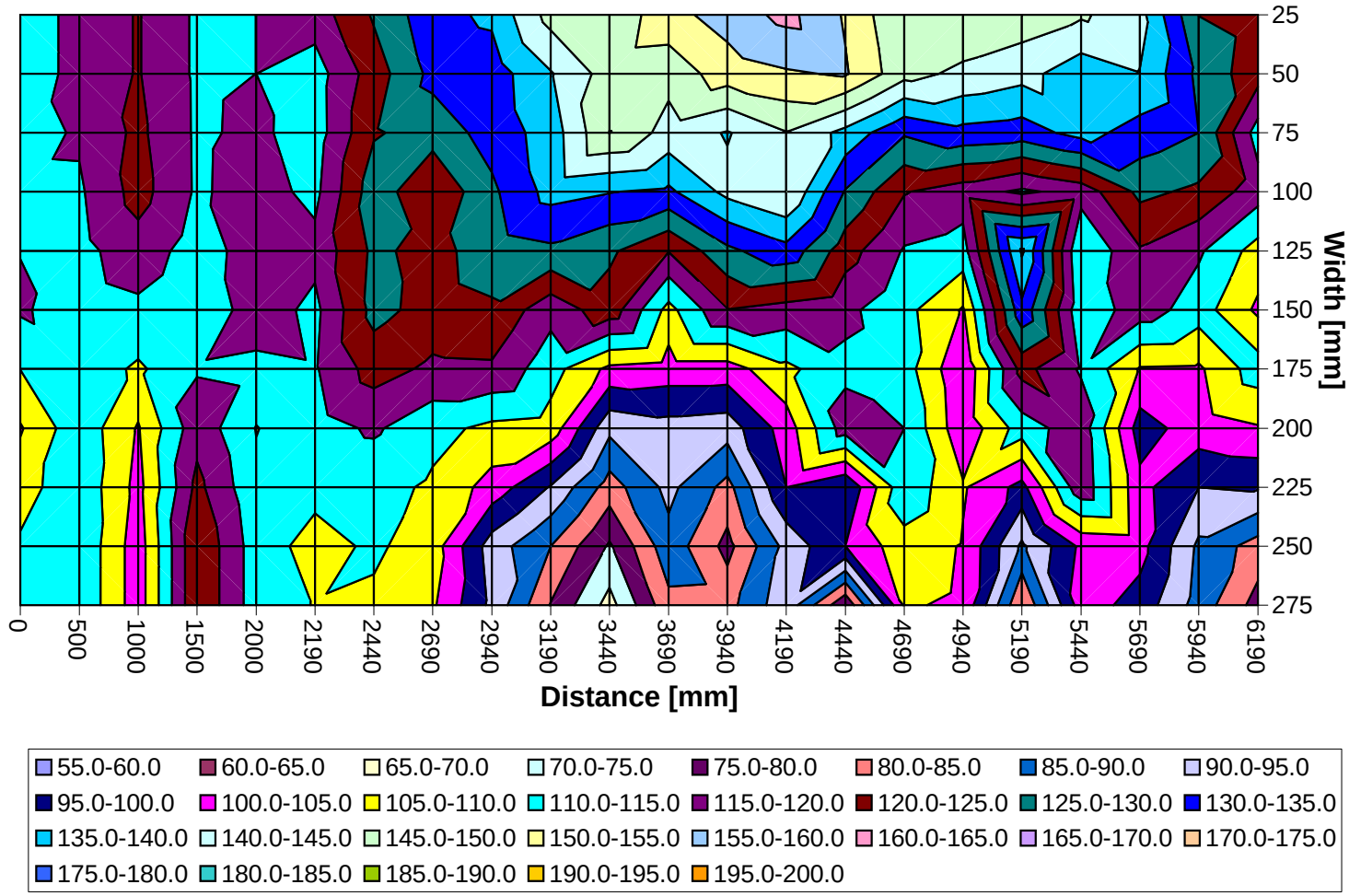

Figure A - 35: Test A5-Sediment levels after Run 3

A.2 TEST B (AVERAGE RADIUS = 3.55 M)

A.2.1 VELOCITY RELATED

A.2.1.1 TEST B1 (F_R = 0.1)

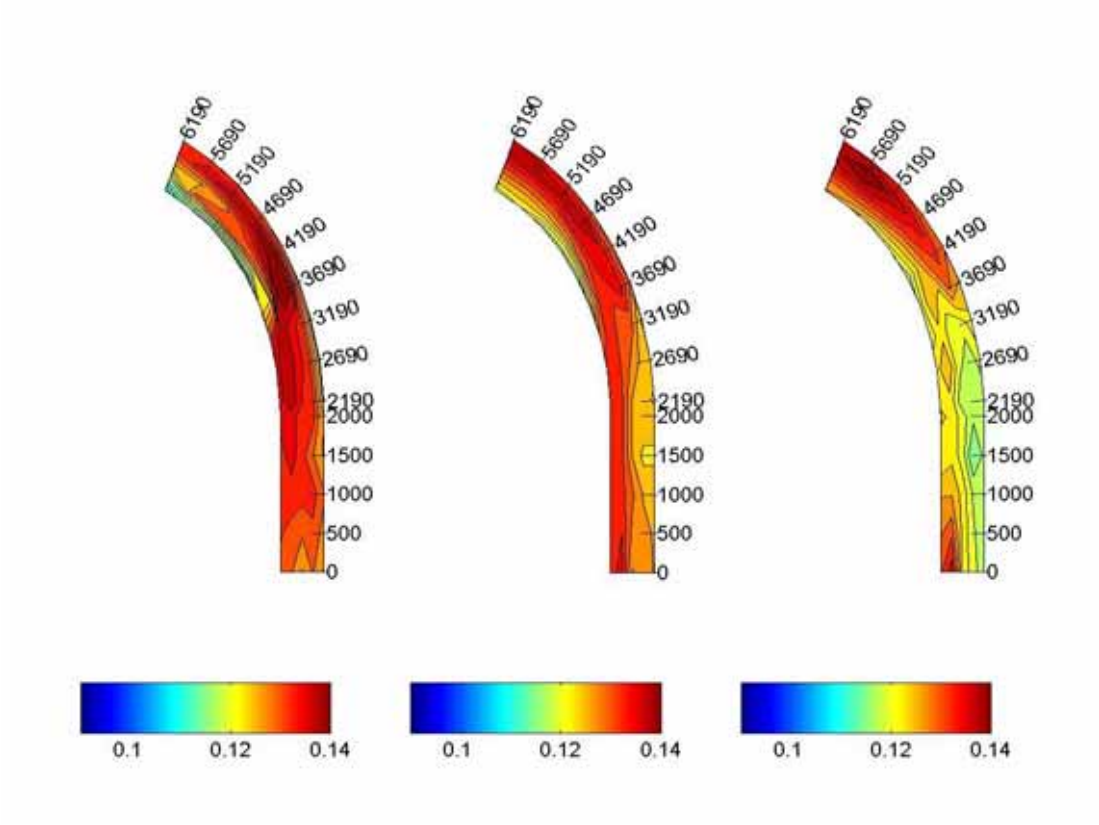

Figure A - 36: Test B1-Velocity distribution in the horisontal plane measured at 70, 50 and 30 mm

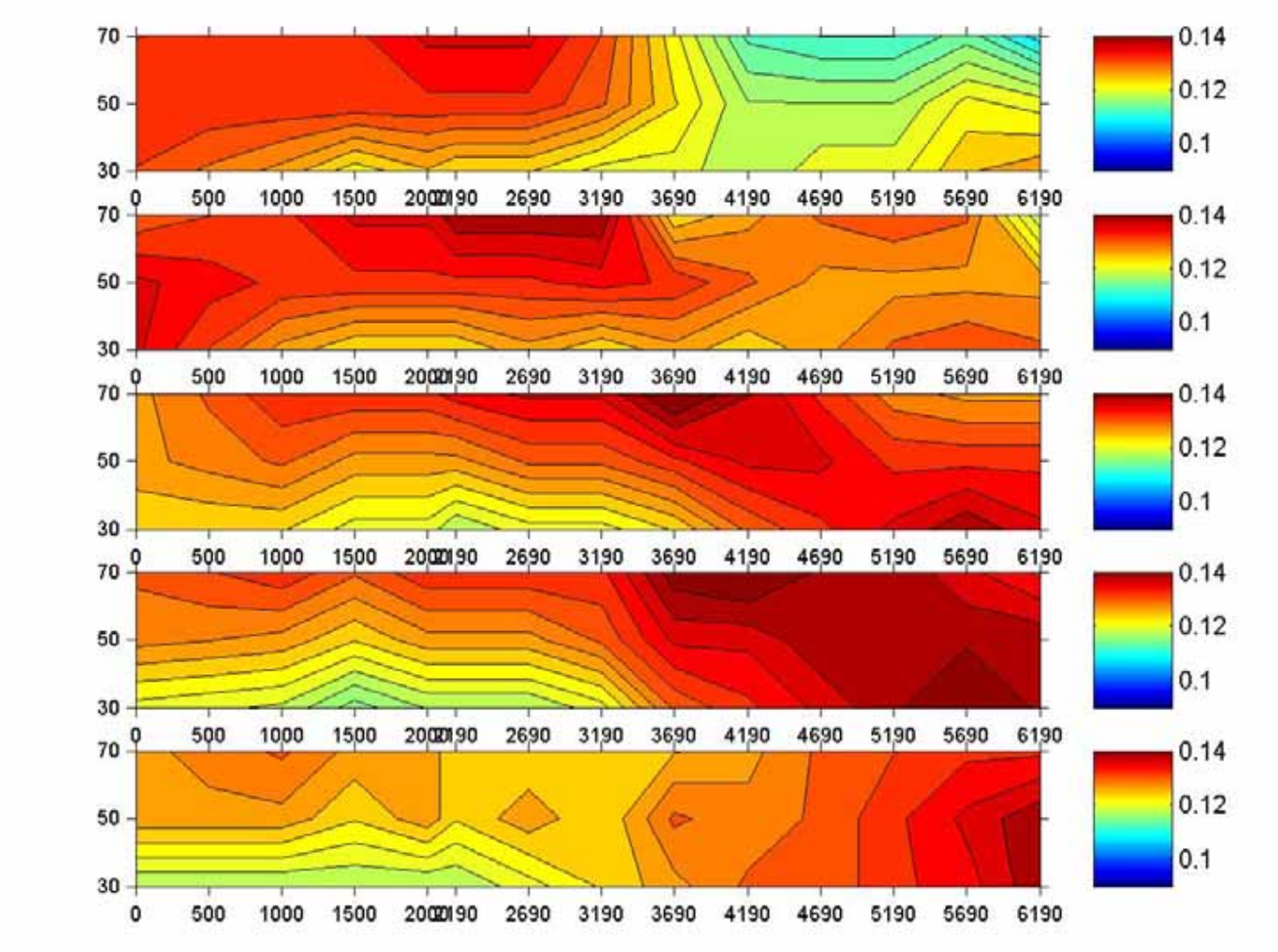

Figure A - 37: Test B1-Velocity distribution in the vertical plane

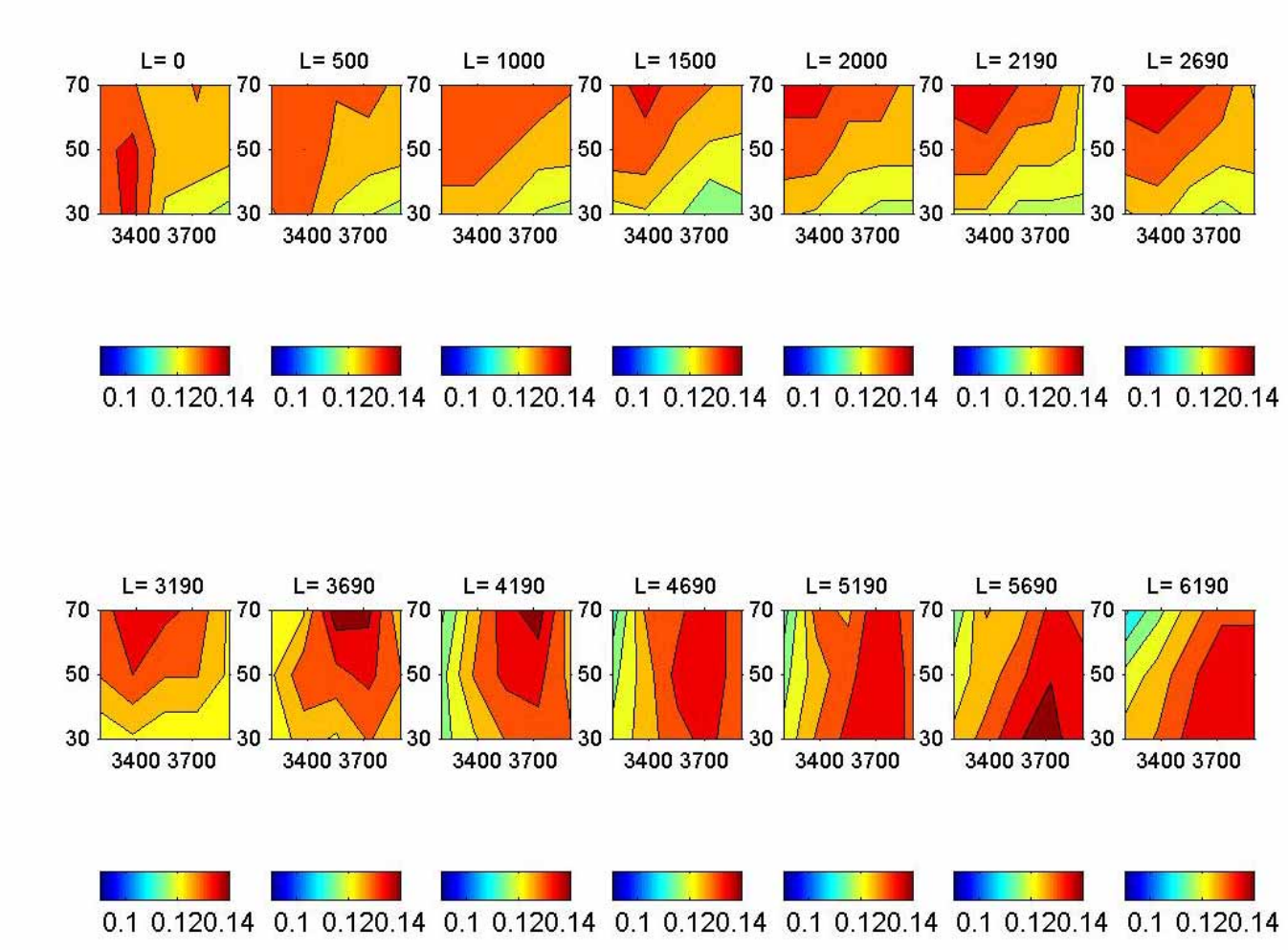

Figure A - 38: Test B1-Cross-sectional velocity distribution

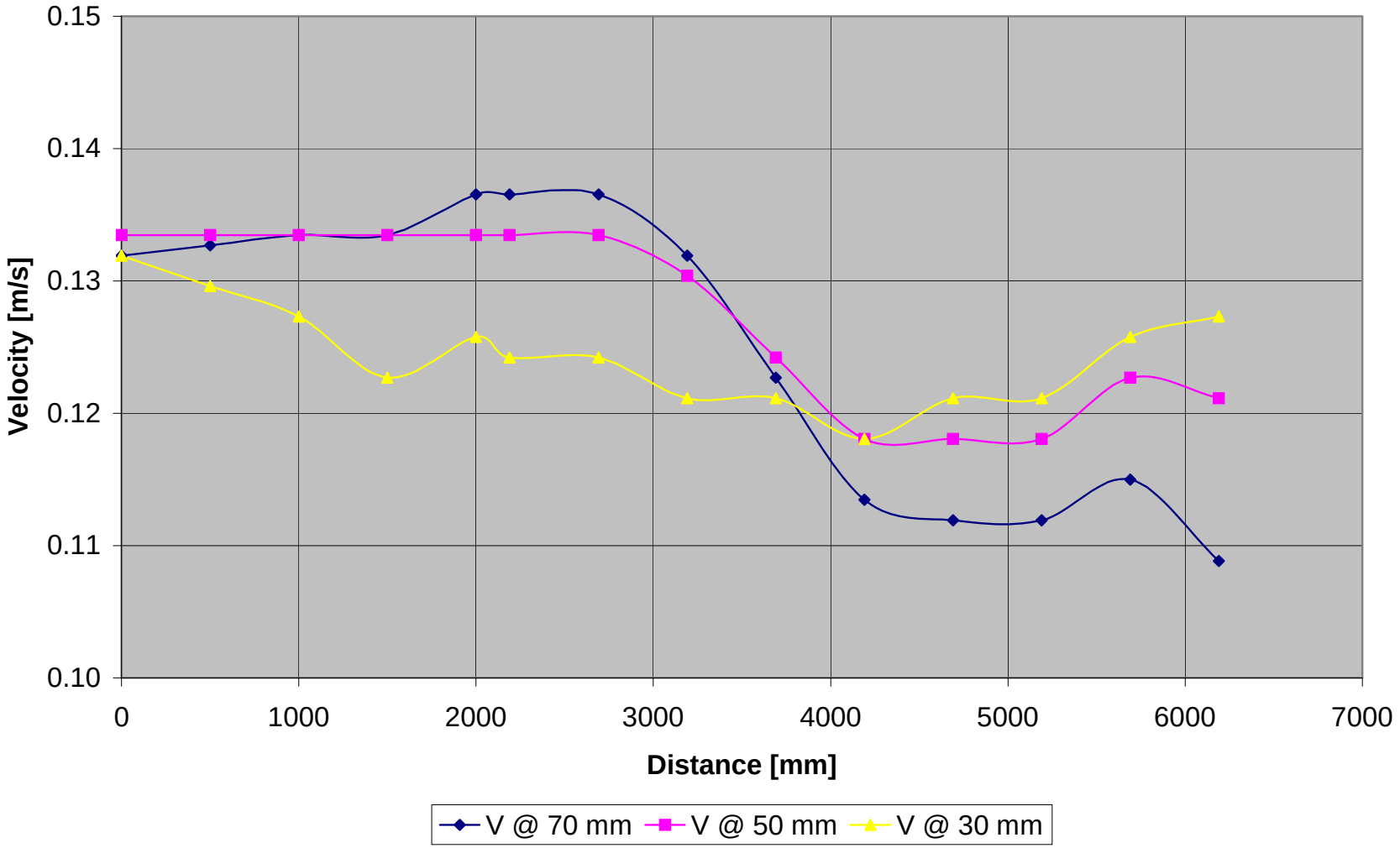

Figure A - 39: Test B1-Vertical velocity distribution measured at 50 mm from inner bank of bend

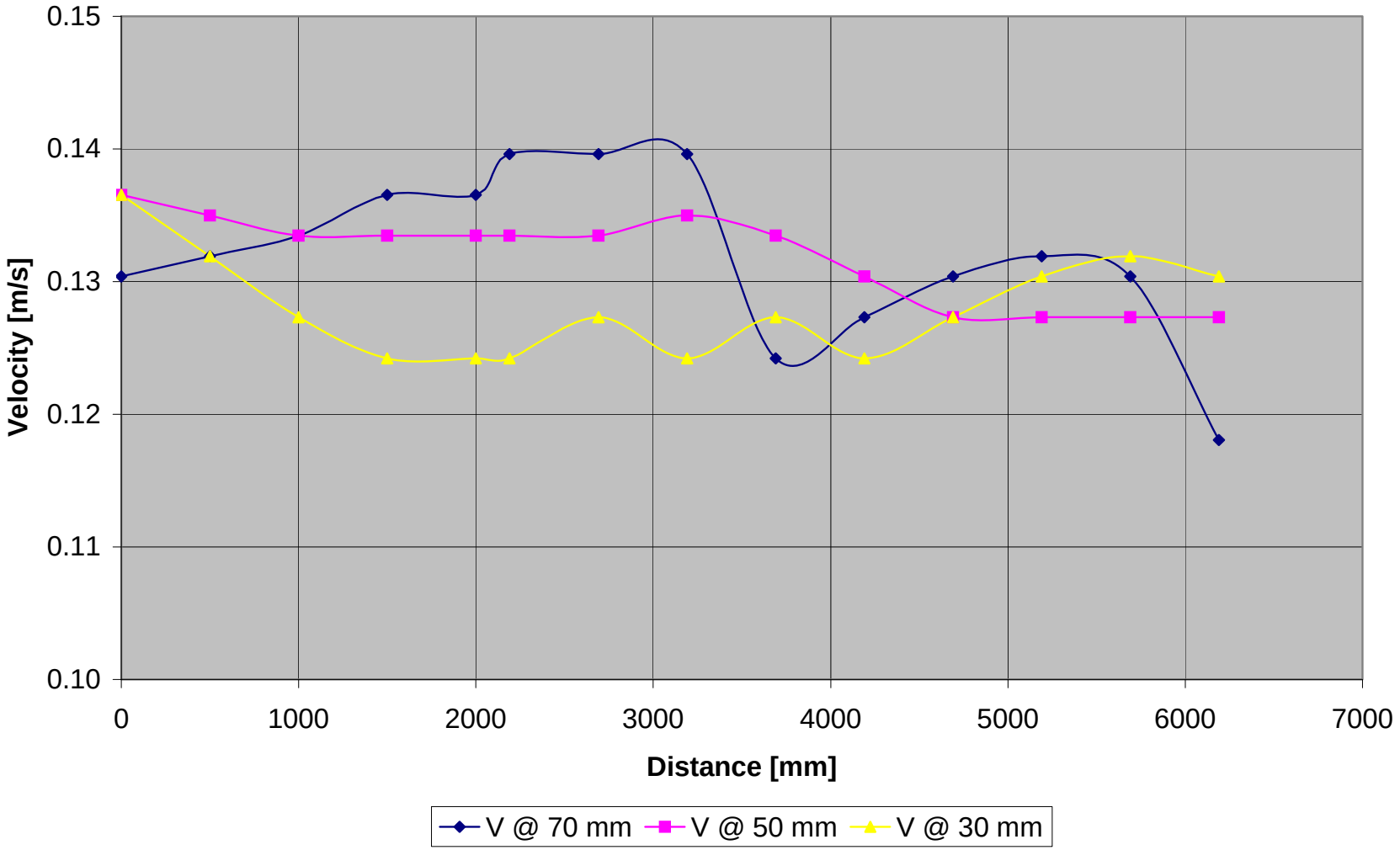

Figure A - 40: Test B1-Vertical velocity distribution measured at 100 mm from inner bank of bend

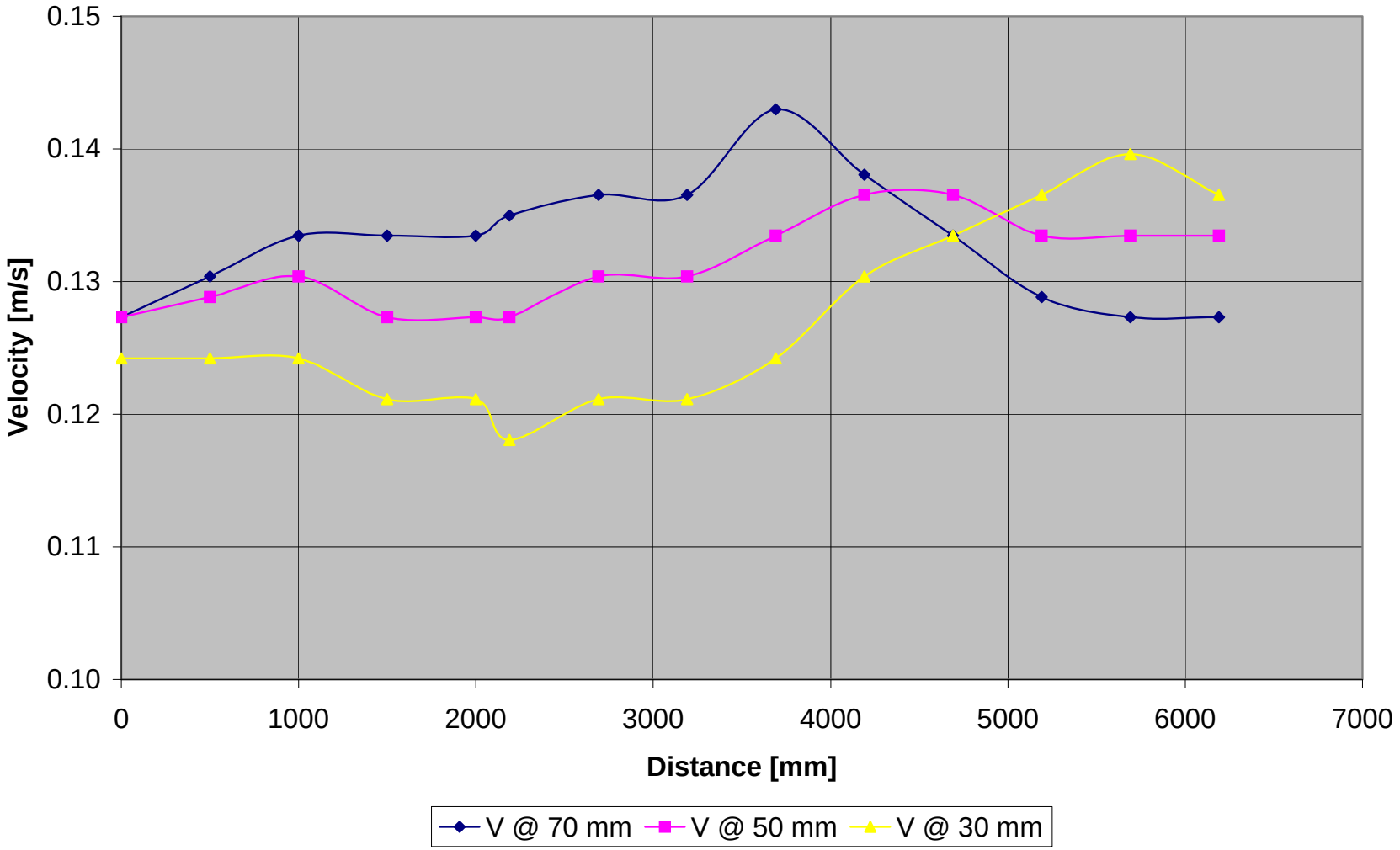

Figure A - 41: Test B1-Vertical velocity distribution measured at 150 mm from inner bank of bend

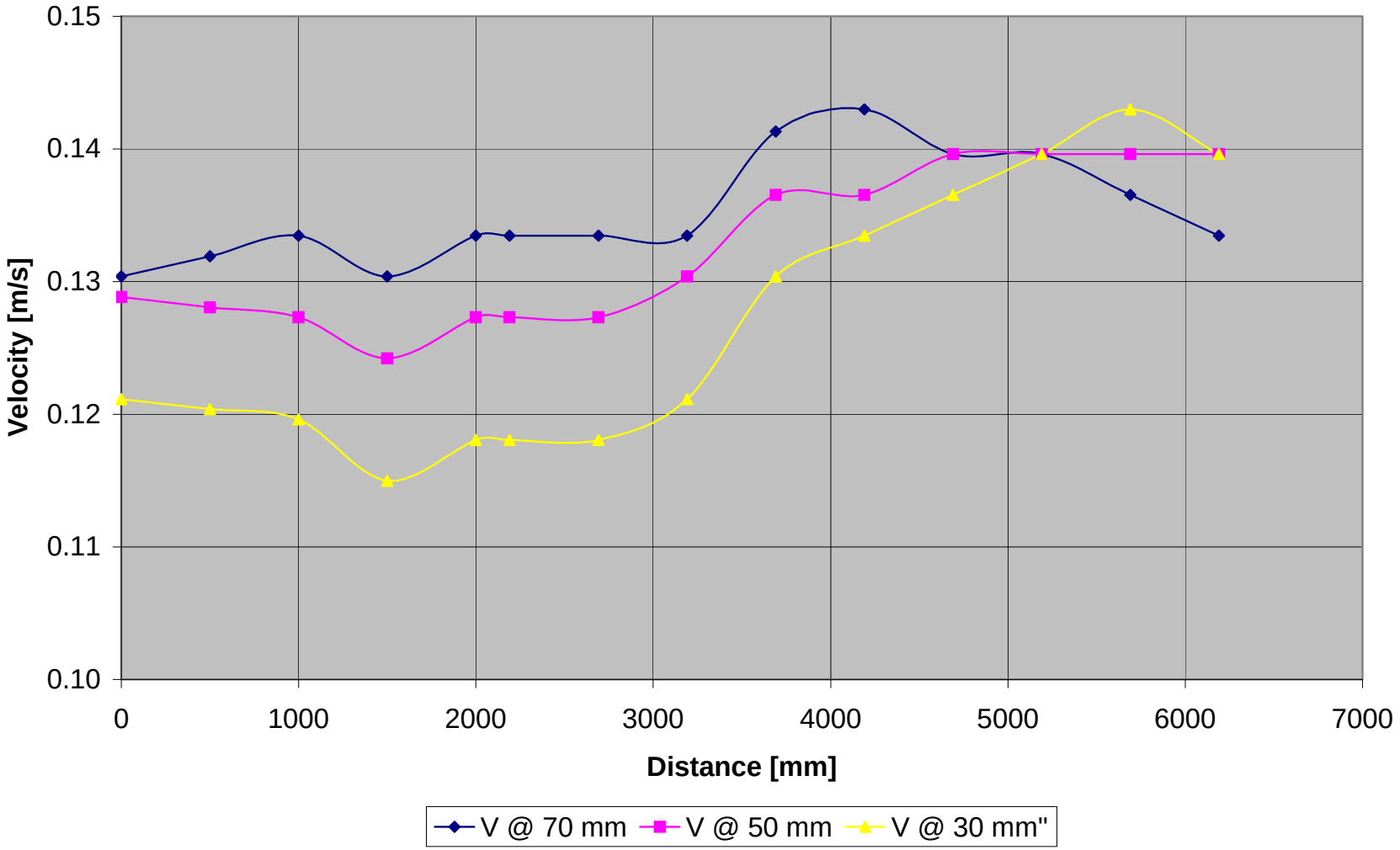

Figure A - 42: Test B1-Vertical velocity distribution measured at 200 mm from inner bank of bend

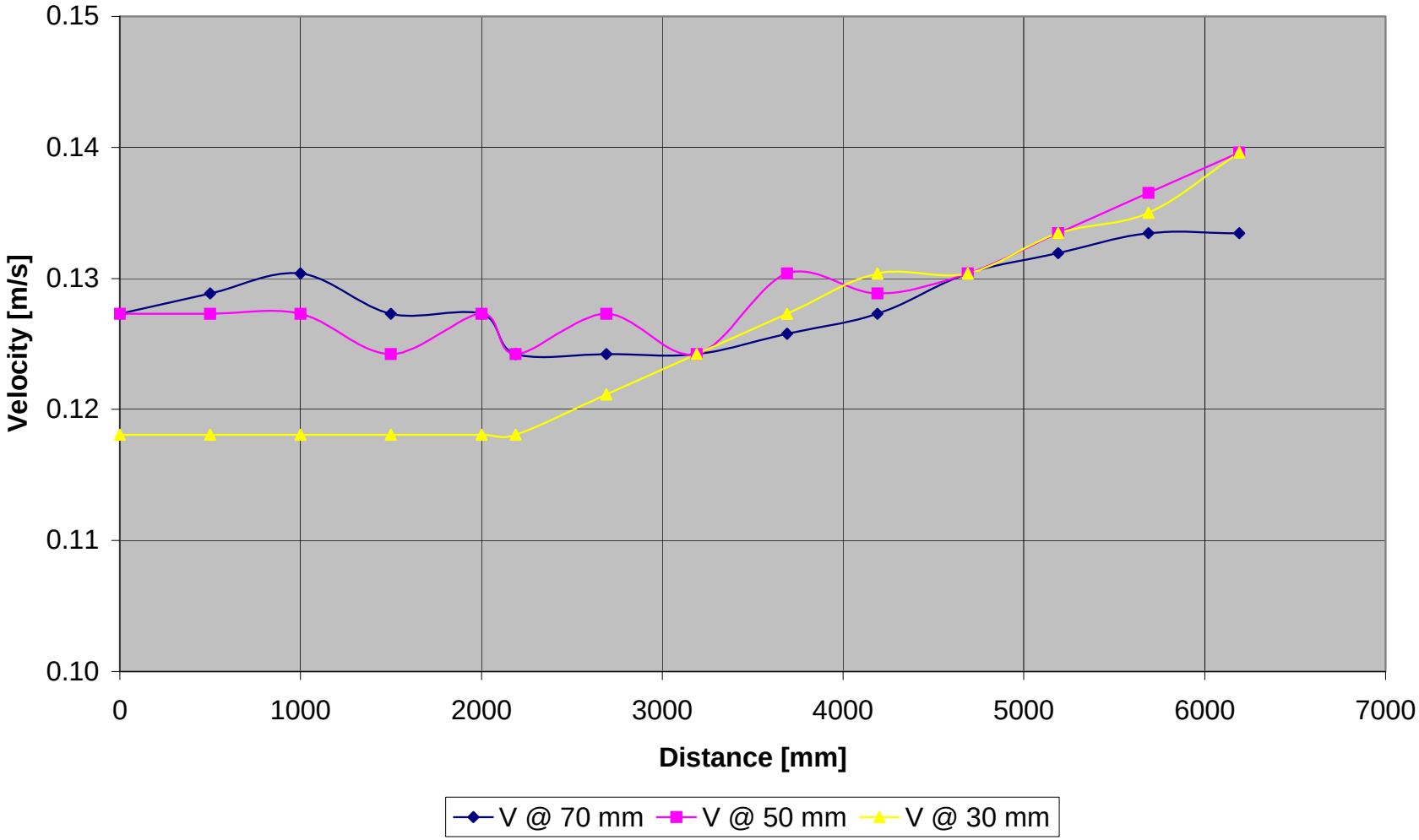

Figure A - 43: Test B1-Vertical velocity distribution measured at 250 mm from inner bank of bend

	Point	1	2	3	4	5	6	7	8	9	10	11	12	13	14
Width	L	0	500	1000	1500	2000	2190	2690	3190	3690	4190	4690	5190	5690	6190
	h														
50	70	0.132	0.133	0.133	0.133	0.137	0.137	0.137	0.132	0.123	0.113	0.112	0.112	0.115	0.109
	50	0.133	0.133	0.133	0.133	0.133	0.133	0.133	0.130	0.124	0.118	0.118	0.118	0.123	0.121
	30	0.132	0.130	0.127	0.123	0.126	0.124	0.124	0.121	0.121	0.118	0.121	0.121	0.126	0.127
100	70	0.130	0.132	0.133	0.137	0.137	0.140	0.140	0.140	0.124	0.127	0.130	0.132	0.130	0.118
	50	0.137	0.135	0.133	0.133	0.133	0.133	0.133	0.135	0.133	0.130	0.127	0.127	0.127	0.127
	30	0.137	0.132	0.127	0.124	0.124	0.124	0.127	0.124	0.127	0.124	0.127	0.130	0.132	0.130
150	70	0.127	0.130	0.133	0.133	0.133	0.135	0.137	0.137	0.143	0.138	0.133	0.129	0.127	0.127
	50	0.127	0.129	0.130	0.127	0.127	0.127	0.130	0.130	0.133	0.137	0.137	0.133	0.133	0.133
	30	0.124	0.124	0.124	0.121	0.121	0.118	0.121	0.121	0.124	0.130	0.133	0.137	0.140	0.137
200	70	0.130	0.132	0.133	0.130	0.133	0.133	0.133	0.133	0.141	0.143	0.140	0.140	0.137	0.133
	50	0.129	0.128	0.127	0.124	0.127	0.127	0.127	0.130	0.137	0.137	0.140	0.140	0.140	0.140
	30	0.121	0.120	0.120	0.115	0.118	0.118	0.118	0.121	0.130	0.133	0.137	0.140	0.143	0.140
250															
	70	0.127	0.129	0.130	0.127	0.127	0.124	0.124	0.124	0.126	0.127	0.130	0.132	0.133	0.133
	50	0.127	0.127	0.127	0.124	0.127	0.124	0.127	0.124	0.130	0.129	0.130	0.133	0.137	0.140
	30	0.118	0.118	0.118	0.118	0.118	0.118	0.121	0.124	0.127	0.130	0.130	0.133	0.135	0.140

Table A - 9: Test B1-Measured velocities [m/s]

A.2.1.2 TEST B2 (F_R = 0.3)

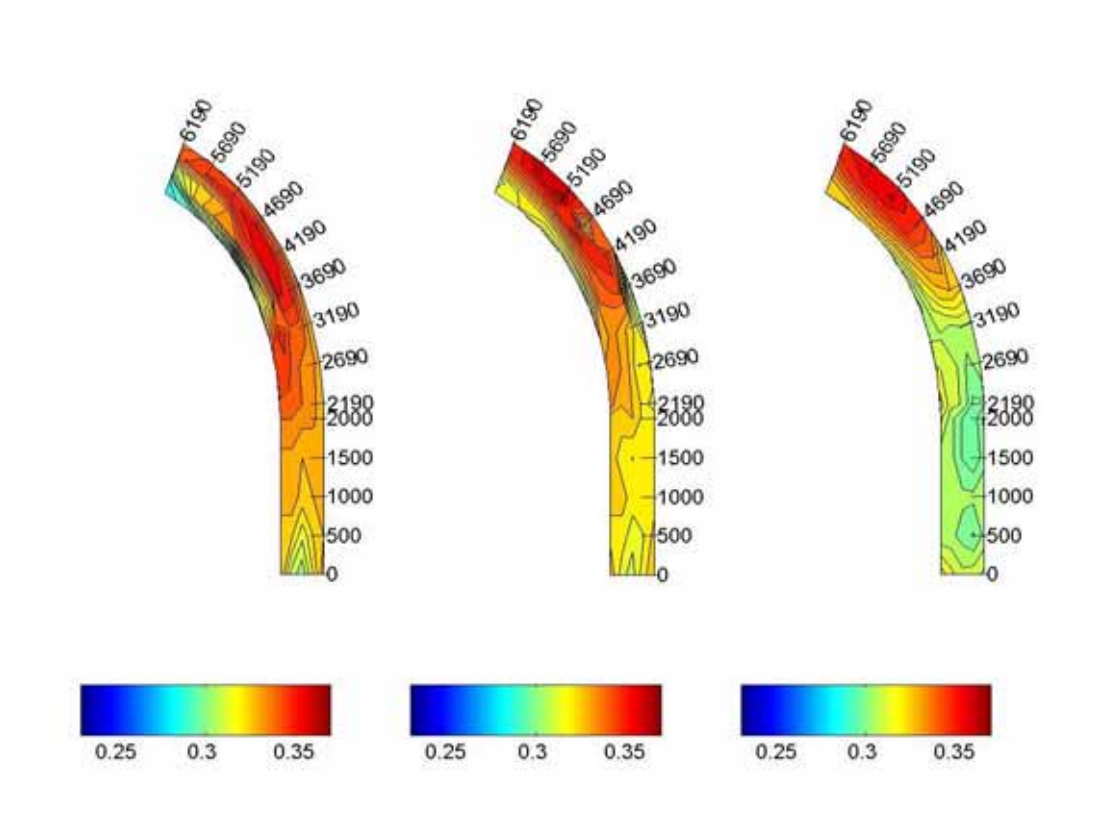

Figure A - 44: Test B2-Velocity distribution in a horizontal plane measured at 70 mm

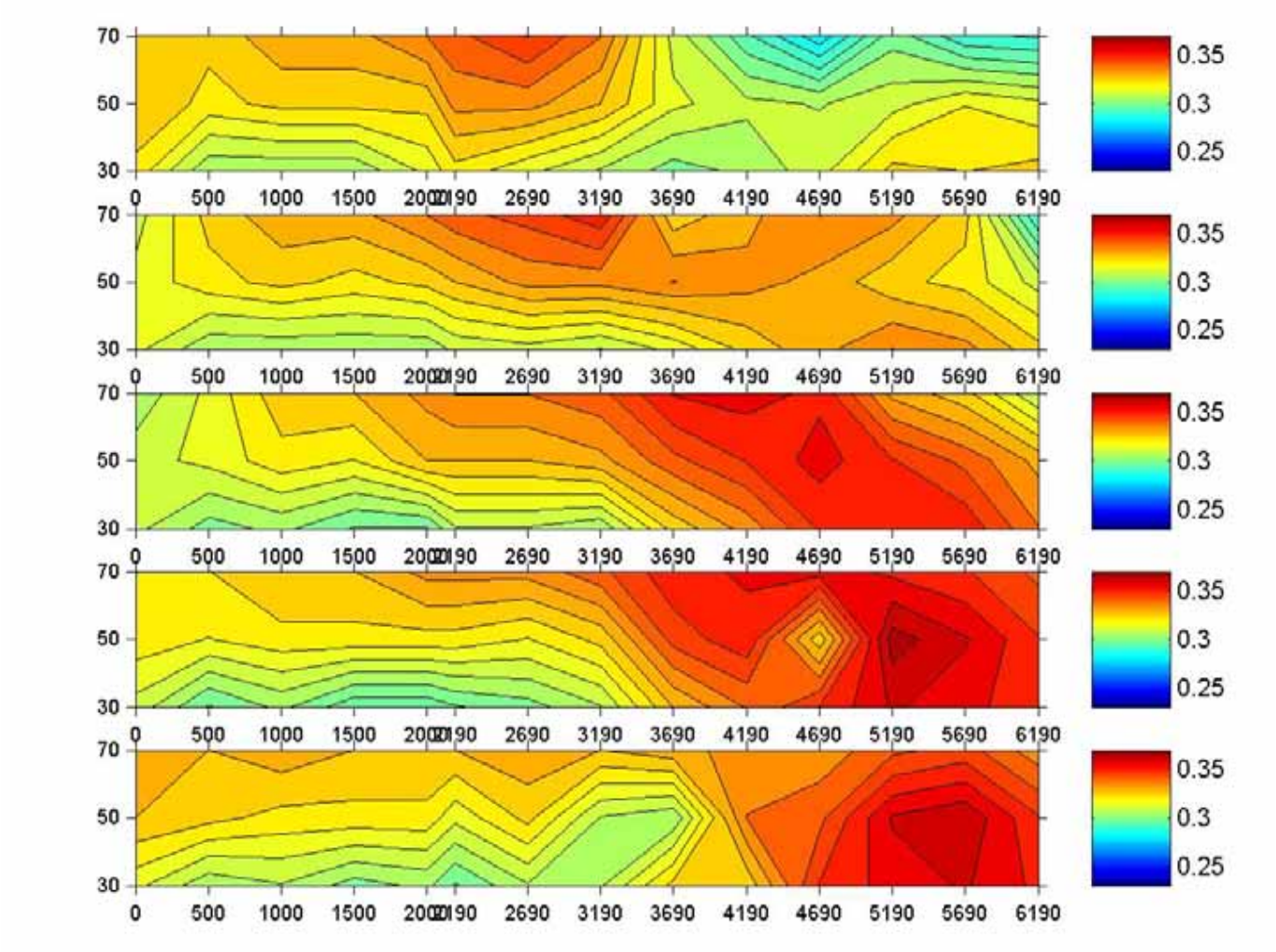

Figure A - 45: Test B2-Velocity distribution in the vertical plane

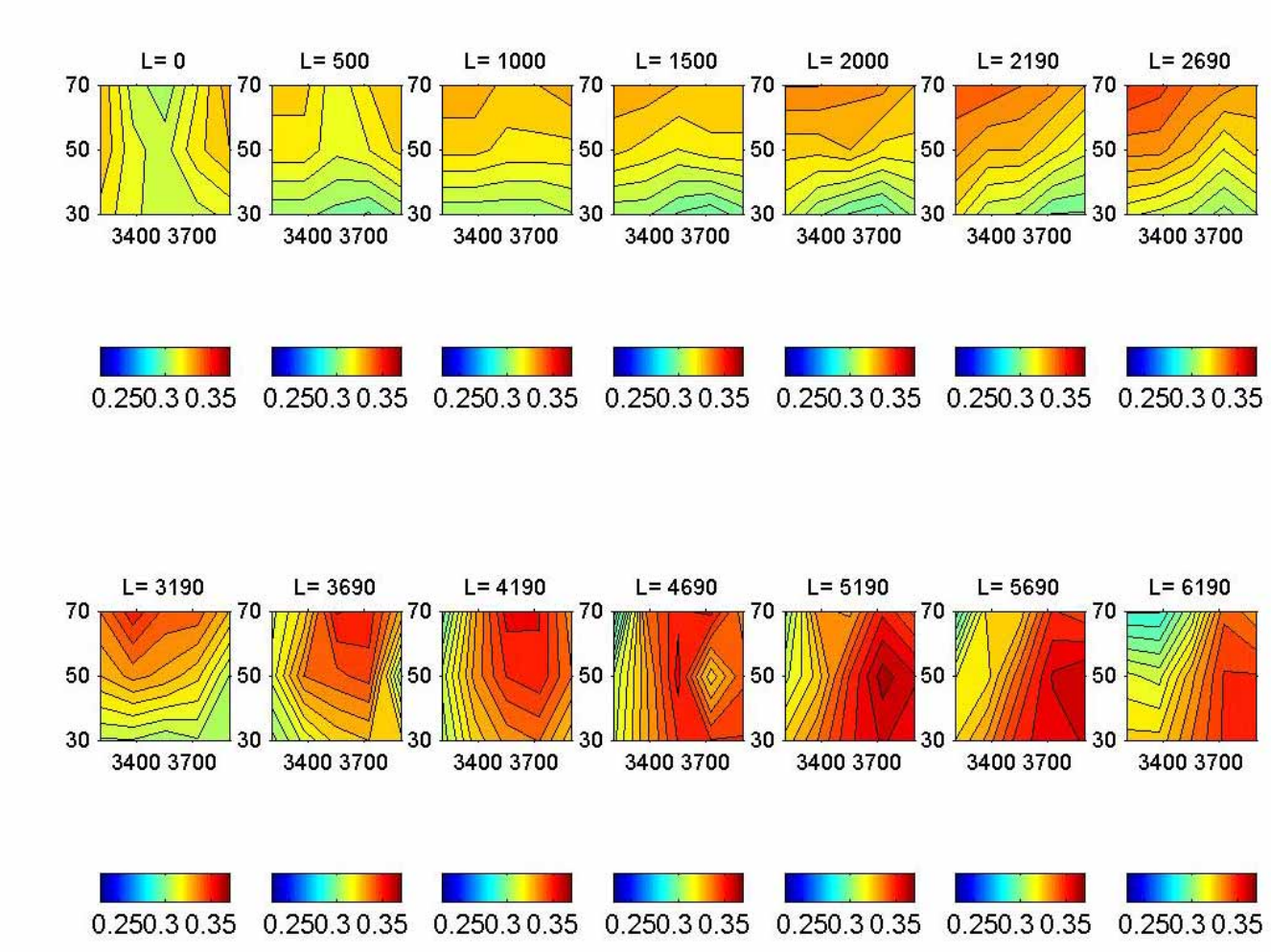

Figure A - 46: Test B2-Cross-sectional velocity distribution

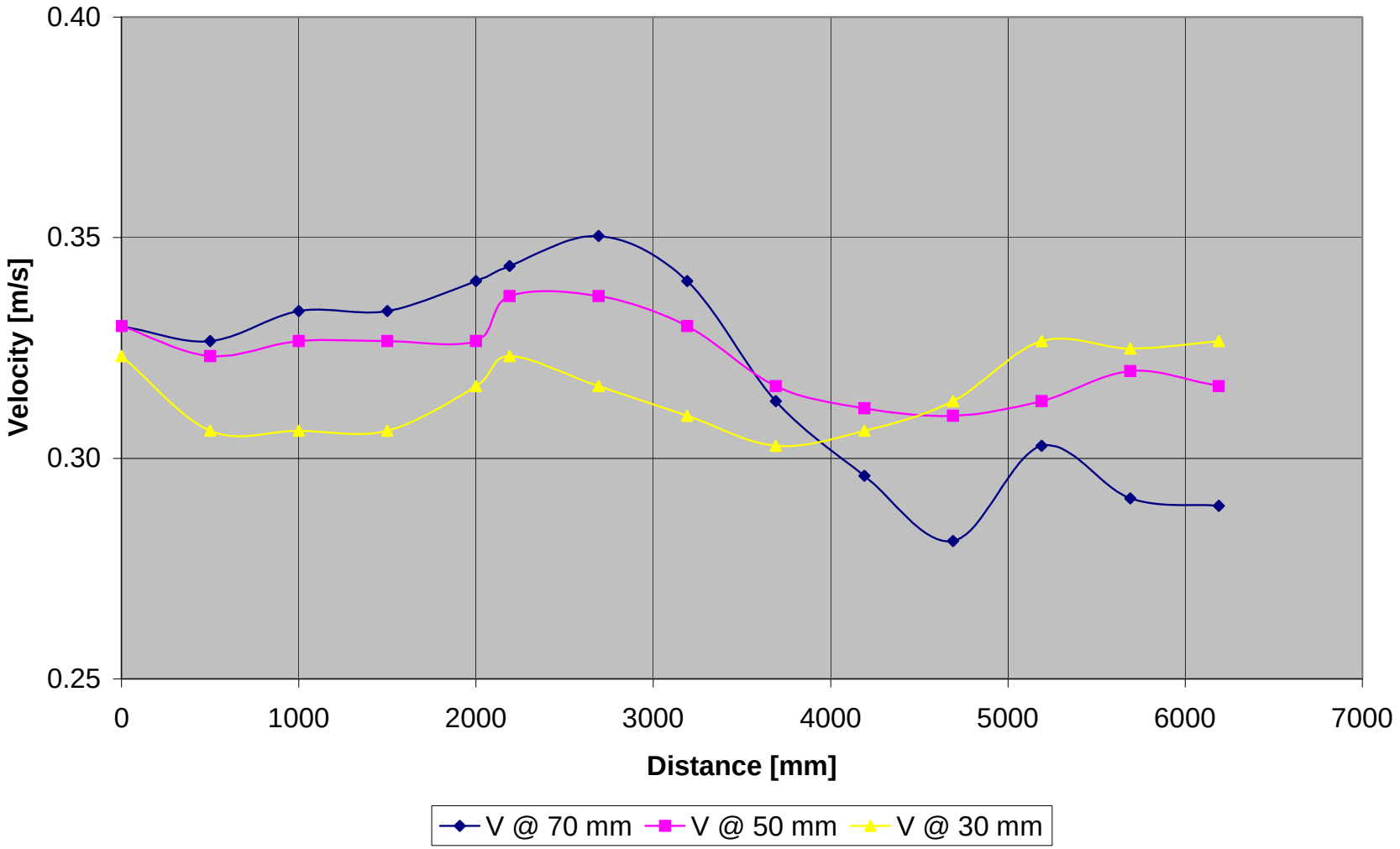

Figure A - 47: Test B2-Vertical velocity distribution measured at 50 mm from inner bank of bend

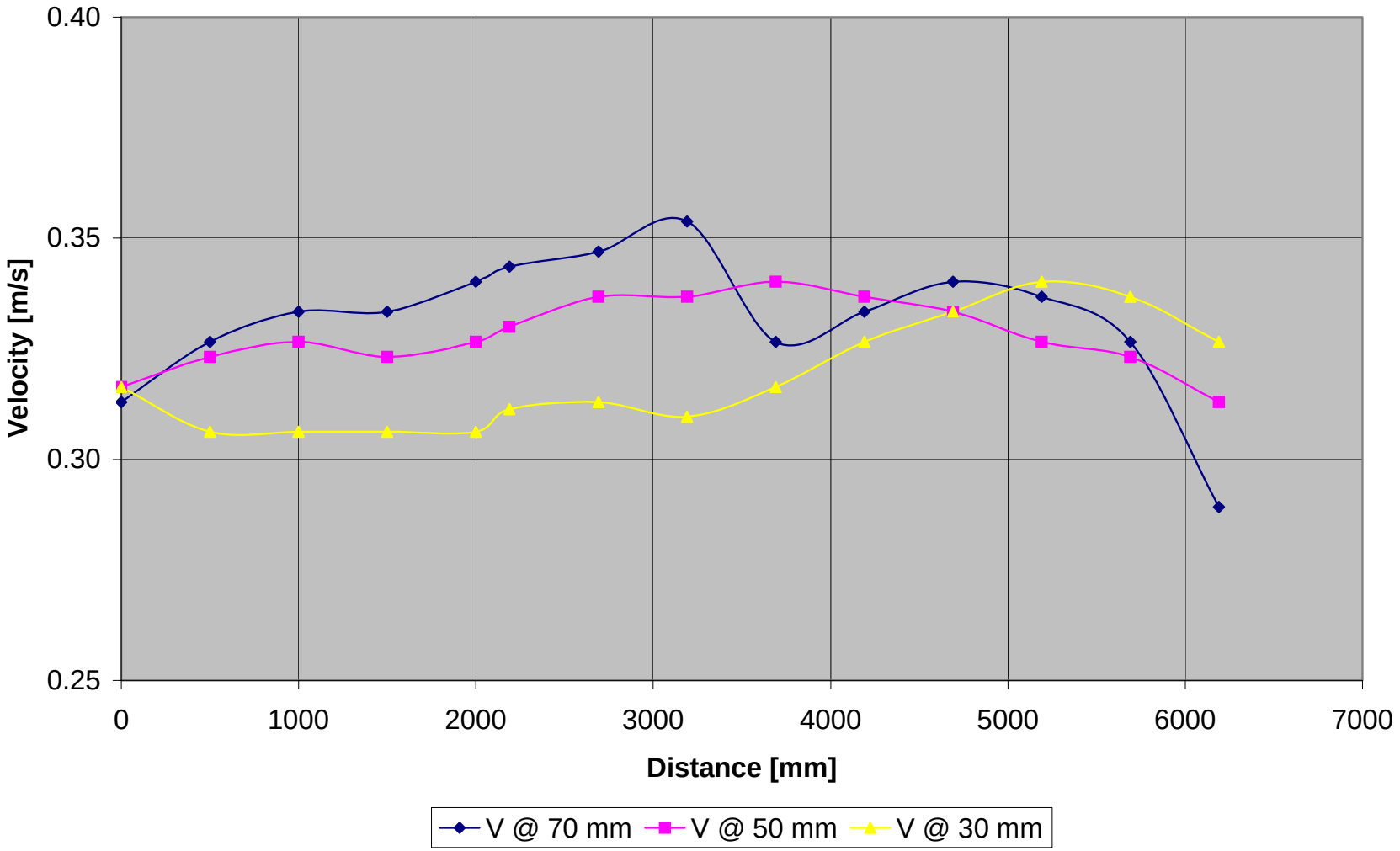

Figure A - 48: Test B2-Vertical velocity distribution measured at 100 mm from inner bank of bend

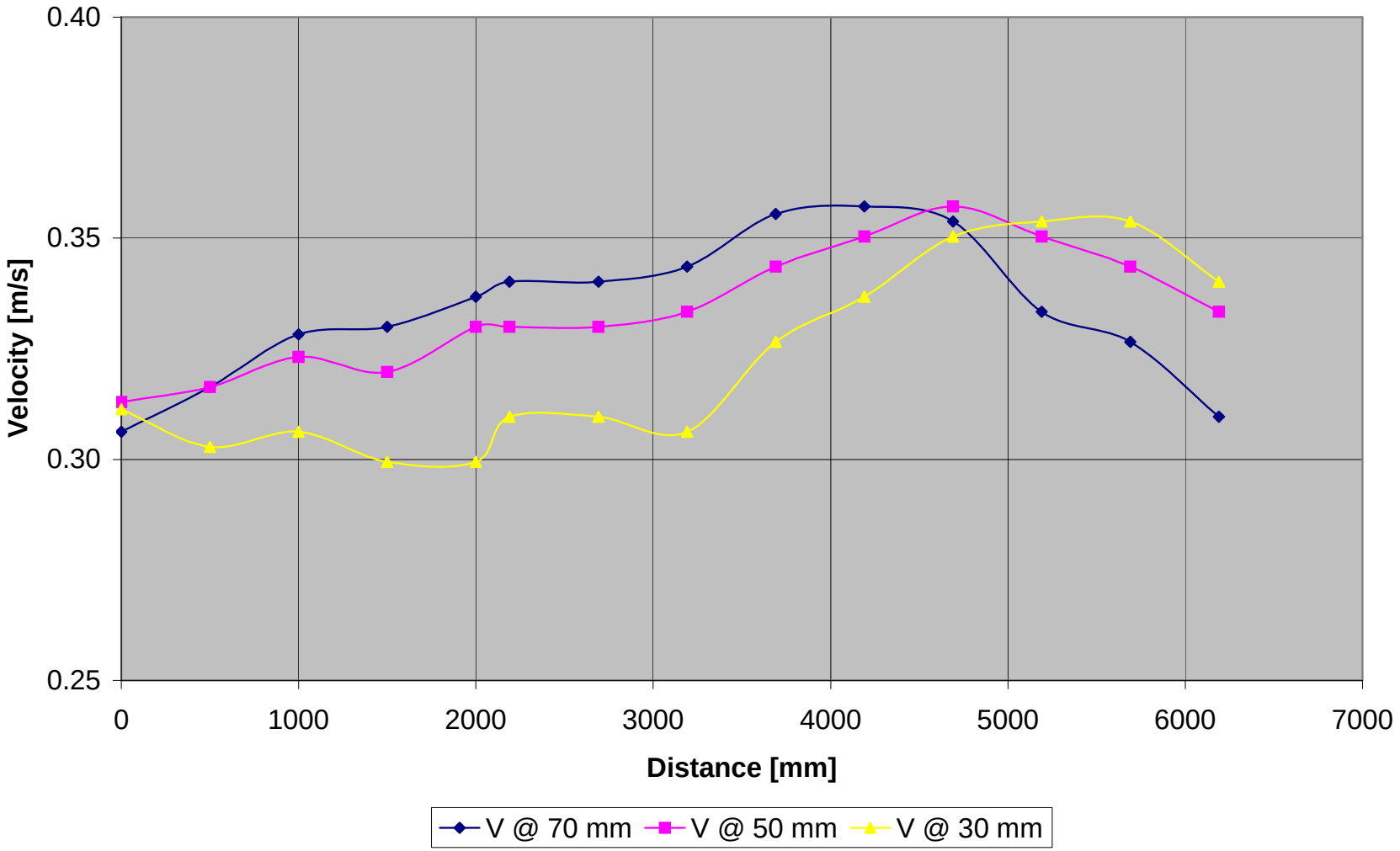

Figure A - 49: Test B2-Vertical velocity distribution measured at 150 mm from inner bank of bend

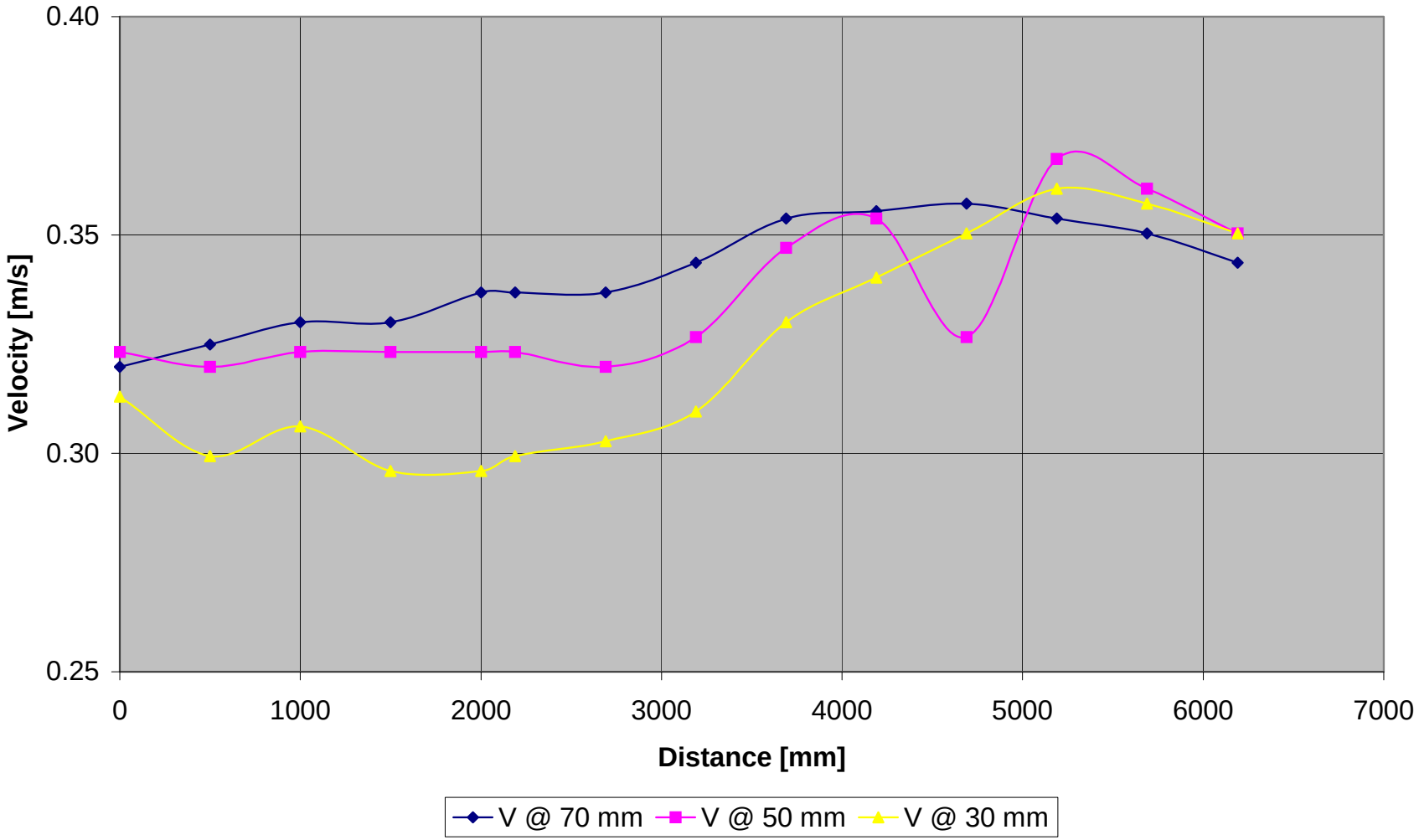

Figure A - 50: Test B2-Vertical velocity distribution measured at 200 mm from inner bank of bend

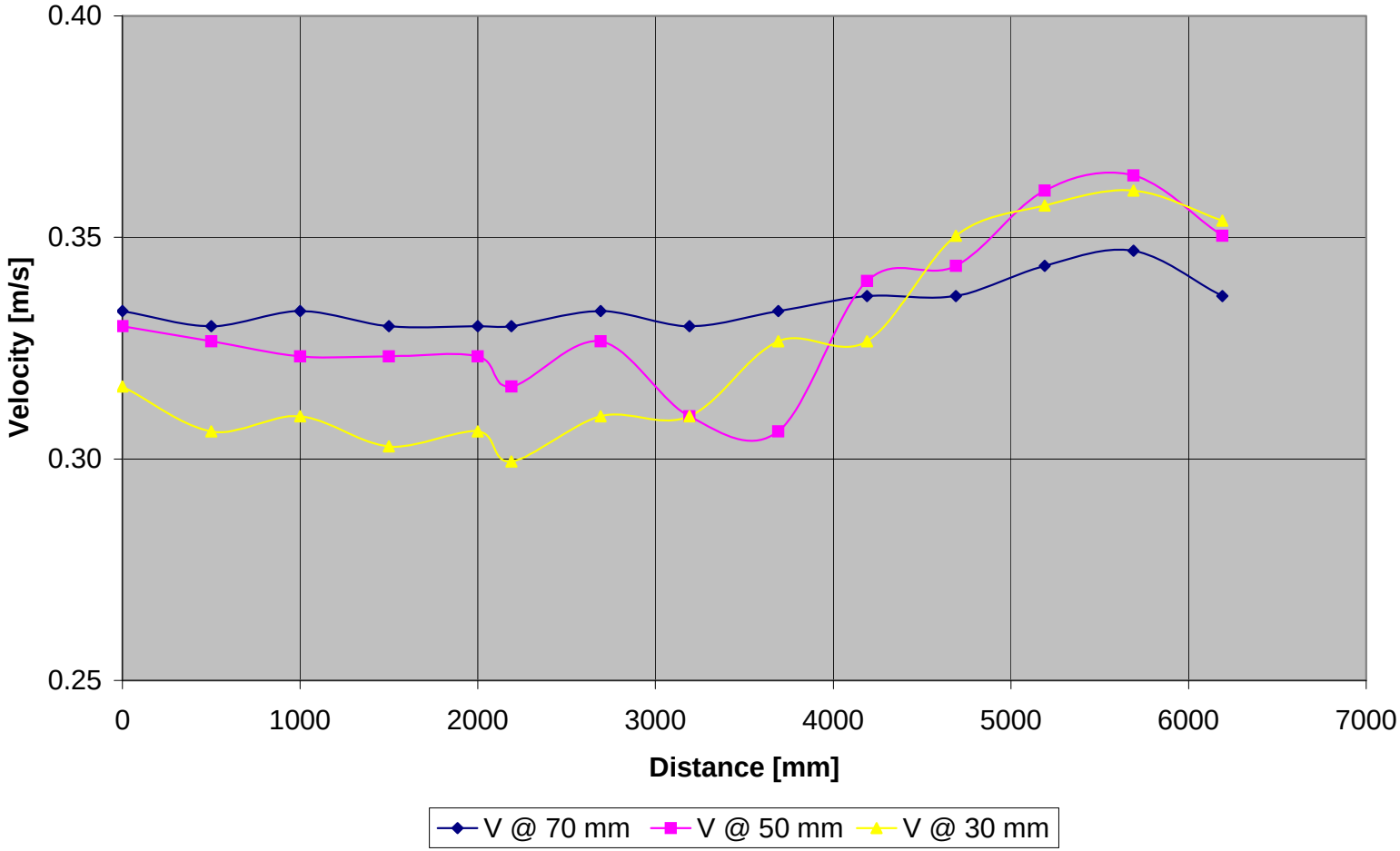

Figure A - 51: Test B2-Vertical velocity distribution measured at 250 mm from inner bank of bend

	Point	1	2	3	4	5	6	7	8	9	10	11	12	13	14
Width	**L**	**0**	**500**	**1000**	**1500**	**2000**	**2190**	**2690**	**3190**	**3690**	**4190**	**4690**	**5190**	**5690**	**6190**
	h														
50	**70**	0.330	0.327	0.333	0.333	0.340	0.344	0.350	0.340	0.313	0.296	0.281	0.303	0.291	0.289
	50	0.330	0.323	0.327	0.327	0.327	0.337	0.337	0.330	0.316	0.311	0.310	0.313	0.320	0.316
	30	0.323	0.306	0.306	0.306	0.316	0.323	0.316	0.310	0.303	0.306	0.313	0.327	0.325	0.327
100	**70**	0.313	0.327	0.333	0.333	0.340	0.344	0.347	0.354	0.327	0.333	0.340	0.337	0.327	0.289
	50	0.316	0.323	0.327	0.323	0.327	0.330	0.337	0.337	0.340	0.337	0.333	0.327	0.323	0.313
	30	0.316	0.306	0.306	0.306	0.306	0.311	0.313	0.310	0.316	0.327	0.333	0.340	0.337	0.327
150	**70**	0.306	0.316	0.328	0.330	0.337	0.340	0.340	0.344	0.356	0.357	0.354	0.333	0.327	0.310
	50	0.313	0.316	0.323	0.320	0.330	0.330	0.330	0.333	0.344	0.350	0.357	0.350	0.344	0.333
	30	0.311	0.303	0.306	0.299	0.299	0.310	0.310	0.306	0.327	0.337	0.350	0.354	0.354	0.340
200	**70**	0.320	0.325	0.330	0.330	0.337	0.337	0.337	0.344	0.354	0.356	0.357	0.354	0.350	0.344
	50	0.323	0.320	0.323	0.323	0.323	0.323	0.320	0.327	0.347	0.354	0.327	0.367	0.361	0.350
	30	0.313	0.299	0.306	0.296	0.296	0.299	0.303	0.310	0.330	0.340	0.350	0.361	0.357	0.350
250															
	70	0.333	0.330	0.333	0.330	0.330	0.330	0.333	0.330	0.333	0.337	0.337	0.344	0.347	0.337
	50	0.330	0.327	0.323	0.323	0.323	0.316	0.327	0.310	0.306	0.340	0.344	0.361	0.364	0.350
	30	0.316	0.306	0.310	0.303	0.306	0.299	0.310	0.310	0.327	0.327	0.350	0.357	0.361	0.354

Table A - 10: Test B2-Measured velocities [m/s]

A.2.1.3 TEST B3 (F_R = 0.5)

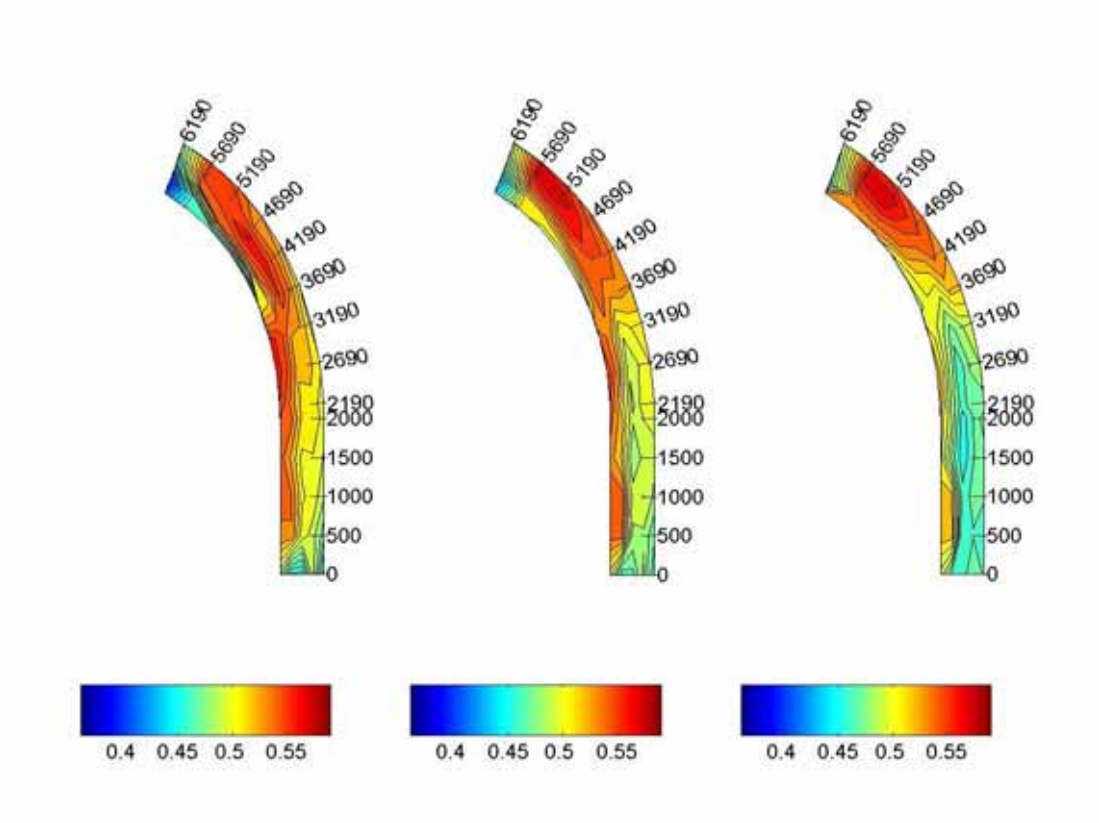

Figure A - 52: Test B3-Velocity distribution in the horizontal plane measured at 70, 50 and 30 mm

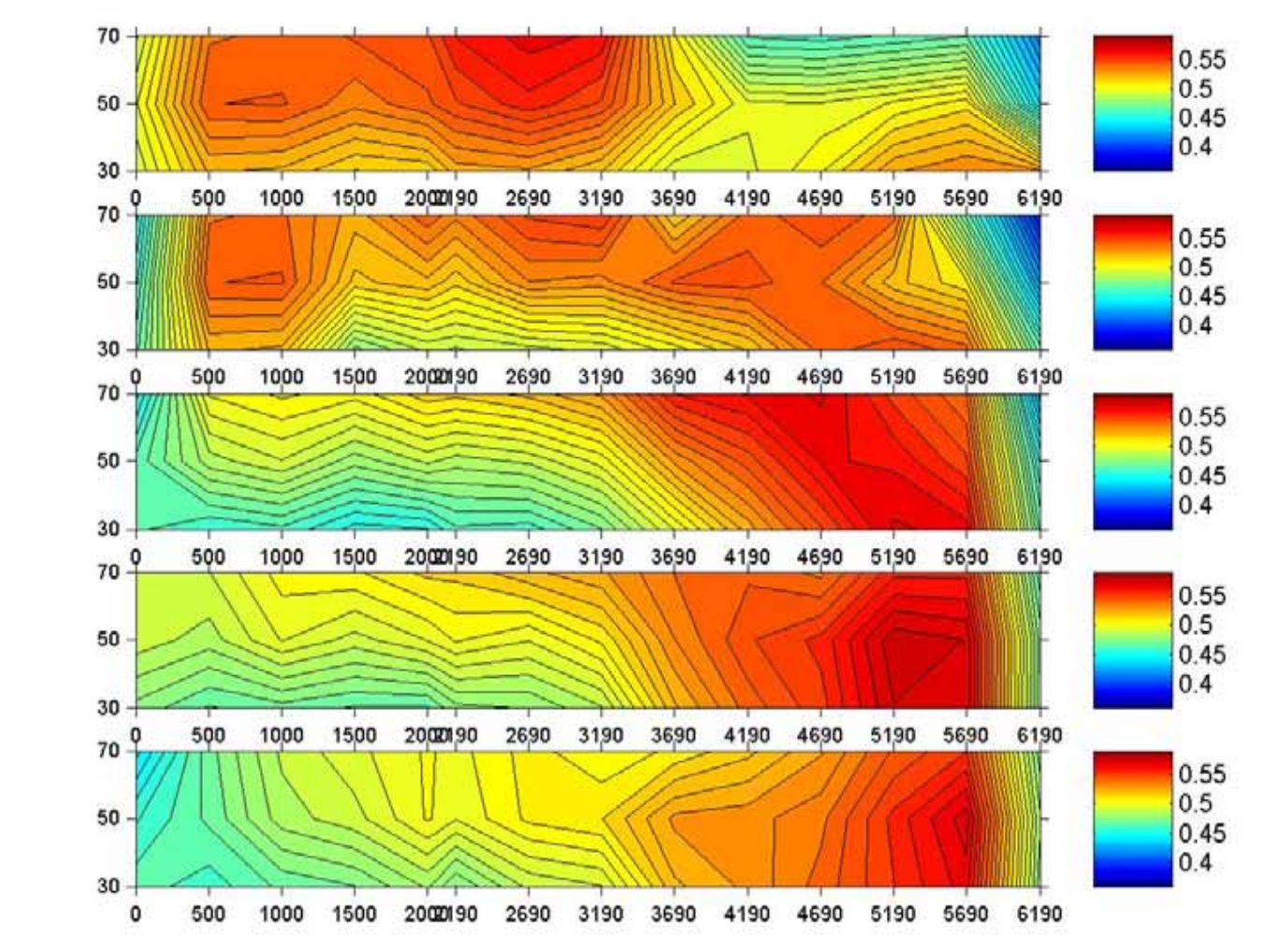

Figure A - 53: Test B3-Velocity distribution in the vertical plane

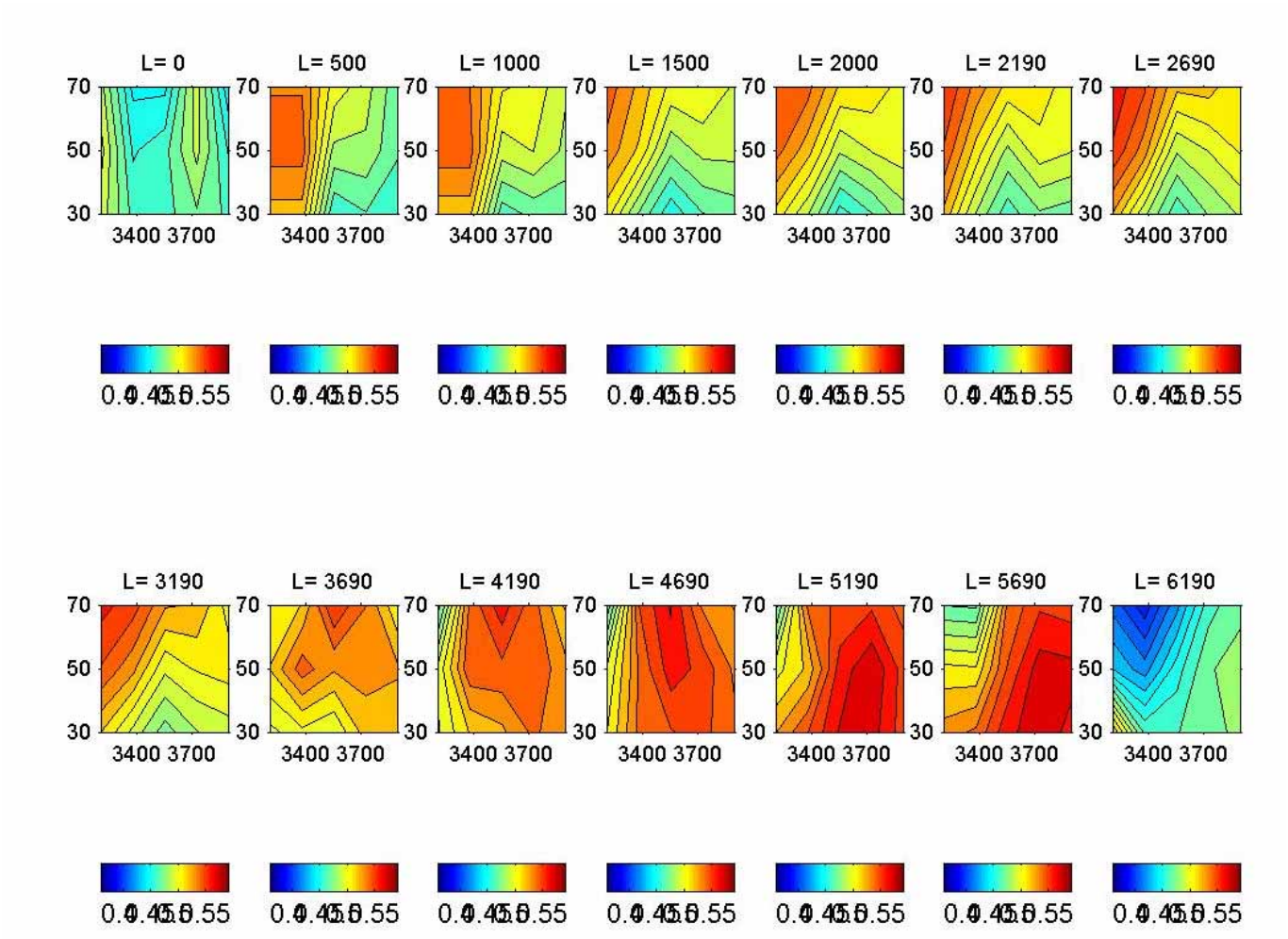

Figure A - 54: Test B3-Cross-sectional velocity distribution

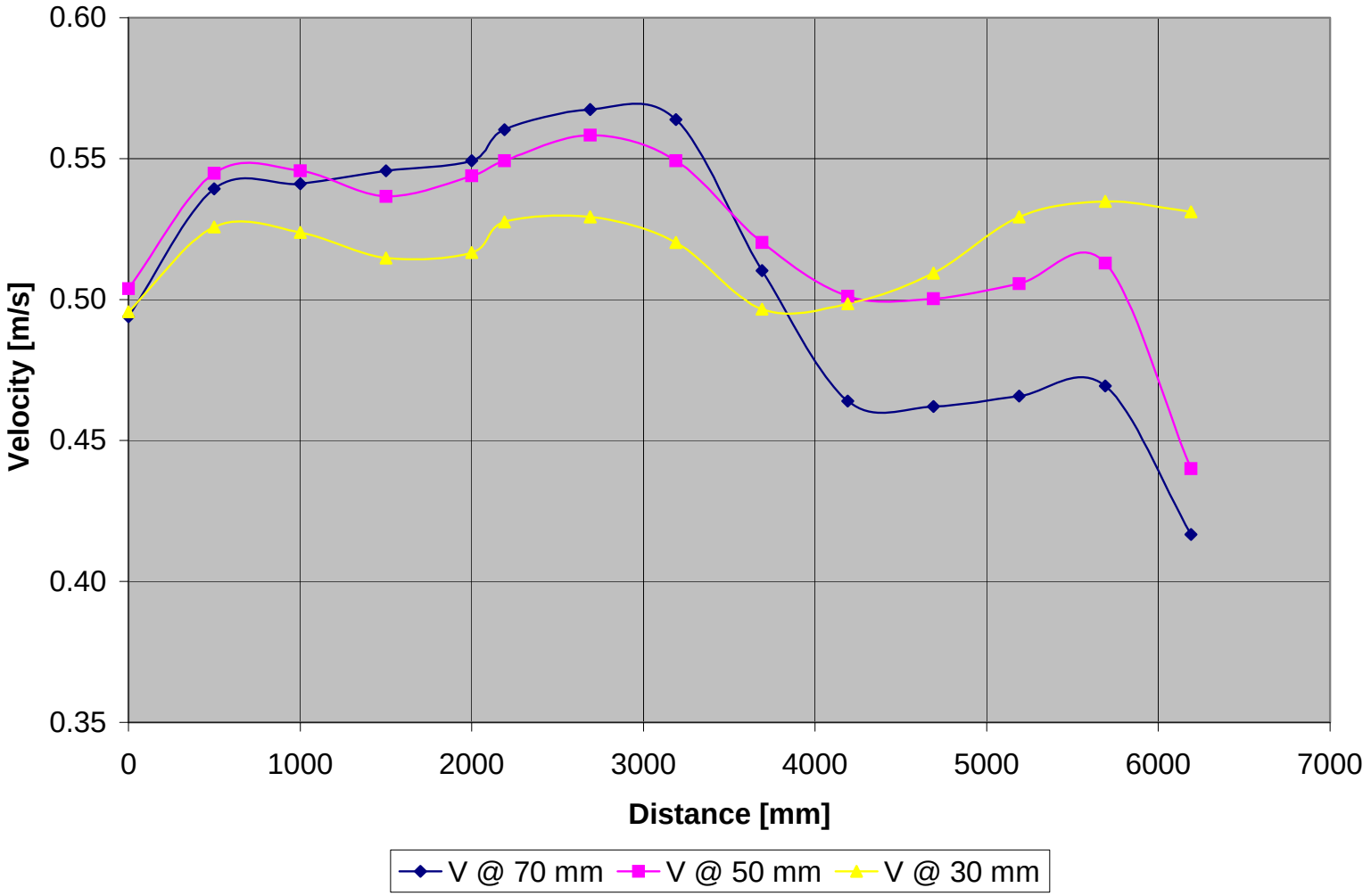

Figure A - 55: Test B3-Vertical velocity distribution measured at 50 mm from inner bank of bend

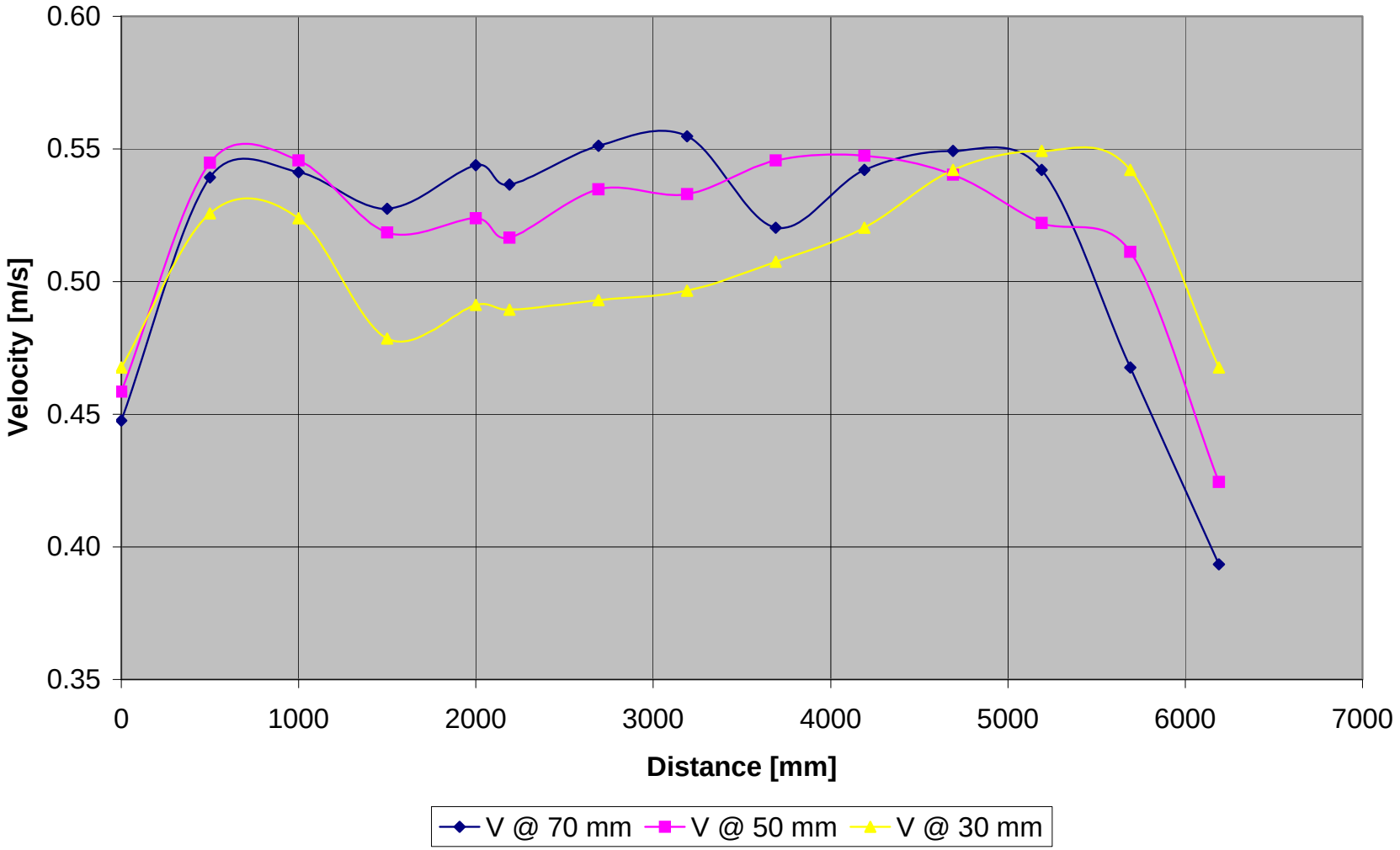

Figure A - 56: Test B3-Vertical velocity distribution measured at 100 mm from inner bank of bend

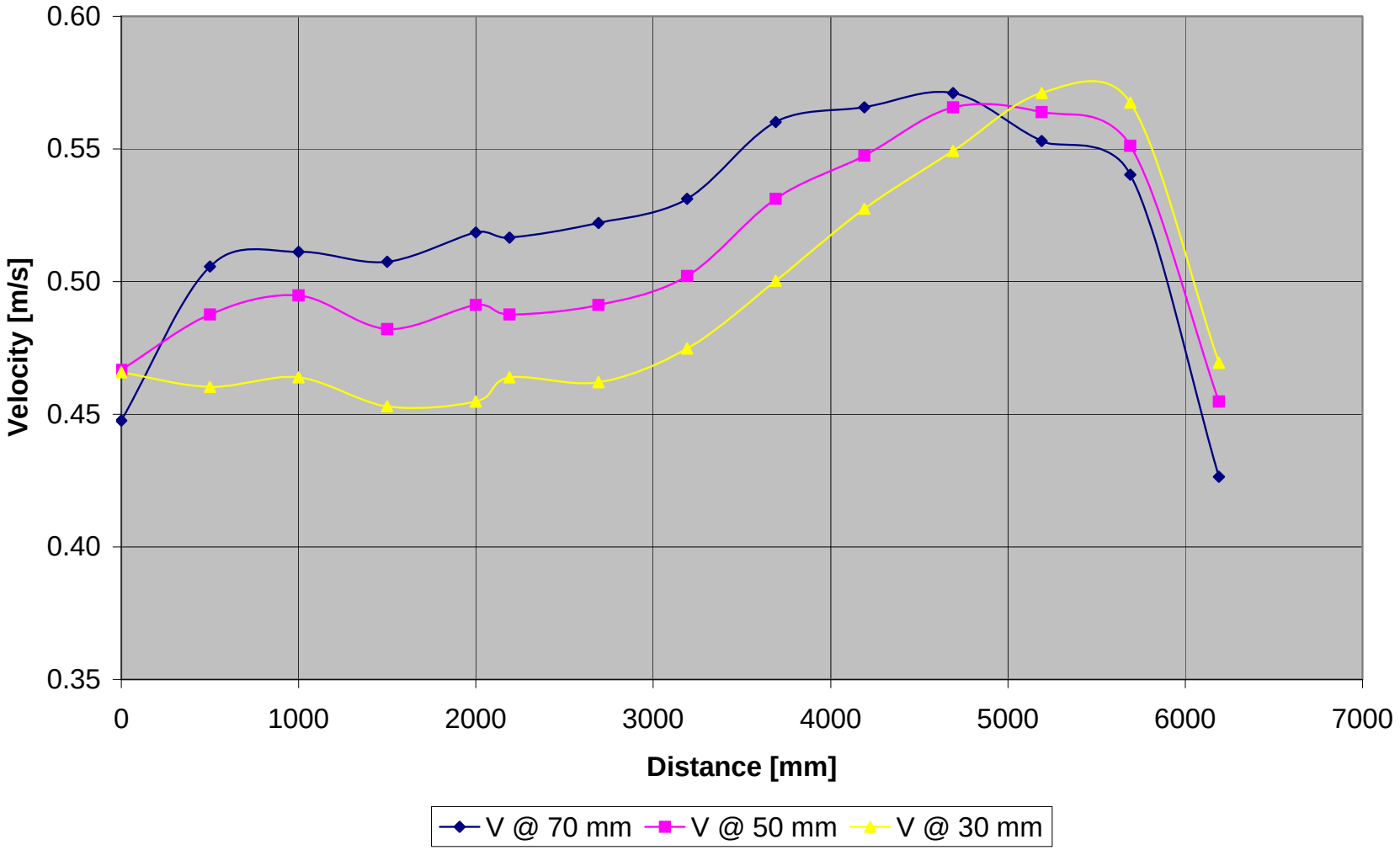

Figure A - 57: Test B3-Vertical velocity distribution measured at 150 mm from inner bank of bend

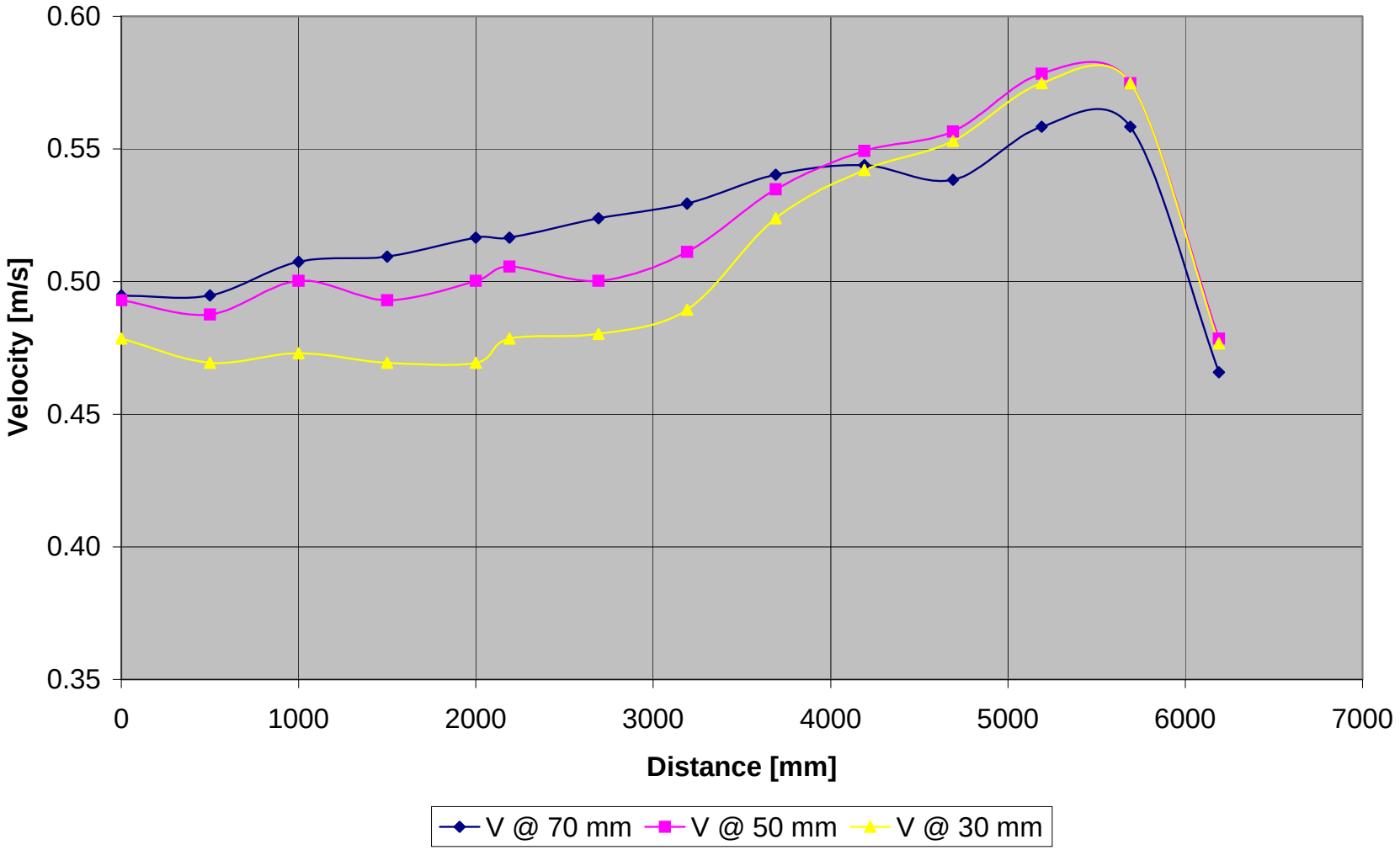

Figure A - 58: Test B3-Vertical velocity distribution measured at 200 mm from inner bank of bend

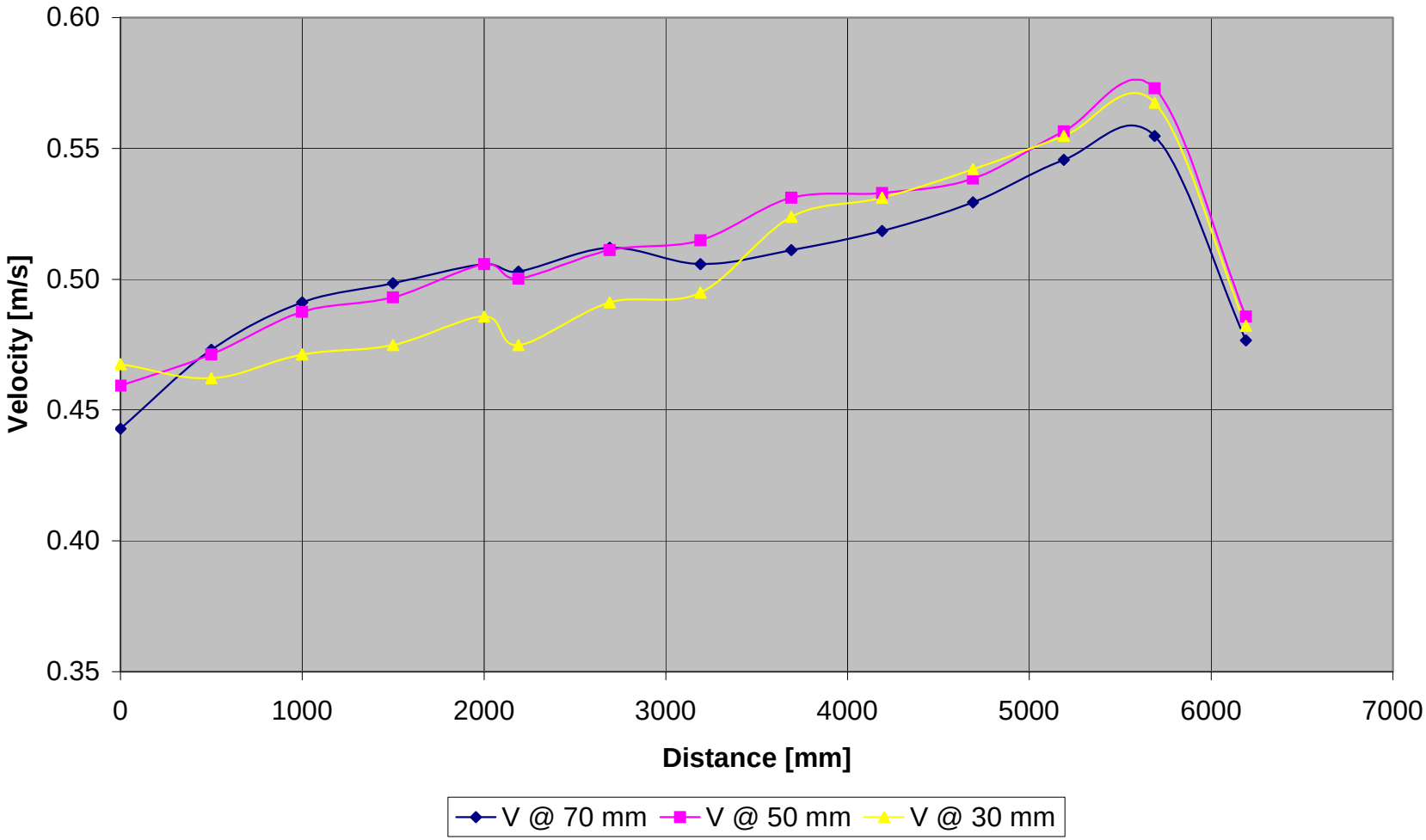

Figure A - 59: Test B3-Vertical velocity distribution measured at 250 mm from inner bank of bend

	Point	1	2	3	4	5	6	7	8	9	10	11	12	13	14
Width	**L**	**0**	**500**	**1000**	**1500**	**2000**	**2190**	**2690**	**3190**	**3690**	**4190**	**4690**	**5190**	**5690**	**6190**
	h														
50	**70**	0.494	0.539	0.541	0.546	0.549	0.560	0.567	0.564	0.510	0.464	0.462	0.466	0.469	0.417
	50	0.504	0.545	0.546	0.537	0.544	0.549	0.558	0.549	0.520	0.501	0.500	0.506	0.513	0.440
	30	0.496	0.526	0.524	0.515	0.517	0.528	0.529	0.520	0.497	0.498	0.509	0.529	0.535	0.531
100	**70**	0.448	0.539	0.541	0.528	0.544	0.537	0.551	0.555	0.520	0.542	0.549	0.542	0.468	0.393
	50	0.458	0.545	0.546	0.518	0.524	0.517	0.535	0.533	0.546	0.548	0.540	0.522	0.511	0.424
	30	0.468	0.526	0.524	0.478	0.491	0.489	0.493	0.497	0.508	0.520	0.542	0.549	0.542	0.468
150	**70**	0.448	0.506	0.511	0.508	0.518	0.517	0.522	0.531	0.560	0.566	0.571	0.553	0.540	0.426
	50	0.467	0.488	0.495	0.482	0.491	0.488	0.491	0.502	0.531	0.548	0.566	0.564	0.551	0.455
	30	0.466	0.460	0.464	0.453	0.455	0.464	0.462	0.475	0.500	0.528	0.549	0.571	0.567	0.469
200	**70**	0.495	0.495	0.508	0.509	0.517	0.517	0.524	0.529	0.540	0.544	0.538	0.558	0.558	0.466
	50	0.493	0.488	0.500	0.493	0.500	0.506	0.500	0.511	0.535	0.549	0.557	0.578	0.575	0.478
	30	0.478	0.469	0.473	0.469	0.469	0.478	0.480	0.489	0.524	0.542	0.553	0.575	0.575	0.477
250															
	70	0.443	0.473	0.491	0.498	0.506	0.503	0.512	0.506	0.511	0.518	0.529	0.546	0.555	0.477
	50	0.459	0.471	0.488	0.493	0.506	0.500	0.511	0.515	0.531	0.533	0.538	0.557	0.573	0.486
	30	0.468	0.462	0.471	0.475	0.486	0.475	0.491	0.495	0.524	0.531	0.542	0.555	0.567	0.482

Table A - 11: Test B3-Measured velocities [m/s]

A.2.1.4 TEST B4 (F_R = 0.7)

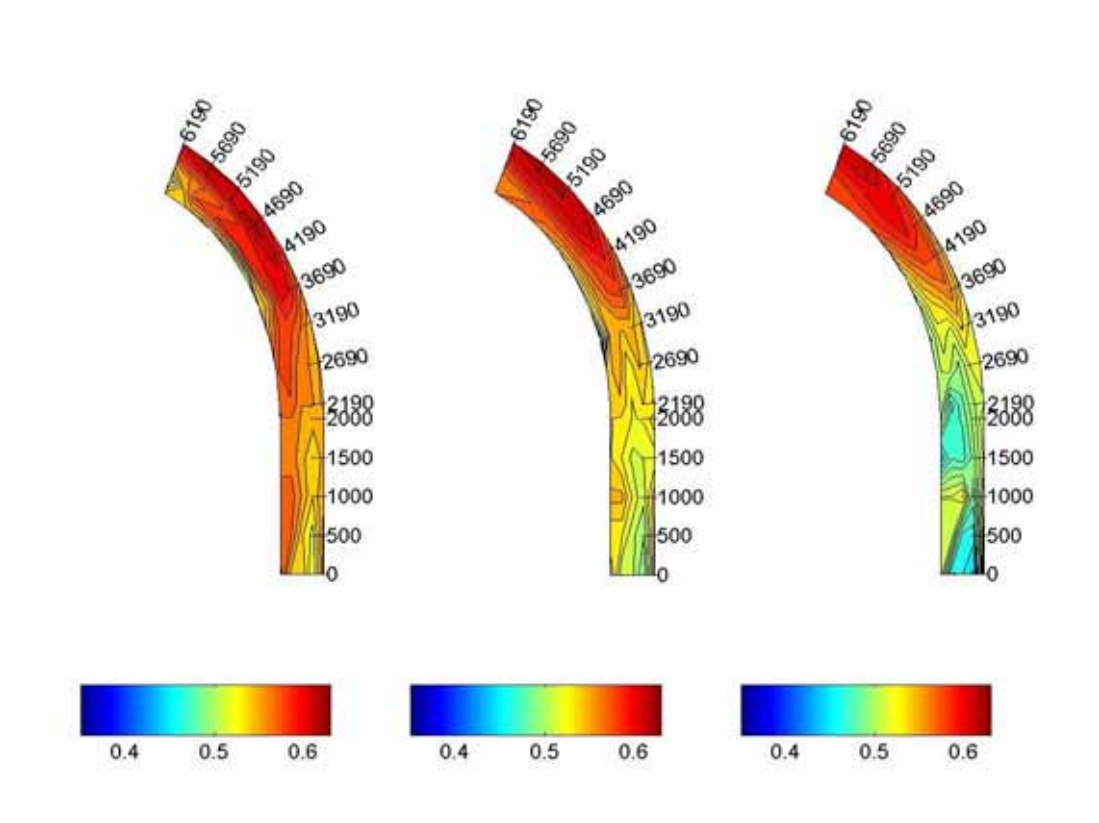

Figure A - 60: Test B4-Velocity distribution in the horisontal plane measured at 70, 50 and 30 mm

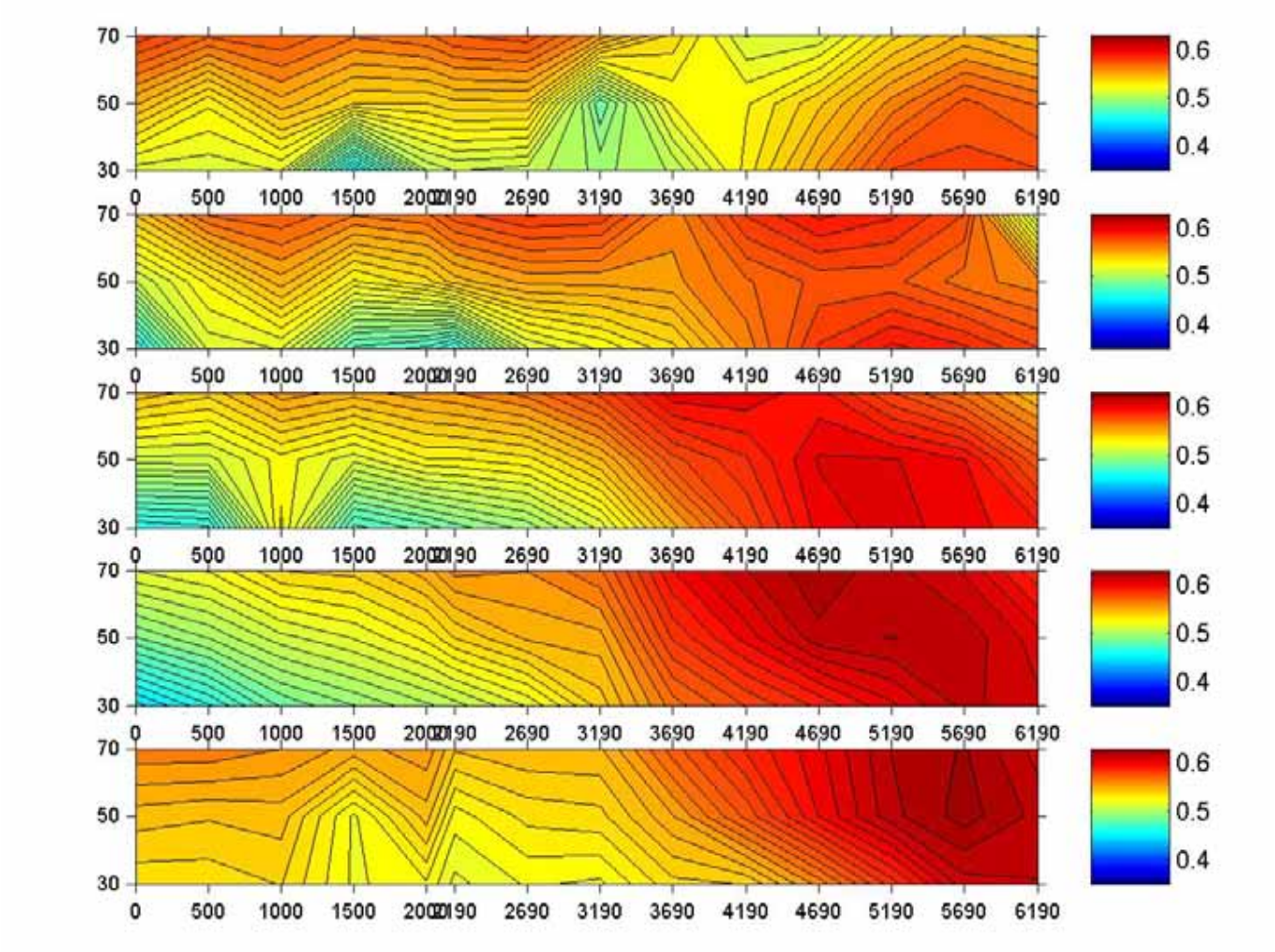

Figure A - 61: Test B4-Velocity distribution in the vertical plane

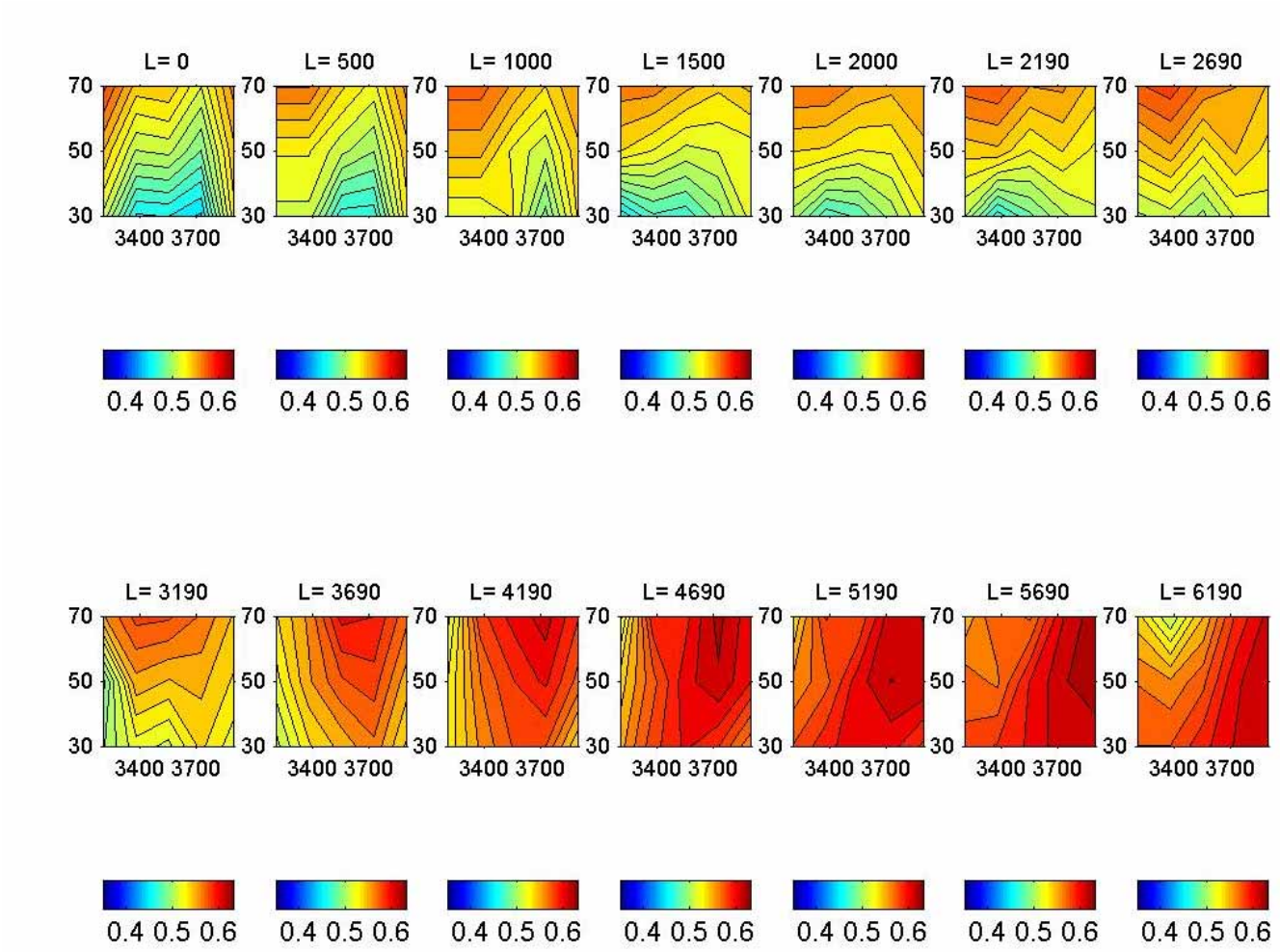

Figure A - 62: Test B4-Cross-sectional velocity distribution

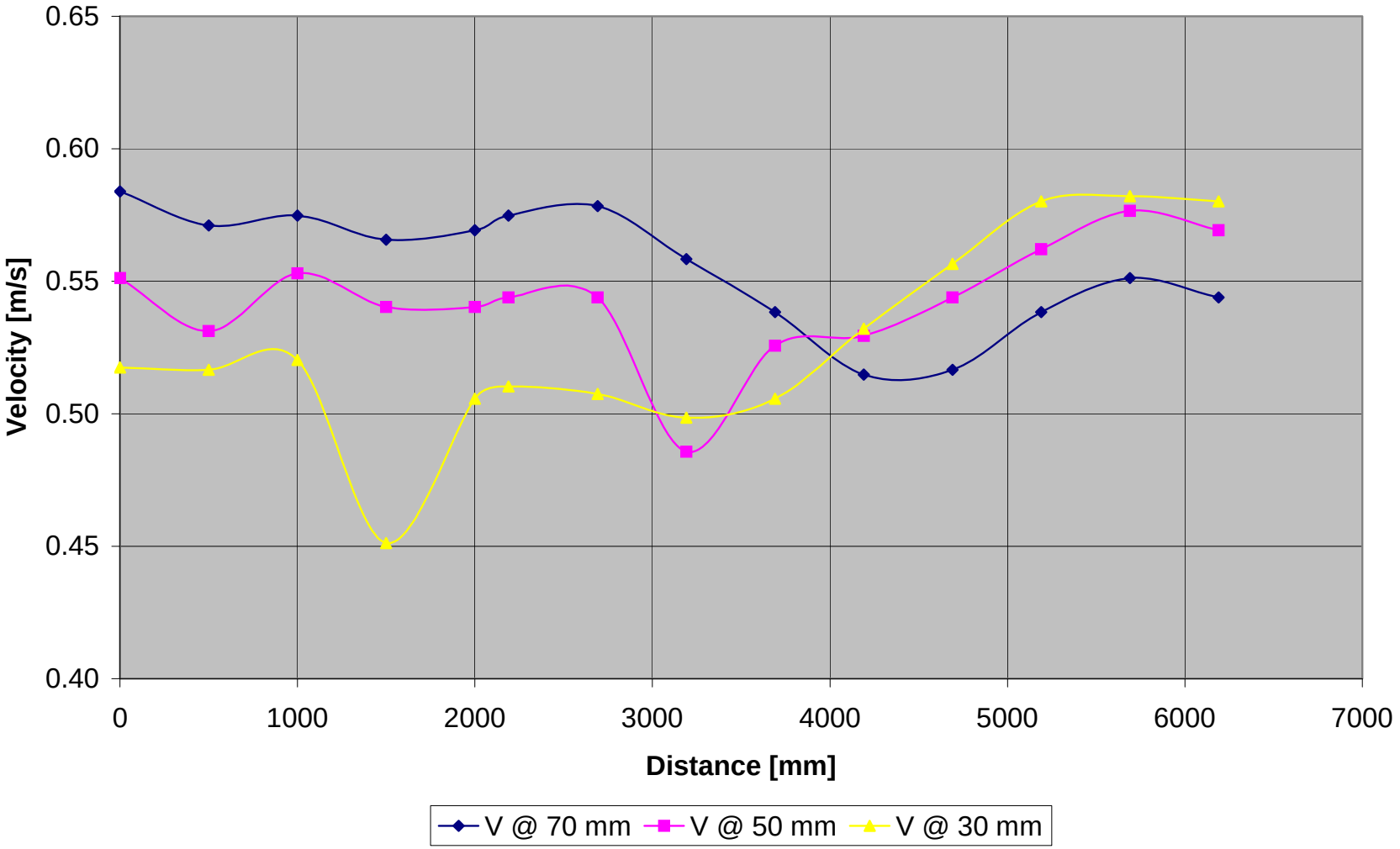

Figure A - 63: Test B4-Vertical velocity distribution measured at 50 mm from inner bank of bend

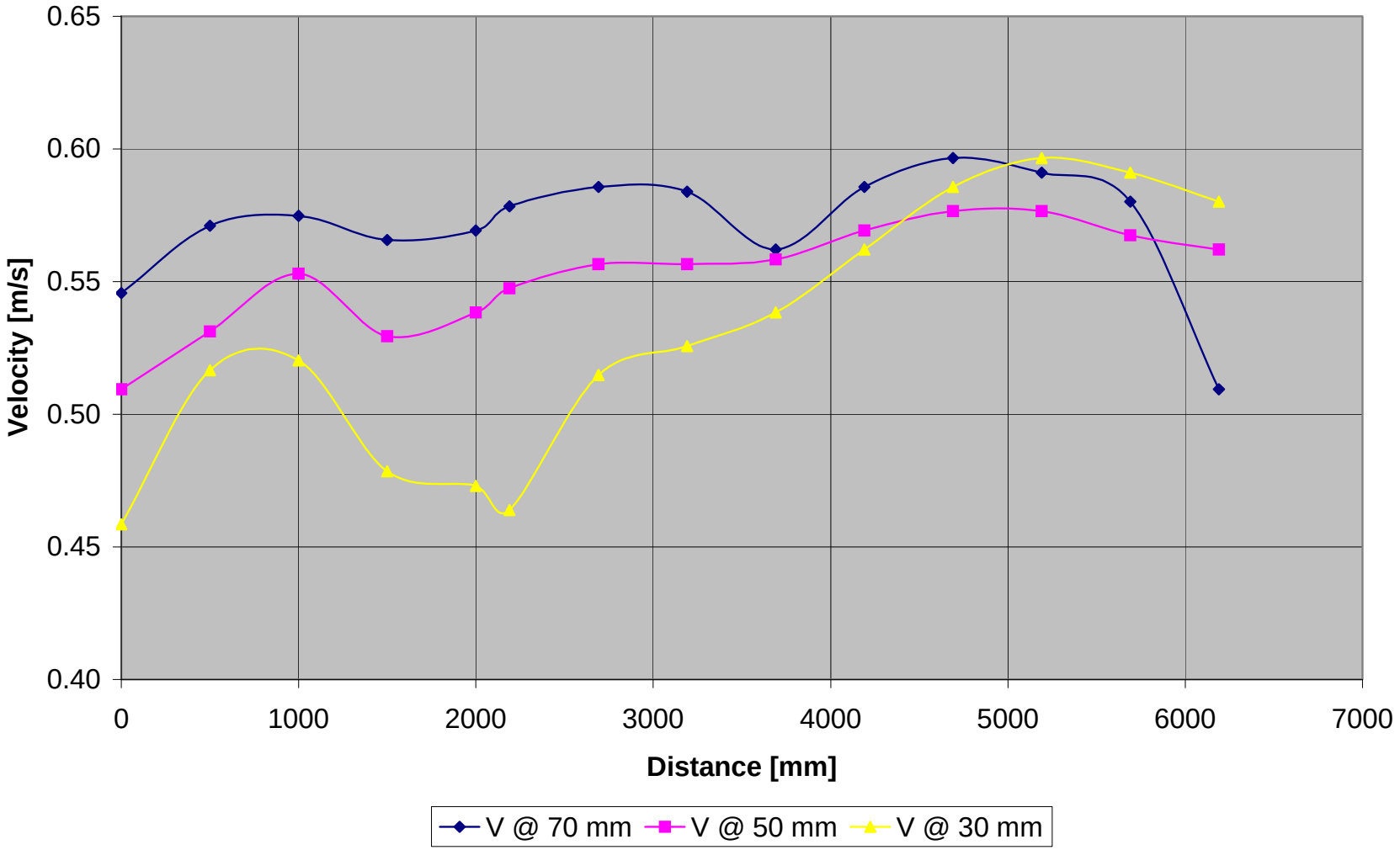

Figure A - 64: Test B4-Vertical velocity distribution measured at 100 mm from inner bank of bend

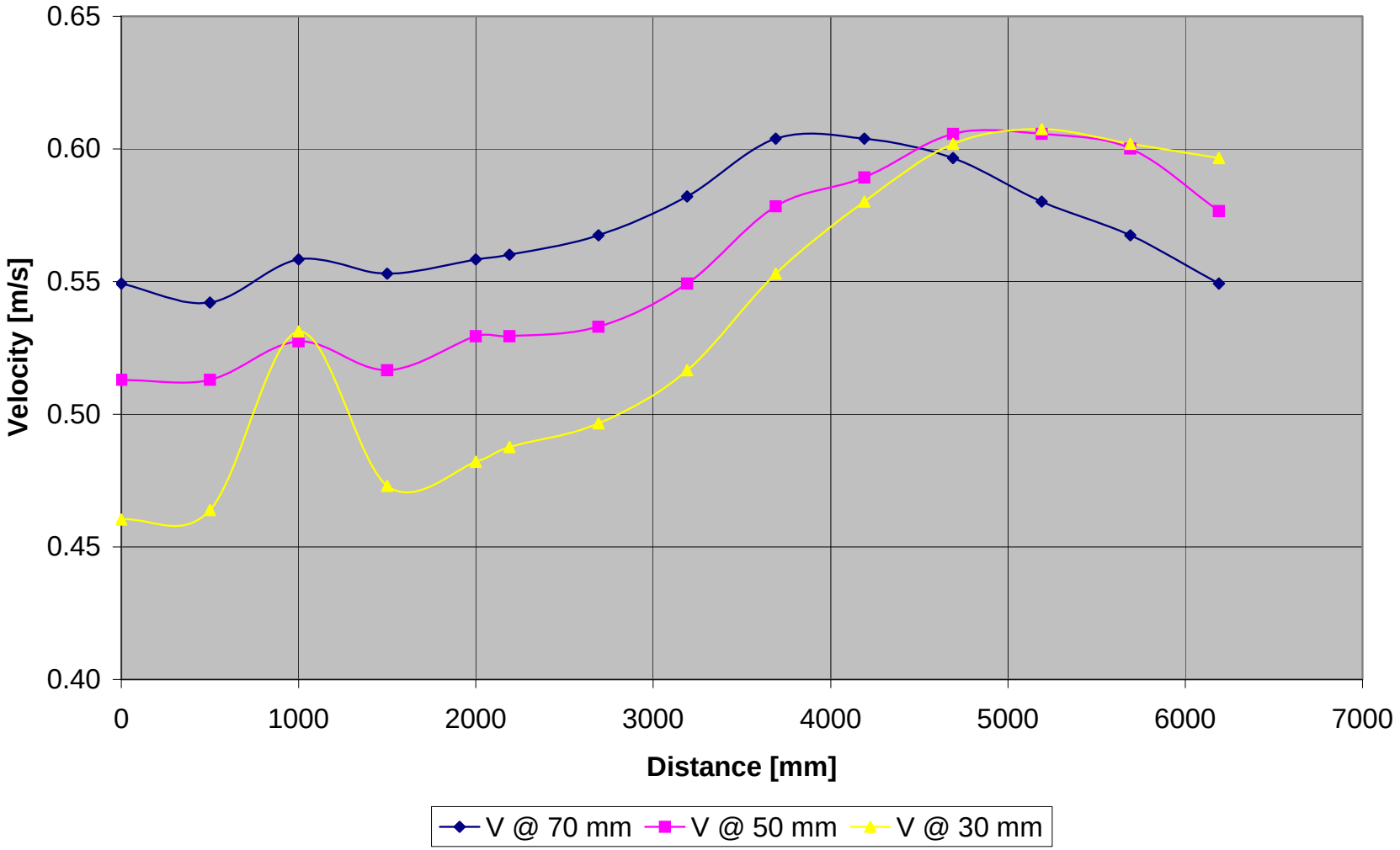

Figure A - 65: Test B4-Vertical velocity distribution measured at 150 mm from inner bank of bend

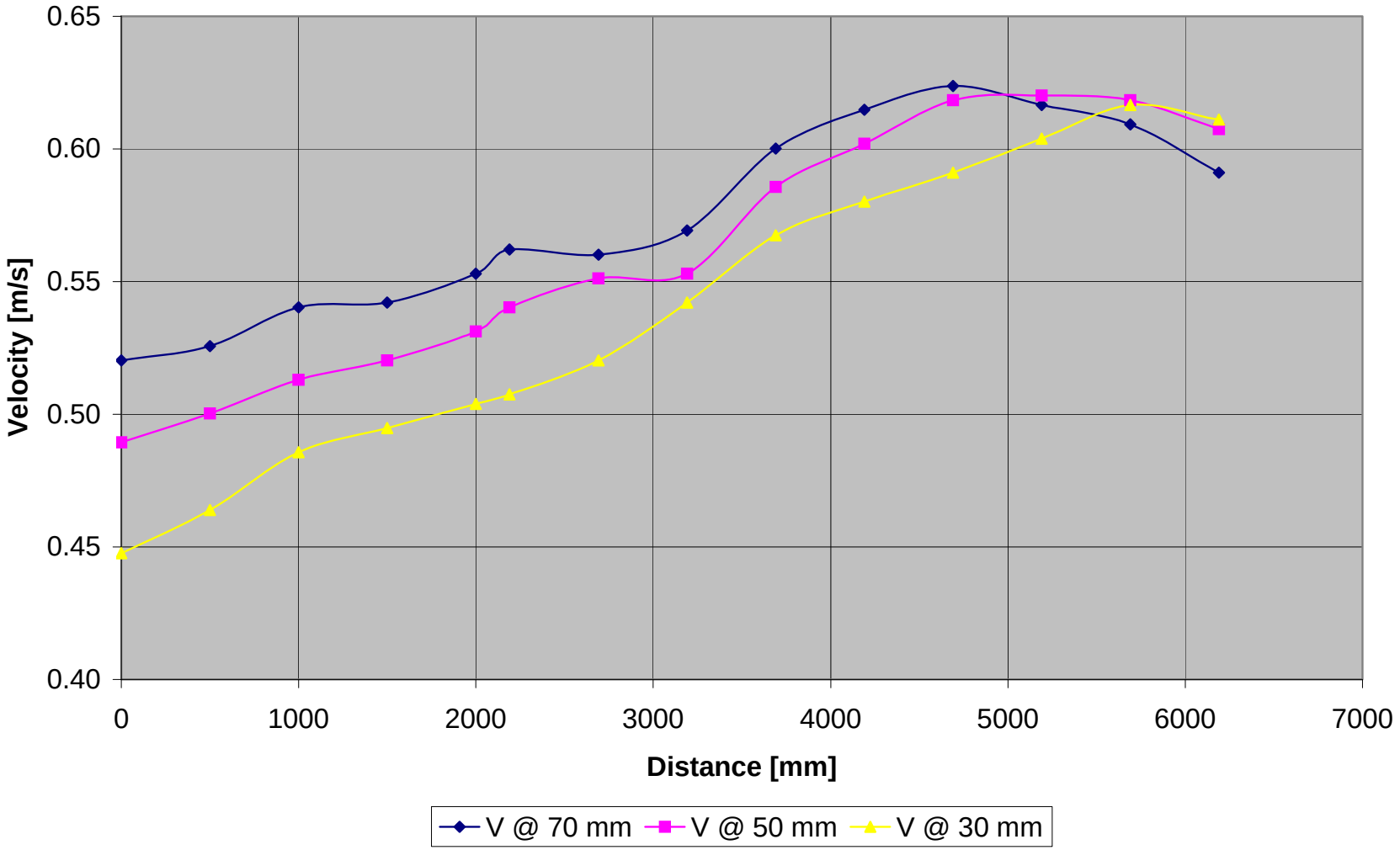

Figure A - 66: Test B4-Vertical velocity distribution measured at 200 mm from inner bank of bend

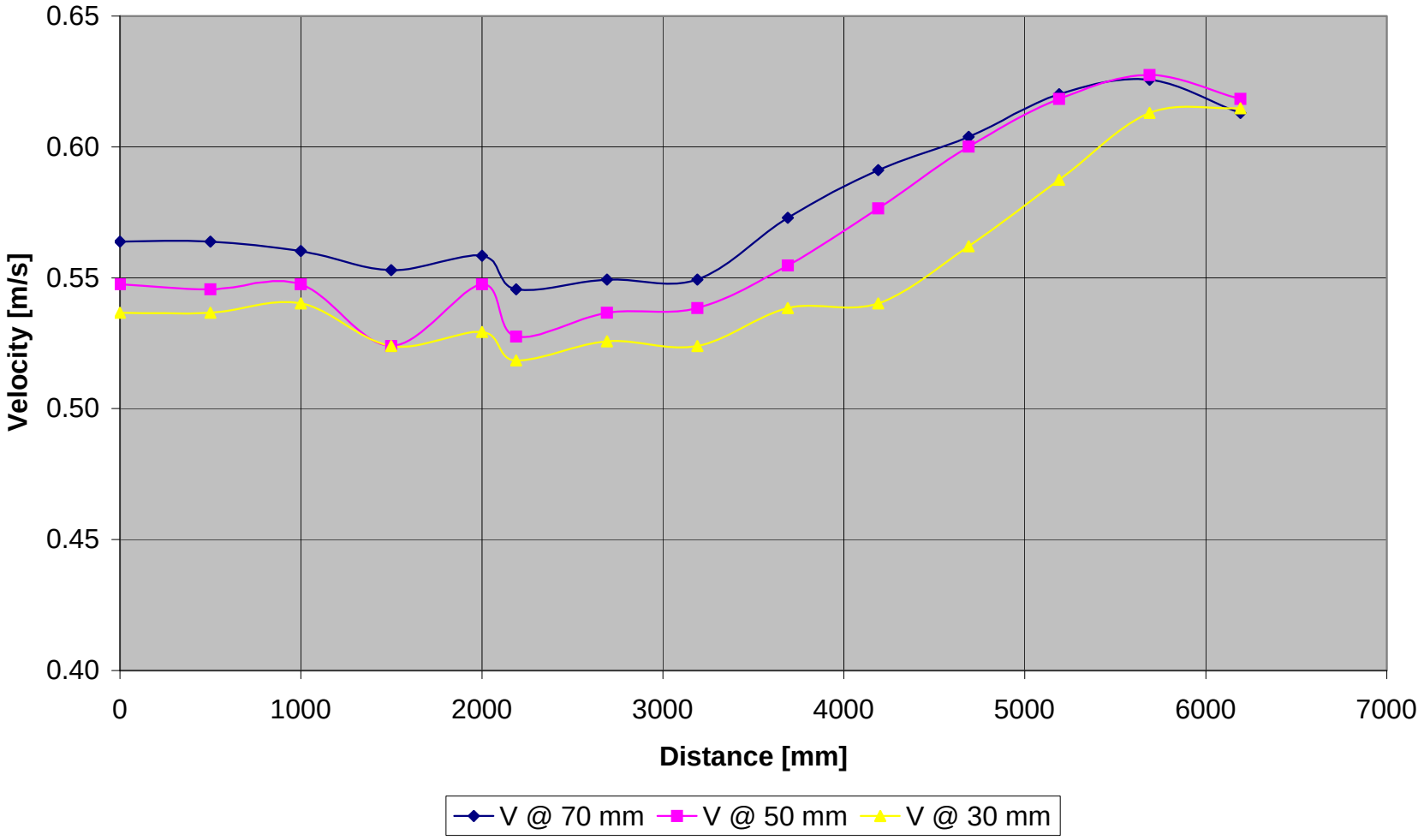

Figure A - 67: Test B4-Vertical velocity distribution measured at 250 mm from inner bank of bend

	Point	1	2	3	4	5	6	7	8	9	10	11	12	13	14
Width	L	0	500	1000	1500	2000	2190	2690	3190	3690	4190	4690	5190	5690	6190
	h														
50	70	0.584	0.571	0.575	0.566	0.569	0.575	0.578	0.558	0.538	0.515	0.517	0.538	0.551	0.544
	50	0.551	0.531	0.553	0.540	0.540	0.544	0.544	0.486	0.526	0.529	0.544	0.562	0.577	0.569
	30	0.518	0.517	0.520	0.451	0.506	0.510	0.508	0.498	0.506	0.532	0.557	0.580	0.582	0.580
100	70	0.546	0.571	0.575	0.566	0.569	0.578	0.586	0.584	0.562	0.586	0.597	0.591	0.580	0.509
	50	0.509	0.531	0.553	0.529	0.538	0.548	0.557	0.557	0.558	0.569	0.577	0.577	0.567	0.562
	30	0.458	0.517	0.520	0.478	0.473	0.464	0.515	0.526	0.538	0.562	0.586	0.597	0.591	0.580
150	70	0.549	0.542	0.558	0.553	0.558	0.560	0.567	0.582	0.604	0.604	0.597	0.580	0.567	0.549
	50	0.513	0.513	0.528	0.517	0.529	0.529	0.533	0.549	0.578	0.589	0.606	0.606	0.600	0.577
	30	0.460	0.464	0.531	0.473	0.482	0.488	0.497	0.517	0.553	0.580	0.602	0.607	0.602	0.597
200	70	0.520	0.526	0.540	0.542	0.553	0.562	0.560	0.569	0.600	0.615	0.624	0.617	0.609	0.591
	50	0.489	0.500	0.513	0.520	0.531	0.540	0.551	0.553	0.586	0.602	0.618	0.620	0.618	0.607
	30	0.448	0.464	0.486	0.495	0.504	0.508	0.520	0.542	0.567	0.580	0.591	0.604	0.617	0.611
250															
	70	0.564	0.564	0.560	0.553	0.558	0.546	0.549	0.549	0.573	0.591	0.604	0.620	0.626	0.613
	50	0.548	0.546	0.548	0.524	0.548	0.528	0.537	0.538	0.555	0.577	0.600	0.618	0.627	0.618
	30	0.537	0.537	0.540	0.524	0.529	0.518	0.526	0.524	0.538	0.540	0.562	0.587	0.613	0.615

Table A - 12: Test B4-Measured velocities [m/s]

A.2.2 SEDIMENT RELATED

A.2.2.1 TEST B5 (F_R = 0.3)

L	Width										
	25	50	75	100	125	150	175	200	225	250	275
0	84.3	84.3	84.5	84.7	88.2	91.6	92.9	94.1	91.3	88.5	88.5
500	86.2	86.2	88.3	90.3	86.2	82.0	89.7	97.3	99.6	101.9	101.9
1000	88.7	88.7	88.9	89.1	88.0	86.9	87.0	87.0	84.7	82.3	82.3
1500	91.1	91.1	89.2	87.2	90.1	93.0	90.4	87.8	86.0	84.2	84.2
2000	90.7	90.7	91.5	92.3	91.9	91.4	89.0	86.5	85.9	85.3	85.3
2190	89.1	90.0	87.0	84.1	81.8	83.8	85.8	81.6	87.1	81.0	83.6
2440	95.0	96.0	89.7	92.3	91.3	87.1	89.3	89.4	86.0	79.2	83.2
2690	97.4	91.5	94.6	94.4	90.5	89.3	89.0	87.2	81.1	76.0	70.7
2940	95.0	92.0	85.5	88.8	87.4	92.4	96.2	93.6	93.1	89.3	81.2
3190	82.0	88.4	96.5	95.0	88.9	91.6	88.3	90.0	85.8	84.2	82.4
3440	99.2	98.4	94.6	90.9	94.8	90.7	94.8	94.2	86.9	79.0	70.4
3690	93.0	97.5	94.6	88.6	94.8	92.5	73.3	65.5	86.5	70.0	74.8
3940	102.1	95.6	104.5	106.2	100.7	92.3	79.5	74.4	76.6	81.0	84.4
4190	94.3	98.9	100.0	100.0	106.7	102.0	96.0	83.4	82.3	82.8	85.0
4440	95.0	100.6	105.0	103.7	99.7	93.3	101.4	103.2	91.5	80.7	76.3
4690	98.8	105.3	108.9	110.0	110.0	108.0	105.5	105.4	97.1	92.2	87.3
4940	103.8	101.3	104.5	106.6	106.6	98.0	90.3	92.6	92.3	98.5	93.4
5190	97.6	103.3	108.4	106.3	106.3	105.8	93.2	87.8	93.0	92.3	94.3
5440	104.1	105.4	108.0	114.3	114.3	101.8	101.2	94.3	91.0	87.4	93.0
5690	108.0	103.4	102.0	106.8	106.8	109.2	103.0	91.7	82.7	86.2	87.0

Table A - 13: Test B5-Sediment levels (zero readings)

L	Width										
	25	50	75	100	125	150	175	200	225	250	275
0	91.4	91.4	90.9	90.4	85.9	81.3	74.3	67.3	74.7	82.0	82.0
500	94.1	94.1	94.5	94.9	93.3	91.6	95.8	100.0	93.7	87.3	87.3
1000	96.1	96.1	97.3	98.5	97.4	96.2	95.4	94.6	90.6	86.5	86.5
1500	90.5	90.5	92.2	93.8	95.8	97.8	91.1	84.3	84.4	84.5	84.5
2000	89.4	89.4	90.4	91.3	88.8	86.2	83.1	80.0	81.4	82.8	82.8
2190	86.1	81.3	83.9	92.7	92.6	84.5	80.8	80.0	83.0	81.2	75.5
2440	91.1	83.6	83.2	86.9	80.4	81.2	87.2	86.2	92.3	88.3	82.6
2690	93.8	96.3	91.6	87.1	76.8	77.6	84.4	87.9	83.2	86.7	82.6
2940	91.2	93.8	89.5	94.0	90.5	84.4	84.7	84.5	76.8	76.4	67.1
3190	88.6	91.9	86.5	85.1	87.8	89.3	83.6	84.1	79.0	75.2	70.2
3440	103.5	96.2	96.2	96.3	98.0	88.1	72.6	65.0	70.3	79.8	65.8
3690	100.4	103.5	102.4	101.0	103.2	99.5	86.3	81.2	78.0	66.2	62.2
3940	101.0	98.9	101.0	106.8	91.2	77.6	76.8	78.7	78.0	76.1	65.8
4190	104.2	111.7	100.0	95.2	98.2	94.9	91.1	82.2	74.2	68.2	66.1
4440	108.2	100.5	98.3	101.5	111.8	111.1	101.5	95.6	86.7	75.3	67.0
4690	108.4	107.2	107.3	109.8	105.7	94.3	90.8	88.8	83.1	80.0	78.6
4940	113.5	104.6	109.2	101.5	95.9	92.4	96.5	97.0	90.5	82.7	77.5
5190	108.0	106.0	108.2	108.8	97.3	95.2	91.5	88.3	94.0	83.3	79.4
5440	106.2	95.6	98.6	101.2	114.5	111.7	103.0	94.7	82.1	83.6	85.0
5690	114.3	122.2	118.8	113.4	95.2	91.8	88.5	86.1	94.4	94.4	92.2

Table A - 14: Test B5-Sediment levels (Run 1)

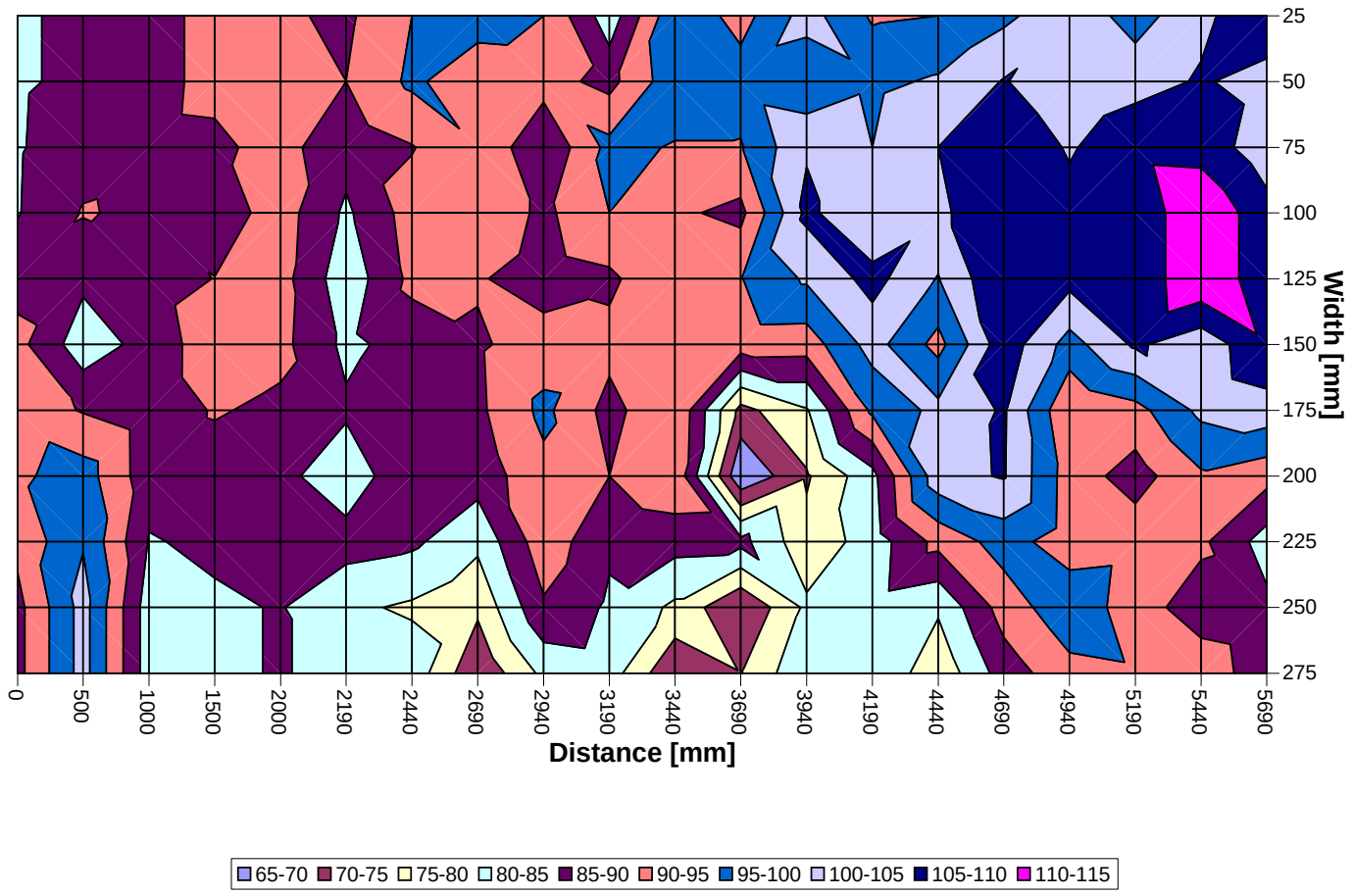

Figure A - 68: Test B5-Sediment levels after Run 1

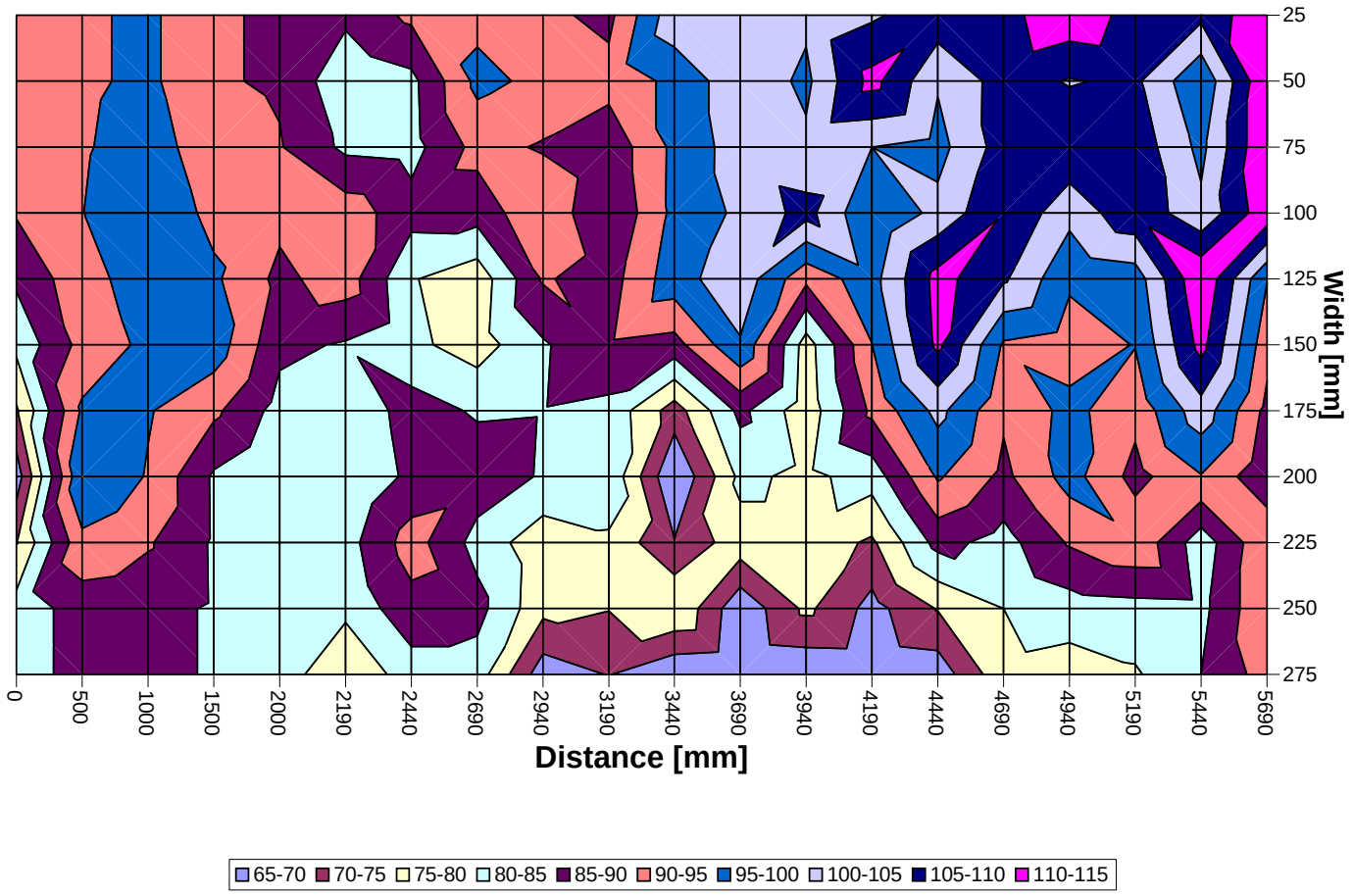

Figure A - 69: Test B5-Sediment levels after Run 2

A.3 TEST C (AVERAGE RADIUS = 4.55 m)

A.3.1 VELOCITY RELATED

A.3.1.1 TEST C1 (F_R = 0.1)

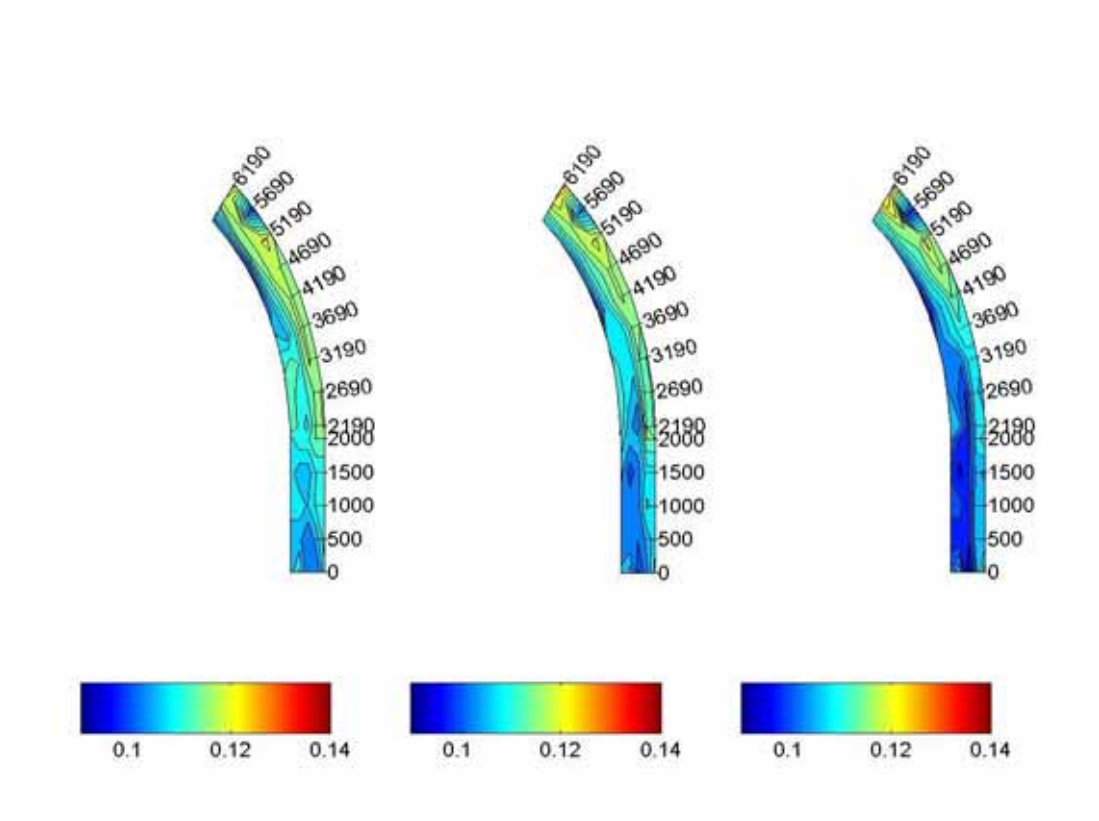

Figure A - 70: Test C1-Velocity distribution in the horisontal plane measured at 70, 50 and 30 mm

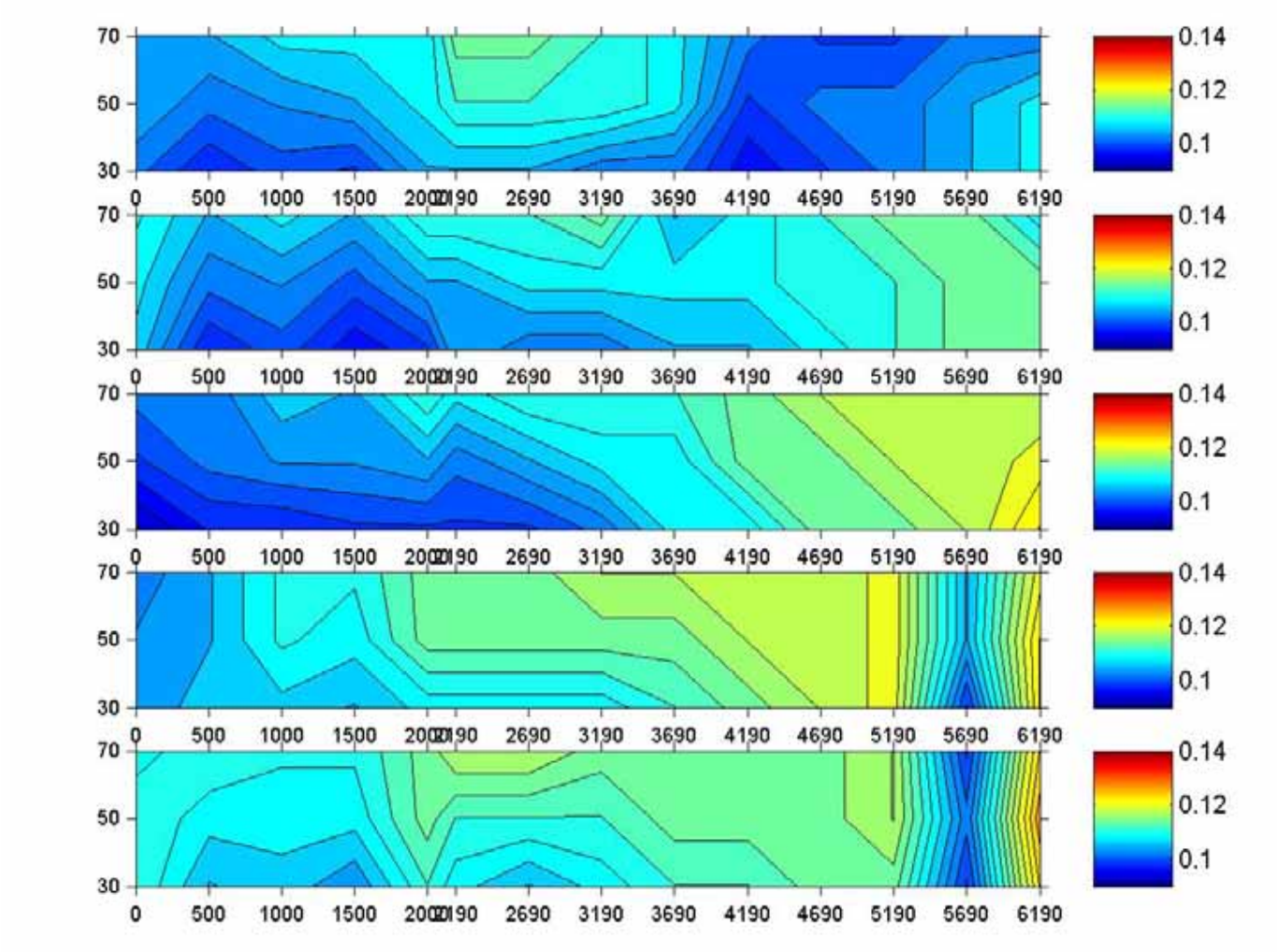

Figure A - 71: Test C1-Velocity distribution in the vertical plane

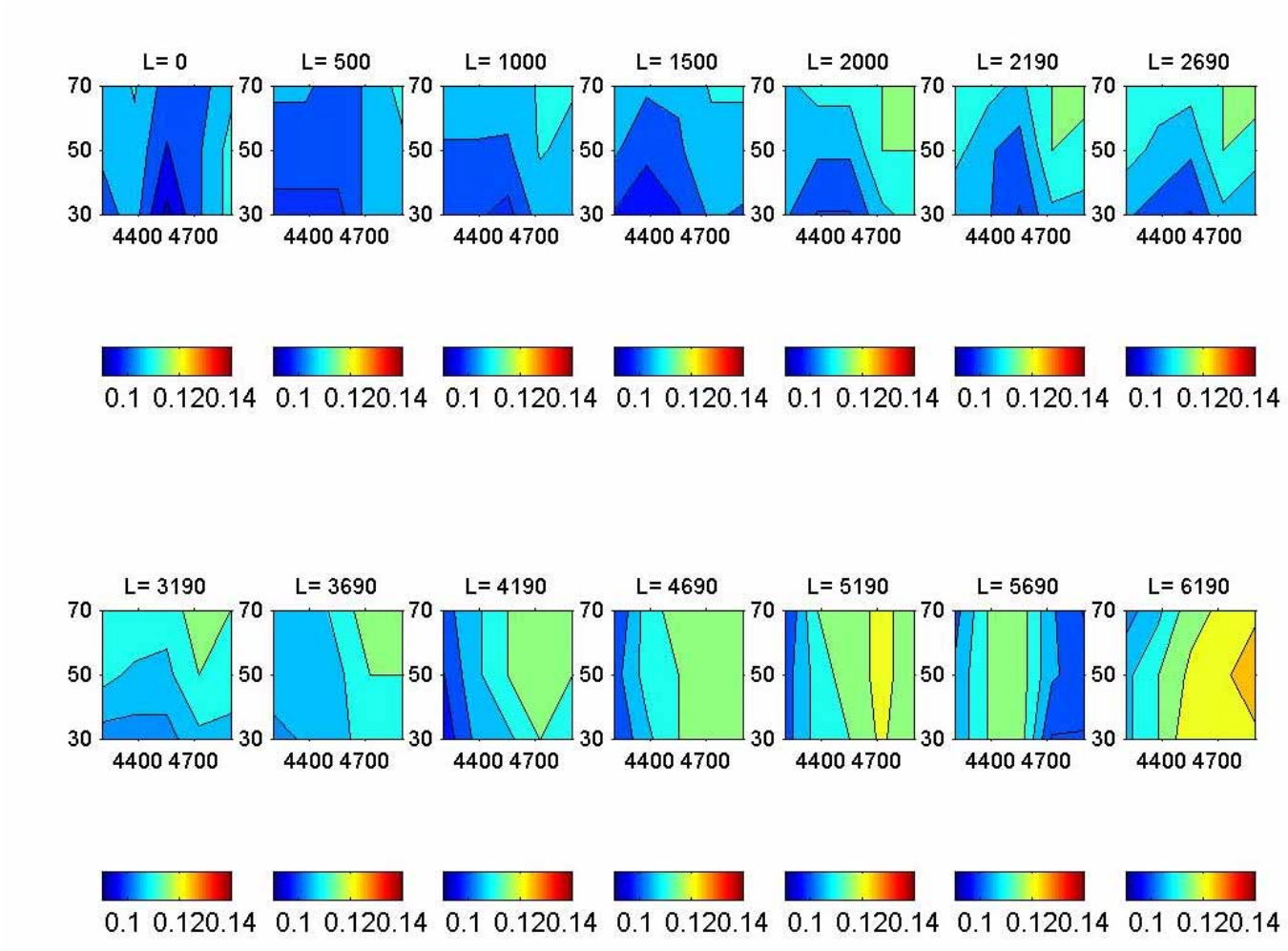

Figure A - 72: Test C1-Cross-sectional velocity distribution

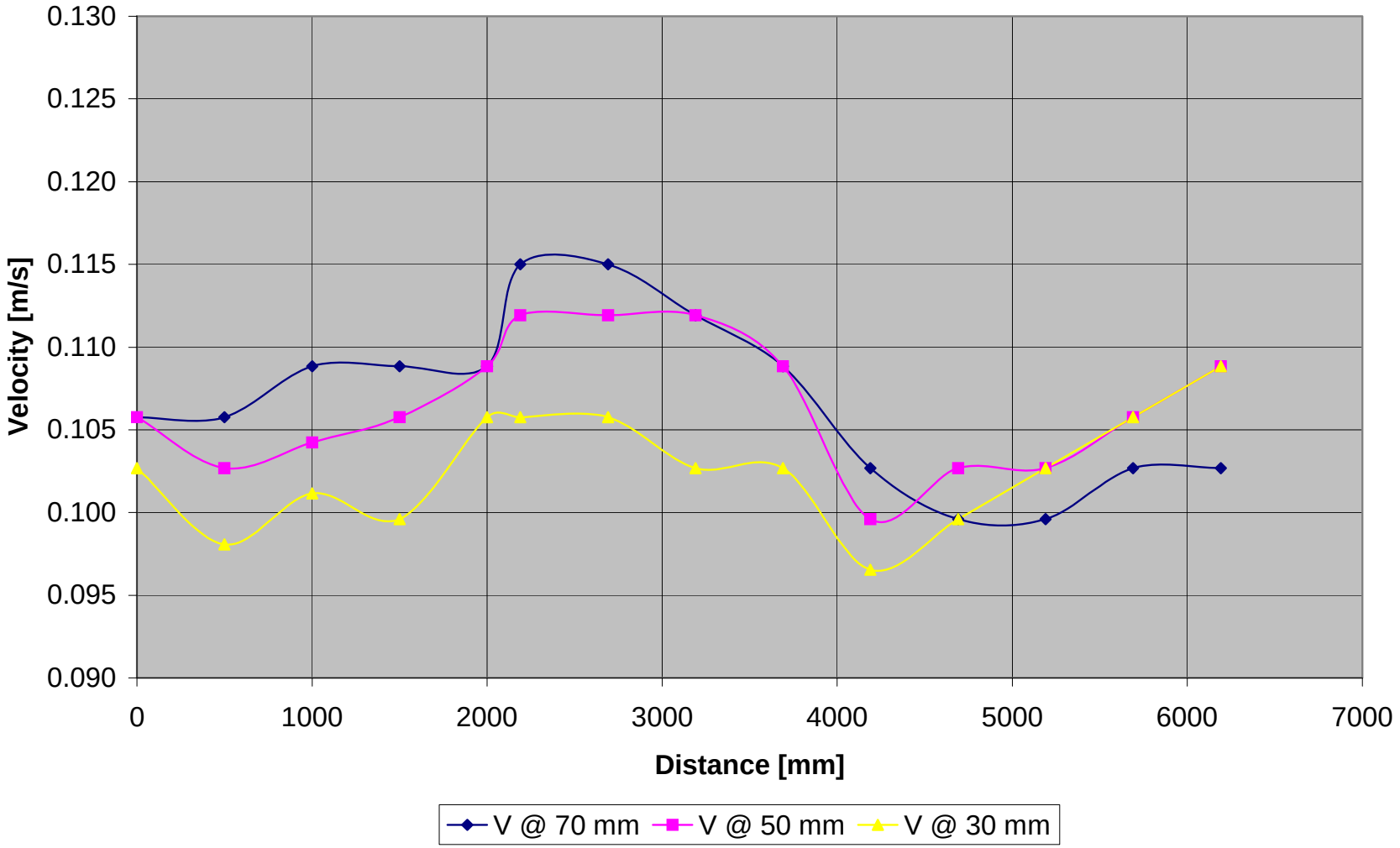

Figure A - 73: Test C1-Vertical velocity distribution measured at 50 mm from inner bank of bend

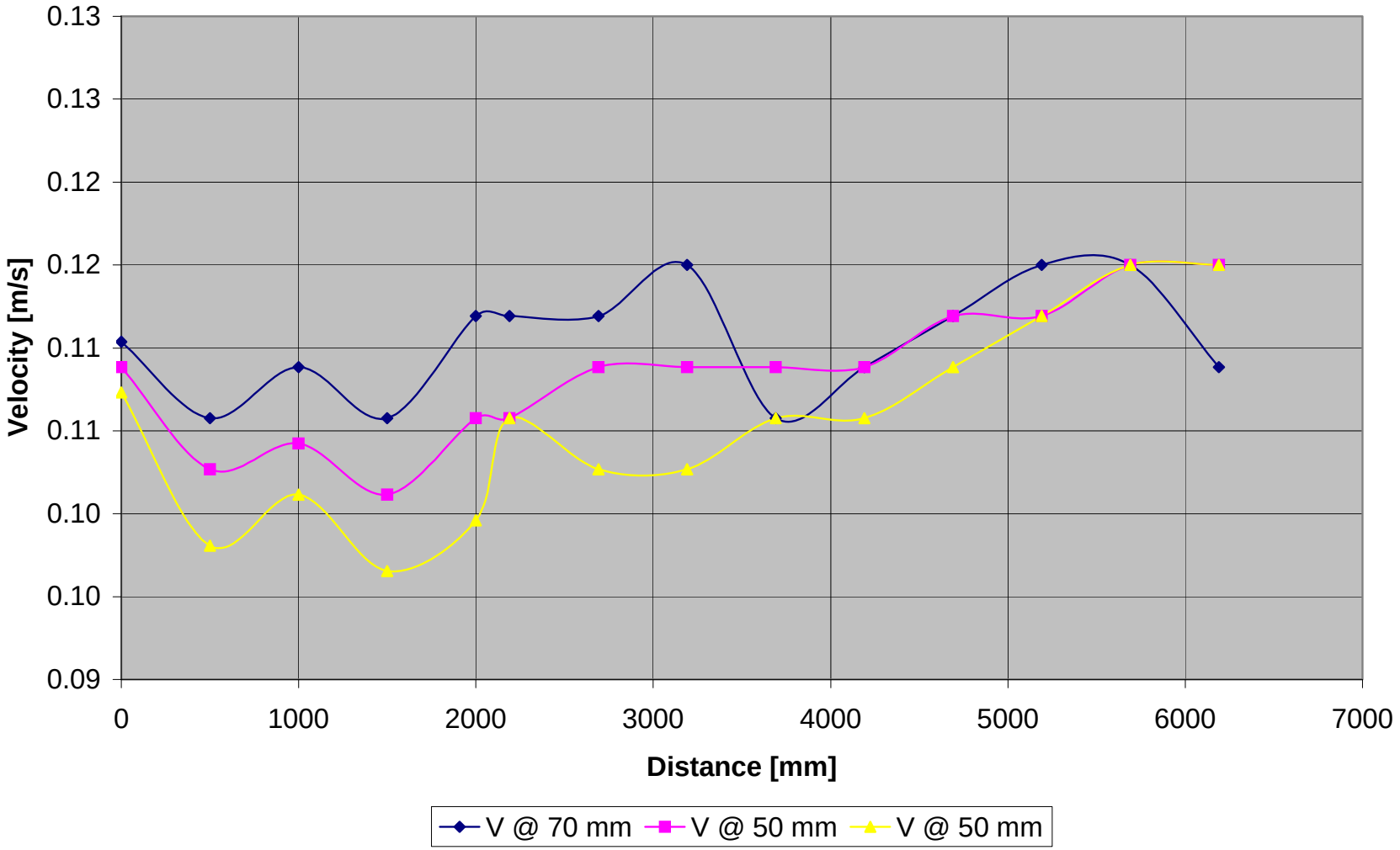

Figure A - 74: Test C1-Vertical velocity distribution measured at 100 mm from inner bank of bend

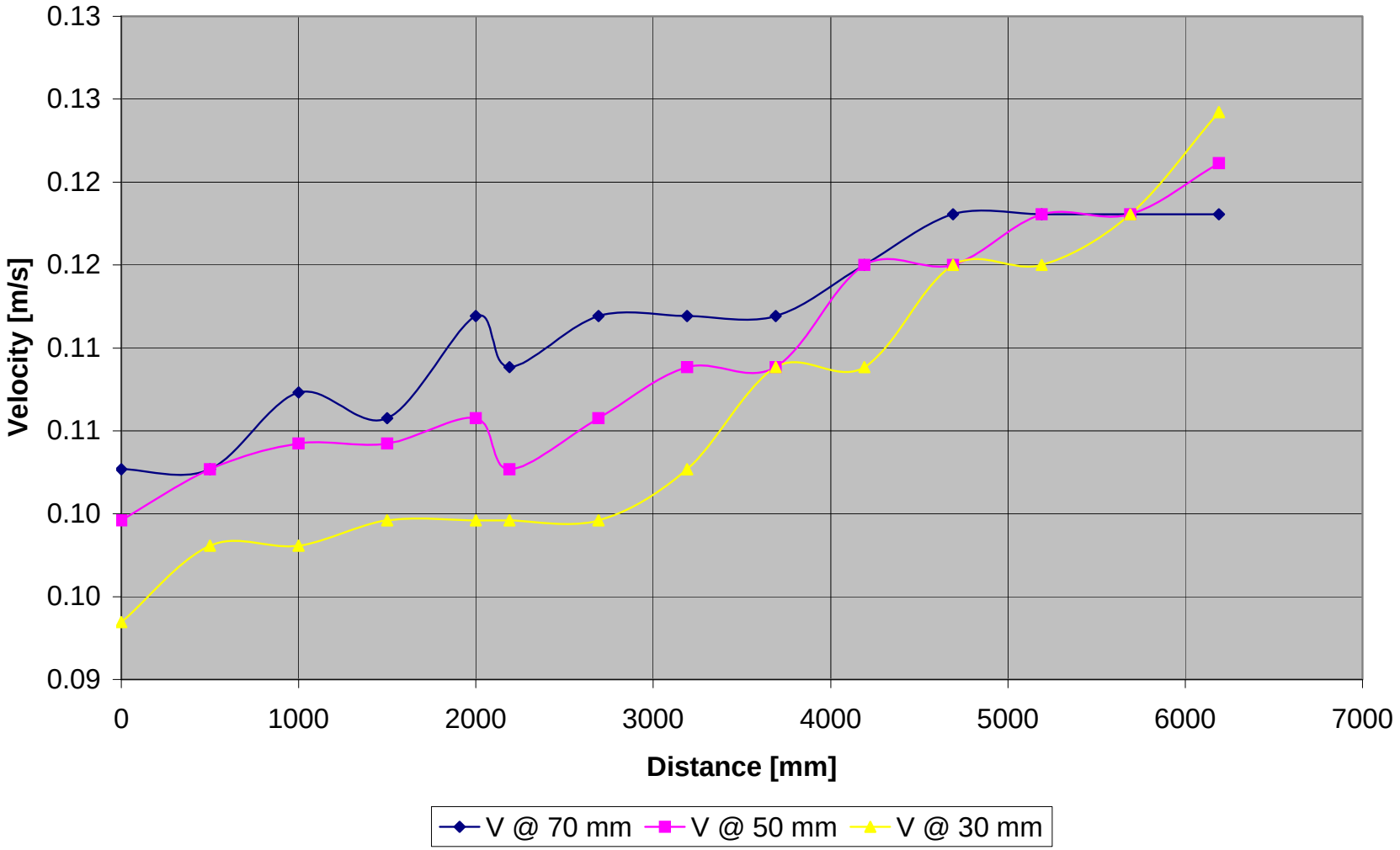

Figure A - 75: Test C1-Vertical velocity distribution measured at 150 mm from inner bank of bend

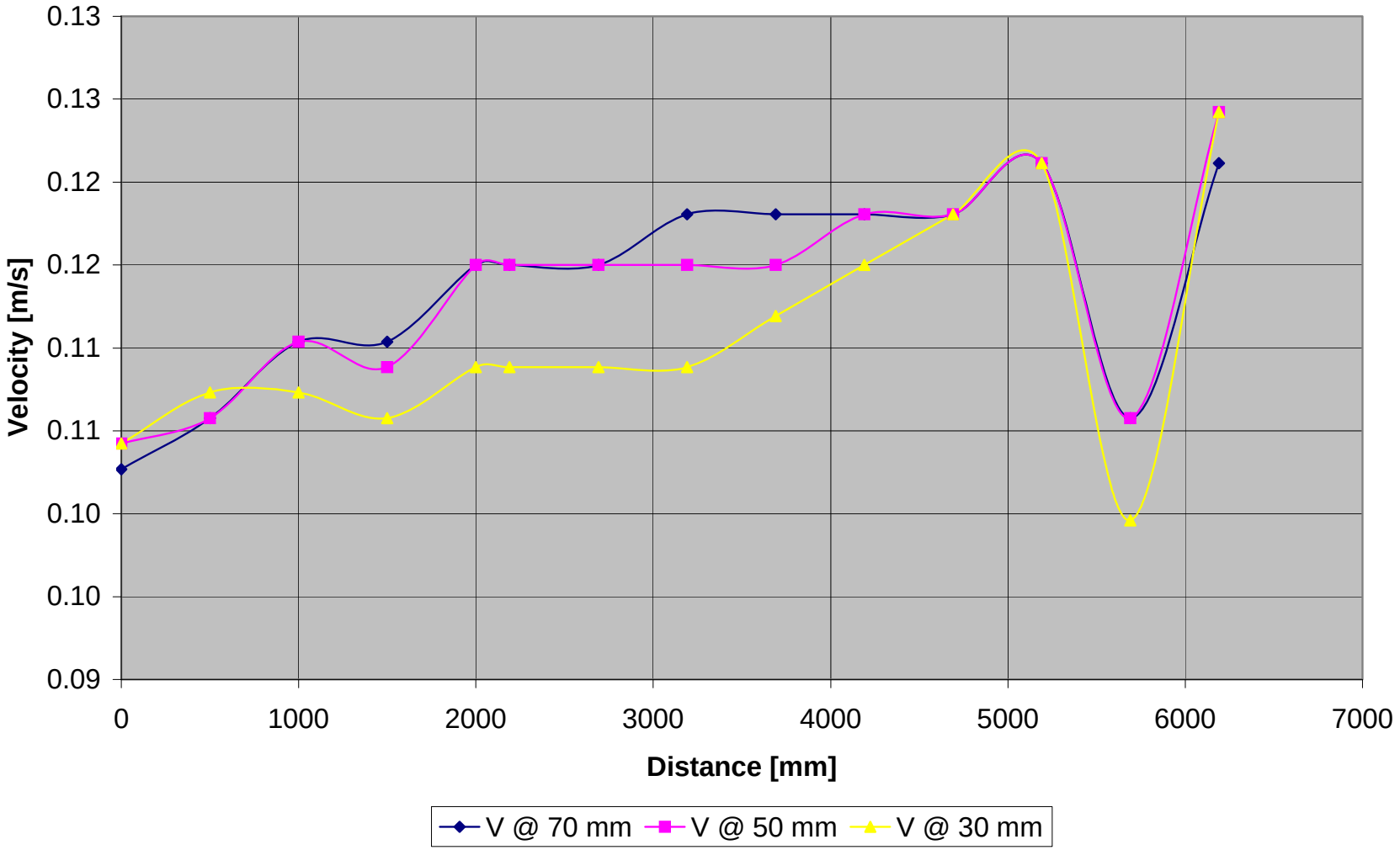

Figure A - 76: Test C1-Vertical velocity distribution measured at 200 mm from inner bank of bend

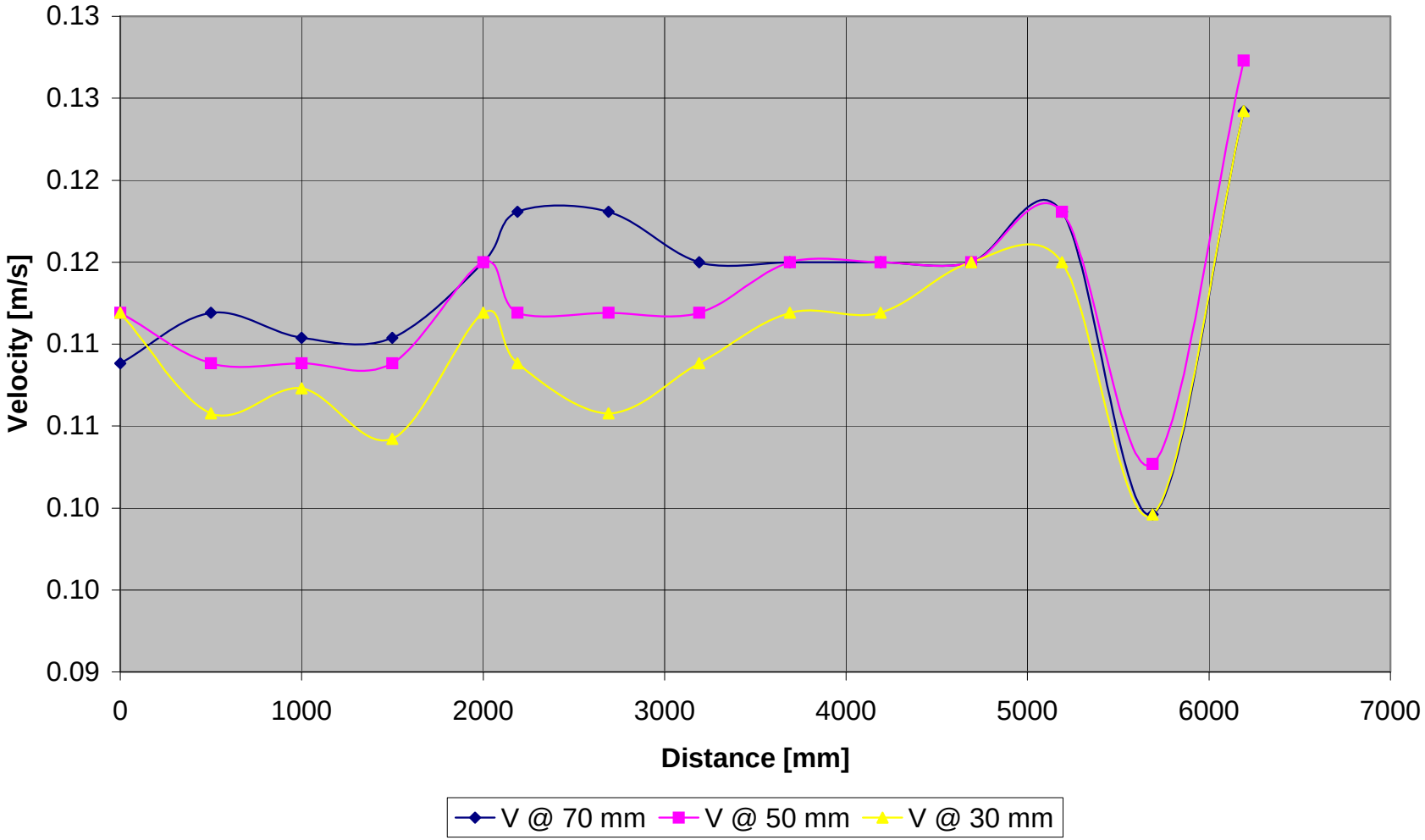

Figure A - 77: Test C1-Vertical velocity distribution measured at 250 mm from inner bank of bend

	Point	1	2	3	4	5	6	7	8	9	10	11	12	13	14	15
Width	**L**	**0**	**500**	**1000**	**1500**	**2000**	**2190**	**2690**	**3190**	**3690**	**4190**	**4690**	**5190**	**5690**	**6190**	**6690**
	h															
50	**70**	0.106	0.106	0.109	0.109	0.109	0.115	0.115	0.112	0.109	0.103	0.100	0.100	0.103	0.103	0.100
	50	0.106	0.103	0.104	0.106	0.109	0.112	0.112	0.112	0.109	0.100	0.103	0.103	0.106	0.109	0.106
	30	0.103	0.098	0.101	0.100	0.106	0.106	0.106	0.103	0.103	0.097	0.100	0.103	0.106	0.109	0.109
100	**70**	0.110	0.106	0.109	0.106	0.112	0.112	0.112	0.115	0.106	0.109	0.112	0.115	0.115	0.109	0.106
	50	0.109	0.103	0.104	0.101	0.106	0.106	0.109	0.109	0.109	0.109	0.112	0.112	0.115	0.115	0.106
	30	0.107	0.098	0.101	0.097	0.100	0.106	0.103	0.103	0.106	0.106	0.109	0.112	0.115	0.115	0.109
150	**70**	0.103	0.103	0.107	0.106	0.112	0.109	0.112	0.112	0.112	0.115	0.118	0.118	0.118	0.118	0.118
	50	0.100	0.103	0.104	0.104	0.106	0.103	0.106	0.109	0.109	0.115	0.115	0.118	0.118	0.121	0.121
	30	0.093	0.098	0.098	0.100	0.100	0.100	0.100	0.103	0.109	0.109	0.115	0.115	0.118	0.124	0.121
200	**70**	0.103	0.106	0.110	0.110	0.115	0.115	0.115	0.118	0.118	0.118	0.118	0.121	0.106	0.121	0.121
	50	0.104	0.106	0.110	0.109	0.115	0.115	0.115	0.115	0.115	0.118	0.118	0.121	0.106	0.124	0.124
	30	0.104	0.107	0.107	0.106	0.109	0.109	0.109	0.109	0.112	0.115	0.118	0.121	0.100	0.124	0.124
250																
	70	0.109	0.112	0.110	0.110	0.115	0.118	0.118	0.115	0.115	0.115	0.115	0.118	0.100	0.124	0.124
	50	0.112	0.109	0.109	0.109	0.115	0.112	0.112	0.112	0.115	0.115	0.115	0.118	0.103	0.127	0.124
	30	0.112	0.106	0.107	0.104	0.112	0.109	0.106	0.109	0.112	0.112	0.115	0.115	0.100	0.124	0.124

Table A - 15: Test C1-Measured velocities [m/s]

A.3.1.2 TEST C2 (F_R = 0.3)

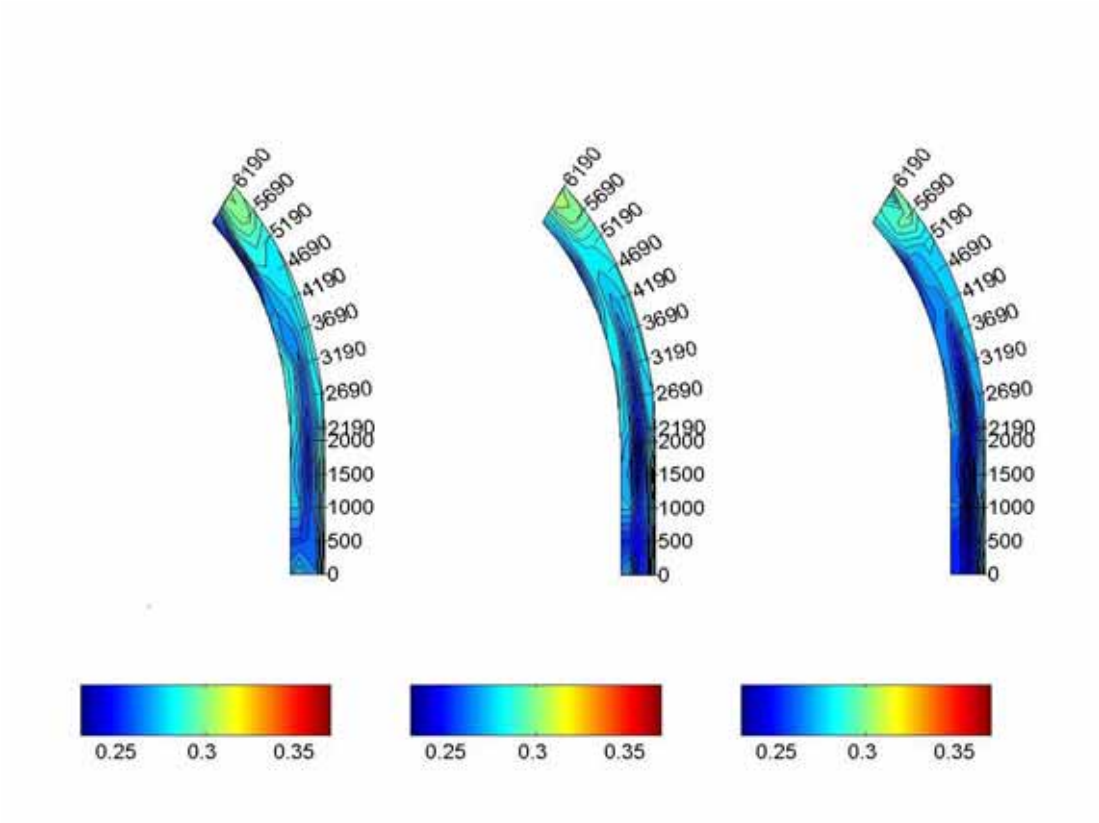

Figure A - 78: Test C2-Velocity distribution in the horisontal plane measured at 70, 50 and 30 mm

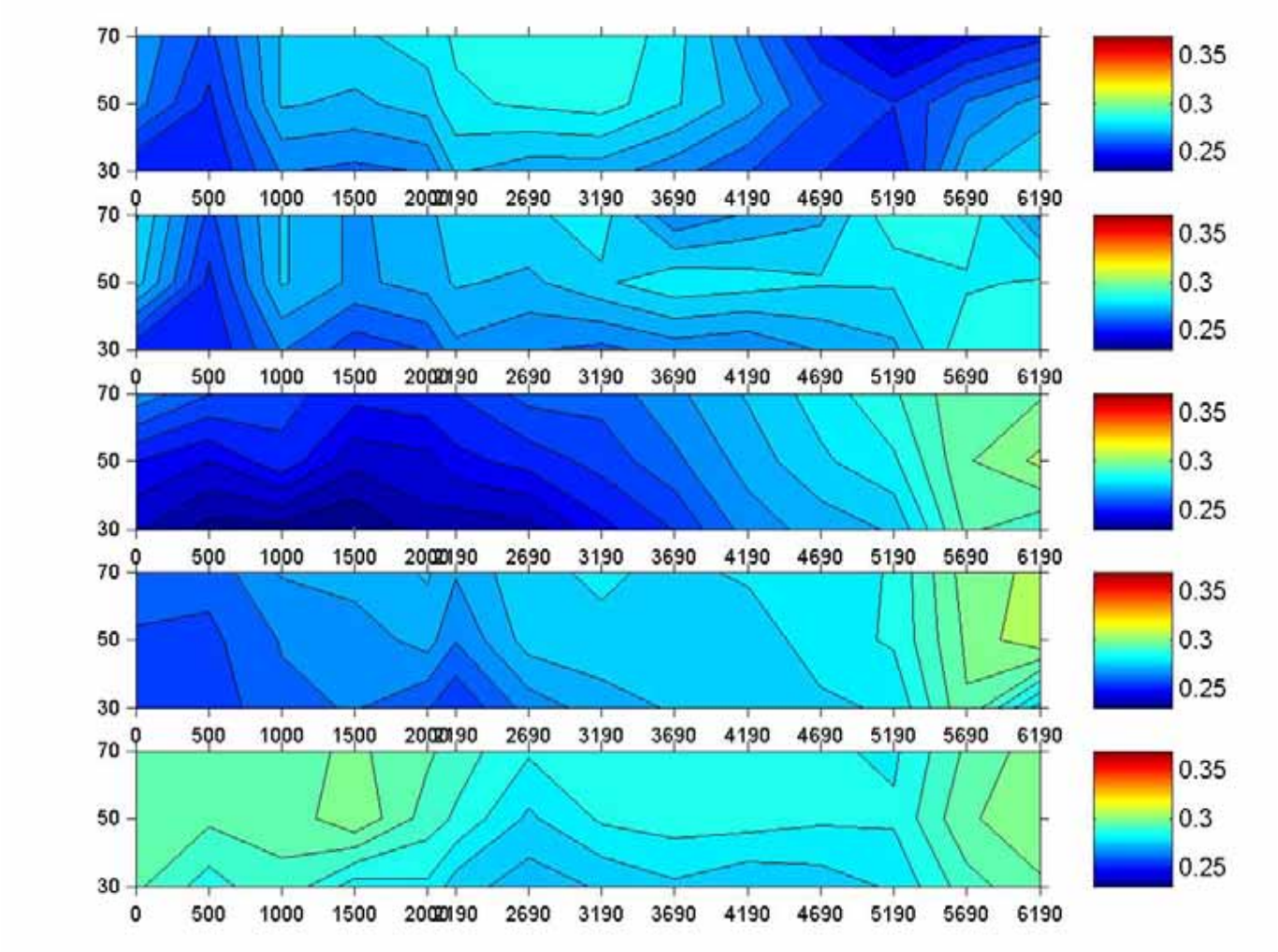

Figure A - 79: Test C2-Velocity distribution in the vertical plane

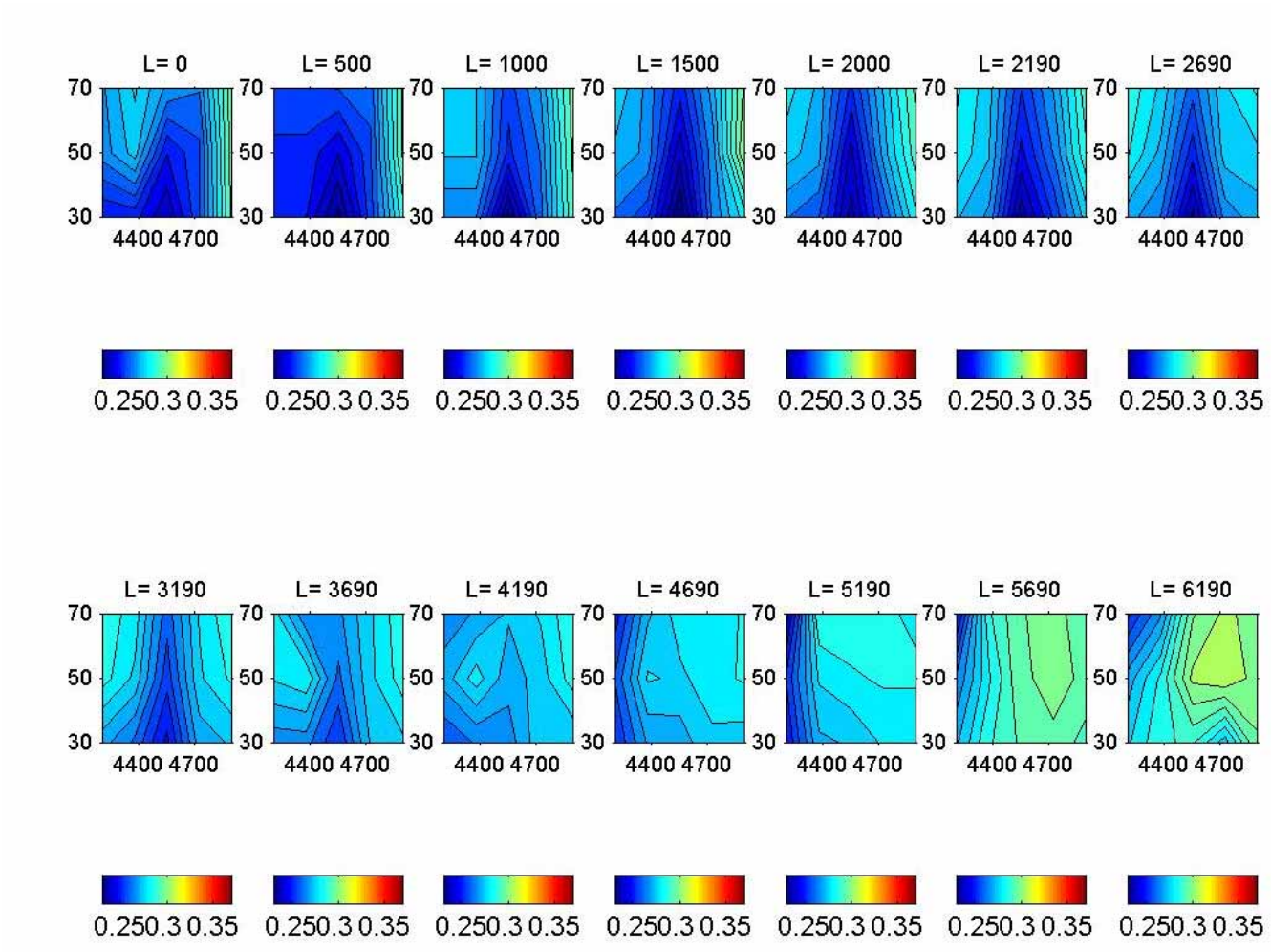

Figure A - 80: Test C2-Cross-sectional velocity distribution

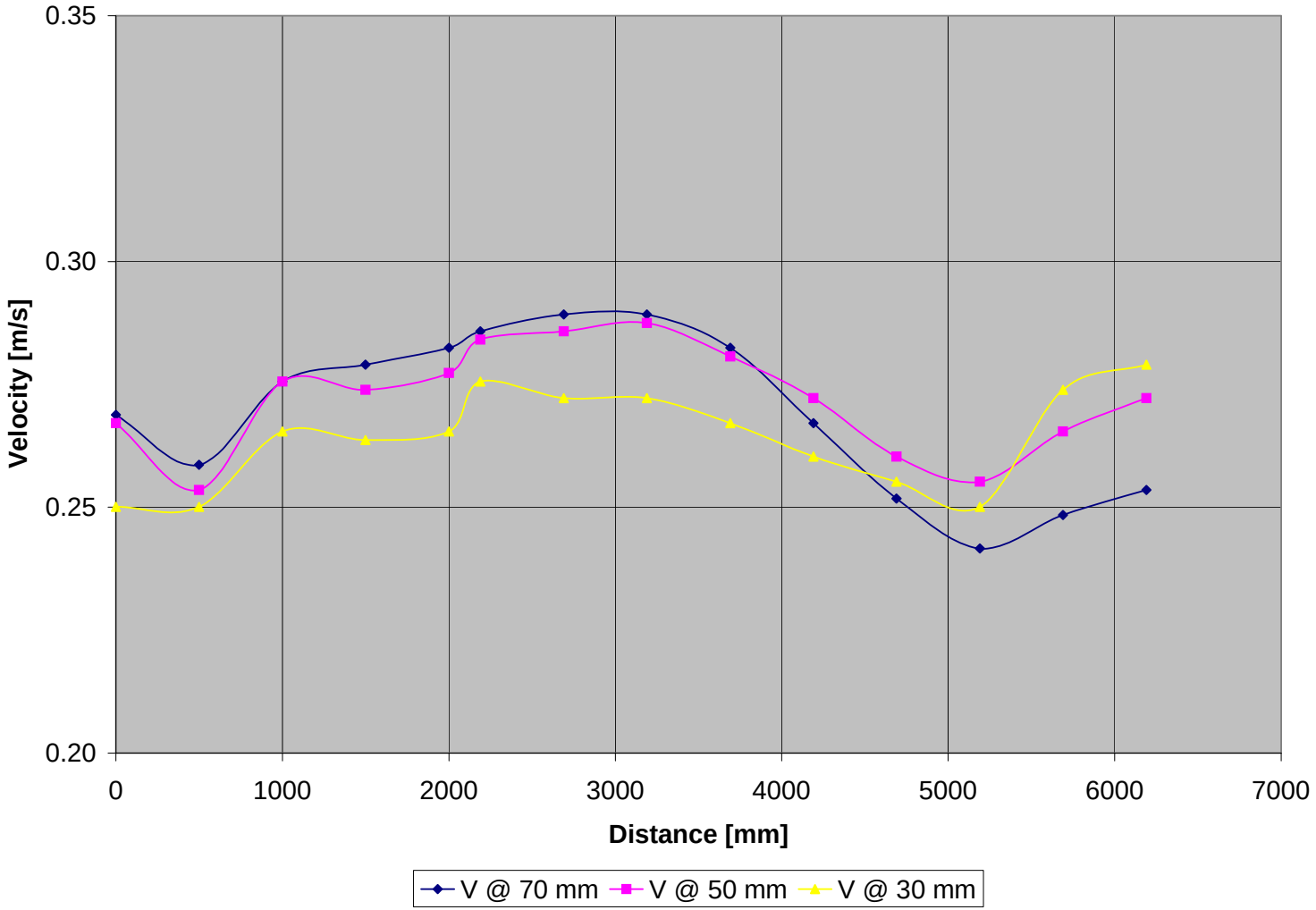

Figure A - 81: Test C2-Vertical velocity distribution measured at 50 mm from inner bank of bend

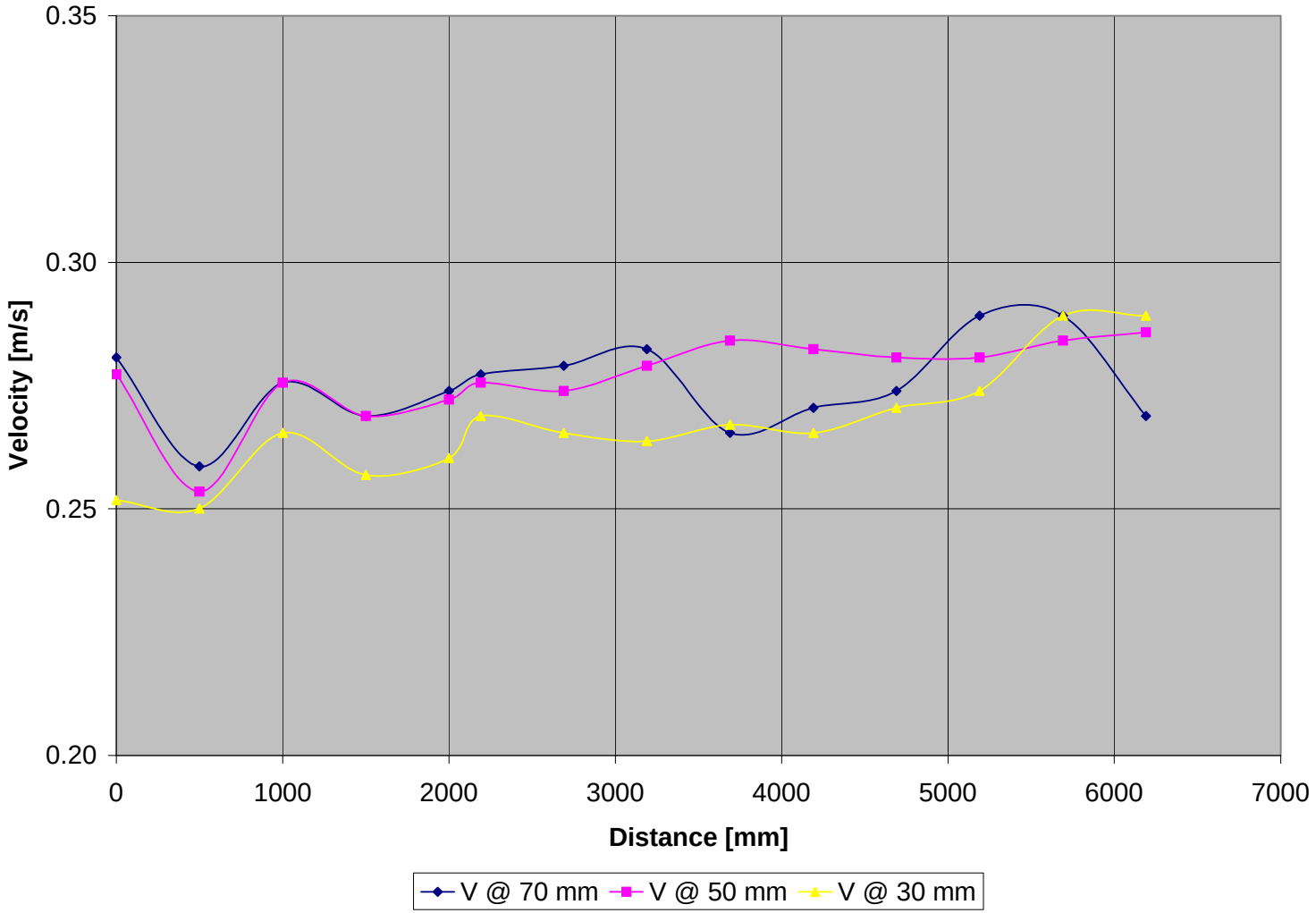

Figure A - 82: Test C2-Vertical velocity distribution measured at 100 mm from inner bank of bend

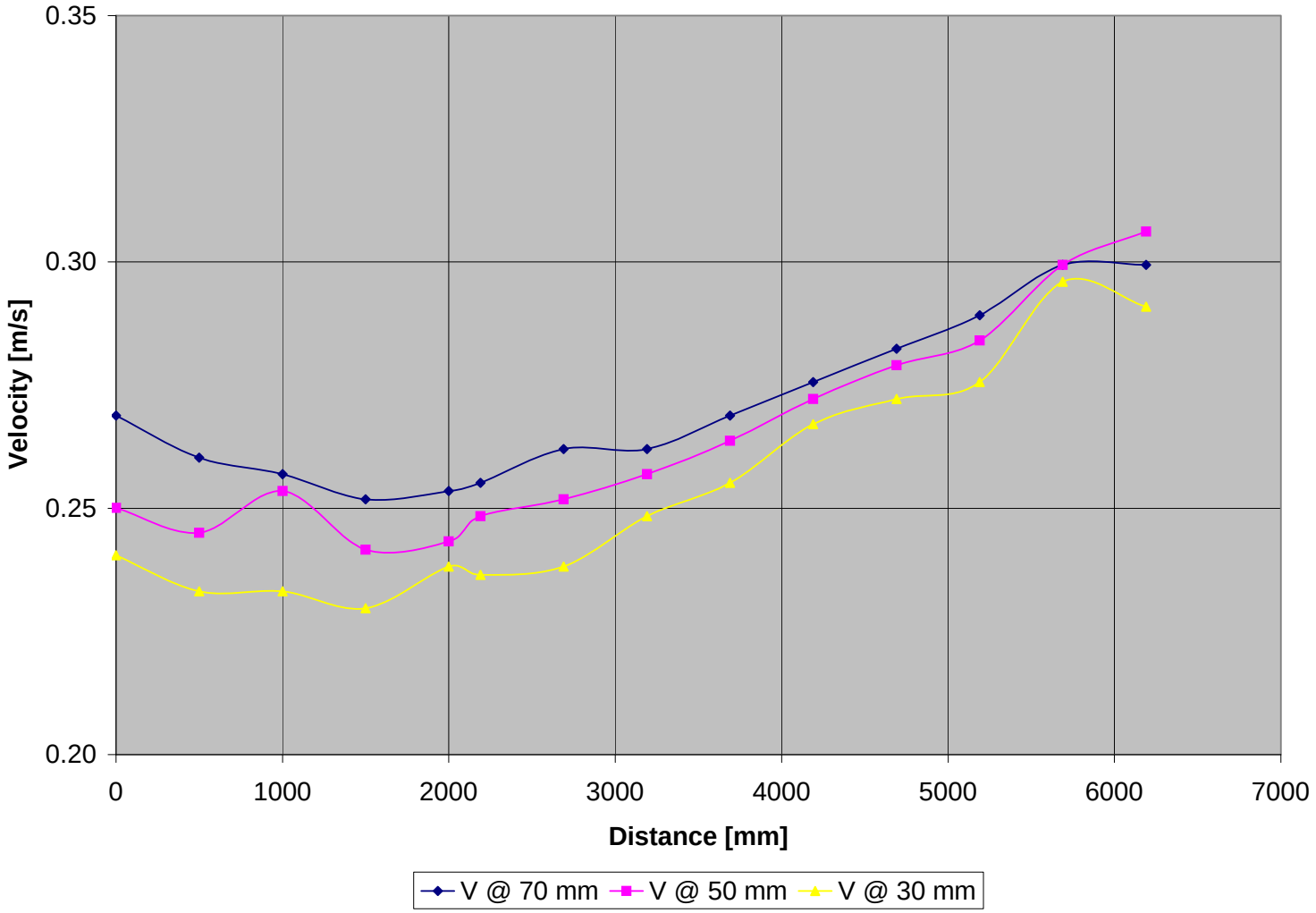

Figure A - 83: Test C2-Vertical velocity distribution measured at 150 mm from inner bank of bend

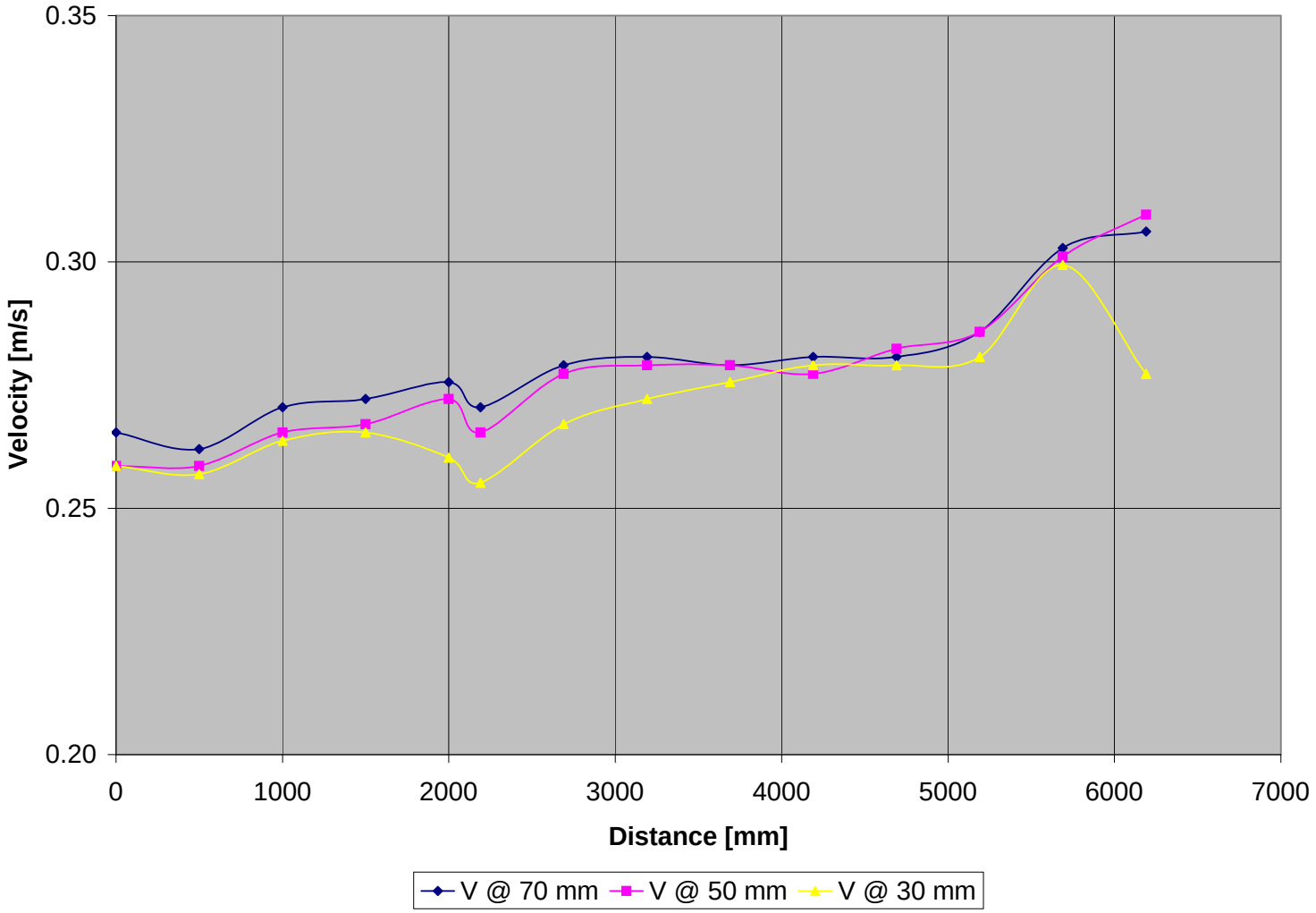

Figure A - 84: Test C2-Vertical velocity distribution measured at 200 mm from inner bank of bend

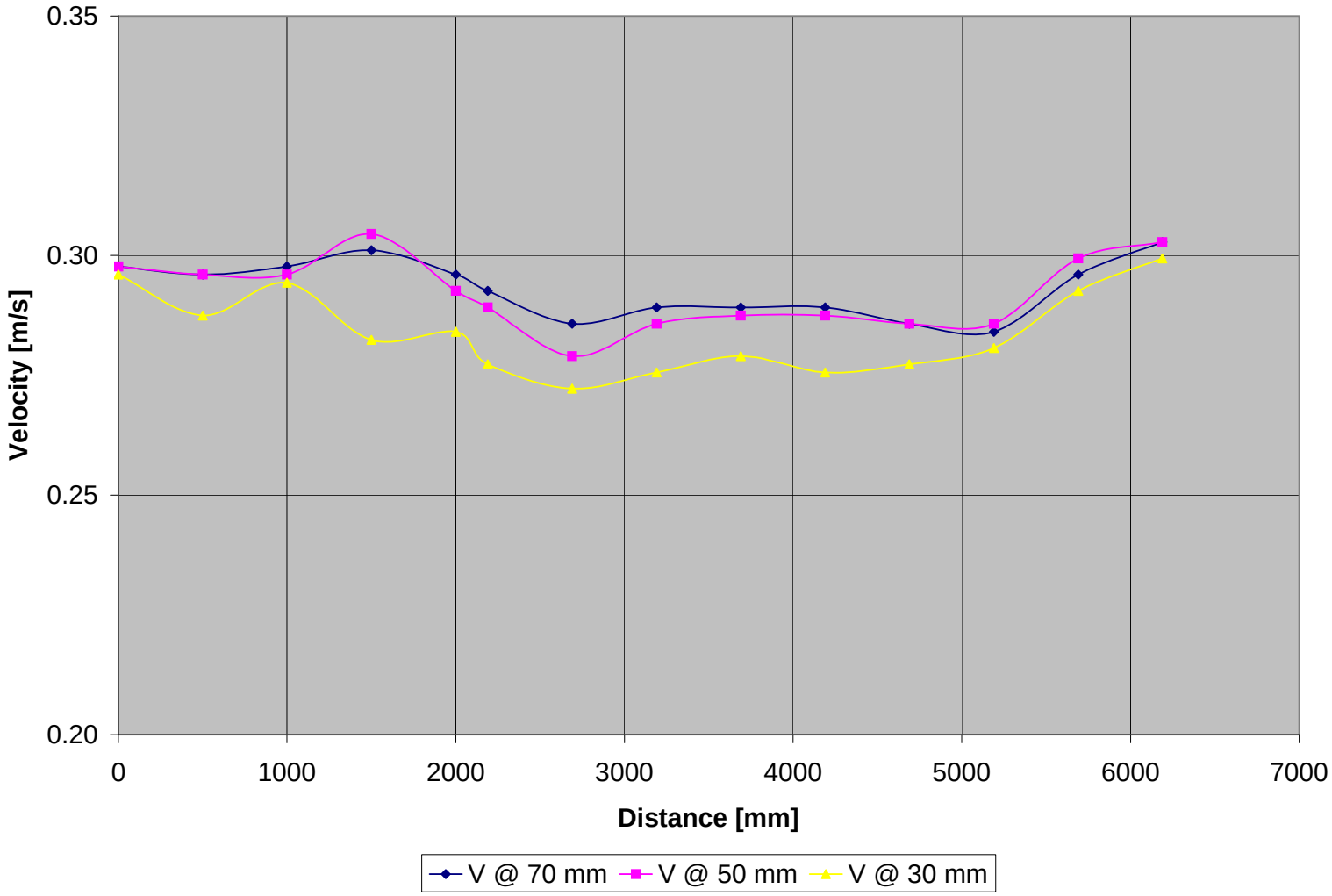

Figure A - 85: Test C2-Vertical velocity distribution measured at 250 mm from inner bank of bend

	Point	1	2	3	4	5	6	7	8	9	10	11	12	13	14
Width	L	0	500	1000	1500	2000	2190	2690	3190	3690	4190	4690	5190	5690	6190
	h														
50	70	0.269	0.259	0.276	0.279	0.282	0.286	0.289	0.289	0.282	0.267	0.252	0.242	0.248	0.254
	50	0.267	0.254	0.276	0.274	0.277	0.284	0.286	0.288	0.281	0.272	0.260	0.255	0.265	0.272
	30	0.250	0.250	0.265	0.264	0.265	0.276	0.272	0.272	0.267	0.260	0.255	0.250	0.274	0.279
100	70	0.281	0.259	0.276	0.269	0.274	0.277	0.279	0.282	0.265	0.271	0.274	0.289	0.289	0.269
	50	0.277	0.254	0.276	0.269	0.272	0.276	0.274	0.279	0.284	0.282	0.281	0.281	0.284	0.286
	30	0.252	0.250	0.265	0.257	0.260	0.269	0.265	0.264	0.267	0.265	0.271	0.274	0.289	0.289
150	70	0.269	0.260	0.257	0.252	0.254	0.255	0.262	0.262	0.269	0.276	0.282	0.289	0.299	0.299
	50	0.250	0.245	0.254	0.242	0.243	0.248	0.252	0.257	0.264	0.272	0.279	0.284	0.299	0.306
	30	0.240	0.233	0.233	0.230	0.238	0.237	0.238	0.248	0.255	0.267	0.272	0.276	0.296	0.291
200	70	0.265	0.262	0.271	0.272	0.276	0.271	0.279	0.281	0.279	0.281	0.281	0.286	0.303	0.306
	50	0.259	0.259	0.265	0.267	0.272	0.265	0.277	0.279	0.279	0.277	0.282	0.286	0.301	0.310
	30	0.259	0.257	0.264	0.265	0.260	0.255	0.267	0.272	0.276	0.279	0.279	0.281	0.299	0.277
250															
	70	0.298	0.296	0.298	0.301	0.296	0.293	0.286	0.289	0.289	0.289	0.286	0.284	0.296	0.303
	50	0.298	0.296	0.296	0.305	0.293	0.289	0.279	0.286	0.288	0.288	0.286	0.286	0.299	0.303
	30	0.296	0.288	0.294	0.282	0.284	0.277	0.272	0.276	0.279	0.276	0.277	0.281	0.293	0.299

Table A - 16: Test C2-Measured velocities [m/s]

A.3.1.3 TEST C3 (F_R = 0.5)

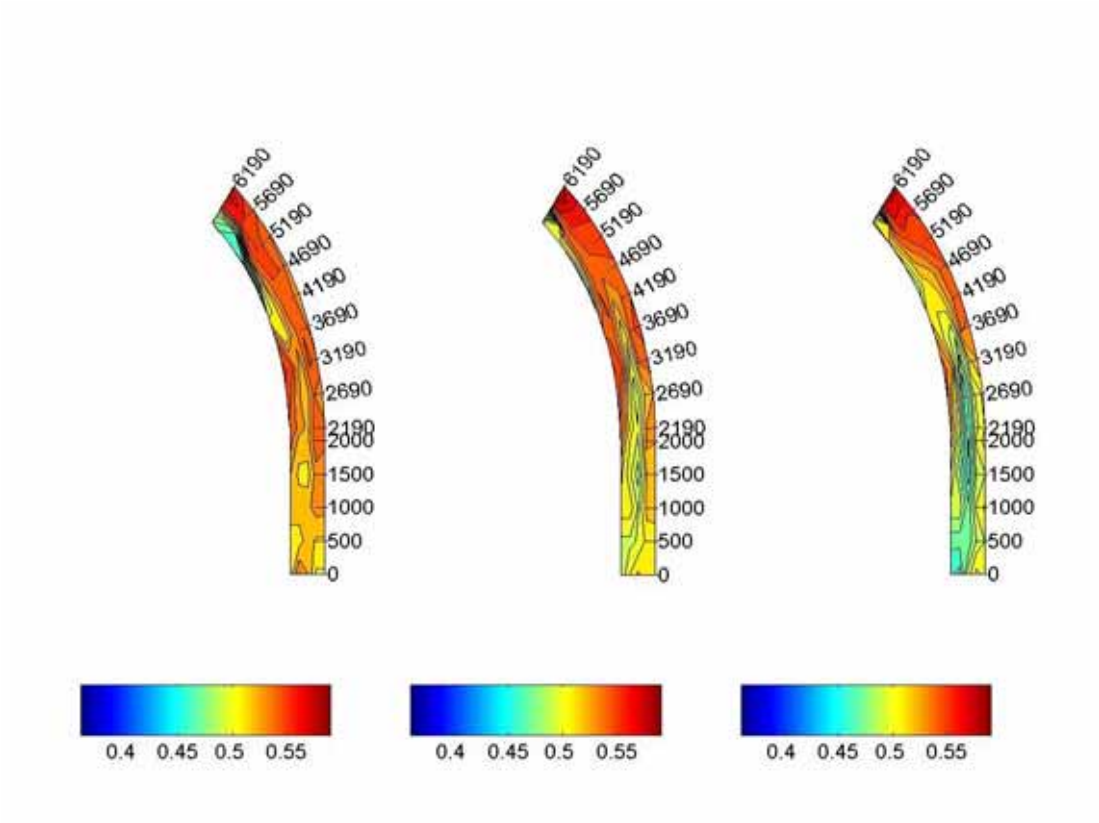

Figure A - 86: Test C3-Velocity distribution in the horisontal plane measured at 70, 50 and 30 mm

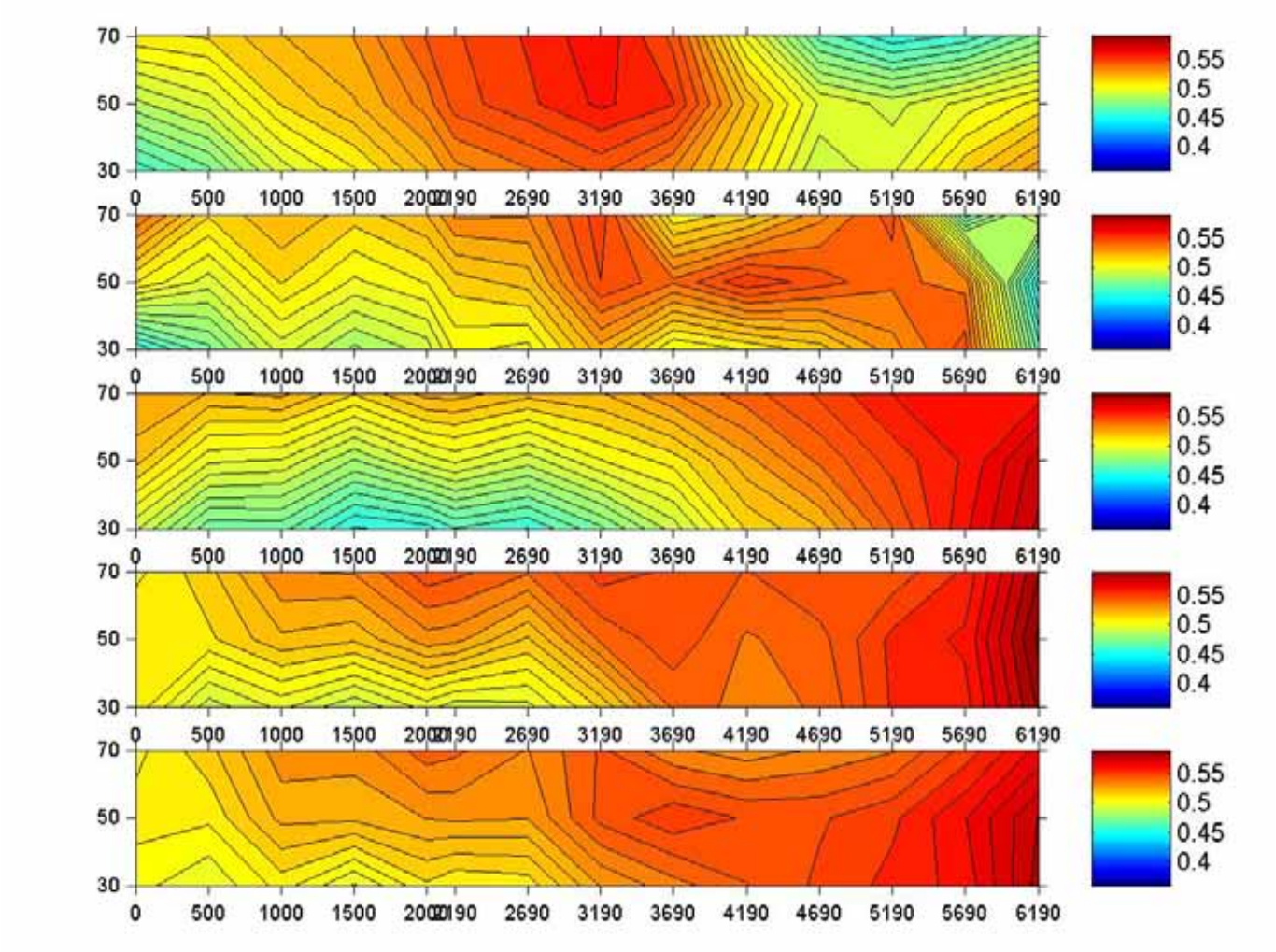

Figure A - 87: Test C3-Velocity distribution in the vertical plane

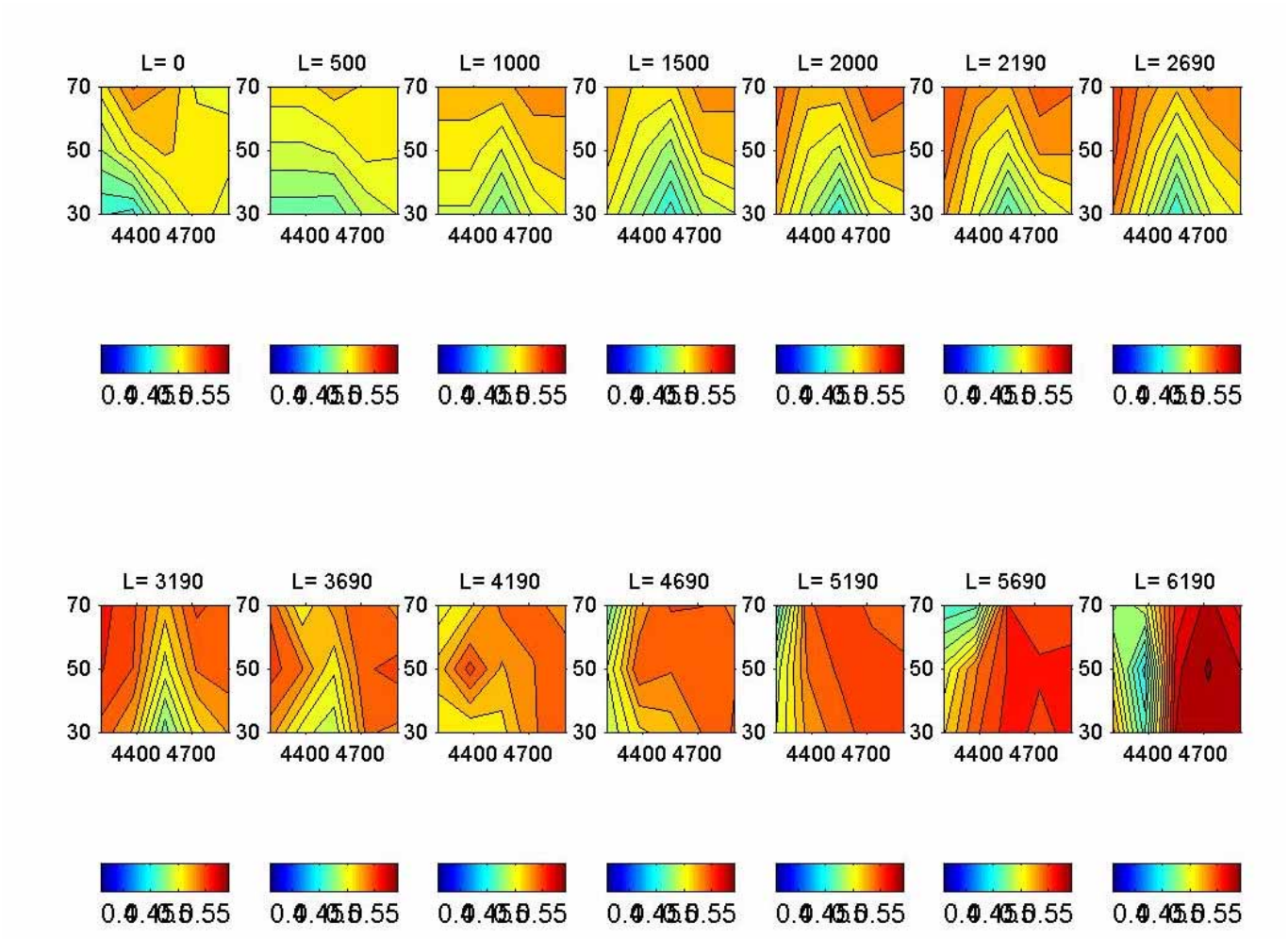

Figure A - 88: Test C3-Cross-sectional velocity distribution

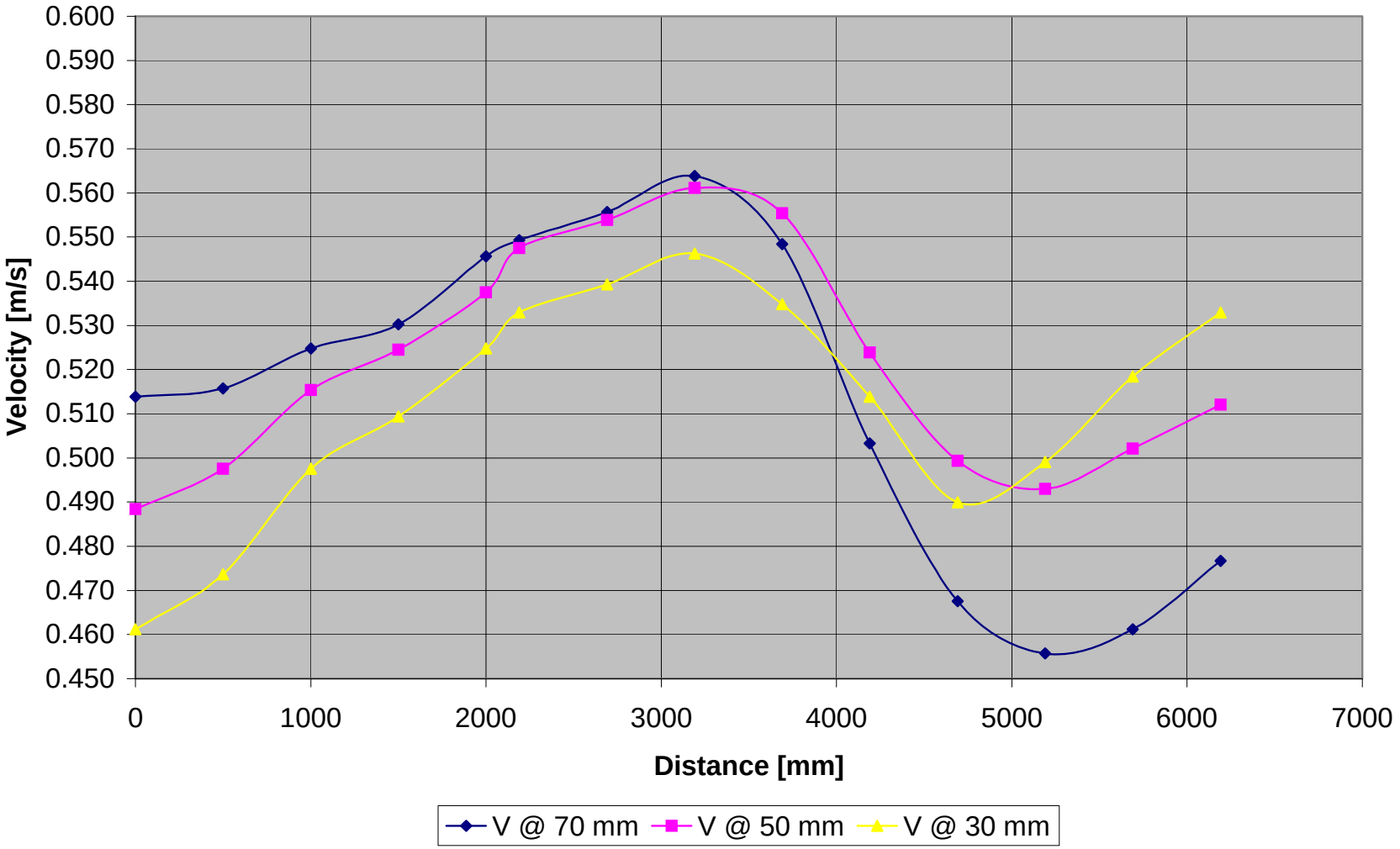

Figure A - 89: Test C3-Vertical velocity distribution measured at 50 mm from inner bank of bend

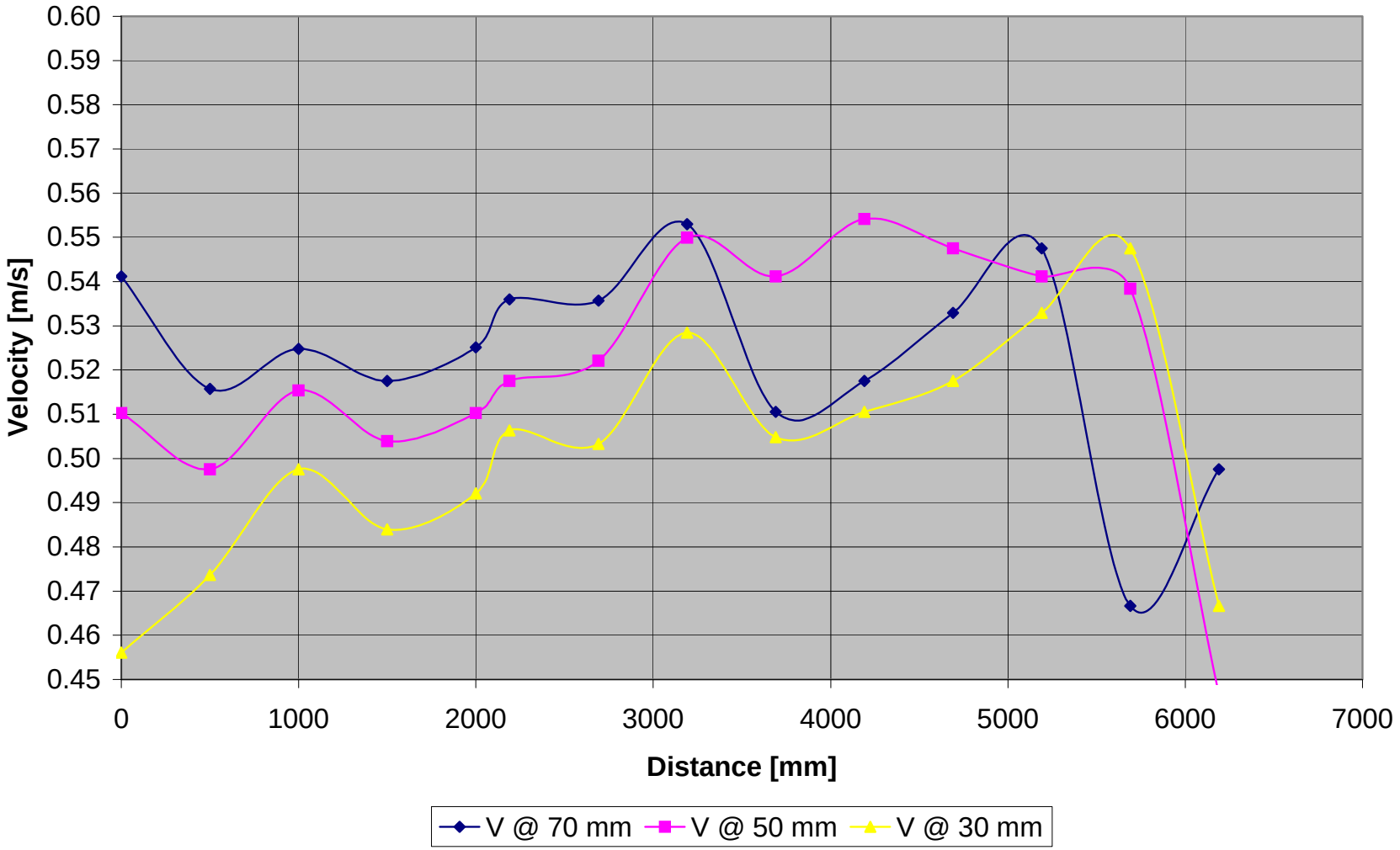

Figure A - 90: Test C3-Vertical velocity distribution measured at 100 mm from inner bank of bend

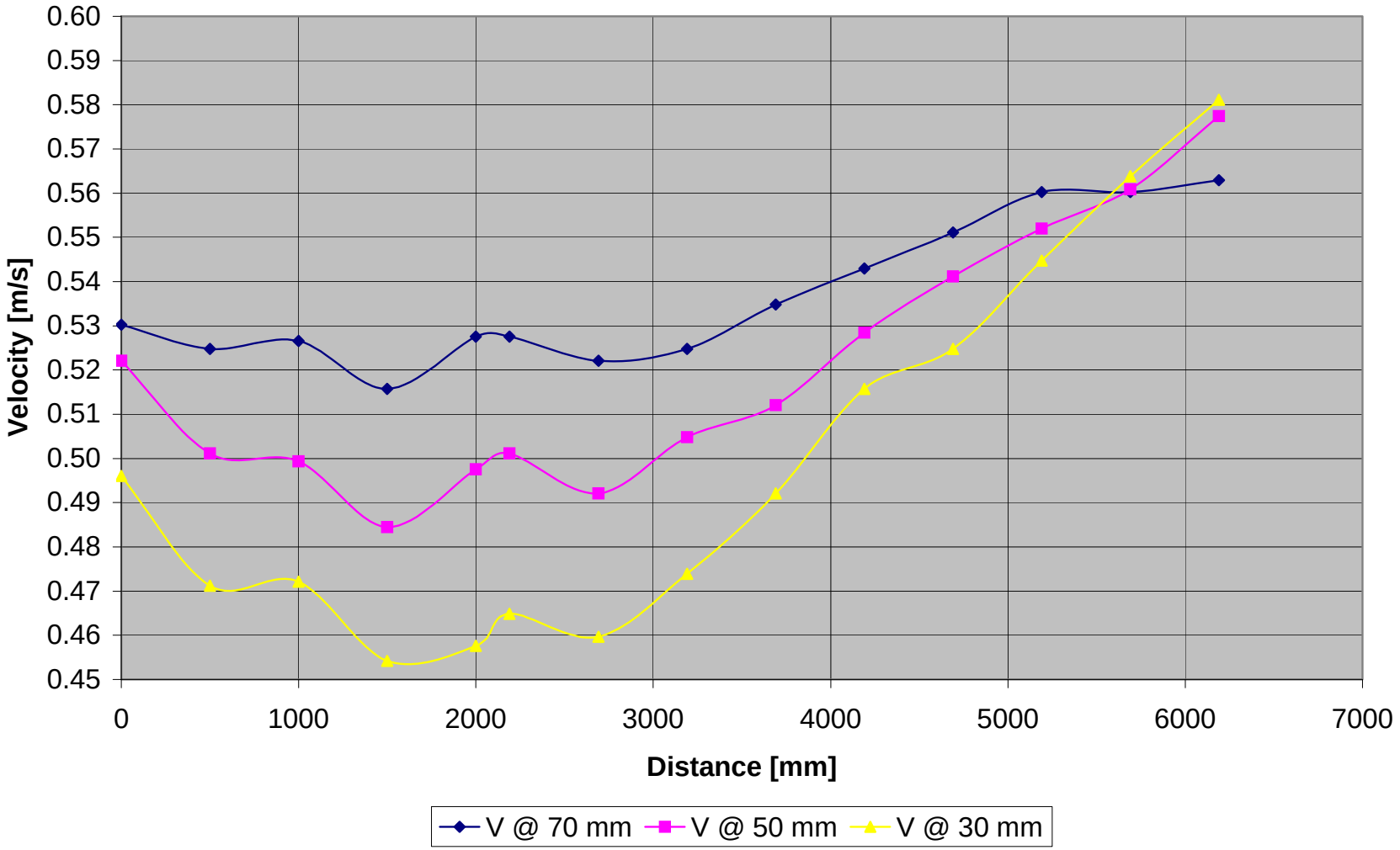

Figure A - 91: Test C3-Vertical velocity distribution measured at 150 mm from inner bank of bend

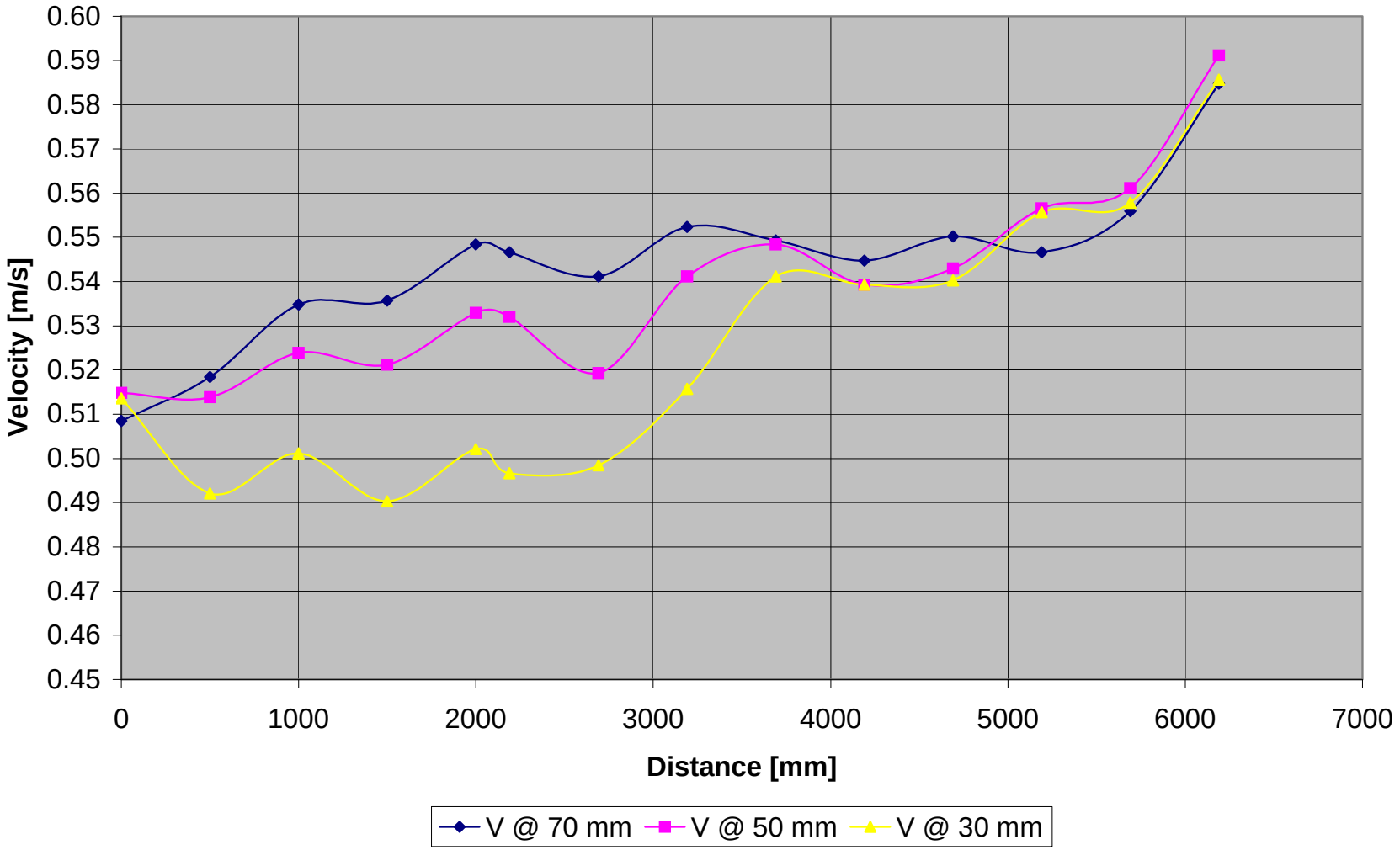

Figure A - 92: Test C3-Vertical velocity distribution measured at 200 mm from inner bank of bend

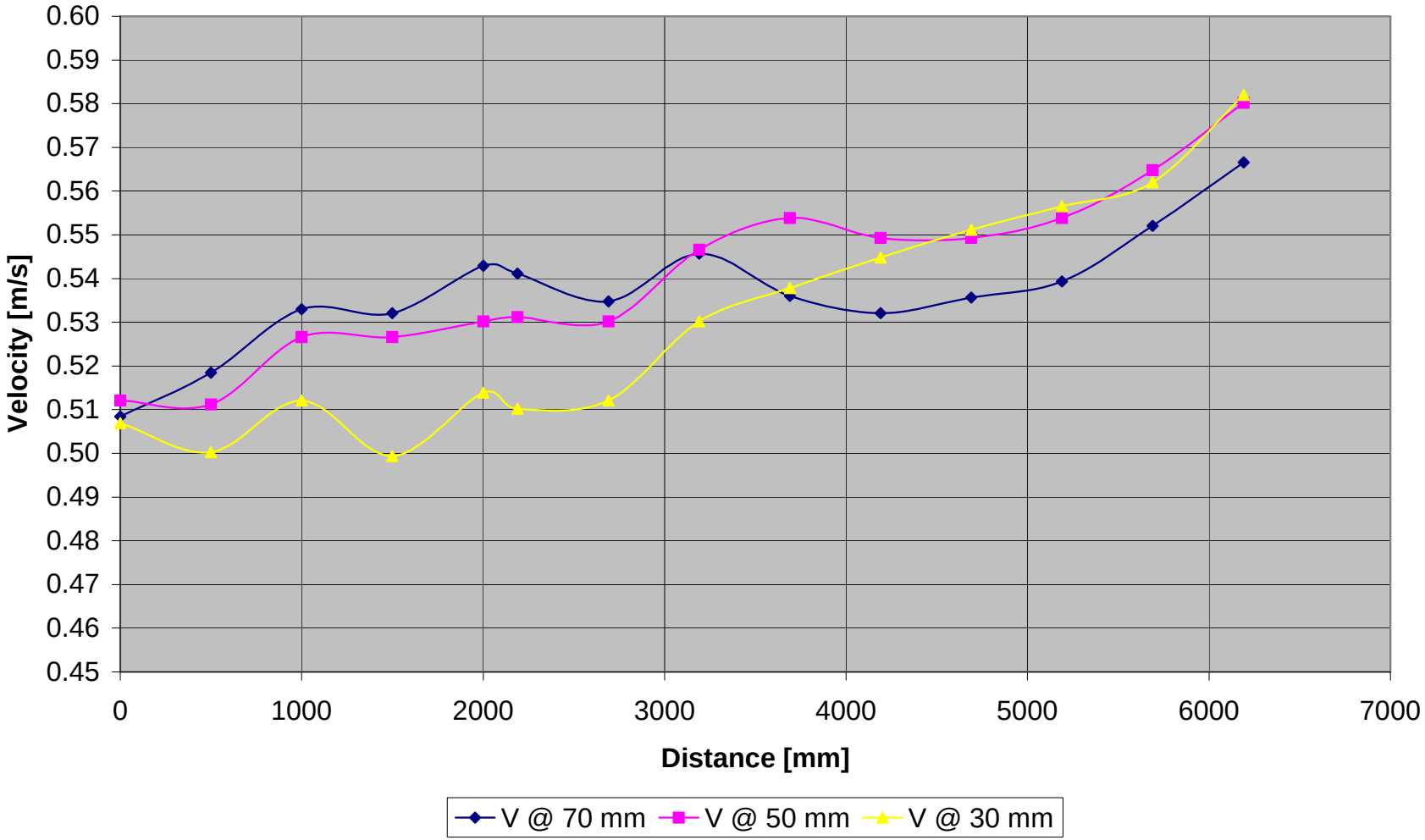

Figure A - 93: Test C3-Vertical velocity distribution measured at 250 mm from inner bank of bend

	Point	1	2	3	4	5	6	7	8	9	10	11	12	13	14
Width	**L**	**0**	**500**	**1000**	**1500**	**2000**	**2190**	**2690**	**3190**	**3690**	**4190**	**4690**	**5190**	**5690**	**6190**
	h														
50	**70**	0.514	0.516	0.525	0.530	0.546	0.549	0.556	0.564	0.548	0.503	0.468	0.456	0.461	0.477
	50	0.488	0.498	0.515	0.524	0.538	0.548	0.554	0.561	0.555	0.524	0.499	0.493	0.502	0.512
	30	0.461	0.474	0.498	0.509	0.525	0.533	0.539	0.546	0.535	0.514	0.490	0.499	0.518	0.533
100	**70**	0.541	0.516	0.525	0.518	0.525	0.536	0.536	0.553	0.511	0.518	0.533	0.548	0.467	0.498
	50	0.510	0.498	0.515	0.504	0.510	0.518	0.522	0.550	0.541	0.554	0.548	0.541	0.538	0.447
	30	0.456	0.474	0.498	0.484	0.492	0.506	0.503	0.528	0.505	0.511	0.518	0.533	0.548	0.467
150	**70**	0.530	0.525	0.527	0.516	0.528	0.528	0.522	0.525	0.535	0.543	0.551	0.560	0.560	0.563
	50	0.522	0.501	0.499	0.485	0.498	0.501	0.492	0.505	0.512	0.528	0.541	0.552	0.561	0.577
	30	0.496	0.471	0.472	0.454	0.458	0.465	0.460	0.474	0.492	0.516	0.525	0.545	0.564	0.581
200	**70**	0.508	0.518	0.535	0.536	0.548	0.547	0.541	0.552	0.549	0.545	0.550	0.547	0.556	0.585
	50	0.515	0.514	0.524	0.521	0.533	0.532	0.519	0.541	0.548	0.539	0.543	0.557	0.561	0.591
	30	0.514	0.492	0.501	0.490	0.502	0.497	0.498	0.516	0.541	0.539	0.540	0.556	0.558	0.586
250															
	70	0.508	0.518	0.533	0.532	0.543	0.541	0.535	0.546	0.536	0.532	0.536	0.539	0.552	0.567
	50	0.512	0.511	0.527	0.527	0.530	0.531	0.530	0.547	0.554	0.549	0.549	0.554	0.565	0.580
	30	0.507	0.500	0.512	0.499	0.514	0.510	0.512	0.530	0.538	0.545	0.551	0.557	0.562	0.582

Table A - 17: Test C3-Measured velocities [m/s]

A.3.1.4 TEST C4 (F_R = 0.7)

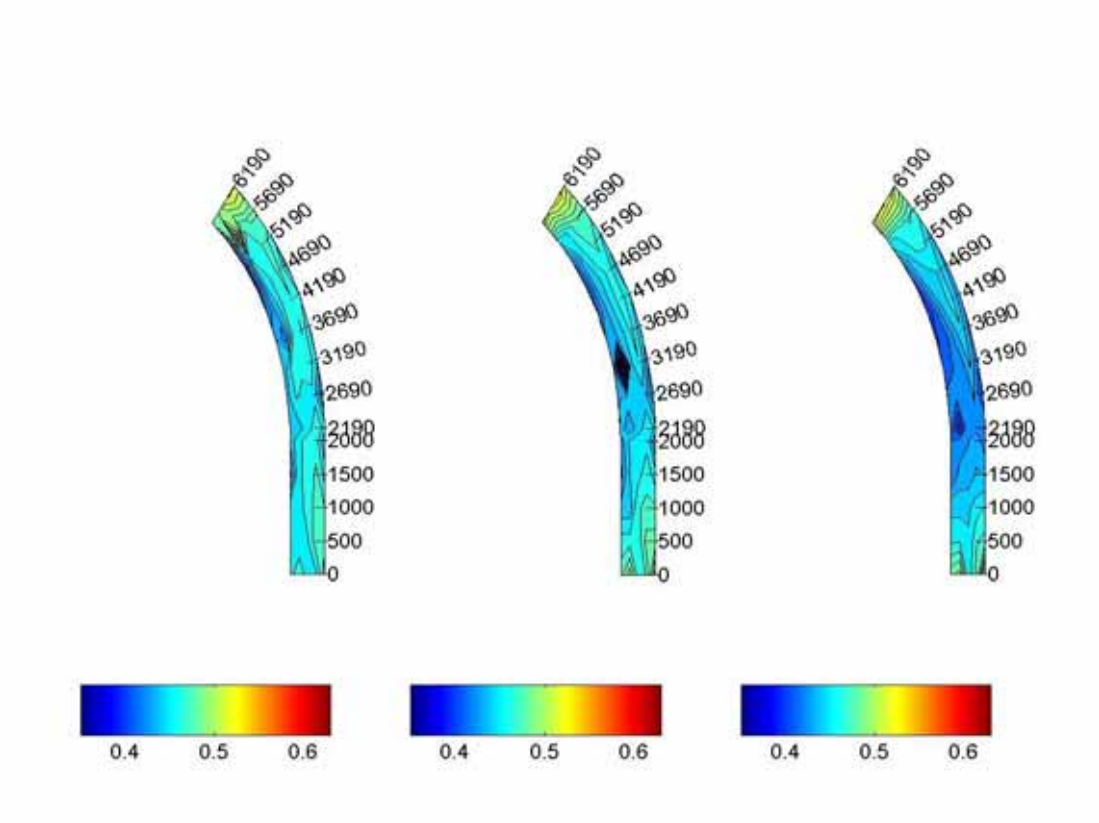

Figure A - 94: Test C4-Velocity distribution in the horisontal plane measured at 70, 50 and 30 mm

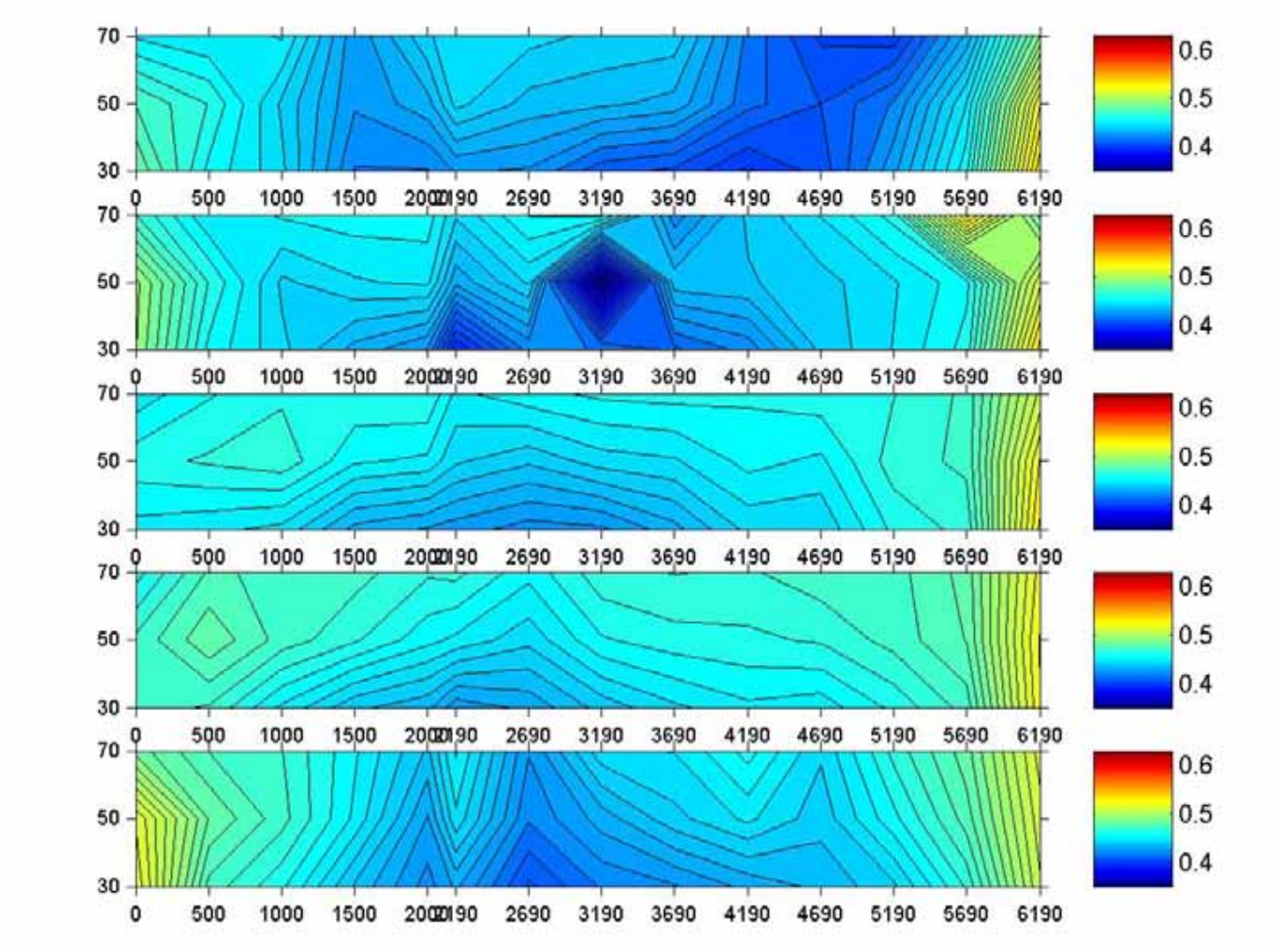

Figure A - 95: Test C4-Velocity distribution in the vertical plane

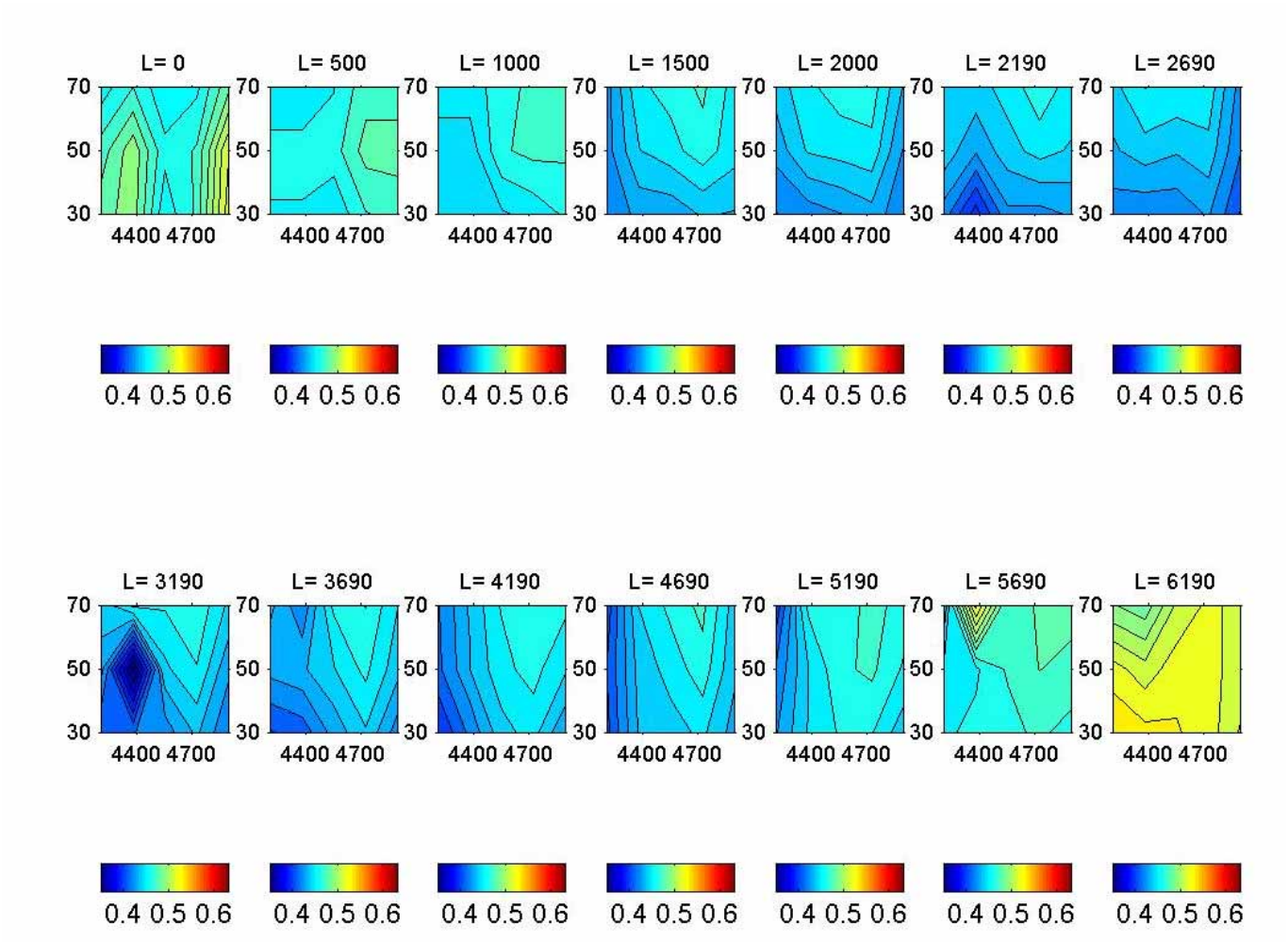

Figure A - 96: Test C4-Cross-sectional velocity distribution

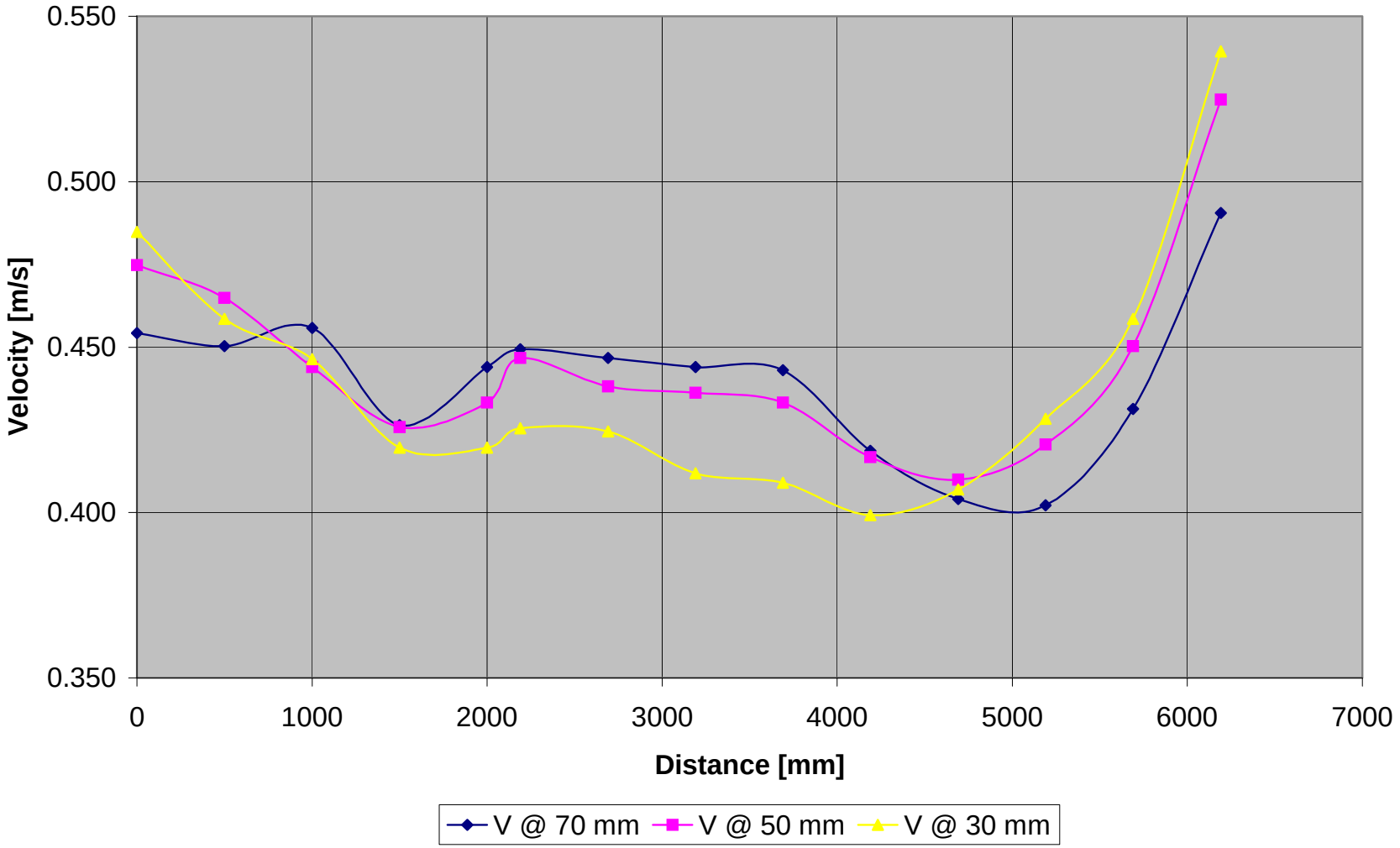

Figure A - 97: Test C4-Vertical velocity distribution measured at 50 mm from inner bank of bend

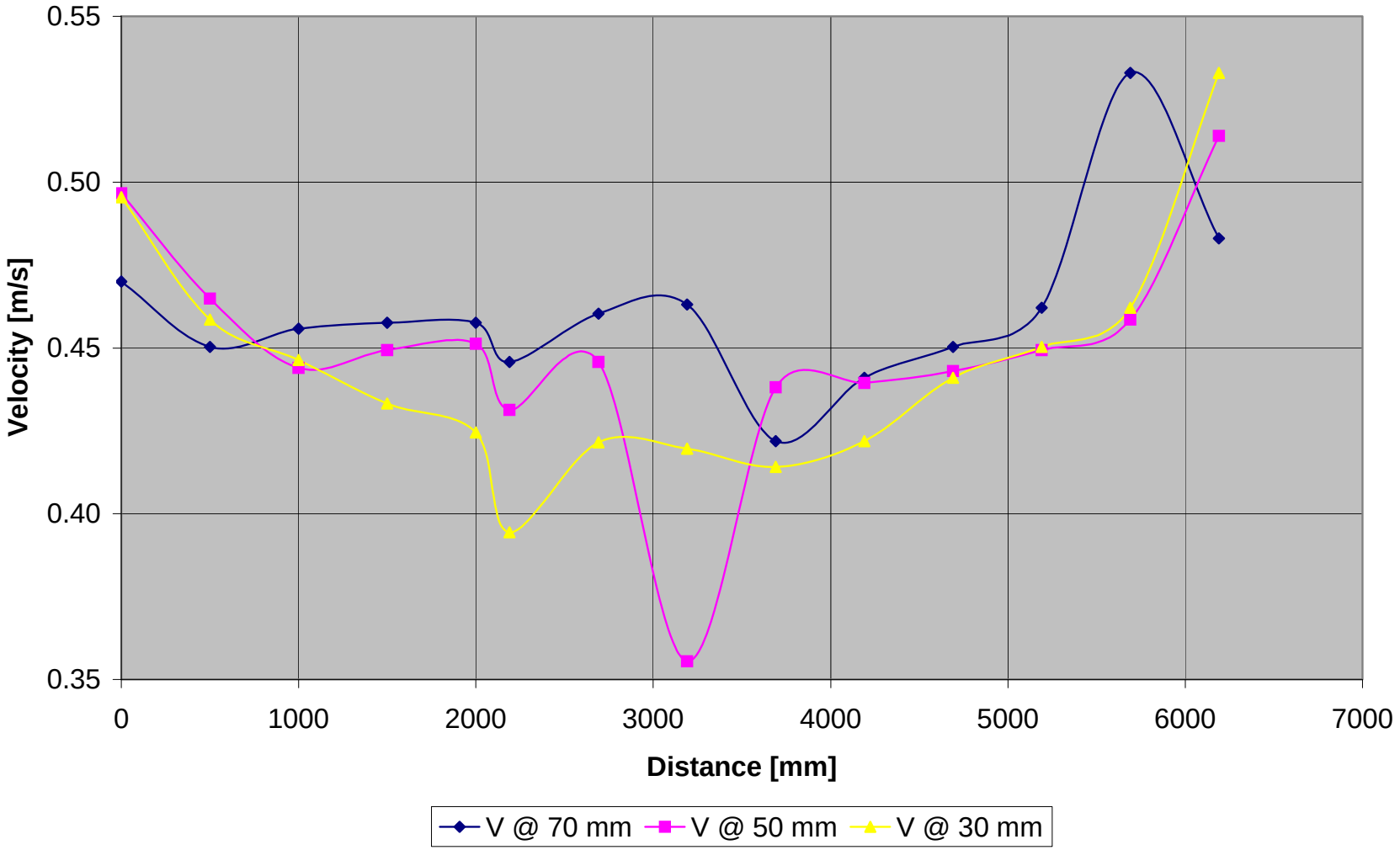

Figure A - 98: Test C4-Vertical velocity distribution measured at 100 mm from inner bank of bend

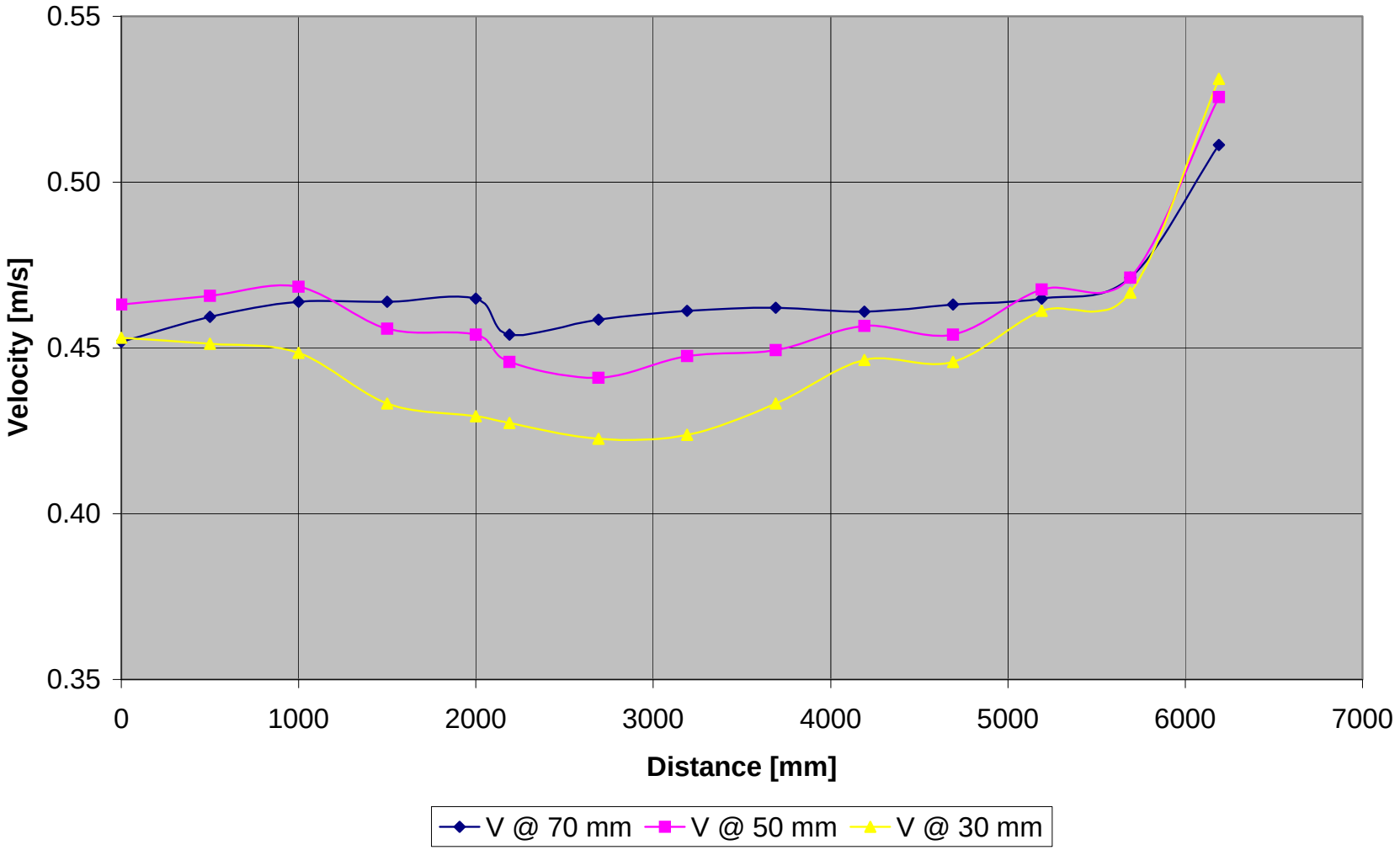

Figure A - 99: Test C4-Vertical velocity distribution measured at 150 mm from inner bank of bend

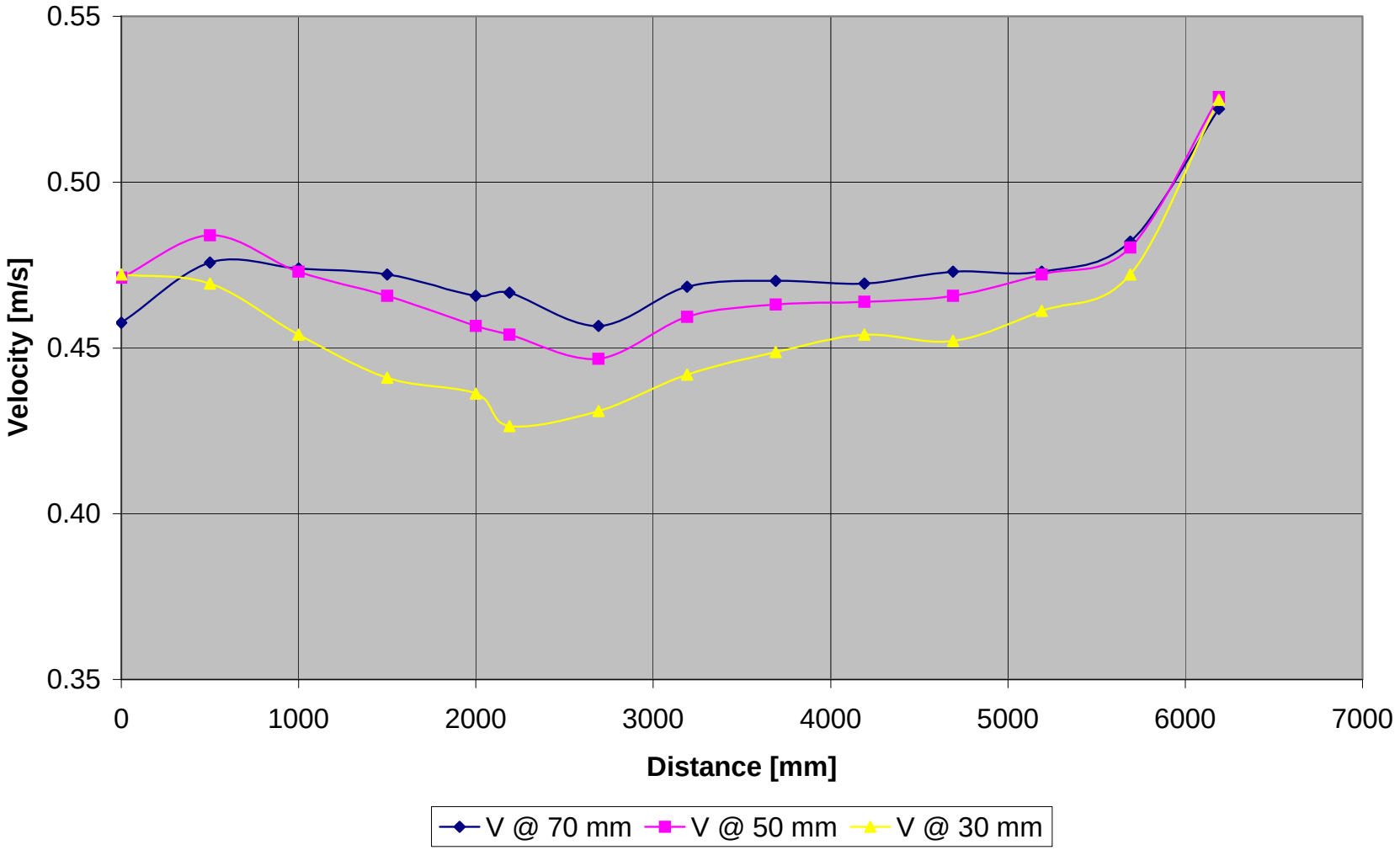

Figure A - 100: Test C4-Vertical velocity distribution measured at 200 mm from inner bank of bend

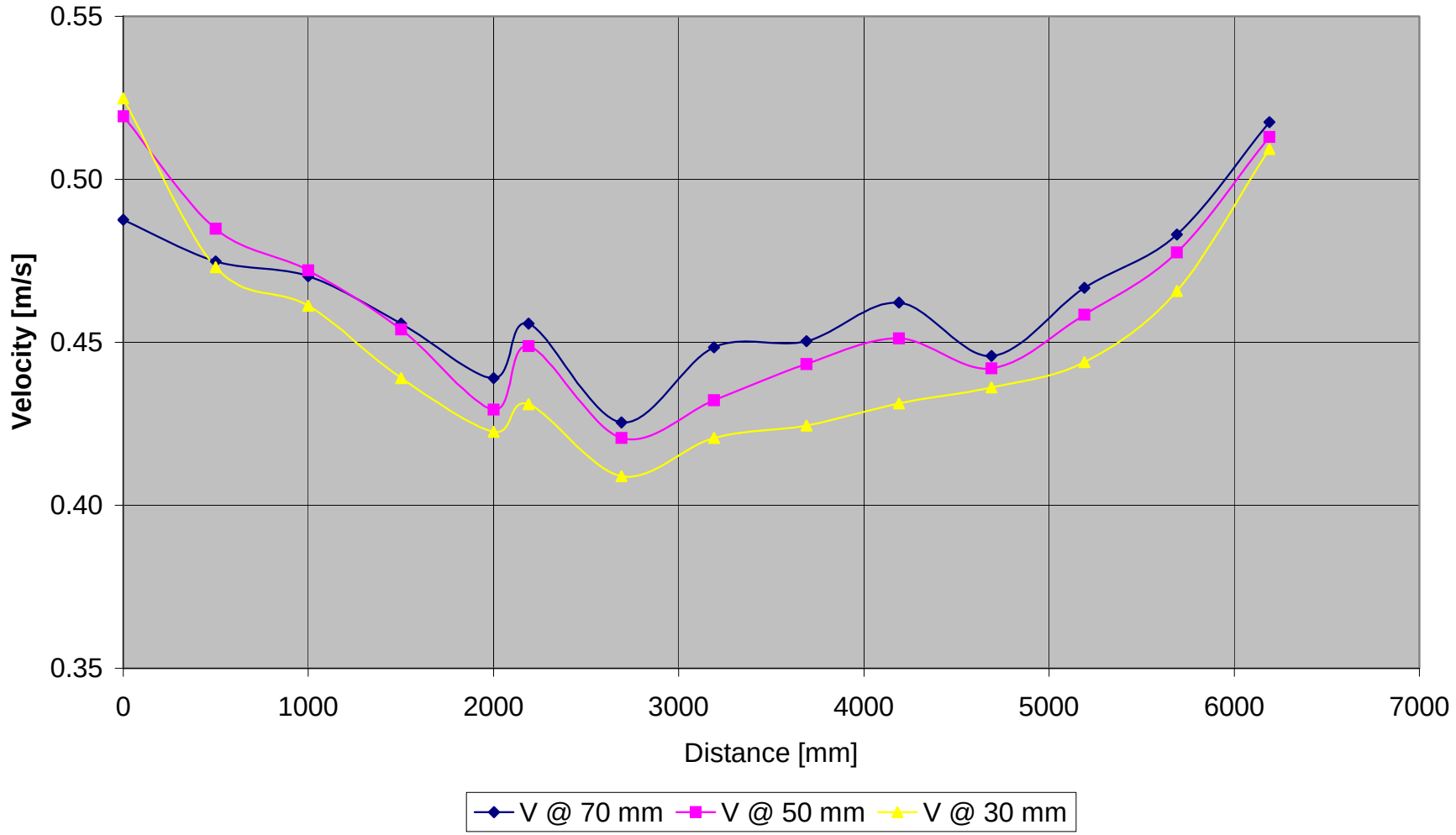

Figure A - 101: Test C4-Vertical velocity distribution measured at 250 mm from inner bank of bend

	Point	1	2	3	4	5	6	7	8	9	10	11	12	13	14
Width	**L**	**0**	**500**	**1000**	**1500**	**2000**	**2190**	**2690**	**3190**	**3690**	**4190**	**4690**	**5190**	**5690**	**6190**
	h														
50	**70**	0.454	0.450	0.456	0.426	0.444	0.449	0.447	0.444	0.443	0.419	0.404	0.402	0.431	0.491
	50	0.475	0.465	0.444	0.426	0.433	0.447	0.438	0.436	0.433	0.417	0.410	0.421	0.450	0.525
	30	0.485	0.458	0.446	0.420	0.420	0.425	0.424	0.412	0.409	0.399	0.407	0.428	0.458	0.539
100	**70**	0.470	0.450	0.456	0.458	0.458	0.446	0.460	0.463	0.422	0.441	0.450	0.462	0.533	0.483
	50	0.497	0.465	0.444	0.449	0.451	0.431	0.446	0.356	0.438	0.439	0.443	0.449	0.458	0.514
	30	0.495	0.458	0.446	0.433	0.424	0.394	0.422	0.420	0.414	0.422	0.441	0.450	0.462	0.533
150	**70**	0.452	0.459	0.464	0.464	0.465	0.454	0.458	0.461	0.462	0.461	0.463	0.465	0.471	0.511
	50	0.463	0.466	0.468	0.456	0.454	0.446	0.441	0.448	0.449	0.457	0.454	0.468	0.471	0.526
	30	0.453	0.451	0.448	0.433	0.429	0.427	0.423	0.424	0.433	0.446	0.446	0.461	0.467	0.531
200	**70**	0.458	0.476	0.474	0.472	0.466	0.467	0.457	0.468	0.470	0.469	0.473	0.473	0.482	0.522
	50	0.471	0.484	0.473	0.466	0.457	0.454	0.447	0.459	0.463	0.464	0.466	0.472	0.480	0.526
	30	0.472	0.469	0.454	0.441	0.436	0.426	0.431	0.442	0.449	0.454	0.452	0.461	0.472	0.525
250															
	70	0.488	0.475	0.470	0.456	0.439	0.456	0.425	0.448	0.450	0.462	0.446	0.467	0.483	0.518
	50	0.519	0.485	0.472	0.454	0.429	0.449	0.421	0.432	0.443	0.451	0.442	0.458	0.478	0.513
	30	0.525	0.473	0.461	0.439	0.423	0.431	0.409	0.421	0.424	0.431	0.436	0.444	0.466	0.509

Table A - 18: Test C4-Measured velocities [m/s]

A.3.2 SEDIMENT RELATED

A.3.2.1 TEST C5 (F_R = 0.3)

L	Width										
	25	50	75	100	125	150	175	200	225	250	275
0	137.8	137.8	136.5	135.2	134.2	133.2	133.6	133.9	132.6	131.2	131.2
500	149.8	149.8	149.0	148.1	147.1	146.0	143.8	141.5	140.0	138.5	138.5
1000	150.1	150.1	149.2	148.3	148.0	147.7	147.7	147.6	146.3	145.0	145.0
1500	142.6	142.6	143.6	144.5	145.6	146.6	146.6	146.5	146.1	145.7	145.7
2000	150.6	150.6	148.8	146.9	146.5	146.1	144.9	143.6	143.3	142.9	142.9
2190	159.5	156.0	155.2	154.6	153.3	152.0	152.2	151.0	148.9	148.6	150.0
2440	158.9	156.2	155.1	154.3	150.8	153.1	149.2	152.4	152.7	152.0	151.0
2690	168.1	156.9	153.0	152.0	152.1	150.8	150.5	152.1	150.6	150.0	149.2
2940	154.7	148.6	148.6	150.5	148.8	148.2	148.3	148.7	148.9	148.6	147.9
3190	149.0	145.1	143.1	146.4	142.8	140.0	139.2	138.7	138.6	137.5	140.0
3440	139.4	140.5	138.1	139.9	135.2	134.8	136.5	135.8	136.3	135.6	138.8
3690	145.6	146.1	143.0	142.6	140.9	142.0	143.3	141.9	141.7	141.5	142.7
3940	151.9	148.5	145.0	145.4	144.8	143.8	143.3	144.5	145.3	145.4	146.6
4190	153.4	150.8	148.4	146.5	146.0	147.0	143.9	143.5	143.4	144.2	144.4
4440	143.8	138.4	140.0	142.1	142.0	142.9	143.6	143.5	145.0	146.8	148.0
4690	151.0	144.9	145.5	146.7	145.3	144.3	144.5	144.3	144.8	144.0	144.7
4940	153.4	144.7	146.5	147.2	147.0	149.5	147.7	148.0	147.6	147.5	146.5
5190	160.8	153.4	150.7	152.6	154.0	154.3	154.5	155.3	154.0	153.9	154.8
5440	162.5	149.0	150.0	148.6	147.7	148.6	150.1	150.5	150.8	151.4	151.9
5690	159.0	148.6	148.8	148.5	148.2	146.8	148.4	149.2	150.0	149.5	150.0
5940	162.0	159.0	158.2	157.0	155.9	154.4	155.5	153.9	154.2	154.3	157.2
6190	159.3	155.5	156.9	155.4	154.8	153.5	151.4	150.5	150.0	150.1	149.6

Table A - 19: Test C5-Sediment levels (zero readings)

L	Width										
	25	50	75	100	125	150	175	200	225	250	275
0	131.4	131.4	134.4	137.4	135.0	132.6	132.5	132.3	128.0	123.7	123.7
500	136.6	136.6	140.4	144.2	145.6	146.9	141.7	136.5	133.7	130.9	130.9
1000	132.8	132.8	130.8	128.7	133.9	139.1	146.6	154.0	149.6	145.2	145.2
1500	141.4	141.4	140.0	138.6	143.3	147.9	143.2	138.5	140.8	143.1	143.1
2000	146.9	146.9	146.4	145.9	142.0	138.0	139.2	140.3	142.8	145.2	145.2
2190	150.8	152.9	152.5	145.8	148.7	145.0	136.7	133.9	134.5	138.3	140.5
2440	153.6	151.9	144.9	140.8	133.4	132.8	142.4	150.6	141.8	137.4	126.9
2690	164.8	163.2	158.0	156.5	158.7	147.6	151.3	141.8	146.0	142.6	138.8
2940	155.9	159.2	145.9	142.0	148.8	143.1	132.2	122.2	123.0	127.4	127.8
3190	153.4	149.5	150.3	145.1	140.9	135.5	147.0	148.9	137.9	134.3	131.5
3440	144.4	142.2	135.9	135.7	139.1	135.4	136.4	145.0	133.4	135.6	134.9
3690	149.3	140.3	140.1	142.6	139.8	136.0	137.0	141.8	140.2	140.3	131.8
3940	149.9	145.7	147.8	145.8	149.0	148.1	149.3	146.2	136.6	128.8	127.7
4190	152.3	144.6	149.1	153.7	148.6	141.1	136.3	135.4	131.1	134.2	132.5
4440	143.1	140.6	144.7	146.6	148.3	149.5	140.0	134.9	131.8	135.0	140.6
4690	150.3	145.5	143.0	149.6	135.0	131.5	135.4	138.4	136.9	134.1	126.5
4940	154.0	150.3	154.0	148.6	155.0	152.5	152.0	145.7	138.6	130.2	122.9
5190	154.3	150.4	160.7	151.9	146.7	155.8	162.8	152.9	141.5	134.5	139.3
5440	152.9	141.7	143.2	141.5	140.0	145.9	159.3	152.9	144.8	143.0	143.4
5690	159.4	150.3	149.5	159.8	156.2	153.3	147.7	140.5	134.7	142.4	142.3
5940	162.9	155.8	156.2	155.1	153.8	152.7	148.8	143.9	132.1	132.7	131.5
6190	147.0	146.3	154.7	156.8	151.5	140.7	135.5	126.8	126.2	133.2	137.9

Table A - 20: Test C5-Sediment levels (Run 1)

L	Width										
	25	50	75	100	125	150	175	200	225	250	275
0	146.8	146.8	141.5	136.2	139.1	142.0	140.2	138.3	136.4	134.5	134.5
500	139.0	139.0	137.7	136.3	136.5	136.6	134.9	133.1	132.9	132.6	132.6
1000	145.4	145.4	146.4	147.3	150.0	152.6	143.9	135.2	132.7	130.2	130.2
1500	139.0	139.0	134.8	130.5	136.2	141.9	147.4	152.8	153.0	153.1	153.1
2000	143.6	143.6	142.2	140.8	145.1	149.3	149.0	148.6	147.9	147.2	147.2
2190	158.3	152.9	150.2	145.7	148.1	147.7	147.4	145.4	143.0	139.0	134.2
2440	160.8	150.2	148.4	147.0	141.7	147.6	144.5	144.8	135.5	135.4	138.2
2690	140.5	144.6	143.5	150.8	152.7	151.2	144.6	138.2	136.5	136.9	139.0
2940	158.8	157.9	148.7	139.6	142.6	143.8	136.8	131.0	129.7	125.1	119.6
3190	163.9	151.1	142.8	144.5	152.5	150.0	148.9	144.3	140.1	133.0	128.6
3440	146.2	141.6	153.5	148.0	145.5	138.3	130.2	124.0	125.9	134.5	132.1
3690	145.4	150.5	149.2	147.0	140.0	140.1	141.5	131.0	126.7	119.5	107.8
3940	148.5	139.8	140.2	143.7	144.6	143.0	142.3	138.9	131.2	129.0	129.6
4190	149.6	151.5	156.0	145.4	153.2	148.5	140.7	134.5	123.2	115.5	111.8
4440	151.1	151.2	145.8	152.1	151.8	142.3	130.7	123.5	131.4	129.0	130.9
4690	149.5	144.9	146.9	151.2	146.1	142.5	143.9	136.3	133.2	131.1	122.7
4940	143.3	142.2	155.7	159.3	153.0	141.8	137.8	140.0	133.4	130.3	127.1
5190	151.2	153.9	153.4	145.1	138.2	139.9	137.2	135.2	144.0	143.6	141.5
5440	152.2	153.4	151.5	164.6	156.8	144.0	136.4	131.2	124.8	122.9	131.0
5690	151.1	161.7	158.6	155.2	154.1	140.5	128.3	112.2	97.8	98.5	106.3
5940	162.2	152.0	151.9	160.8	156.5	145.3	139.8	134.7	122.8	116.0	113.6
6190	155.5	155.9	155.2	157.7	157.0	131.4	129.0	127.9	124.9	118.8	119.8

Table A - 21: Test C5-Sediment levels (Run 2)

L	Width										
	25	50	75	100	125	150	175	200	225	250	275
0	141.1	141.1	147.6	154.1	146.9	139.7	141.7	143.6	136.5	129.4	129.4
500	146.0	146.0	147.1	148.2	142.7	137.1	136.9	136.7	137.2	137.6	137.6
1000	139.3	139.3	142.5	145.6	146.9	148.2	145.0	141.7	144.9	148.0	148.0
1500	131.1	131.1	136.6	142.0	143.9	145.8	143.5	141.2	138.2	135.1	135.1
2000	132.8	132.8	138.2	143.5	145.1	146.6	143.2	139.7	142.7	145.7	145.7
2190	127.0	136.0	139.6	143.2	140.4	135.5	135.7	145.0	143.0	141.4	144.1
2440	153.9	153.4	152.9	146.0	145.0	151.5	138.7	132.0	133.4	135.6	133.6
2690	151.0	147.1	146.0	142.4	148.7	145.3	141.0	139.5	132.7	137.2	135.2
2940	164.3	165.5	157.0	141.9	132.7	141.2	147.2	145.2	138.6	137.4	135.2
3190	160.7	153.6	150.0	146.5	141.7	139.6	145.3	144.5	138.6	123.4	117.5
3440	145.6	157.6	149.3	138.4	138.6	140.8	139.6	136.7	127.8	119.4	115.0
3690	154.8	145.8	133.1	130.0	135.0	140.8	136.8	135.2	130.6	126.2	120.3
3940	150.1	144.8	155.0	147.1	139.2	131.8	135.1	134.0	125.5	113.3	119.8
4190	149.1	148.2	153.8	146.4	152.0	143.5	140.0	134.3	129.3	123.7	121.1
4440	149.3	154.0	143.5	137.8	143.7	138.4	130.8	132.5	127.7	121.4	124.0
4690	148.1	145.2	152.0	152.7	149.3	143.1	132.4	139.6	132.2	130.0	122.0
4940	148.5	151.2	151.3	154.3	146.2	136.4	131.4	137.2	144.0	143.7	143.1
5190	161.2	148.9	145.6	149.0	144.2	144.7	135.4	131.5	123.2	123.5	126.9
5440	161.3	158.2	158.8	161.5	160.7	154.5	142.9	137.0	136.0	133.0	132.5
5690	158.5	159.6	159.7	151.4	151.9	148.3	144.6	139.5	126.5	112.6	114.0
5940	160.0	157.6	146.7	146.5	149.7	138.6	130.3	127.1	125.9	118.2	117.8
6190	158.9	165.6	157.4	148.0	140.9	128.6	124.3	130.3	122.4	105.1	103.6

Table A - 22: Test C5-Sediment levels (Run 3)

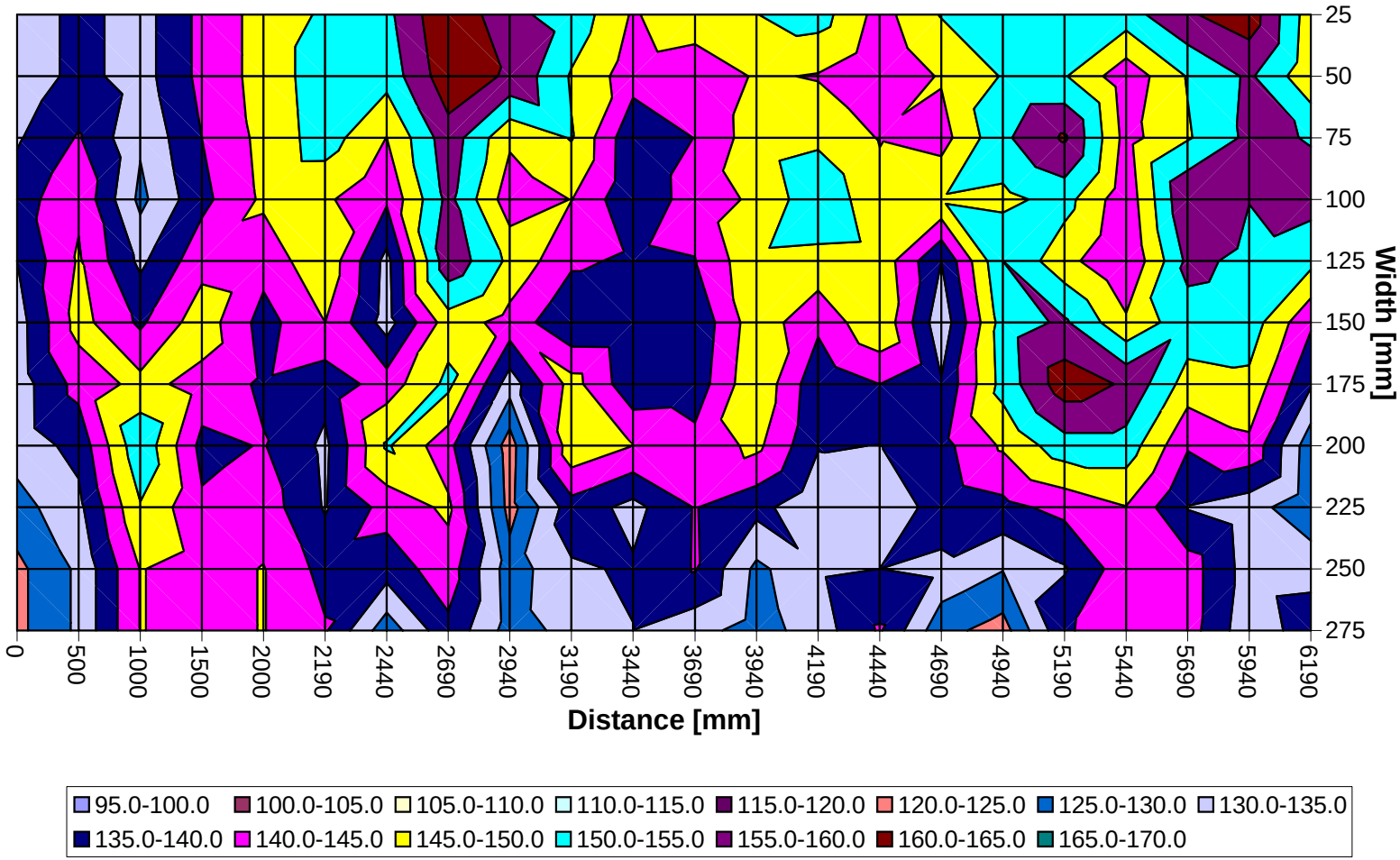

Figure A - 102: Test C5-Sediment levels after Run 1

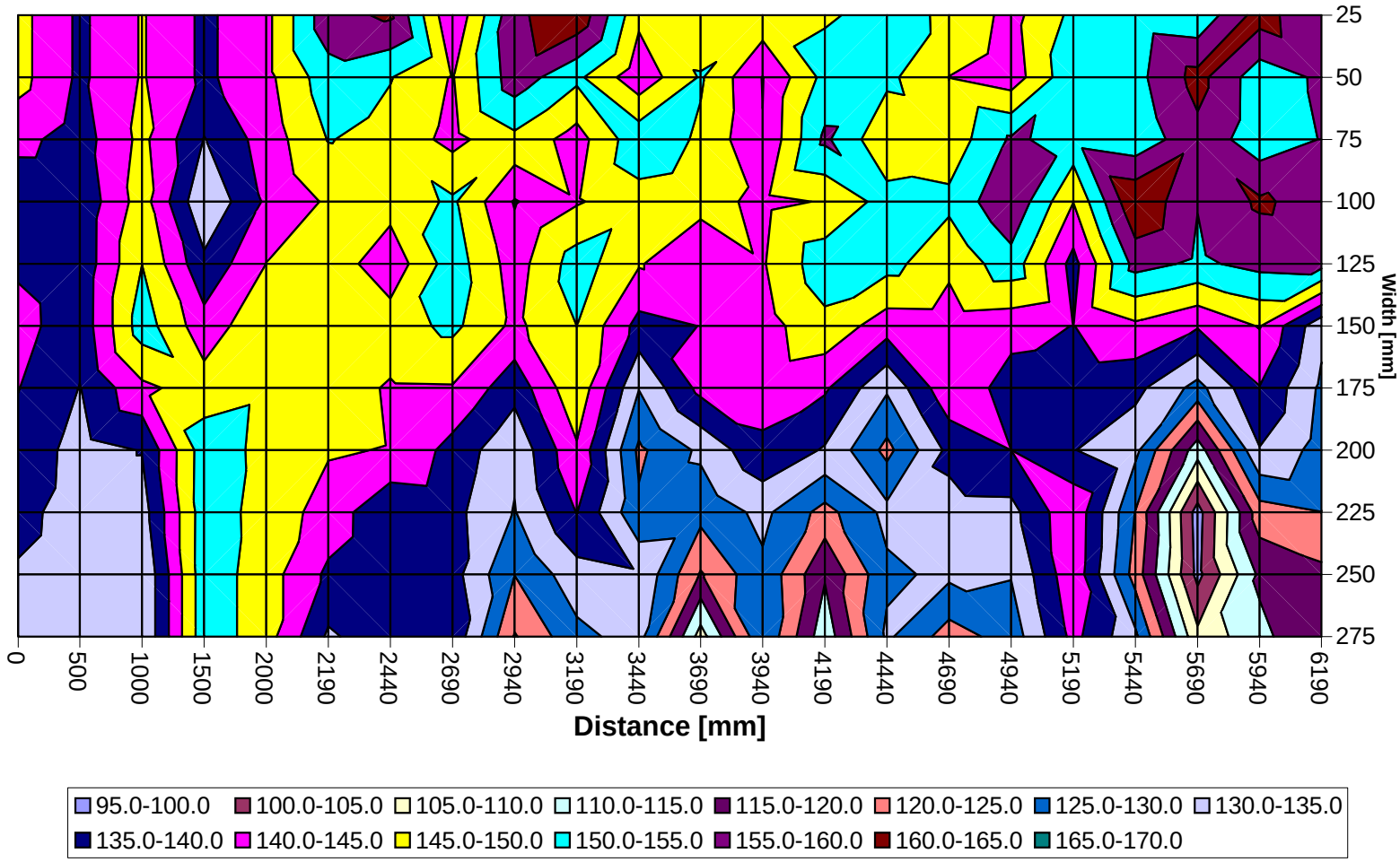

Figure A - 103: Test C5-Sediment levels after Run 2

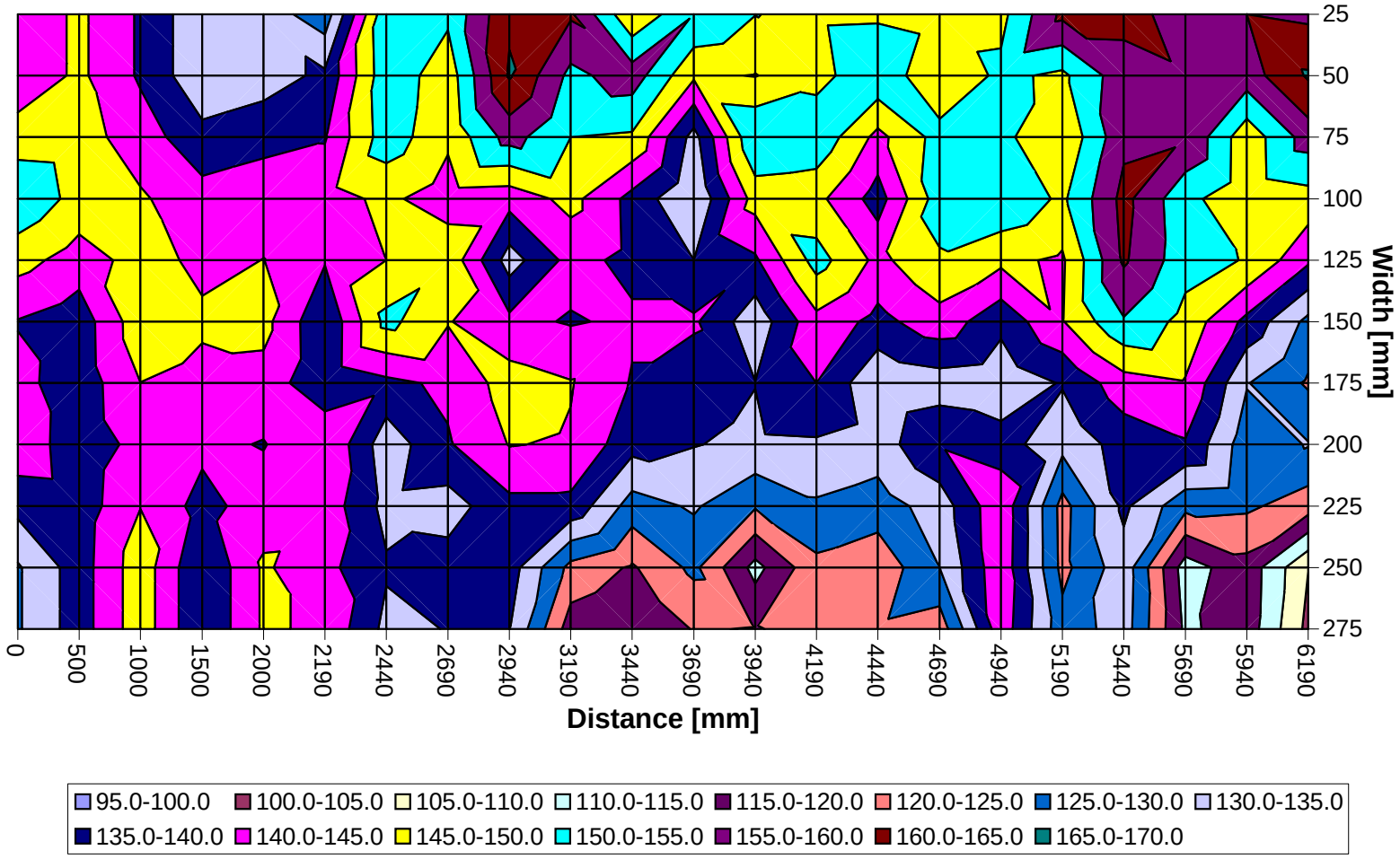

Figure A - 104: Test C5-Sediment levels after Run 3

APPENDIX B-DIVERSION ANGLE

APPENDIX B-DIVERSION ANGLE

CONTENTS

LIST OF FIGURES

LIST OF TABLES

Page

B.1 TEST D (Θ = 20˚)

B.1.1 TEST D1 (F_R = 0.3)

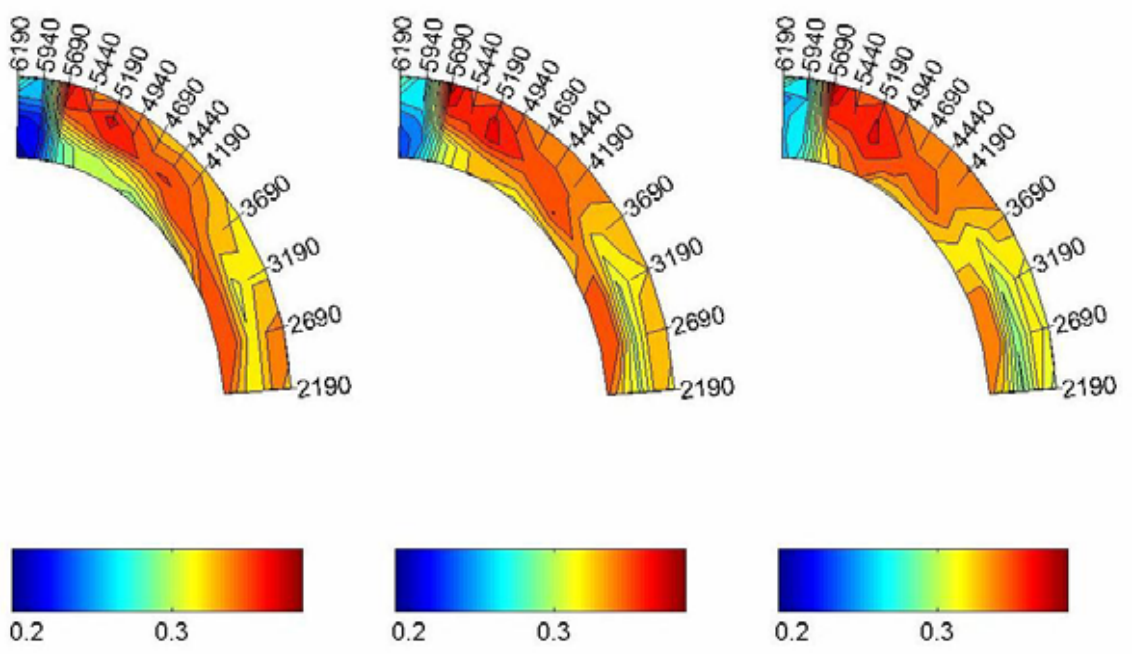

Figure B - 1: Test D1-Velocity distribution in the horizontal plane measured at 70, 50 and 30 mm

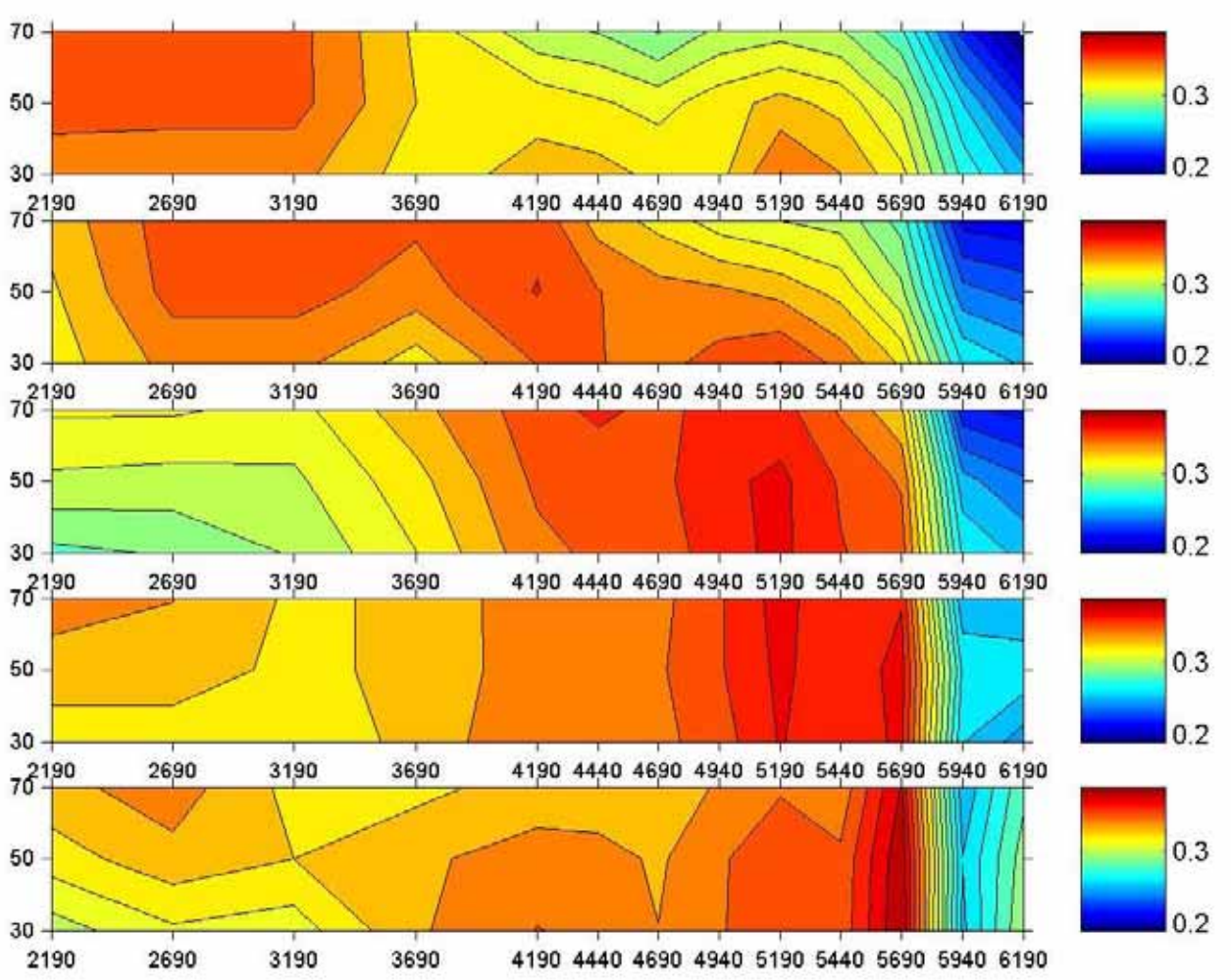

Figure B - 2: Test D1-Velocity distribution in the vertical plane

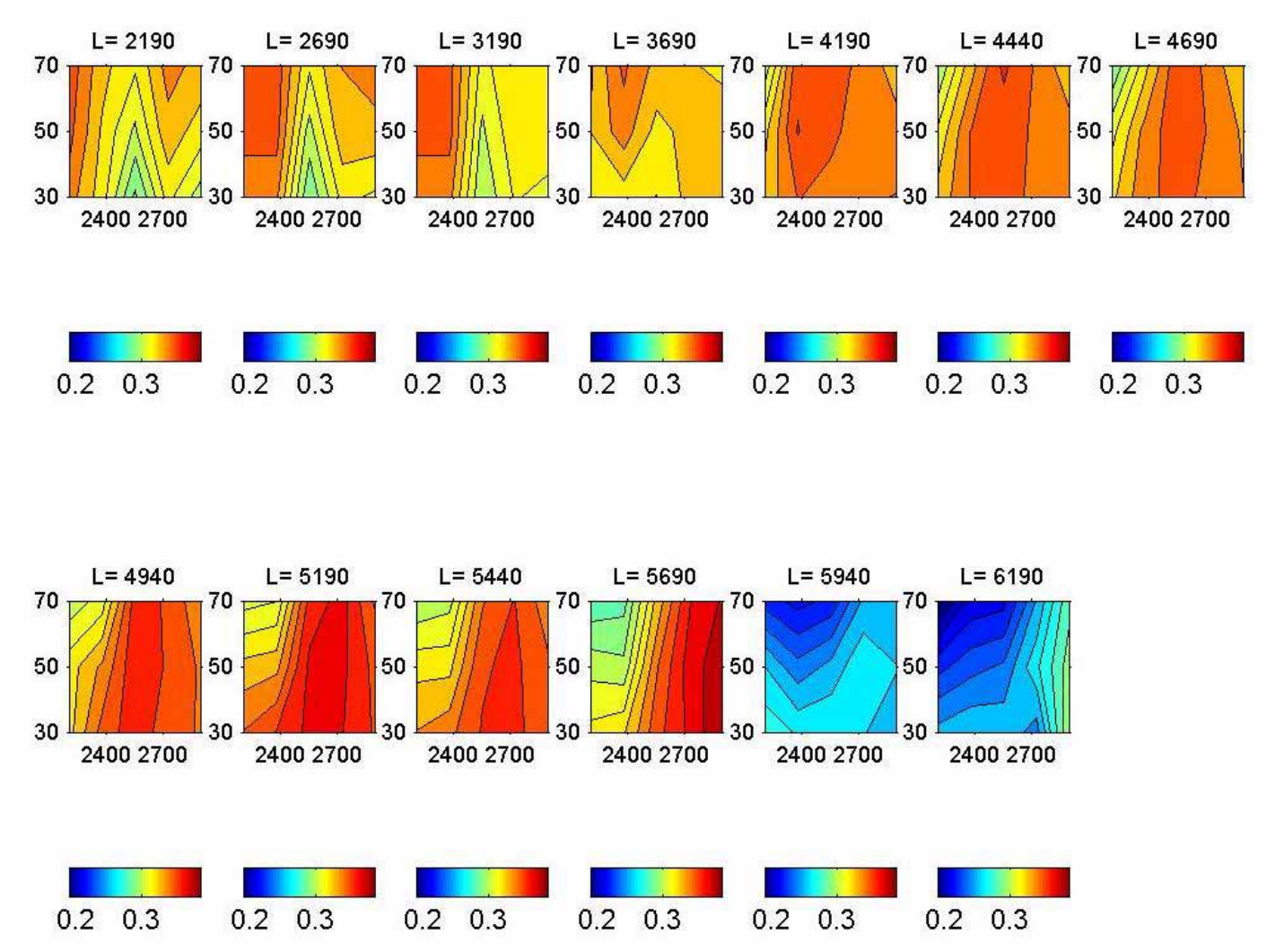

Figure B - 3: Test D1-Cross-sectional velocity distribution

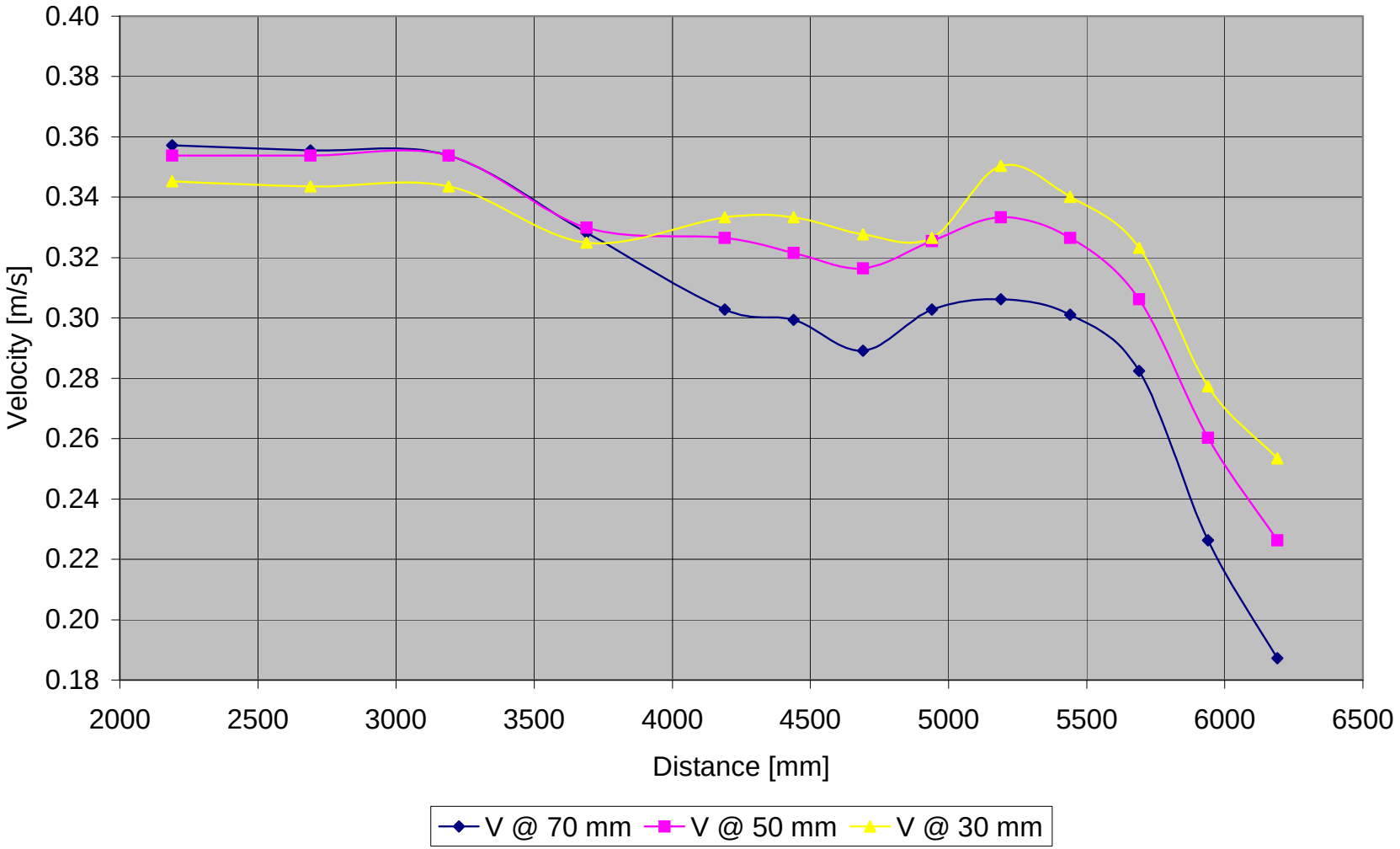

Figure B - 4: Test D1-Vertical velocity distribution measured at 50 mm from inner bank of bend

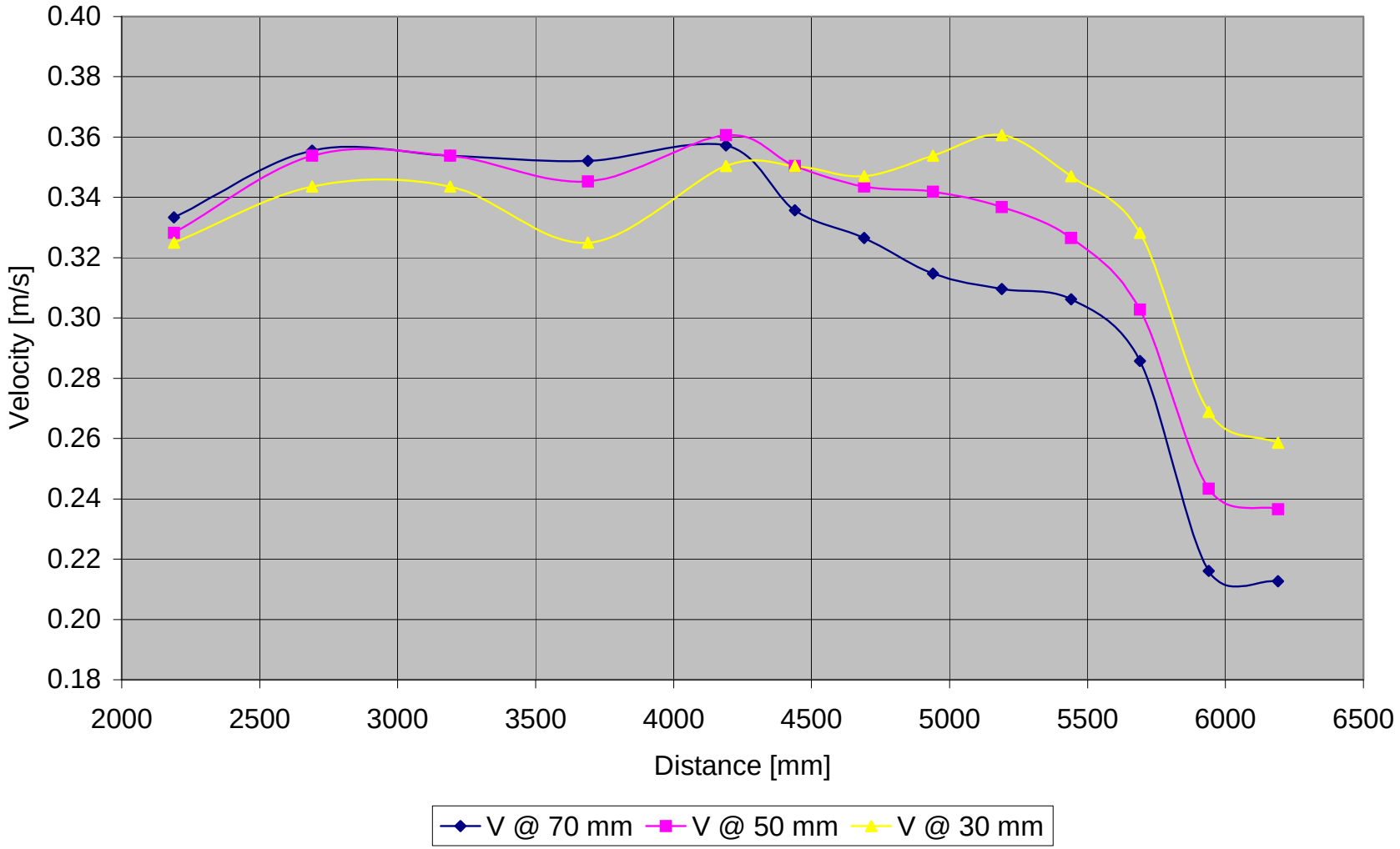

Figure B - 5: Test D1-Vertical velocity distribution measured at 100 mm from inner bank of bend

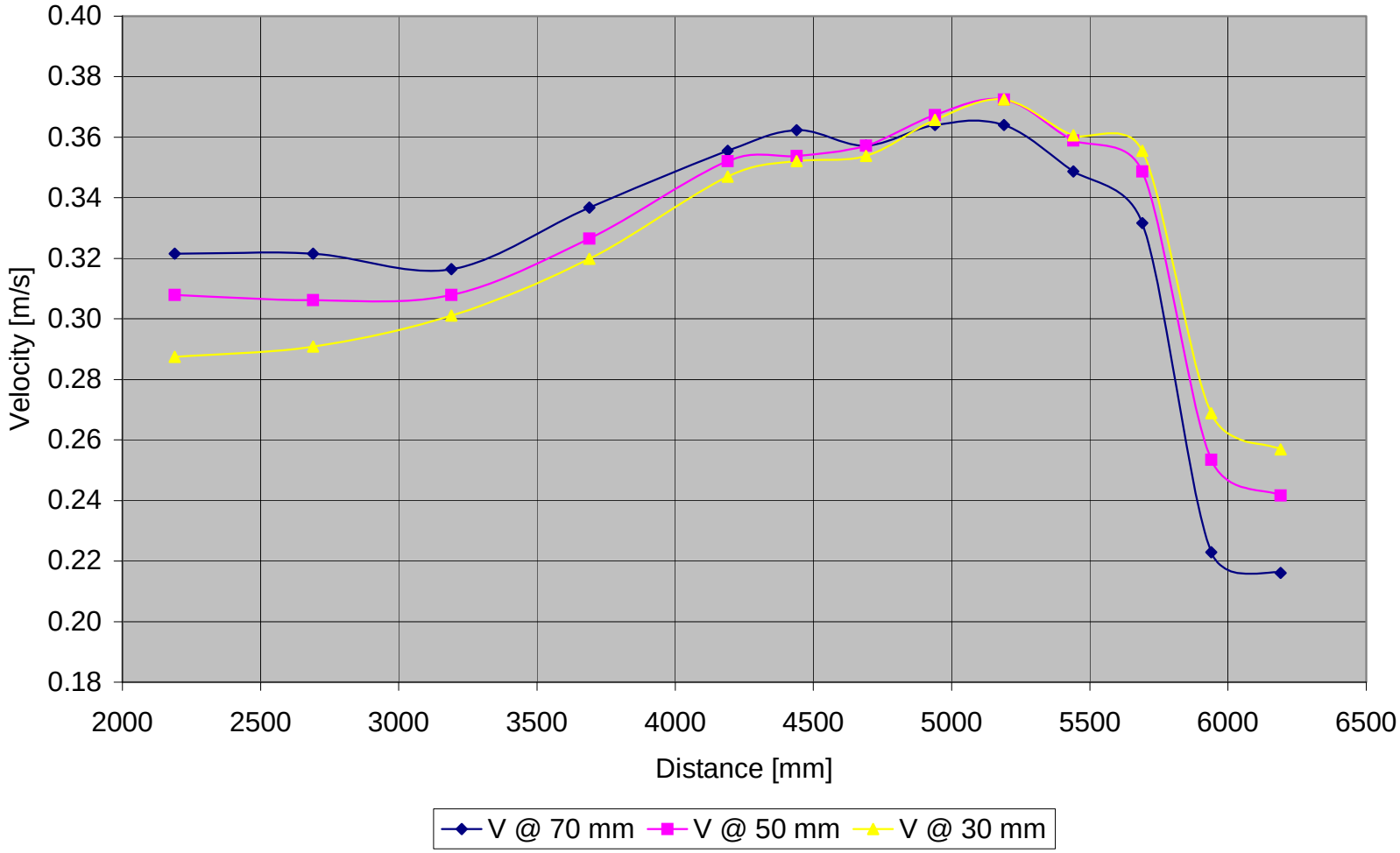

Figure B - 6: Test D1-Vertical velocity distribution measured at 150 mm from inner bank of bend

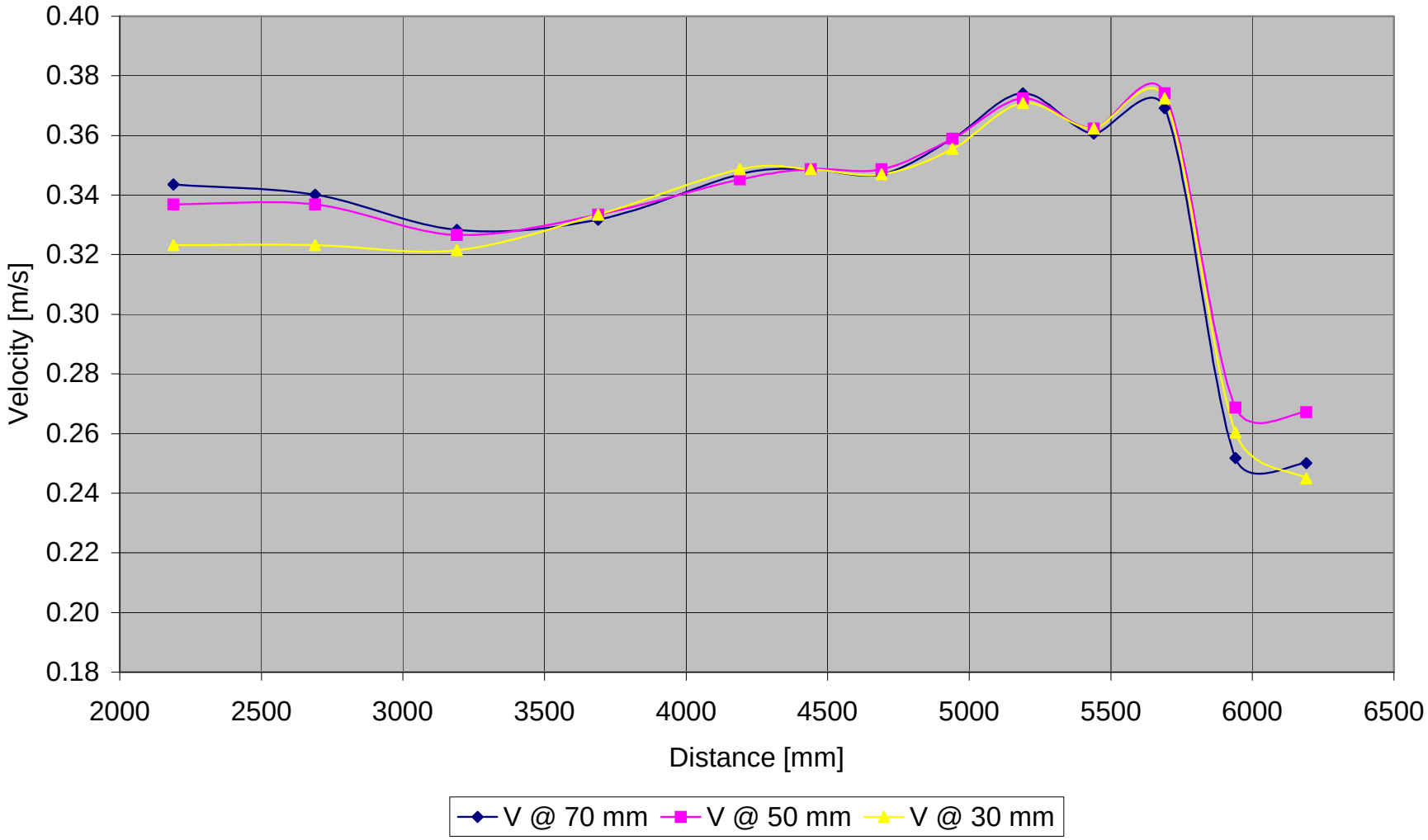

Figure B - 7: Test D1-Vertical velocity distribution measured at 200 mm from inner bank of bend

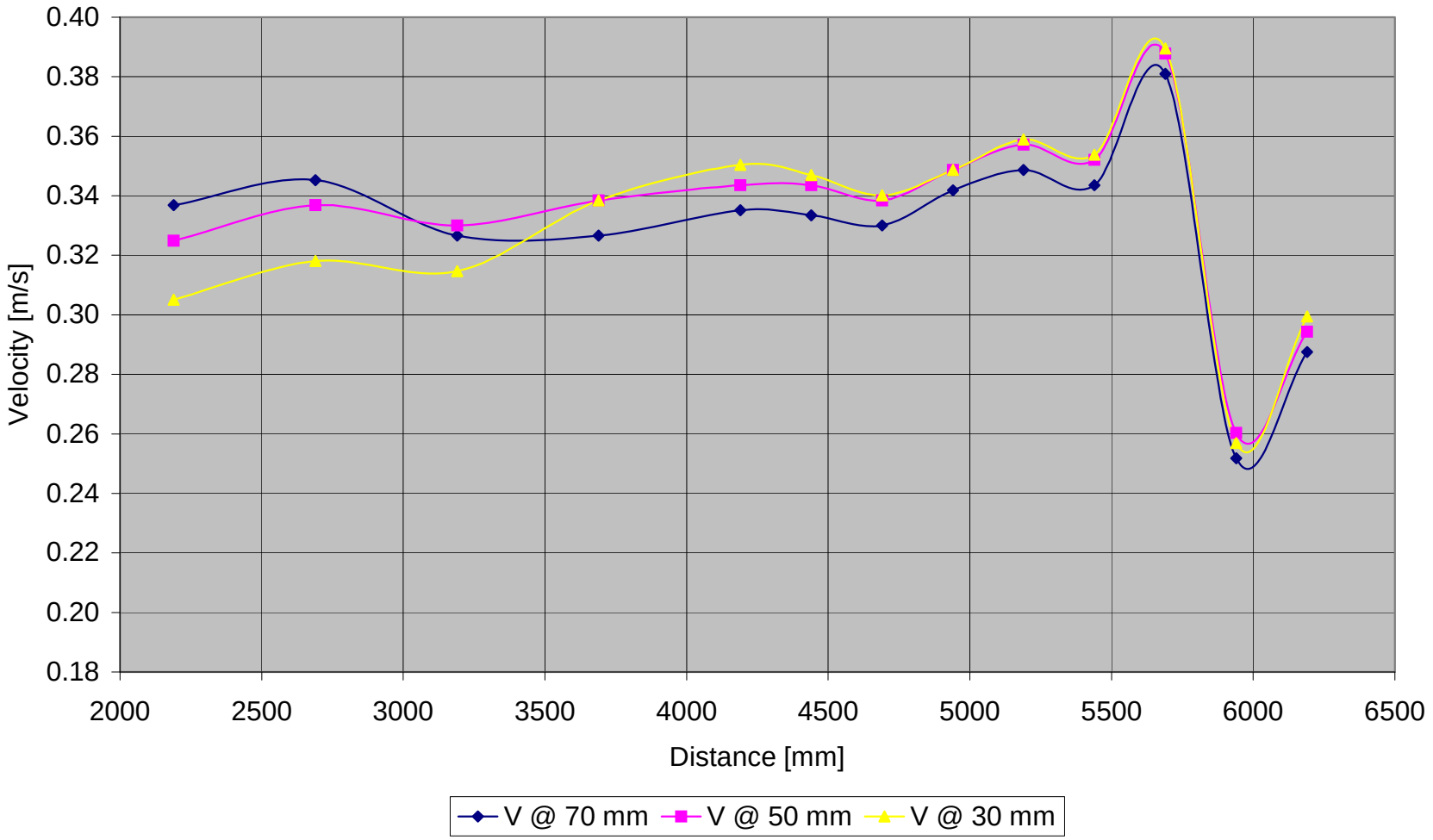

Figure B - 8: Test D1-Vertical velocity distribution measured at 250 mm from inner bank of bend

	Point	6	7	8	9	10	10A	11	11A	12	12A	13	13A	14
Width	**L**	**2190**	**2690**	**3190**	**3690**	**4190**	**4440**	**4690**	**4940**	**5190**	**5440**	**5690**	**5940**	**6190**
	h													
50	**70**	0.357	0.356	0.354	0.328	0.303	0.299	0.289	0.303	0.306	0.301	0.282	0.226	0.187
	50	0.354	0.354	0.354	0.330	0.327	0.322	0.316	0.325	0.333	0.327	0.306	0.260	0.226
	30	0.345	0.344	0.344	0.325	0.333	0.333	0.328	0.327	0.350	0.340	0.323	0.277	0.254
100	**70**	0.333	0.356	0.354	0.352	0.357	0.336	0.327	0.315	0.310	0.306	0.286	0.216	0.213
	50	0.328	0.354	0.354	0.345	0.361	0.350	0.344	0.342	0.337	0.327	0.303	0.243	0.237
	30	0.325	0.344	0.344	0.325	0.350	0.350	0.347	0.354	0.361	0.347	0.328	0.269	0.259
150	**70**	0.322	0.322	0.316	0.337	0.356	0.362	0.357	0.364	0.364	0.349	0.332	0.223	0.216
	50	0.308	0.306	0.308	0.327	0.352	0.354	0.357	0.367	0.373	0.359	0.349	0.254	0.242
	30	0.288	0.291	0.301	0.320	0.347	0.352	0.354	0.366	0.373	0.361	0.356	0.269	0.257
200	**70**	0.344	0.340	0.328	0.332	0.347	0.349	0.347	0.359	0.374	0.361	0.369	0.252	0.250
	50	0.337	0.337	0.327	0.333	0.345	0.349	0.349	0.359	0.373	0.362	0.374	0.269	0.267
	30	0.323	0.323	0.322	0.333	0.349	0.349	0.347	0.356	0.371	0.362	0.373	0.260	0.245
250														
	70	0.337	0.345	0.327	0.327	0.335	0.333	0.330	0.342	0.349	0.344	0.381	0.252	0.288
	50	0.325	0.337	0.330	0.339	0.344	0.344	0.339	0.349	0.357	0.352	0.388	0.260	0.294
	30	0.305	0.318	0.315	0.339	0.350	0.347	0.340	0.349	0.359	0.354	0.390	0.257	0.299

Table B - 1: Test D1- Measured velocities [m/s]

B.1.2 TEST D2 (F_R = 0.5)

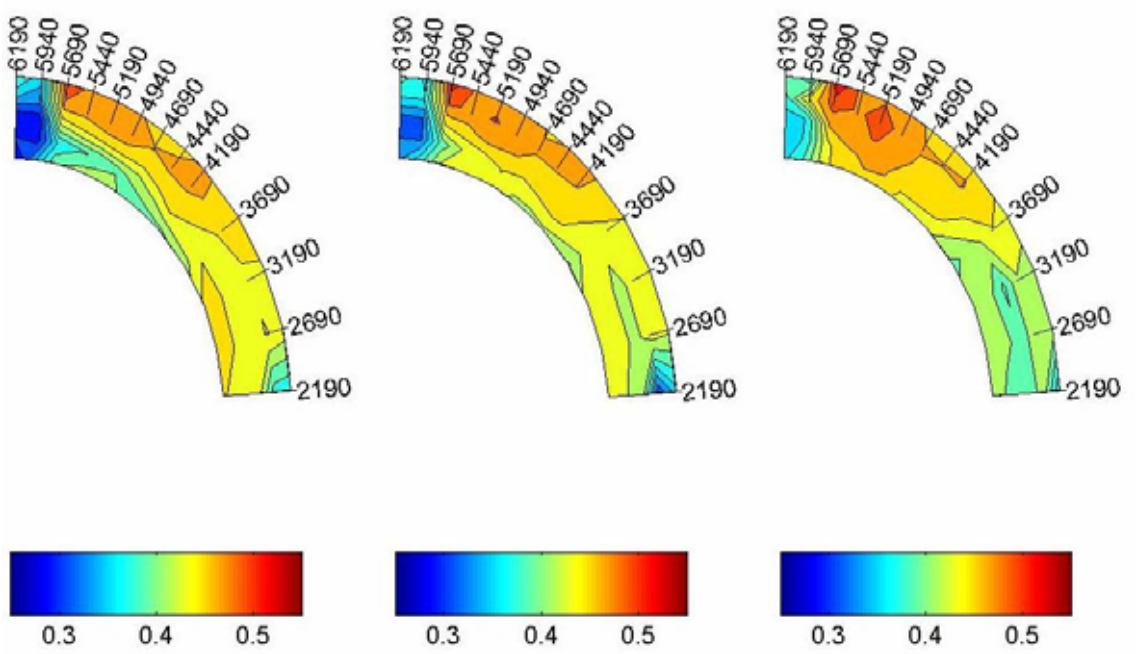

Figure B - 9: Test D2-Velocity distribution in the horizontal plane measured at 70, 50 and 30 mm

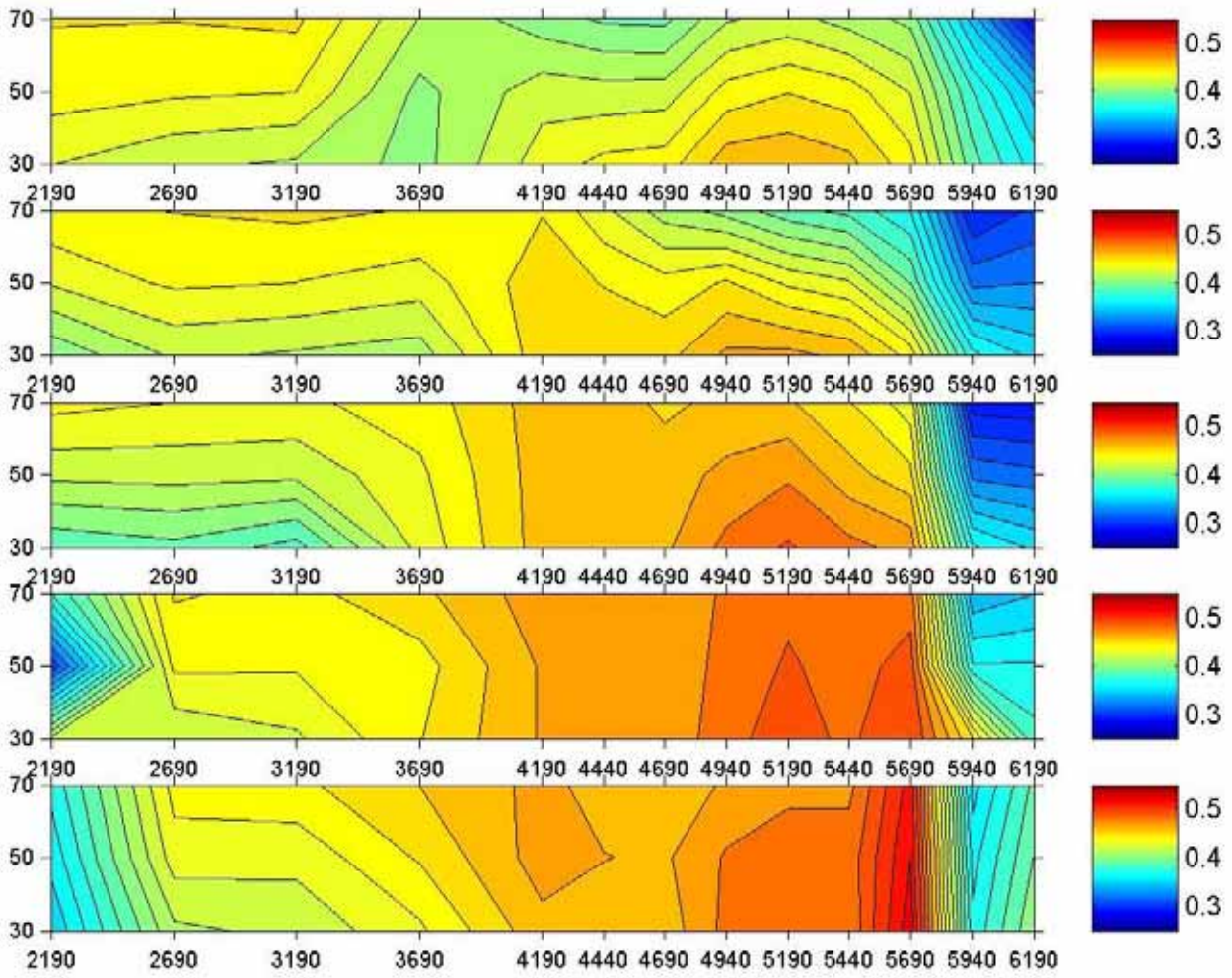

Figure B - 10: Test D2-Velocity distribution in the vertical plane

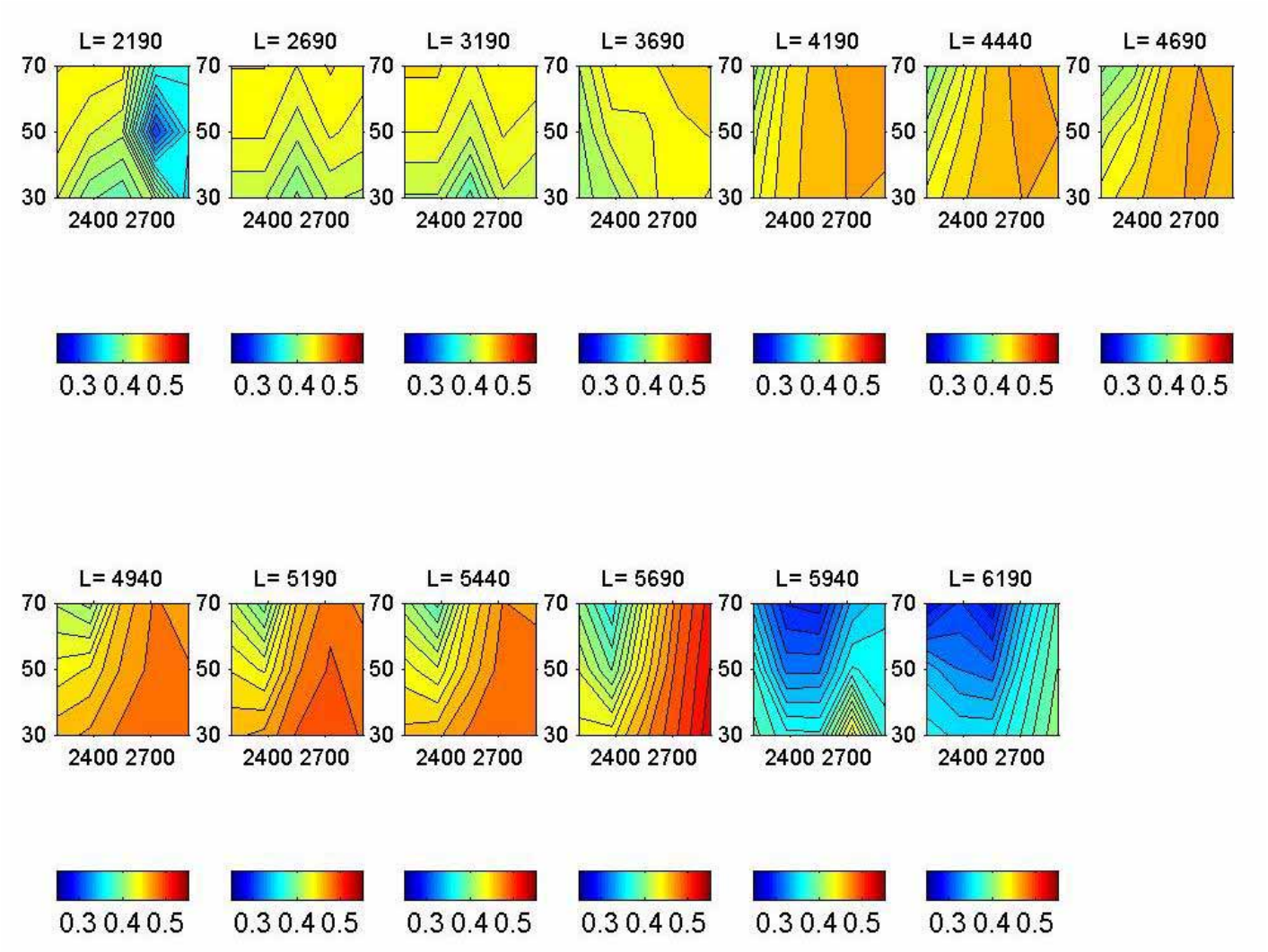

Figure B - 11: Test D2-Cross-sectional velocity distribution

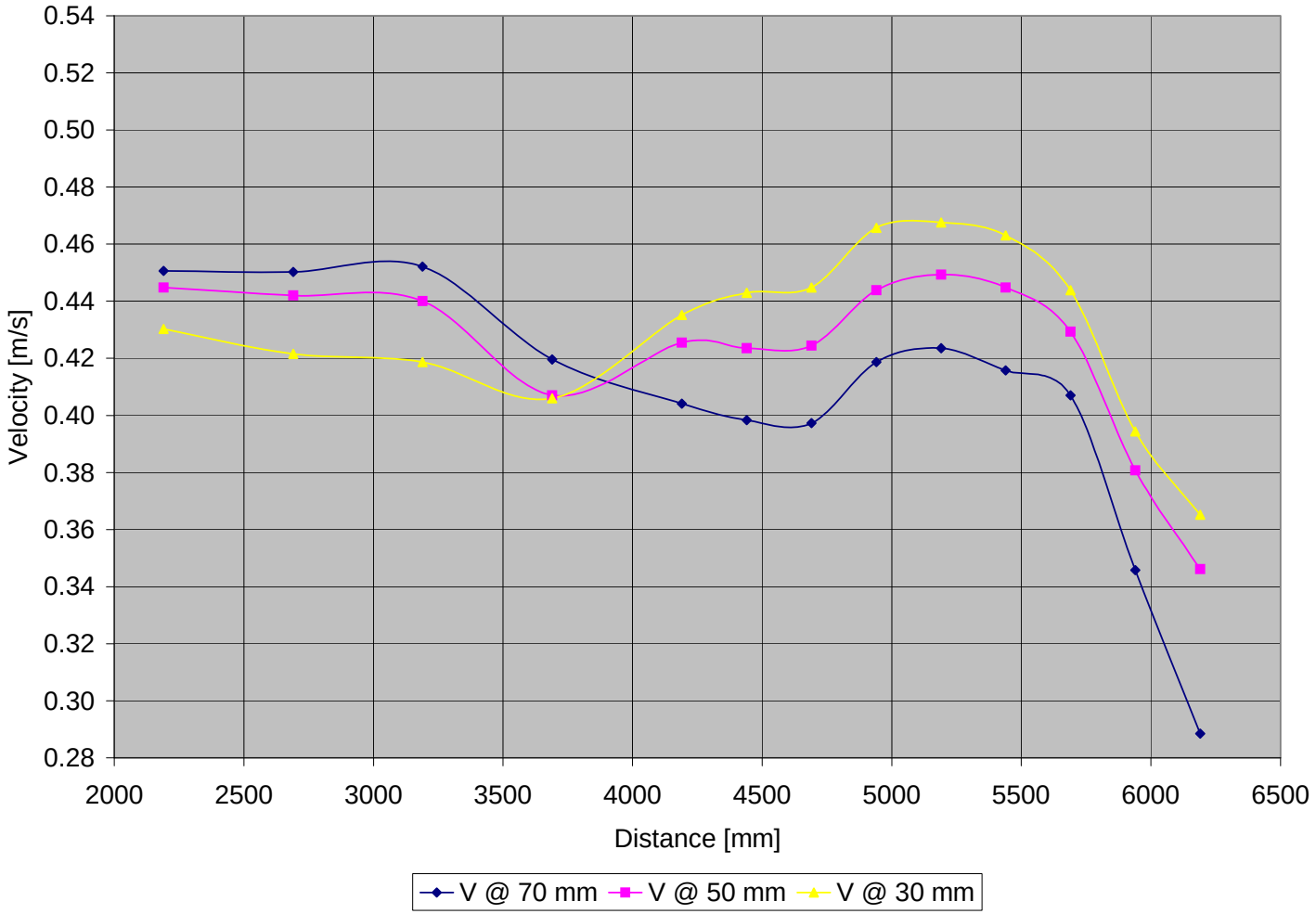

Figure B - 12: Test D2-Vertical velocity distribution measured at 50 mm from inner bank of bend

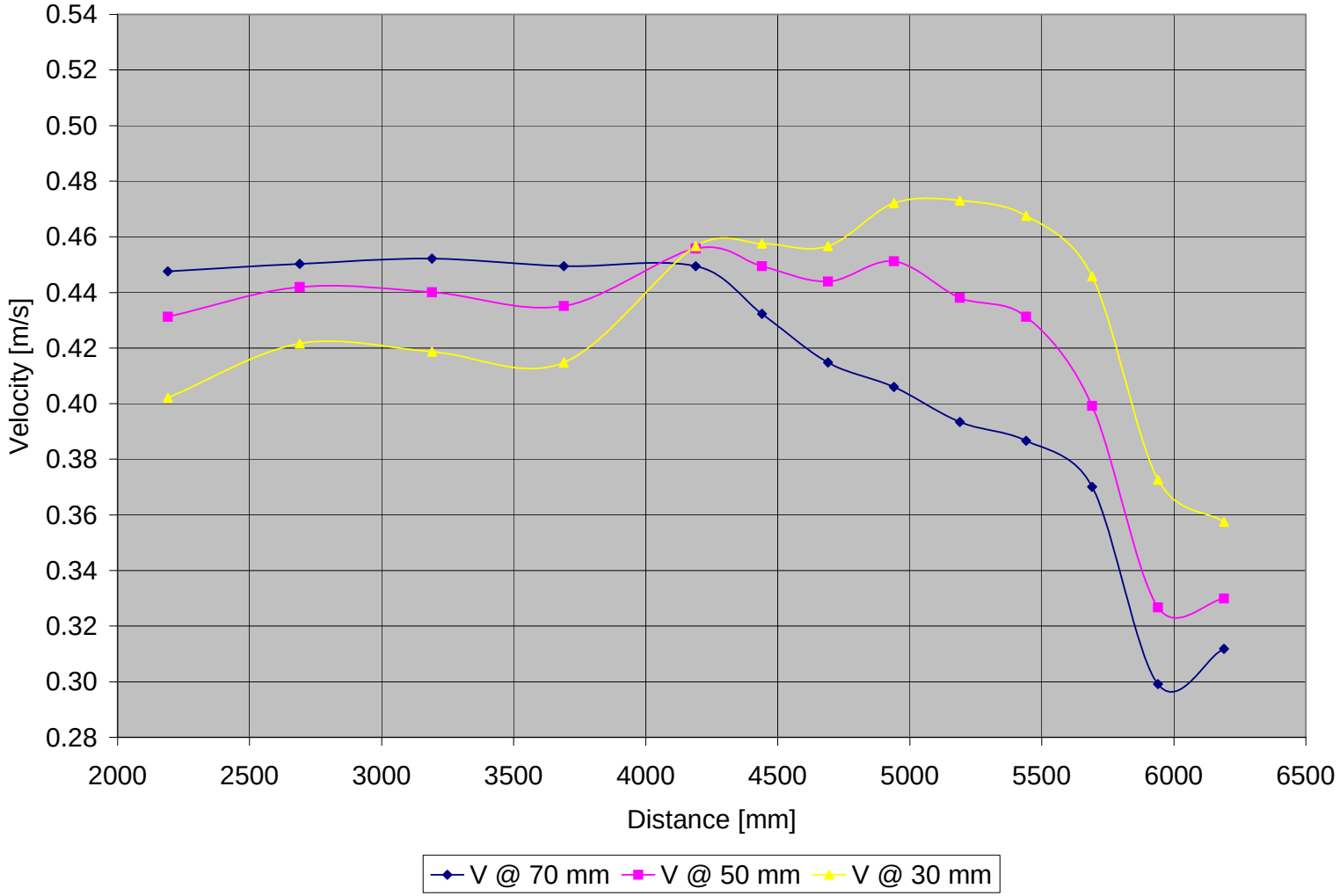

Figure B - 13: Test D2-Vertical velocity distribution measured at 100 mm from inner bank of bend

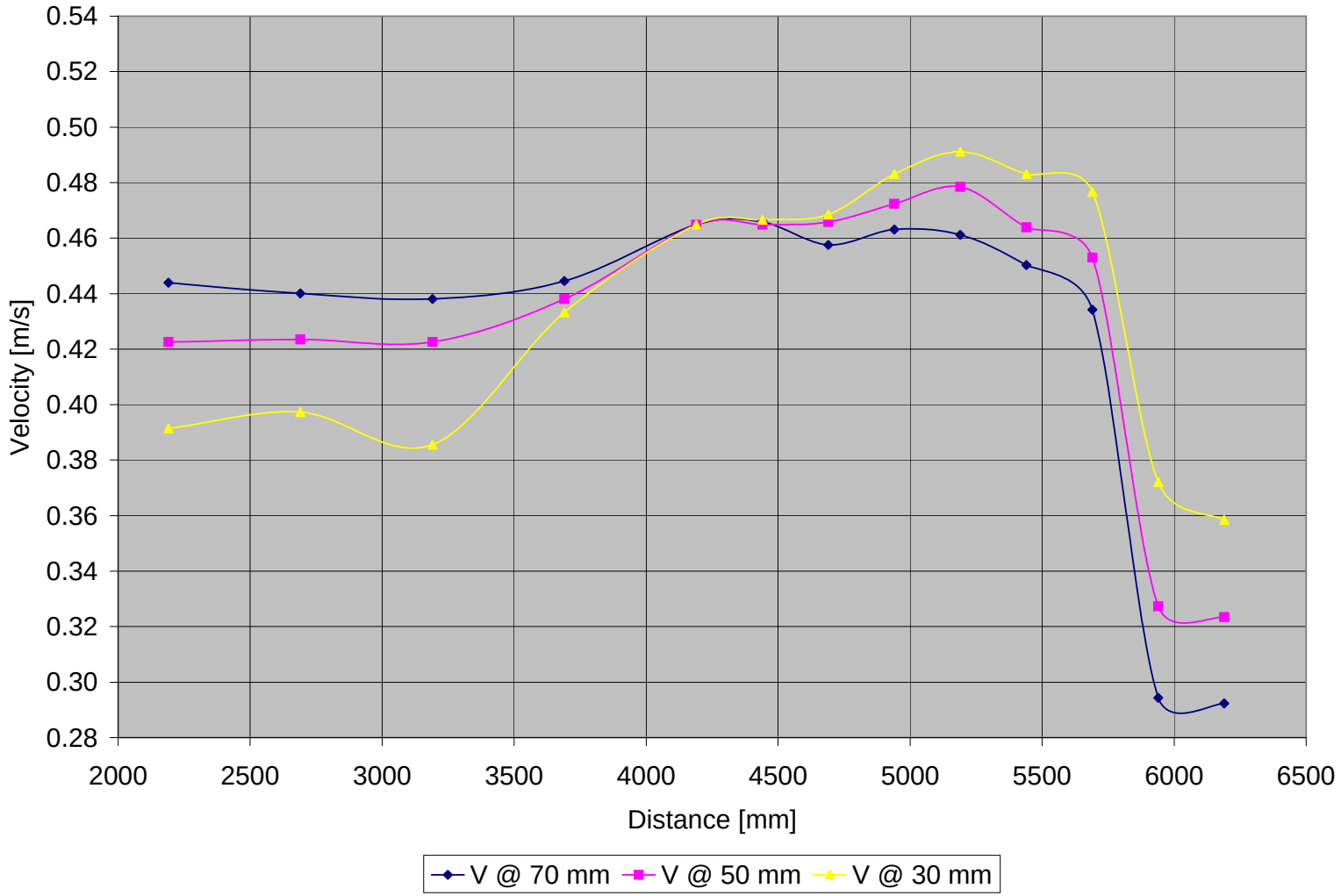

Figure B - 14: Test D2-Vertical velocity distribution measured at 150 mm from inner bank of bend

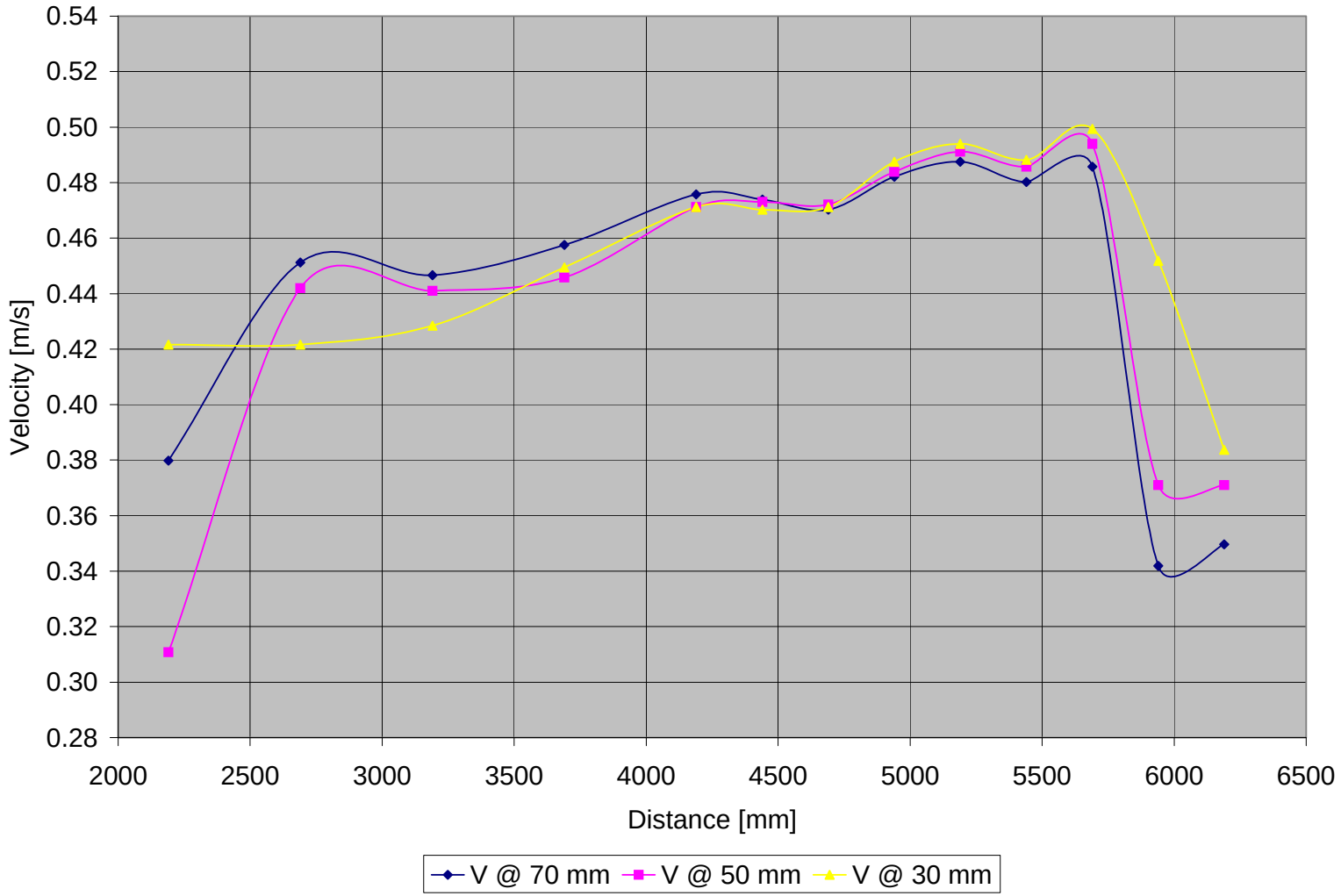

Figure B - 15: Test D2-Vertical velocity distribution measured at 200 mm from inner bank of bend

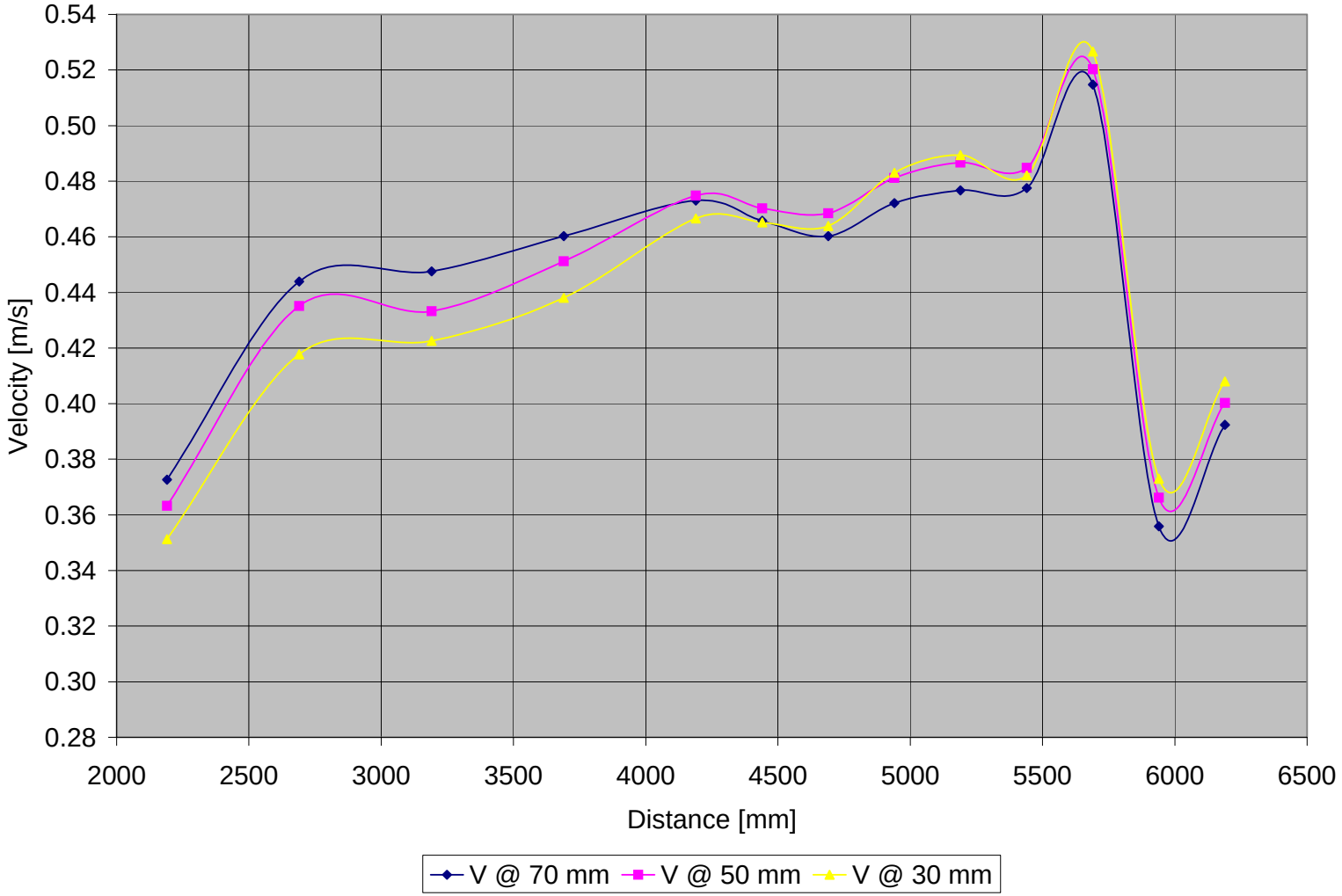

Figure B - 16: Test D2-Vertical velocity distribution measured at 250 mm from inner bank of bend

	Point	6	7	8	9	10	10A	11	11A	12	12A	13	13A	14
Width	L	2190	2690	3190	3690	4190	4440	4690	4940	5190	5440	5690	5940	6190
	h													
50	70	0.451	0.450	0.452	0.420	0.404	0.398	0.397	0.419	0.424	0.416	0.407	0.346	0.288
	50	0.445	0.442	0.440	0.407	0.425	0.424	0.424	0.444	0.449	0.445	0.429	0.381	0.346
	30	0.430	0.422	0.419	0.406	0.435	0.443	0.445	0.466	0.468	0.463	0.444	0.394	0.365
100	70	0.448	0.450	0.452	0.449	0.449	0.432	0.415	0.406	0.393	0.387	0.370	0.299	0.312
	50	0.431	0.442	0.440	0.435	0.456	0.449	0.444	0.451	0.438	0.431	0.399	0.327	0.330
	30	0.402	0.422	0.419	0.415	0.457	0.458	0.457	0.472	0.473	0.468	0.446	0.373	0.357
150	70	0.444	0.440	0.438	0.445	0.465	0.466	0.458	0.463	0.461	0.450	0.434	0.294	0.292
	50	0.423	0.424	0.423	0.438	0.465	0.465	0.466	0.472	0.478	0.464	0.453	0.327	0.323
	30	0.391	0.397	0.386	0.433	0.465	0.467	0.468	0.483	0.491	0.483	0.477	0.372	0.358
200	70	0.380	0.451	0.447	0.458	0.476	0.474	0.470	0.482	0.488	0.480	0.486	0.342	0.350
	50	0.311	0.442	0.441	0.446	0.471	0.473	0.472	0.484	0.491	0.486	0.494	0.371	0.371
	30	0.422	0.422	0.428	0.449	0.471	0.470	0.471	0.488	0.494	0.488	0.499	0.452	0.384
250														
	70	0.373	0.444	0.448	0.460	0.473	0.466	0.460	0.472	0.477	0.478	0.515	0.356	0.392
	50	0.363	0.435	0.433	0.451	0.475	0.470	0.468	0.481	0.487	0.485	0.520	0.366	0.400
	30	0.351	0.418	0.423	0.438	0.467	0.465	0.464	0.483	0.489	0.482	0.527	0.373	0.408

Table B - 2: Test D2-Measured velocities [m/s]

B.1.3 TEST D3 (F_R = 0.7)

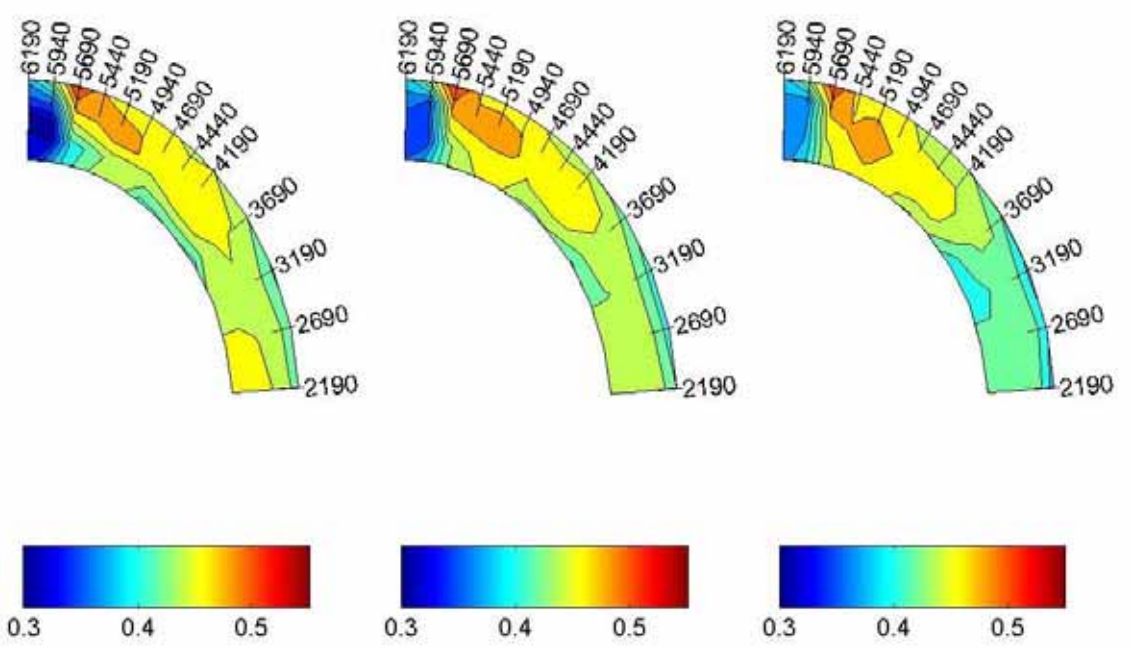

Figure B - 17: Test D3-Velocity distribution in the horizontal plane measured at 70, 50 and 30 mm

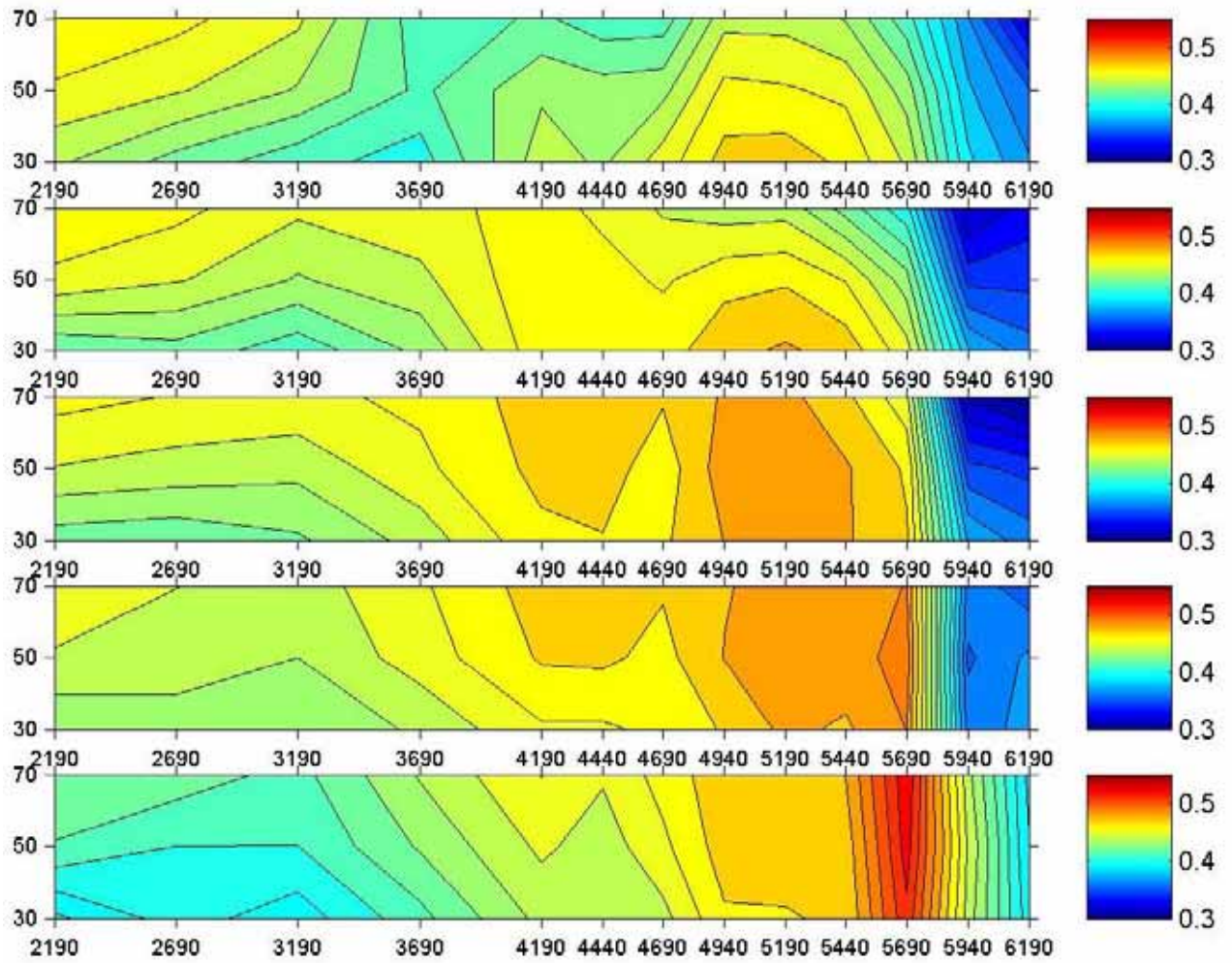

Figure B - 18: Test D3-Velocity distribution in the vertical plane

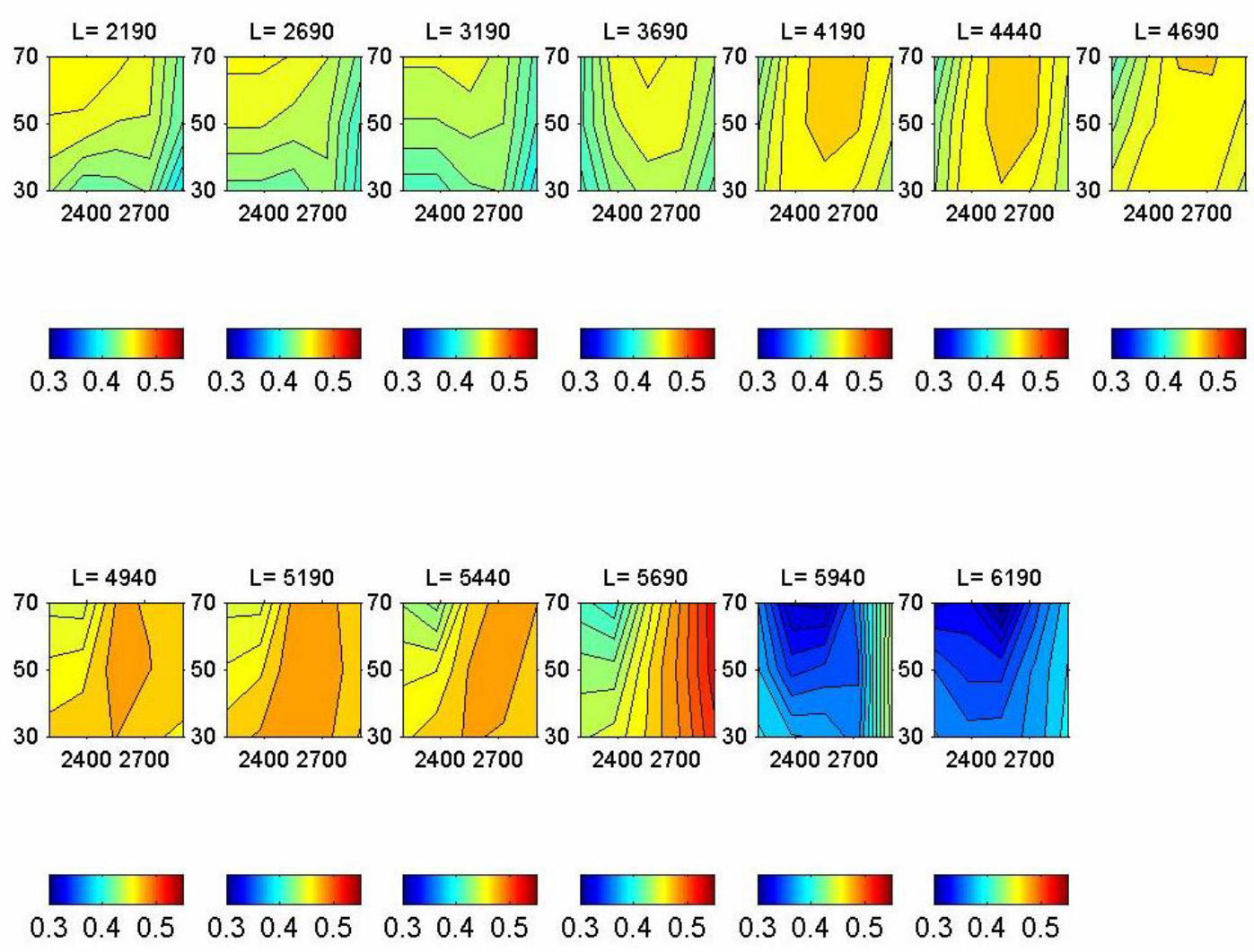

Figure B - 19: Test D3-Cross-sectional velocity distribution

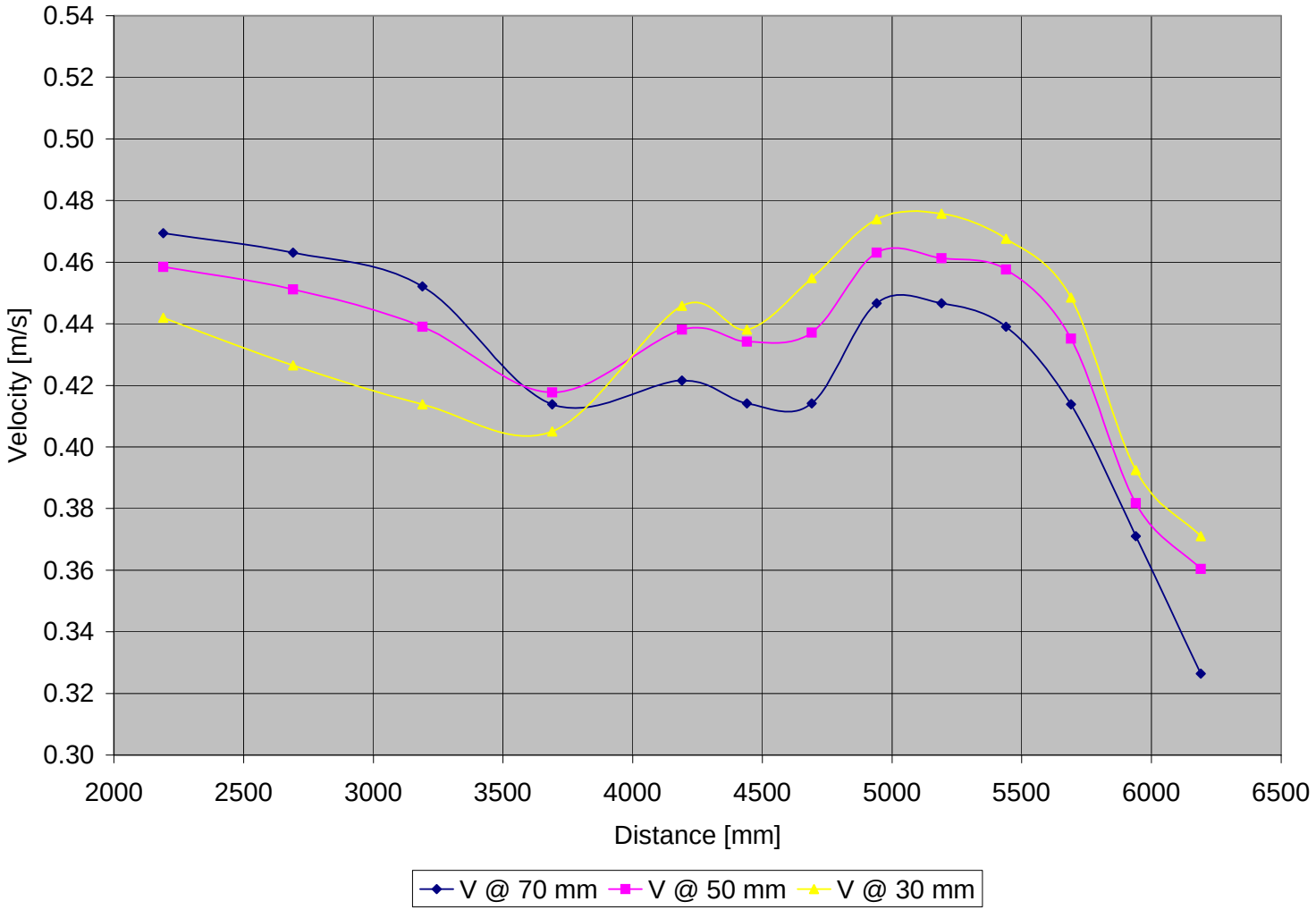

Figure B - 20: Test D3-Vertical velocity distribution measured at 50 mm from inner bank of bend

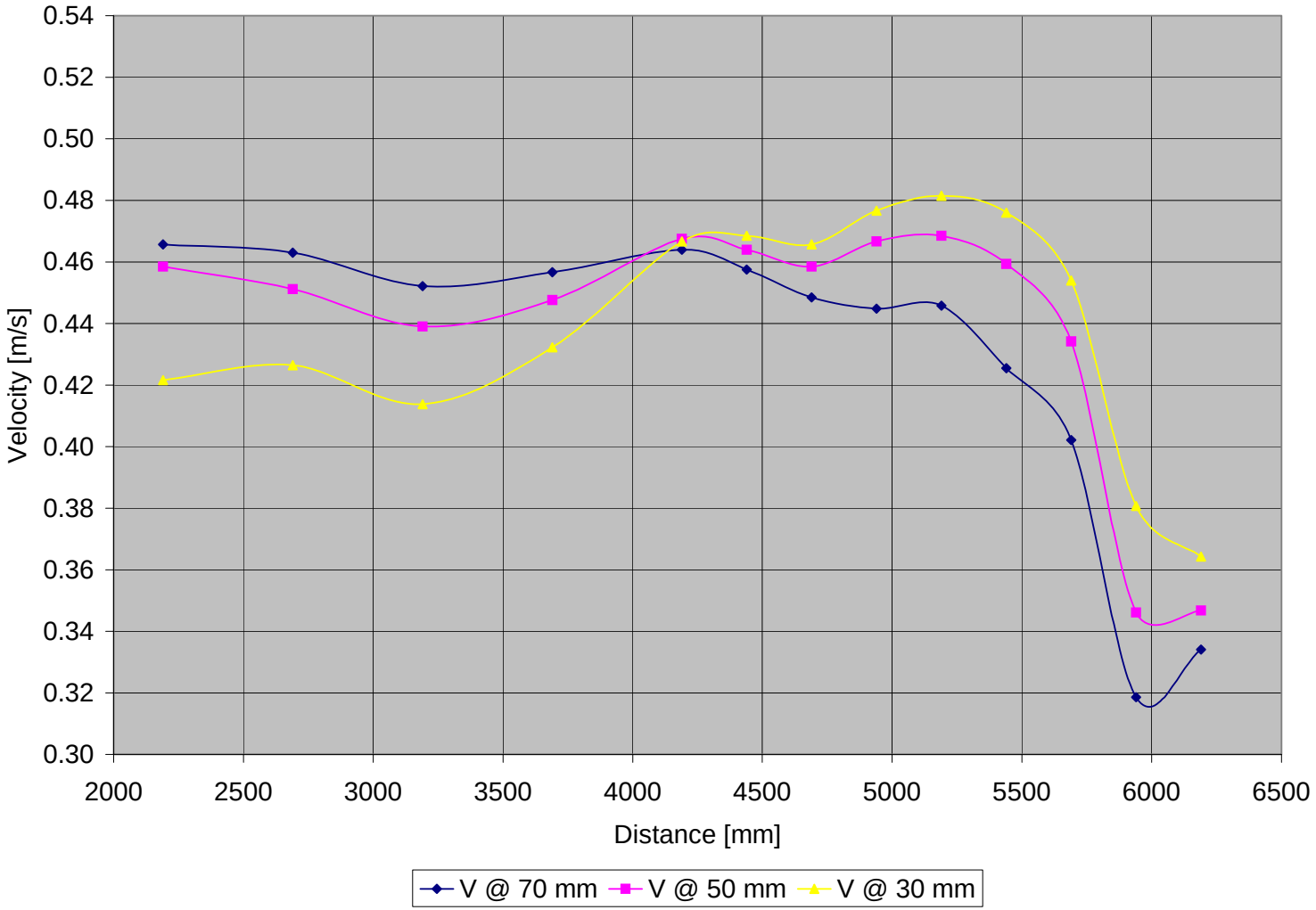

Figure B - 21: Test D3-Vertical velocity distribution measured at 100 mm from inner bank of bend

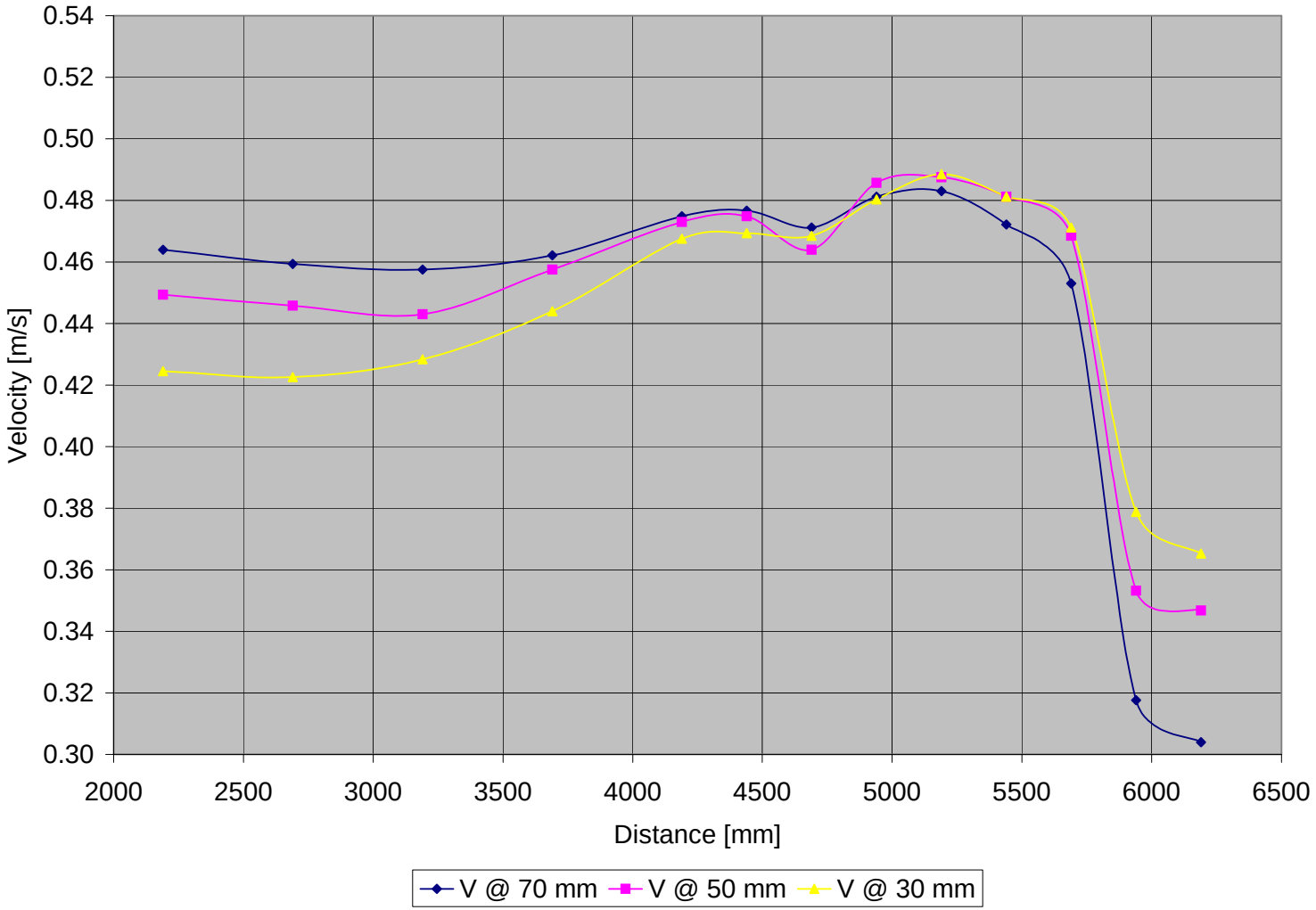

Figure B - 22: Test D3-Vertical velocity distribution measured at 150 mm from inner bank of bend

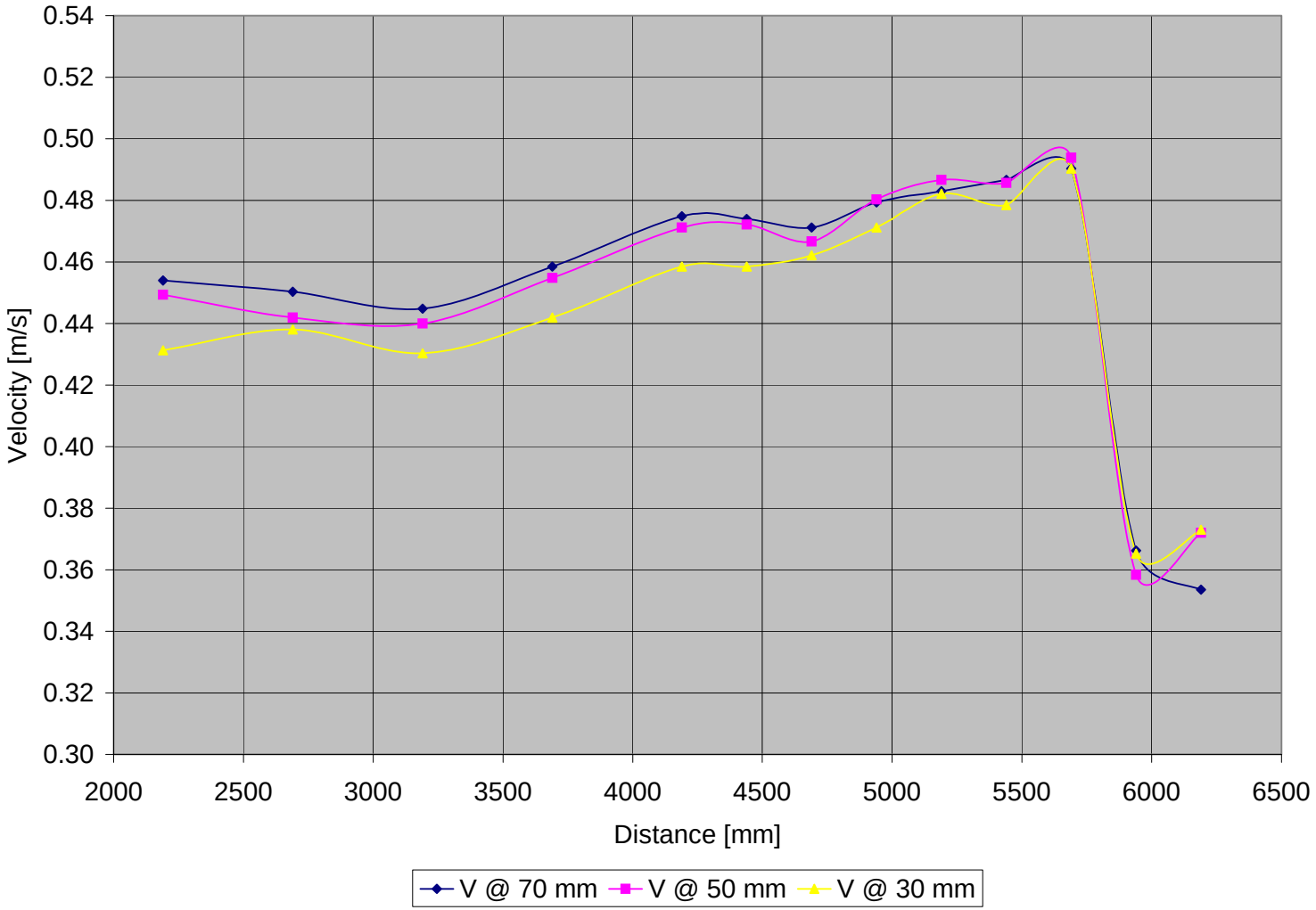

Figure B - 23: Test D3-Vertical velocity distribution measured at 200 mm from inner bank of bend

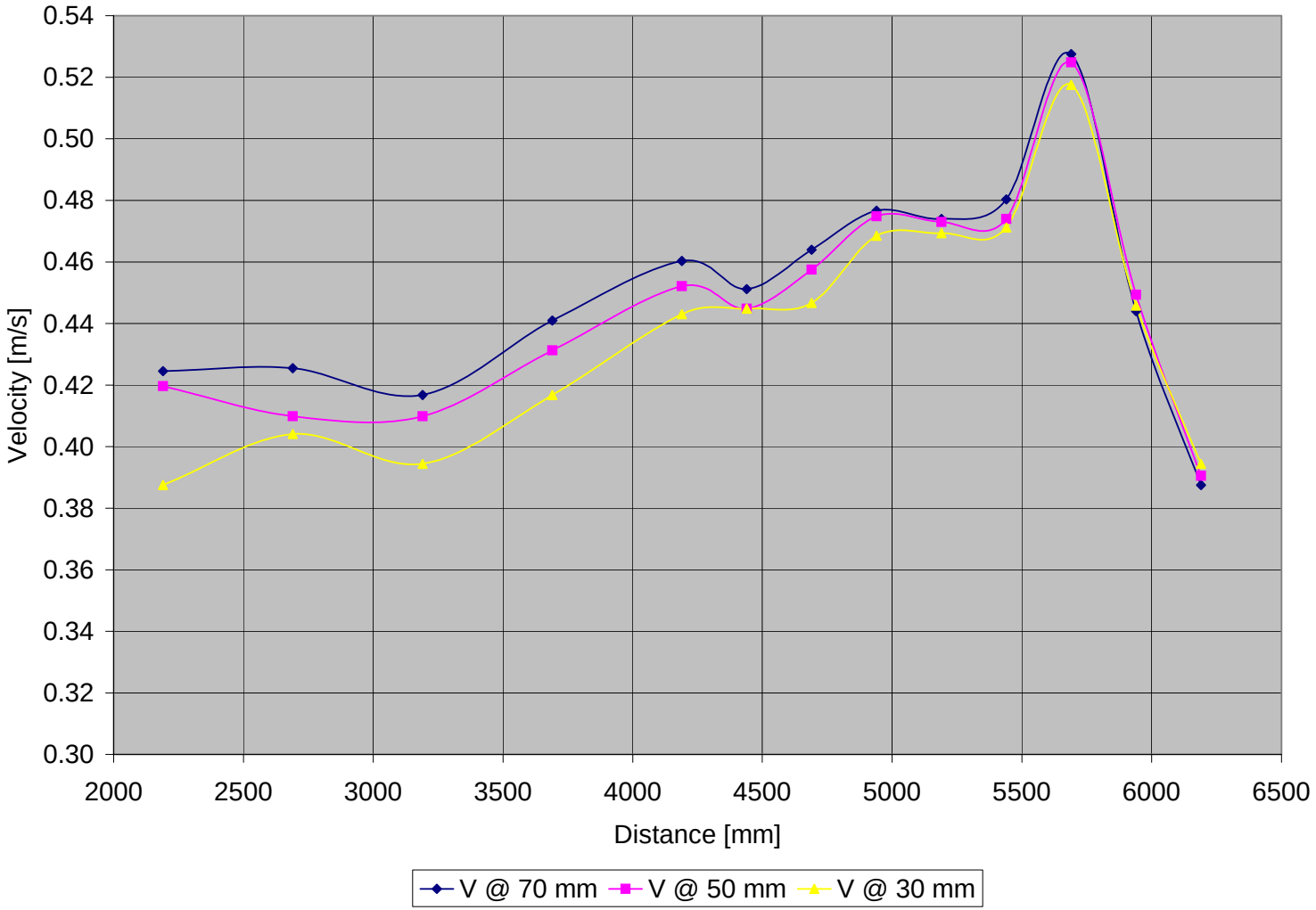

Figure B - 24: Test D3-Vertical velocity distribution measured at 250 mm from inner bank of bend

	Point	6	7	8	9	10	10A	11	11A	12	12A	13	13A	14
Width	L	2190	2690	3190	3690	4190	4440	4690	4940	5190	5440	5690	5940	6190
	h													
50	70	0.469	0.463	0.452	0.414	0.422	0.414	0.414	0.447	0.447	0.439	0.414	0.371	0.326
	50	0.458	0.451	0.439	0.418	0.438	0.434	0.437	0.463	0.461	0.458	0.435	0.382	0.360
	30	0.442	0.426	0.414	0.405	0.446	0.438	0.455	0.474	0.476	0.468	0.448	0.392	0.371
100	70	0.466	0.463	0.452	0.457	0.464	0.458	0.448	0.445	0.446	0.425	0.402	0.319	0.334
	50	0.458	0.451	0.439	0.448	0.468	0.464	0.458	0.467	0.468	0.459	0.434	0.346	0.347
	30	0.422	0.426	0.414	0.432	0.467	0.468	0.466	0.477	0.481	0.476	0.454	0.381	0.364
150	70	0.464	0.459	0.458	0.462	0.475	0.477	0.471	0.481	0.483	0.472	0.453	0.318	0.304
	50	0.449	0.446	0.443	0.458	0.473	0.475	0.464	0.486	0.488	0.481	0.468	0.353	0.347
	30	0.424	0.423	0.428	0.444	0.468	0.469	0.468	0.480	0.488	0.481	0.471	0.379	0.365
200	70	0.454	0.450	0.445	0.458	0.475	0.474	0.471	0.479	0.483	0.487	0.490	0.366	0.354
	50	0.449	0.442	0.440	0.455	0.471	0.472	0.467	0.480	0.487	0.486	0.494	0.358	0.372
	30	0.431	0.438	0.430	0.442	0.458	0.458	0.462	0.471	0.482	0.478	0.490	0.365	0.373
250														
	70	0.424	0.425	0.417	0.441	0.460	0.451	0.464	0.477	0.474	0.480	0.528	0.444	0.388
	50	0.420	0.410	0.410	0.431	0.452	0.445	0.458	0.475	0.473	0.474	0.525	0.449	0.390
	30	0.388	0.404	0.394	0.417	0.443	0.445	0.447	0.468	0.469	0.471	0.518	0.446	0.394

Table B - 3: Test D3- Measured velocities [m/s]

B.2 TEST E (Θ = 35˚)

B.2.1 TEST E1 (F_R = 0.3)

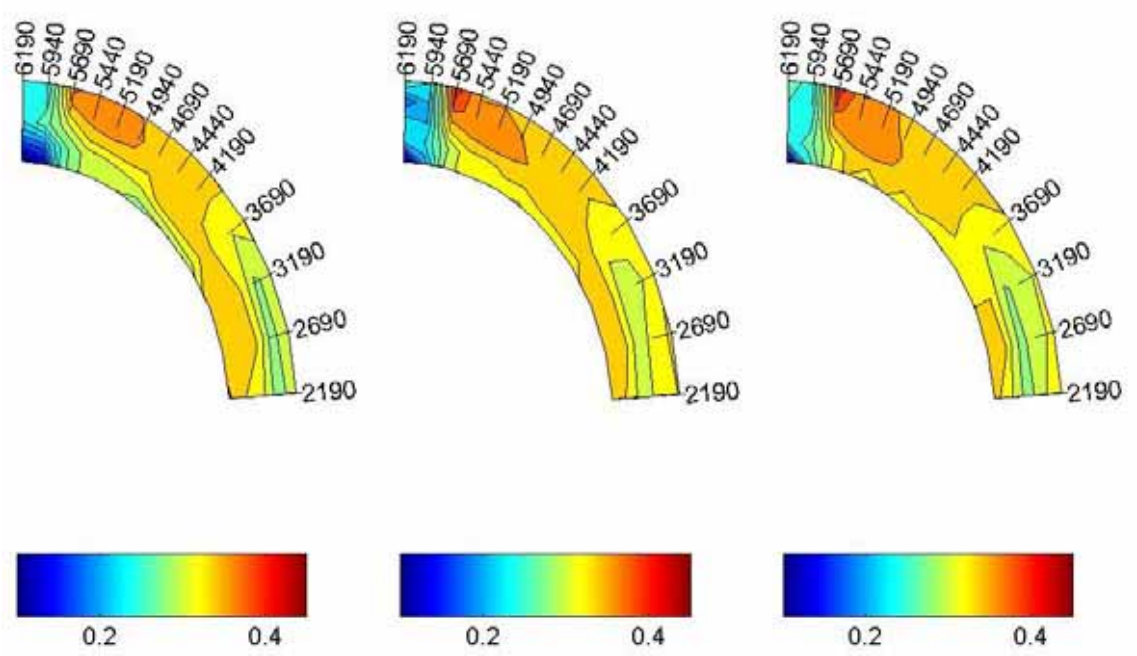

Figure B - 25: Test E1-Velocity distribution in the horizontal plane measured at 70, 50 and 30 mm

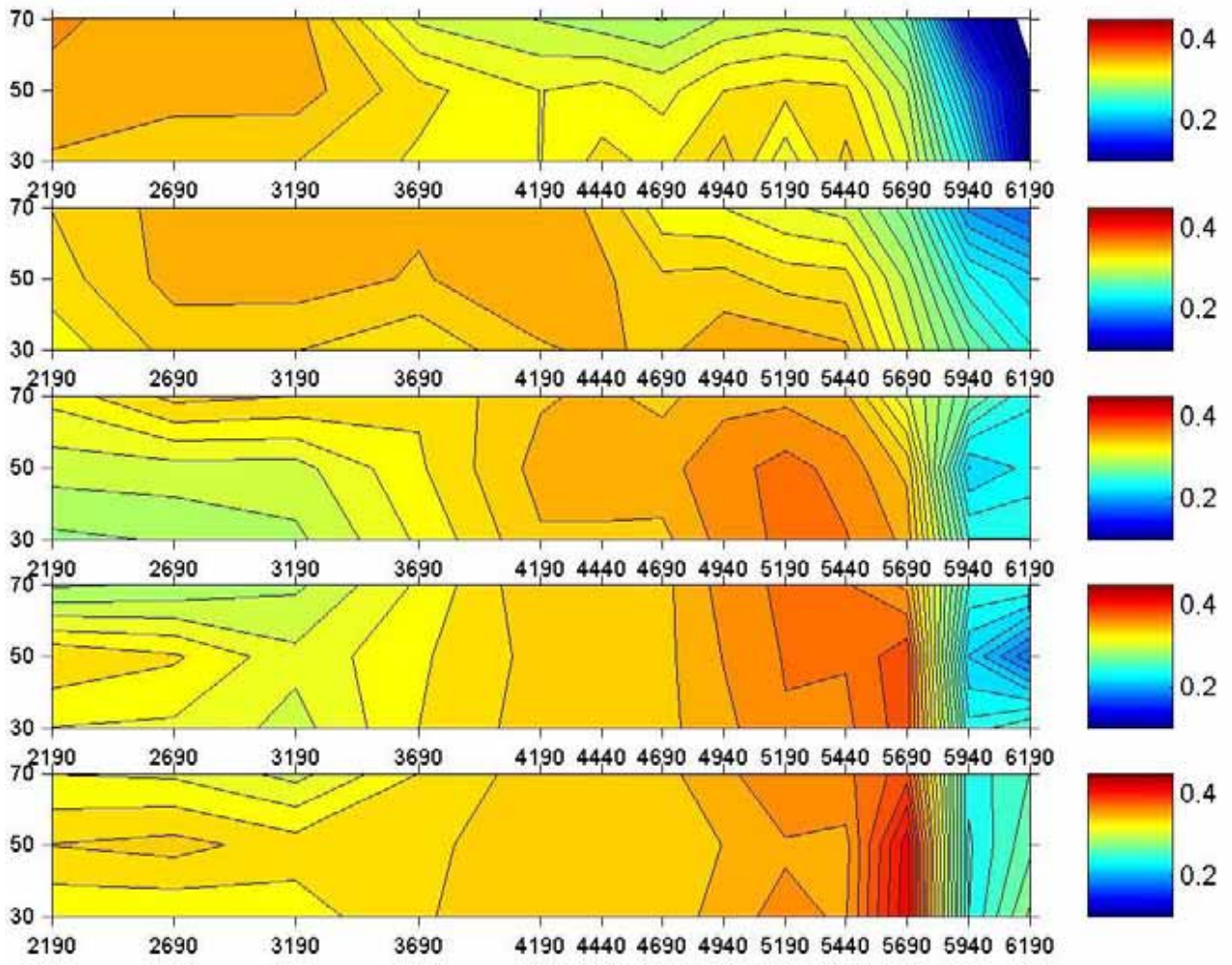

Figure B - 26: Test E1-Velocity distribution in the vertical plane

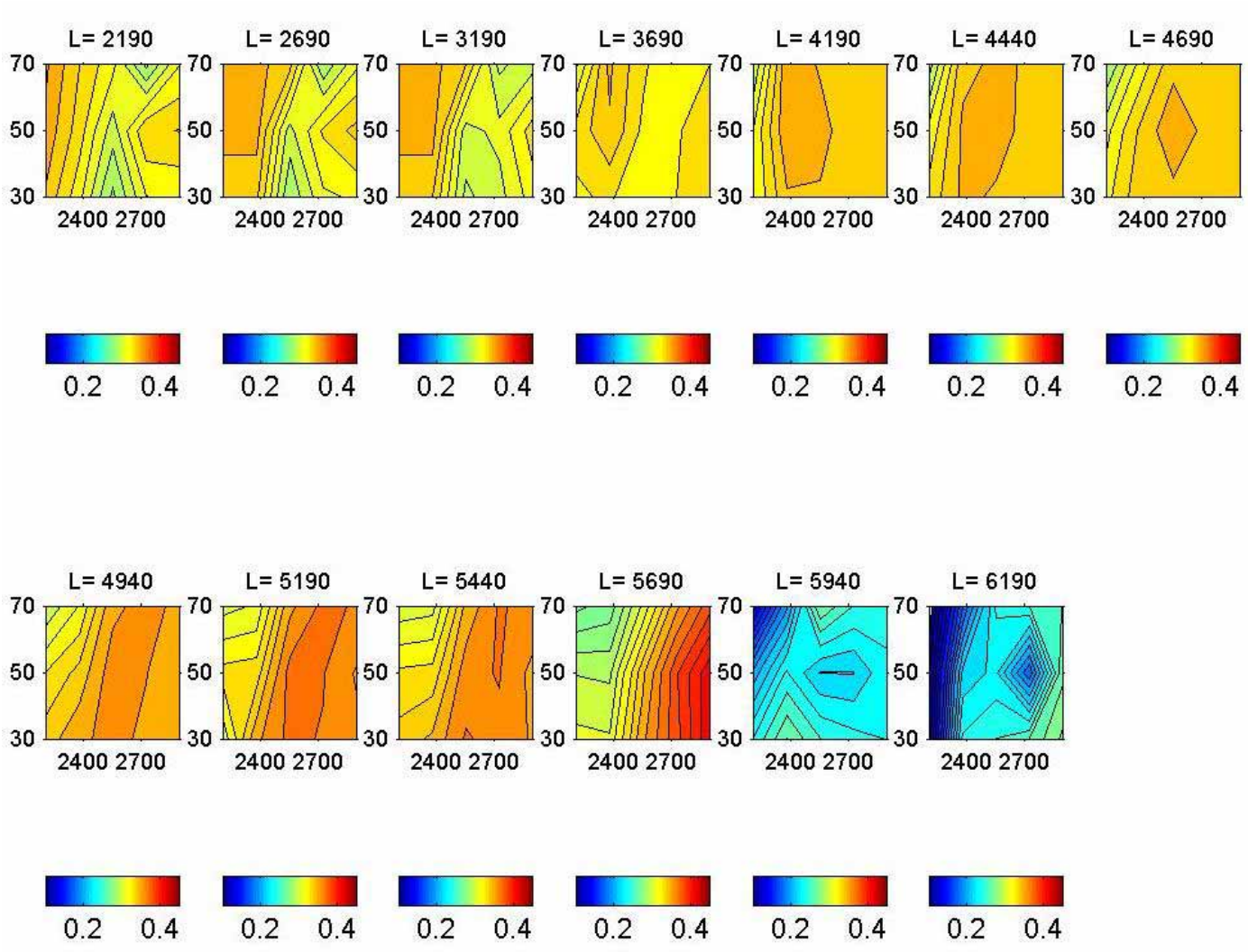

Figure B - 27: Test E1-Cross-sectional velocity distribution

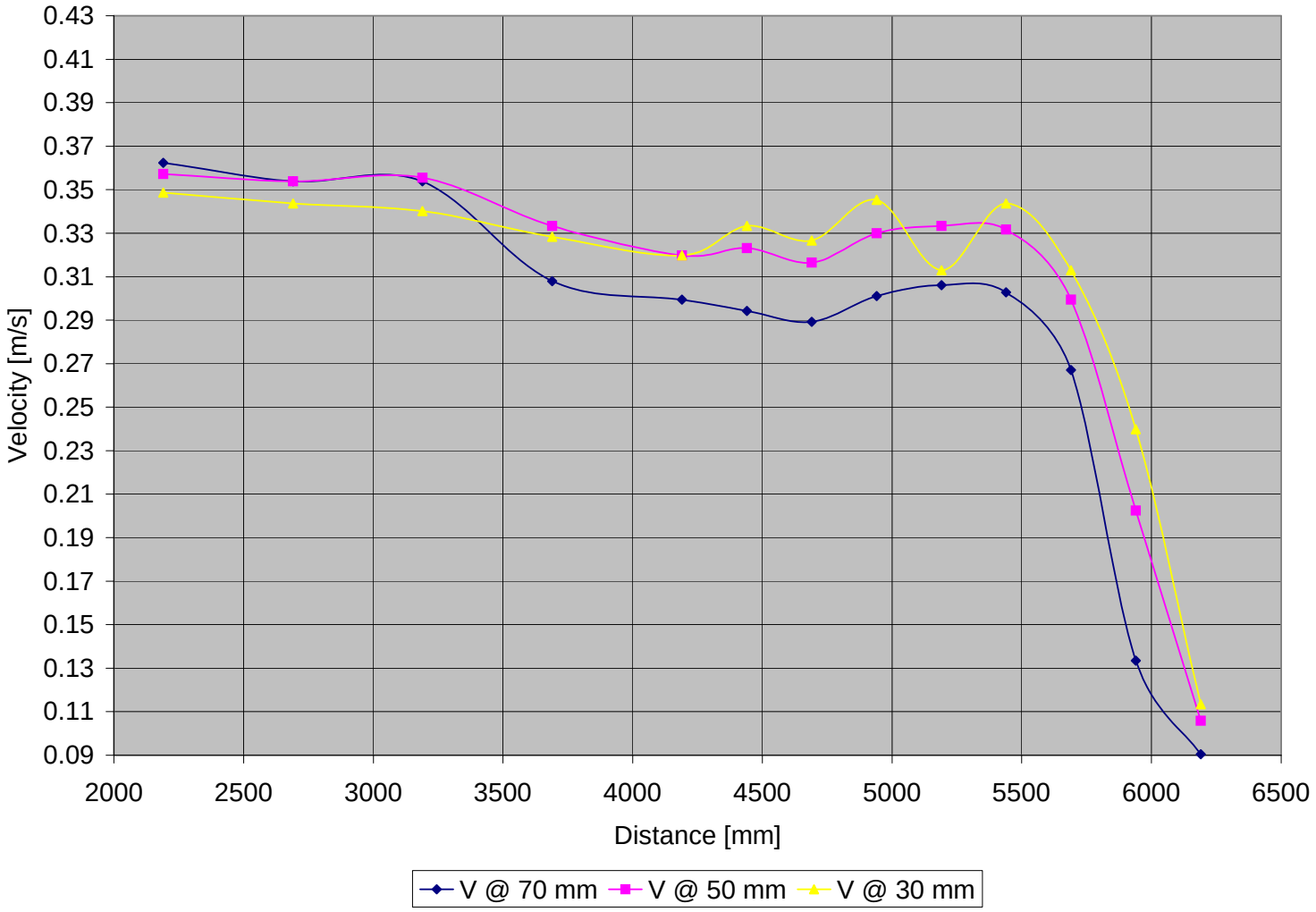

Figure B - 28: Test E1-Vertical velocity distribution measured at 50 mm from inner bank of bend

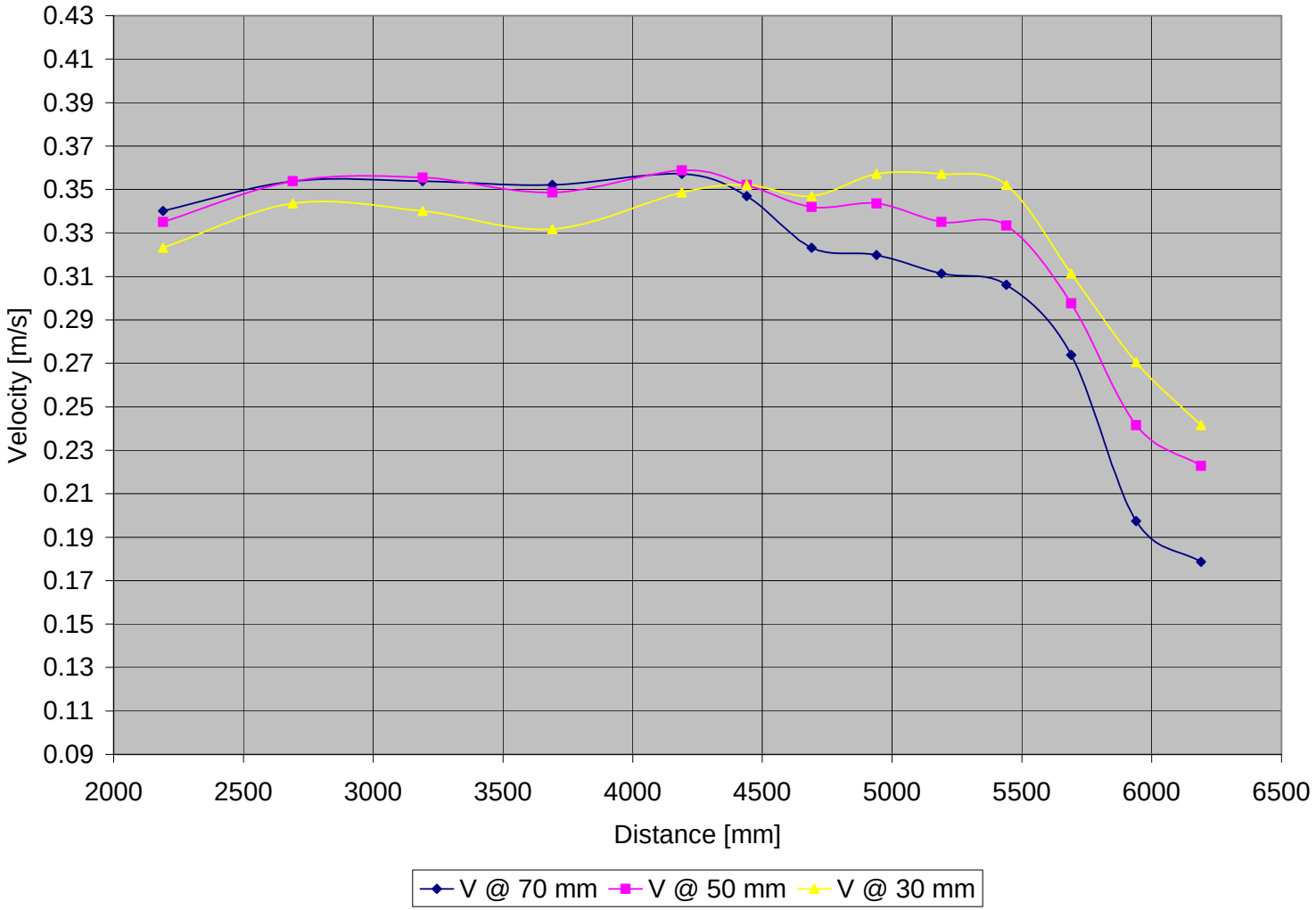

Figure B - 29: Test E1-Vertical velocity distribution measured at 100 mm from inner bank of bend

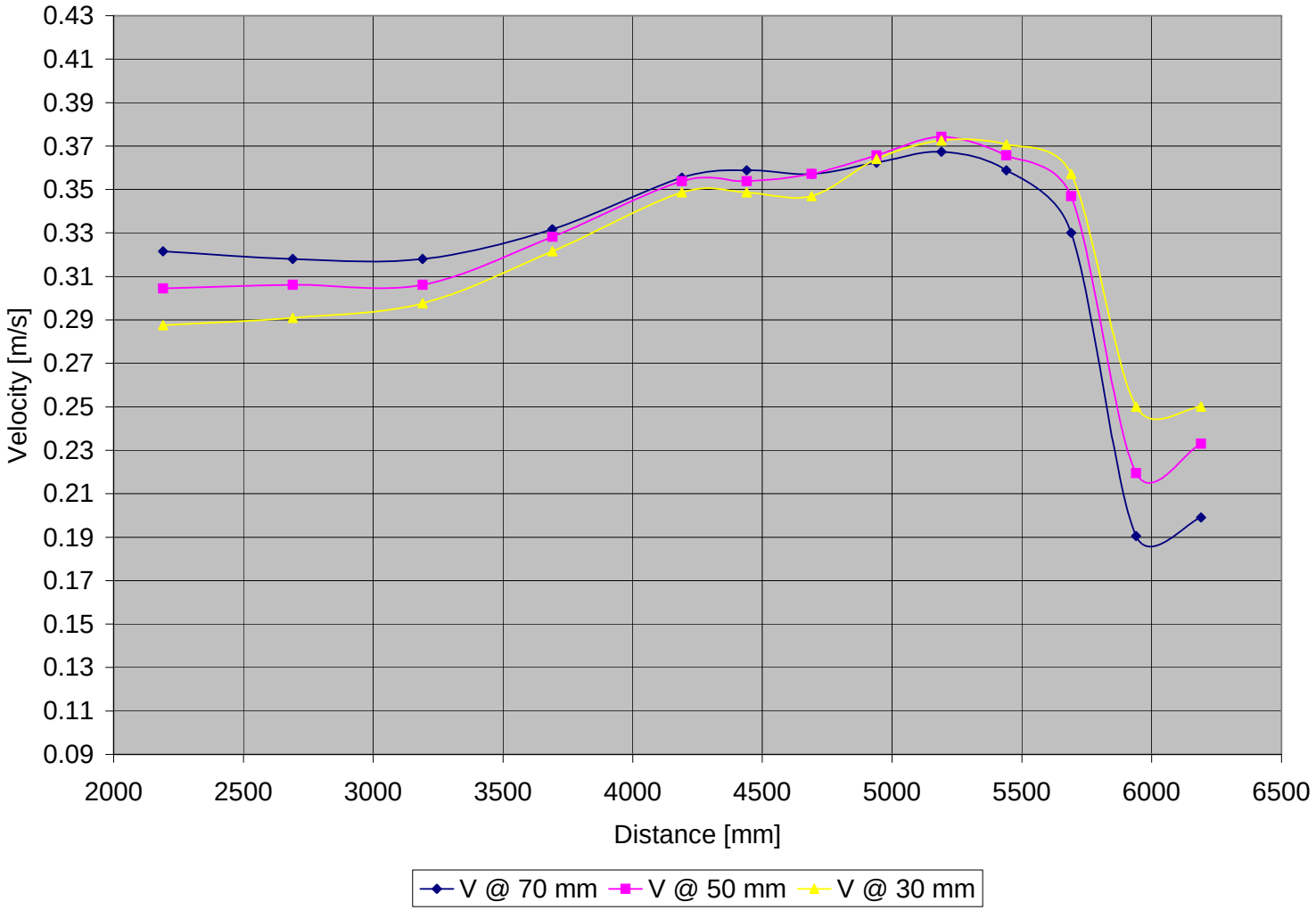

Figure B - 30: Test E1-Vertical velocity distribution measured at 150 mm from inner bank of bend

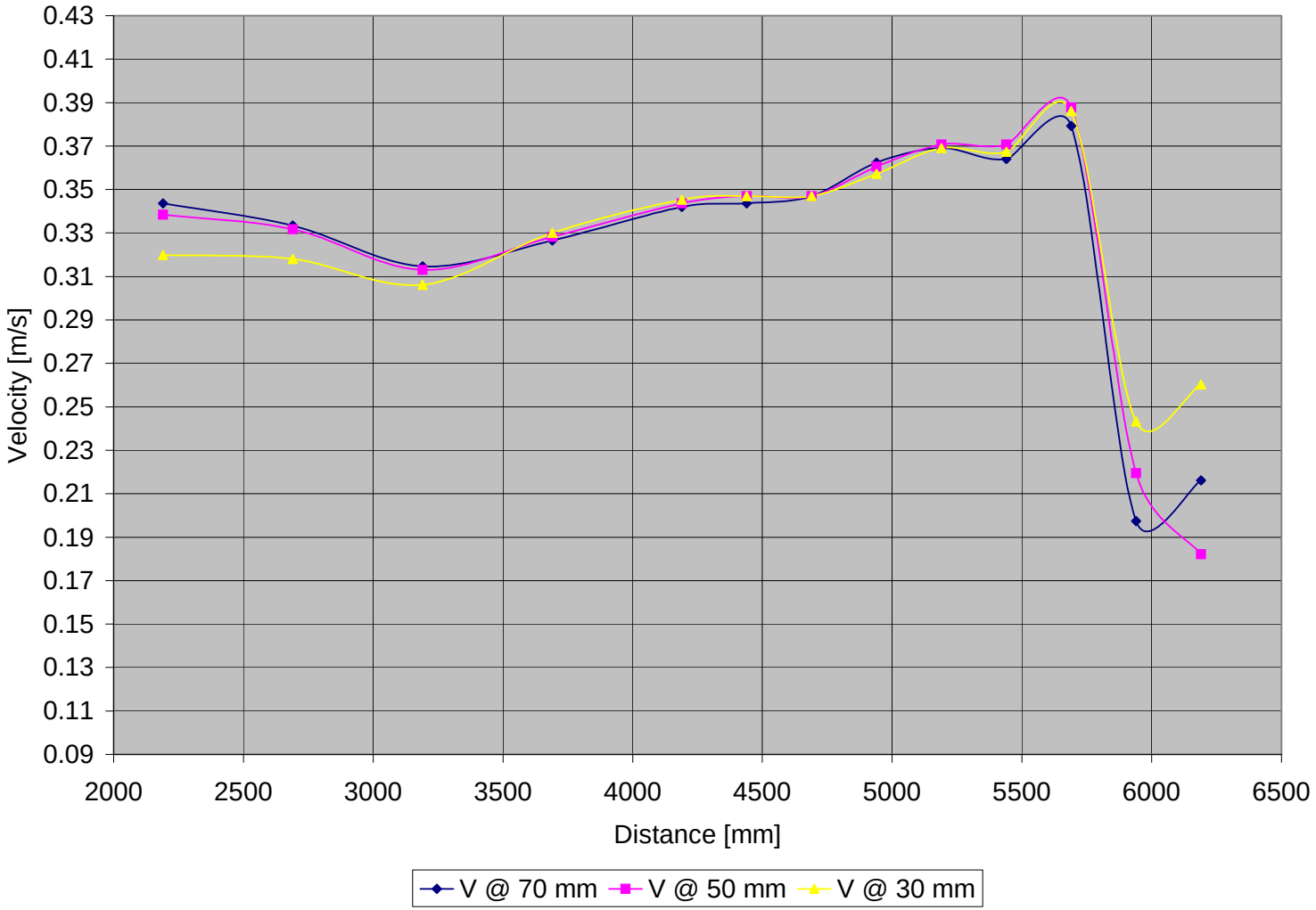

Figure B - 31: Test E1-Vertical velocity distribution measured at 200 mm from inner bank of bend

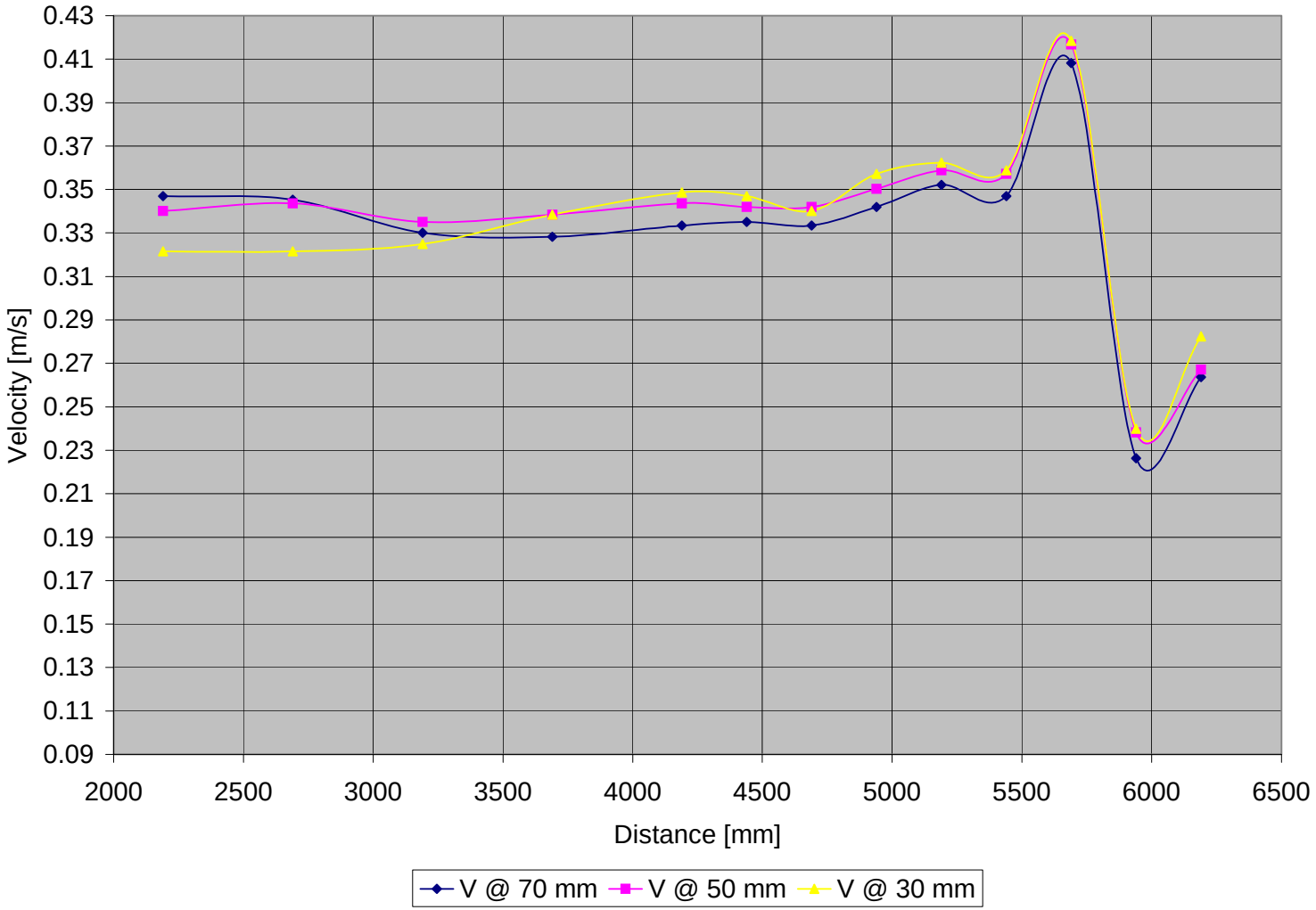

Figure B - 32: Test E1-Vertical velocity distribution measured at 250 mm from inner bank of bend

	Point	6	7	8	9	10	10A	11	11A	12	12A	13	13A	14
Width	L	2190	2690	3190	3690	4190	4440	4690	4940	5190	5440	5690	5940	6190
	h													
50	70	0.362	0.354	0.354	0.308	0.299	0.294	0.289	0.301	0.306	0.303	0.267	0.133	0.090
	50	0.357	0.354	0.356	0.333	0.320	0.323	0.316	0.330	0.333	0.332	0.299	0.203	0.106
	30	0.349	0.344	0.340	0.328	0.320	0.333	0.327	0.345	0.313	0.344	0.313	0.240	0.113
100	70	0.340	0.354	0.354	0.352	0.357	0.347	0.323	0.320	0.311	0.306	0.274	0.197	0.179
	50	0.335	0.354	0.356	0.349	0.359	0.352	0.342	0.344	0.335	0.333	0.298	0.242	0.223
	30	0.323	0.344	0.340	0.332	0.349	0.352	0.347	0.357	0.357	0.352	0.311	0.271	0.242
150	70	0.322	0.318	0.318	0.332	0.356	0.359	0.357	0.362	0.367	0.359	0.330	0.191	0.199
	50	0.305	0.306	0.306	0.328	0.354	0.354	0.357	0.366	0.374	0.366	0.347	0.220	0.233
	30	0.288	0.291	0.298	0.322	0.349	0.349	0.347	0.364	0.373	0.371	0.357	0.250	0.250
200	70	0.344	0.333	0.315	0.327	0.342	0.344	0.347	0.362	0.369	0.364	0.379	0.197	0.216
	50	0.339	0.332	0.313	0.328	0.344	0.347	0.347	0.361	0.371	0.371	0.388	0.220	0.182
	30	0.320	0.318	0.306	0.330	0.345	0.347	0.347	0.357	0.369	0.367	0.386	0.243	0.260
250														
	70	0.347	0.345	0.330	0.328	0.333	0.335	0.333	0.342	0.352	0.347	0.408	0.226	0.264
	50	0.340	0.344	0.335	0.339	0.344	0.342	0.342	0.350	0.359	0.357	0.417	0.238	0.267
	30	0.322	0.322	0.325	0.339	0.349	0.347	0.340	0.357	0.362	0.359	0.418	0.240	0.282

Table B - 4: Test E1- Measured velocities [m/s]

B.2.2 TEST E2 (F_R = 0.5)

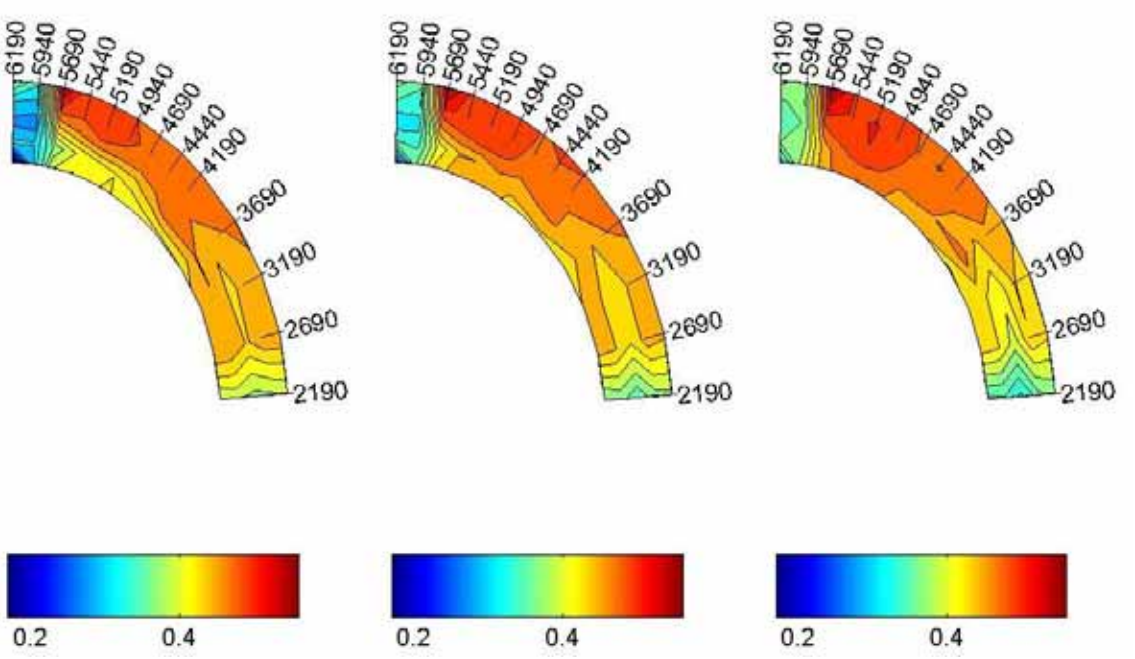

Figure B - 33: Test E2-Velocity distribution in the horizontal plane measured at 70, 50 and 30 mm

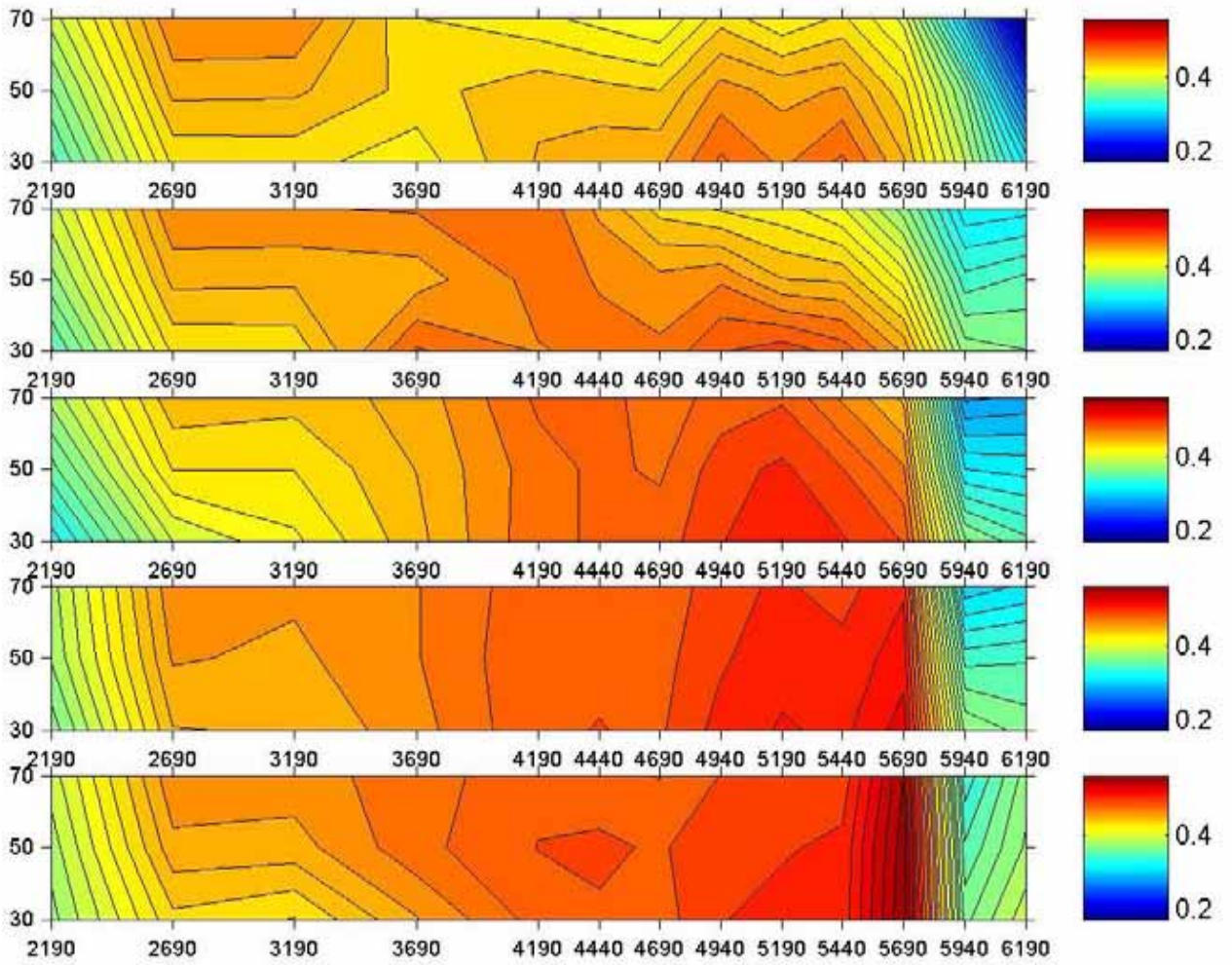

Figure B - 34: Test E2-Velocity distribution in the vertical plane

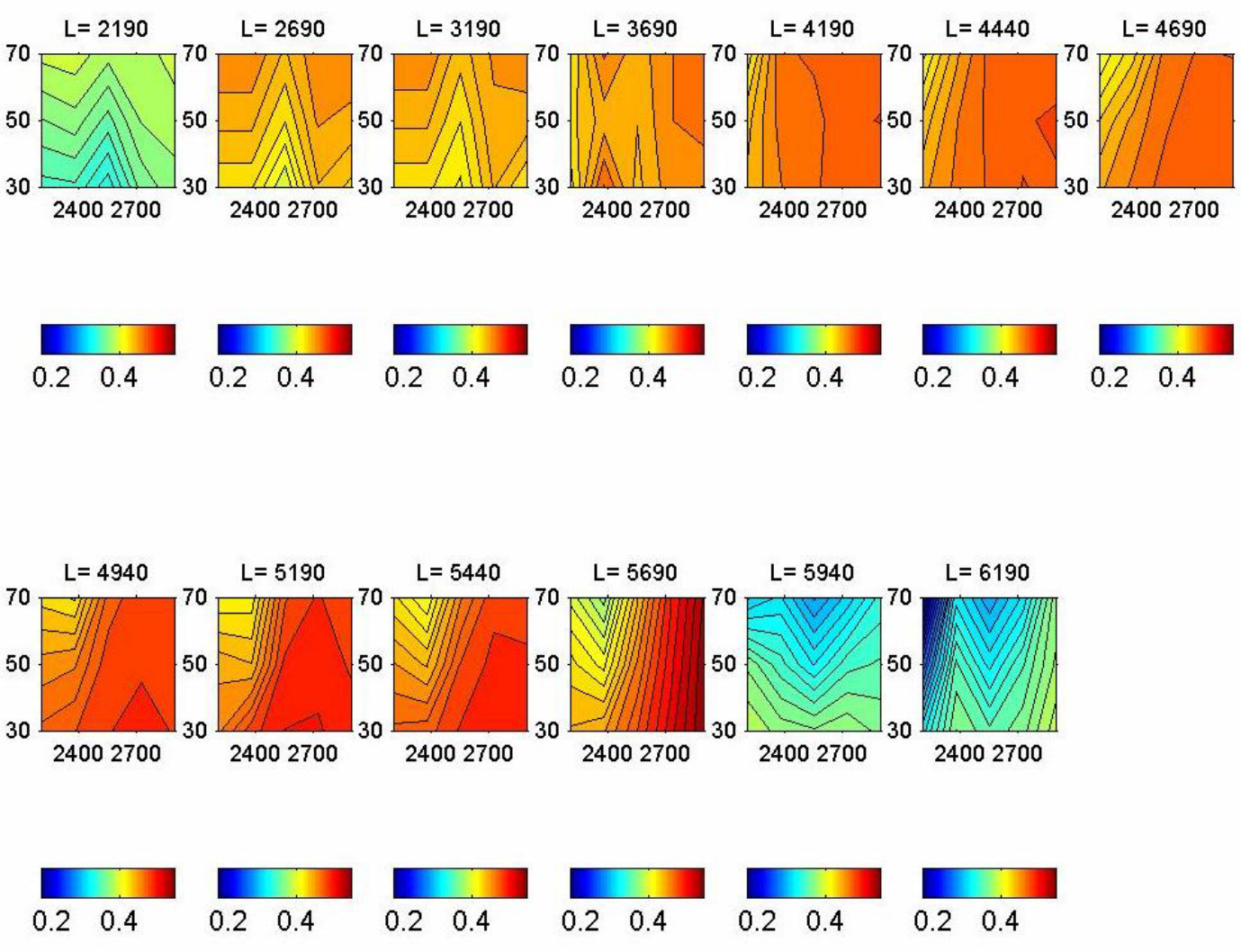

Figure B - 35: Test E2-Cross-sectional velocity distribution

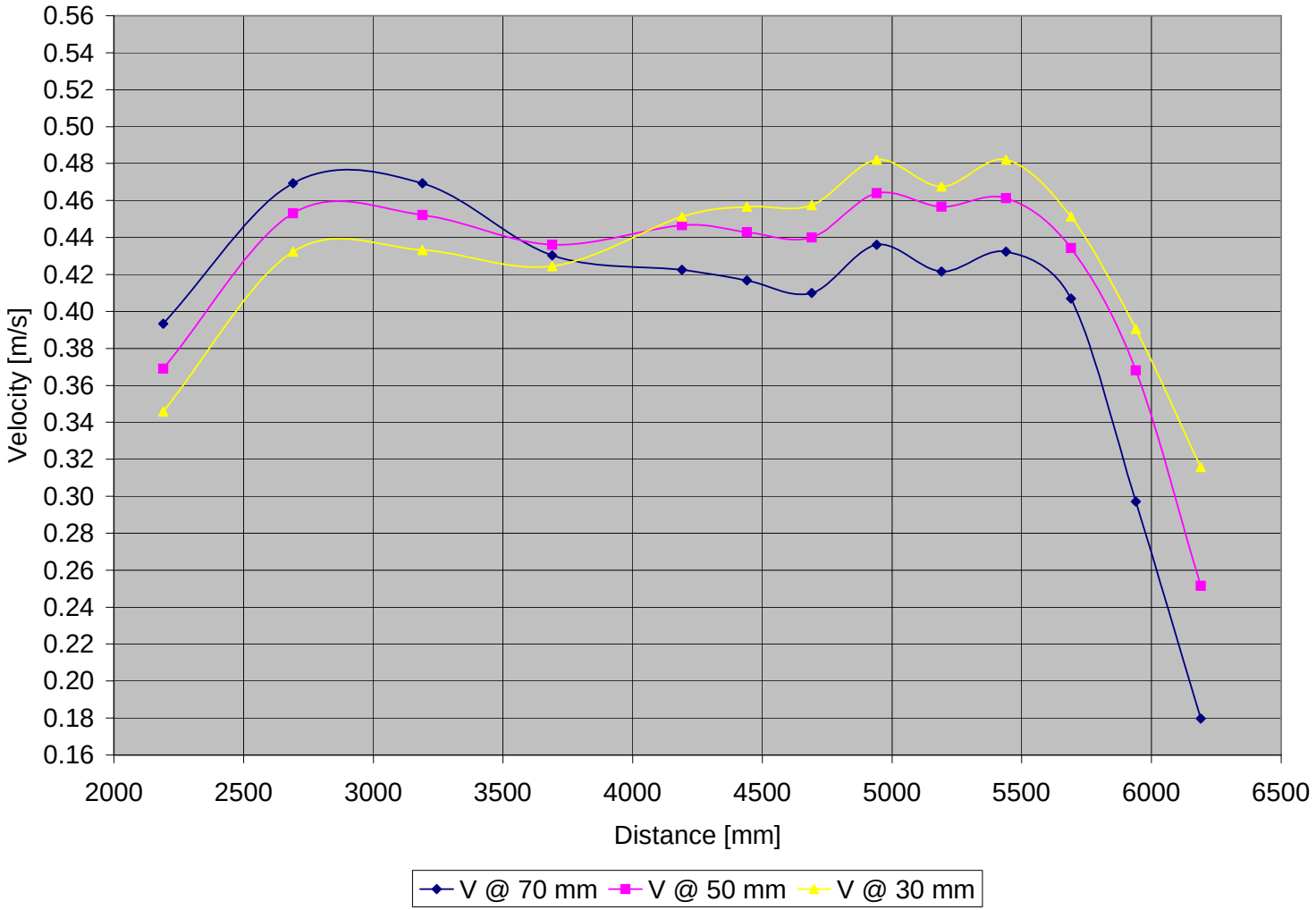

Figure B - 36: Test E2-Vertical velocity distribution measured at 50 mm from inner bank of bend

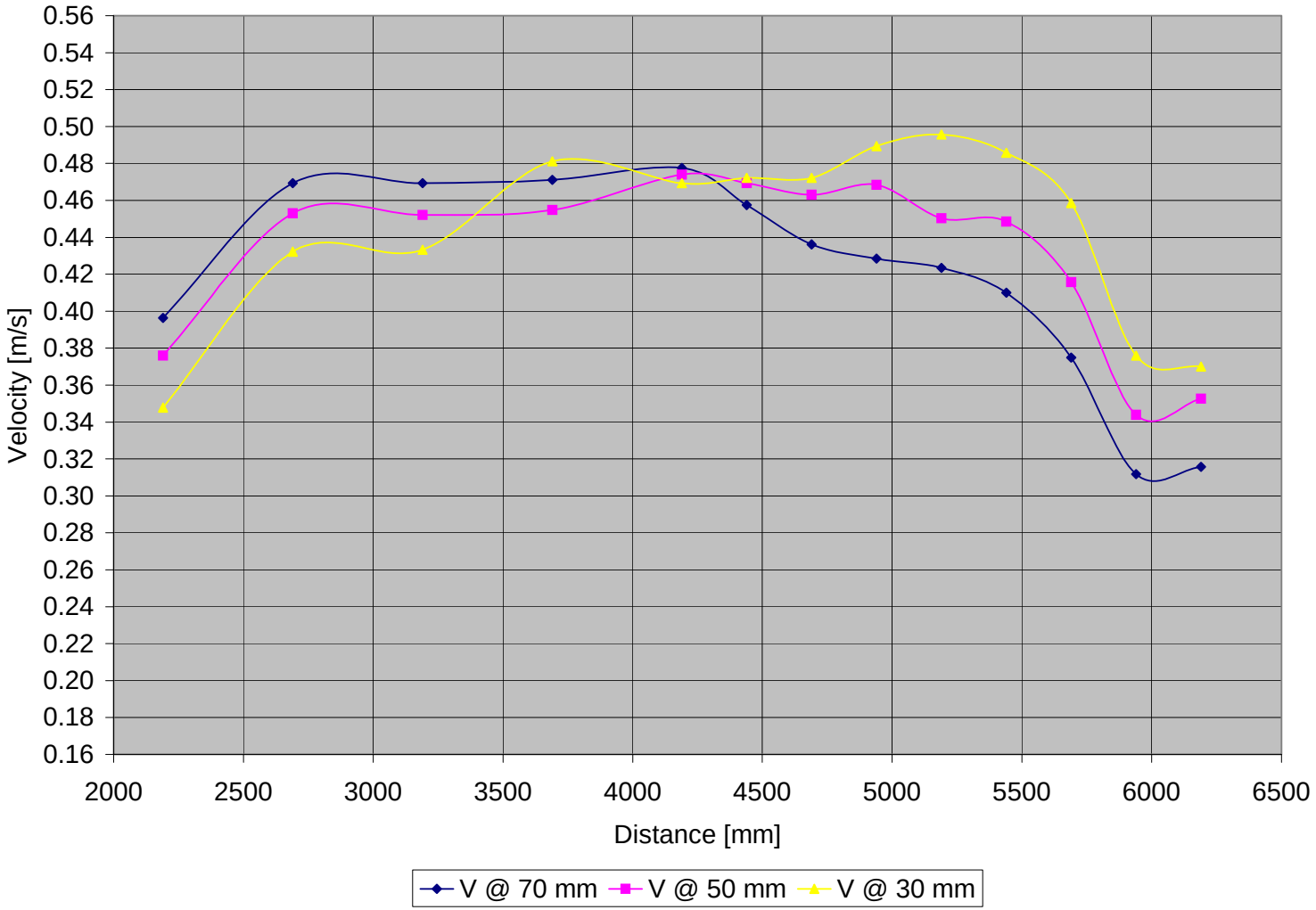

Figure B - 37: Test E2-Vertical velocity distribution measured at 100 mm from inner bank of bend

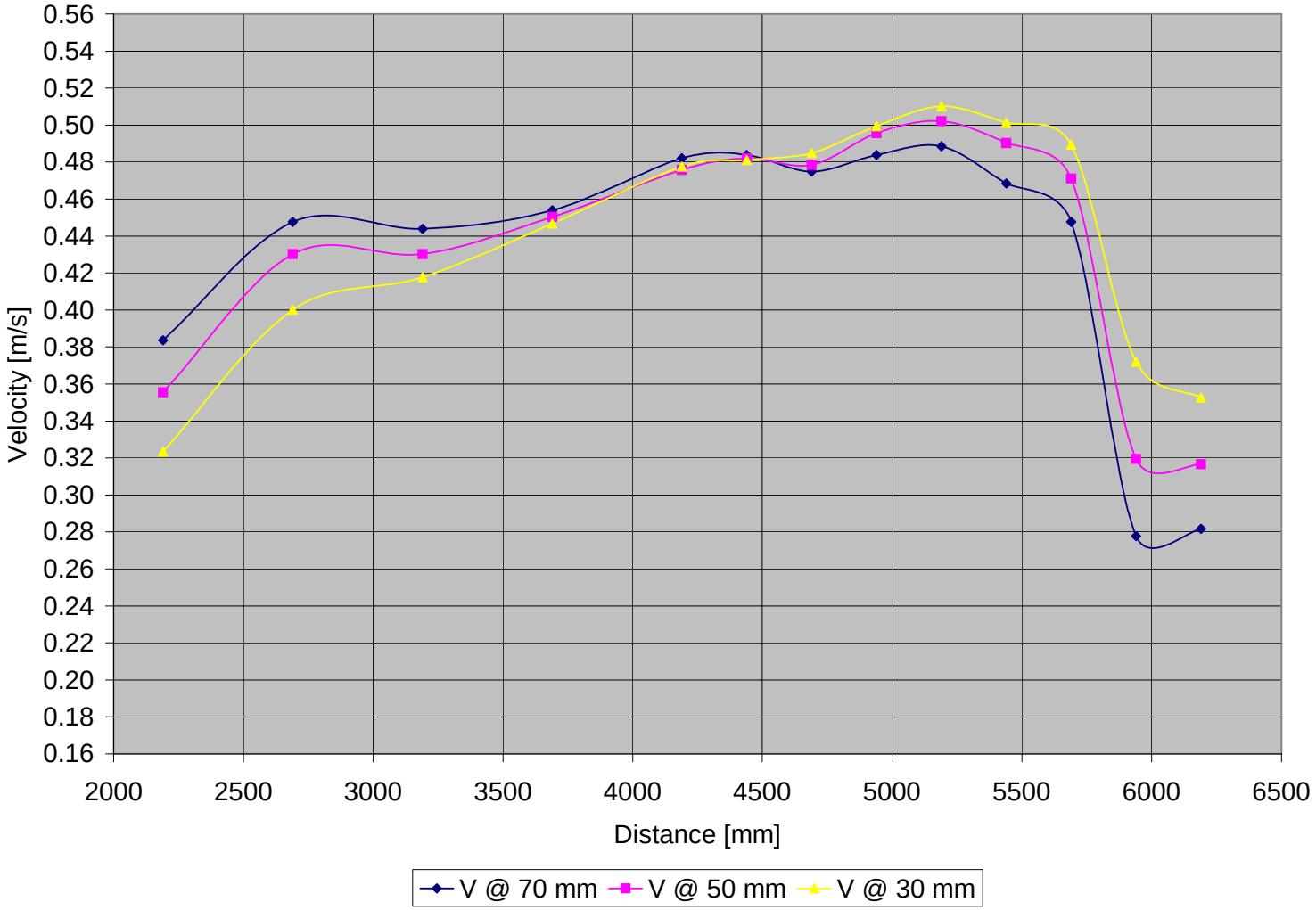

Figure B - 38: Test E2-Vertical velocity distribution measured at 150 mm from inner bank of bend

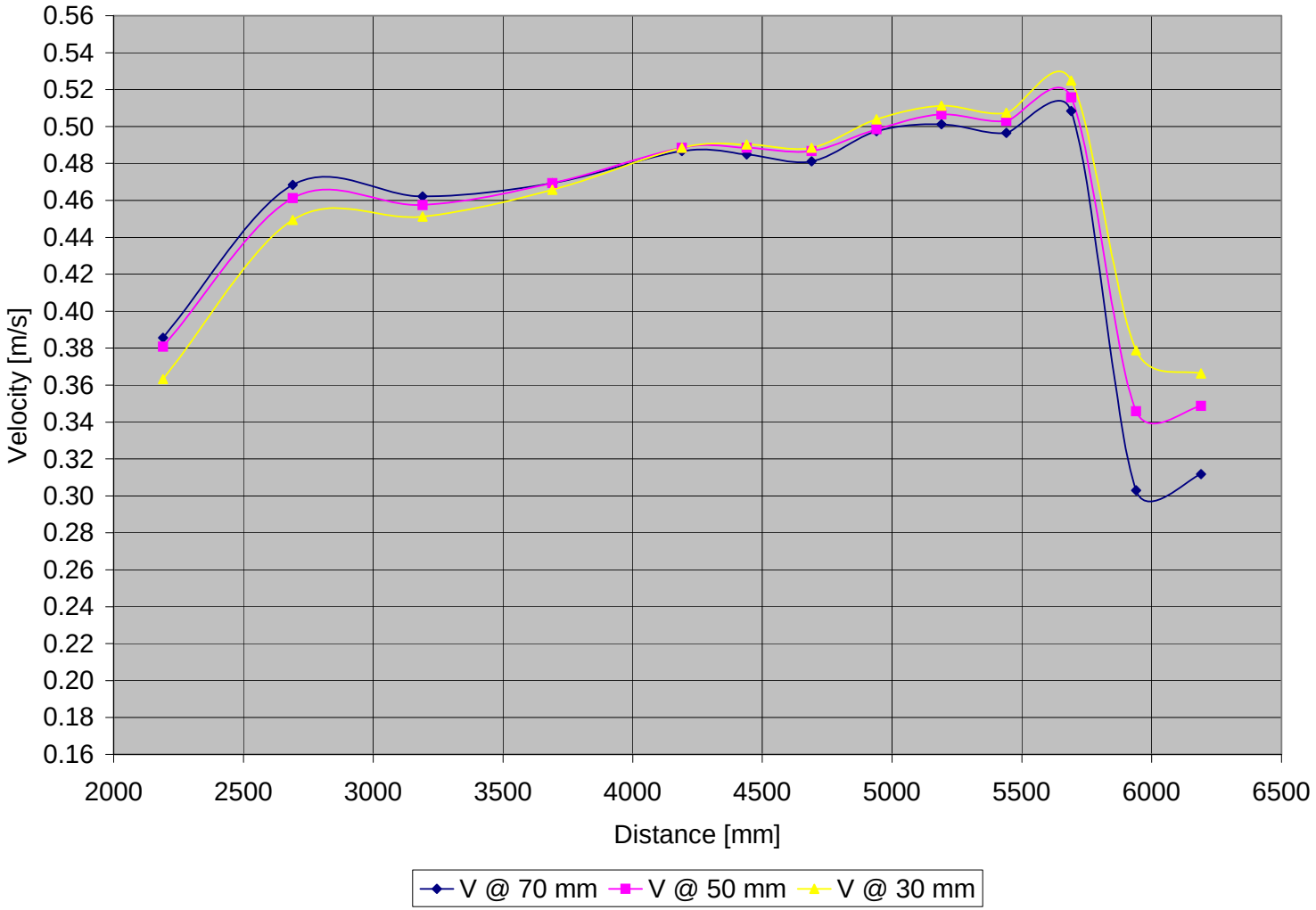

Figure B - 39: Test E2-Vertical velocity distribution measured at 200 mm from inner bank of bend

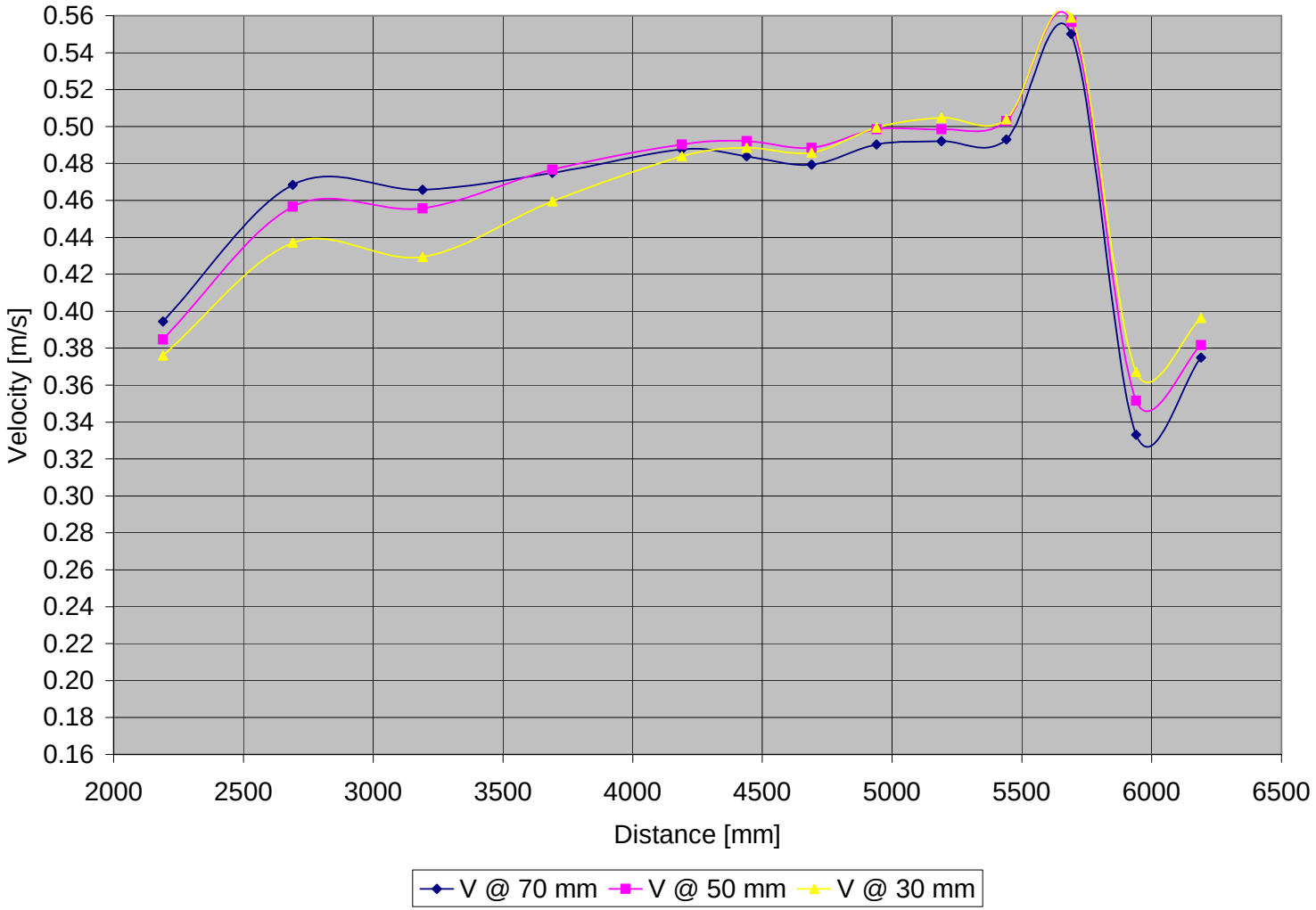

Figure B - 40: Test E2-Vertical velocity distribution measured at 250 mm from inner bank of bend

	Point	6	7	8	9	10	10A	11	11A	12	12A	13	13A	14
Width	L	2190	2690	3190	3690	4190	4440	4690	4940	5190	5440	5690	5940	6190
	h													
50	70	0.393	0.469	0.469	0.430	0.423	0.417	0.410	0.436	0.422	0.432	0.407	0.297	0.180
	50	0.369	0.453	0.452	0.436	0.447	0.443	0.440	0.464	0.457	0.461	0.434	0.368	0.252
	30	0.346	0.432	0.433	0.424	0.451	0.457	0.458	0.482	0.468	0.482	0.451	0.390	0.316
100	70	0.396	0.469	0.469	0.471	0.478	0.458	0.436	0.428	0.424	0.410	0.375	0.312	0.316
	50	0.376	0.453	0.452	0.455	0.474	0.469	0.463	0.468	0.450	0.448	0.416	0.344	0.353
	30	0.348	0.432	0.433	0.481	0.469	0.472	0.472	0.489	0.496	0.486	0.458	0.376	0.370
150	70	0.384	0.448	0.444	0.454	0.482	0.484	0.475	0.484	0.488	0.468	0.448	0.278	0.282
	50	0.356	0.430	0.430	0.450	0.476	0.482	0.478	0.496	0.502	0.490	0.471	0.320	0.317
	30	0.323	0.400	0.418	0.447	0.478	0.481	0.485	0.499	0.510	0.501	0.489	0.372	0.353
200	70	0.386	0.468	0.462	0.469	0.487	0.485	0.481	0.498	0.501	0.497	0.508	0.303	0.312
	50	0.381	0.461	0.458	0.469	0.488	0.488	0.487	0.498	0.507	0.503	0.516	0.346	0.349
	30	0.363	0.449	0.451	0.466	0.488	0.490	0.488	0.504	0.511	0.508	0.525	0.379	0.366
250														
	70	0.394	0.468	0.466	0.475	0.488	0.484	0.479	0.490	0.492	0.493	0.550	0.333	0.375
	50	0.385	0.457	0.456	0.477	0.490	0.492	0.488	0.498	0.498	0.503	0.557	0.352	0.382
	30	0.376	0.437	0.429	0.459	0.484	0.488	0.486	0.499	0.505	0.504	0.559	0.367	0.396

Table B - 5: Test E2- Measured velocities [m/s]

B.2.3 TEST E3 (F_R = 0.7)

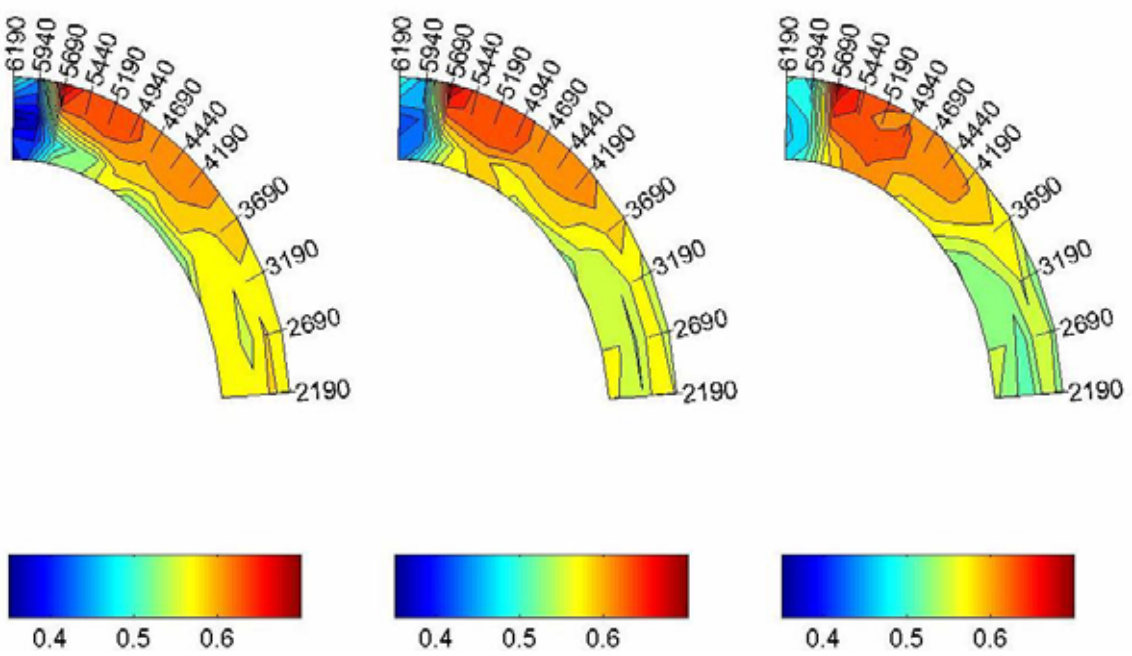

Figure B - 41: Test E3-Velocity distribution in the horizontal plane measured at 70, 50 and 30 mm

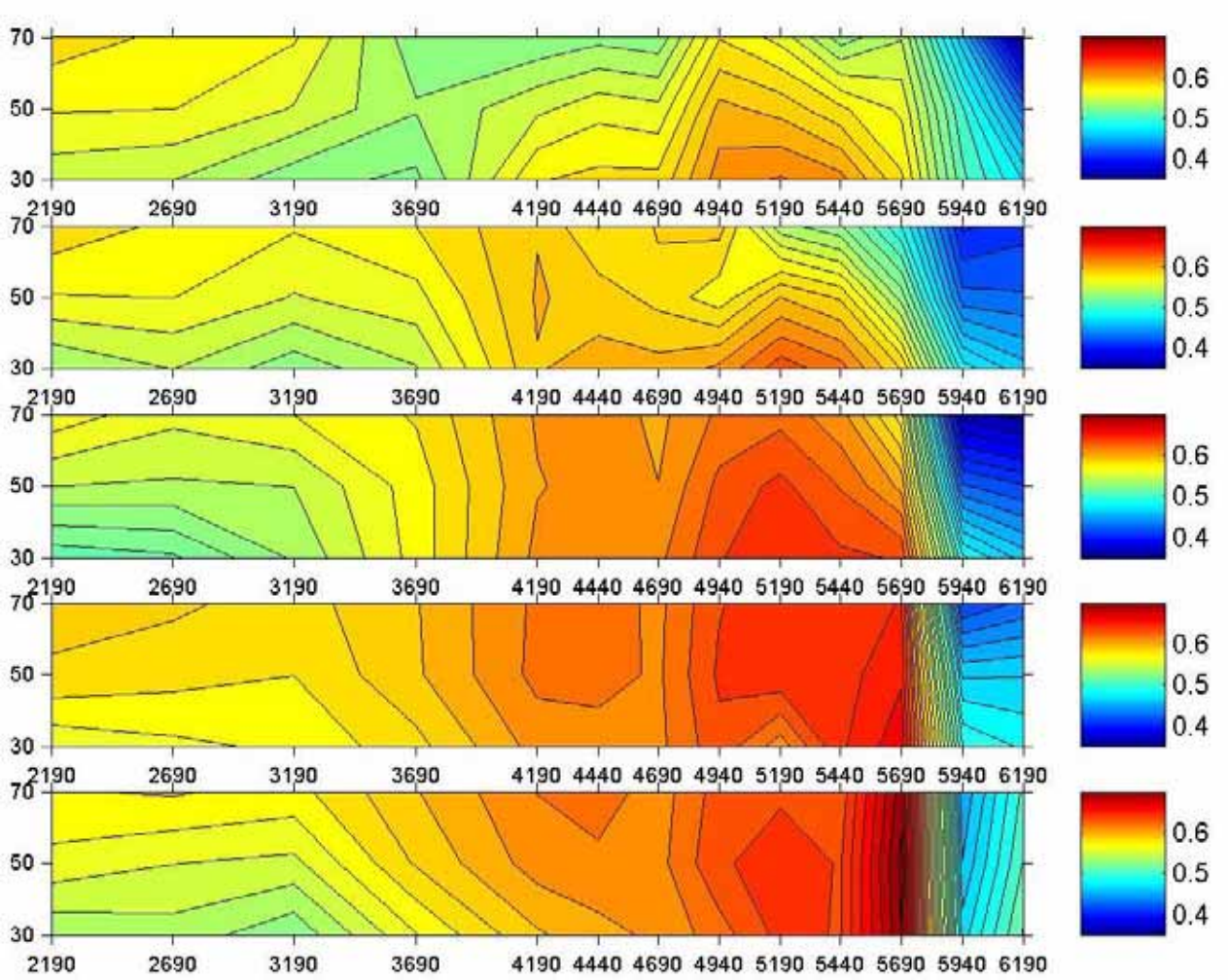

Figure B - 42: Test E3-Velocity distribution in the vertical plane

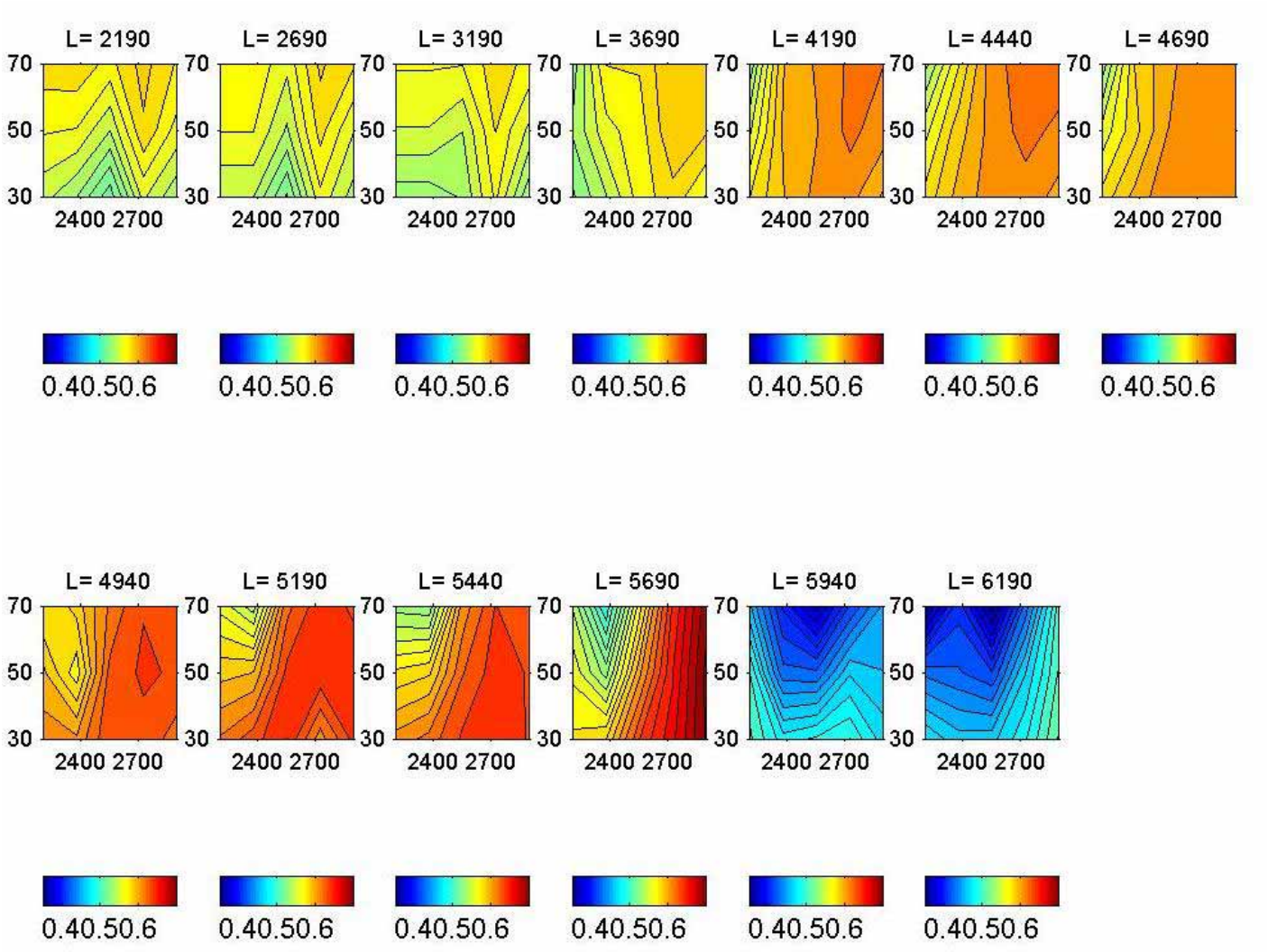

Figure B - 43: Test E3-Cross-sectional velocity distribution

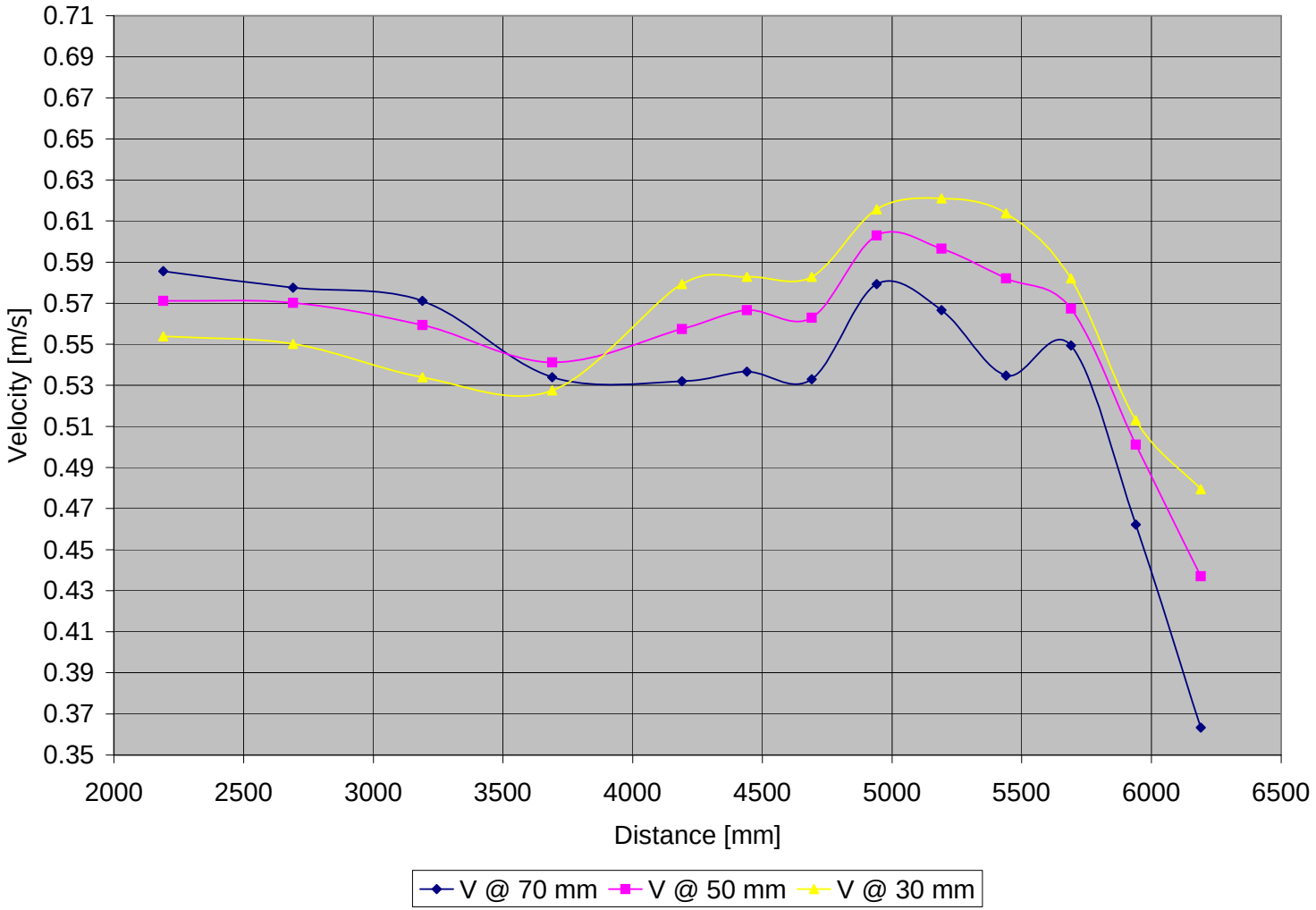

Figure B - 44: Test E3-Vertical velocity distribution measured at 50 mm from inner bank of bend

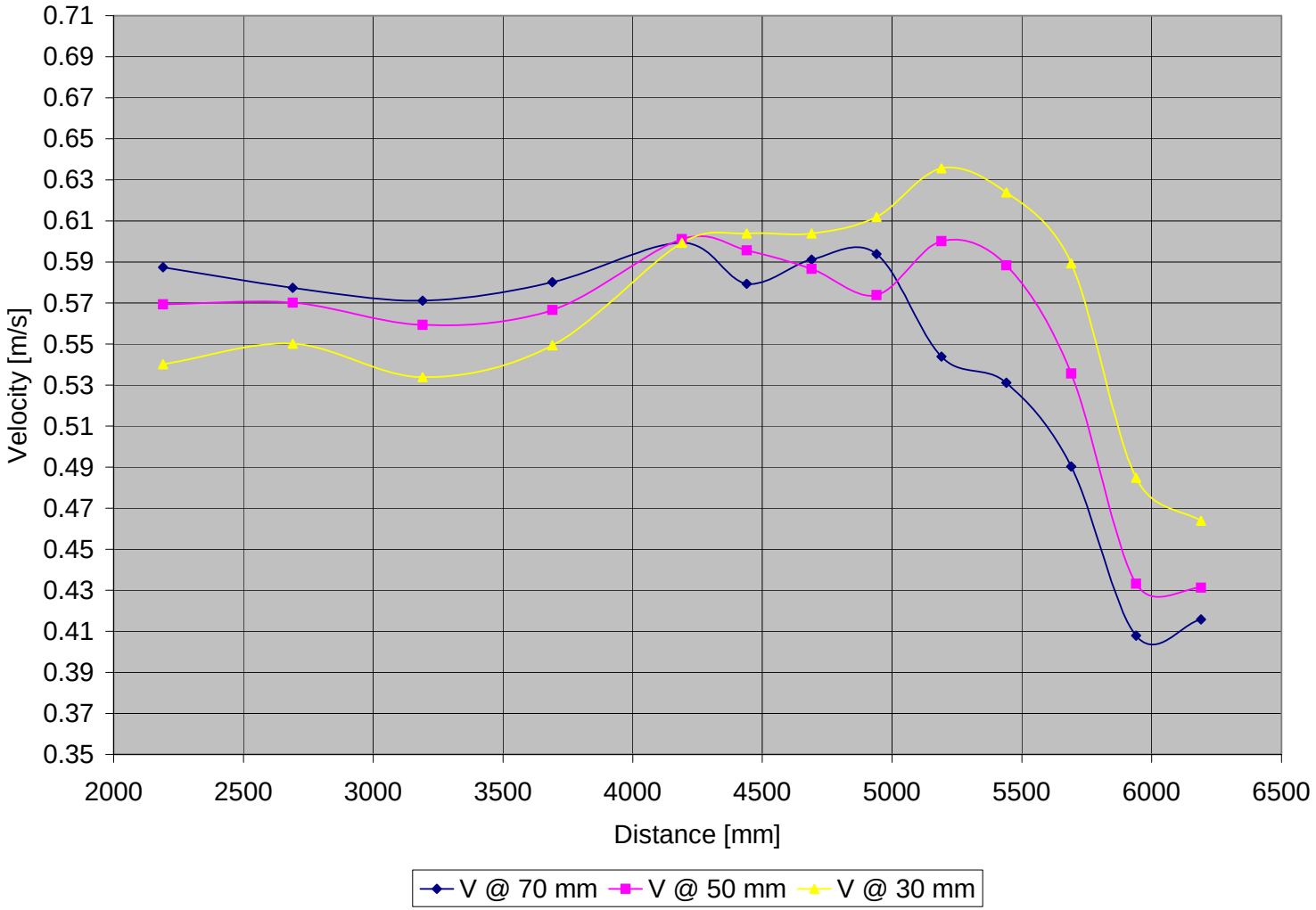

Figure B - 45: Test E3-Vertical velocity distribution measured at 100 mm from inner bank of bend

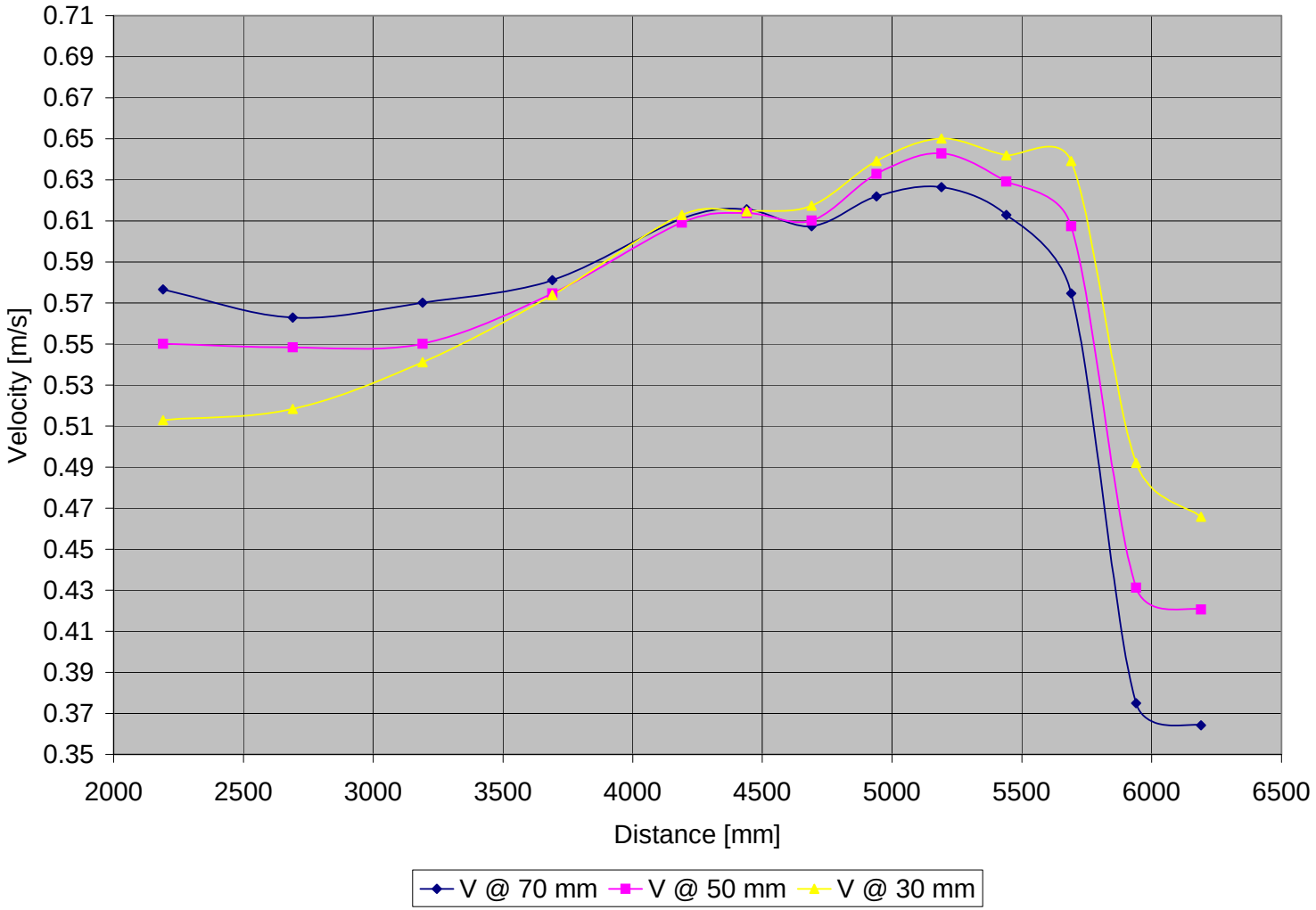

Figure B - 46: Test E3-Vertical velocity distribution measured at 150 mm from inner bank of bend

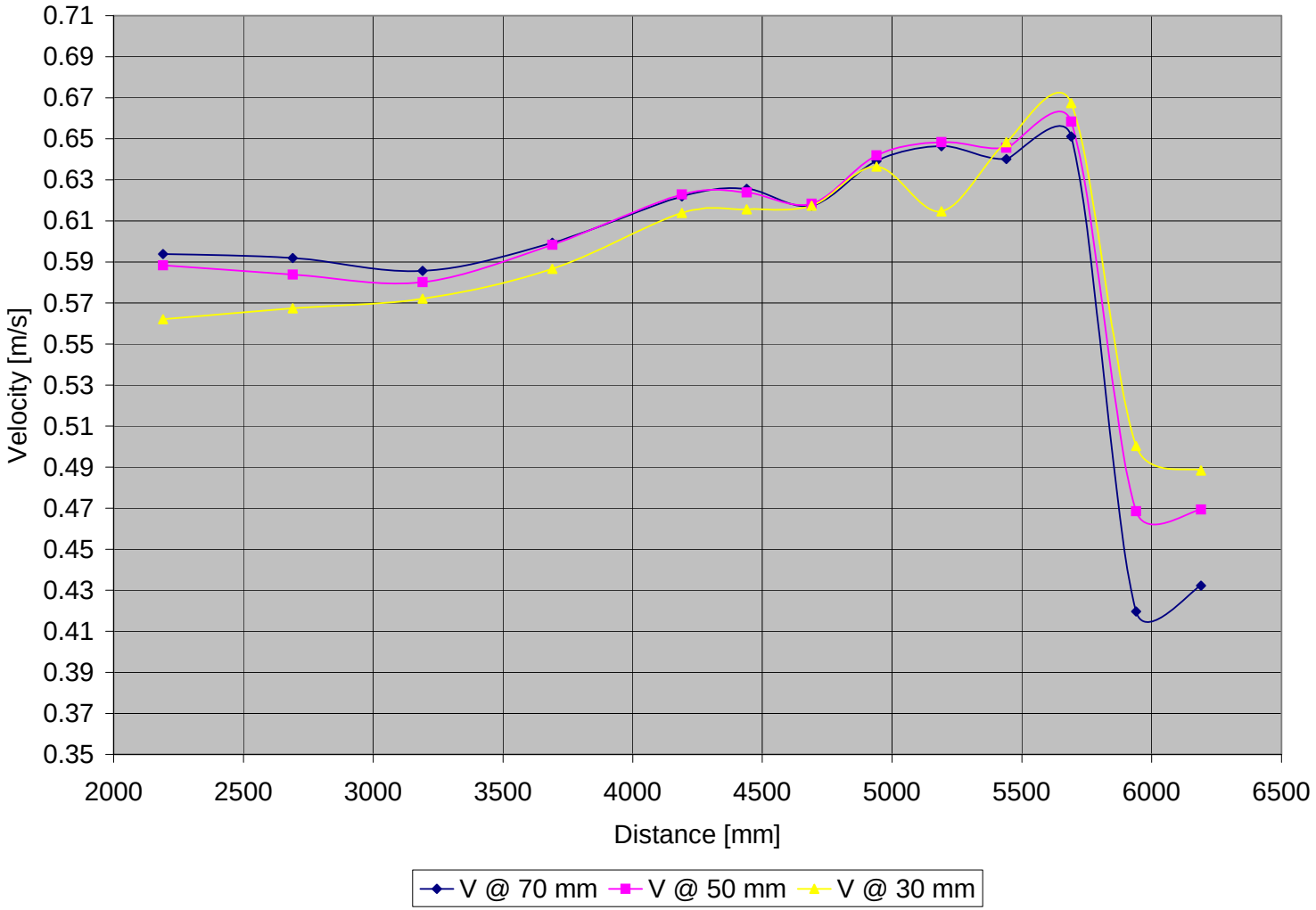

Figure B - 47: Test E3-Vertical velocity distribution measured at 200 mm from inner bank of bend

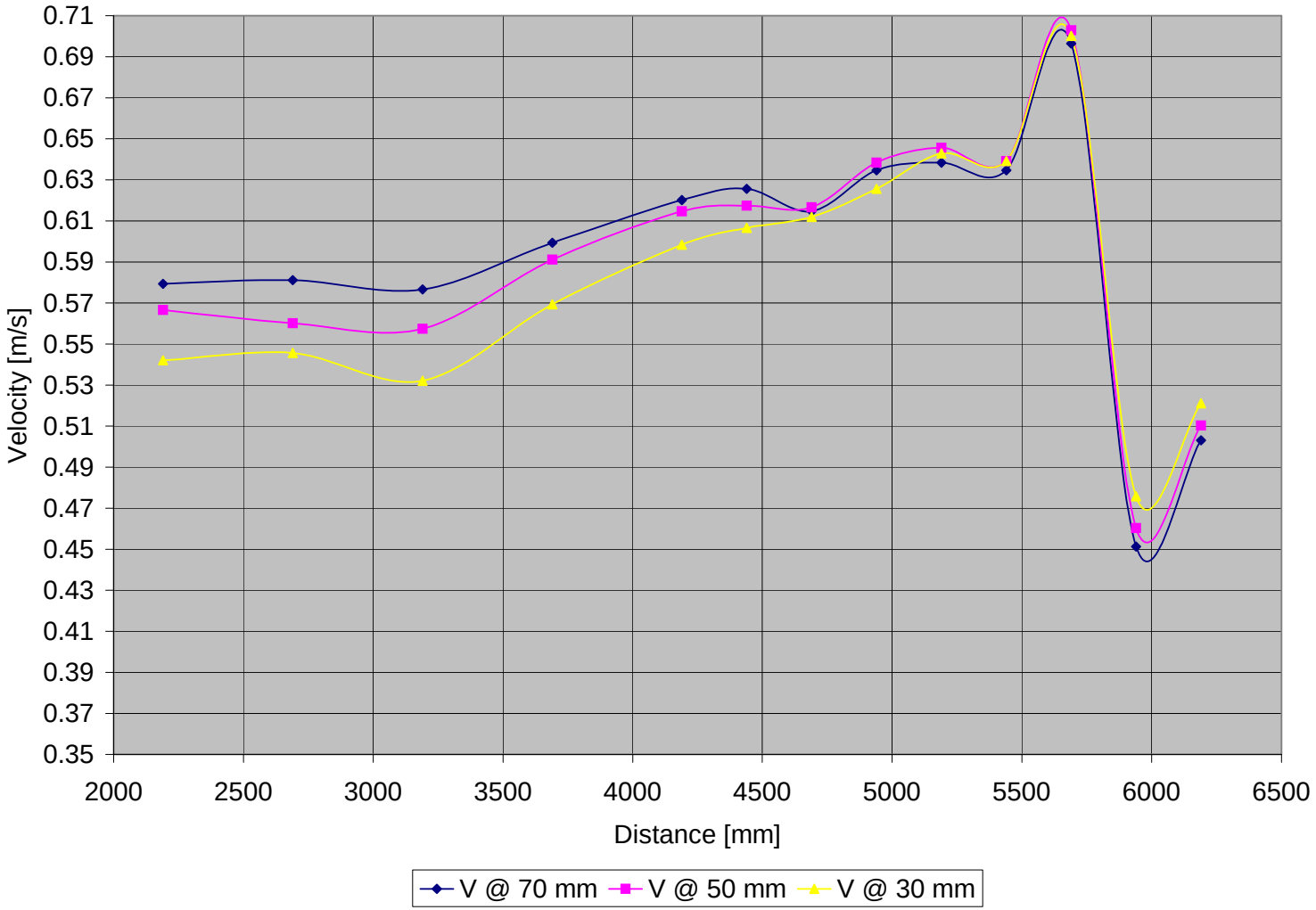

Figure B - 48: Test E3-Vertical velocity distribution measured at 250 mm from inner bank of bend

	Point	6	7	8	9	10	10A	11	11A	12	12A	13	13A	14
Width	L	2190	2690	3190	3690	4190	4440	4690	4940	5190	5440	5690	5940	6190
	h													
50	70	0.586	0.577	0.571	0.534	0.532	0.537	0.533	0.579	0.567	0.535	0.549	0.462	0.363
	50	0.571	0.570	0.559	0.541	0.557	0.567	0.563	0.603	0.597	0.582	0.567	0.501	0.437
	30	0.554	0.550	0.534	0.528	0.579	0.583	0.583	0.616	0.621	0.614	0.582	0.513	0.479
100	70	0.587	0.577	0.571	0.580	0.599	0.579	0.591	0.594	0.544	0.531	0.490	0.408	0.416
	50	0.569	0.570	0.559	0.567	0.601	0.596	0.587	0.574	0.600	0.588	0.536	0.433	0.431
	30	0.540	0.550	0.534	0.549	0.599	0.604	0.604	0.612	0.636	0.624	0.589	0.485	0.464
150	70	0.577	0.563	0.570	0.581	0.611	0.616	0.607	0.622	0.627	0.613	0.575	0.375	0.364
	50	0.550	0.548	0.550	0.575	0.609	0.614	0.610	0.633	0.643	0.629	0.607	0.431	0.421
	30	0.513	0.518	0.541	0.574	0.613	0.615	0.617	0.639	0.650	0.642	0.639	0.492	0.466
200	70	0.594	0.592	0.586	0.599	0.622	0.626	0.617	0.639	0.647	0.640	0.651	0.420	0.432
	50	0.588	0.584	0.580	0.598	0.623	0.624	0.618	0.642	0.648	0.646	0.658	0.468	0.469
	30	0.562	0.567	0.572	0.587	0.614	0.616	0.617	0.637	0.615	0.648	0.667	0.500	0.488
250														
	70	0.579	0.581	0.577	0.599	0.620	0.626	0.615	0.635	0.638	0.635	0.696	0.451	0.503
	50	0.567	0.560	0.557	0.591	0.615	0.617	0.617	0.638	0.646	0.639	0.703	0.460	0.510
	30	0.542	0.546	0.532	0.569	0.598	0.607	0.612	0.626	0.643	0.639	0.700	0.476	0.521

Table B - 6: Test E3- Measured velocities [m/s]

B.2.4 TEST E4 (F_R = 0.3 ; DDR = 0)

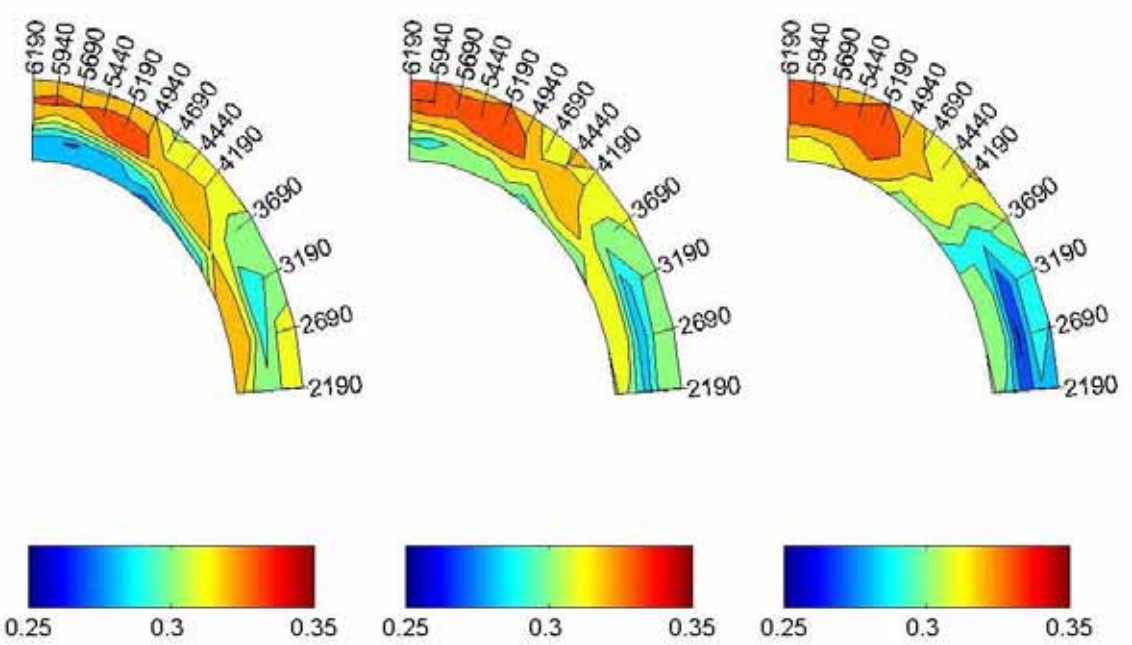

Figure B - 49: Test E4-Velocity distribution in the horizontal plane measured at 70, 50 and 30 mm

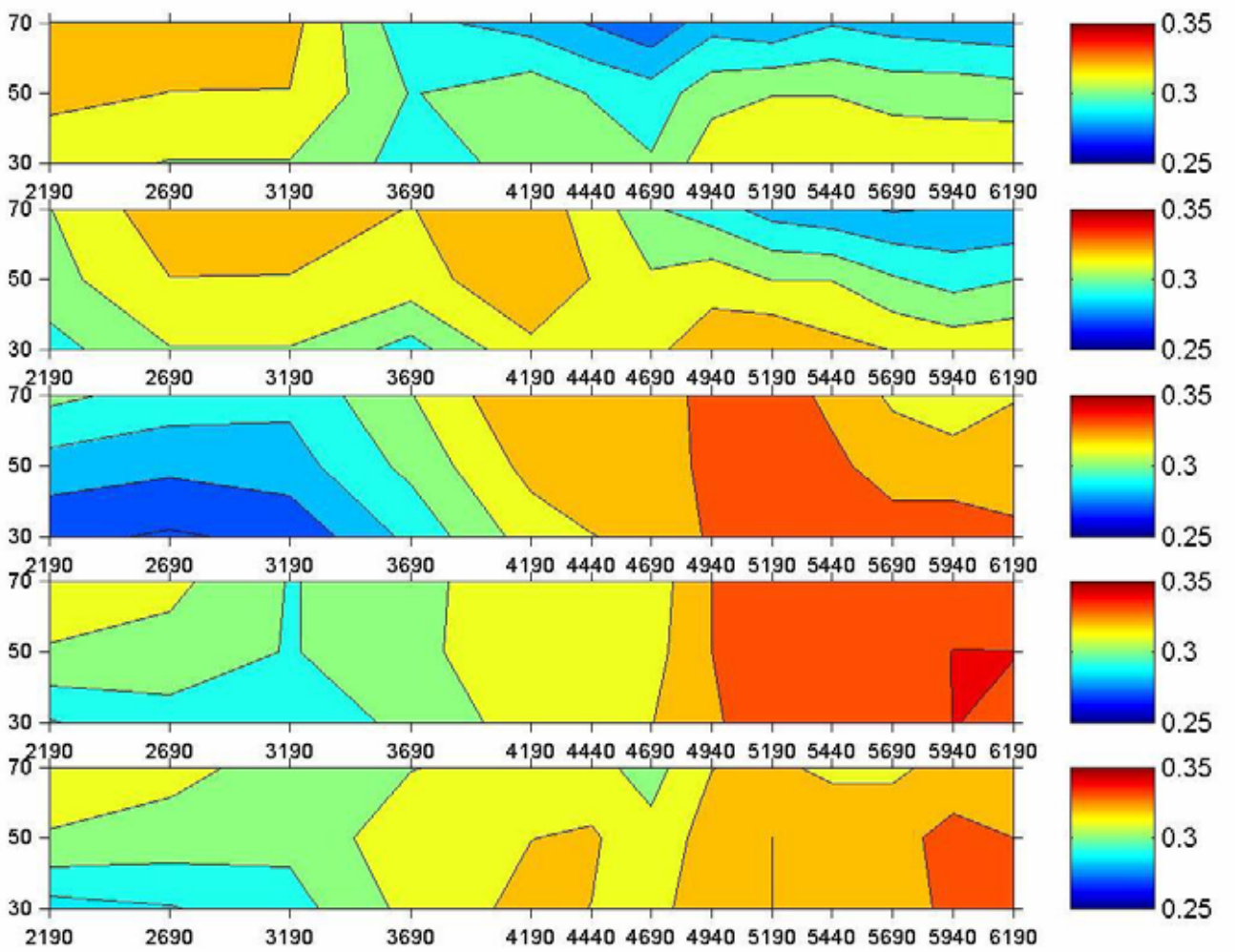

Figure B - 50: Test E4-Velocity distribution in the vertical plane

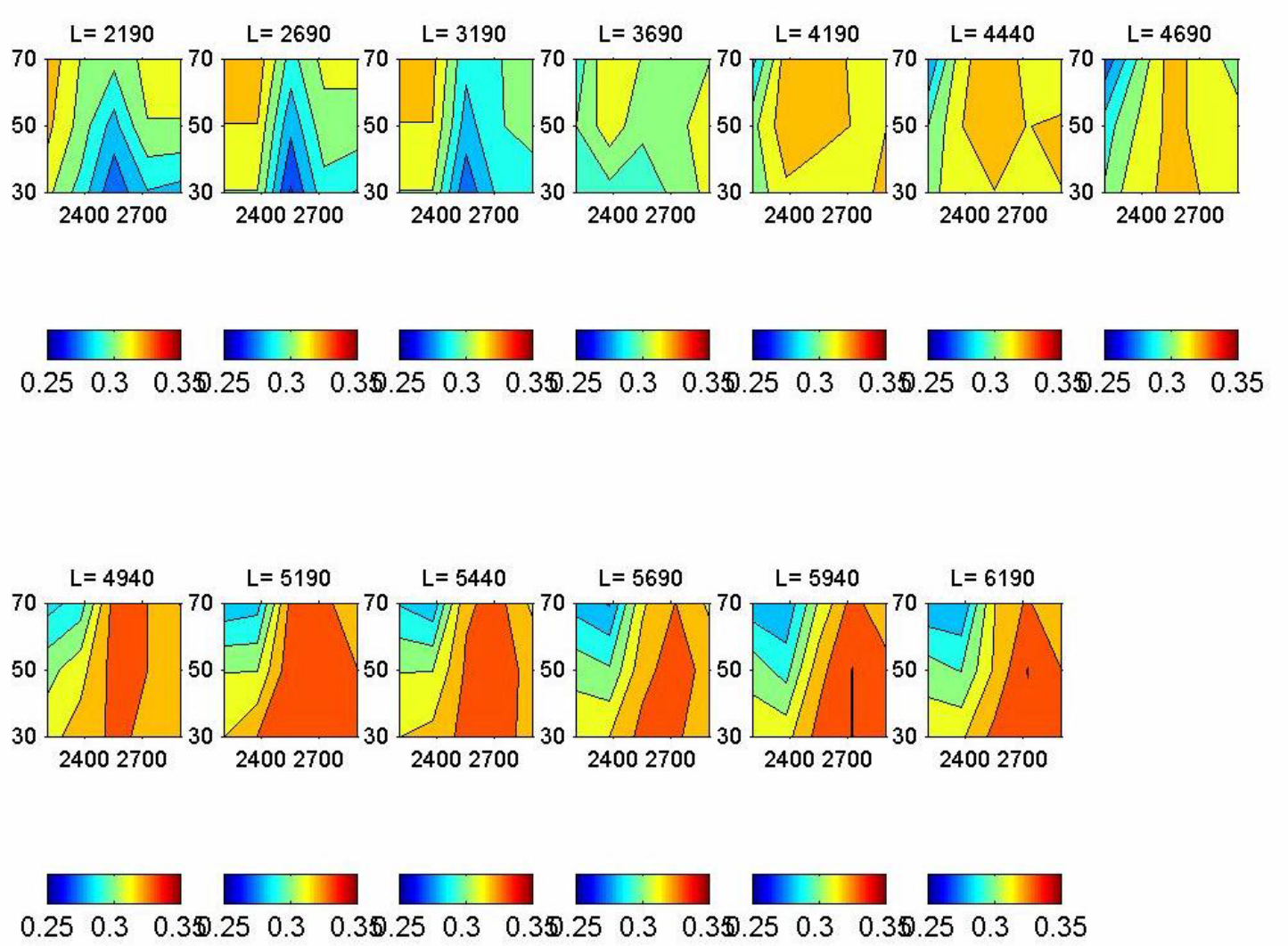

Figure B - 51: Test E4-Cross-sectional velocity distribution

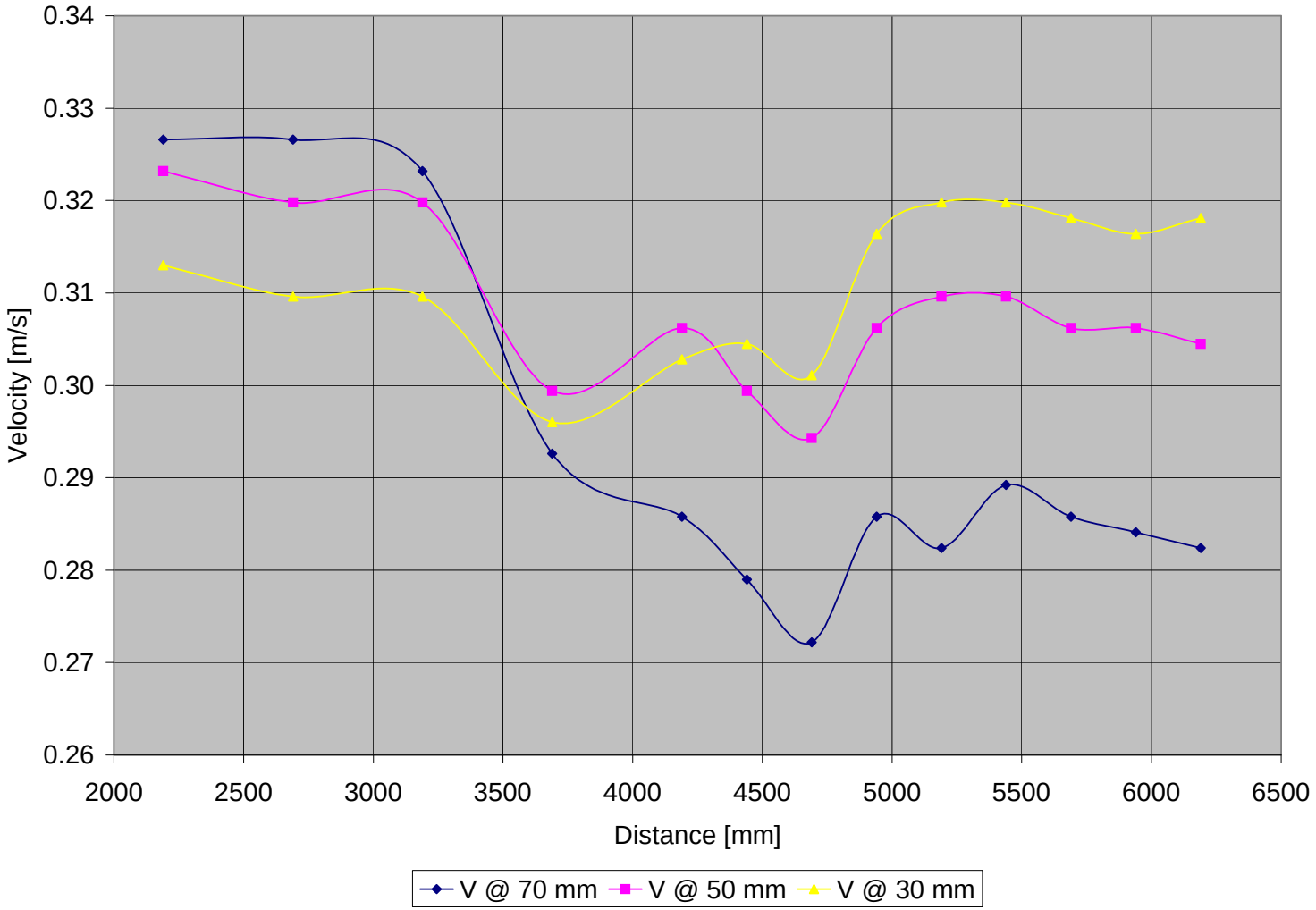

Figure B - 52: Test E4-Vertical velocity distribution measured at 50 mm from inner bank of bend

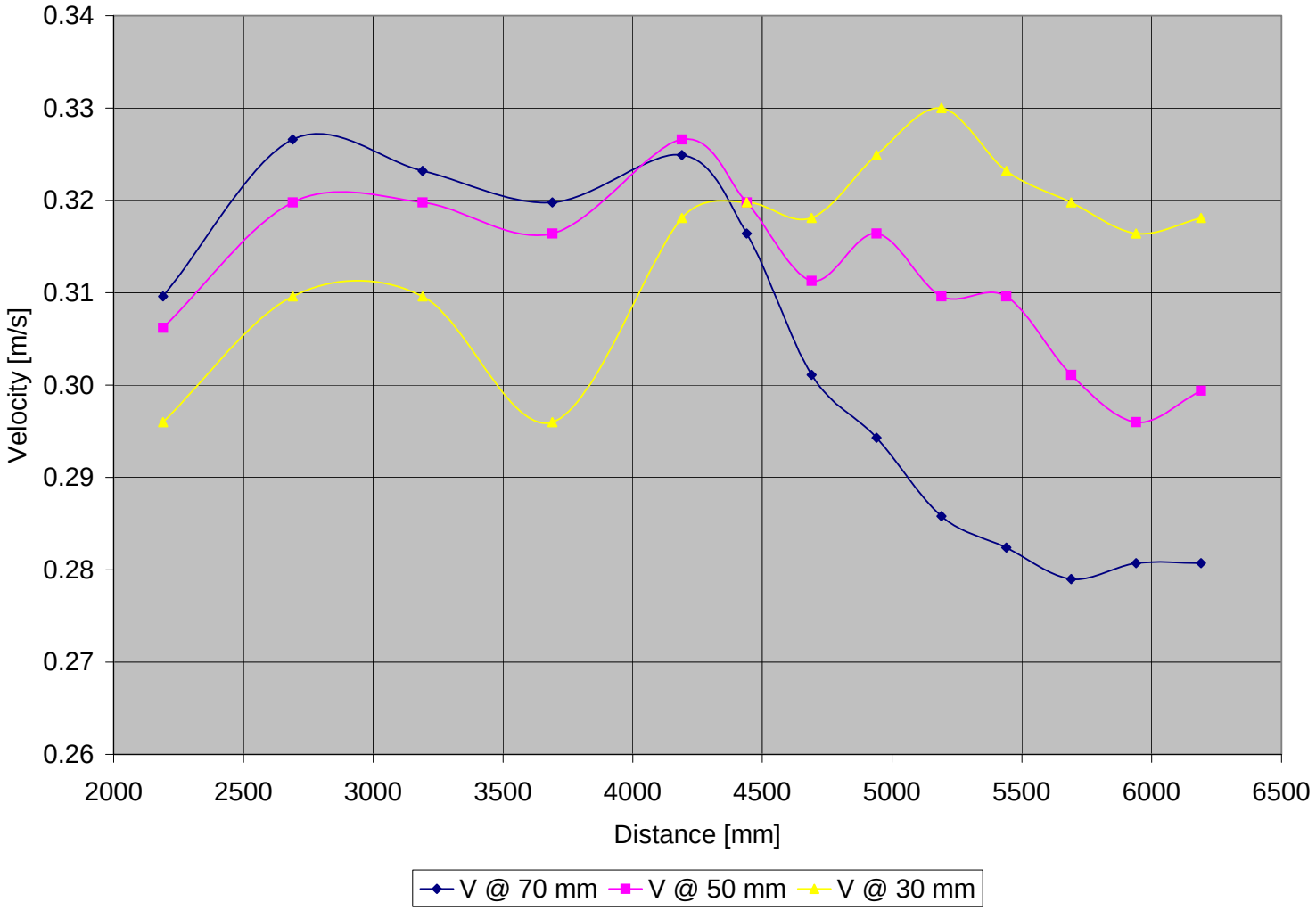

Figure B - 53: Test E4-Vertical velocity distribution measured at 100 mm from inner bank of bend

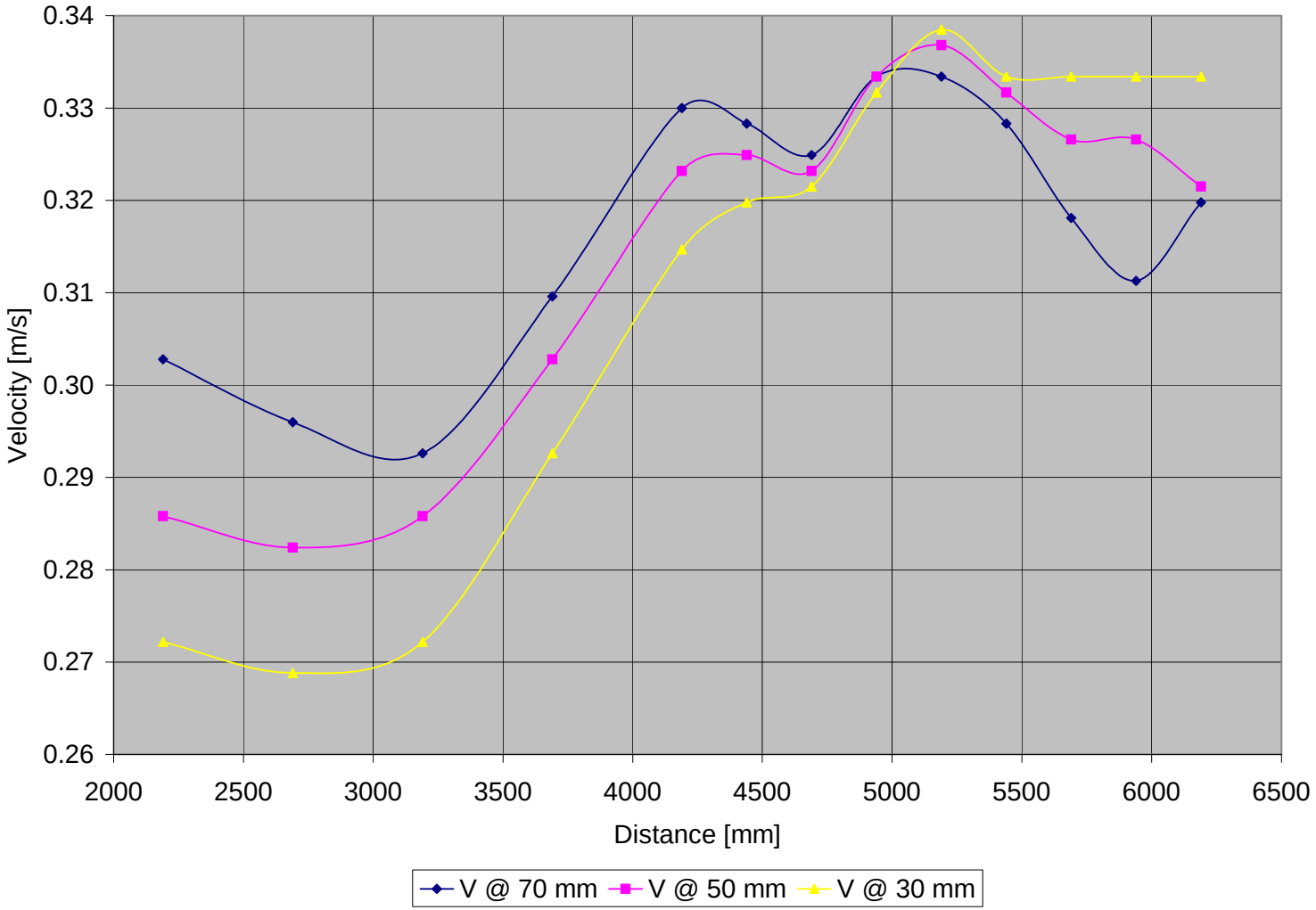

Figure B - 54: Test E4-Vertical velocity distribution measured at 150 mm from inner bank of bend

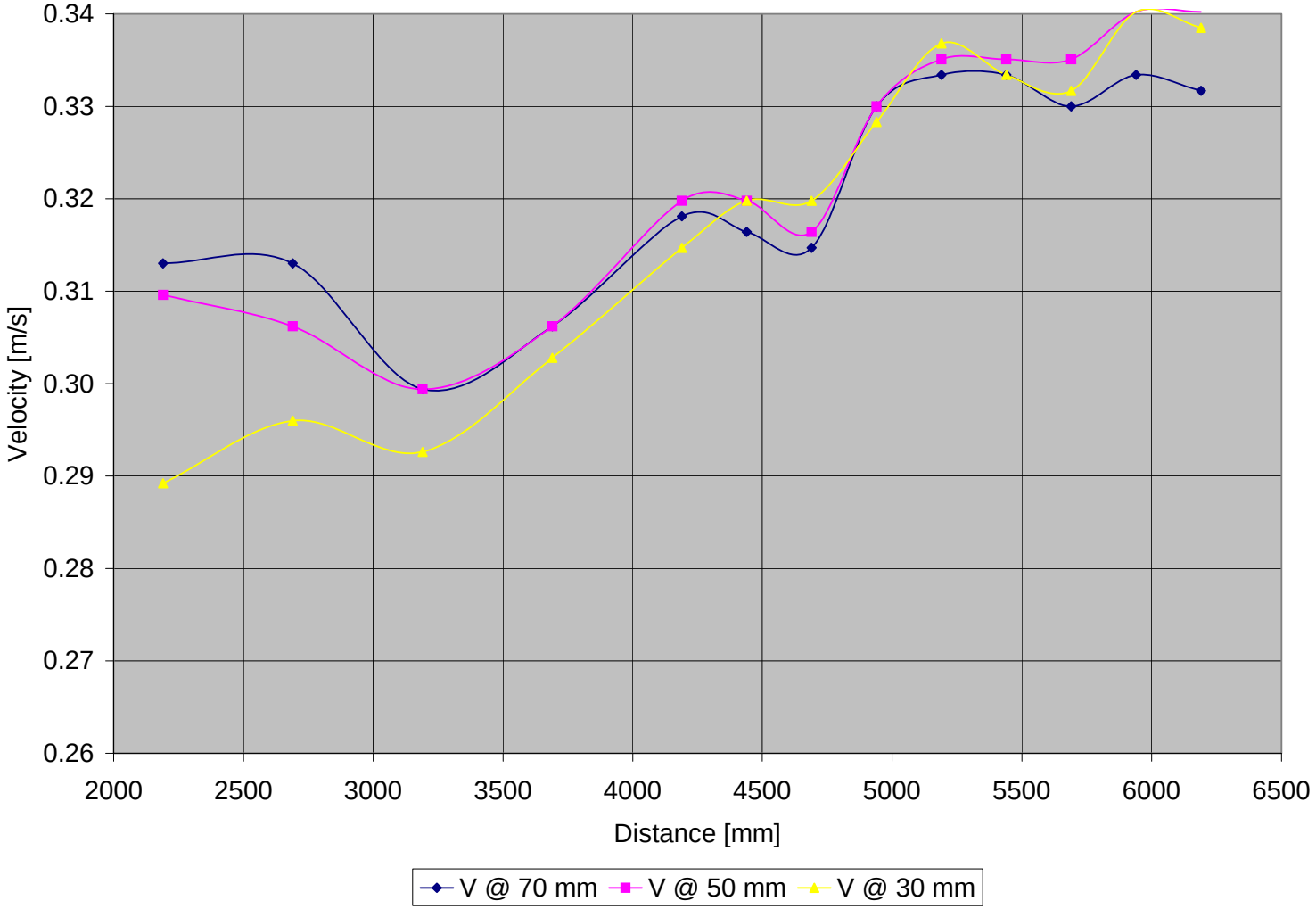

Figure B - 55: Test E4-Vertical velocity distribution measured at 200 mm from inner bank of bend

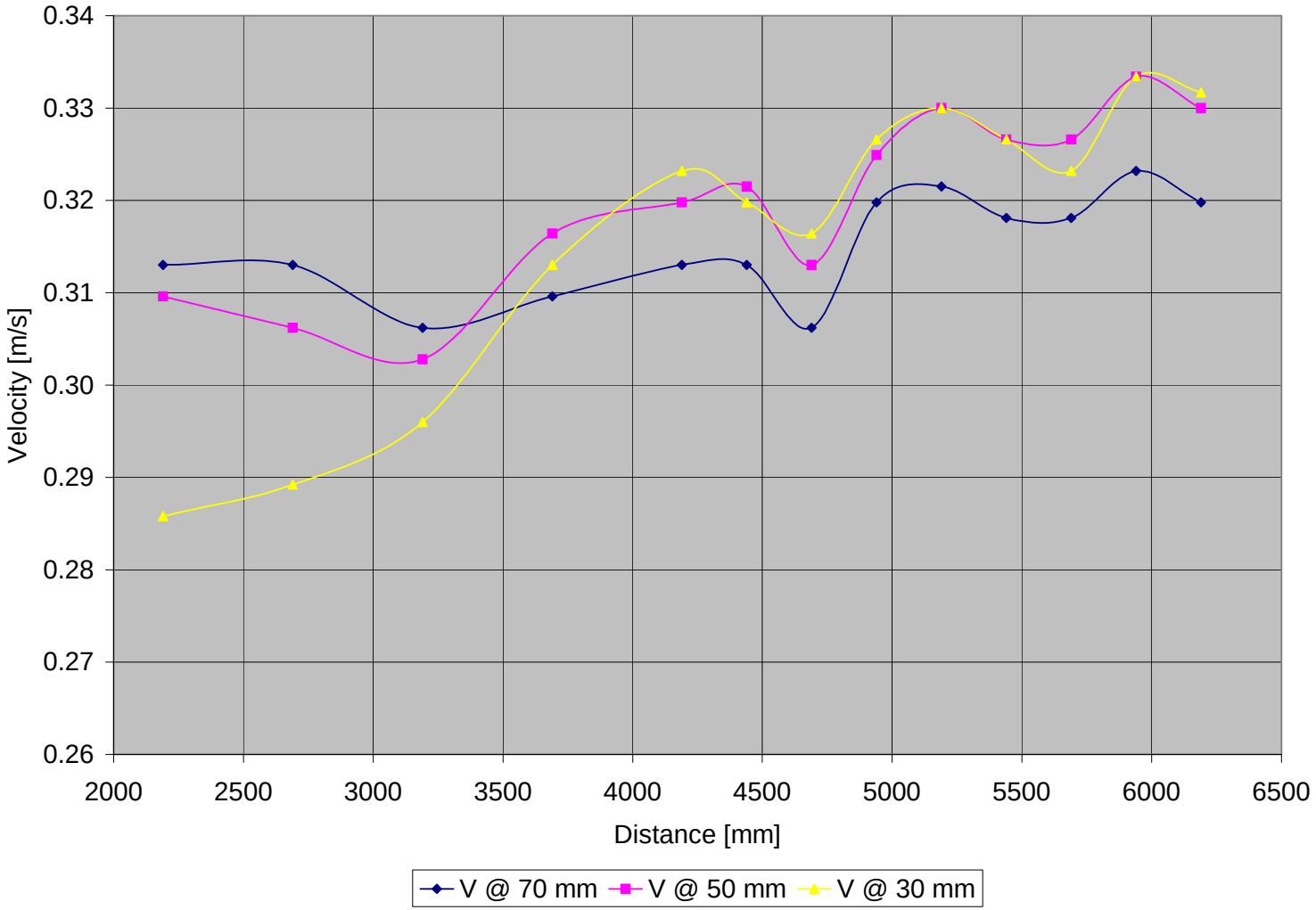

Figure B - 56: Test E4-Vertical velocity distribution measured at 250 mm from inner bank of bend

	Point	6	7	8	9	10	10A	11	11A	12	12A	13	13A	14
Width	L	2190	2690	3190	3690	4190	4440	4690	4940	5190	5440	5690	5940	6190
	h													
50	70	0.327	0.327	0.323	0.293	0.286	0.279	0.272	0.286	0.282	0.289	0.286	0.284	0.282
	50	0.323	0.320	0.320	0.299	0.306	0.299	0.294	0.306	0.310	0.310	0.306	0.306	0.305
	30	0.313	0.310	0.310	0.296	0.303	0.305	0.301	0.316	0.320	0.320	0.318	0.316	0.318
100	70	0.310	0.327	0.323	0.320	0.325	0.316	0.301	0.294	0.286	0.282	0.279	0.281	0.281
	50	0.306	0.320	0.320	0.316	0.327	0.320	0.311	0.316	0.310	0.310	0.301	0.296	0.299
	30	0.296	0.310	0.310	0.296	0.318	0.320	0.318	0.325	0.330	0.323	0.320	0.316	0.318
150	70	0.303	0.296	0.293	0.310	0.330	0.328	0.325	0.333	0.333	0.328	0.318	0.311	0.320
	50	0.286	0.282	0.286	0.303	0.323	0.325	0.323	0.333	0.337	0.332	0.327	0.327	0.322
	30	0.272	0.269	0.272	0.293	0.315	0.320	0.322	0.332	0.339	0.333	0.333	0.333	0.333
200	70	0.313	0.313	0.299	0.306	0.318	0.316	0.315	0.330	0.333	0.333	0.330	0.333	0.332
	50	0.310	0.306	0.299	0.306	0.320	0.320	0.316	0.330	0.335	0.335	0.335	0.340	0.340
	30	0.289	0.296	0.293	0.303	0.315	0.320	0.320	0.328	0.337	0.333	0.332	0.340	0.339
250														
	70	0.313	0.313	0.306	0.310	0.313	0.313	0.306	0.320	0.322	0.318	0.318	0.323	0.320
	50	0.310	0.306	0.303	0.316	0.320	0.322	0.313	0.325	0.330	0.327	0.327	0.333	0.330
	30	0.286	0.289	0.296	0.313	0.323	0.320	0.316	0.327	0.330	0.327	0.323	0.333	0.332

Table B - 7: Test E4- Measured velocities [m/s]

B.3 TEST F (Θ = 50˚)

B.3.1 TEST F1 (F_R = 0.3)

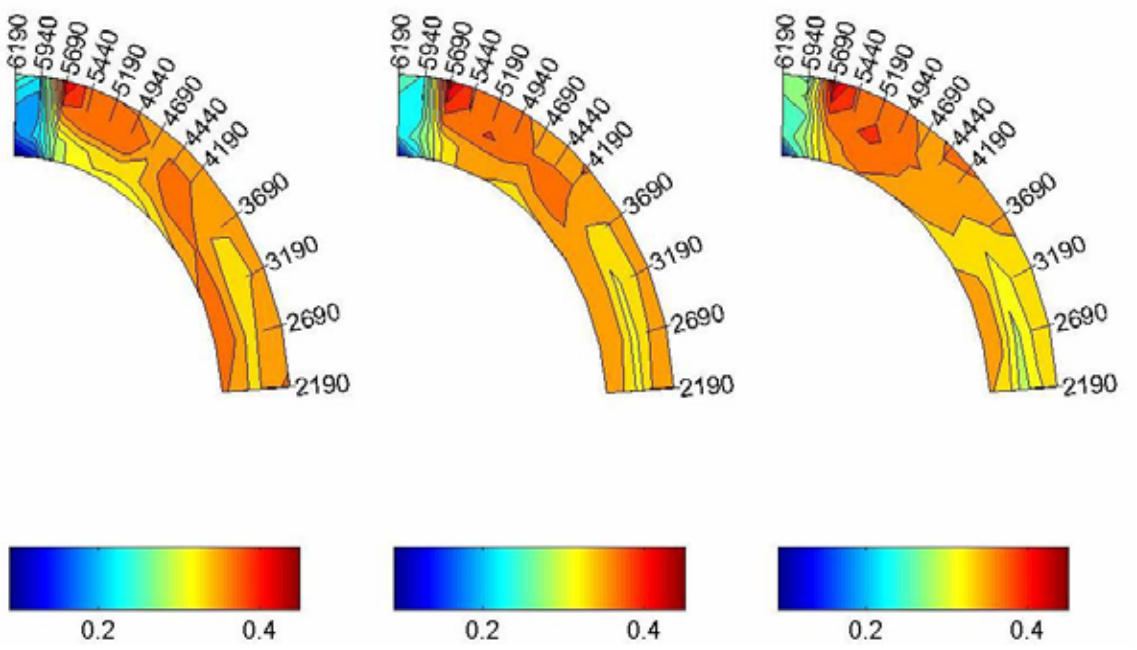

Figure B - 57: Test F1-Velocity distribution in the horizontal plane measured at 70, 50 and 30 mm

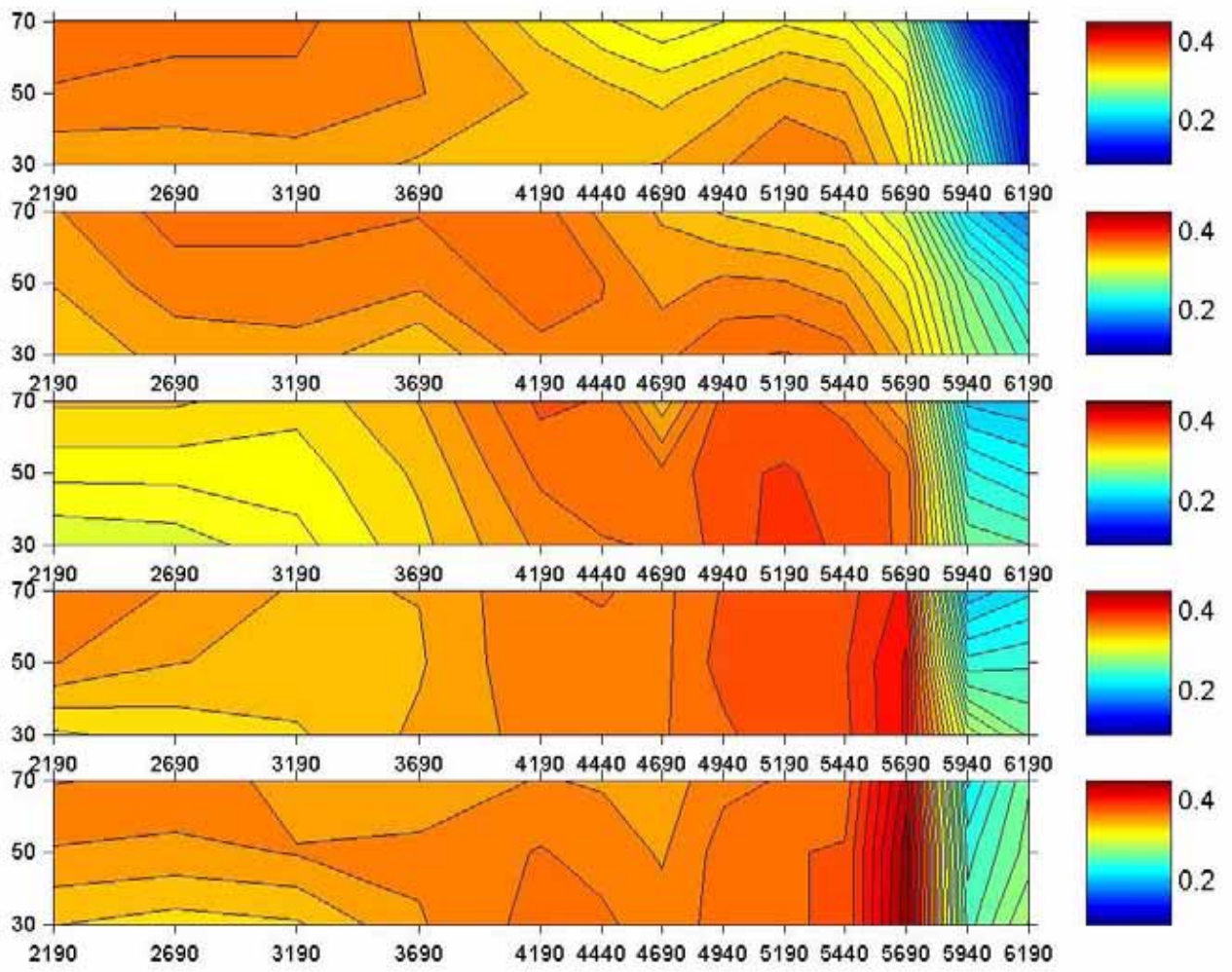

Figure B - 58: Test F1-Velocity distribution in the vertical plane

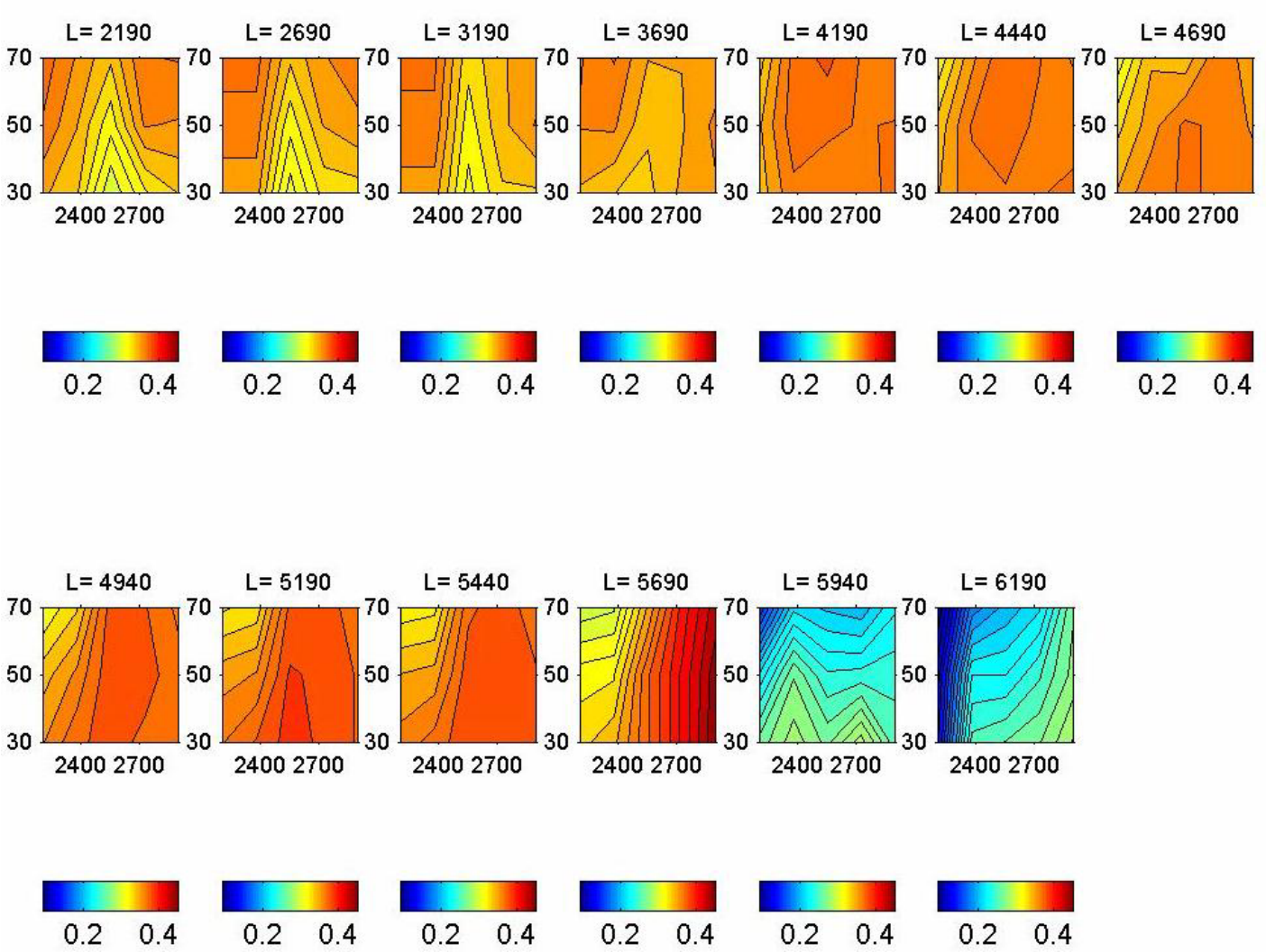

Figure B - 59: Test F1-Cross-sectional velocity distribution

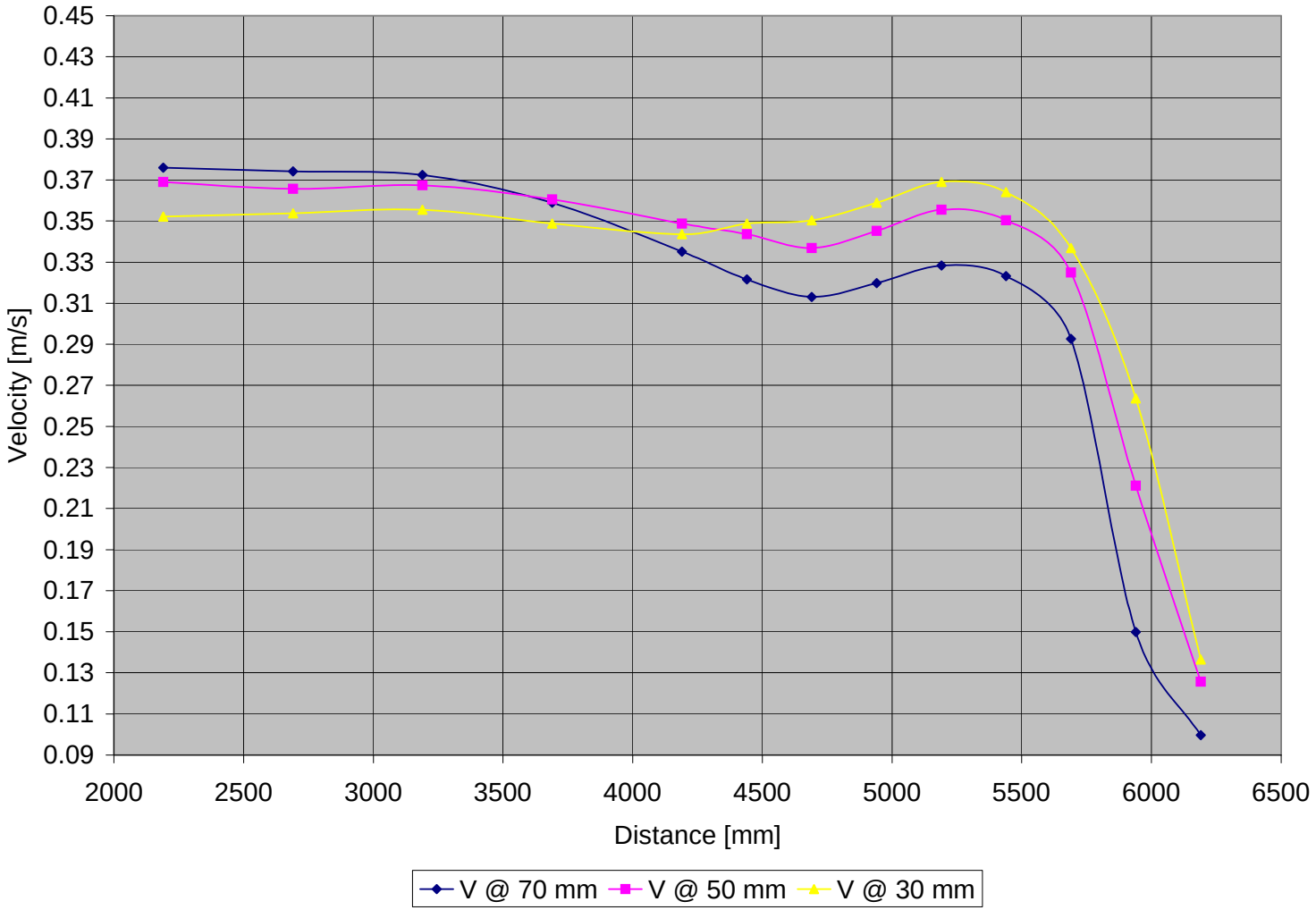

Figure B - 60: Test F1-Vertical velocity distribution measured at 50 mm from inner bank of bend

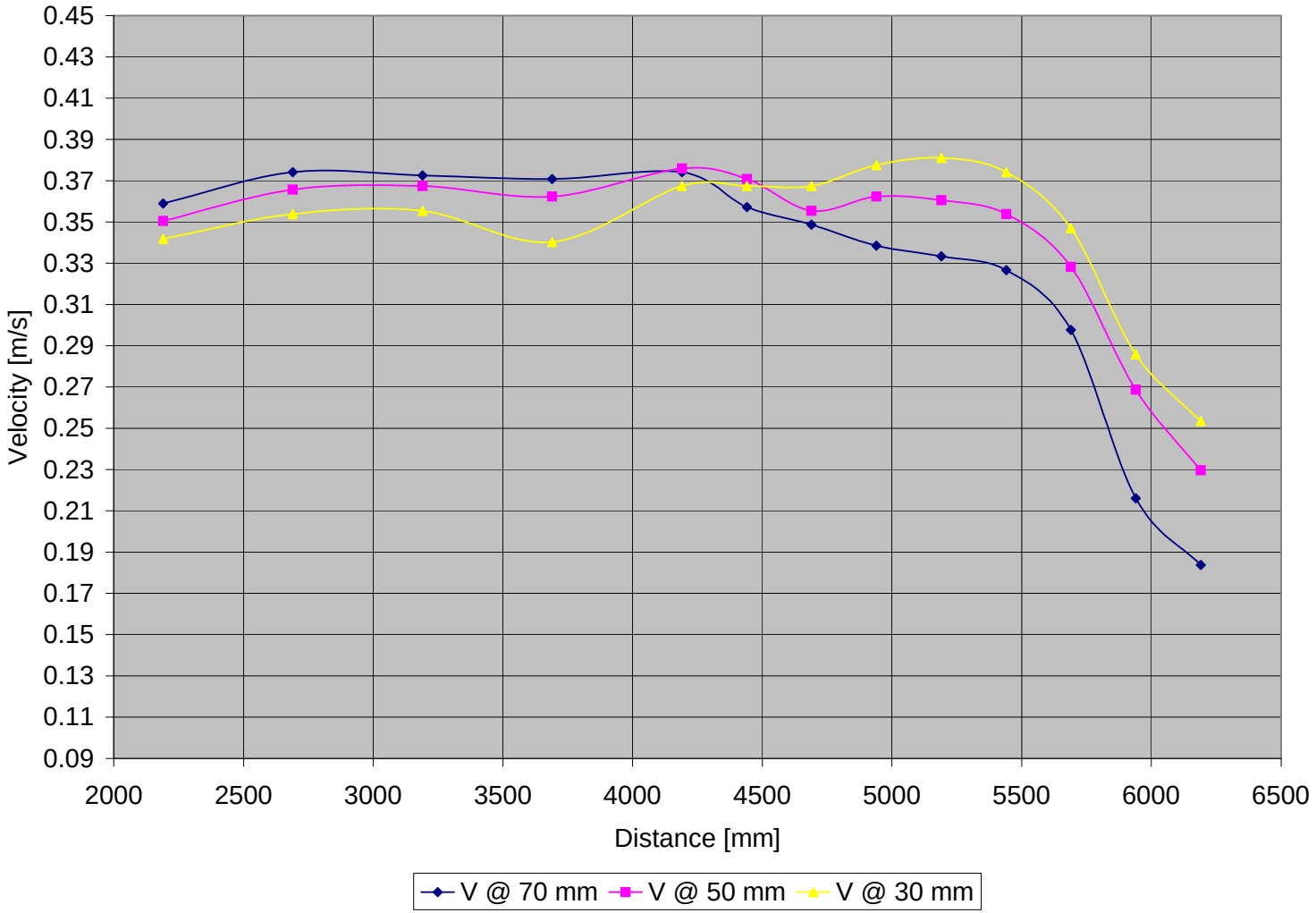

Figure B - 61: Test F1-Vertical velocity distribution measured at 100 mm from inner bank of bend

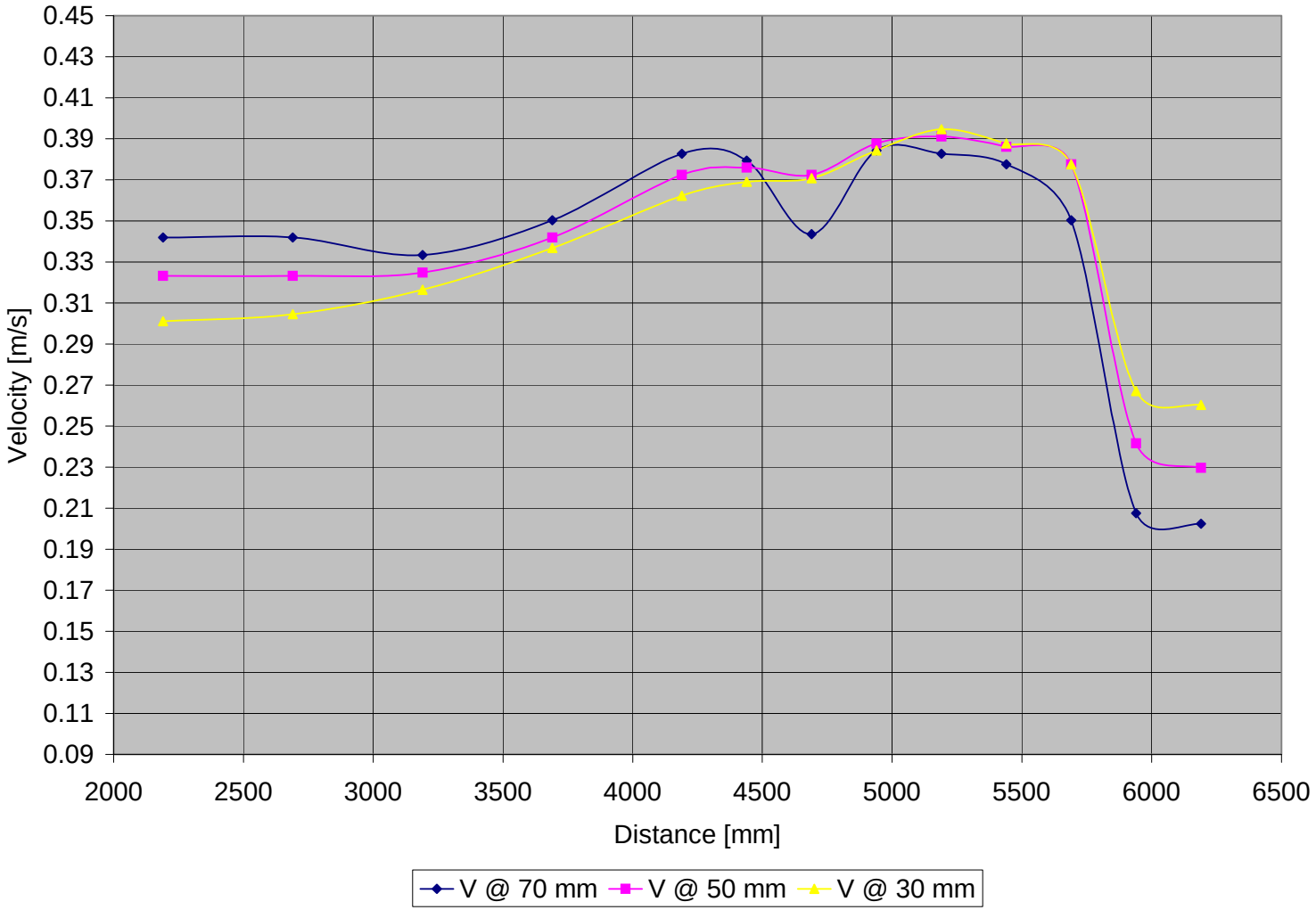

Figure B - 62: Test F1-Vertical velocity distribution measured at 150 mm from inner bank of bend

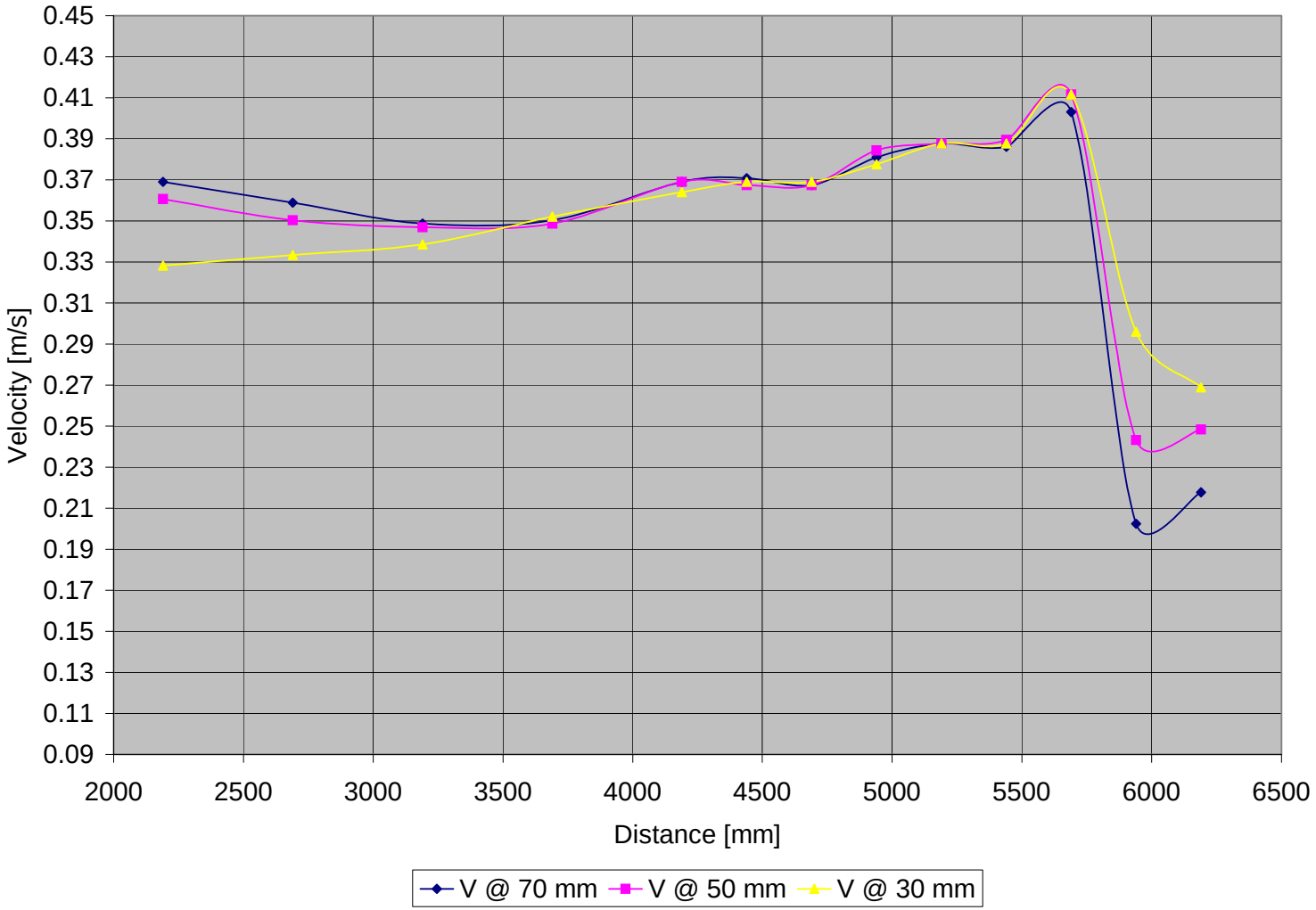

Figure B - 63: Test F1-Vertical velocity distribution measured at 200 mm from inner bank of bend

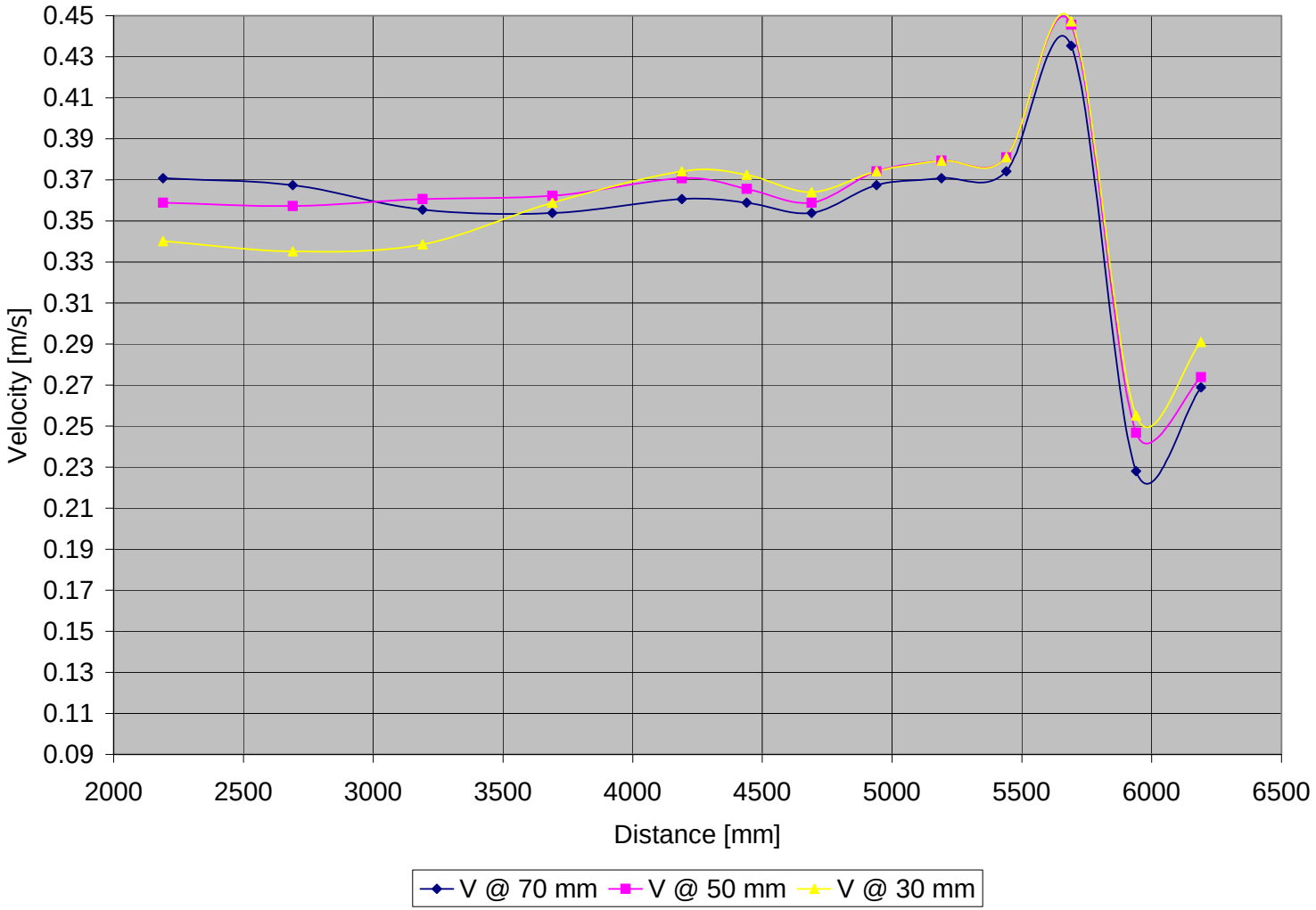

Figure B - 64: Test F1-Vertical velocity distribution measured at 250 mm from inner bank of bend

	Point	6	7	8	9	10	10A	11	11A	12	12A	13	13A	14
Width	**L**	**2190**	**2690**	**3190**	**3690**	**4190**	**4440**	**4690**	**4940**	**5190**	**5440**	**5690**	**5940**	**6190**
	h													
50	**70**	0.376	0.374	0.373	0.359	0.335	0.322	0.313	0.320	0.328	0.323	0.293	0.150	0.100
	50	0.369	0.366	0.367	0.361	0.349	0.344	0.337	0.345	0.356	0.350	0.325	0.221	0.126
	30	0.352	0.354	0.356	0.349	0.344	0.349	0.350	0.359	0.369	0.364	0.337	0.264	0.137
100	**70**	0.359	0.374	0.373	0.371	0.374	0.357	0.349	0.339	0.333	0.327	0.298	0.216	0.184
	50	0.350	0.366	0.367	0.362	0.376	0.371	0.356	0.362	0.361	0.354	0.328	0.269	0.230
	30	0.342	0.354	0.356	0.340	0.367	0.367	0.367	0.378	0.381	0.374	0.347	0.286	0.254
150	**70**	0.342	0.342	0.333	0.350	0.383	0.379	0.344	0.384	0.383	0.378	0.350	0.208	0.203
	50	0.323	0.323	0.325	0.342	0.373	0.376	0.373	0.388	0.391	0.386	0.378	0.242	0.230
	30	0.301	0.305	0.316	0.337	0.362	0.369	0.371	0.384	0.395	0.388	0.378	0.267	0.260
200	**70**	0.369	0.359	0.349	0.350	0.369	0.371	0.367	0.381	0.388	0.386	0.403	0.203	0.218
	50	0.361	0.350	0.347	0.349	0.369	0.367	0.367	0.384	0.388	0.390	0.412	0.243	0.248
	30	0.328	0.333	0.339	0.352	0.364	0.369	0.369	0.378	0.388	0.388	0.412	0.296	0.269
250														
	70	0.371	0.367	0.356	0.354	0.361	0.359	0.354	0.367	0.371	0.374	0.435	0.228	0.269
	50	0.359	0.357	0.361	0.362	0.371	0.366	0.359	0.374	0.379	0.381	0.446	0.247	0.274
	30	0.340	0.335	0.339	0.359	0.374	0.373	0.364	0.374	0.379	0.381	0.447	0.255	0.291

Table B - 8: Test F1- Measured velocities [m/s]

B.3.2 TEST F2 (F_R = 0.5)

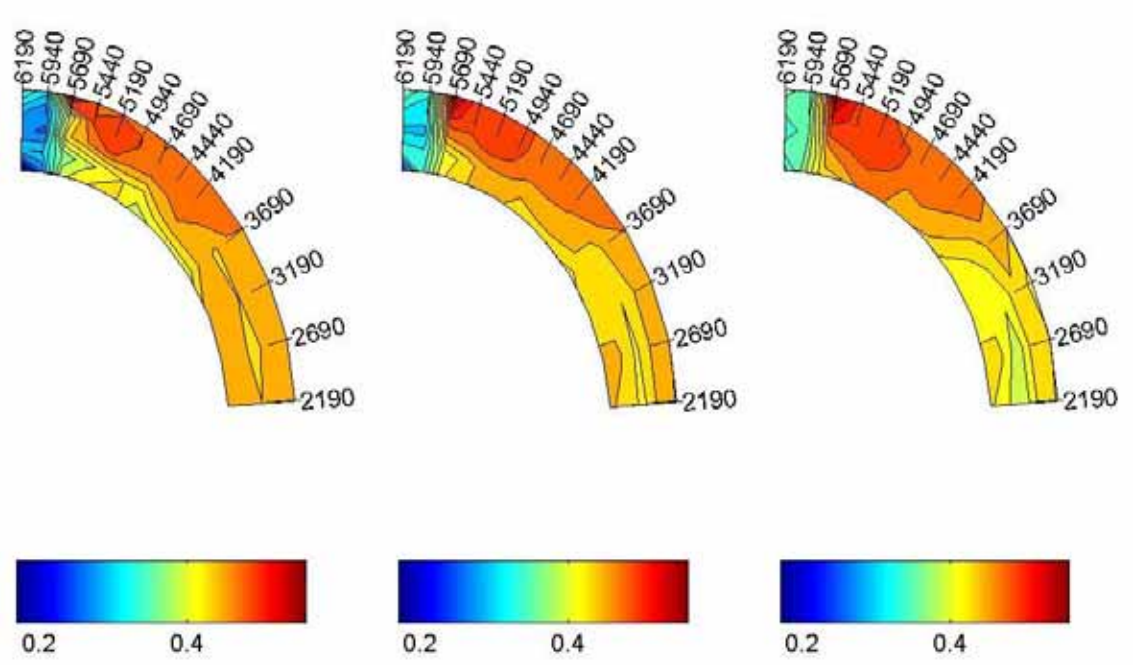

Figure B - 65: Test F2-Velocity distribution in the horizontal plane measured at 70, 50 and 30 mm

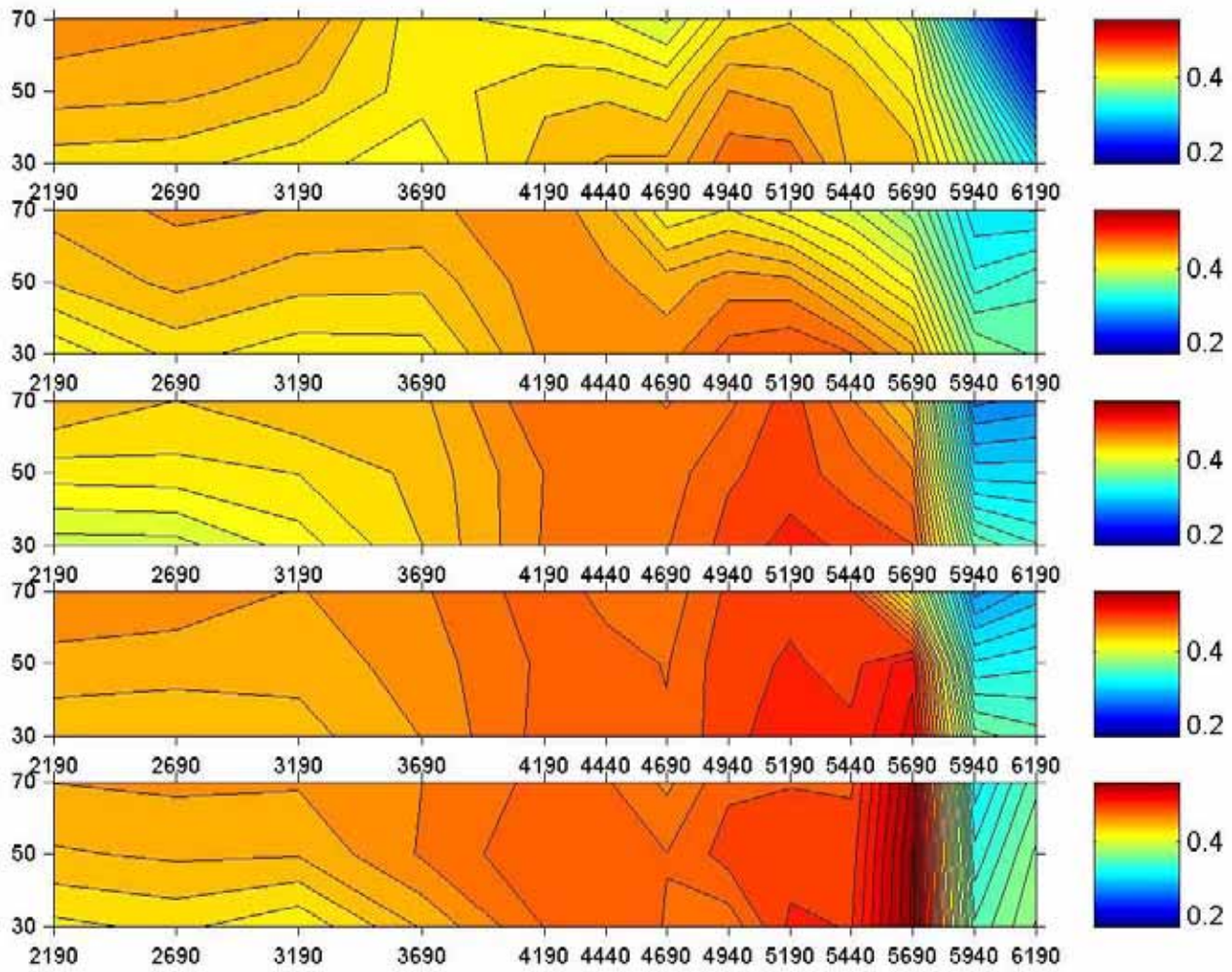

Figure B - 66: Test F2-Velocity distribution in the vertical plane

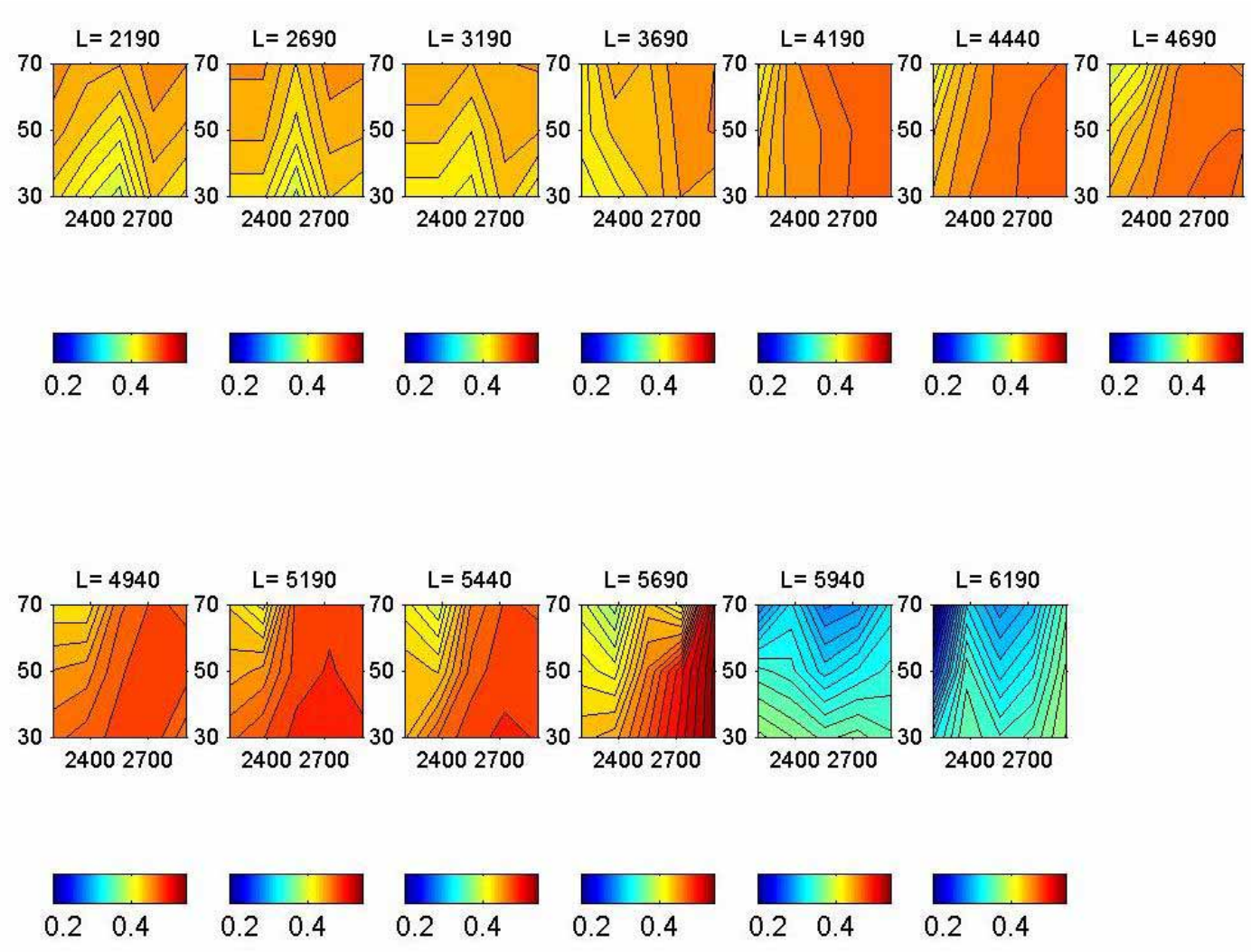

Figure B - 67: Test F2-Cross-sectional velocity distribution

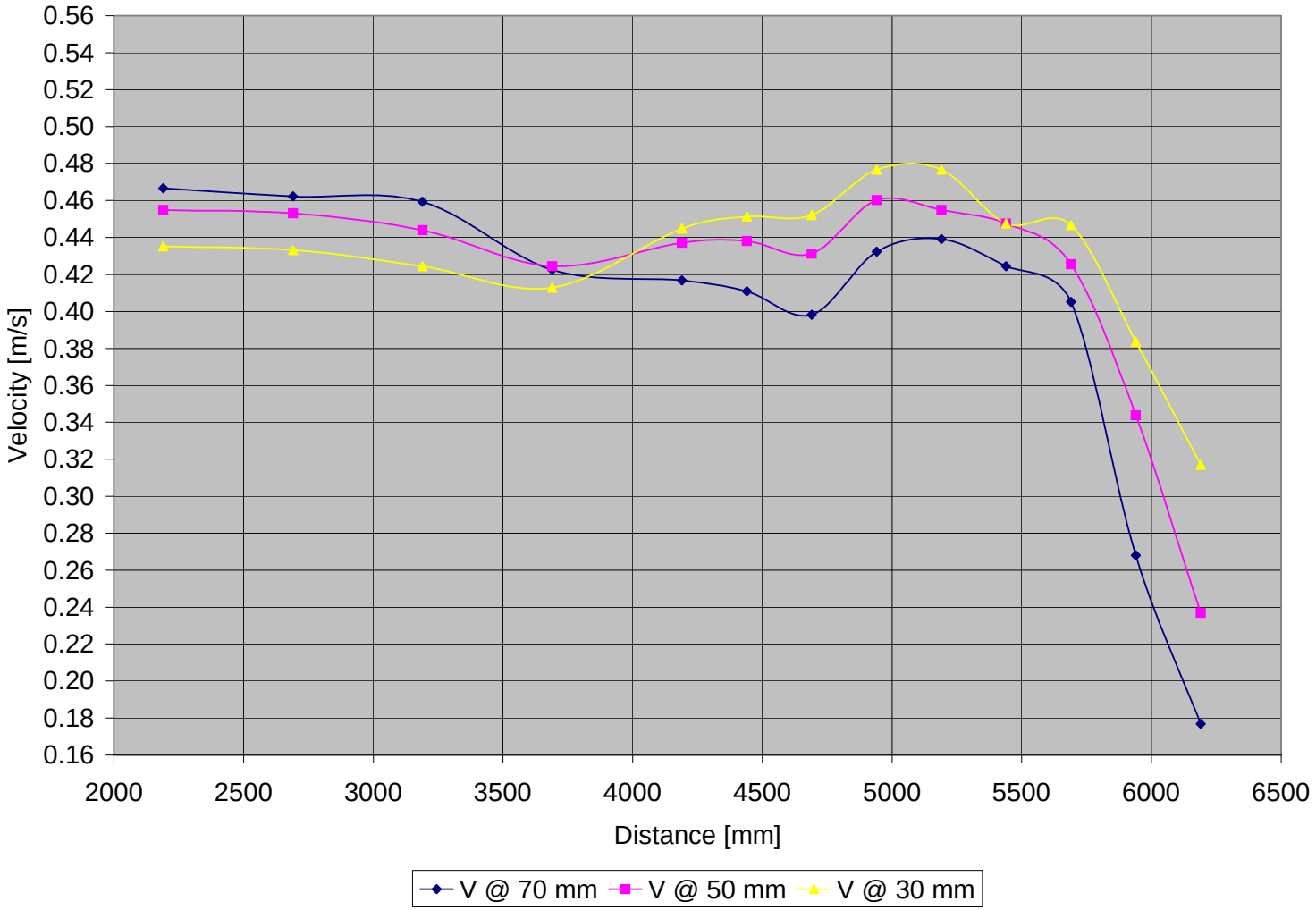

Figure B - 68: Test F2-Vertical velocity distribution measured at 50 mm from inner bank of bend

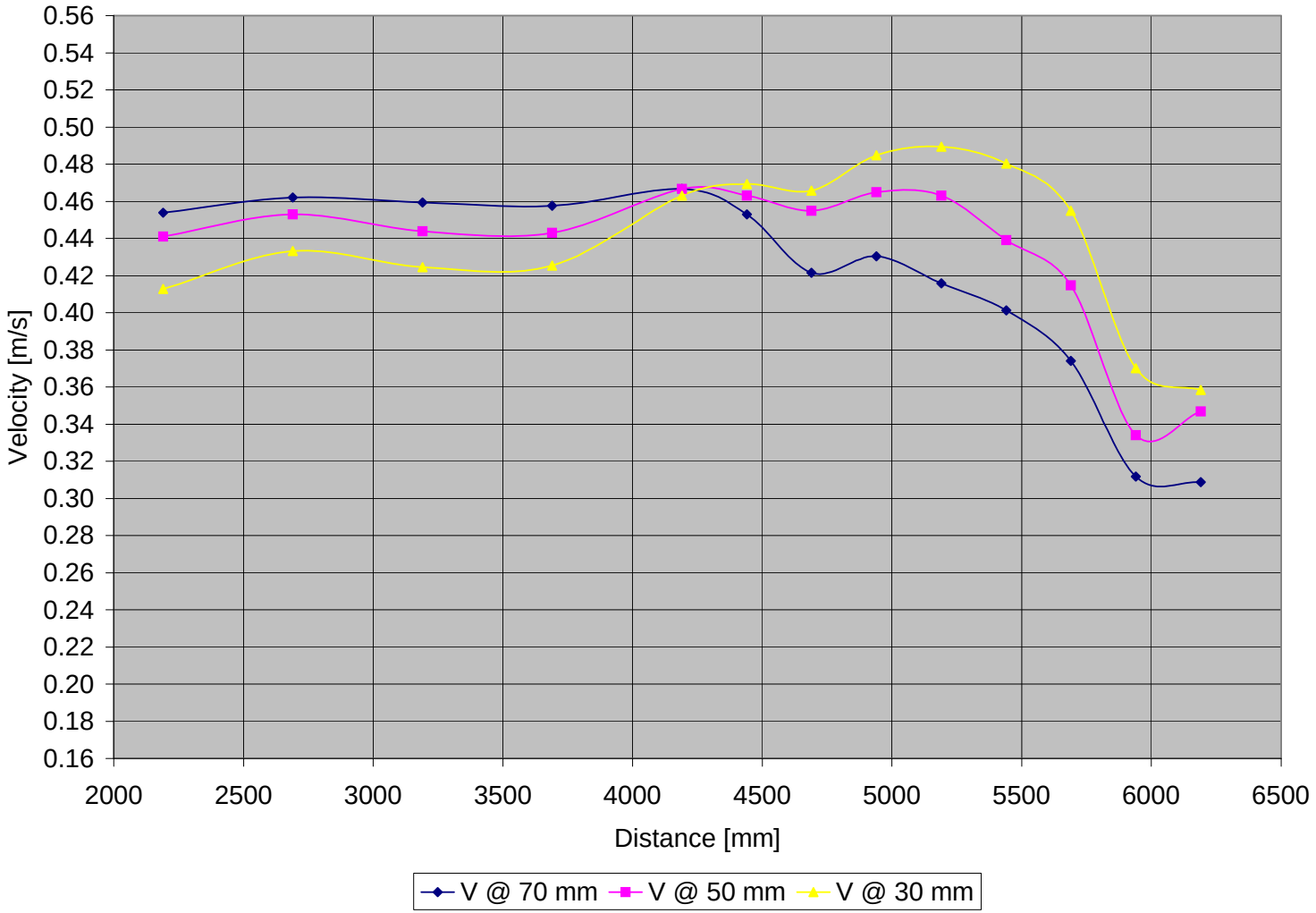

Figure B - 69: Test F2-Vertical velocity distribution measured at 100 mm from inner bank of bend

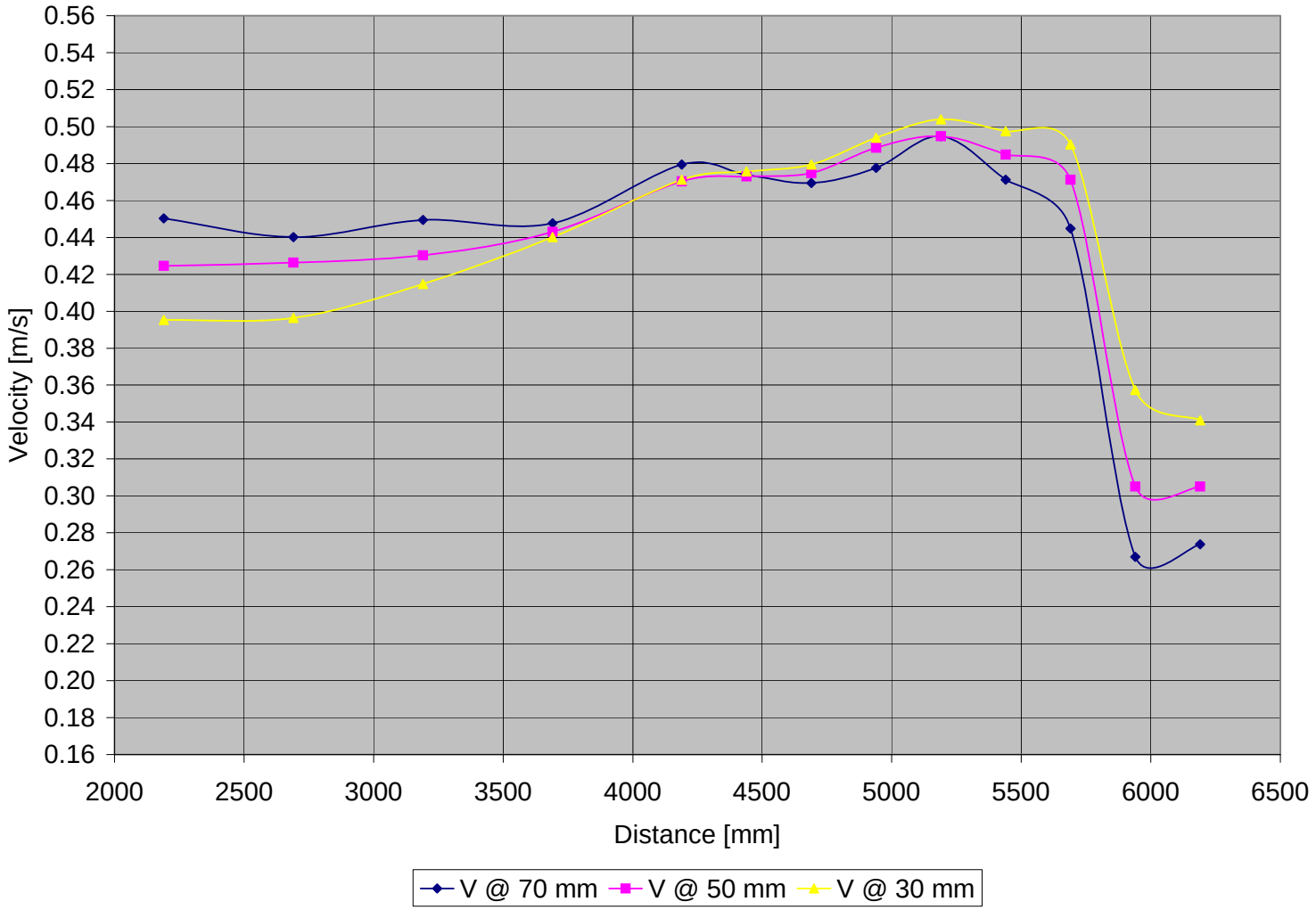

Figure B - 70: Test F2-Vertical velocity distribution measured at 150 mm from inner bank of bend

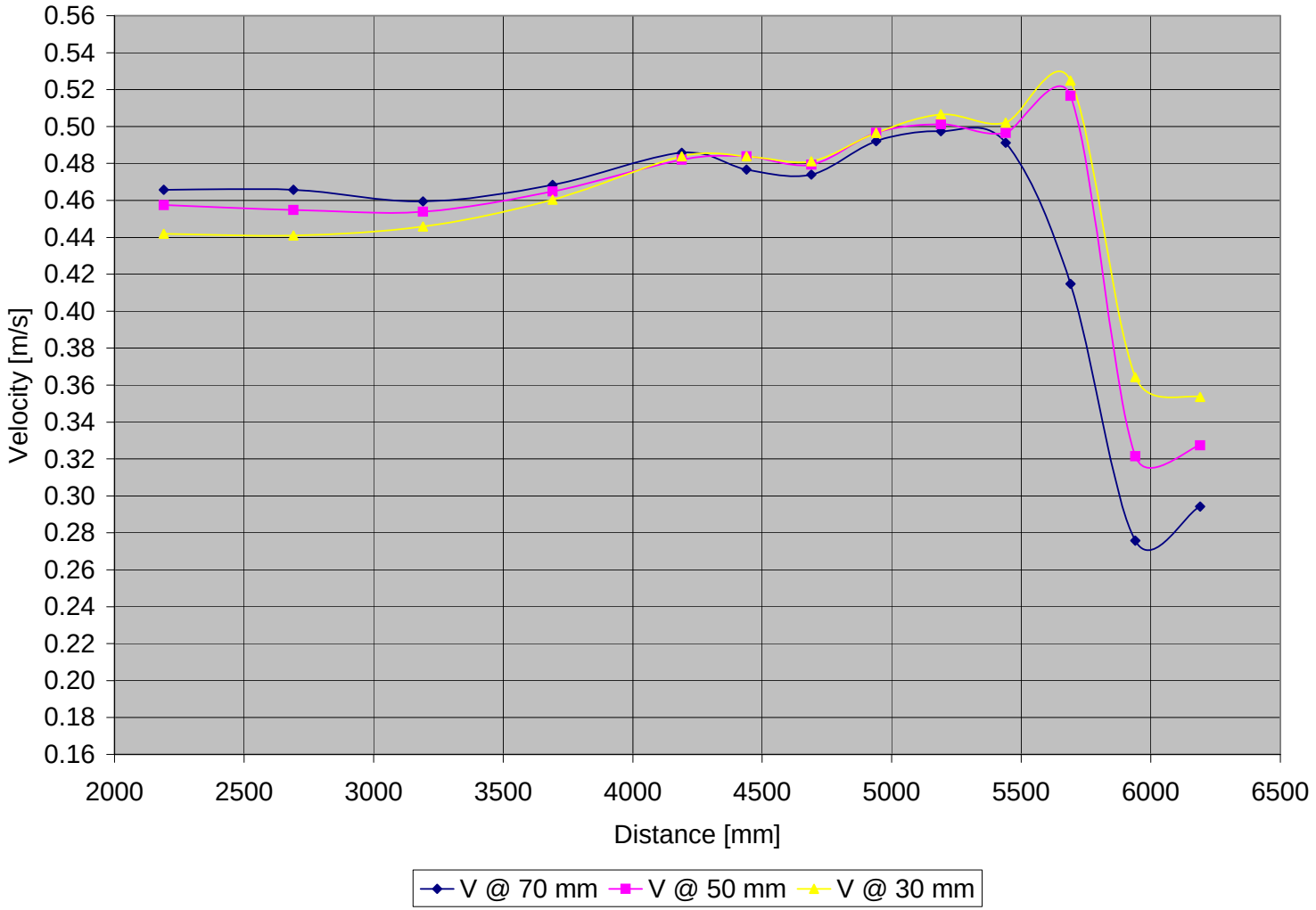

Figure B - 71: Test F2-Vertical velocity distribution measured at 200 mm from inner bank of bend

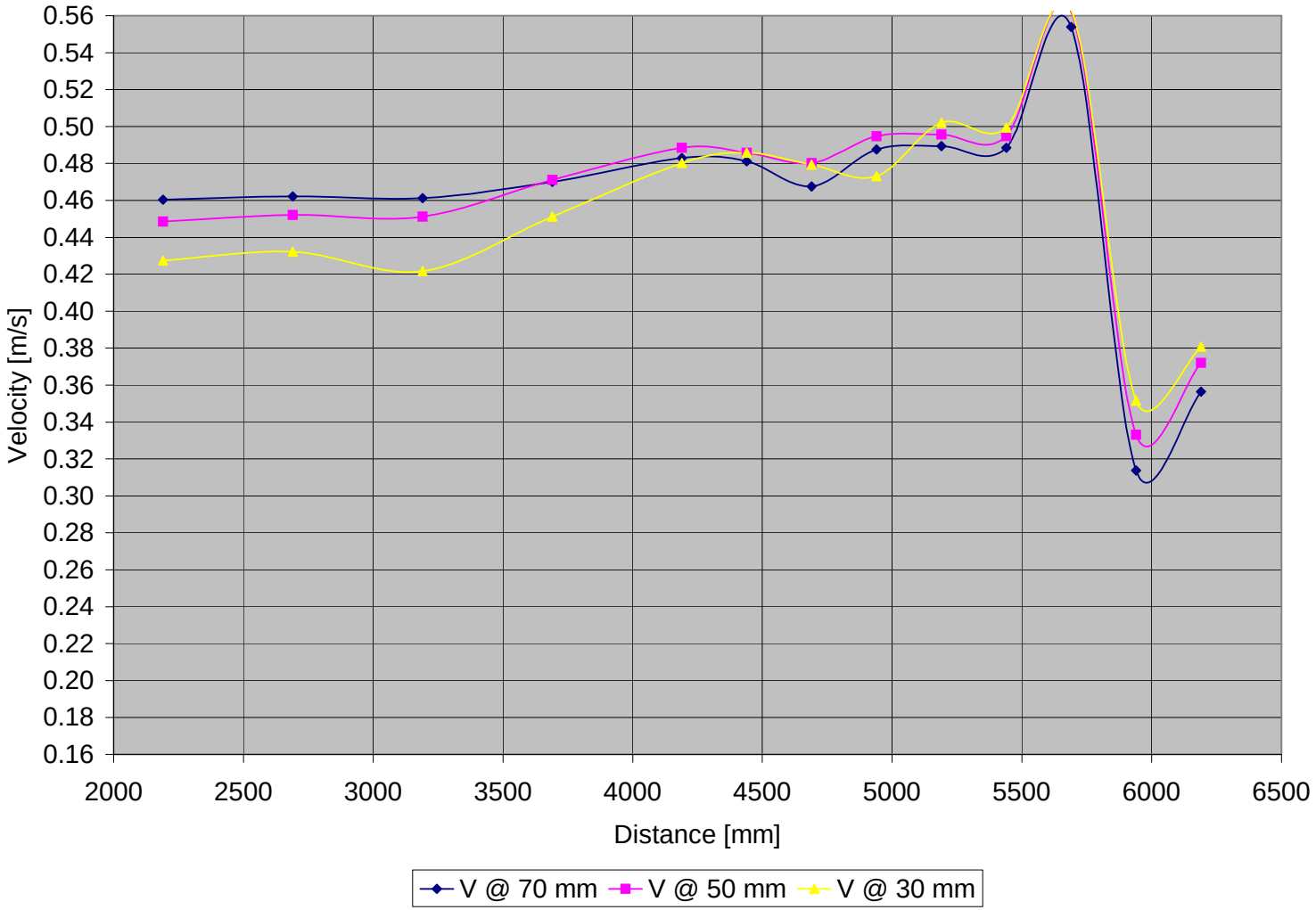

Figure B - 72: Test F2-Vertical velocity distribution measured at 250 mm from inner bank of bend

	Point	6	7	8	9	10	10A	11	11A	12	12A	13	13A	14
Width	L	2190	2690	3190	3690	4190	4440	4690	4940	5190	5440	5690	5940	6190
	h													
50	70	0.467	0.462	0.459	0.423	0.417	0.411	0.398	0.432	0.439	0.424	0.405	0.268	0.177
	50	0.455	0.453	0.444	0.424	0.437	0.438	0.431	0.460	0.455	0.448	0.425	0.344	0.237
	30	0.435	0.433	0.424	0.413	0.445	0.451	0.452	0.477	0.477	0.448	0.447	0.384	0.317
100	70	0.454	0.462	0.459	0.458	0.467	0.453	0.422	0.430	0.416	0.401	0.374	0.312	0.309
	50	0.441	0.453	0.444	0.443	0.467	0.463	0.455	0.465	0.463	0.439	0.415	0.334	0.347
	30	0.413	0.433	0.424	0.425	0.463	0.469	0.466	0.485	0.489	0.480	0.455	0.370	0.358
150	70	0.450	0.440	0.449	0.448	0.479	0.474	0.469	0.478	0.495	0.471	0.445	0.267	0.274
	50	0.424	0.426	0.430	0.443	0.470	0.473	0.475	0.488	0.495	0.485	0.471	0.305	0.305
	30	0.395	0.396	0.415	0.440	0.471	0.476	0.479	0.494	0.504	0.498	0.490	0.357	0.341
200	70	0.466	0.466	0.459	0.468	0.486	0.477	0.474	0.492	0.498	0.491	0.415	0.276	0.294
	50	0.458	0.455	0.454	0.465	0.482	0.484	0.479	0.497	0.501	0.497	0.517	0.322	0.327
	30	0.442	0.441	0.446	0.460	0.484	0.484	0.481	0.497	0.507	0.502	0.525	0.364	0.354
250														
	70	0.460	0.462	0.461	0.470	0.483	0.481	0.468	0.488	0.489	0.488	0.554	0.314	0.356
	50	0.448	0.452	0.451	0.471	0.488	0.486	0.480	0.495	0.496	0.495	0.562	0.333	0.372
	30	0.427	0.432	0.422	0.451	0.480	0.486	0.479	0.473	0.502	0.499	0.563	0.352	0.381

Table B - 9: Test F2- Measured velocities [m/s]

B.3.3 TEST F3 (F_R = 0.7)

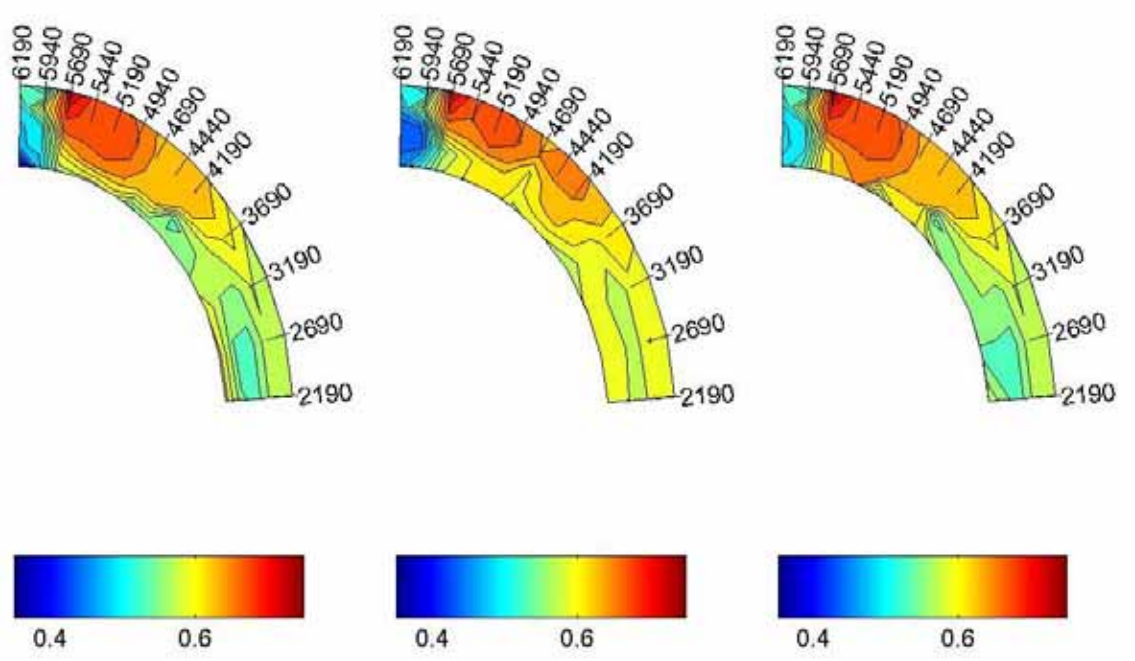

Figure B - 73: Test F3-Velocity distribution in the horizontal plane measured at 70, 50 and 30 mm

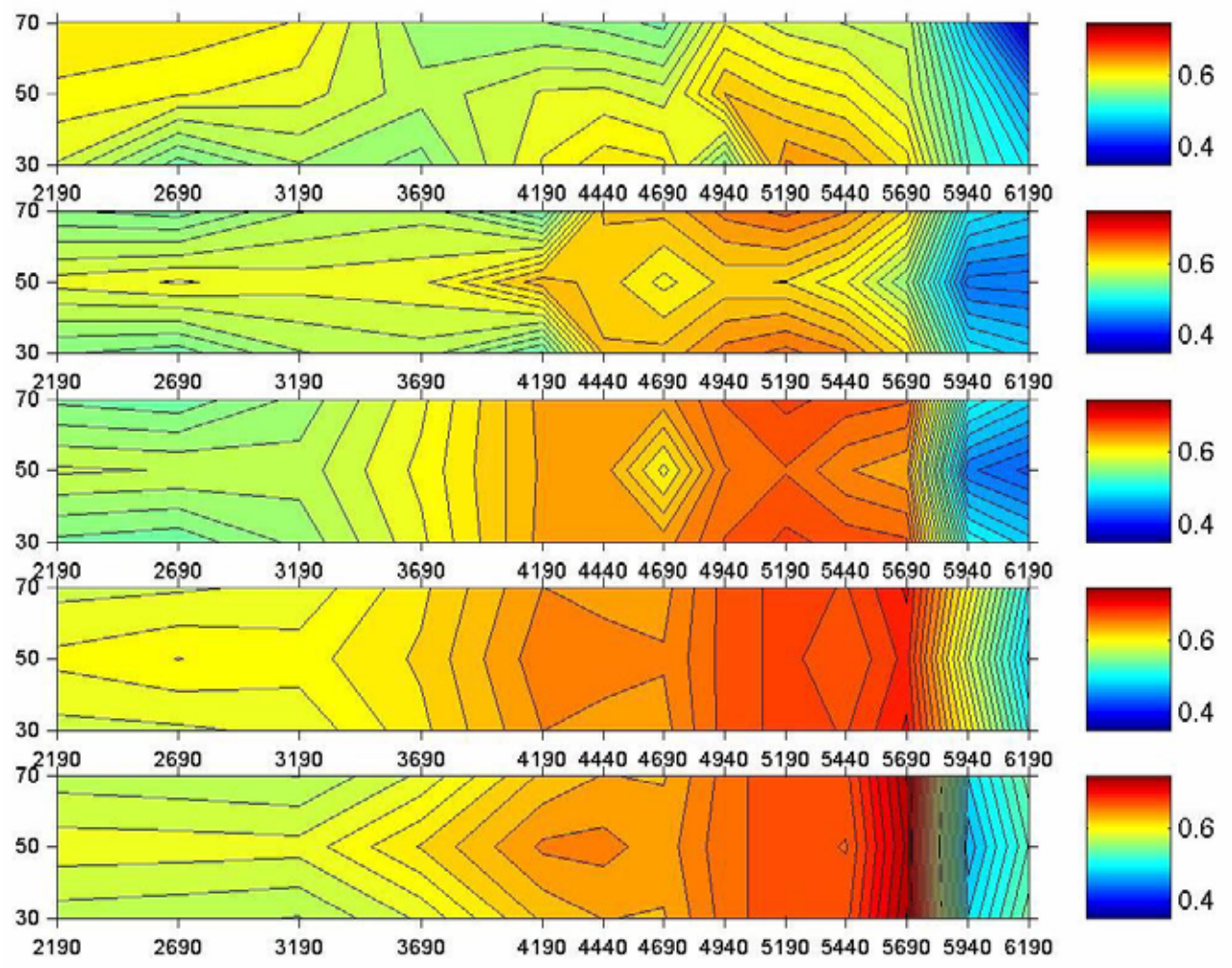

Figure B - 74: Test F3-Velocity distribution in the vertical plane

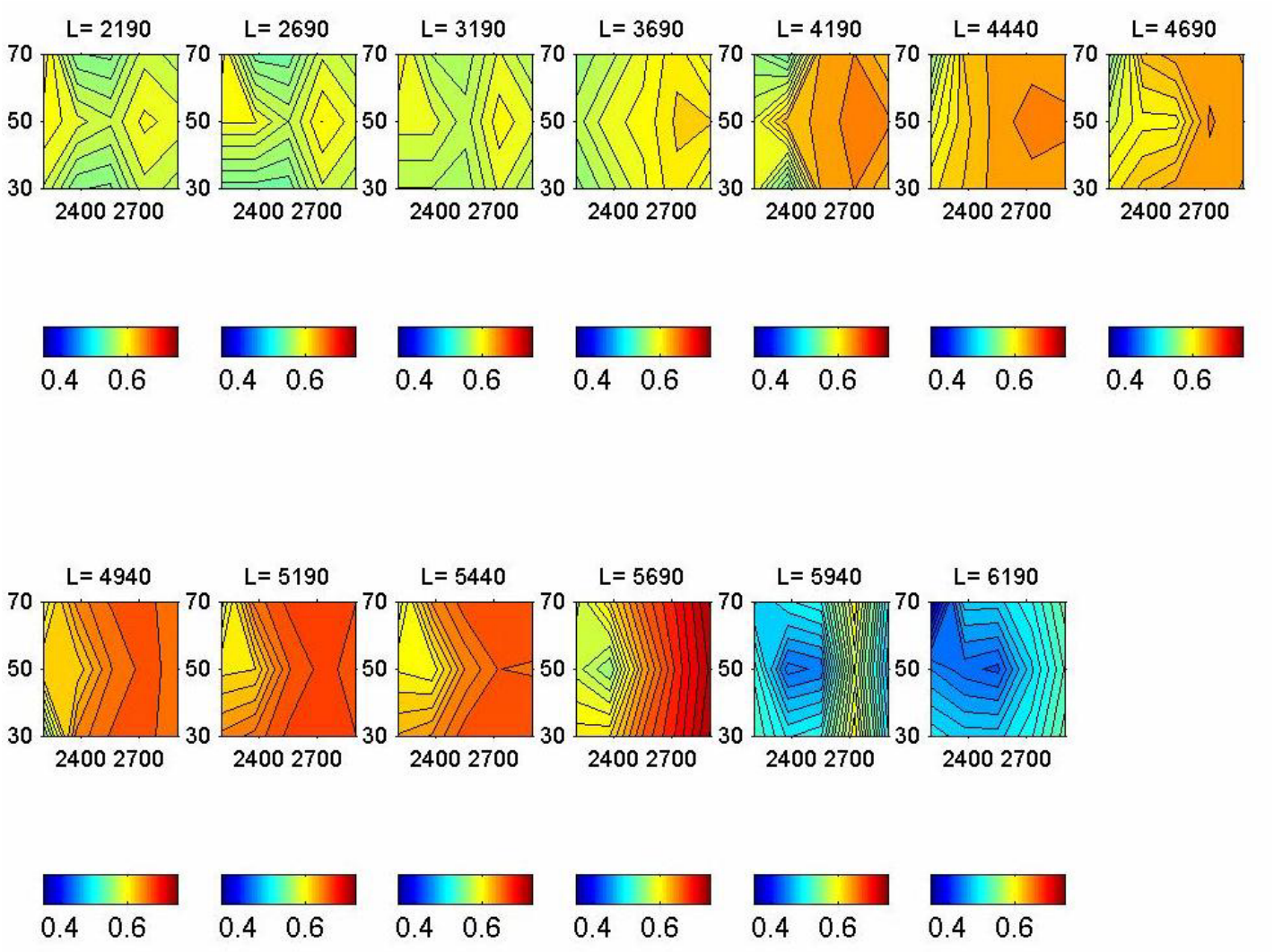

Figure B - 75: Test F3-Cross-sectional velocity distribution

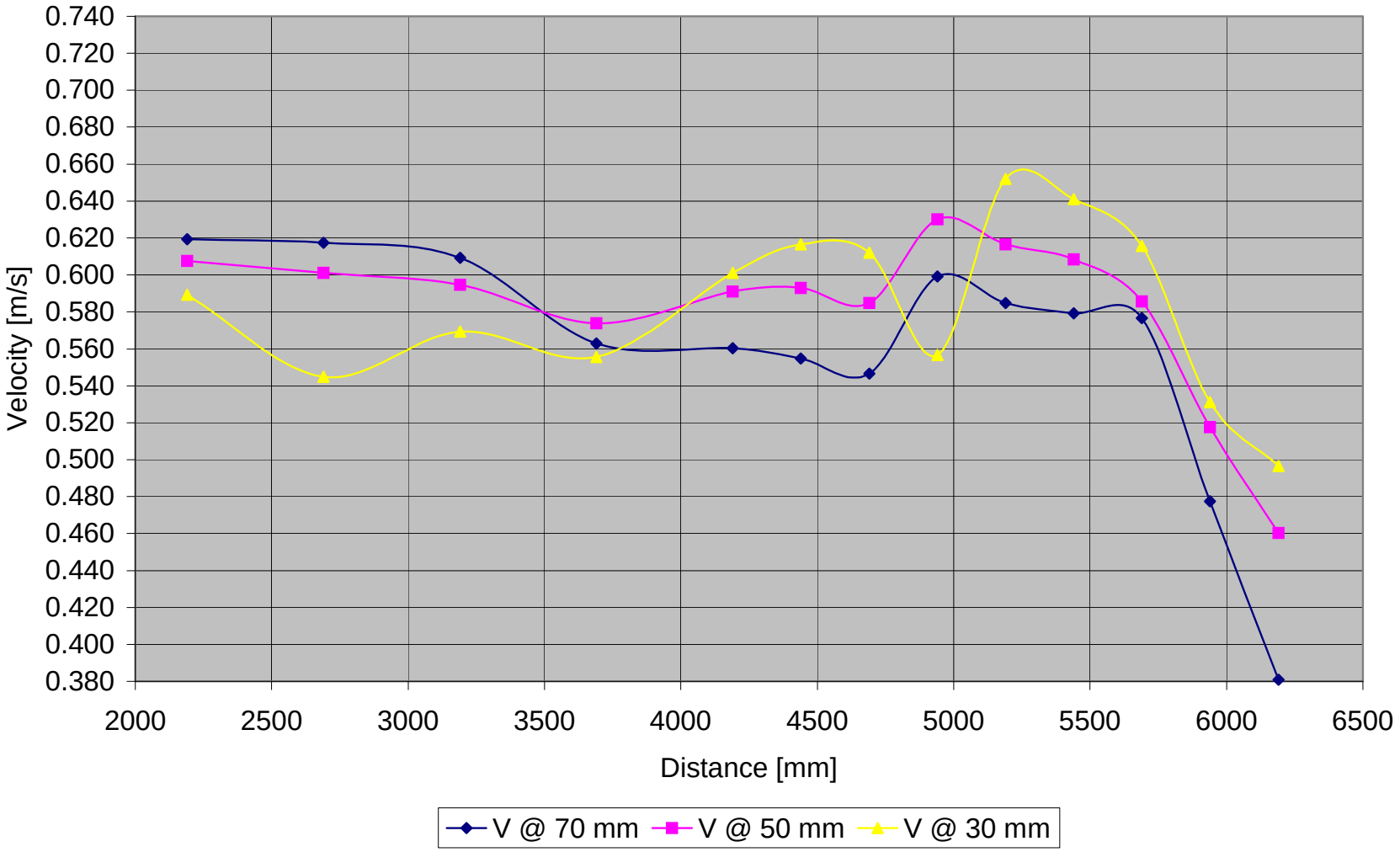

Figure B - 76: Test F3-Vertical velocity distribution measured at 50 mm from inner bank of bend

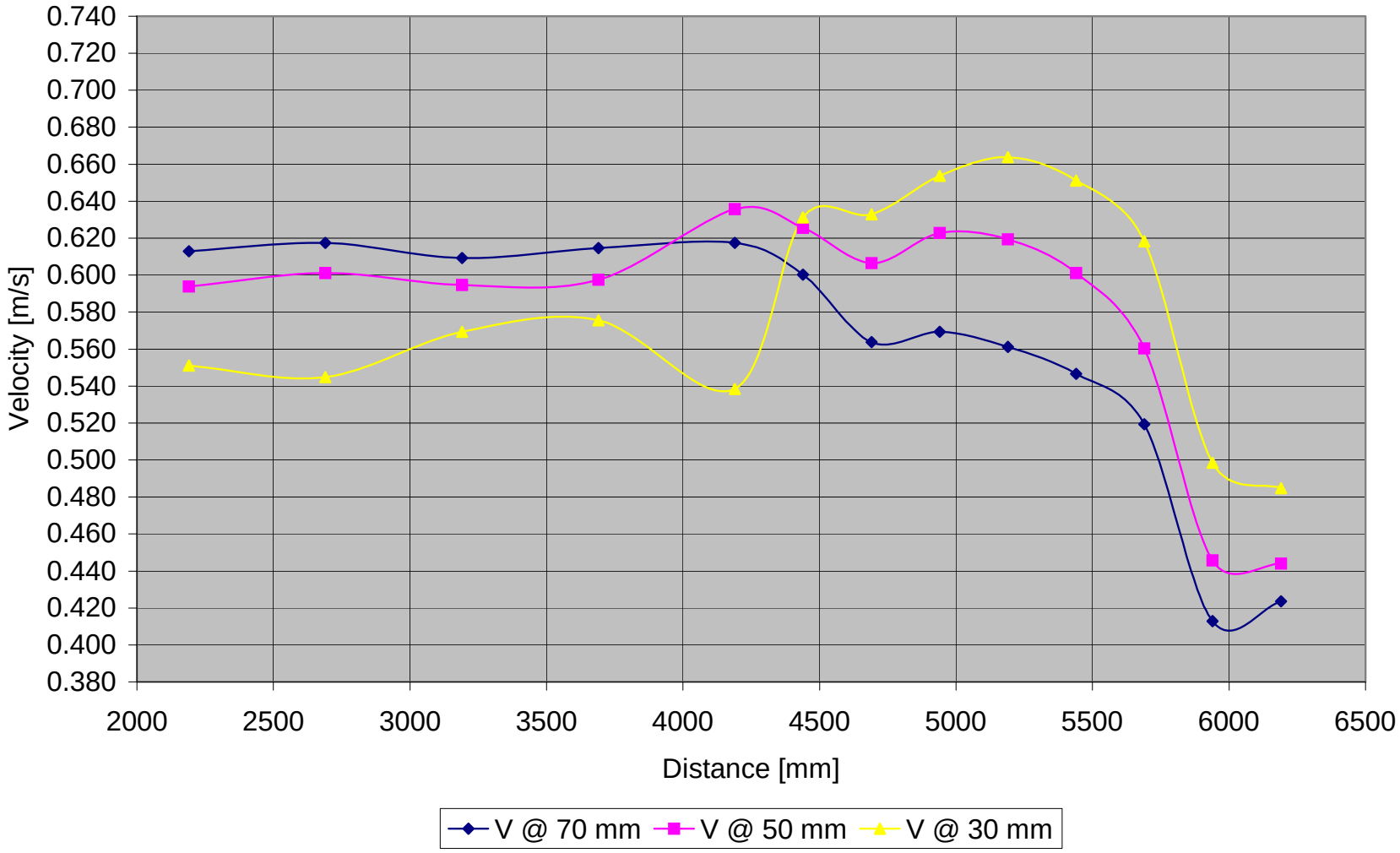

Figure B - 77: Test F3-Vertical velocity distribution measured at 100 mm from inner bank of bend

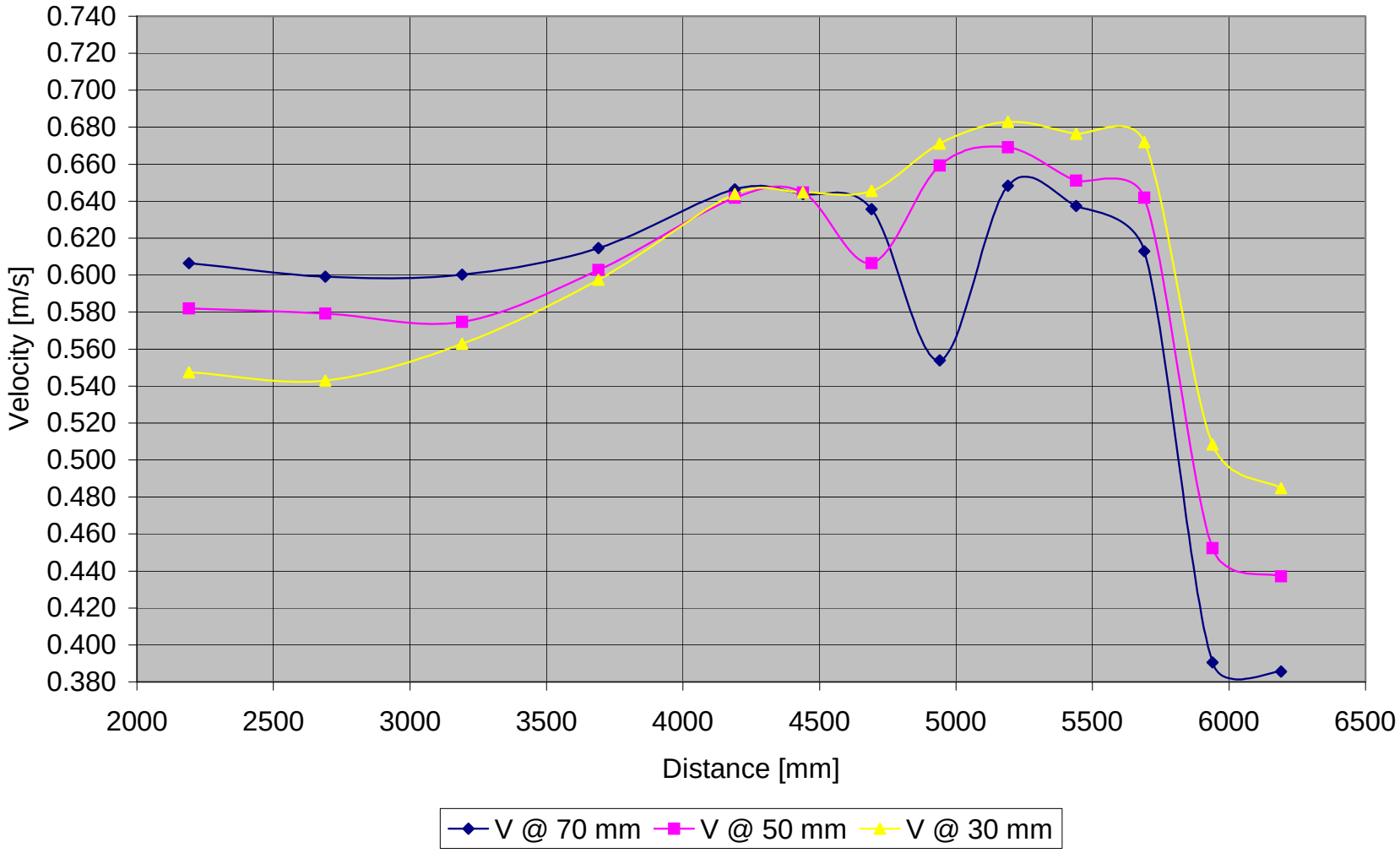

Figure B - 78: Test F3-Vertical velocity distribution measured at 150 mm from inner bank of bend

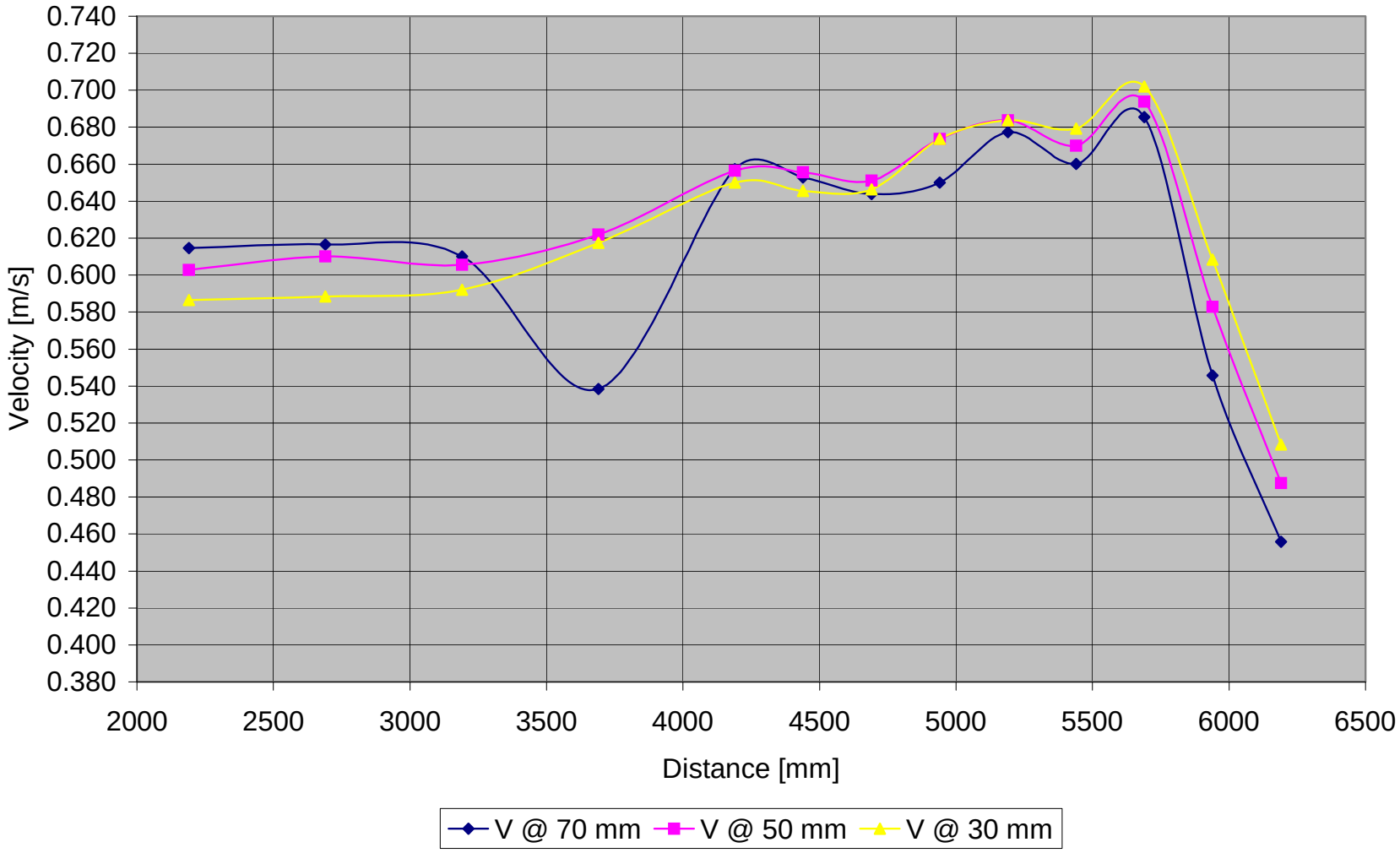

Figure B - 79: Test F3-Vertical velocity distribution measured at 200 mm from inner bank of bend

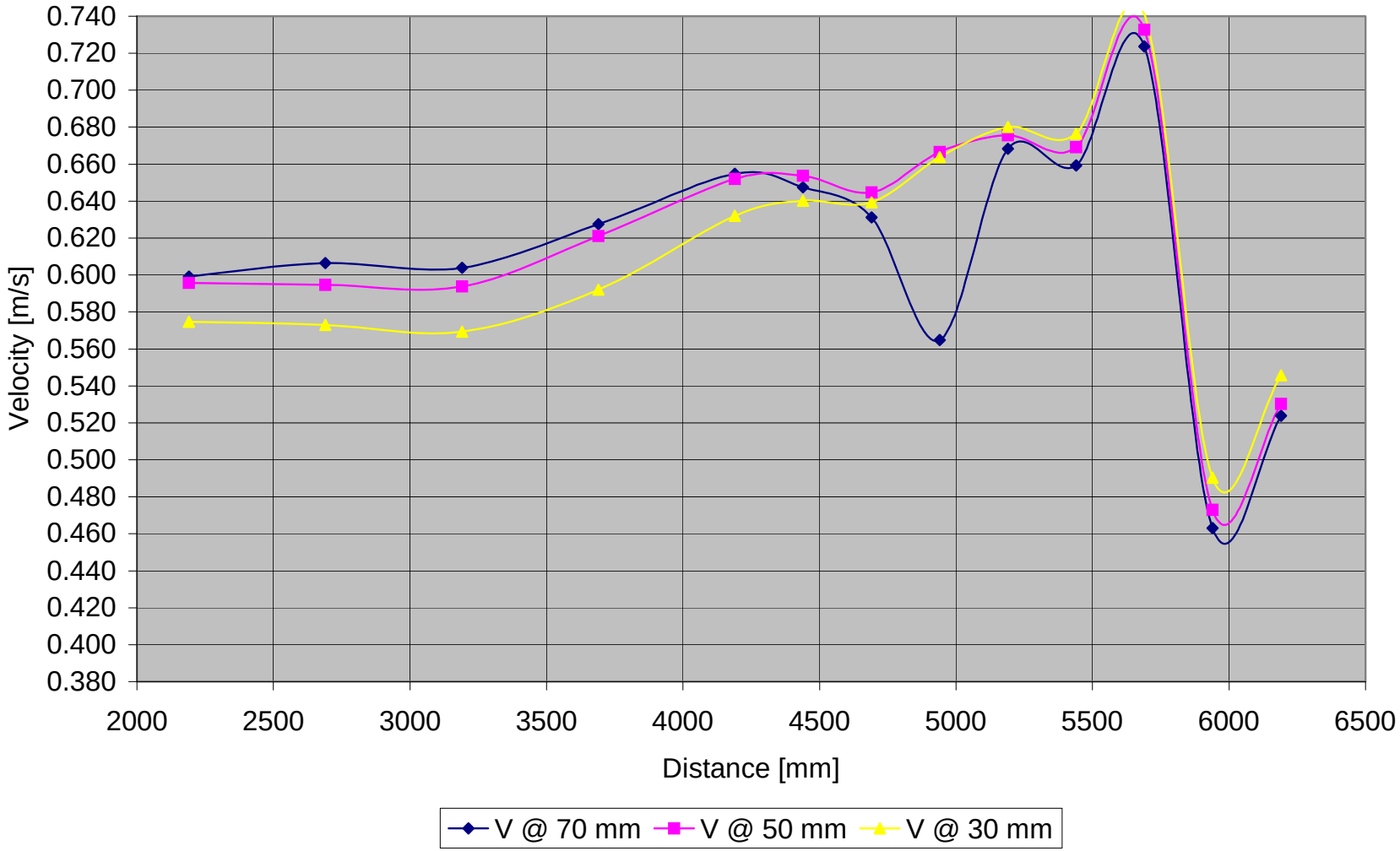

Figure B - 80: Test F3-Vertical velocity distribution measured at 250 mm from inner bank of bend

	Point	6	7	8	9	10	10A	11	11A	12	12A	13	13A	14
Width	**L**	**2190**	**2690**	**3190**	**3690**	**4190**	**4440**	**4690**	**4940**	**5190**	**5440**	**5690**	**5940**	**6190**
	h													
50	**70**	0.619	0.617	0.609	0.563	0.560	0.555	0.547	0.599	0.585	0.579	0.577	0.478	0.381
	50	0.607	0.601	0.595	0.574	0.591	0.593	0.585	0.630	0.617	0.608	0.586	0.518	0.460
	30	0.589	0.545	0.569	0.556	0.601	0.617	0.612	0.557	0.652	0.641	0.616	0.531	0.497
100	**70**	0.613	0.617	0.609	0.615	0.617	0.600	0.564	0.569	0.561	0.547	0.519	0.413	0.424
	50	0.594	0.601	0.595	0.597	0.636	0.626	0.607	0.623	0.619	0.601	0.560	0.446	0.444
	30	0.551	0.545	0.569	0.576	0.538	0.631	0.633	0.654	0.664	0.651	0.618	0.498	0.485
150	**70**	0.607	0.599	0.600	0.615	0.647	0.644	0.636	0.554	0.648	0.637	0.613	0.390	0.386
	50	0.582	0.579	0.575	0.603	0.642	0.645	0.607	0.659	0.669	0.651	0.642	0.452	0.437
	30	0.548	0.543	0.563	0.597	0.644	0.645	0.646	0.671	0.683	0.676	0.672	0.508	0.485
200	**70**	0.615	0.617	0.610	0.538	0.657	0.653	0.644	0.650	0.677	0.660	0.686	0.546	0.456
	50	0.603	0.610	0.606	0.622	0.657	0.656	0.651	0.674	0.684	0.670	0.694	0.583	0.488
	30	0.587	0.588	0.592	0.617	0.650	0.646	0.647	0.674	0.684	0.679	0.702	0.608	0.508
250														
	70	0.599	0.607	0.604	0.627	0.655	0.647	0.631	0.565	0.668	0.659	0.724	0.463	0.524
	50	0.596	0.595	0.594	0.621	0.652	0.654	0.645	0.666	0.676	0.669	0.733	0.473	0.530
	30	0.575	0.573	0.569	0.592	0.632	0.640	0.639	0.664	0.680	0.676	0.741	0.490	0.546

Table B - 10: Test F3- Measured velocities [m/s]

B.3.4 TEST F4 (F_R = 0.3 ; DDR = 0)

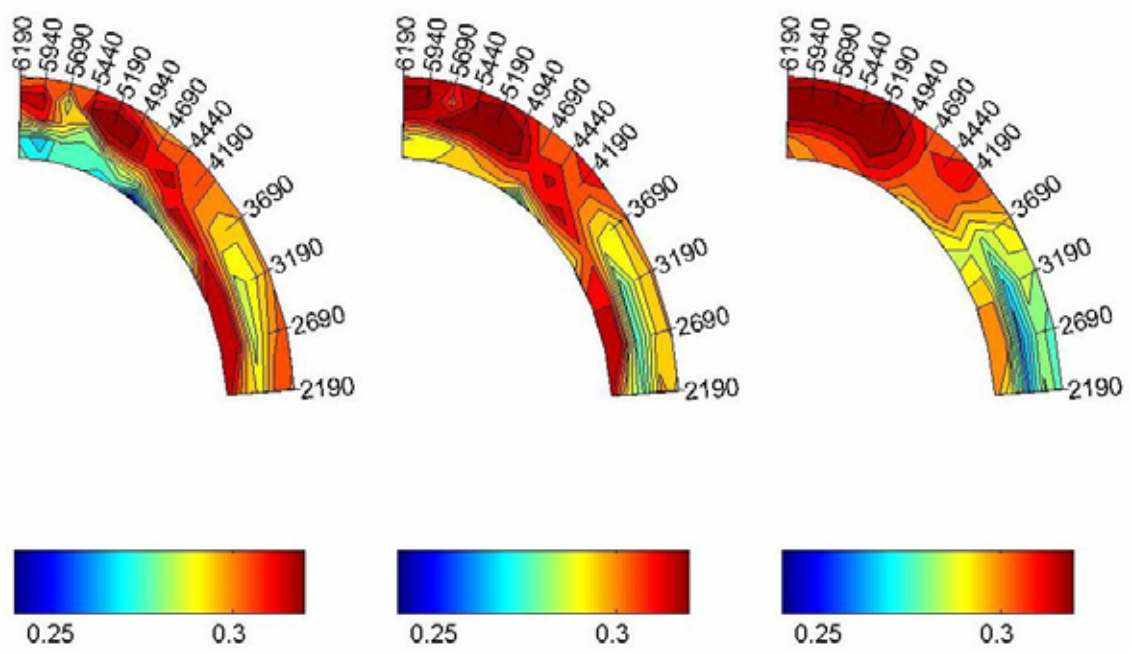

Figure B - 81: Test F4-Velocity distribution in the horizontal plane measured at 70, 50 and 30 mm

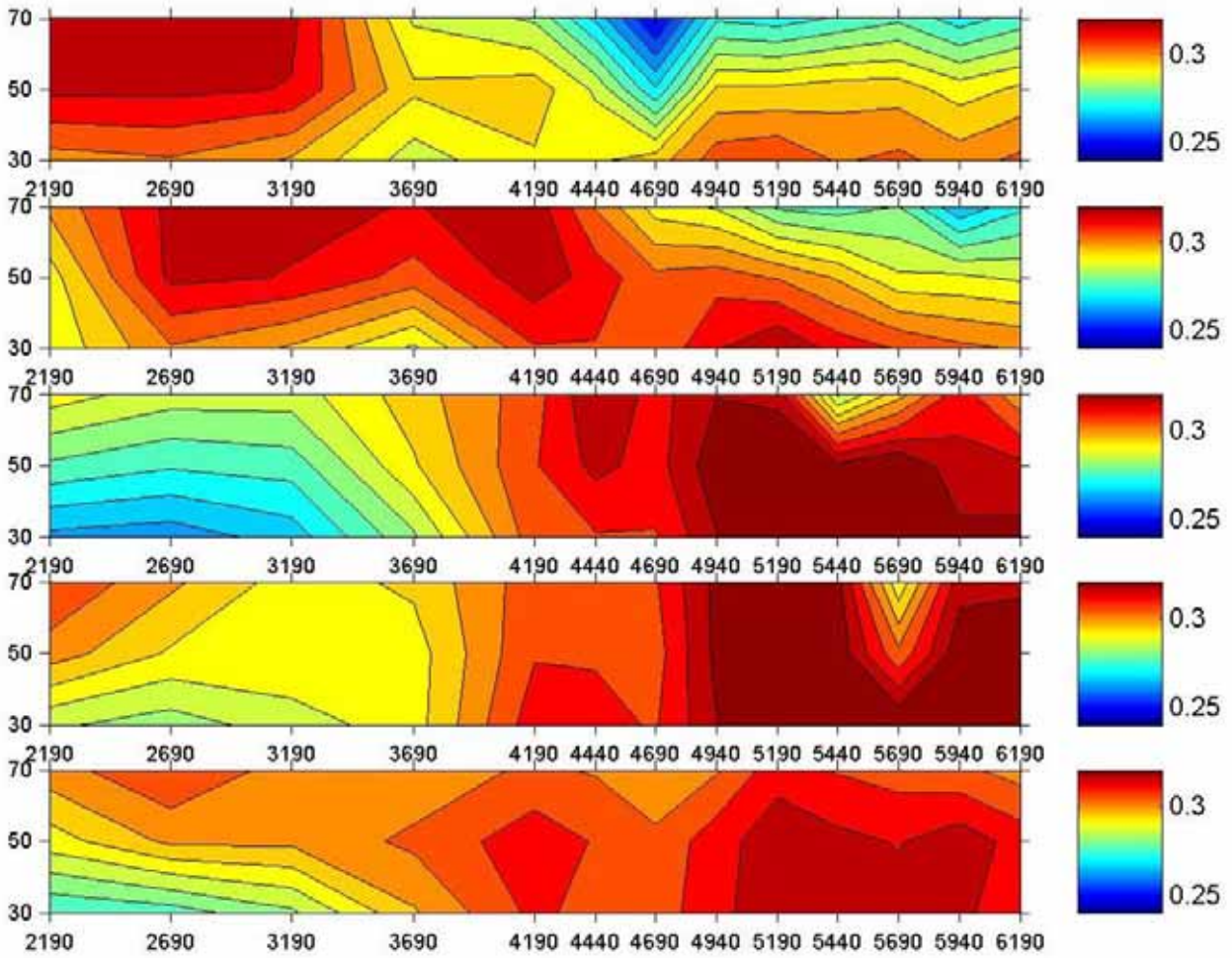

Figure B - 82: Test F4-Velocity distribution in the vertical plane

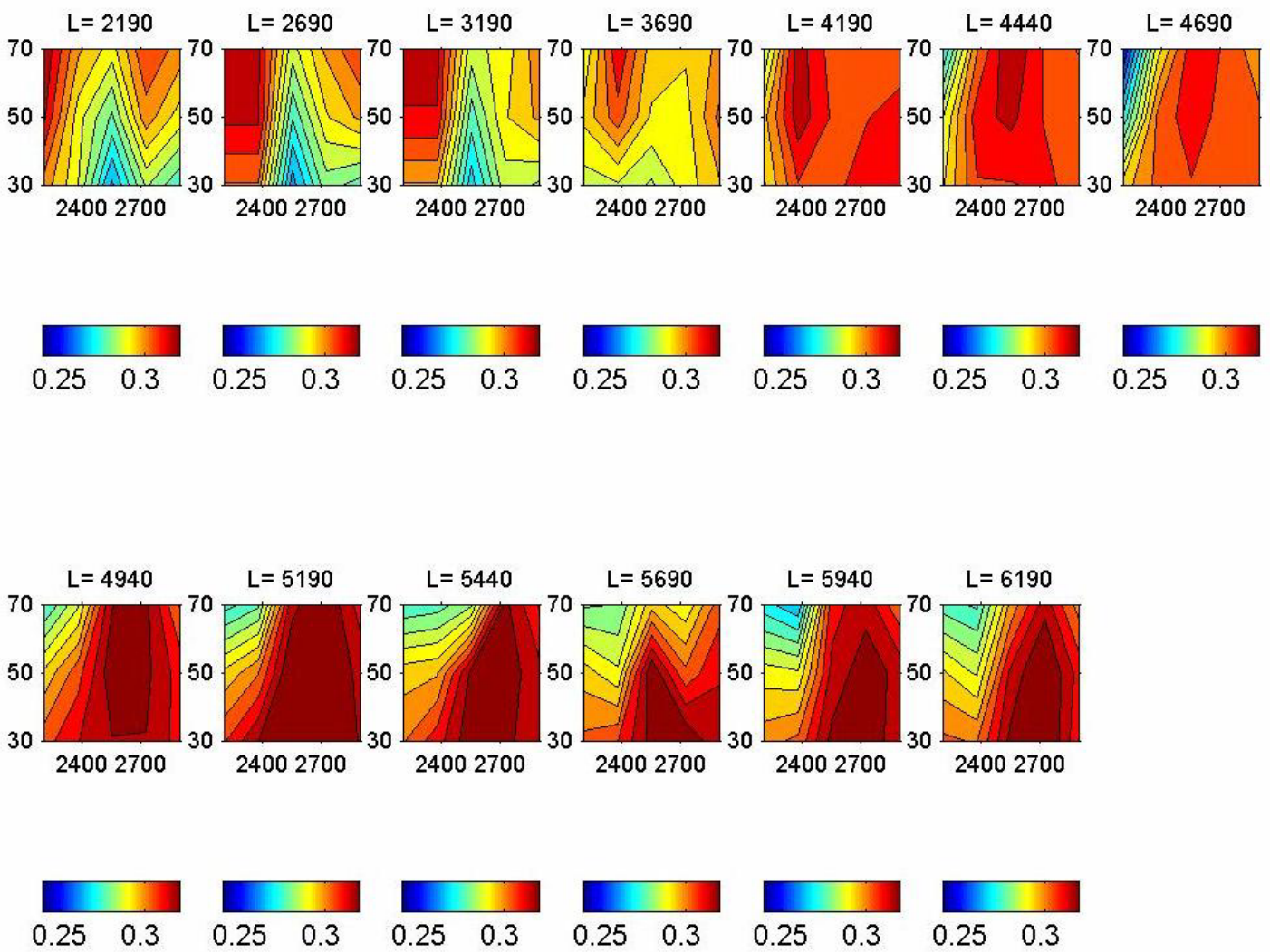

Figure B - 83: Test F4-Cross-sectional velocity distribution

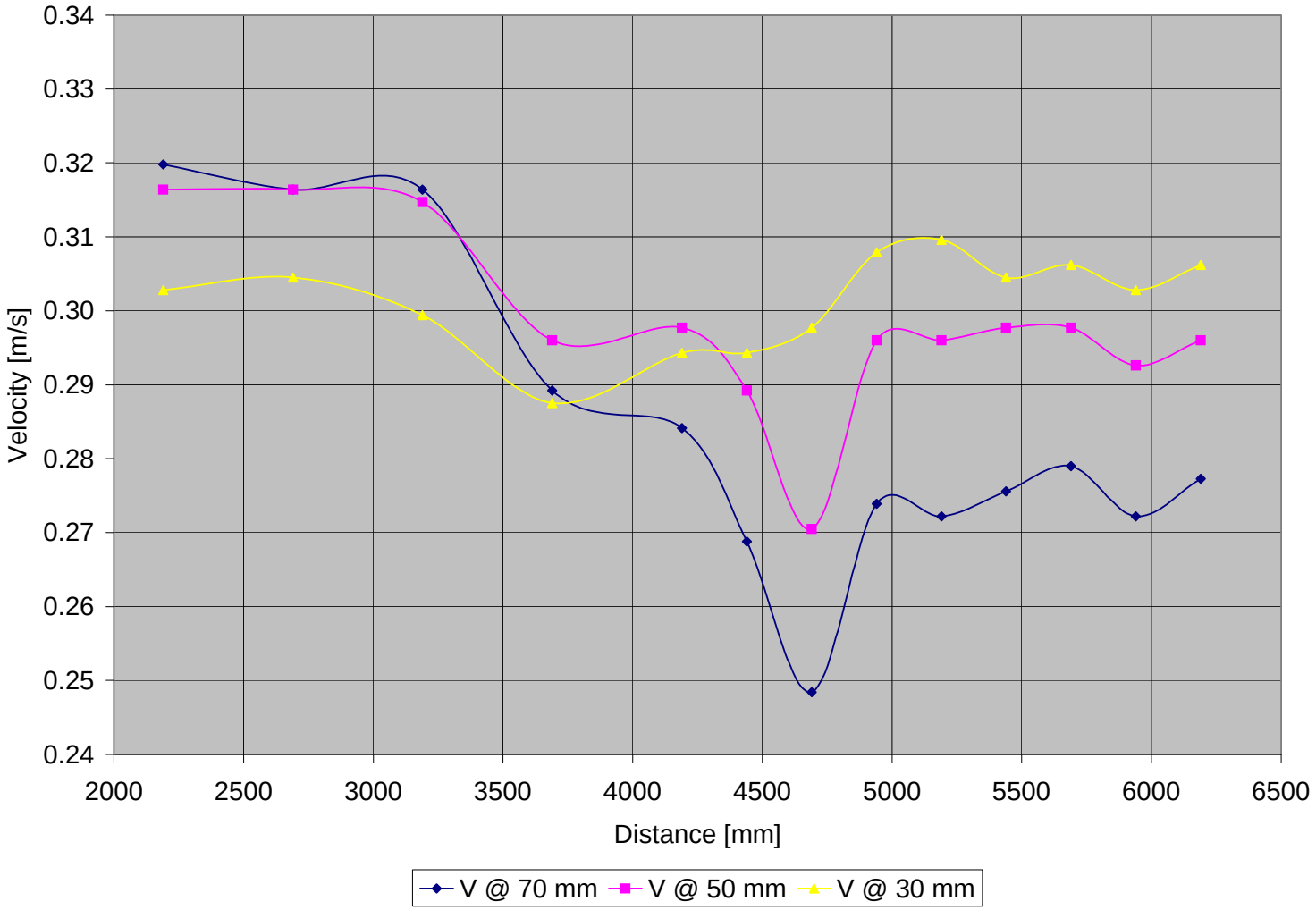

Figure B - 84: Test F4-Vertical velocity distribution measured at 50 mm from inner bank of bend

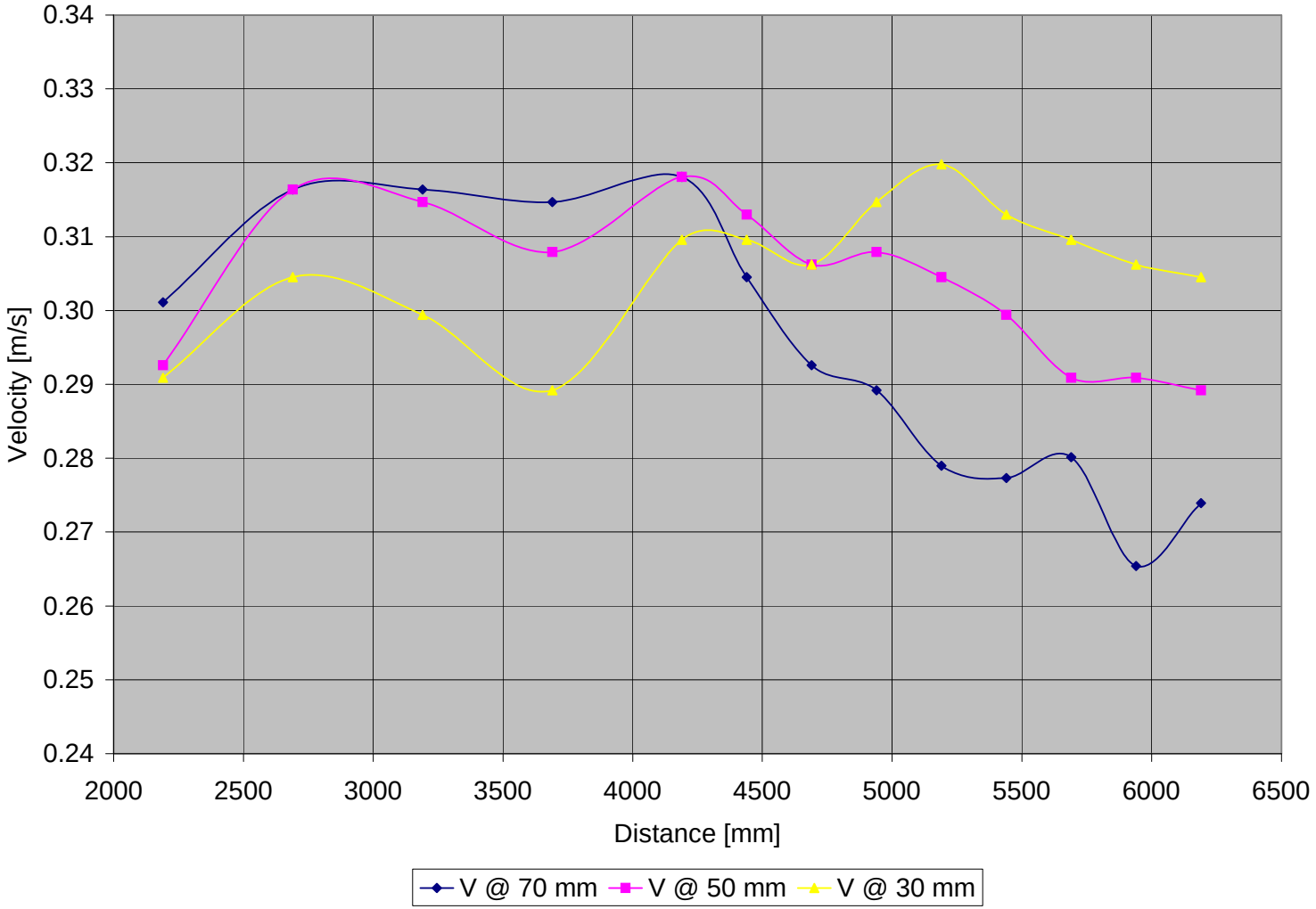

Figure B - 85: Test F4-Vertical velocity distribution measured at 100 mm from inner bank of bend

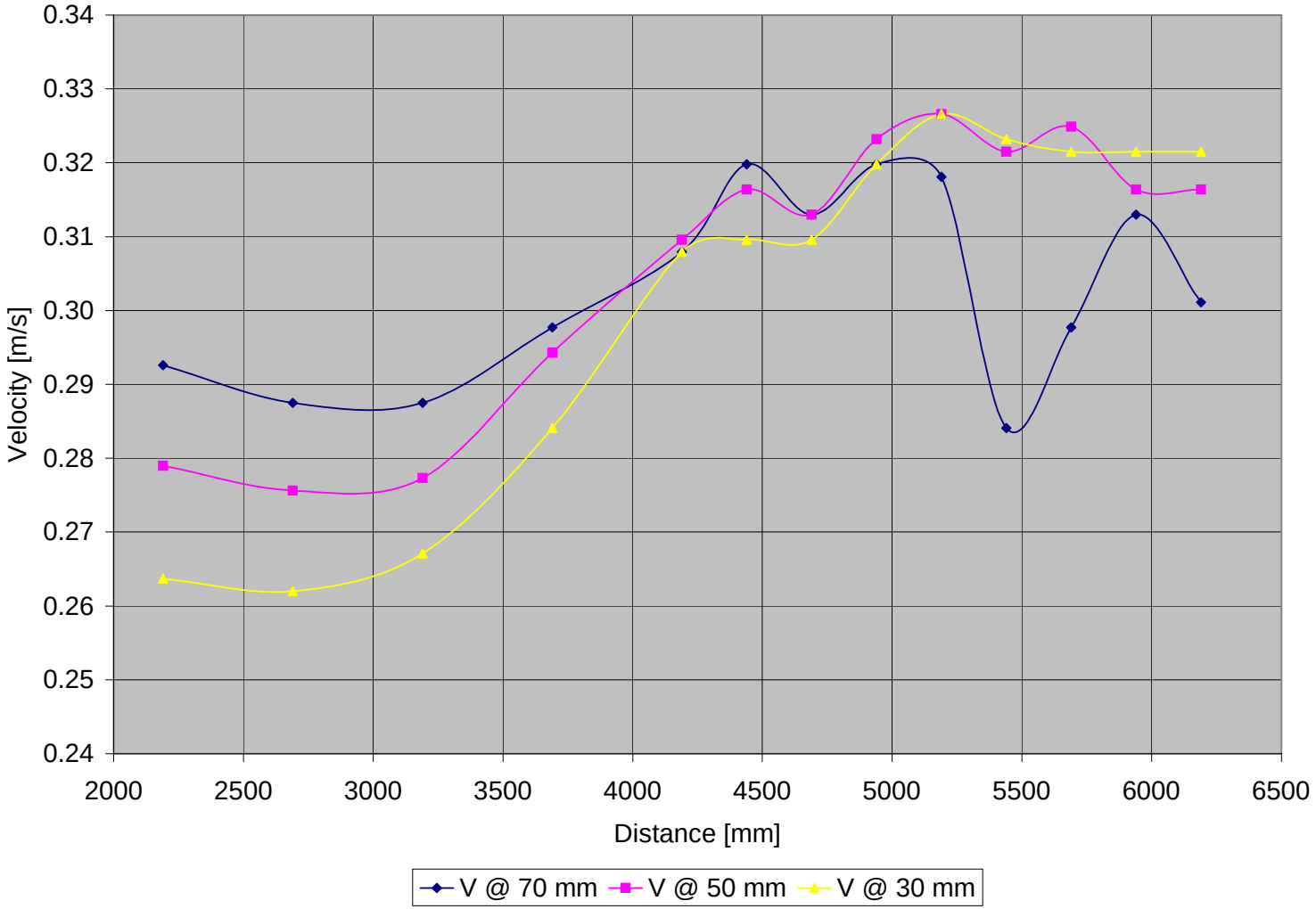

Figure B - 86: Test F4-Vertical velocity distribution measured at 150 mm from inner bank of bend

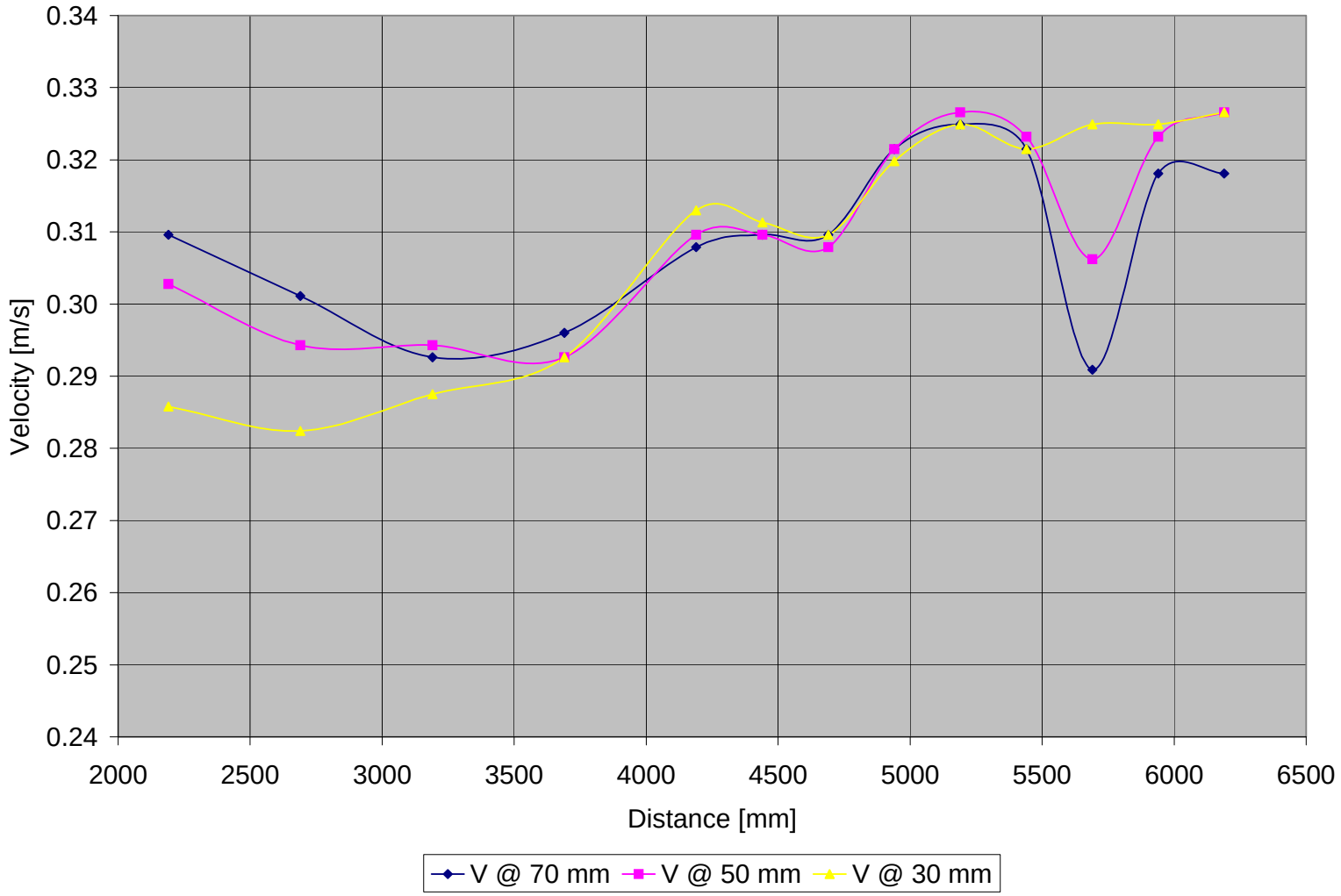

Figure B - 87: Test F4-Vertical velocity distribution measured at 200 mm from inner bank of bend

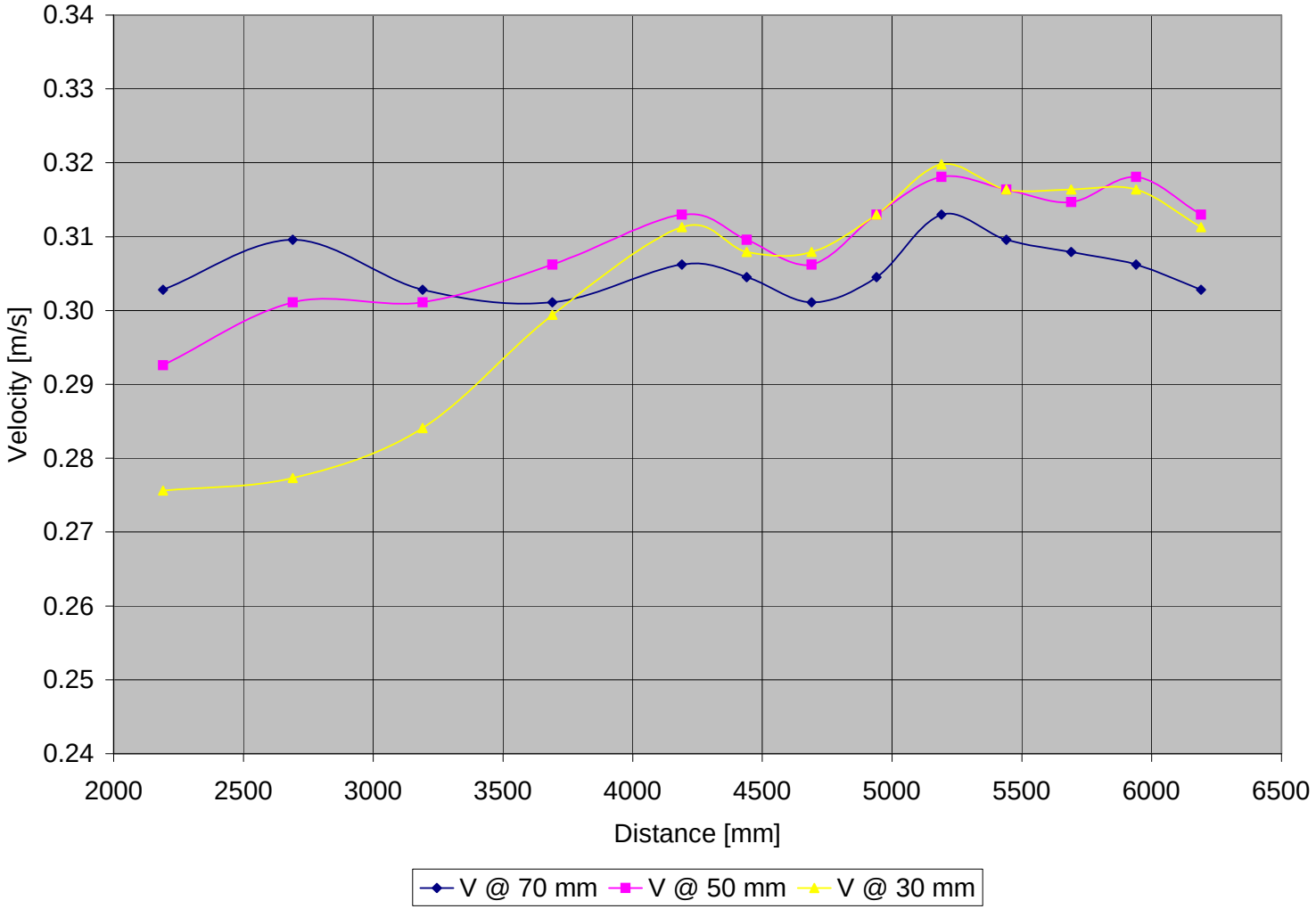

Figure B - 88: Test F4-Vertical velocity distribution measured at 250 mm from inner bank of bend

	Point	6	7	8	9	10	10A	11	11A	12	12A	13	13A	14
Width	**L**	**2190**	**2690**	**3190**	**3690**	**4190**	**4440**	**4690**	**4940**	**5190**	**5440**	**5690**	**5940**	**6190**
	h													
50	**70**	0.320	0.316	0.316	0.289	0.284	0.269	0.248	0.274	0.272	0.276	0.279	0.272	0.277
	50	0.316	0.316	0.315	0.296	0.298	0.289	0.271	0.296	0.296	0.298	0.298	0.293	0.296
	30	0.303	0.305	0.299	0.288	0.294	0.294	0.298	0.308	0.310	0.305	0.306	0.303	0.306
100	**70**	0.301	0.316	0.316	0.315	0.318	0.305	0.293	0.289	0.279	0.277	0.280	0.265	0.274
	50	0.293	0.316	0.315	0.308	0.318	0.313	0.306	0.308	0.305	0.299	0.291	0.291	0.289
	30	0.291	0.305	0.299	0.289	0.310	0.310	0.306	0.315	0.320	0.313	0.310	0.306	0.305
150	**70**	0.293	0.288	0.288	0.298	0.308	0.320	0.313	0.320	0.318	0.284	0.298	0.313	0.301
	50	0.279	0.276	0.277	0.294	0.310	0.316	0.313	0.323	0.327	0.322	0.325	0.316	0.316
	30	0.264	0.262	0.267	0.284	0.308	0.310	0.310	0.320	0.327	0.323	0.322	0.322	0.322
200	**70**	0.310	0.301	0.293	0.296	0.308	0.310	0.310	0.322	0.325	0.322	0.291	0.318	0.318
	50	0.303	0.294	0.294	0.293	0.310	0.310	0.308	0.322	0.327	0.323	0.306	0.323	0.327
	30	0.286	0.282	0.288	0.293	0.313	0.311	0.310	0.320	0.325	0.322	0.325	0.325	0.327
250														
	70	0.303	0.310	0.303	0.301	0.306	0.305	0.301	0.305	0.313	0.310	0.308	0.306	0.303
	50	0.293	0.301	0.301	0.306	0.313	0.310	0.306	0.313	0.318	0.316	0.315	0.318	0.313
	30	0.276	0.277	0.284	0.299	0.311	0.308	0.308	0.313	0.320	0.316	0.316	0.316	0.311

Table B - 11: Test F4- Measured velocities [m/s]

APPENDIX C-NUMERICAL MODELLING

APPENDIX C-NUMERICAL MODELLING

TABLE OF CONTENTS

Page

LIST OF FIGURES

C NUMERICAL SIMULATION RESULTS

C.1 2D SIMULATION

C.1.1 TEST G1 (F_R = 0.1)

Figure C - 1: Test G1-Simulated velocity distribution in the horizontal plane

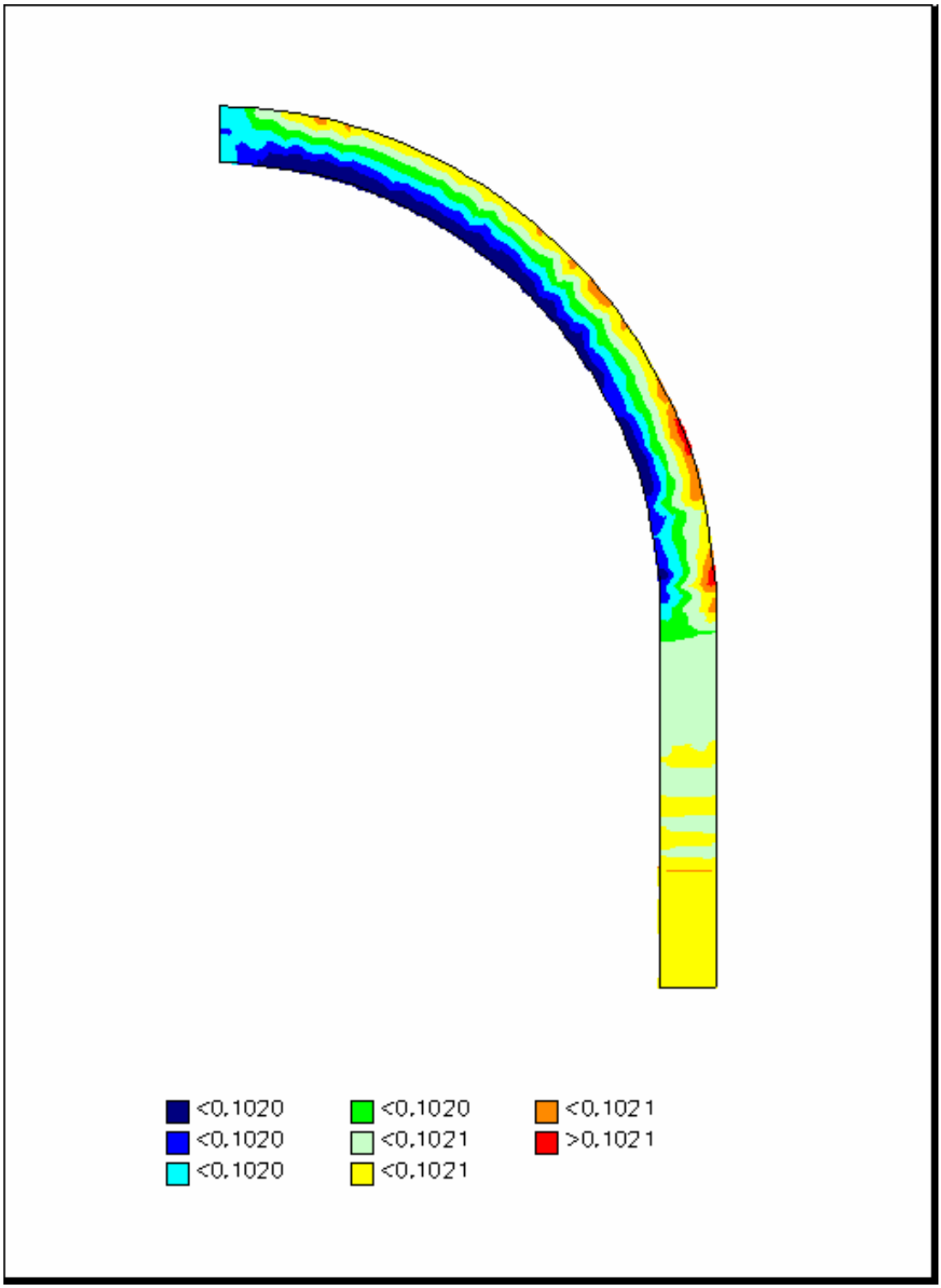

Figure C - 2: Test G1-Simulated water levels

C.1.2 TEST G2 (F_R = 0.3)

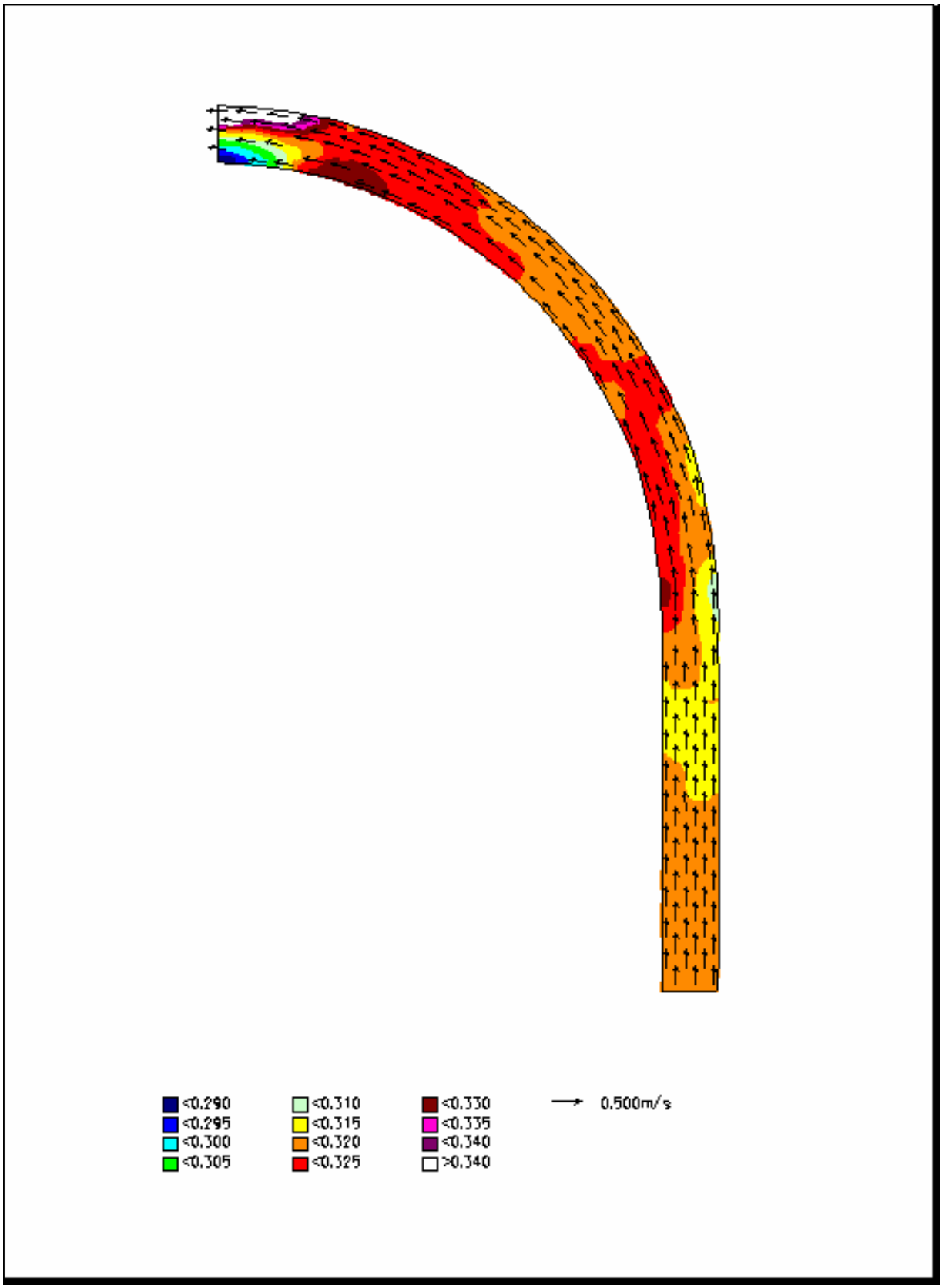

Figure C - 3: Test G2-Simulated velocity distribution in the horizontal plane

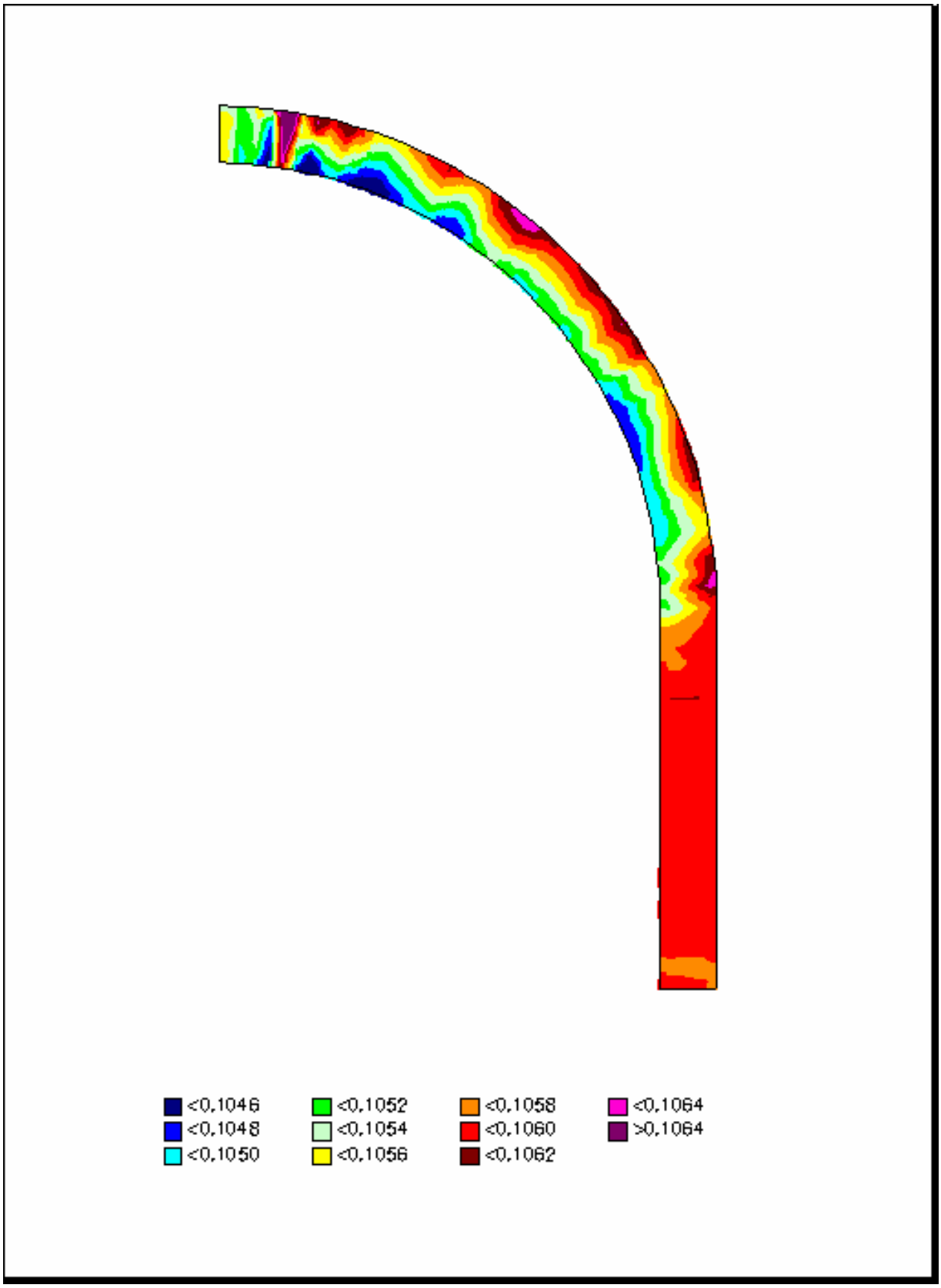

Figure C - 4: Test G2-Simulated water levels

C.1.3 TEST G3 (F_R = 0.5)

Figure C - 5: Test G3-Simulated velocity distribution in the horizontal plane

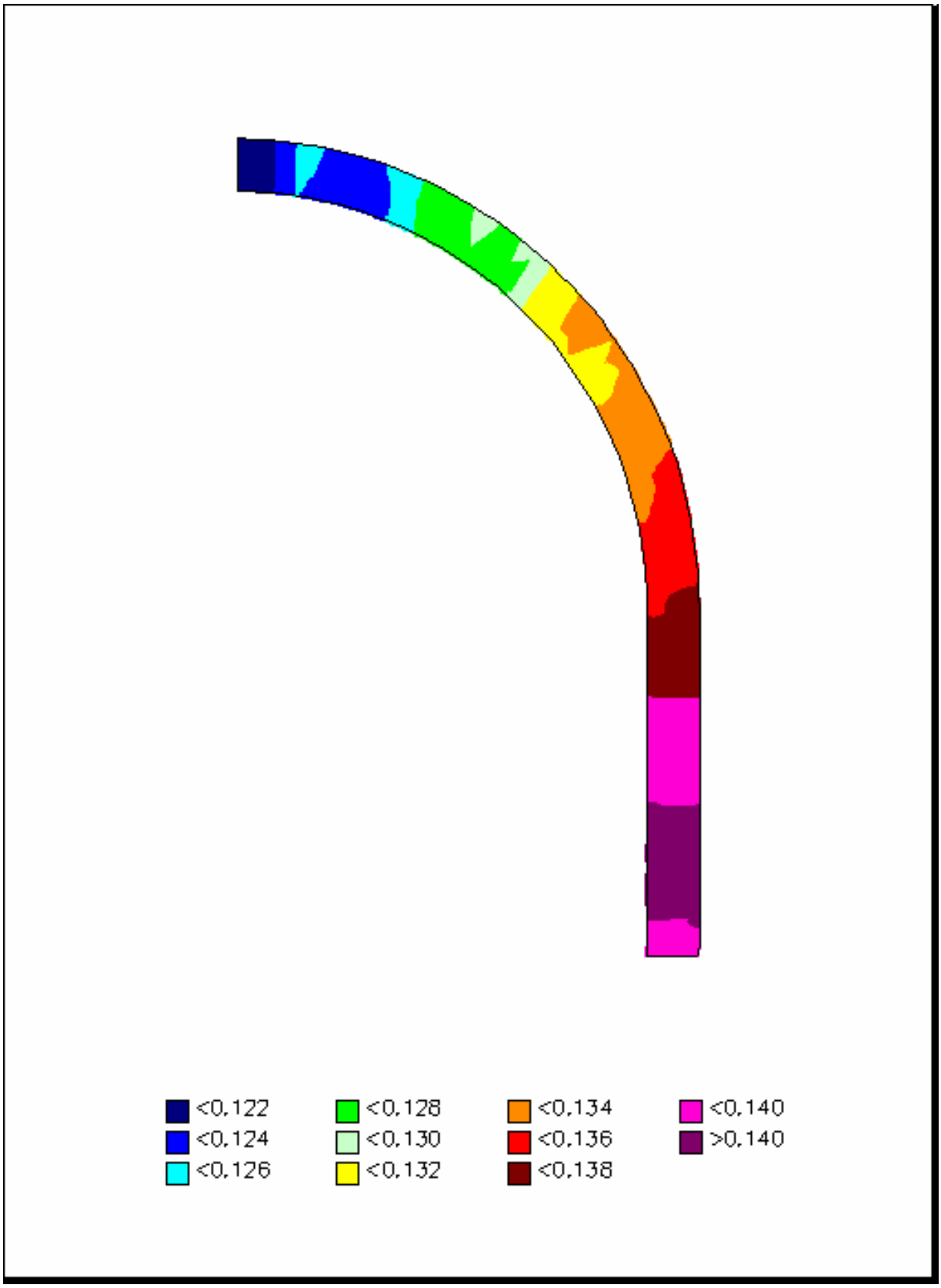

Figure C - 6: Test G3-Simulated water levels

C.2 3D SIMULATION

C.2.1 TEST H1 (F_R = 0.1)

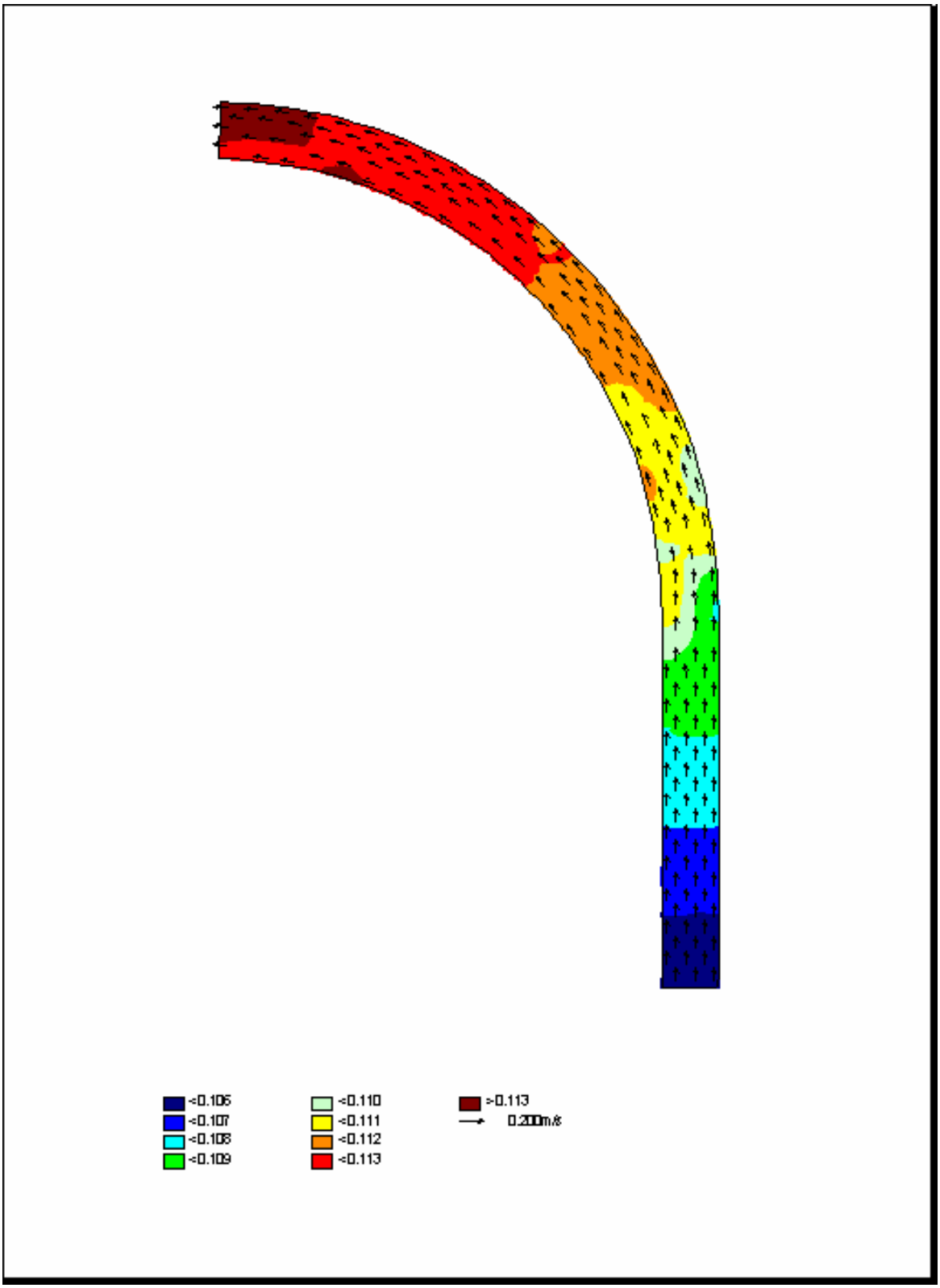

Figure C - 7: Test H1-Simulated velocity distribution in the horizontal plane at surface

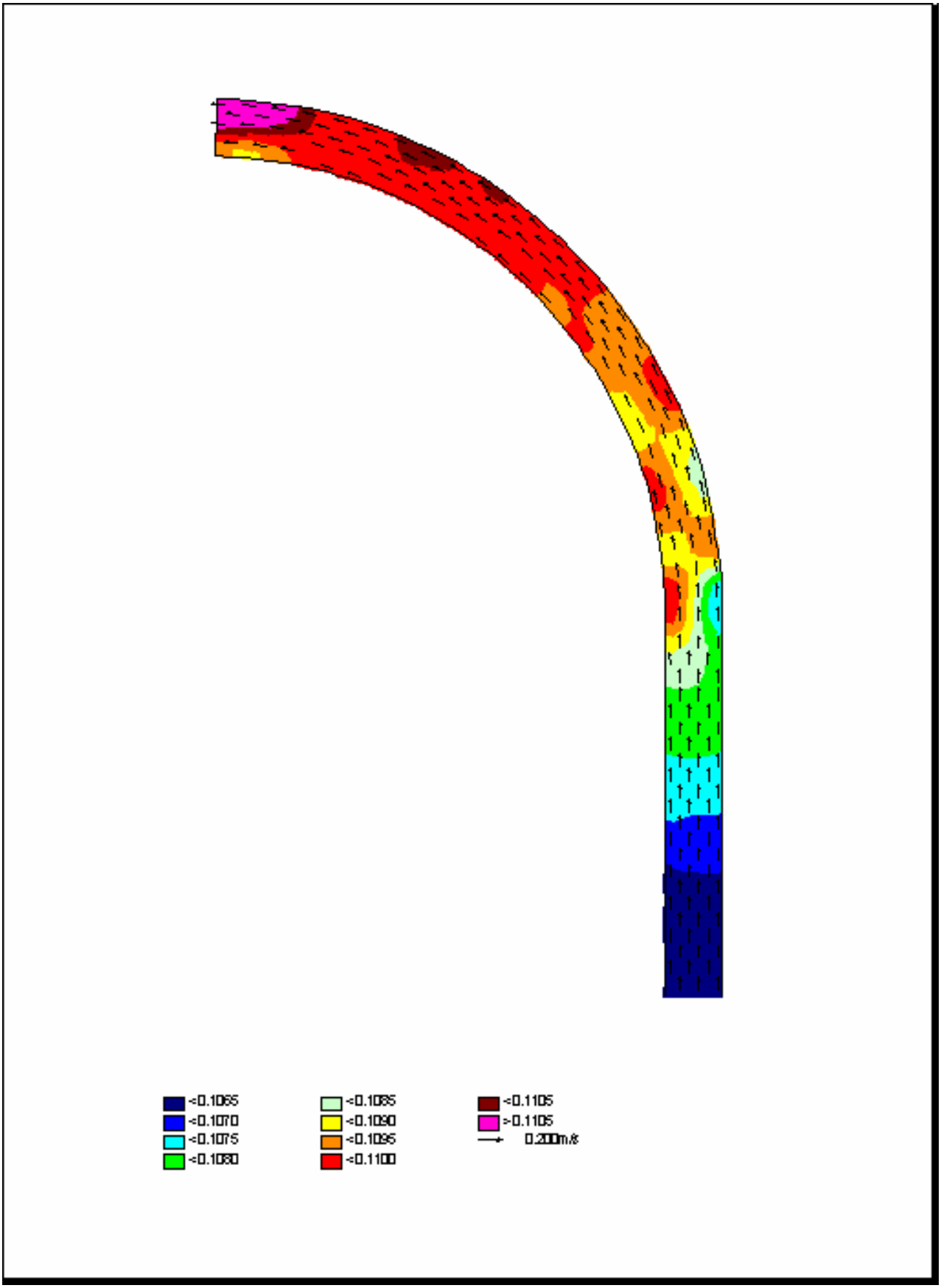

Figure C - 8: Test H1-Simulated velocity distribution in the horizontal plane at 70 mm

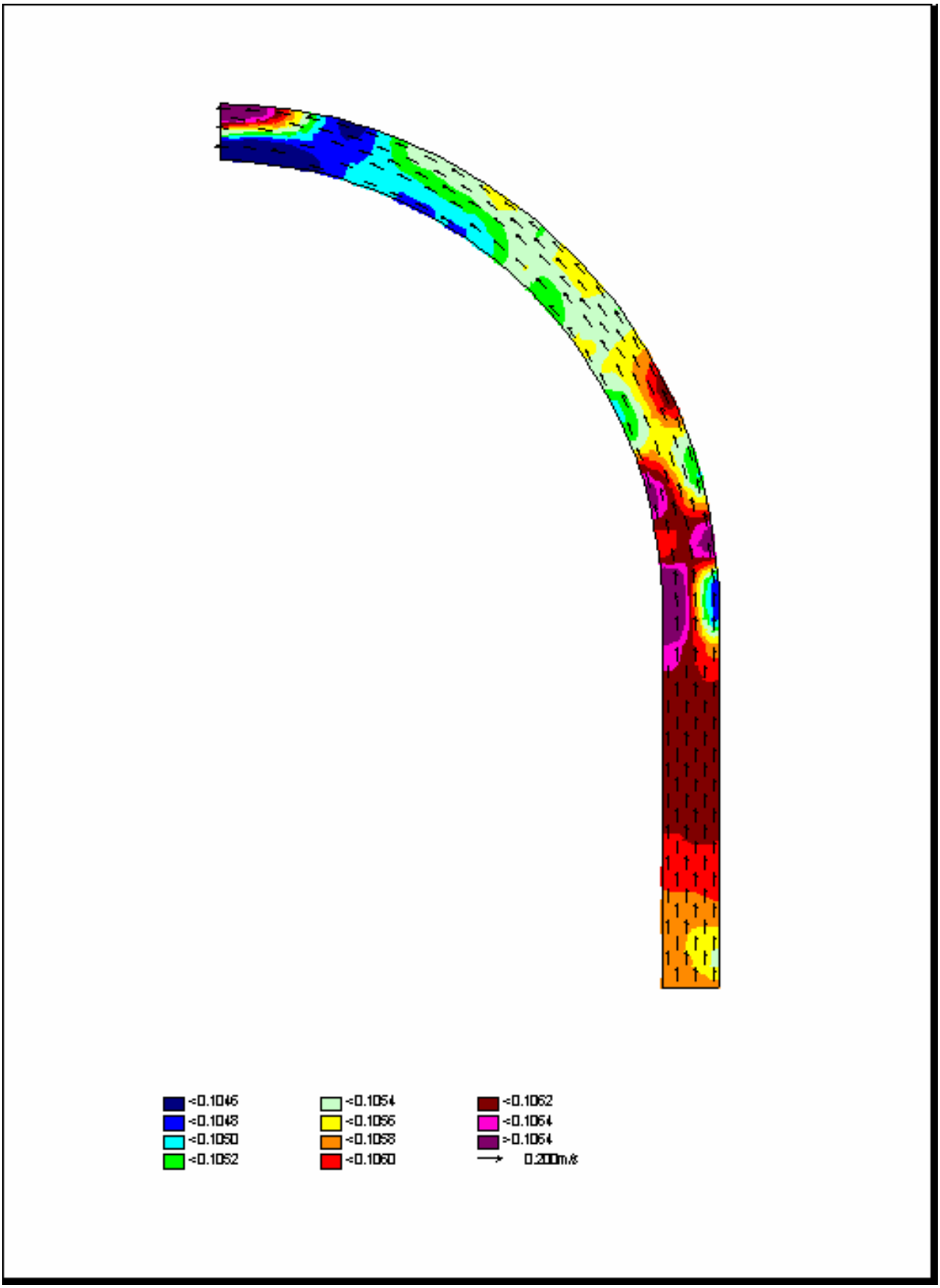

Figure C - 9: Test H1-Simulated velocity distribution in the horizontal plane at 50 mm

Figure C - 10: Test H1-Simulated velocity distribution in the horizontal plane at 30 mm

Figure C - 11: Test H1-Simulated water levels

C.2.2 TEST H2 (F_R = 0.3)

Figure C - 12: Test H2-Simulated velocity distribution in the horizontal plane at surface

Figure C - 13: Test H2-Simulated velocity distribution in the horizontal plane at 70 mm

Figure C - 14: Test H2-Simulated velocity distribution in the horizontal plane at 50 mm

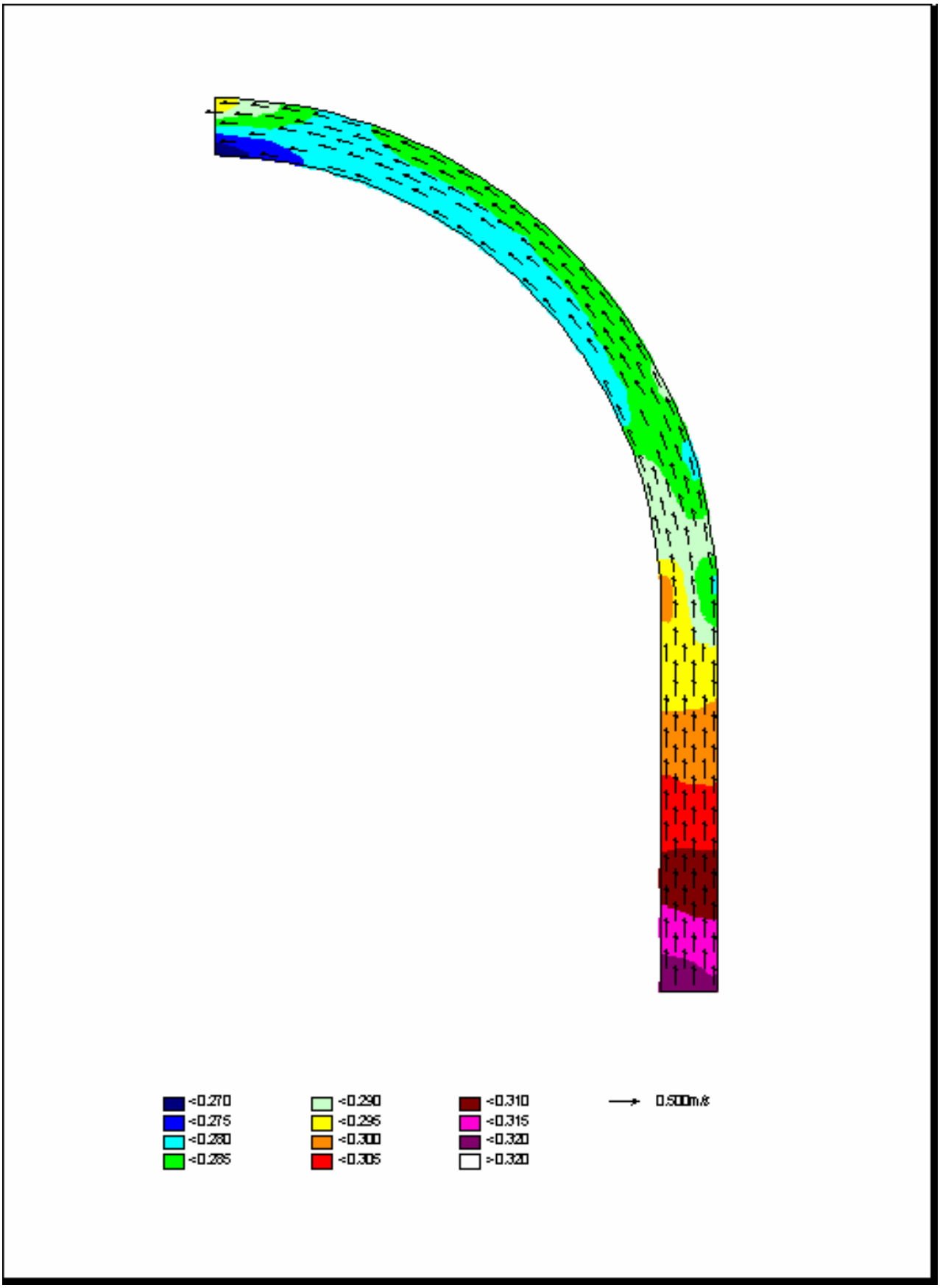

Figure C - 15: Test H2-Simulated velocity distribution in the horizontal plane at 30 mm

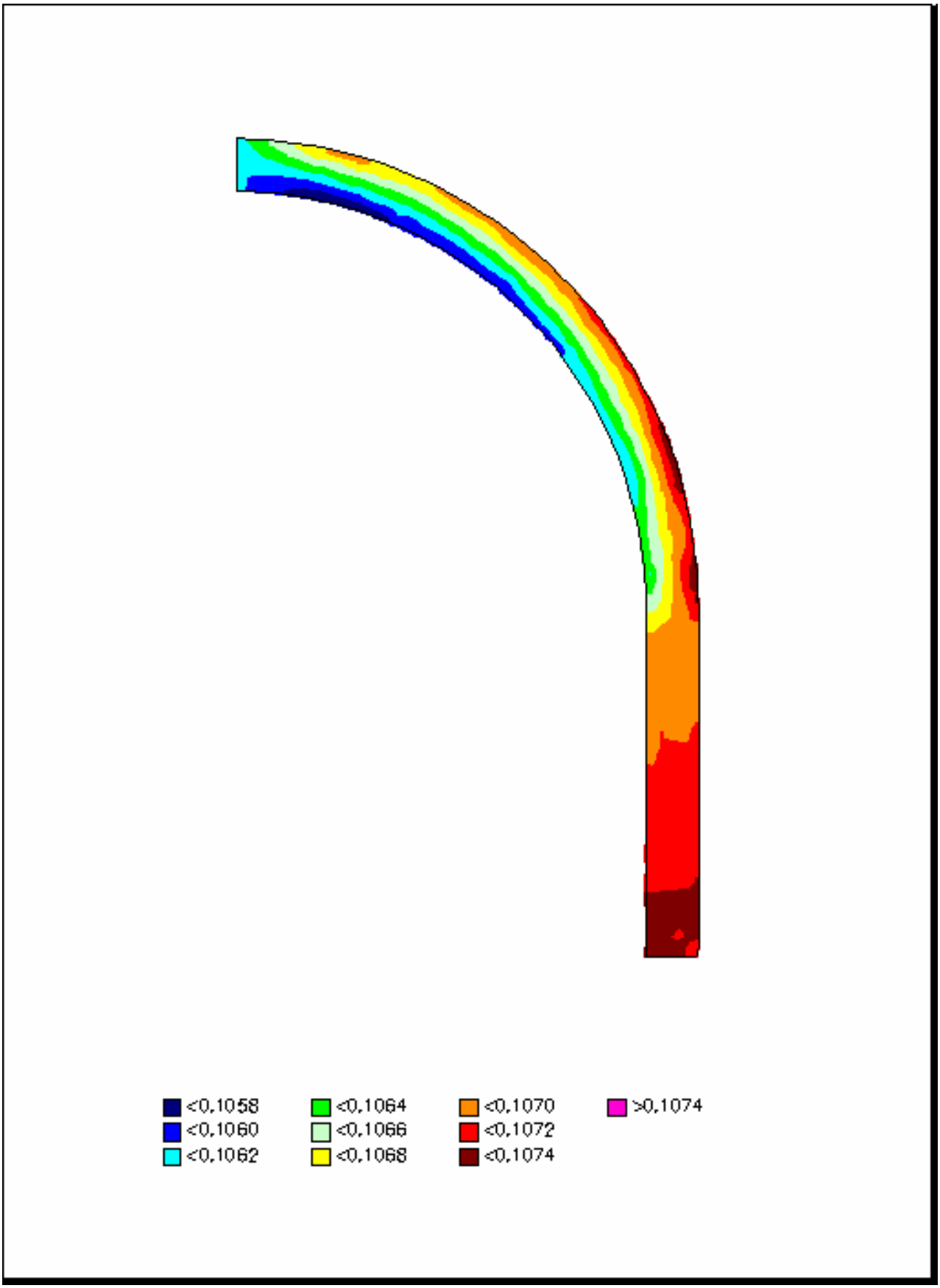

Figure C - 16: Test H2-Simulated water levels

C.2.3 TEST H3 (F_R = 0.5)

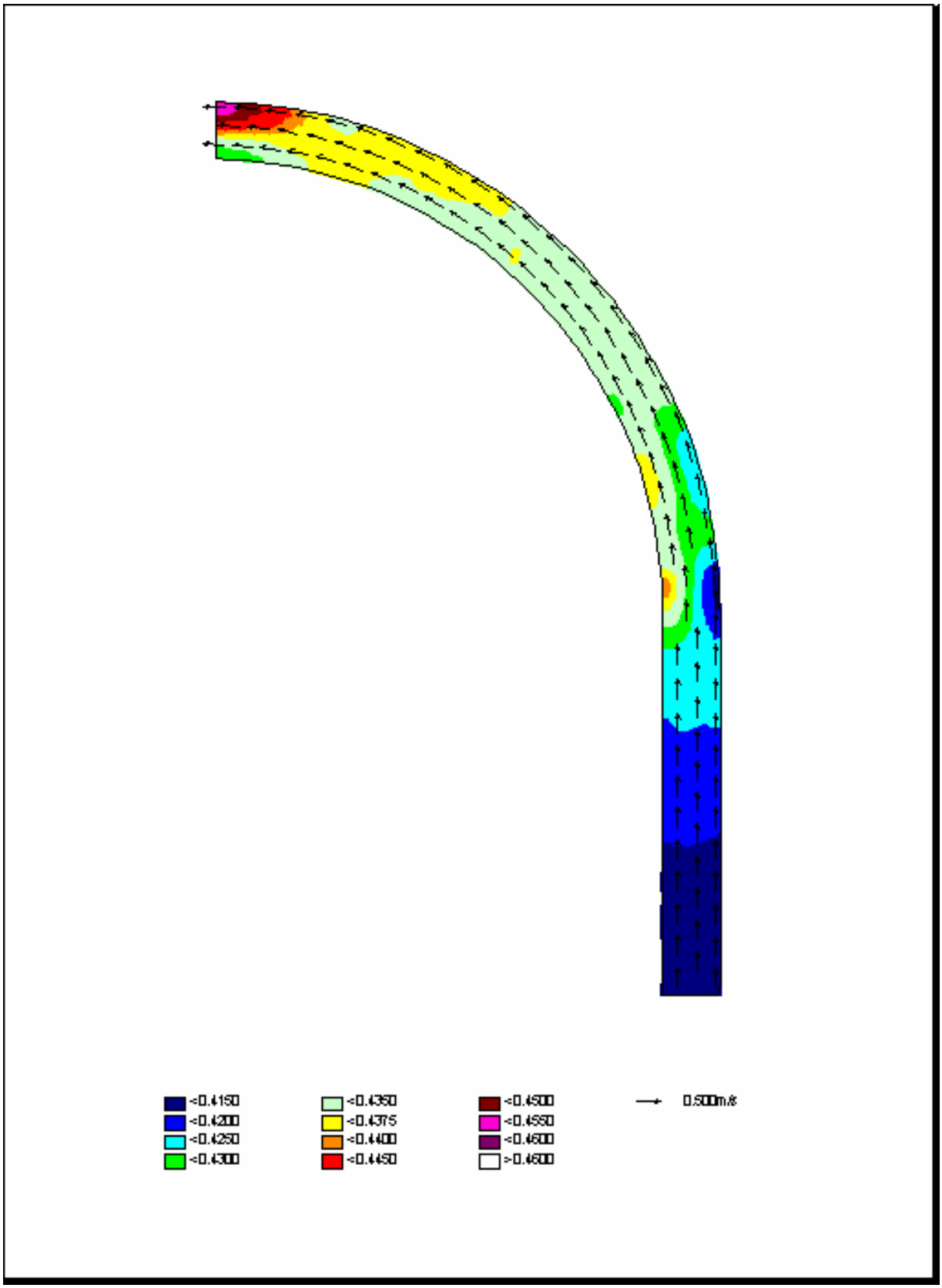

Figure C - 17: Test H3-Simulated velocity distribution in the horizontal plane at surface

Figure C - 18: Test H3-Simulated velocity distribution in the horizontal plane at 70 mm

Figure C - 19: Test H3-Simulated velocity distribution in the horizontal plane at 50 mm

Figure C - 20: Test H3-Simulated velocity distribution in the horizontal plane at 30 mm

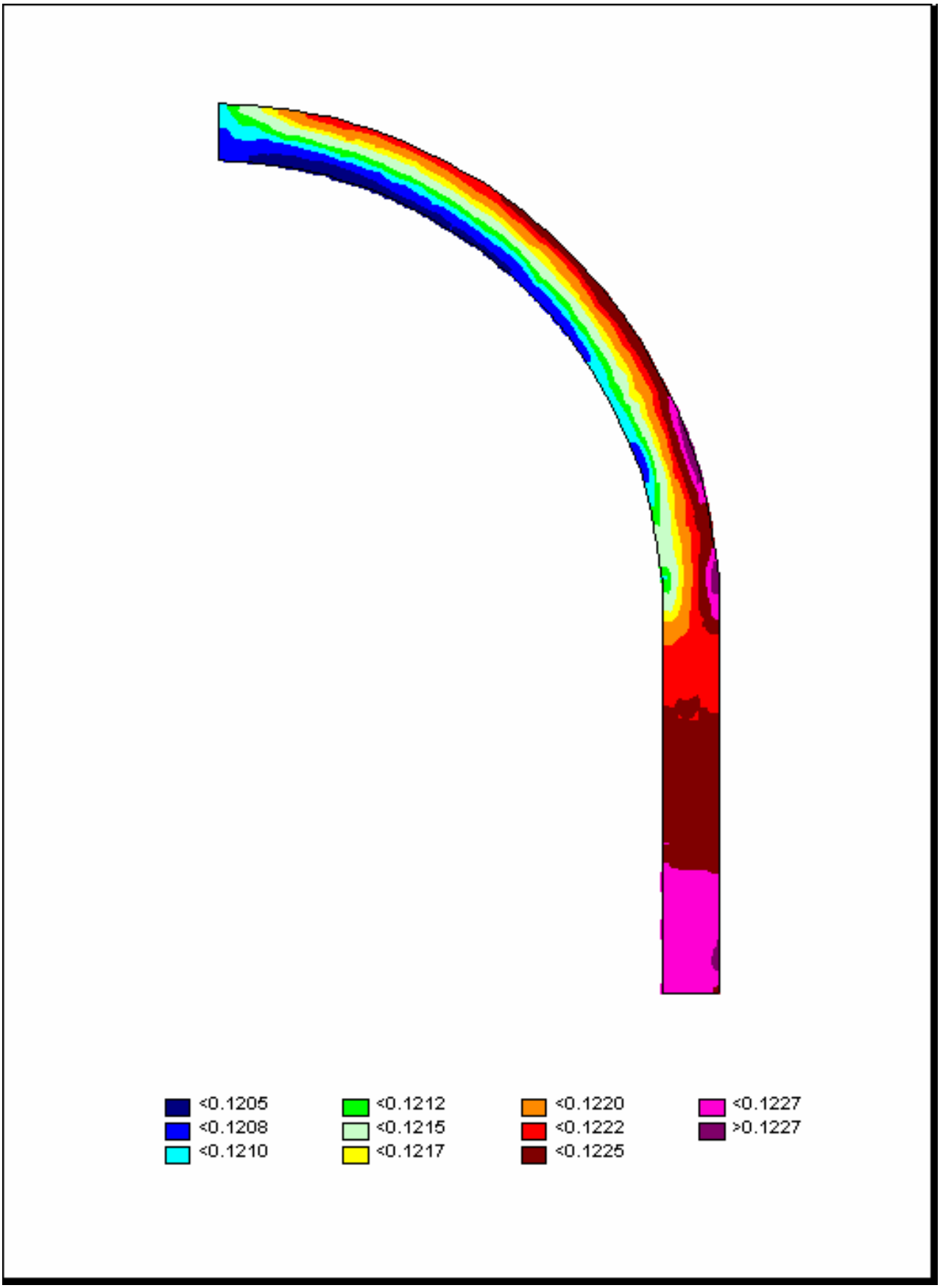

Figure C - 21: Test H3-Simulated water levels

APPENDIX D-LOCATION OF TURNING POINTS FOR TEST A, B AND C

APPENDIX D-LOCATION OF TURNING POINTS FOR TESTS A, B AND C

TABLE OF CONTENTS

LIST OF FIGURES

D.1 TEST A

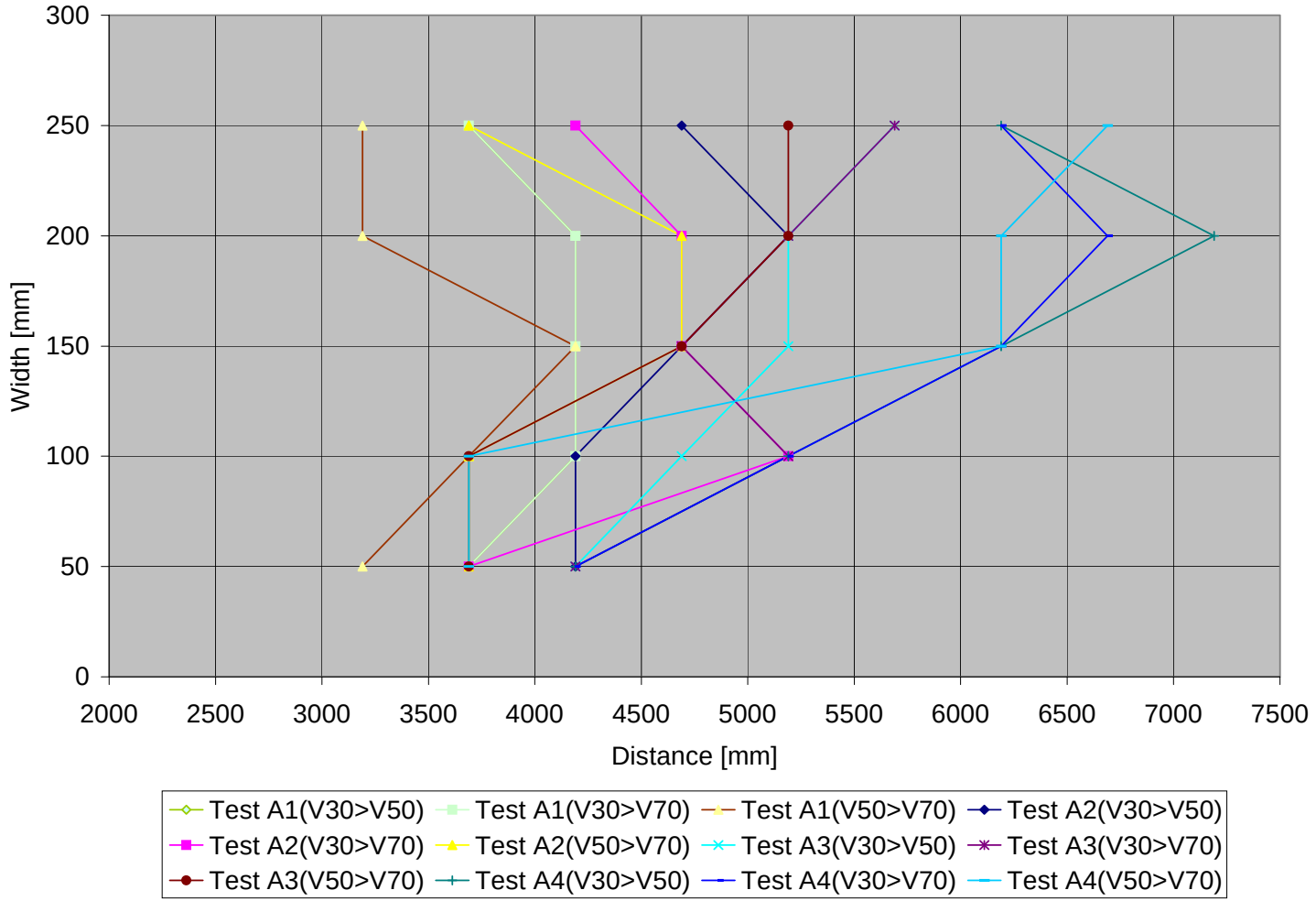

Figure D - 1: Location of turning points where *V30>V50, V30>V70* and *V50>V70* for Test A1, A2, A3 and A4

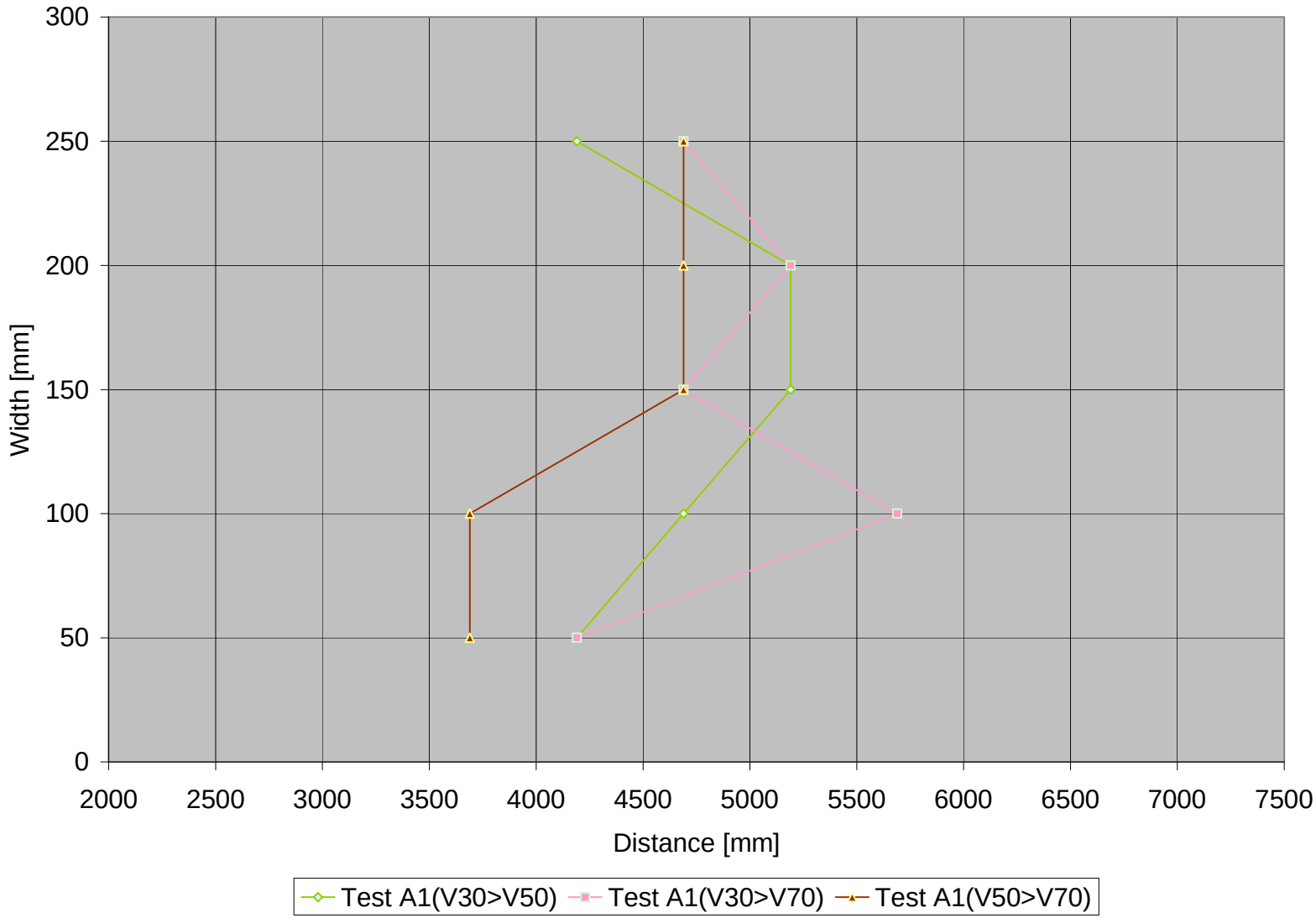

Figure D - 2: Test A1-Location of turning points where *V30>V50*, *V30>V70* and *V50>V70*

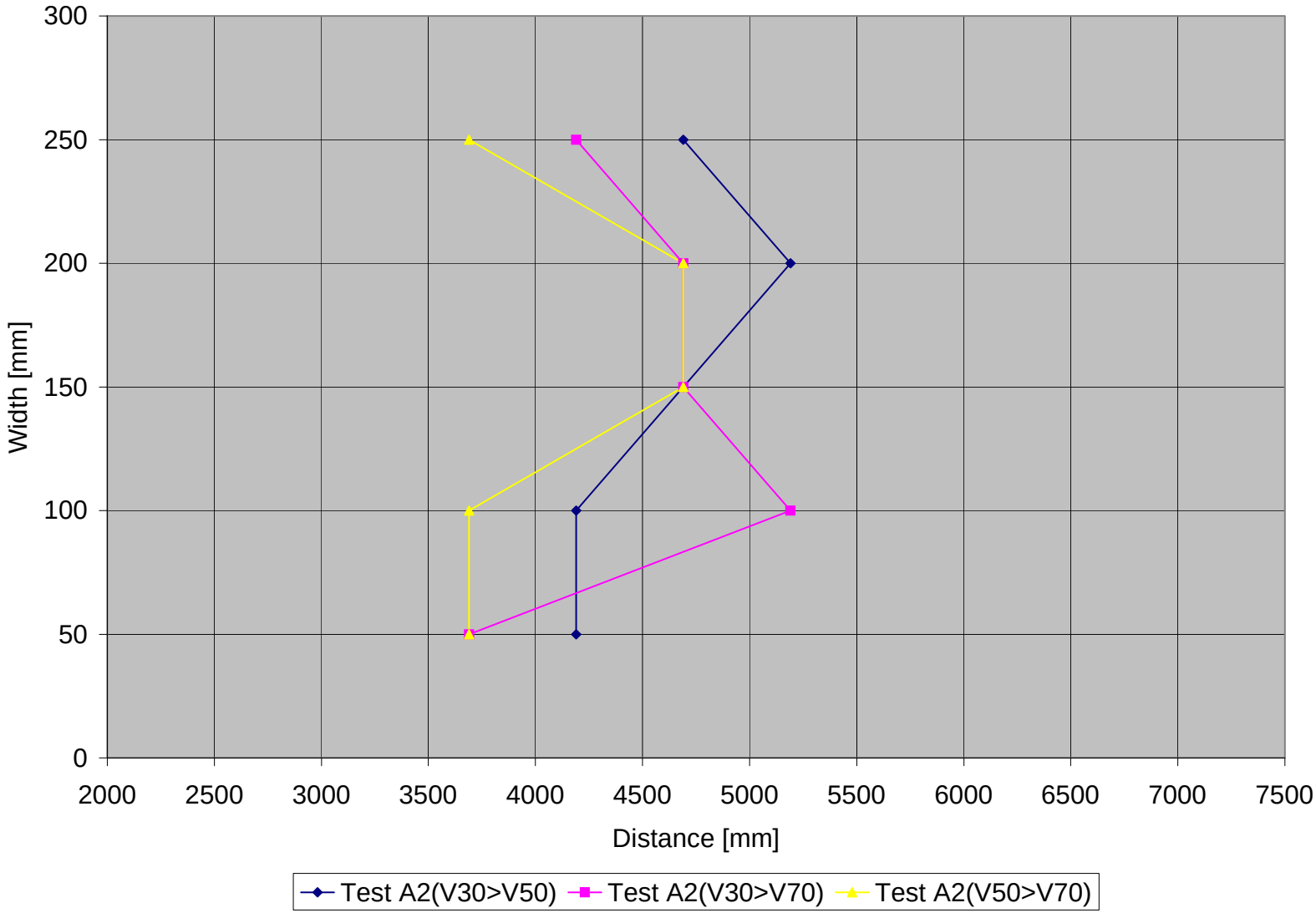

Figure D - 3: Test A2-Location of turning points where *V30>V50*, *V30>V70* and *V50>V70*

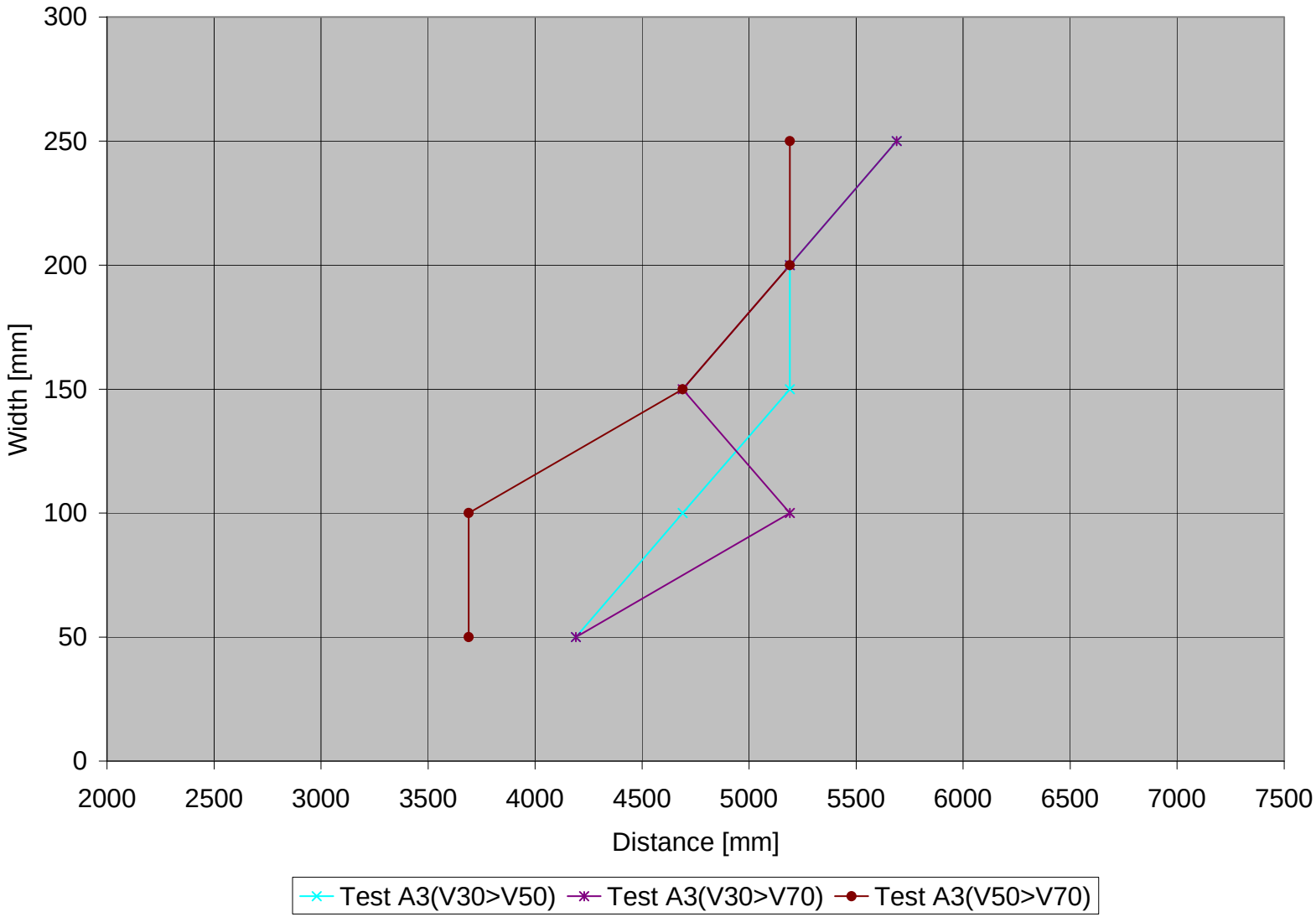

Figure D - 4: Test A3-Location of turning points where *V30>V50*, *V30>V70* and *V50>V70*

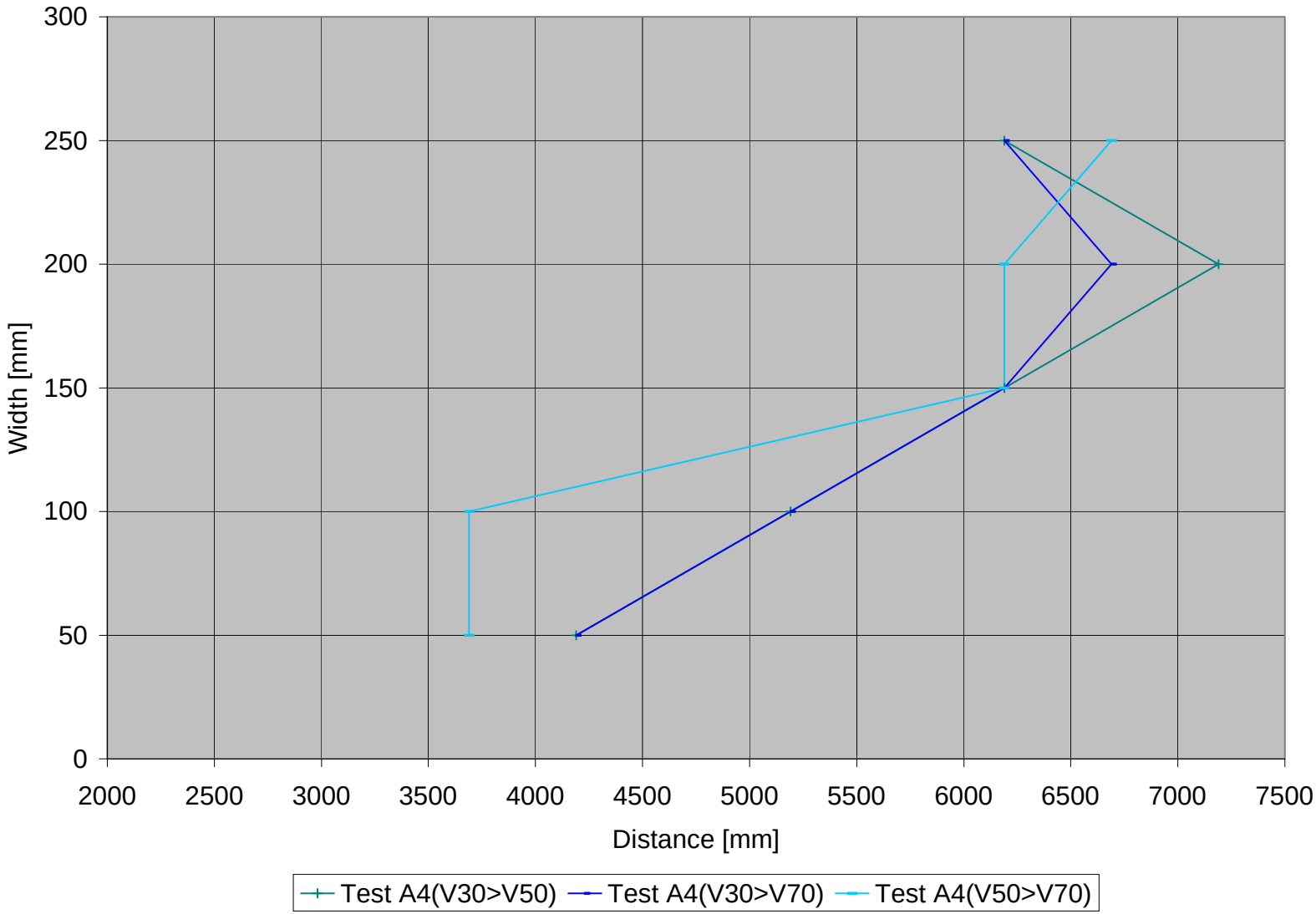

Figure D - 5: Test A4-Location of turning points where *V30>V50*, *V30>V70* and *V50>V70*

D.2 TEST B

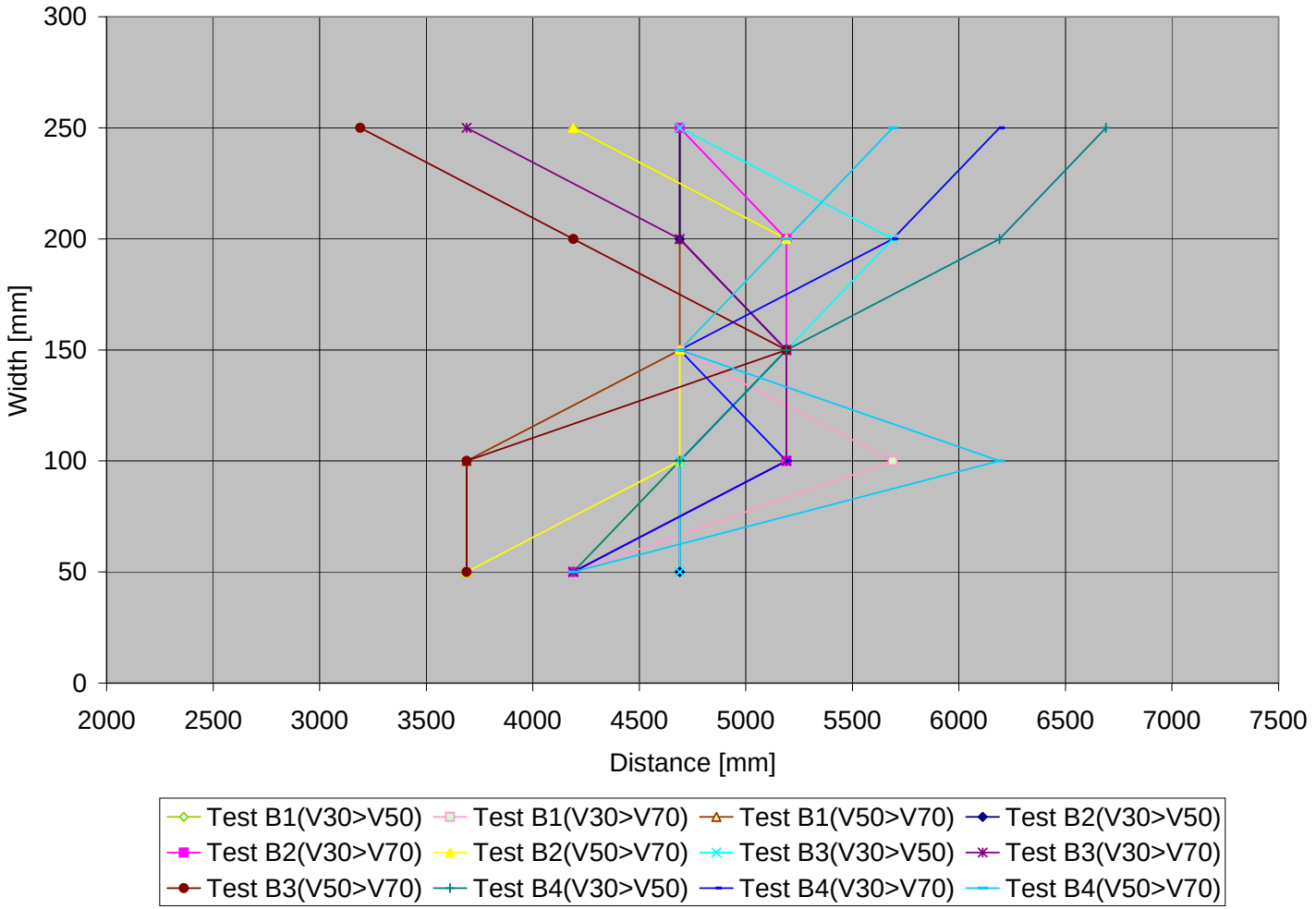

Figure D - 6: Location of turning points where *V30>V50*, *V30>V70* and *V50>V70* for Test B1, B2, B3 and B4

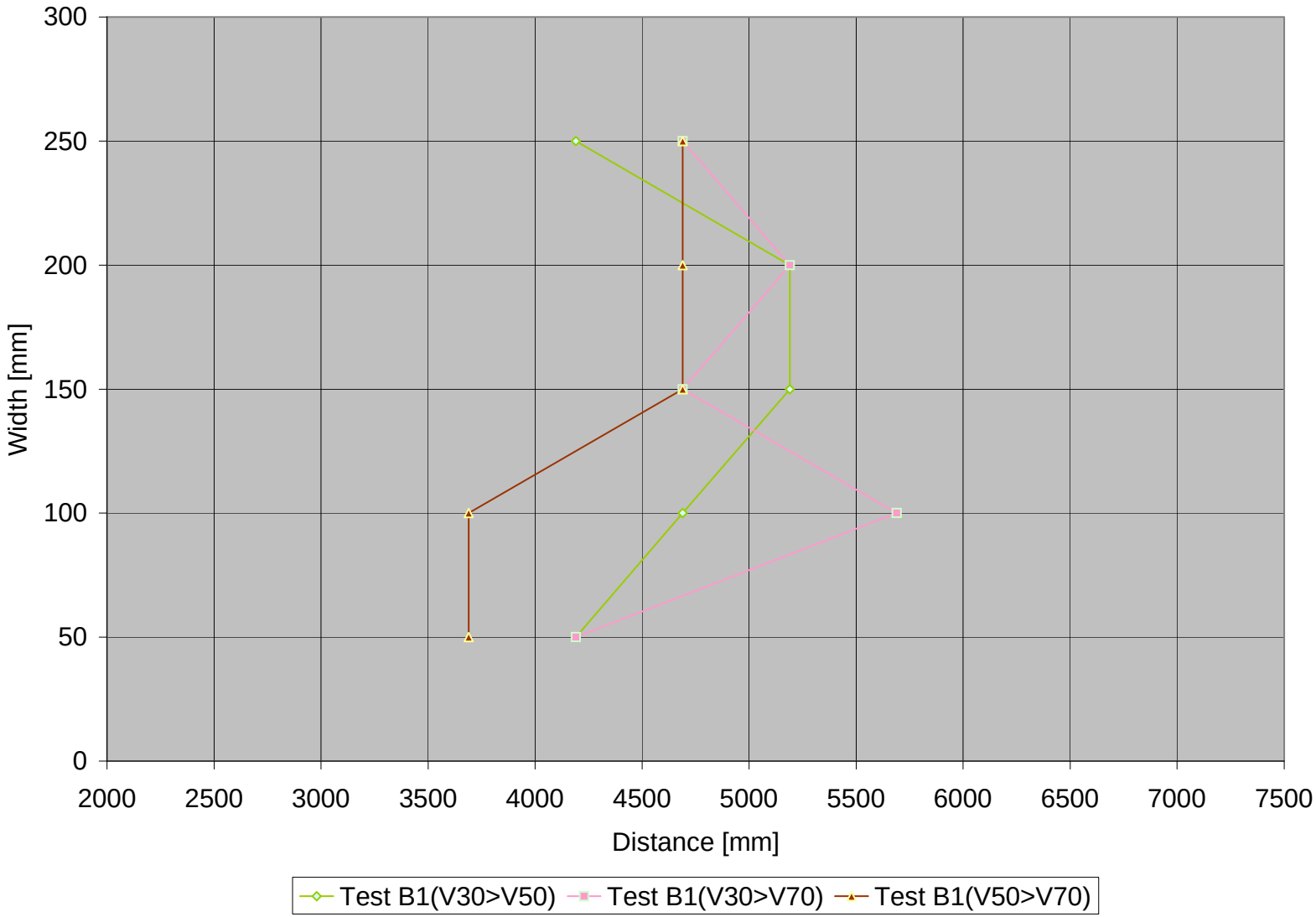

Figure D - 7: Test B1-Location of turning points where *V30>V50*, *V30>V70* and *V50>V70*

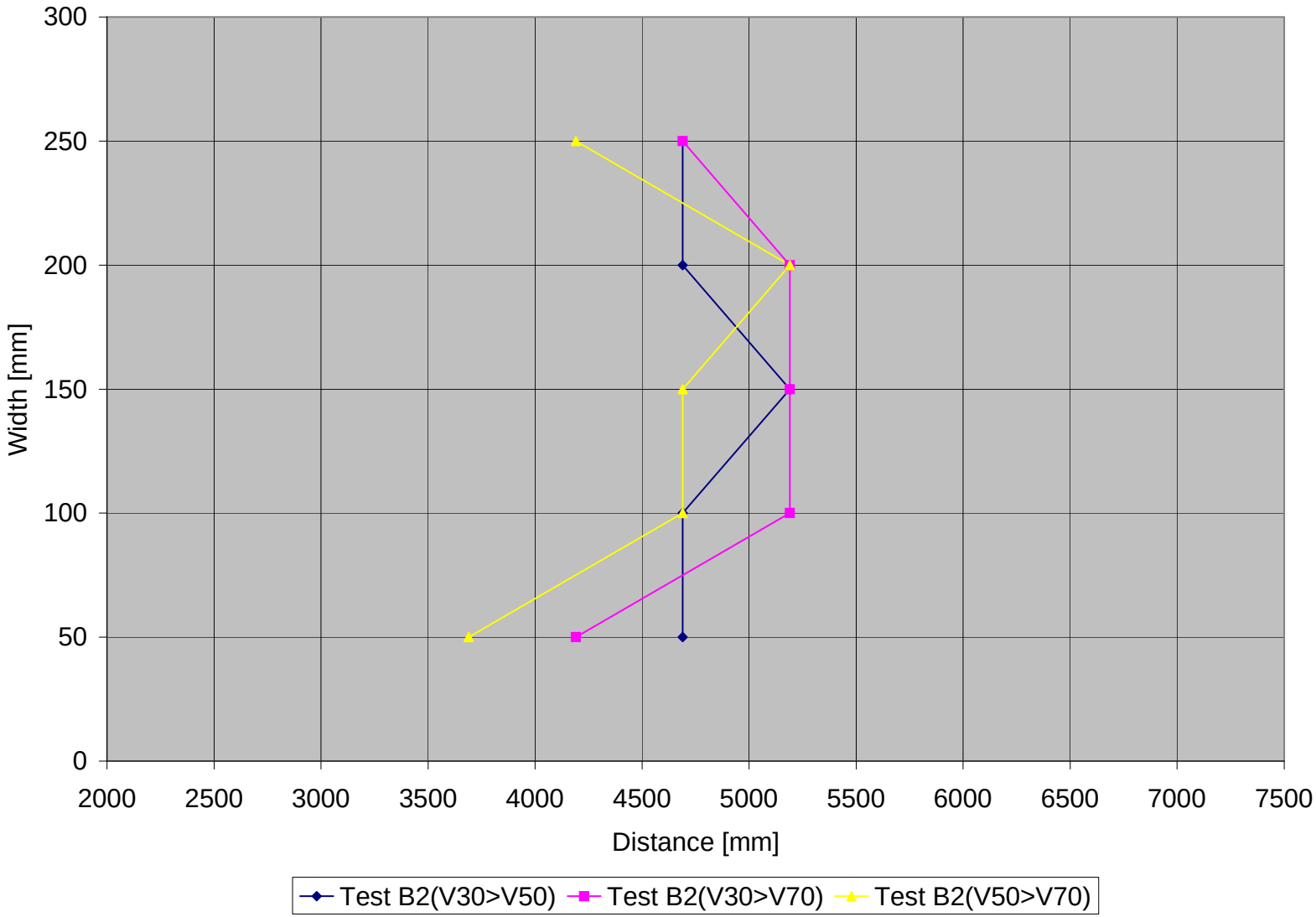

Figure D - 8: Test B2-Location of turning points where *V30>V50*, *V30>V70* and *V50>V70*

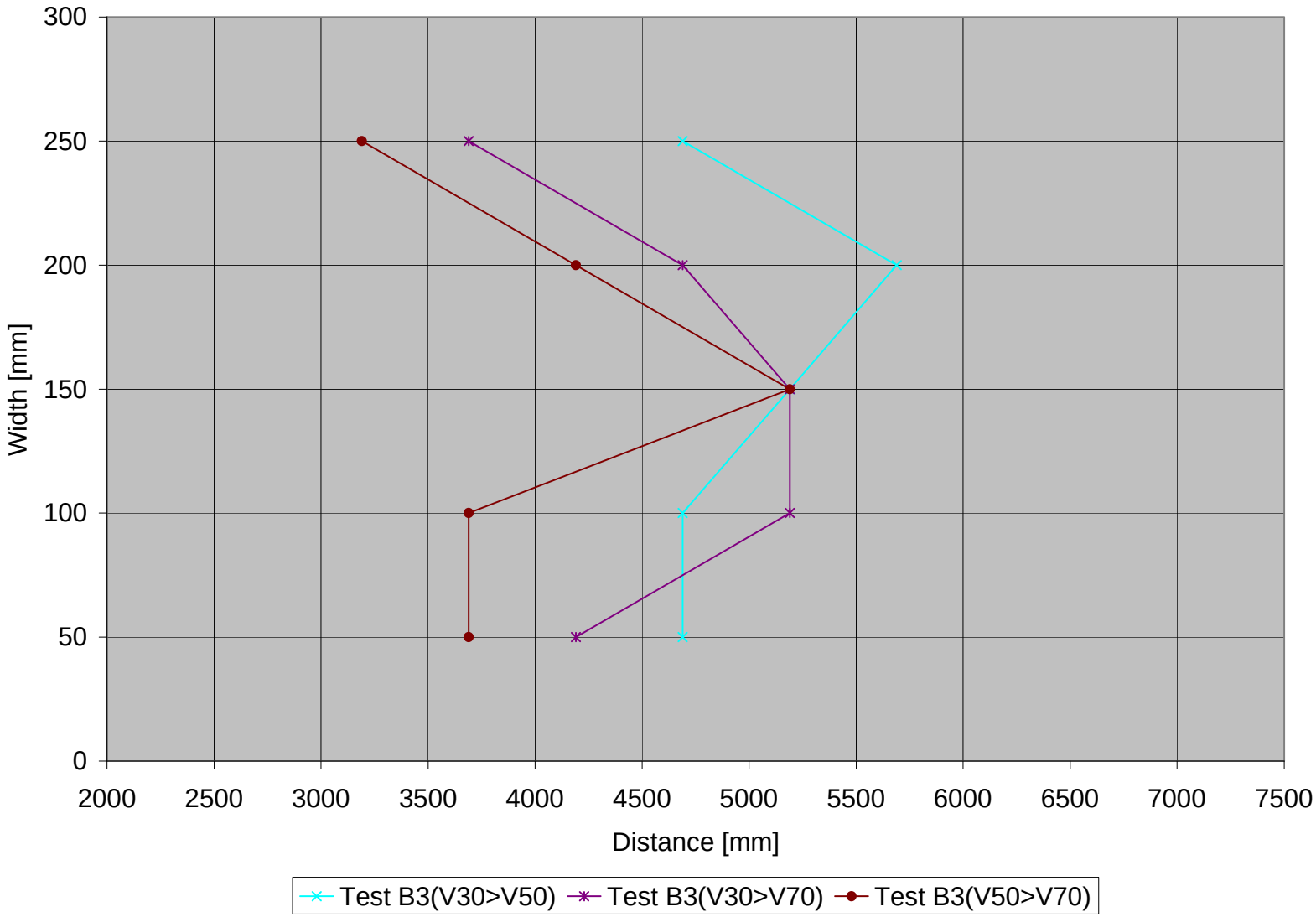

Figure D - 9: Test B3-Location of turning points where *V30>V50*, *V30>V70* and *V50>V70*

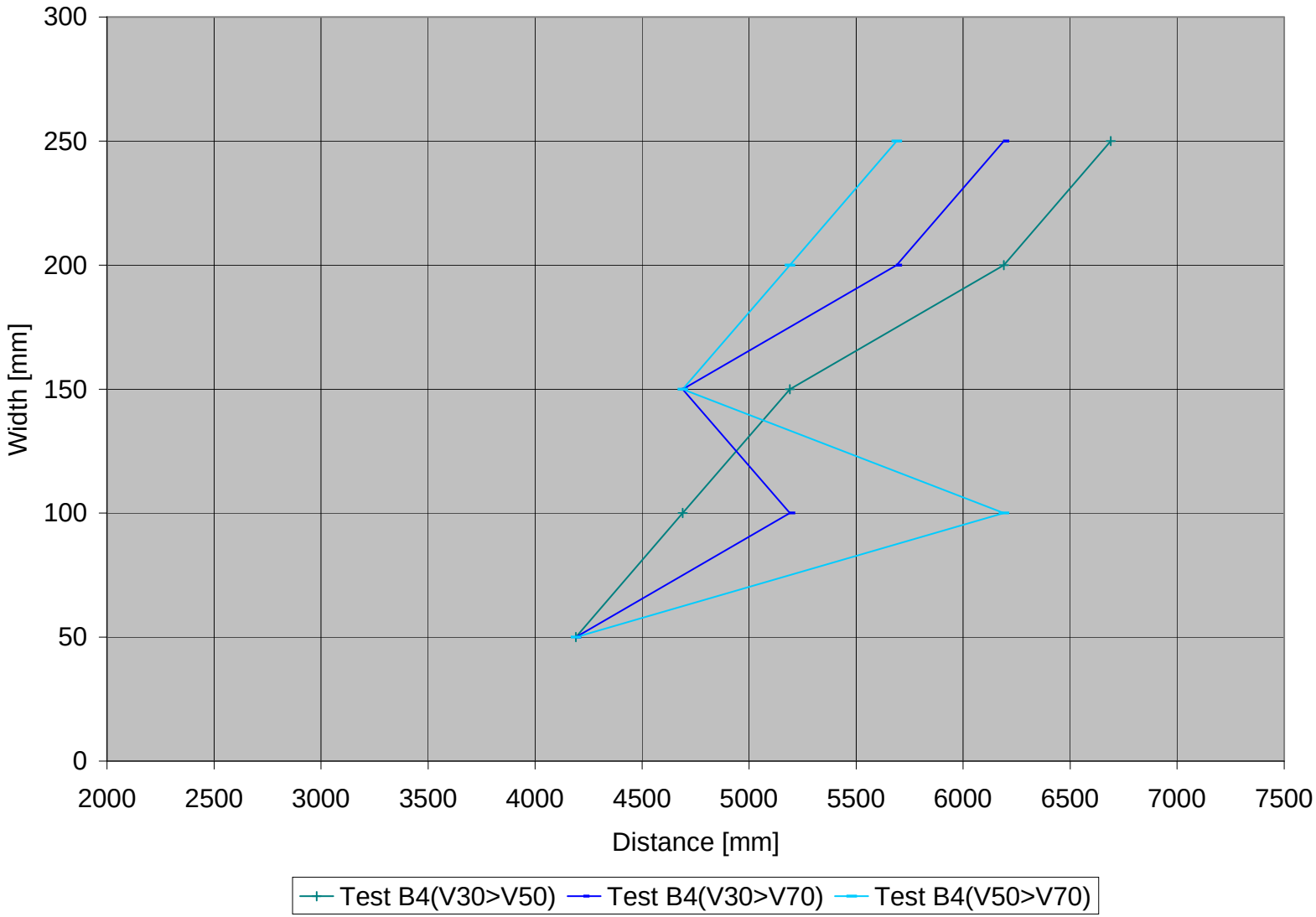

Figure D - 10: Test B4-Location of turning points where *V30>V50*, *V30>V70* and *V50>V70*

D.3 TEST C

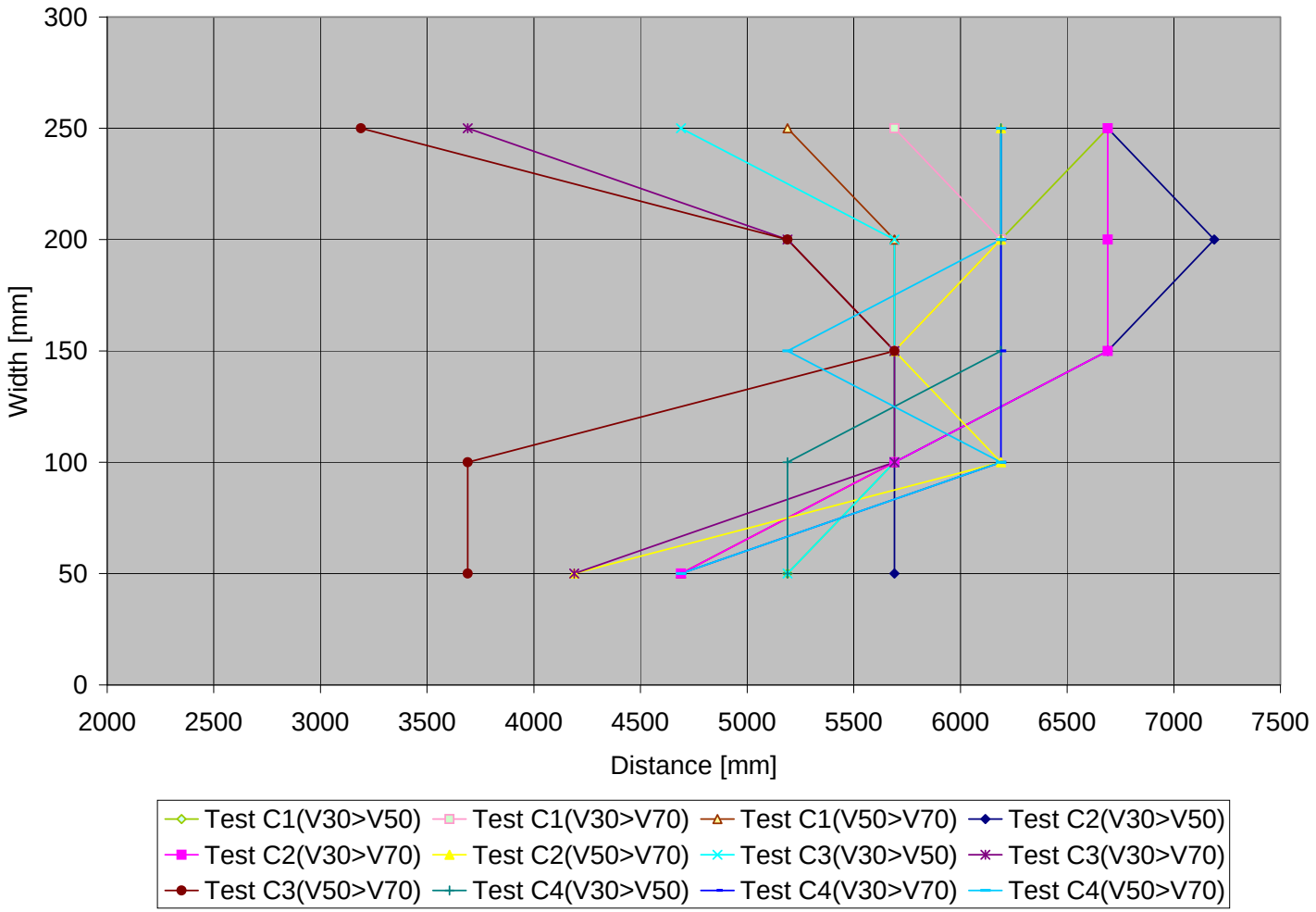

Figure D - 11: Location of turning points where *V30>V50*, *V30>V70* and *V50>V70* for Test C1, C2, C3 and C4

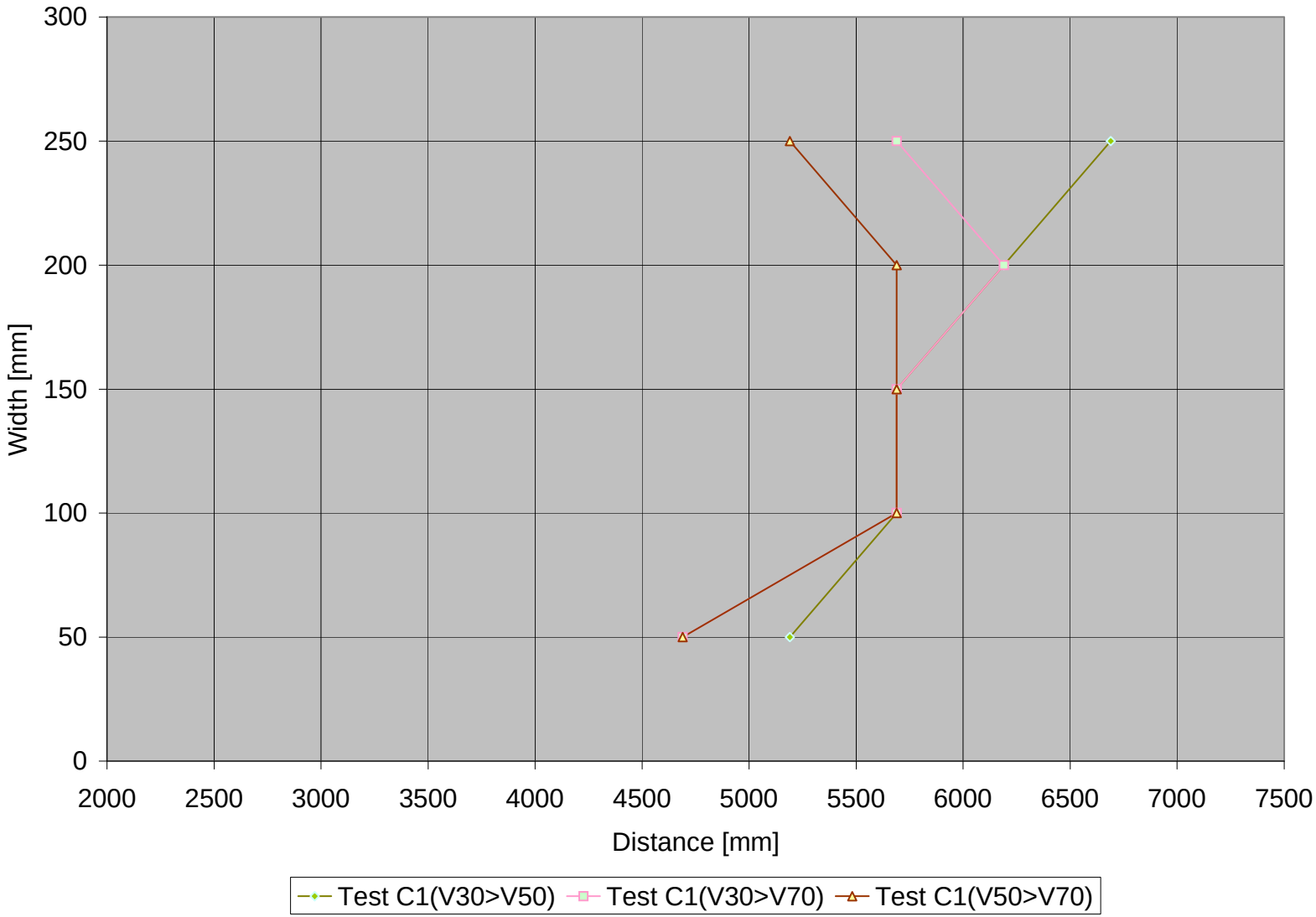

Figure D - 12: Test C1-Location of turning points where *V30>V50*, *V30>V70* and *V50>V70*

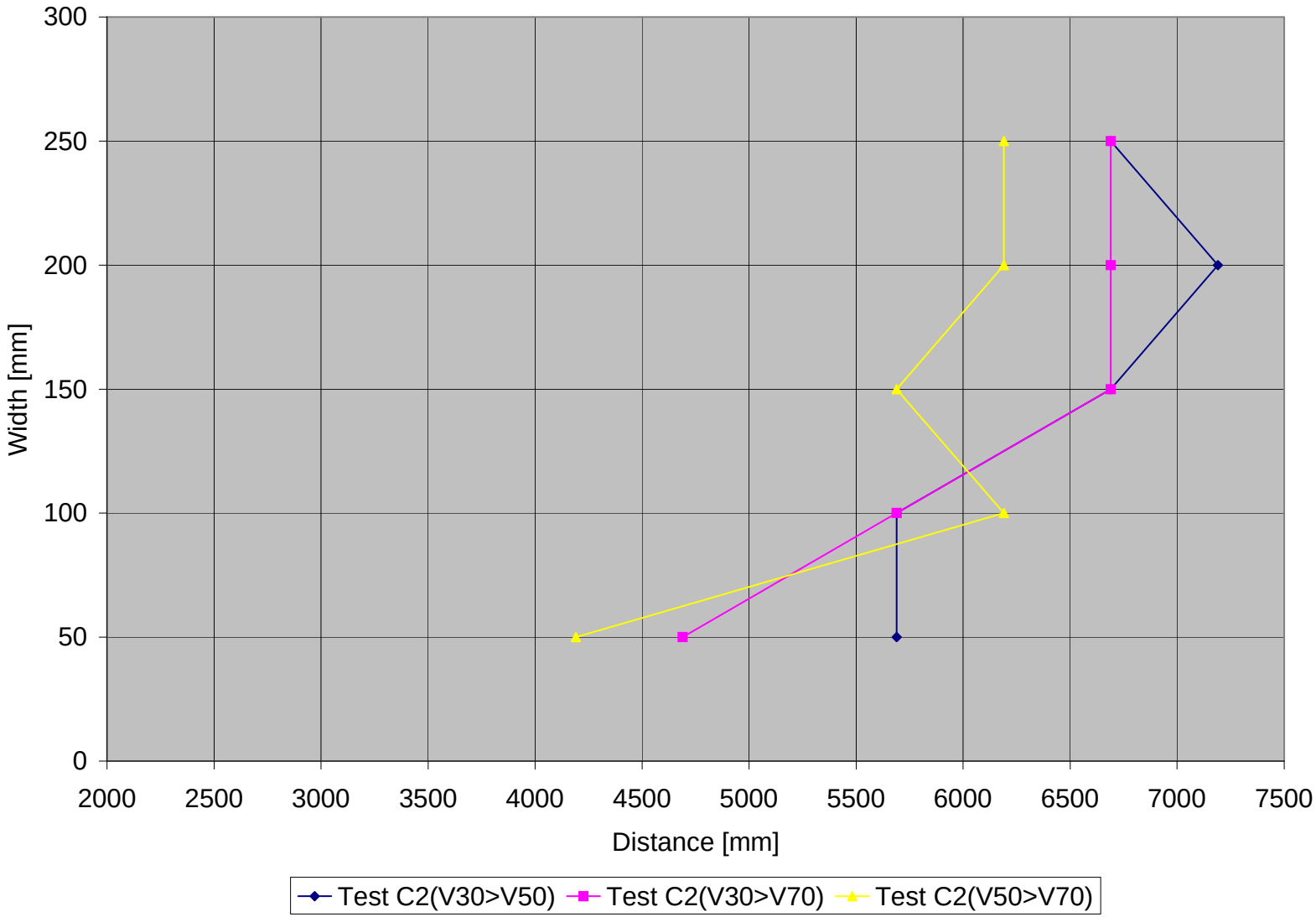

Figure D - 13: Test C2-Location of turning points where *V30>V50*, *V30>V70* and *V50>V70*

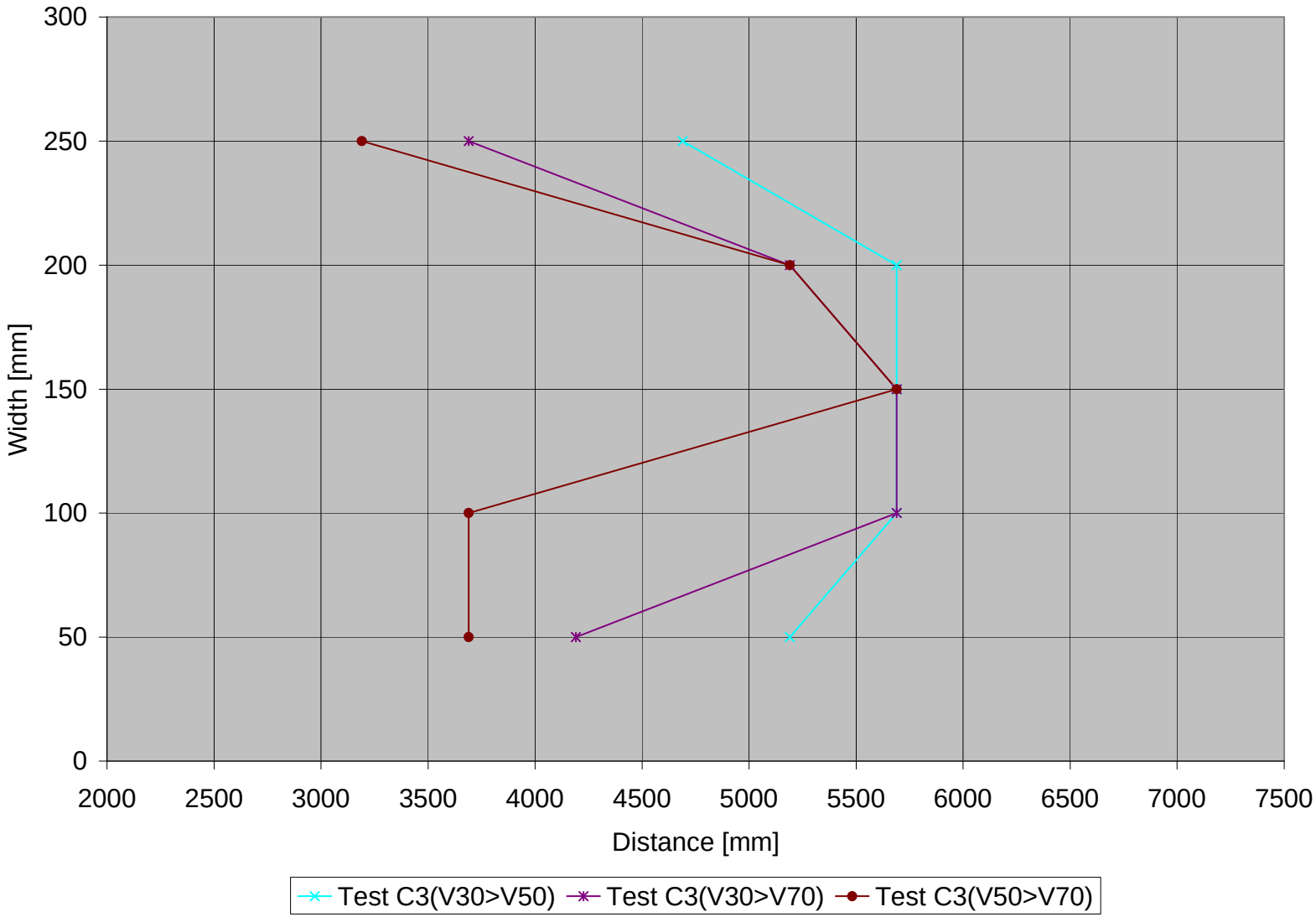

Figure D - 14: Test C3-Location of turning points where *V30>V50*, *V30>V70* and *V50>V70*

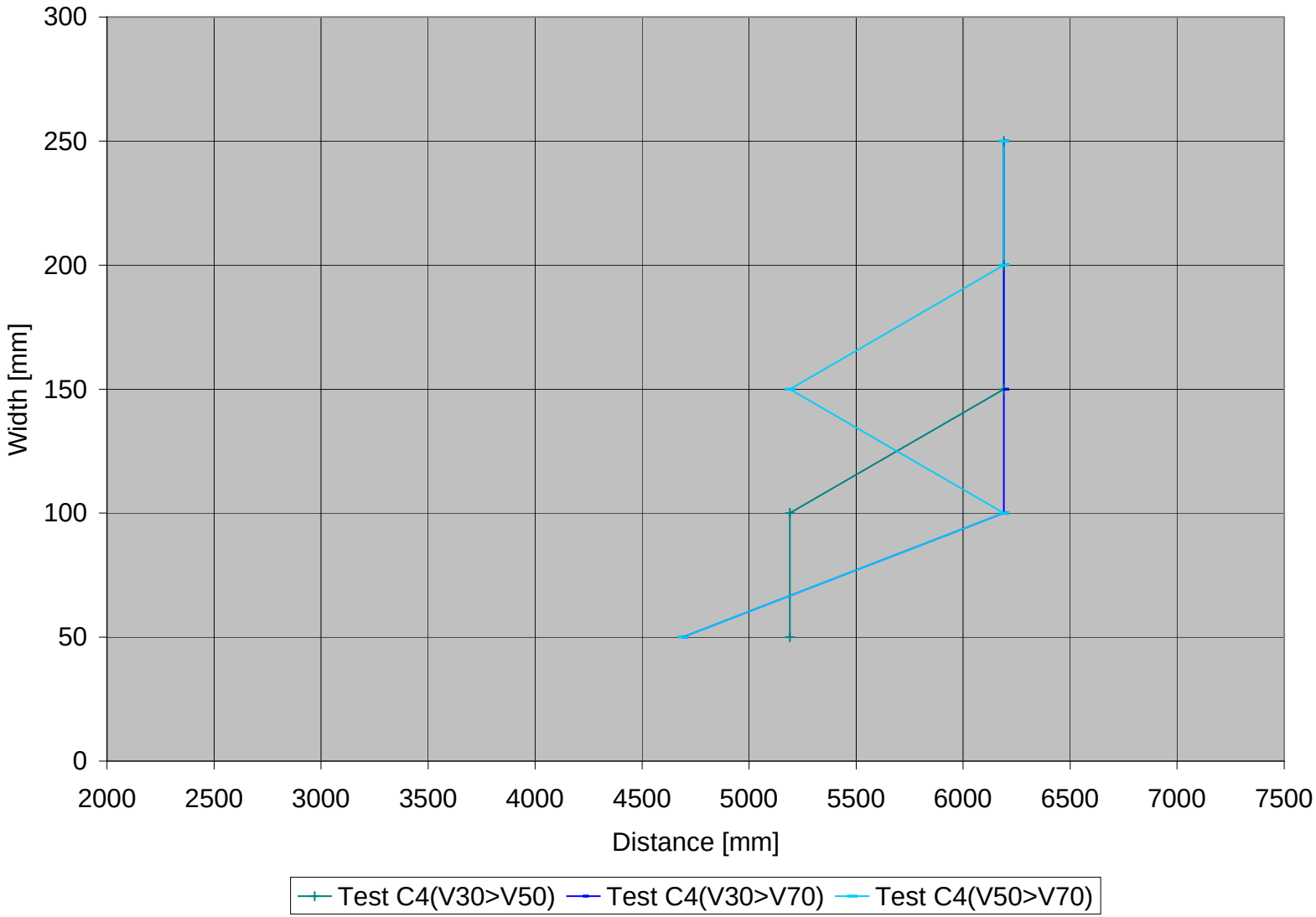

Figure D - 15: Test C4-Location of turning points where *V30>V50*, *V30>V70* and *V50>V70*

APPENDIX E-LOCATION OF TURNING POINTS FOR TEST D, E AND F

APPENDIX E-LOCATION OF TURNING POINTS FOR TESTS D, E AND F

TABLE OF CONTENTS

LIST OF FIGURES

E.1 TEST D

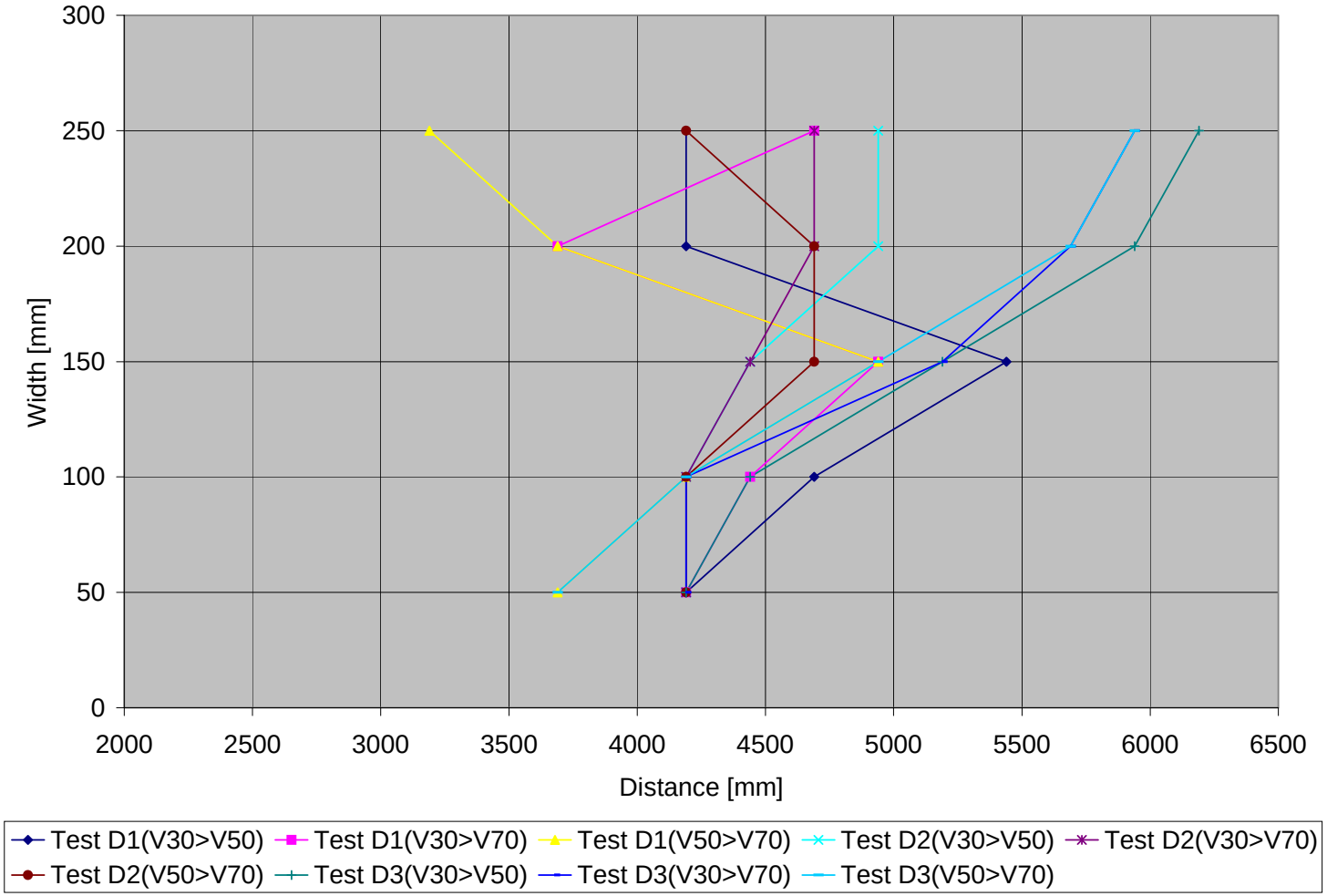

Figure E - 1: Location of turning points where *V30>V50*, *V30>V70* and *V50>V70* for Test D1, D2 and D3

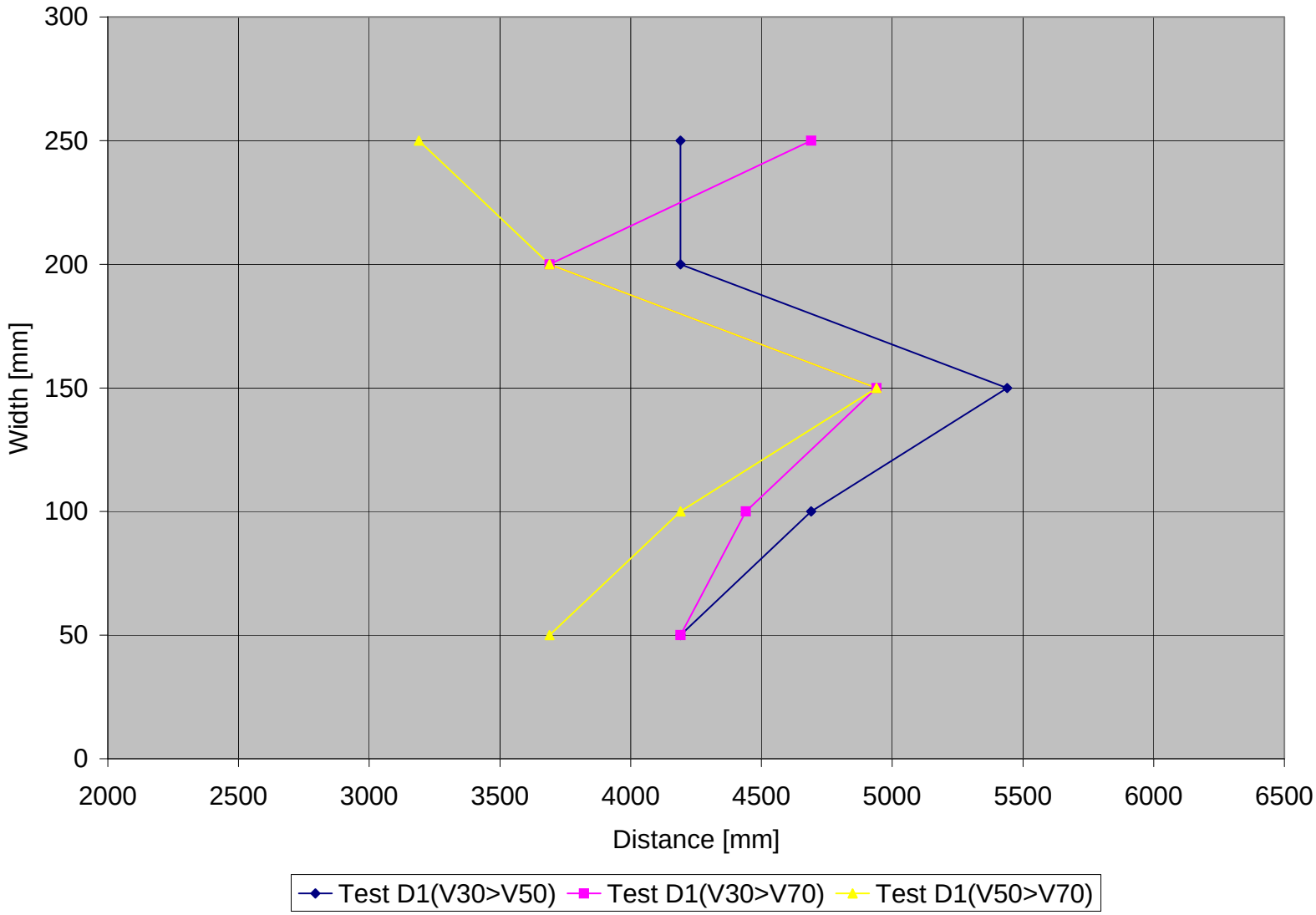

Figure E - 2: Test D1-Location of turning points where *V30>V50*, *V30>V70* and *V50>V70*

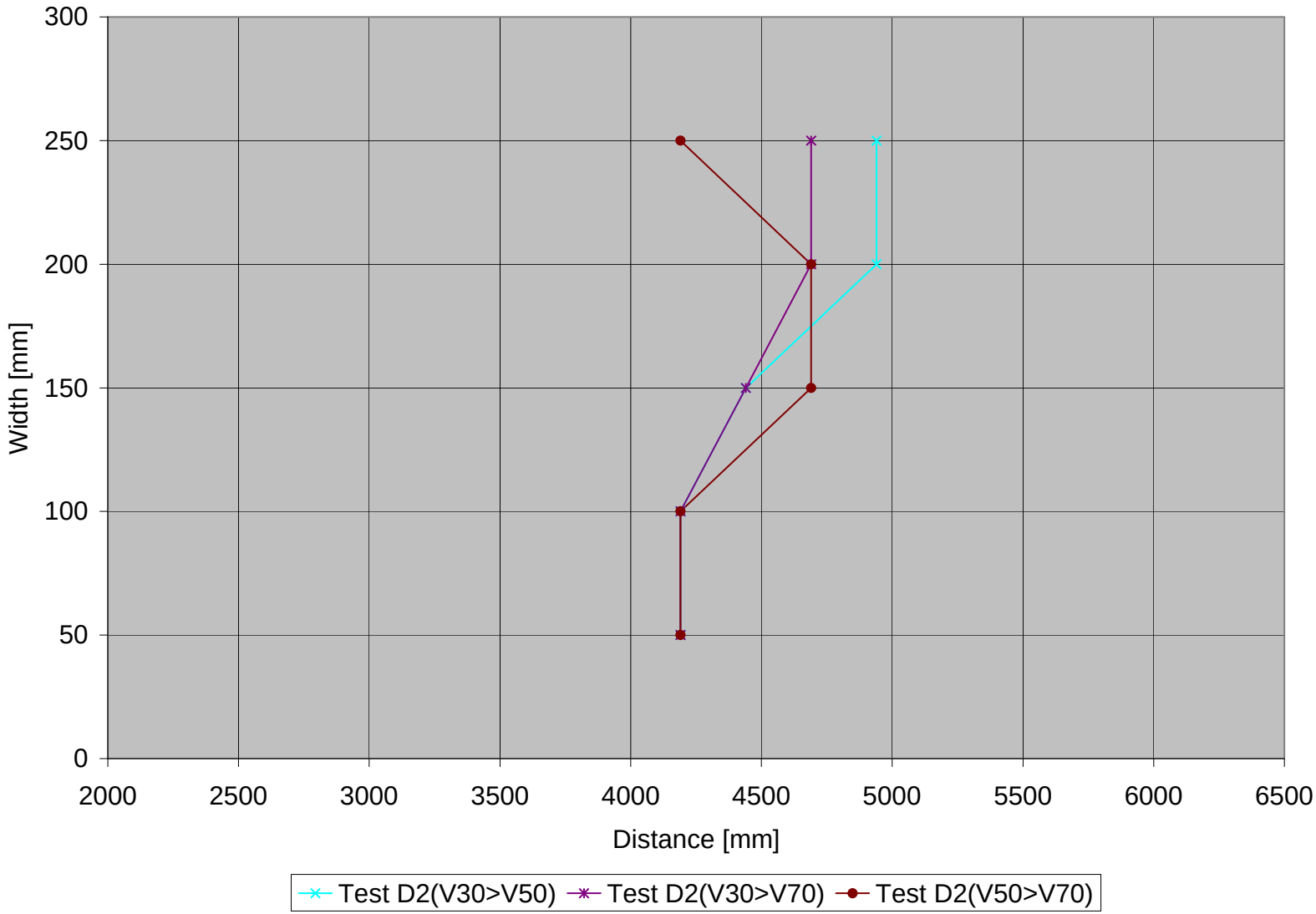

Figure E - 3: Test D2-Location of turning points where *V30>V50*, *V30>V70* and *V50>V70*

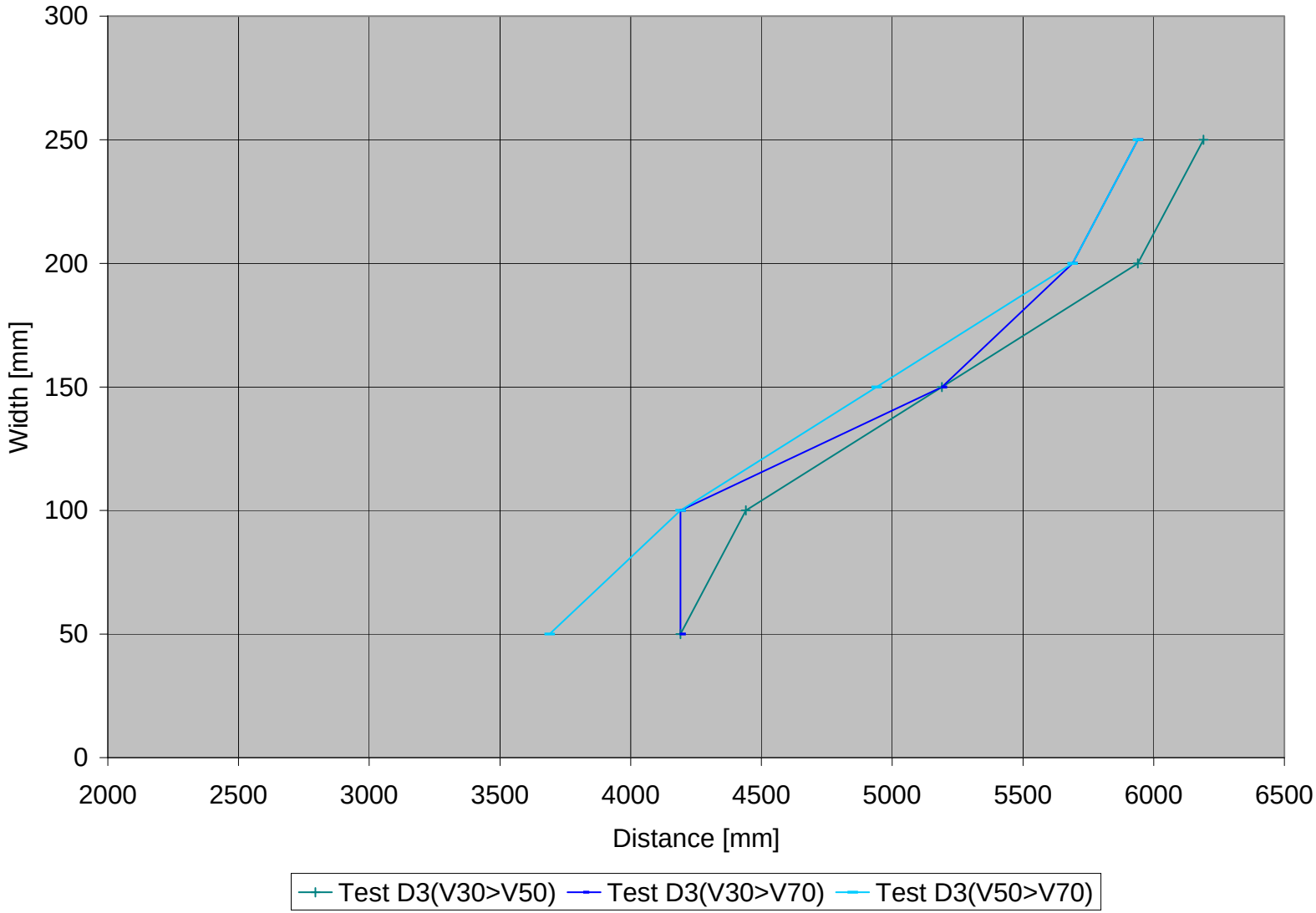

Figure E - 4: Test D3-Location of turning points where *V30>V50*, *V30>V70* and *V50>V70*

E.2 TEST E

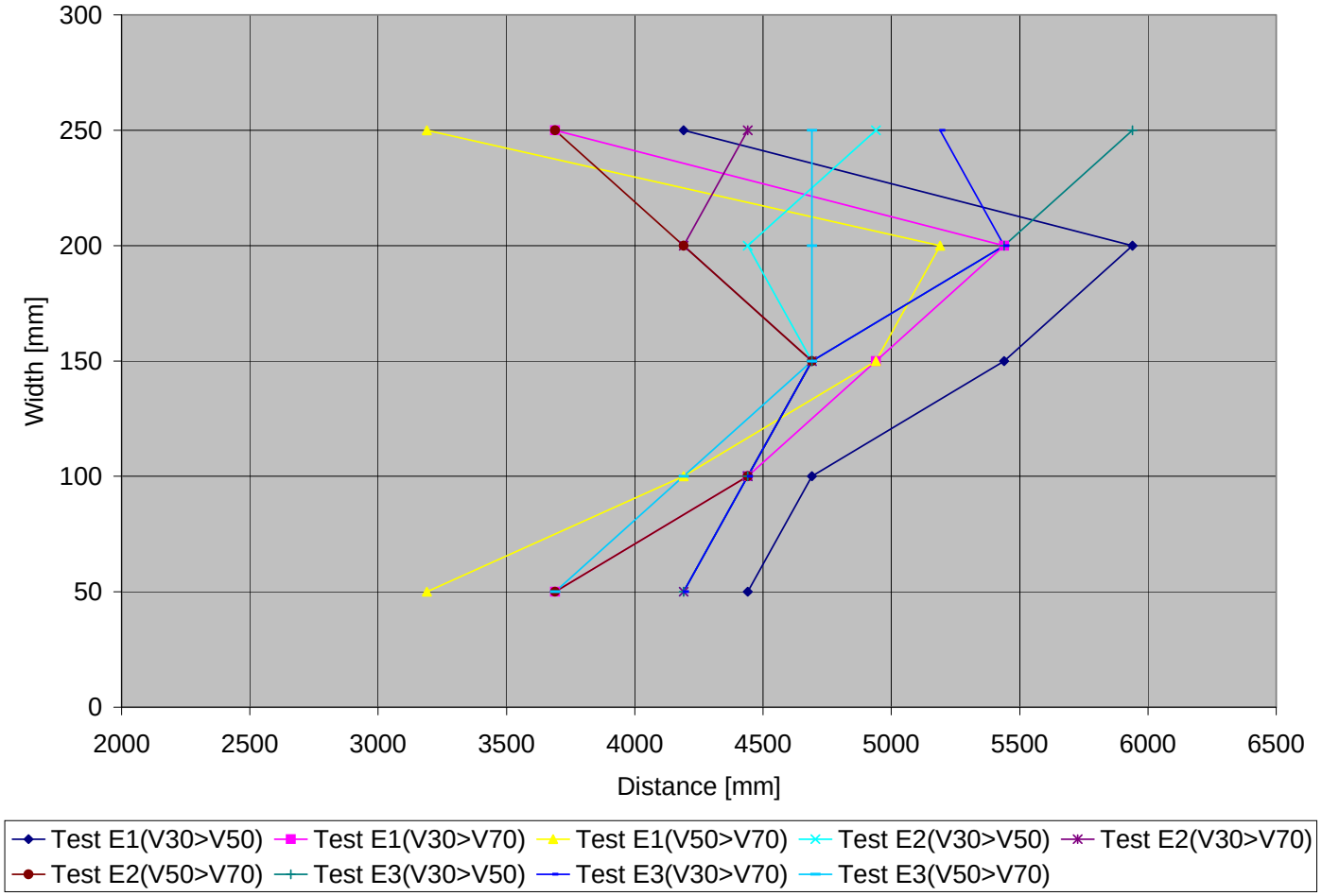

Figure E - 5: Location of turning points where *V30>V50*, *V30>V70* and *V50>V70* for Test E1, E2 and E3

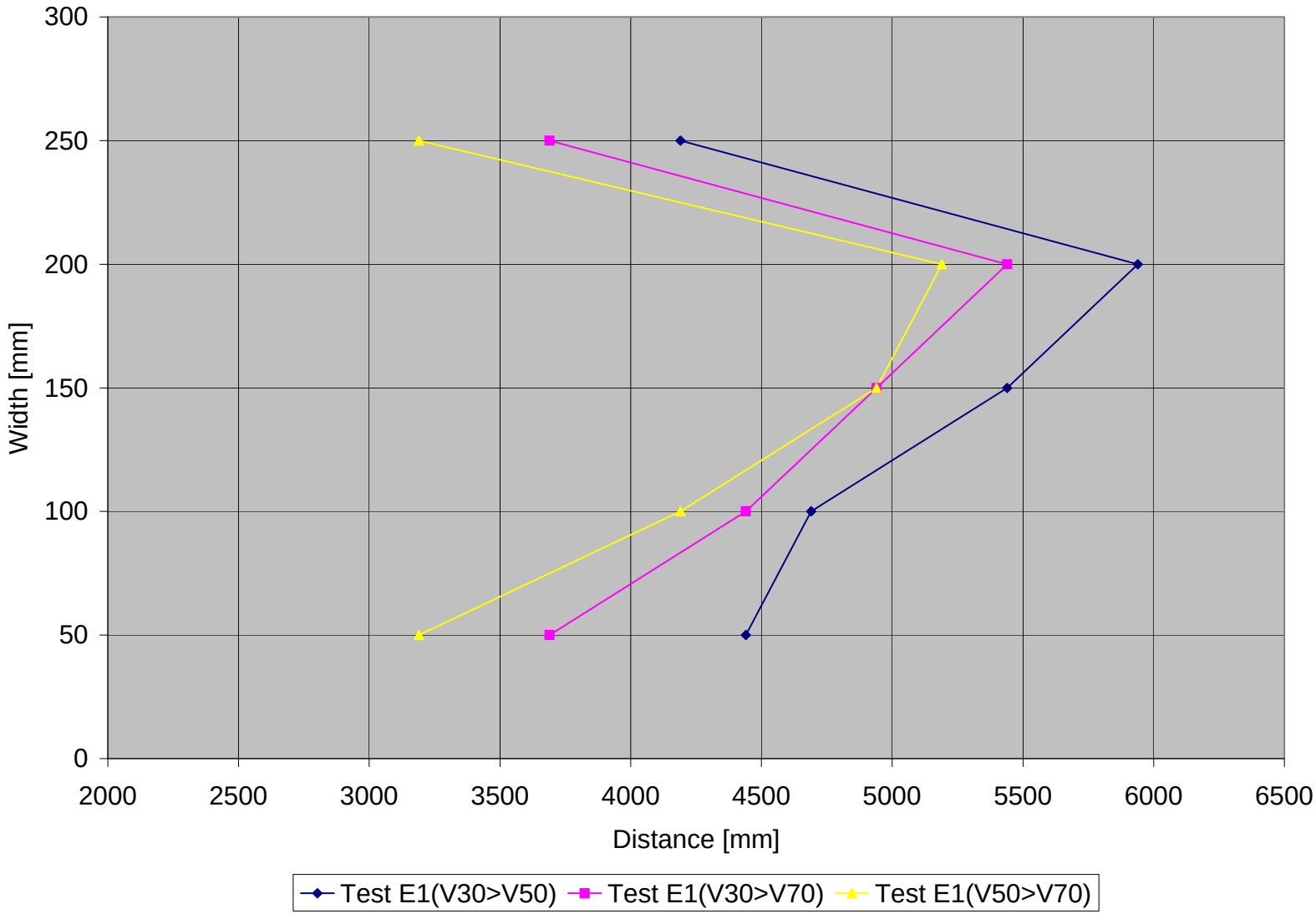

Figure E - 6: Test E1-Location of turning points where *V30>V50*, *V30>V70* and *V50>V70*

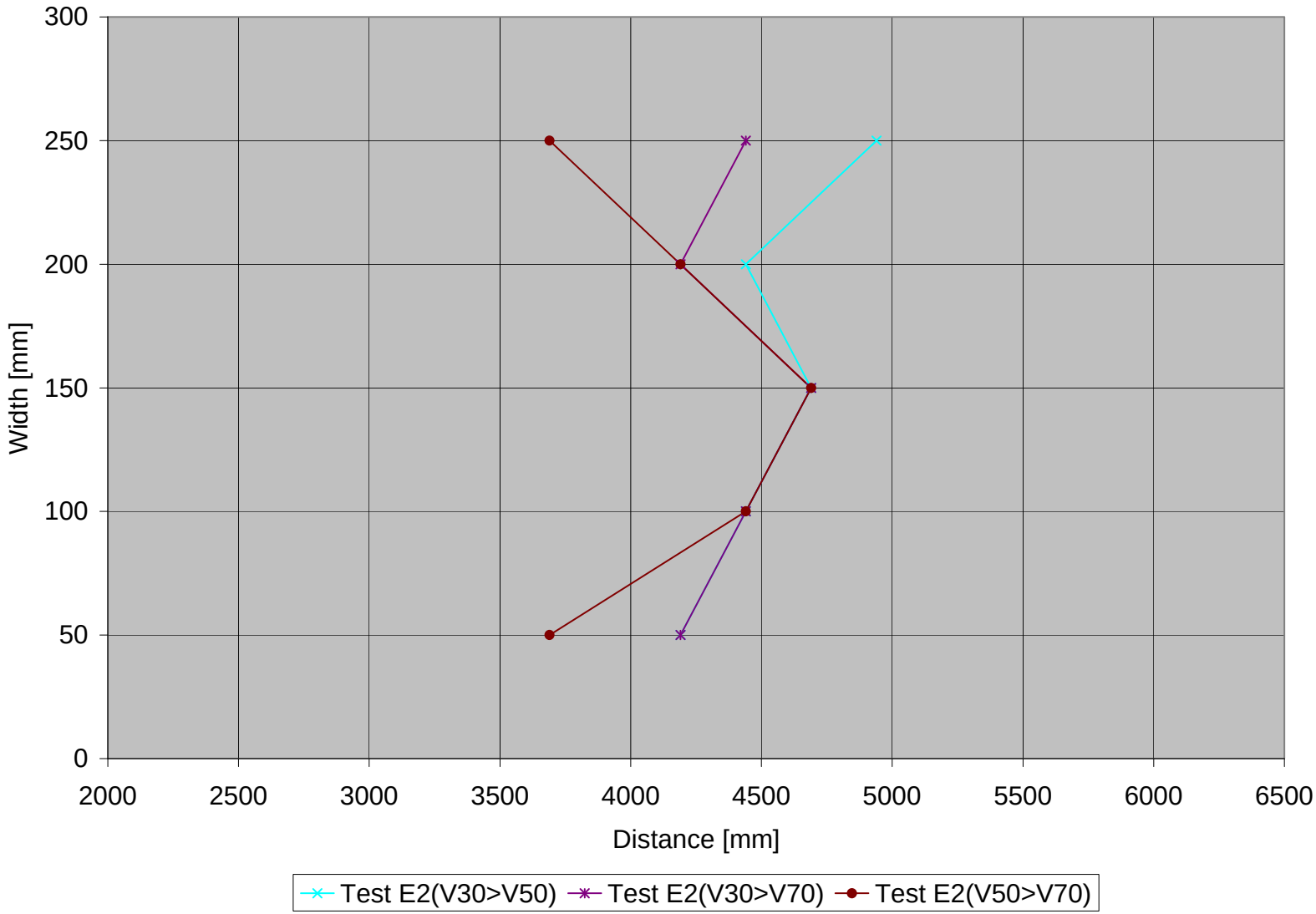

Figure E - 7: Test E2-Location of turning points where *V30>V50*, *V30>V70* and *V50>V70*

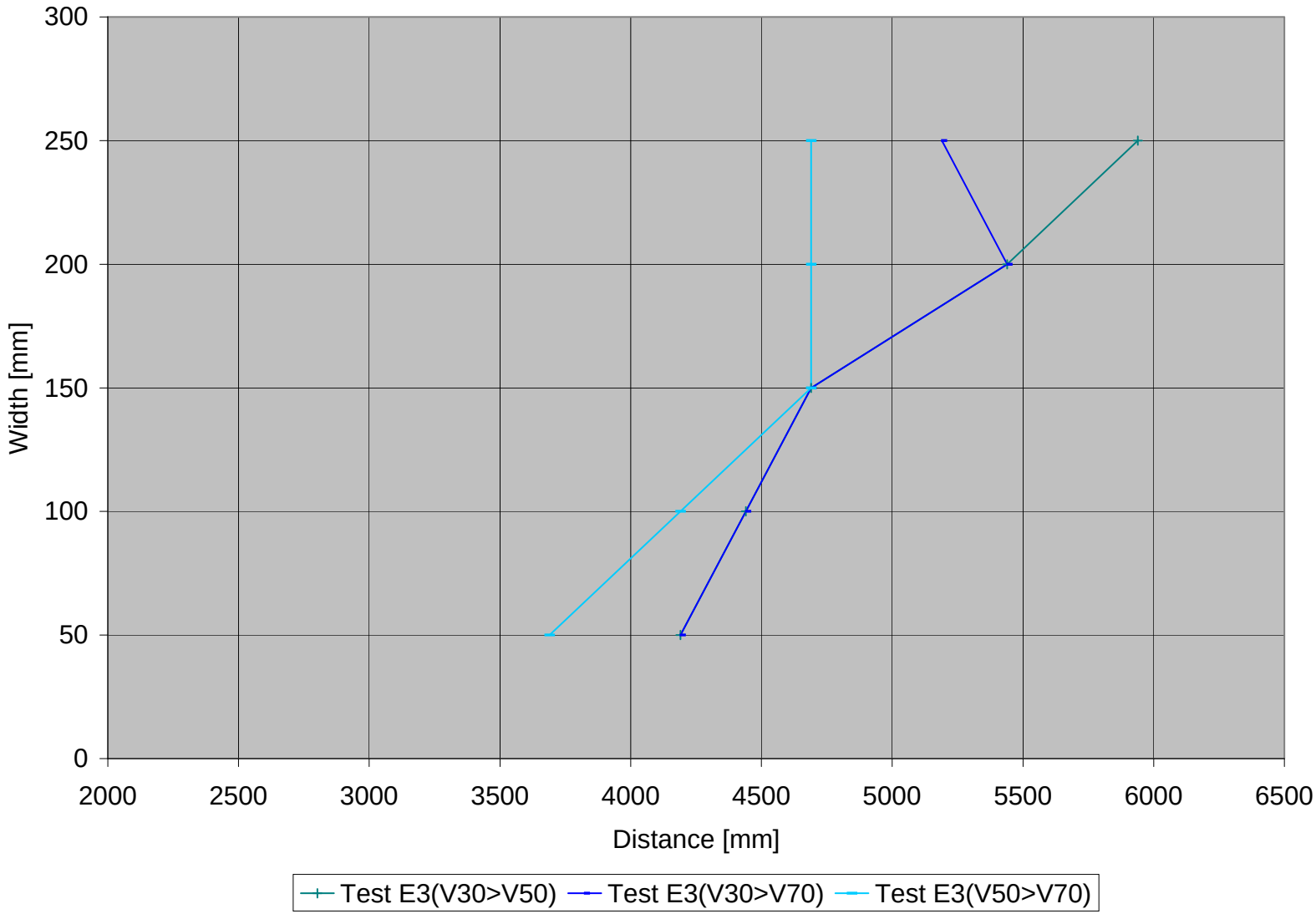

Figure E - 8: Test E3-Location of turning points where *V30>V50*, *V30>V70* and *V50>V70*

E.3 TEST F

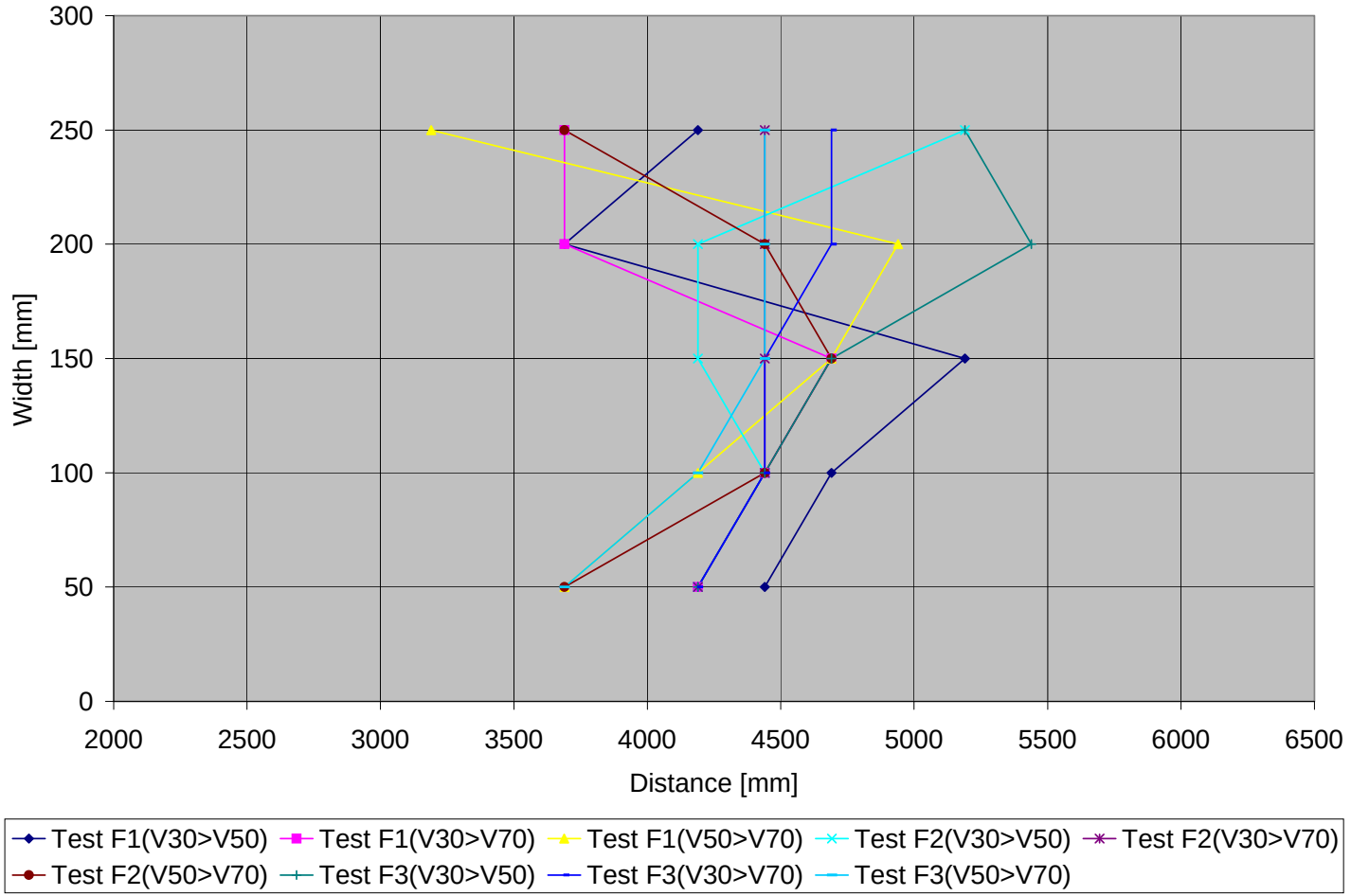

Figure E - 9: Location of turning points where *V30>V50*, *V30>V70* and *V50>V70* for Test F1, F2 and F3

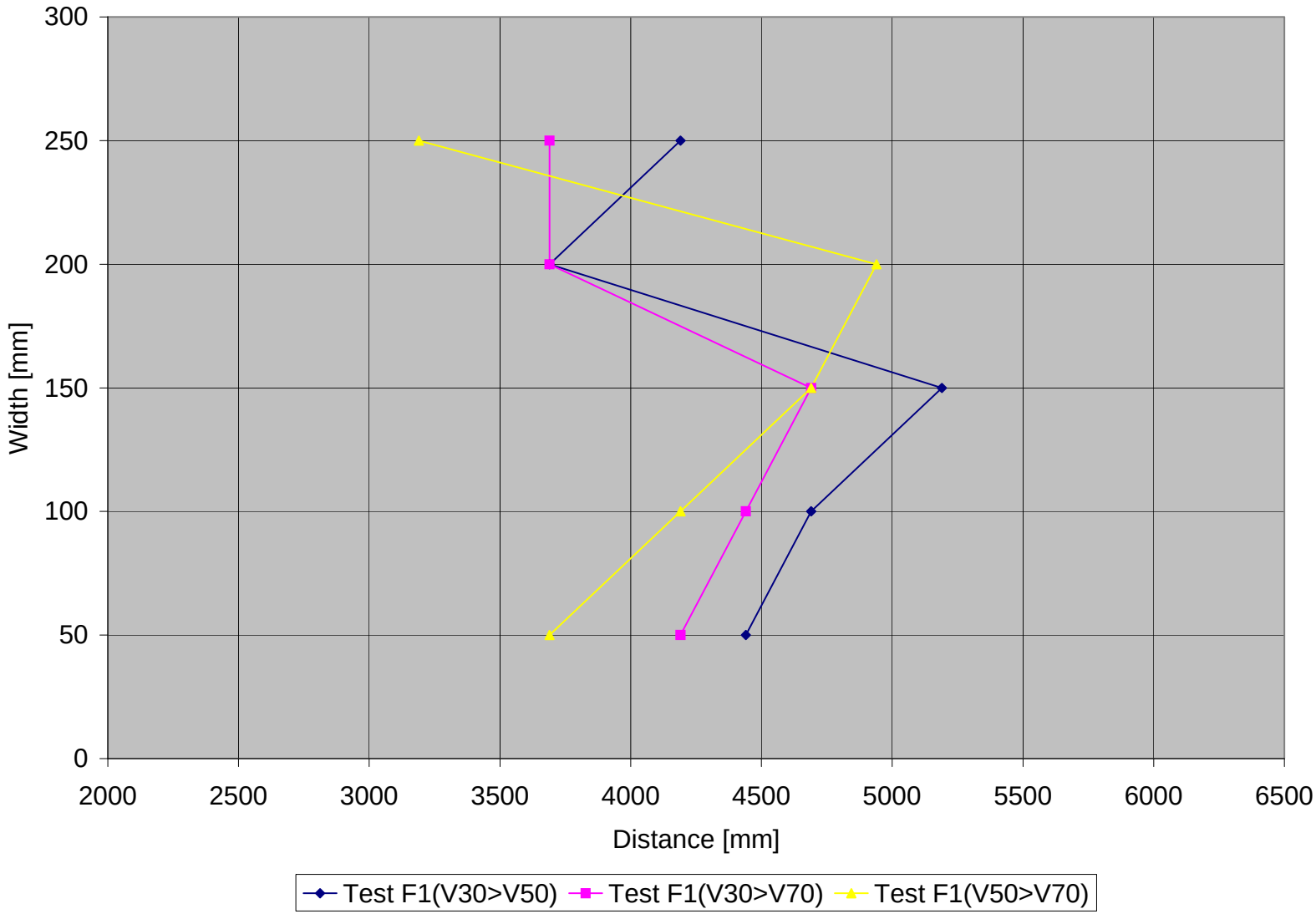

Figure E - 10: Test F1-Location of turning points where *V30>V50*, *V30>V70* and *V50>V70*

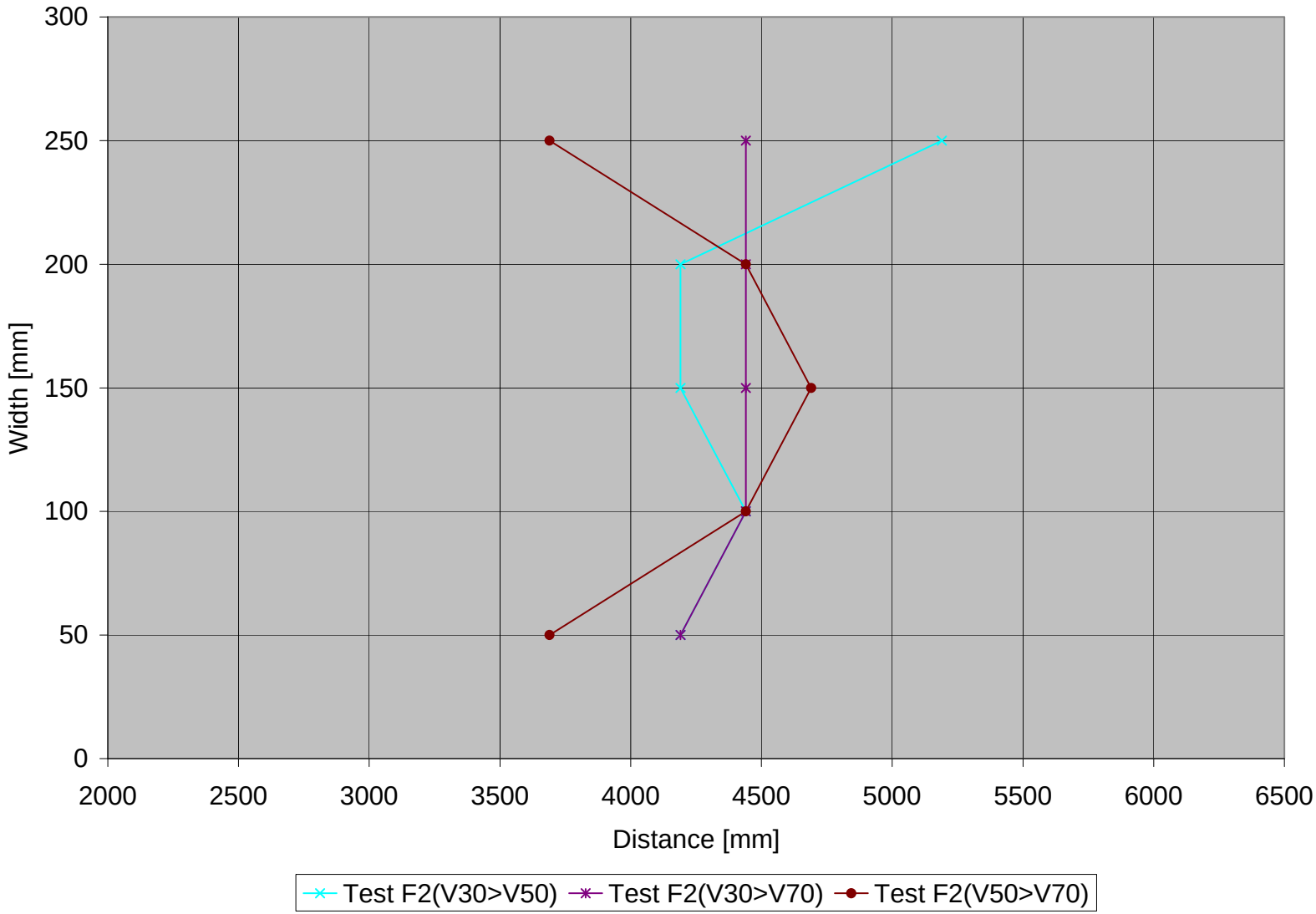

Figure E - 11: Test F2-Location of turning points where *V30>V50*, *V30>V70* and *V50>V70*

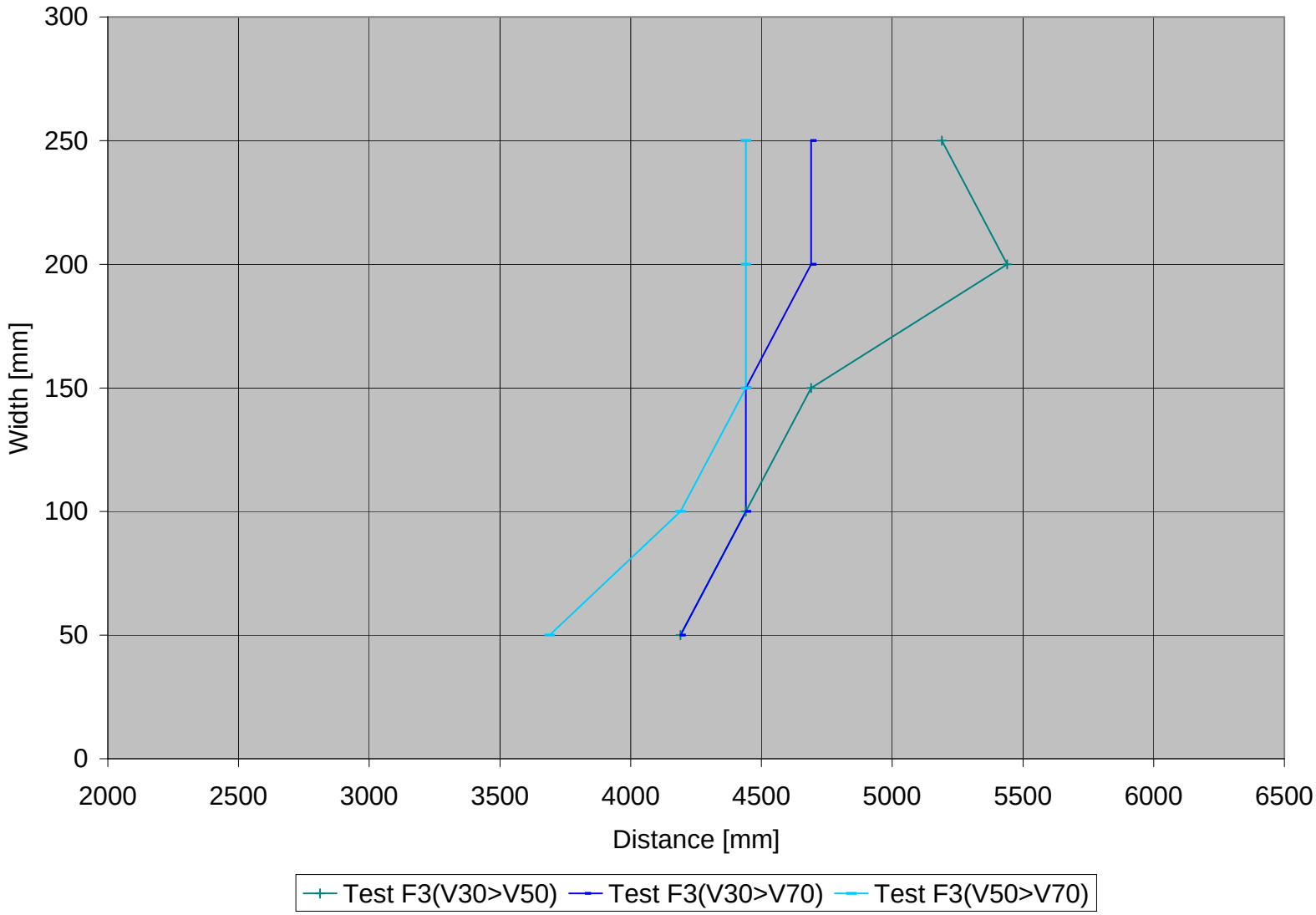

Figure E - 12: Test F3-Location of turning points where *V30>V50*, *V30>V70* and *V50>V70*